AD-A186 938 UNITED STATES - JAPAN SEMINAR ON QUANTUM MECHANICAL 1/7
ASPECTS OF QUANTUM EL (U) MASSACHUSETTS INST OF TECH
CAMBRIDGE RESEARCH LAB OF ELECTRON
UNCLASSIFIED J H SHAPIRO ET AL OCT 87 N00014-87-G-0198 F/G 20/3 NL

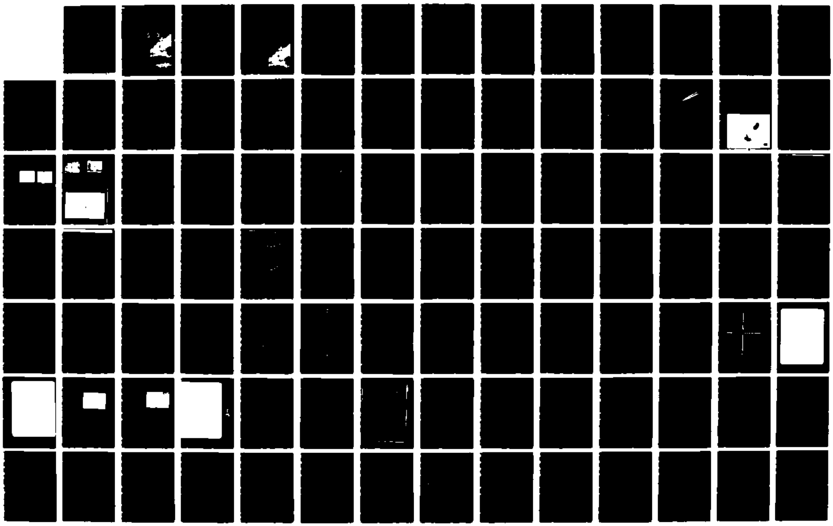

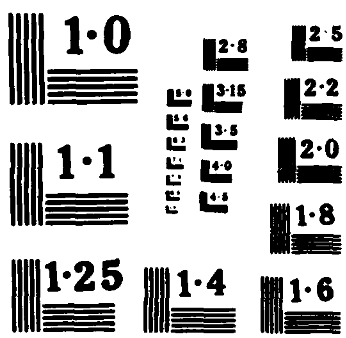
1·0
2·8
2·5
3·15
2·2
3·5
1·1
2·0
4·0
4·5
1·8
1·25
1·4
1·6

(1)

UNITED STATES - JAPAN SEMINAR ON QUANTUM MECHANICAL ASPECTS OF QUANTUM ELECTRONICS

HILTON INN RESORT

MONTEREY, CALIFORNIA

JULY 21-24, 1987

J.H. SHAPIRO

H. TAKUMA

Coordinators

UNITED STATES - JAPAN SEMINAR
ON
QUANTUM MECHANICAL ASPECTS OF QUANTUM ELECTRONICS

HILTON INN RESORT

MONTEREY, CALIFORNIA

JULY 21-24, 1987

J.H. SHAPIRO

H. TAKUMA

Coordinators

Preface

The continuing rapid developments taking place in quantum electronics cut across a wide swath of research activities including atomic and solid-state physics, nonlinear optics and spectroscopy, and quantum light beams and quantum measurements. Strong research programs in these areas presently exist in the United States and Japan. These Proceedings represent summaries and viewgraphs from a U.S.-Japan Seminar entitled "Quantum Mechanical Aspects of Quantum Electronics," which was held from July 21 to July 24, 1987 at the Hilton Inn Resort in Monterey, California. The 1987 Seminar was the fourth in a series on quantum electronics which began in Hakone, Japan in 1977, with meetings in Maui, USA in 1980 and Nara, Japan in 1983. The previous seminars engendered valuable technical ties between researchers in the two countries, which were strengthened and expanded at the Monterey Seminar. The early meetings in the series were centered on the emerging techniques in nonlinear and high-resolution spectroscopy. At the Nara meeting, the emphasis shifted to include major consideration of quantum issues of coherence and incoherence. The 1987 Seminar focused on topics of very current interest, including: neutral atom trapping; ultrahigh stability sources and ultrahigh resolution spectroscopy; squeezed states of light; and nonlinear optics of semiconductors. The spirit and vibrancy with which these topics were discussed was a testimony to the vitality of the U.S.-Japan Seminars. We look forward to another such successful meeting in Japan in 1989 .

Jeffrey H. Shapiro
Hiroshi Takuma

October 1987

Acknowledgements

The 1987 U.S.-Japan Seminar on Quantum Mechanical Aspects of Quantum Electronics was principally supported by grants from the U.S. National Science Foundation and the Japan Society for the Promotion of Science. The preparation and distribution of these Proceedings was supported by the U.S. Office of Naval Research. Additional support for the Seminar arrangements came from the following Corporate Sponsors: Coherent Laser Products, Hoya Optics, IBM, Massachusetts Institute of Technology, Newport Corporation, and Spectra-Physics. Without the support obtained from all of these sources the 1987 Seminar would not have been so successful.

U.S.-JAPAN SEMINAR

Quantum Mechanical Aspects of Quantum Electronics

July 21 — July 24, 1987

Hilton Inn Resort
Monterey, California

PROGRAM

Page No.

		Page No.
11:00 AM	Femtosecond Studies of Hot Carrier Relaxation in GaAs and AlGaAs - E.P. Ippen and J.G. Fujimoto	415
11:40 AM	Exciton Relaxation Phenomena in a Disordered System - M. Aihara	434
2:00 PM	Afternoon Outing: Tour of Monterey Bay Aquarium	

Session VII - Squeezed States II - M.D. Levenson, Chairman

7:30 PM	Generation of Number-Phase Minimum Uncertainty States - Y. Yamamoto, S. Machida, N. Imoto, M. Kitagawa, and G. Bjork	438
8:10 PM	Squeezing via Traveling-Wave Forward Four-Wave Mixing in Atomic Vapors: Comparison with Nondegenerate Theory - P. Kumar	451
8:50 PM	Generating Squeezed Microwave Radiation with a Josephson Parametric Amplifier - B. Yurke	476
9:30 PM	Detecting Squeezed States by Cross-Correlation - Z.Y. Ou, C.K. Hong, and L. Mandel	489

Friday July 24

7:00 AM	Continental Breakfast	

Session VIII - Spectroscopy, Instability and Multistability -
- R.G. Brewer, Chairman

8:30 AM	What Has Been Done and What Will Be Done by Subnatural Linewidth Spectroscopy - H. Takuma, K. Shimizu, and F. Shimizu	503
9:10 AM	Comprehensive Model for Laser Instability in a CO_2 Laser with Gaseous Saturable Absorber - T. Shimizu, M. Tachikawa, and K. Tanii	531
9:50 AM	Recent Progress in Optical Bistability and Tristability - T. Yabuzaki and M. Kitano	552
10:30 AM	Coffee Break	

Principal Sponsors

National Science Foundation

Japan Society for the Promotion of Science

Proceedings Sponsor

U.S. Office of Naval Research

Corporate Sponsors

Coherent Laser Products

Hoya Optics

IBM

MIT

Newport Corporation

Spectra-Physics

Coordinators

J.H. Shapiro - U.S. Coordinator

D.S. Chemla - U.S. Co-Coordinator

H. Takuma - Japan Coordinator

U.S. — JAPAN SEMINAR

Quantum Mechanical Aspects of Quantum Electronics

July 21 - July 24, 1987

Hilton Inn Resort
Monterey, California

LIST OF PARTICIPANTS

Japanese Participants

M. Aihara	Department of Physics, Faculty of Liberal Arts, Yamaguchi University, Yamaguchi 753.
Y. Arakawa	Institute of Industrial Science, University of Tokyo Roppongi 7-22-1, Minato-ku, Tokyo.
E. Hanamura	Department of Applied Physics, University of Tokyo, 7-3-1 Hongo, Bunkyo-ku, Tokyo 113.
N. Imoto	NTT Basic Research Laboratories 3-9-7, Midori-cho, Musashino-shi, Tokyo 180.
S. Kano	Institute for Laser Science, University of Electro-Communications, 1-5-1, Chofugaoka, Chofu-shi, Tokyo 182.
Y. Masumoto	Institute of Physics, University of Tsukuba Sakura-mura, Niihari-gun, Ibaraki-ken, 305.
M. Ohtsu	Graduate School of Nagatsuta, Tokyo Institute of Technology, 1-15-42 Nagatsuta, Midori-ku, Yokohama 227.
F. Shimizu	Department of Applied Physics, University of Tokyo Bunkyo-ku, Tokyo 113.
K. Shimoda	Department of Physics, Keio University 3-4-1 Hiyoshi, Kohoku-ku, Yokohama 223.

Japanese Participants (contd)

M. Tachikawa (T. Shimizu) — Department of Physics, University of Tokyo, 7-3-1 Hongo, Bunkyo-ku, Tokyo 113.

T. Takagahara — NTT Electrical Communication Laboratories, 3-9-11 Midori-cho, Musashino-shi, Tokyo 180.

H. Takuma — Institute for Laser Science, University of Electro-Communications, 1-5-1 Chofugaoka, Chofu-shi, Tokyo 182.

T. Yabuzaki — Department of Physics, Kyoto University, Sakyo-ku, Kyoto 606.

Y. Yamamoto — NTT Electrical Communication Laboratories, 3-9-11 Midori-cho, Musashino-shi, Tokyo 180.

M. Yamanishi — Department of Physical Electronics, Hiroshima University, Saijo-cho, Higashi-Hiroshima 724.

United States Participants

A. Ashkin — AT&T Bell Laboratories, Holmdel, New Jersey 07733

R.G. Brewer — IBM Almaden Research Center, 650 Harry Road, San Jose, California 95120.

R.Y. Chiao — Department of Physics, University of California, Berkeley, California 94720.

D.S. Chemla — AT&T Bell Laboratories, 4E418, Holmdel, New Jersey 07733

E. Garmire — Center for Laser Studies, University of Southern California 1112, Los Angeles, California 90089.

United States Participants (contd)

J.L. Hall	JILA National Bureau of Standards, 325 Broadway, Boulder, Colorado 80303.
E.P. Ippen	Department of Electrical Engineering and Computer Science, Massachusetts Institute of Technology, Cambridge, Mass. 02139.
H.J. Kimble	Department of Physics, University of Texas, Austin, Texas 78712.
S.W. Koch	Optical Sciences Center, University of Arizona, Tucson, Arizona 85721.
M.S. Kruger	Laboratory for Physical Science, 4928 College Avenue, College Park, Maryland 20740.
P. Kumar	Department of Electrical Engineering and Computer Science, Northwestern University, Evanston, Illinois 60201.
M.D. Levenson	IBM Almaden Research Center, 650 Harry Road, San Jose, California 95120.
M. Lindberg	Optical Sciences Center, University of Arizona, Tucson, Arizona 85721.
L. Mandel	Department of Physics and Astronomy, University of Rochester, Rochester, New York 14627.
A. Mooradian	MIT Lincoln Laboratory, Lexington, Massachusetts 02173.
H. Nathel	Lawrence Livermore National Lab, Mail Stop L-43, P.O. Box 808, Livermore, California 94550.
A.V. Nurmikko	Division of Engineering, Brown University, Providence, Rhode Island 02912.
N. Peyghambarian	Optical Sciences Center, University of Arizona, Tucson, Arizona 85721.

United States Participants (contd)

W.D. Phillips	National Bureau of Standards, Gaithersburg, Maryland 20899.
H. Pilloff	Office of Naval Research, Code 1112LO, Arlington, Virginia 22217.
B.L. Schumaker	Jet Propulsion Laboratory, MS 200-122, 4800 Oak Grove Drive, Pasadena, California 91109.
J.H. Shapiro	Department of Electrical Engineering and Computer Science, Massachusetts Institute of Technology, Cambridge, Mass. 02139.
R.M. Shelby	IBM Almaden Research Center, 650 Harry Road, San Jose, California 95120.
R.E. Slusher	AT&T Bell Laboratories 1D368, Murray Hill, New Jersey 07974.
P.A. Wolff	Department of Physics, Massachusetts Institute of Technology, Cambridge, Massachusetts 02139.
N.C. Wong	Research Laboratory of Electronics, Massachusetts Institute of Technology, Cambridge, Massachusetts 02139.
H.P. Yuen	Department of Electrical Engineering and Computer Science, Northwestern University, Evanston, Illinois 60201.
B. Yurke	AT&T Bell Laboratories 1C247, Murray Hill, New Jersey 07974.

Third Country Participants

D.F. Walls	Physics Department, University of Waikato, Hamilton, New Zealand.
Ms. L.-A. Wu	Department of Physics, University of Texas, Austin, Texas 78712.

OPTICAL COOLING AND TRAPPING

William D. Phillips, MET B258, National Bureau of Standards
Gaithersburg, MD 20899

(Summary of presentation at the U. S. - Japan Seminar on Quantum Mechanical Aspects of Quantum Electronics, Montery, CA, July 1987)

Past and present collaborators on work done at NBS Gaithersburg are shown on the 1st slide. Many other groups throughout the world are active in this area and only a fe are mentioned in this talk. The November 1985 issue of J. Opt. Soc. Am. B contains papers from many of these groups. A forthcoming article in Science by Phillips, Gould and Lett reviews much of the recent work.

Some of the motivations for the work are listed in slide 2. In particular, note that efforts to achieve Bose condensation in spin polarized hydrogen have been plagued by problems related to interactions between atoms at high density and atoms adsorbed on the walls of the container. Optical cooling and electromagnetic trapping may be able to address these problems because low temperatures can be achieved, allowing lower densities for Bose condensation, and in a container without material walls.

Slide 3 shows how the resolution of free-bound spectroscopy is limited by the kinetic energy spread of the free atoms. With laser cooled atoms, the free-bound spectroscopic resolution becomes about equal to bound-bound resolution. Slide 4 illustrates how the low energies of laser cooled atoms put collisions between them in a highly qunatum mechanical regime, one which has not been investigated experimentally as yet.

The principle of laser cooling, proposed in 1975 and first demonstrated on trapped ions in 1978, is shown in slide 5. When the laser is tuned below resonance, the atoms absorb the light more strongly when they are moving toward the laser. This results in more absorptions that slow the atoms than ones which accelerate them. In a trap, such as an ion trap, the orbits of the atoms continually bring the atoms toward the laser, so they can be slowed down. In the absence of such trapping, symmetric illumination can accomplish the same thing, as shown in slide 6.

The problem is that the range of velocities over which the force is substantial is only a few meters per second. For a trapped atom going much faster than this, this is not too bad, since the small cooling rate can act over a long period of time. Ion traps hold ions at room temperature or higher energies, but neutral traps (slide 7) are all very shallow and can't hold atoms with energies above about 1 K. Therefore, one must slow the atoms down first, then trap or further cool them.

Slide 8 shows the basic idea of decelerating an atomic beam. A laser beam is directed against an atomic beam and the absorbed photons slow down the atoms. As the atoms slow, their Doppler shift changes and they go out of resonance with the laser. The two major solutions to this problem are to change the frequency of the laser to compensate the change in Doppler shift, and to change the frequency of the atoms (by for example a Zeeman shift).

Slide 9 shows the effect on an atomic beam velocity distribution when nothing is done to compensate the changing Doppler shift. A narrow feature is produced, but little deceleration occurs and only a small part of the distribution is affected. Slides 10 and 11 show the effects of using Zeeman tuning and frequency chirping. These techniques can actually bring the atomic beam virtually to rest. Slide 12 shows a view of our Zeeman tuned cooling apparatus, and the observer position for slide 13 which is a photograph of the stopped beam.

Once the atoms are stopped or going very slowly, the cooling scheme of slide 6 can be used. Slide 14 calculates the damping force on an atom with small velocity. Slide 15 calculates the limiting temperature, balancing the rate of dissipating energy by damping with the rate of gaining energy by the random heating caused by scattering of photons in random directions. Also illustrated is the fact that with a strong motional damping the atoms have a short mean free path and therefore a long diffusion time. This slow diffusion of atoms is the molasses effect. Note that the numbers will be quite different in three dimensions. Slide 16 shows the expected 1-D diffusion time as a function of detuning for this "classical" molasses.

Slide 17 shows our experimental arrangement for observing molasses: Atoms from the atomic beam, slowed by the laser, enter the molasses formed at the interesection of 3 orthogonal pairs of counterpropagating laser beams. Here they "stick" for a long time. Slide 18 is a photograph of the nearly stopped atomic beam and the molasses. Molasses was first observed at Bell Labs in 1985 in pulsed experiments. We achieve higher density by using a continuous process.

Slide 19 shows Phil Gould and Pauld Lett making molasses in our lab, along with a picute of molasses so bright it can be easily seen in daylight, Another picture of molasses is in slide 20.

By sweeping the molasses laser frequency we can measure the molasses brightness as a function of frequency as shown in slide 21. The smooth curve is the predicted behavior of the molasses diffusion time, which should be directly related to the atomic density. Because of additional factors affecting molasses brightness, we also measured the molasses lifetime, the time for atoms to diffuse out of the intersection of the laser beams. The apparatus for this is shown in slide 22. The atomic beam and cooling laser are chopped off, turning off the slow atoms into the molasses, and the fluorescence from the molasses is observed as a function of time.

Slides 23 and 24 show typical loading and decay curves as the source of slow atoms to the molasses is turned on and off. Slide 24 shows a sequence of decay curves as the molasses frequency is scanned, and slide 25 plots the molasses lifetime as a function of frequency for two different powers. The solid curve is the theoretical prediction for classical molasses. The disagreement is strong.

Slide 26 derives the expected drift velocity of atoms in molasses if the laser beams are unbalanced. The exact result for classical molasses indicates a subtantial reduction in the molasses lifetime for a 10% imbalance. Slide 27 shows the experimental results compared to the theory, again with a large disgreement, more than a factor of ten. Slide 28 summarizes possible reasons for the disagreement. Most significant is the

fact that at low power the experimental molasses acts nearly "normal", that is, like classical molasses. None of the possible explanations have given explicit predictions of the experimentally observed behavior.

We now turn to a consideration of dipole forces on atoms in laser fields. Slide 29 shows the origin of the dipole potential in the dressed atom picture. Starting with a ground and excited state g and e, we turn on the laser field, but not the interaction between atoms and laser. The energy levels of atom+field are a ladder of pairs of nearly degenerate states separated by the detuning from resonance. When the interaction is turned on the nearly degenerate states (ground state with n+1 photons and excited state with n photons in the field) are repelled and mixed, being separated by the generalized Rabi frequency. In slide 30 we see the case for both positive and negative detunings of the laser. The atom occupies both dressed levels, but is predominantly in the one which connects adiabatically to the ground state. This is illustrated by the bigger dot. Thus for negative detunings the atom is more often on the level which has its lowest energy at the strongest part of the field. Details of this approach can be found in Dalibard and Cohen-Tannoudji, J. Opt. Soc. B 2, 1701 (1985).

The dipole force can be exploited to make a trap. Slide 31 shows a design suggested by Ashkin in 1978 and recently realized in our laboratory for the first time. Two laser beam with Gaussian intensity profiles are focussed so that they are counterpropagating and diverging at the center of the trap.. For negative detunings the dipole force provides a potential well perpendicular to the symmetry axis, while the radiation pressure or scattering force provides the potential well along the axis.

A number of refinements were needed before the original idea of Ashkin cound be accomplished. Gordon and Ashkin realized that the trap beam alone could not provide the cooling needed to stabilize that trap and that separate cooling was needed (slide 32.) They also realized that the dynamic Stark shifts induced by the trap would inhibit proper cooling. Dalibard, Reynaud and Cohen-Tannoudji suggested alternating the trapping and cooling beams to eliminate this problem (slide 33.) It was also known that the standing wave resulting from the counterpropagating trap beams would cause additional heating due to fluctuations in the strong dipole forces. Dalibard and Cohen-Tannoudji proposed the alternation of the two trap beams to eliminate this effect (slide 34.) Finally, Chu et al. demonstrated the efficient loading of an optical trap from optical molasses. Combining all these ideas we were able to make such a trap, having an volume over which atoms could be captured, of about 10^{-4} cm^3, and a density increase, averaged over the capture volume, on the order of 10^3 or 10^4 compared to the molasses density.

①

OPTICAL COOLING AND TRAPPING

Phillip Gould
Paul Lett
Alan Migdall
John Prodan
— N.B.S. Postdocs

Harold Metcalf
Tom Bergeman
Ivan So
— S.U.N.Y. Stony Brook

Jean Dalibard — Ecole Normale Superieure, Paris

W.D. Phillips — NBS

②

Why Cool and Confine Atoms?

- Spectroscopy - reduce Doppler and Transit Effects
- Bose-Einstein Condensation
  (Lower T → lower n; no walls)
- Quantum Optics
  (trap, cooling physics; cavity QED; statistics)
- Collisions
  (ultra-low energy, molecule and cluster formation)
- Antimatter

③

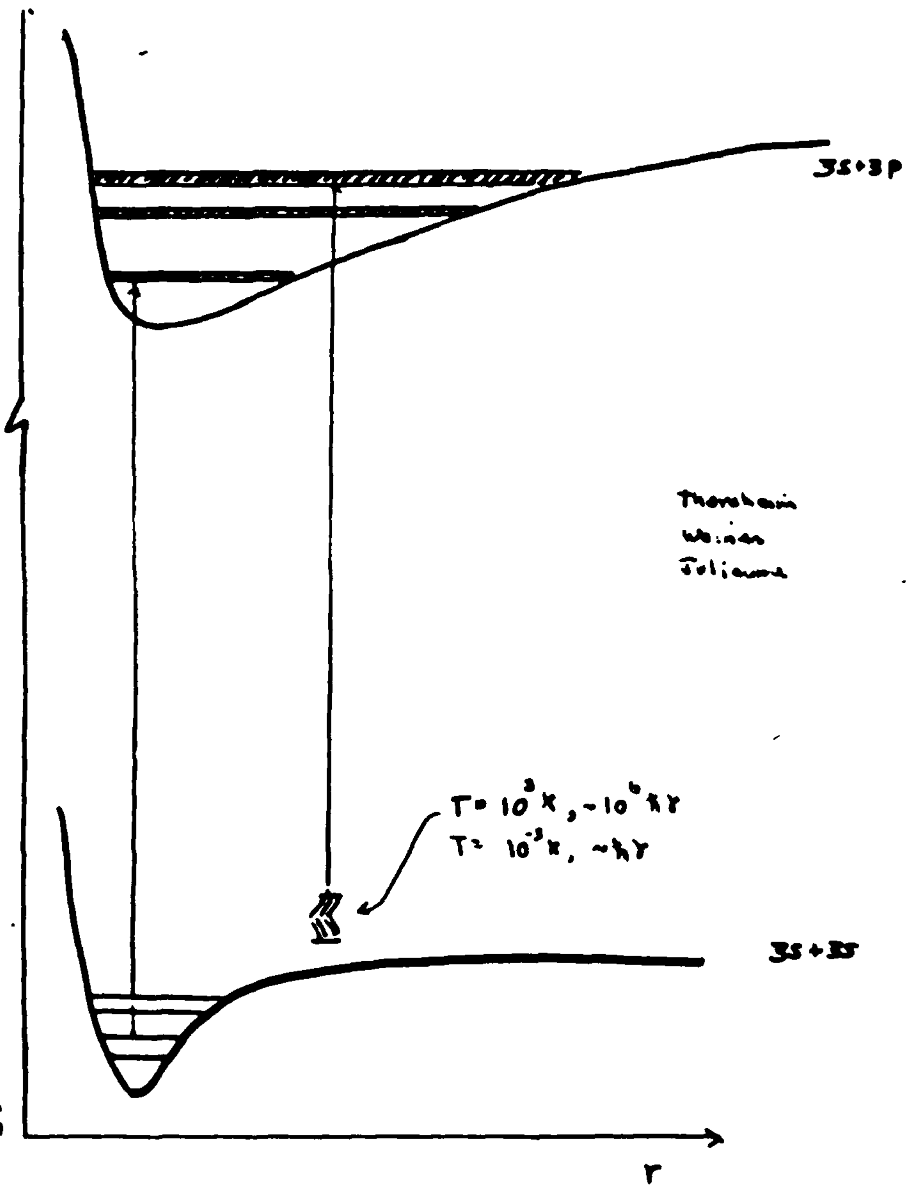

④

de Broglie wavelength

$$\lambda_{dB} = \frac{h}{p}$$

for Na, 10^3 m/s ($T \approx 10^3$ K) $\lambda \approx .15$ Å

1 m/s ($T = 10^{-3}$ K) $\lambda = 150$ Å

Partial waves

$$l \approx 2\pi \cdot \frac{r_{eff}}{\lambda_{dB}}$$

Na^P, $r_{eff} \sim 15$ Å, 10^3 m/s $l \sim 600$

1 m/s $l \approx 1$

6

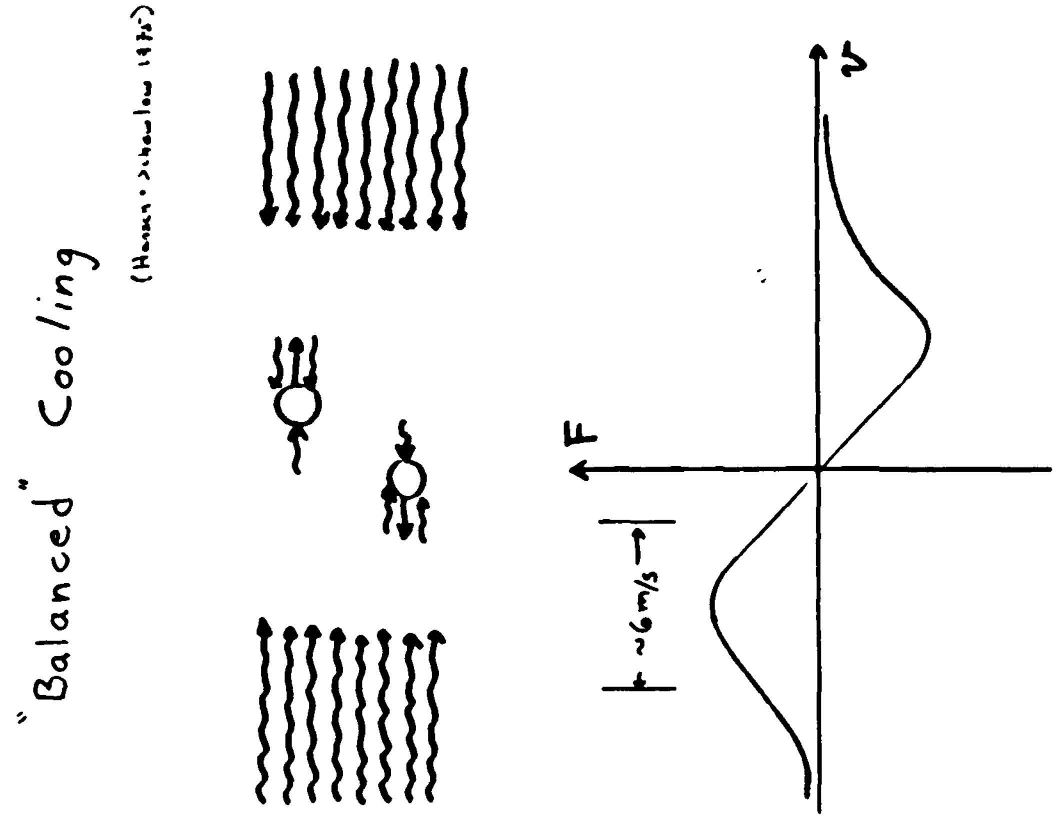

5

Laser Cooling
(Doppler Cooling)

(SCATTERING FORCE)

Hänsch + Schawlow
Wineland + Dehmelt
1975

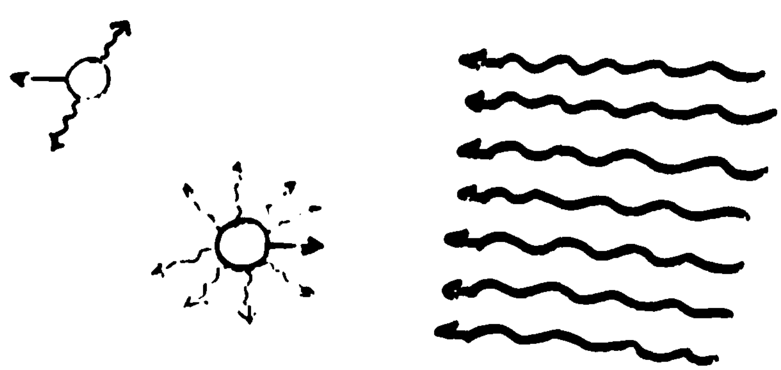

Wineland et al. 1978
Neuhauser et al.

⑦

Neutral Atom Traps

- Magnetic
- Optical
  - Gradient Force
  - Radiation Pressure (Scattering) Force
- Electrostatic
- Hybrid

- Stable Traps are too Shallow ($\lesssim 1$K) to hold most thermal atoms!

⑧

Laser Deceleration (and Cooling) Atomic Beams

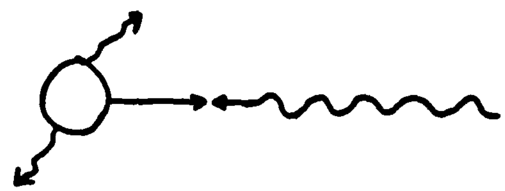

For Na: Δv/photon = 3 cm/s

$v_i \approx 10^5$ cm/s

$N_{phot} \approx 3 \times 10^4$

But! after 100 photons, Doppler shifts off resonance

two solutions (among many)

- Change Laser Frequency (Moscow 1979)
- Change Atomic Frequency (NBS 1981)

10

Zeeman-Tuned Cooling

NBS 1982

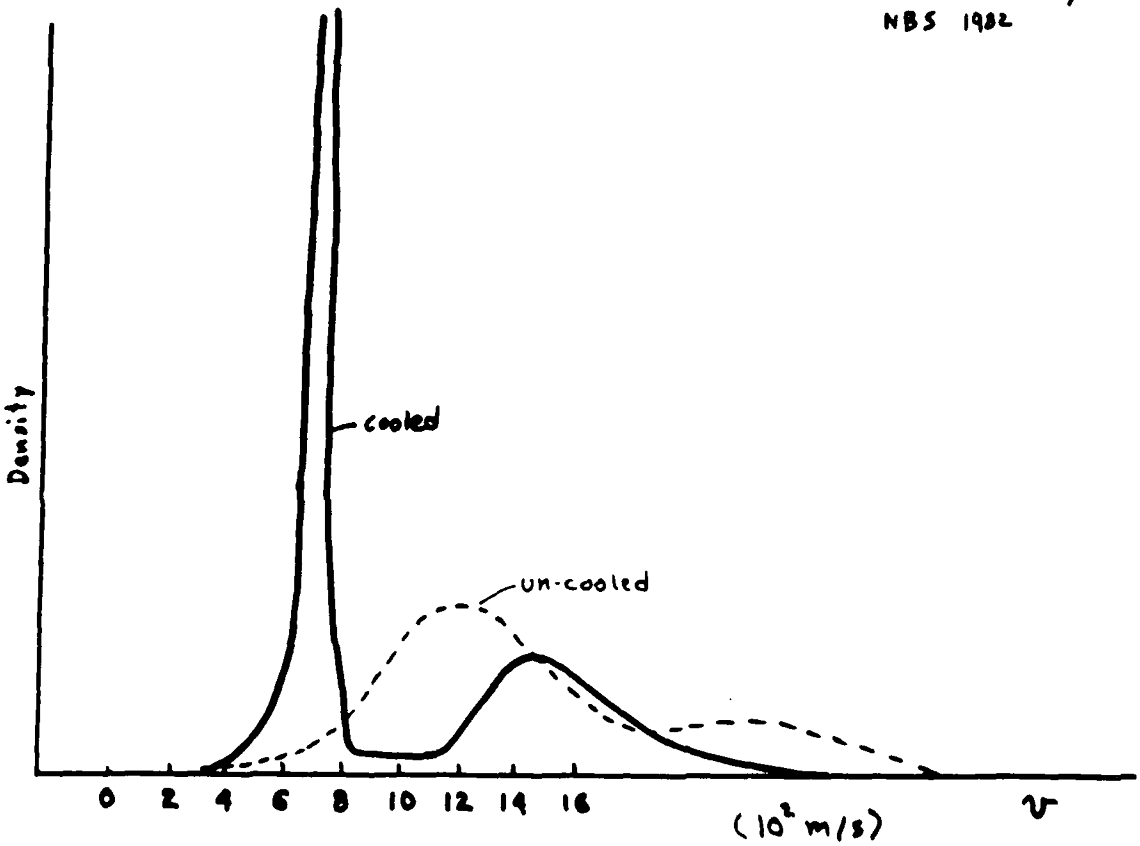

9

Non-Resonant Cooling

(1st expt: Andrews et al 1981)

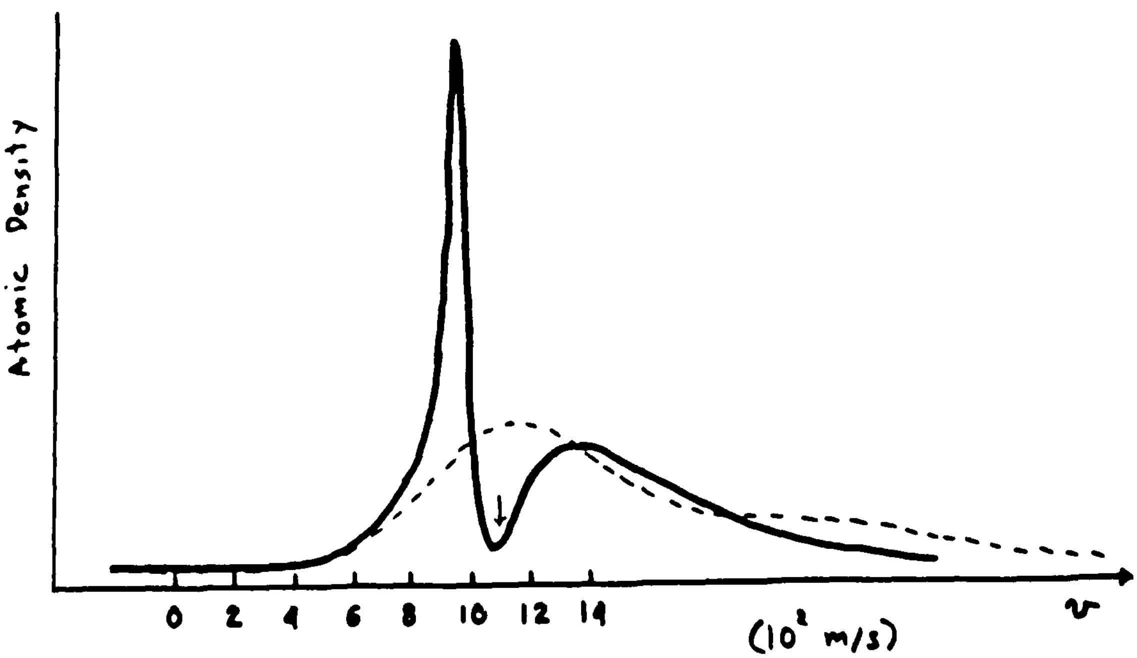

(12)

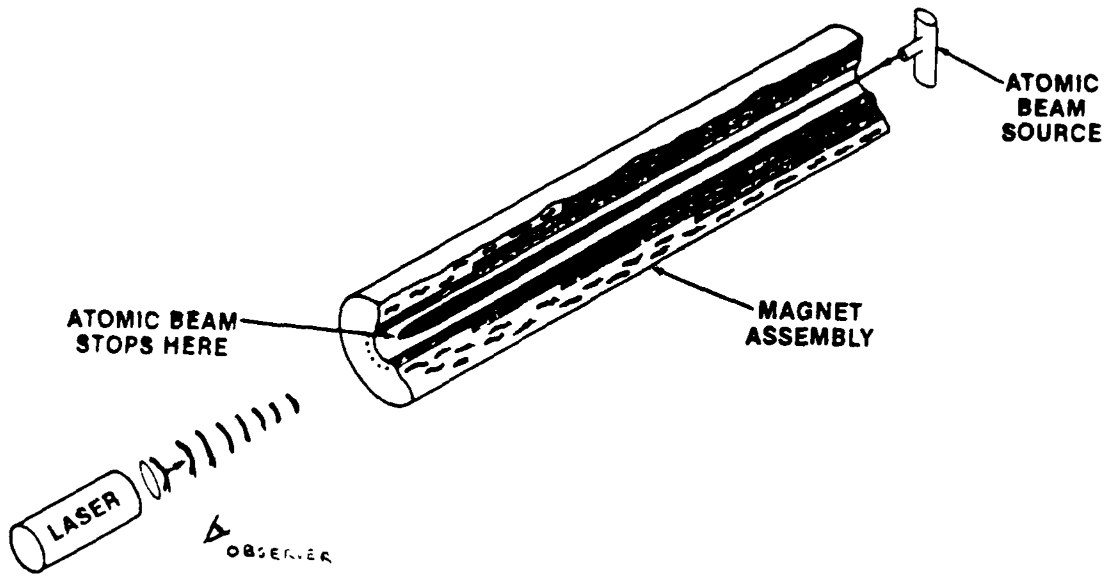

Chirp-Cooling NBS 1983
(1st attempt Moscow 1979)
(Better results NBS-JILA 1985)

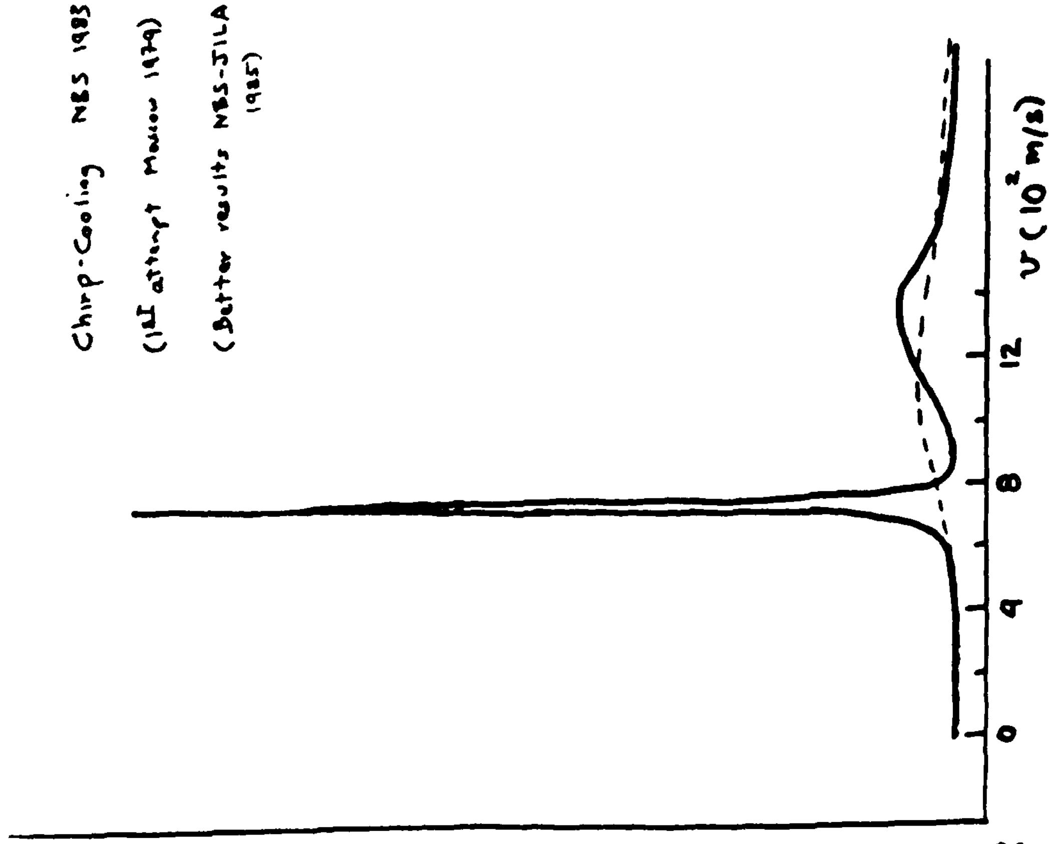

(11)

(13)

(14)

OPTICAL MOLASSES

AT&T 1985
NBS

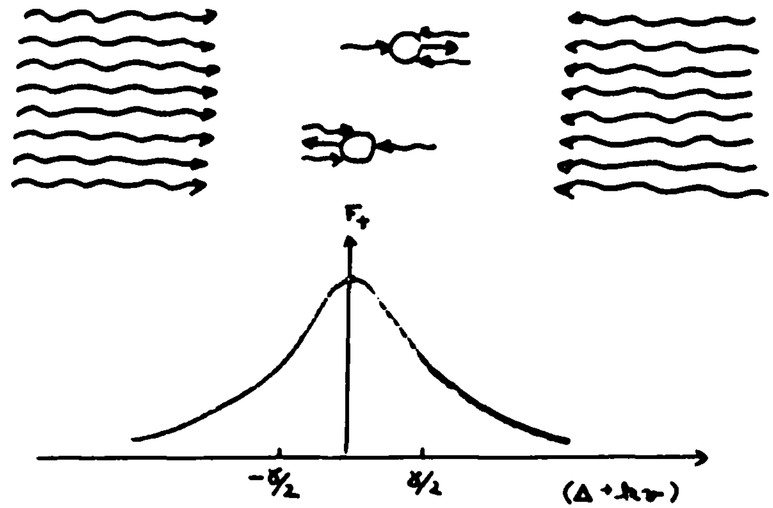

$$F_\pm = \frac{\hbar \gamma k}{2} \frac{I/I_0}{1 + I/I_0 + \left(\frac{\Delta \mp kv}{\gamma/2}\right)^2}$$

$$F_+ - F_- = -\frac{4\hbar k^2\, I/I_0}{\left[1 + I/I_0 + \left(\frac{2\Delta}{\gamma}\right)^2\right]^2} \left(\frac{2\Delta}{\gamma}\right) v \qquad kv \ll \gamma$$

$$F_{max} = -\frac{1}{4}\hbar k^2 v \qquad \left(I/I_0 = 1,\ \Delta = \frac{\gamma}{2}\right)$$

$$F = -\alpha v$$

(For Na $v/\dot{v} \cong 13\ \mu s = \tau_{cool}$)

15

COOLING LIMIT

$$F = -\alpha v$$

$$\dot{E}_{cool} = Fv = -\alpha v^2$$

$$\dot{E}_{heat} = \frac{\dot{p}^2}{2m} = \frac{\hbar^2 k^2}{m} \cdot R_{scatt.}$$

set $\dot{E}_{cool} + \dot{E}_{heat} = 0$, $\frac{1}{2} m v_{th}^2 = \frac{1}{2} k_B T$

$$k_B T = \frac{\hbar\gamma}{4} \frac{1 + I/I_0 + (2\Delta/\gamma)^2}{(2\Delta/\gamma)}$$

$$k_B T_{min} = \frac{\hbar\gamma}{2} \quad \text{at} \quad \Delta = \gamma/2 , \quad I/I_0 \ll 1$$

DIFFUSION (THE MOLASSES EFFECT)

$$\langle x^2 \rangle = l^2 \frac{t}{\tau_l}$$

$$= v_{th}^2 \tau_{cool}^2 \cdot \frac{t}{\tau_{cool}}$$

$$D_x = k_B T / \alpha$$

$$\langle x^2 \rangle = 2 D_x t = \frac{2 k_B T t}{\alpha}$$

$$t_{max} = \frac{4}{27} \frac{\langle x^2 \rangle k^2}{\gamma}$$ (7 sec at 5 mm for Na)

16

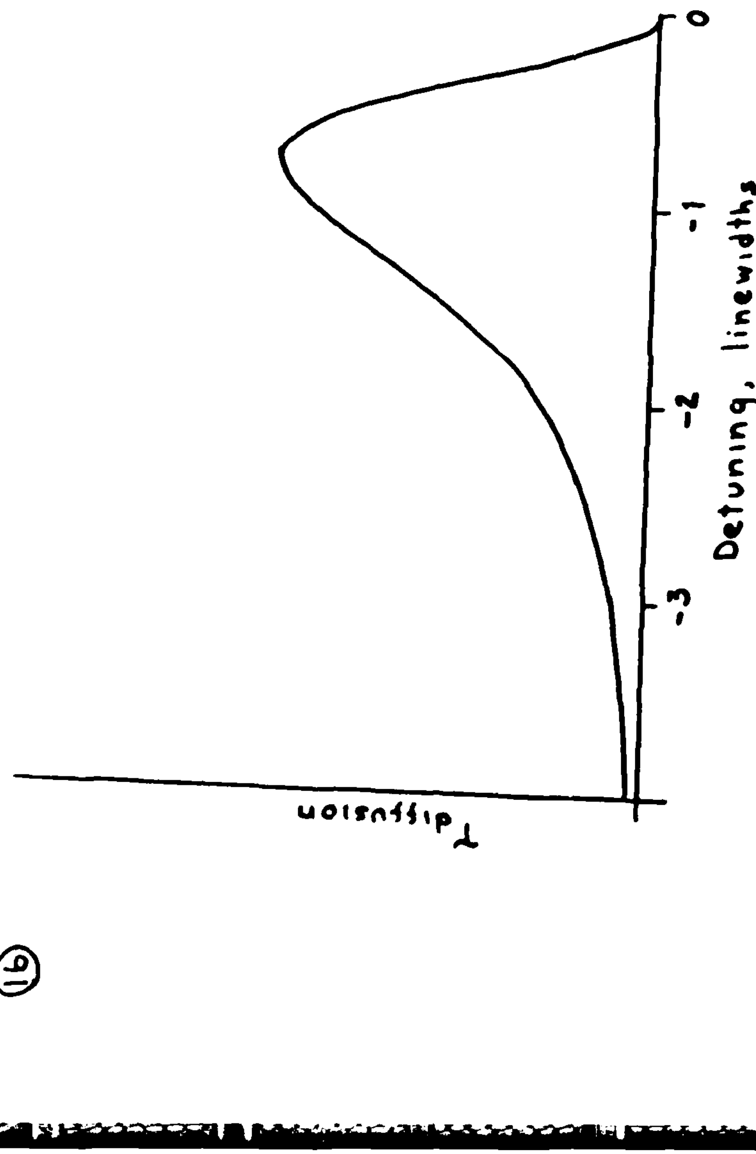

source of ultra-slow atoms

optical molasses

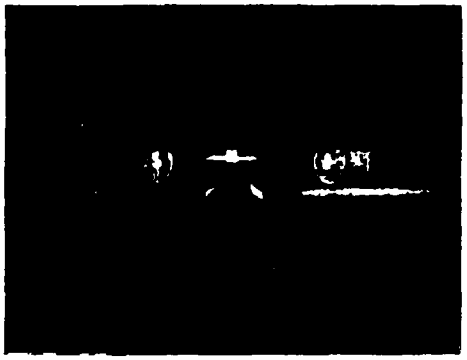

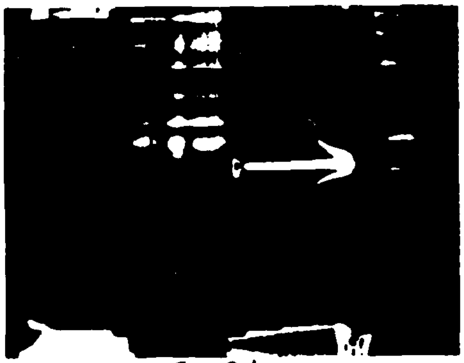

Fig. 9d

81

(17)

Experimental Arrangement For Observing Molasses

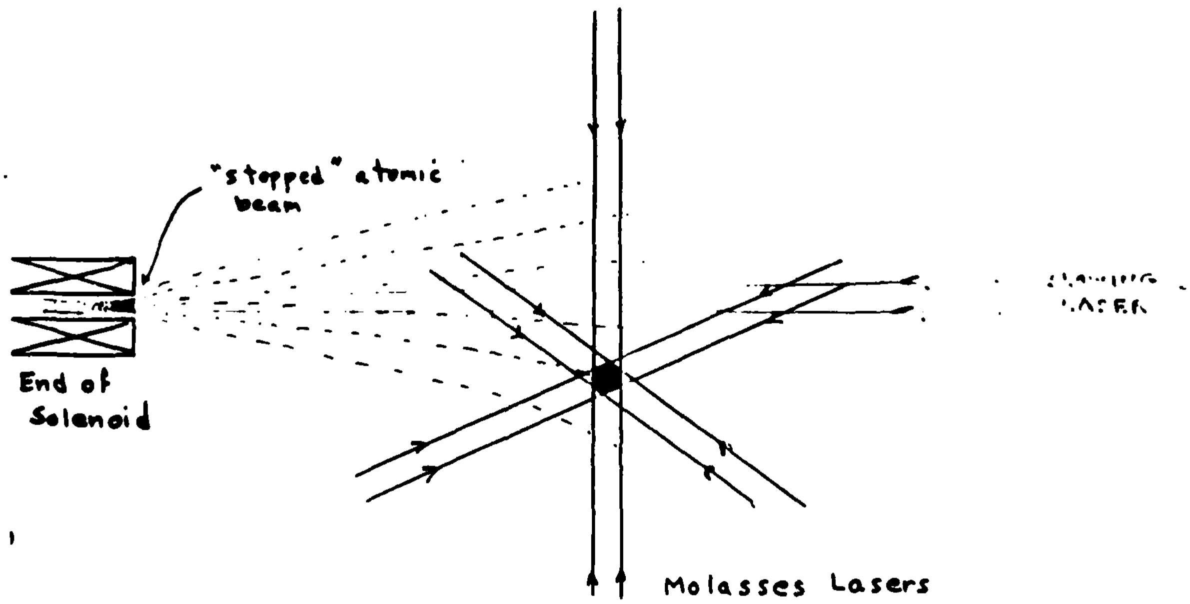

(Earlier pulsed expts: Bell Labs 1985)

(19)

Molasses Apparatus

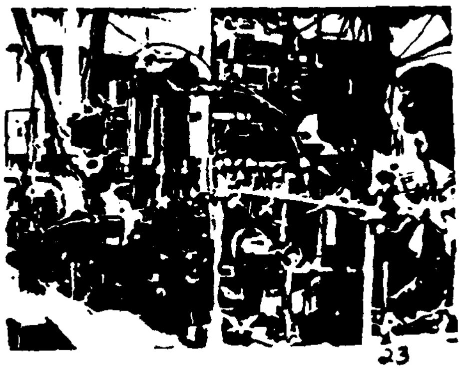

P.L. Gould and P.D. Lett

Optical Molasses in Daylight

(20)

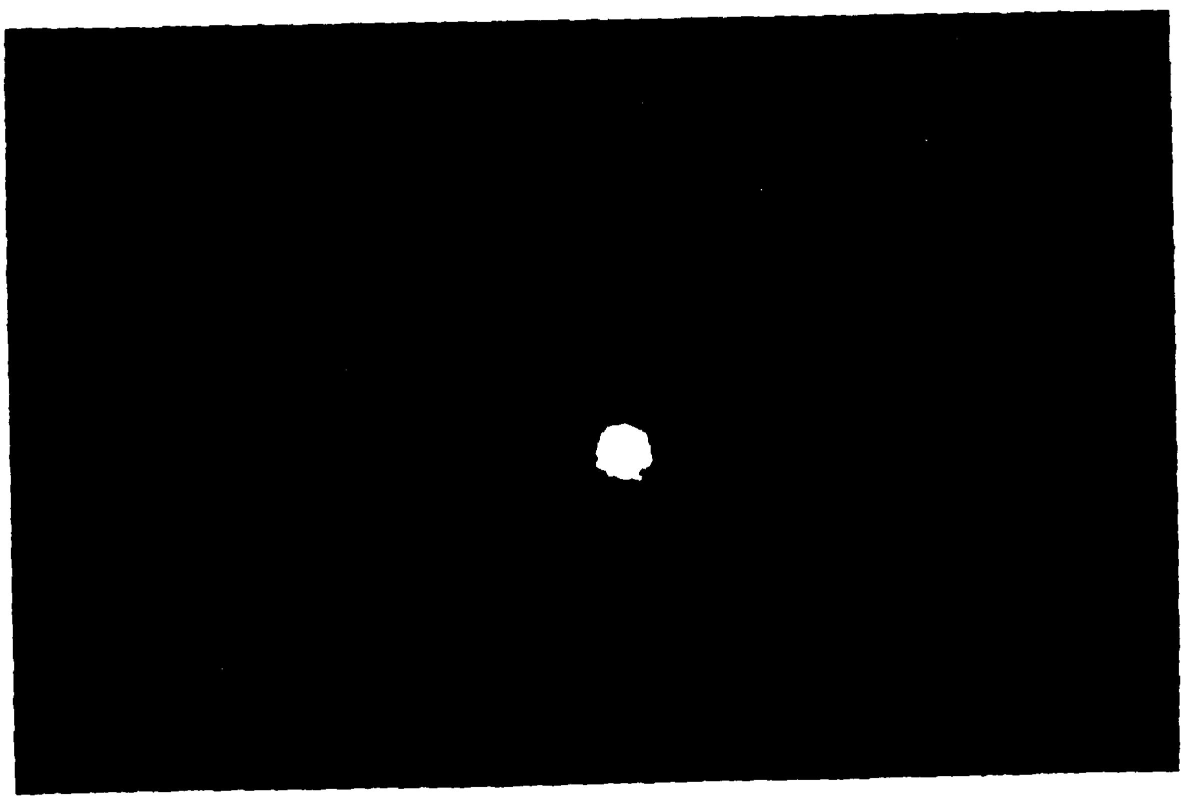

Experimental Arrangement For Observing Molasses

(22)

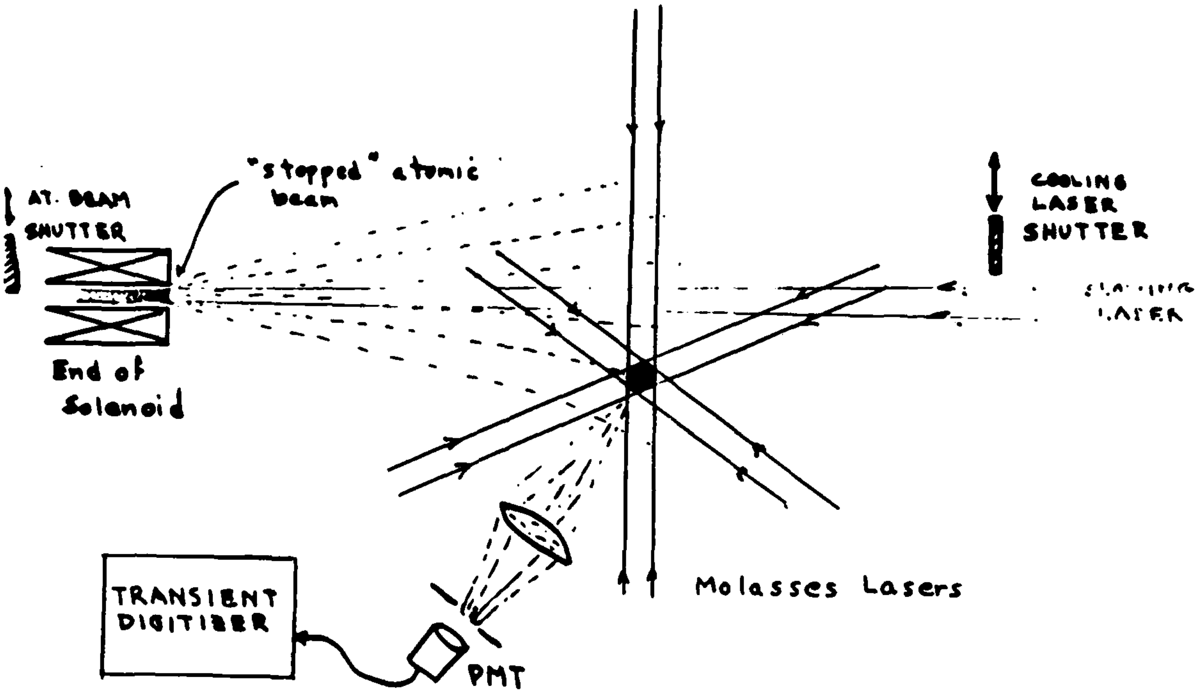

(Earlier, pulsed, expts: Bell Labs, 1985)

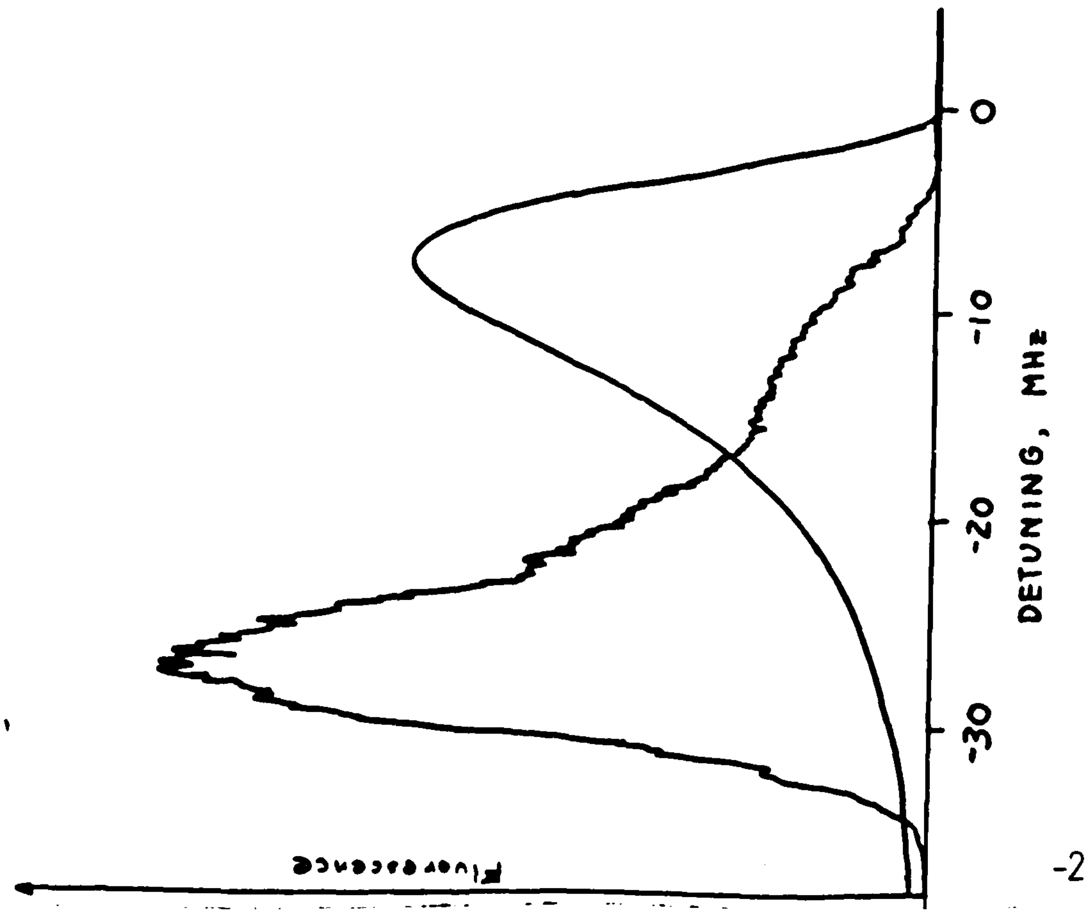

(21)

24

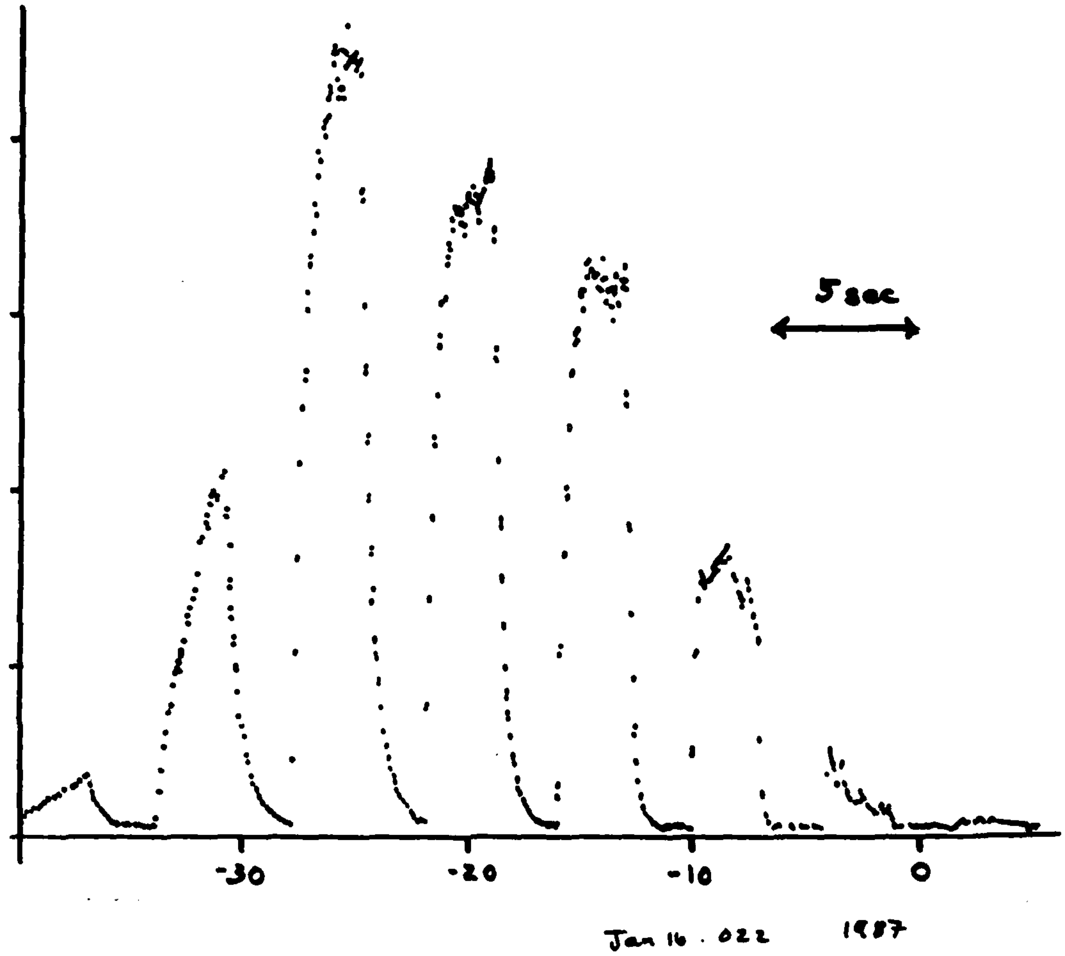
5 sec
-30
-20
-10
0
Jan 16 . 022 1987

23

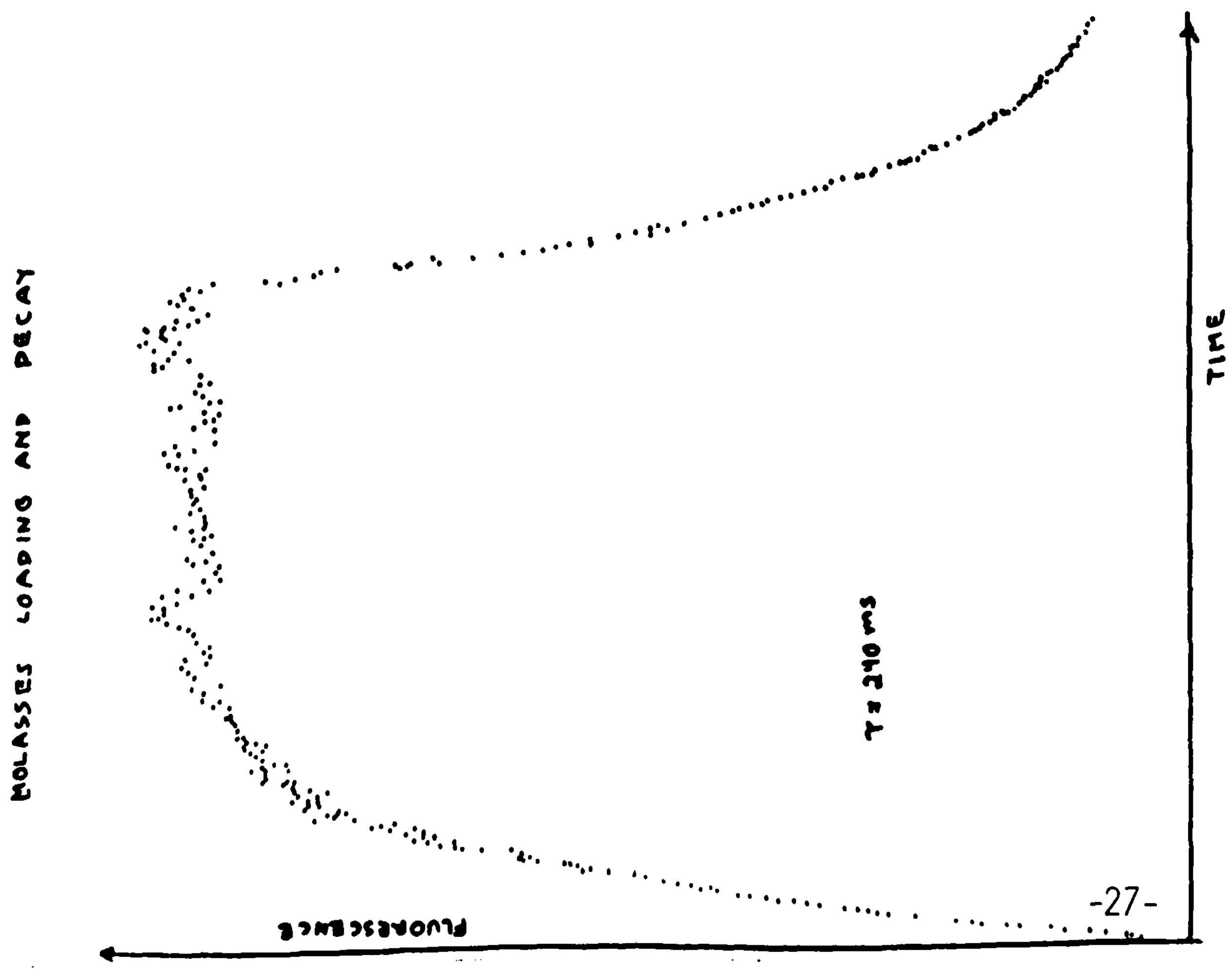
MOLASSES LOADING AND DECAY
τ = 290 ms
TIME
FLUORESCENCE

(26)

Effect of Imbalance

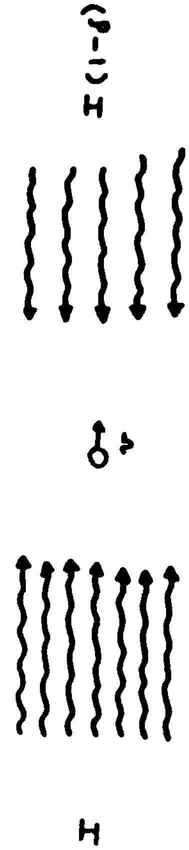

estimate v:

$$F_{unbal} + F_{frict} = 0$$

$$\delta \frac{\hbar k \gamma}{4} - \frac{\hbar k^2 v}{4} = 0 \Rightarrow v = \delta \frac{\gamma}{k}$$

$$\gamma/k = 6\ m/s$$

exact: $$v = \frac{\hbar \gamma}{4k} \; \frac{\frac{1}{4}(1 + I/I_0) + \Delta^2/\gamma^2}{\Delta/\gamma}$$

For optimum molasses ($I/I_0 = 1$, $\Delta = \gamma/2$)

$$v_{drift} = (2.2\ m/s)\ \delta$$

10% imbalance ⇒ 23 ms lifetime in 5 mm

(25)

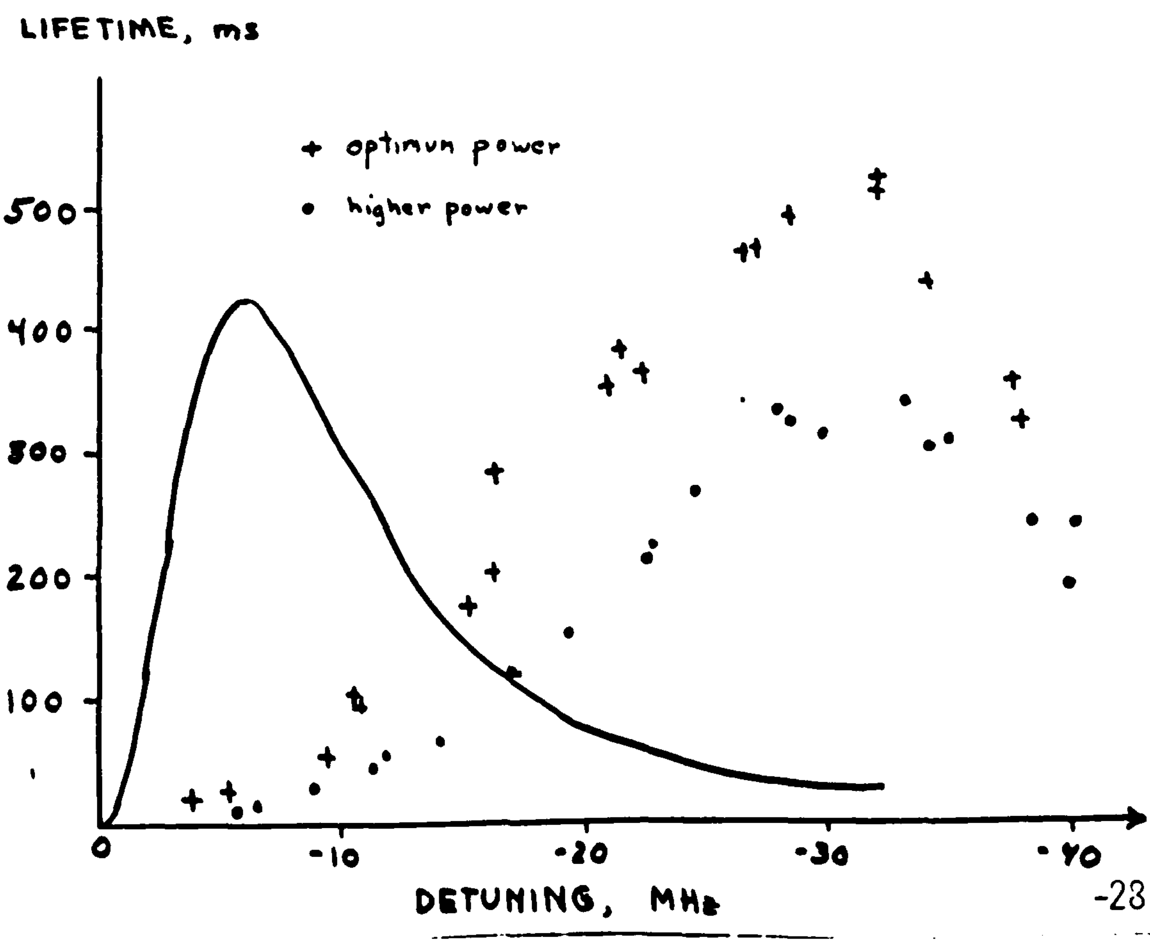

WHY IS EXPERIMENTAL MOLASSES SO STRANGE ?

- At very low power - $I/I_0 \approx 0.01$ it is nearly "normal"
- Saturation and dipole forces not accounted for (but it doesn't help)
- Multiple Levels

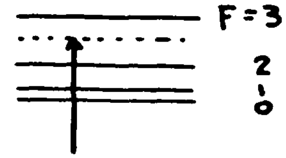

- Multiple States (molasses is sensitive to field and polarization)
- Detailed Motion (Maybe, but not in 1-D)

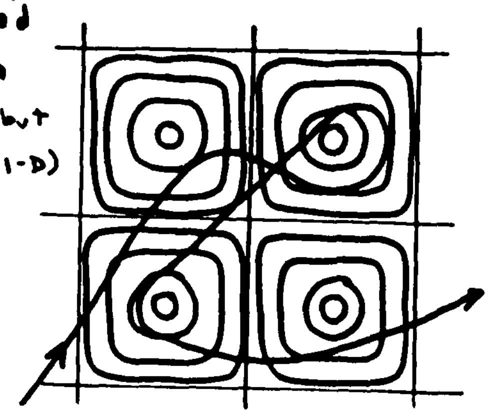

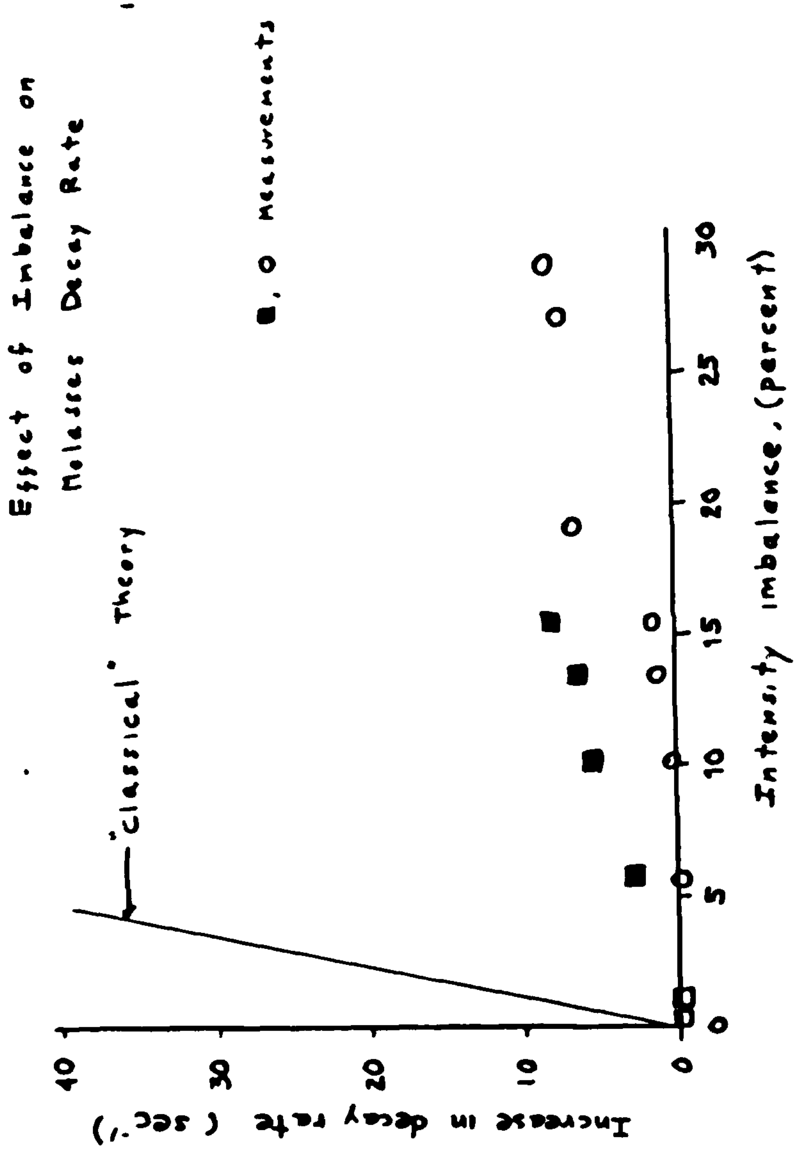

IMBALANCE EFFECT ON MOLASSES LIFETIME

DIPOLE (GRADIENT) FORCE - DRESSED ATOM PICTURE (30)
(COHEN-TANNOUDJI)

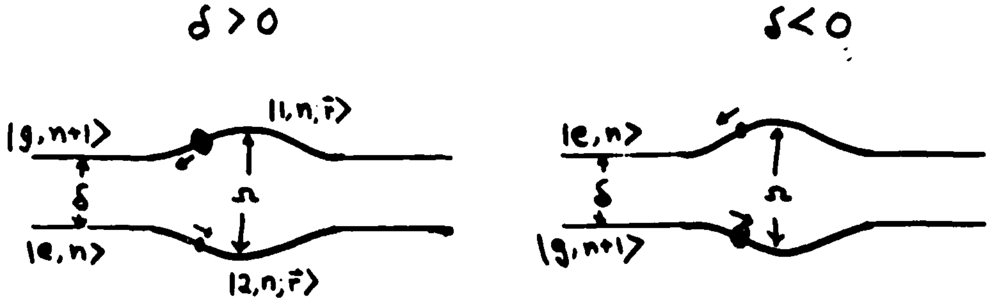

$$\Omega = (\omega_1^2(r) + \delta^2)^{1/2}$$

for large δ: $\Omega \approx \delta + \frac{1}{2}\frac{\omega_1^2}{\delta}$

(29)

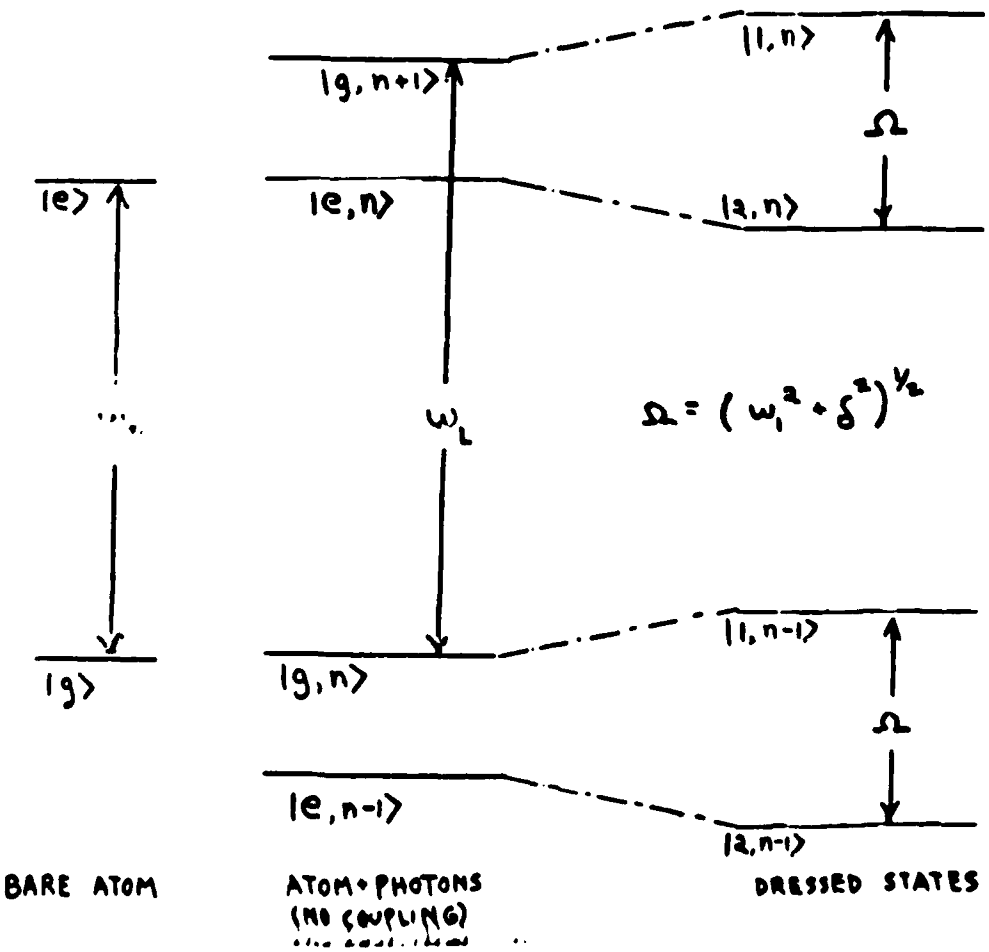

31

2- Focus Trap (Ashkin 1978) NBS 1987

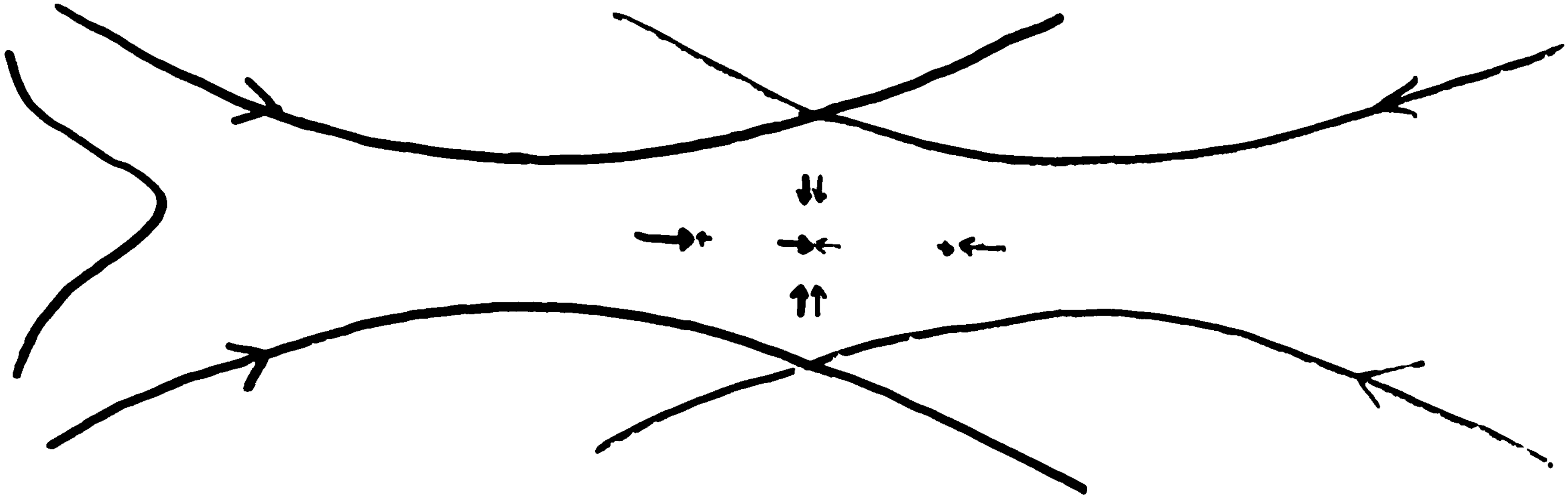

(32)

2- Focus Trap (Ashkin 1978) NBS 1987

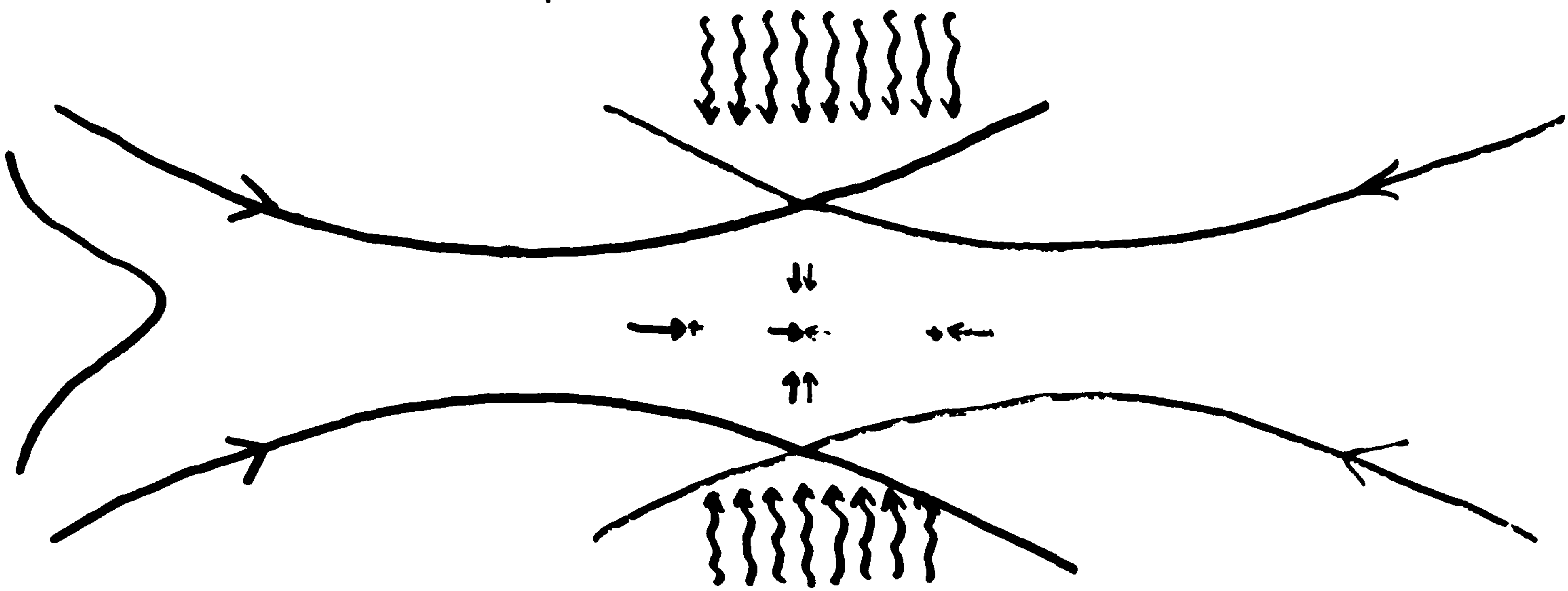

• Separate Cooling Beams (Gordon + Ashkin)

2- Focus Trap (Ashkin 1978) NBS 1987 33

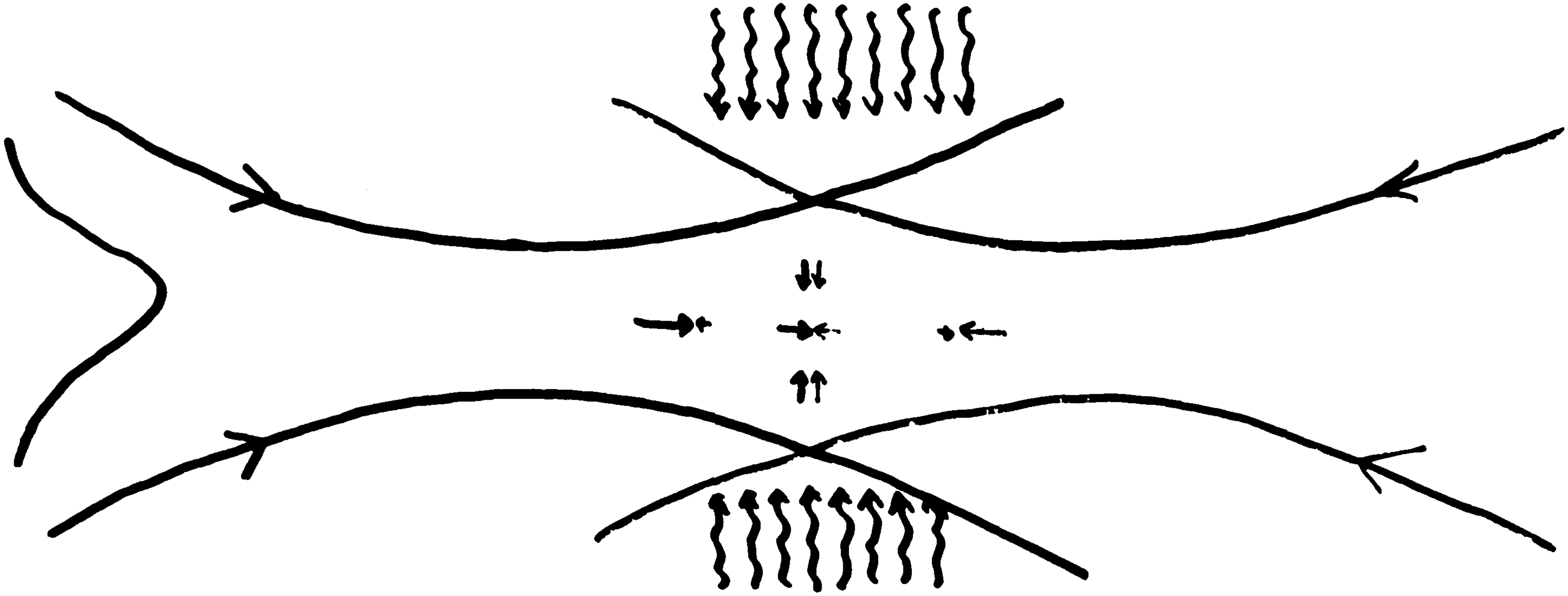

- Separate Cooling Beams (Gordon + Ashkin)
- Alternate Cooling and Trapping (Dalibard, Reynaud + Cohen-Tannoudji)

2- Focus Trap (Ashkin 1978) NBS 1987 34

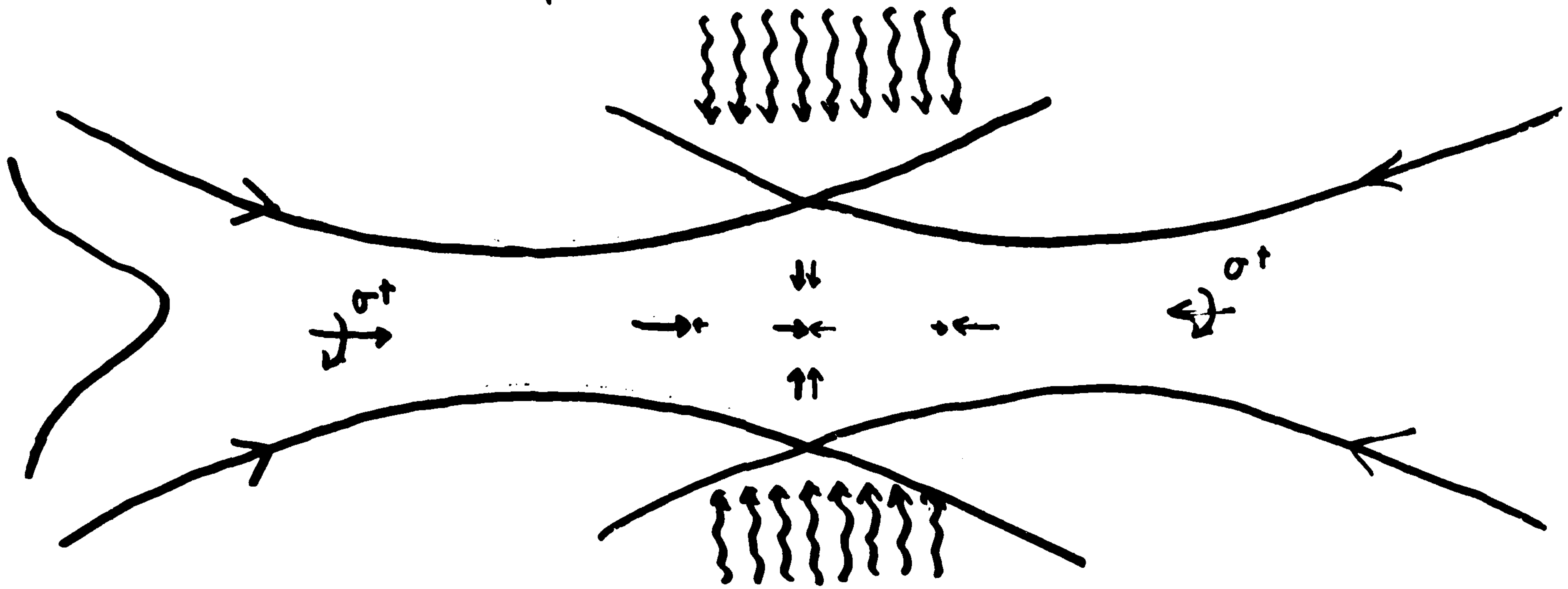

- Separate Cooling Beams (Gordon + Ashkin)
- Alternate Cooling and Trapping (Dalibard, Reynaud + Cohen-Tannoudji)
- Alternate Trapping Beams (Dalibard + Cohen-Tannoudji)

2- Focus Trap (Ashkin 1978) NBS 1987 (35)

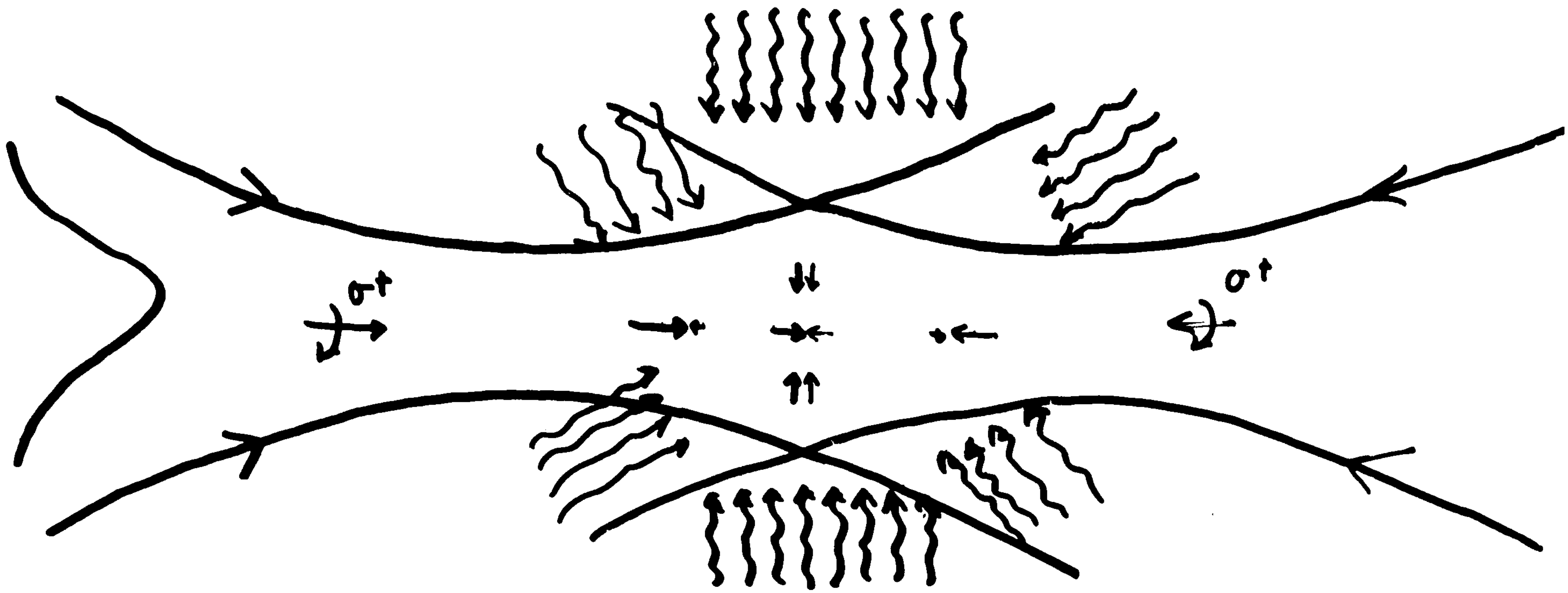

- Separate Cooling Beams (Gordon + Ashkin)
- Alternate Cooling and Trapping (Dalibard, Reynaud + Cohen-Tannoudji)
- Alternate Trapping Beams (Dalibard + Cohen-Tannoudji)
- Load From Molasses (Chu et al.)

NBS: $\sim 10^{-4}\ cm^3$, $\sim 10^4$ density increase in capture volume

Optical Trapping of Neutral Atoms and Dielectric Particles by Radiation Pressure

A. Ashkin, J. E. Bjorkholm and S. Chu
AT&T Bell Laboratories
Holmdel, NJ 07733

SUMMARY

Recently a number of exciting results have been achieved in the field of laser trapping and manipulation of small dielectric particles. Optical trapping and manipulation of Na atoms has been demonstrated at record low temperatures and record densities.

Trapping of submicron Rayleigh particles with diameters down to ≈ 250 Å has been achieved. Individual biological particles such as viruses, bacteria and small organisms have also been manipulated with light. The basic forces involved in trapping all these rather diverse particles are the forces of radiation pressure which come from the momentum of the light itself.

This talk briefly traces the history of the subject, gives some physical feel for the subject, mentions some of the principal results, and gives my perspective on the future. It concludes with a 5 minute tape showing trapping and manipulation of atoms and biological particles.

Force on a Reflecting Mirror

momentum of photon $= \dfrac{h\nu}{c}$

photons/sec $= \dfrac{P}{h\nu}$

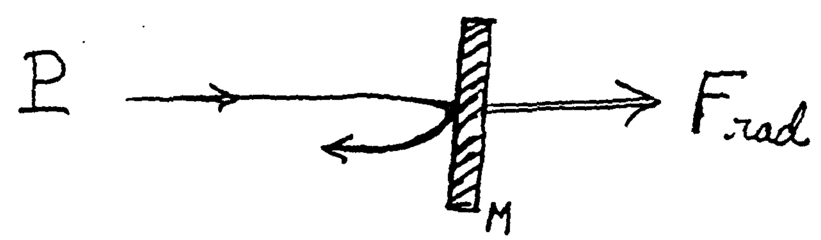

$$F_{rad} = \frac{P}{h\nu}\left(2\,\frac{h\nu}{c}\right) = \frac{2P}{c}$$

1

Forces

Laser Beam, $P = 1$ watt, Focal Spot $\sim \lambda$

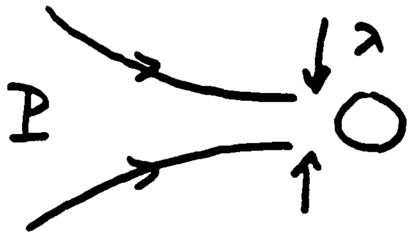

Dielectric Sphere:

$$\text{dia} \sim \lambda = 1/2\ \mu m \quad , \quad m \simeq 10^{-12}\ gm$$

$$F_{rad} = \frac{2P}{c} \simeq 10^{-3}\ \text{dynes.}$$

$$\boxed{\text{Accel } A = \frac{F}{m} \simeq 10^{9}\ cm/sec^{2} = 10^{6}\, g \quad \text{Big !!}}$$

Atoms:

$$\sigma_{scat} \sim \lambda^{2} \qquad m_{atom} \sim 10^{10}\ \text{smaller}$$

$$\boxed{A \text{ large in spite of saturation}}$$

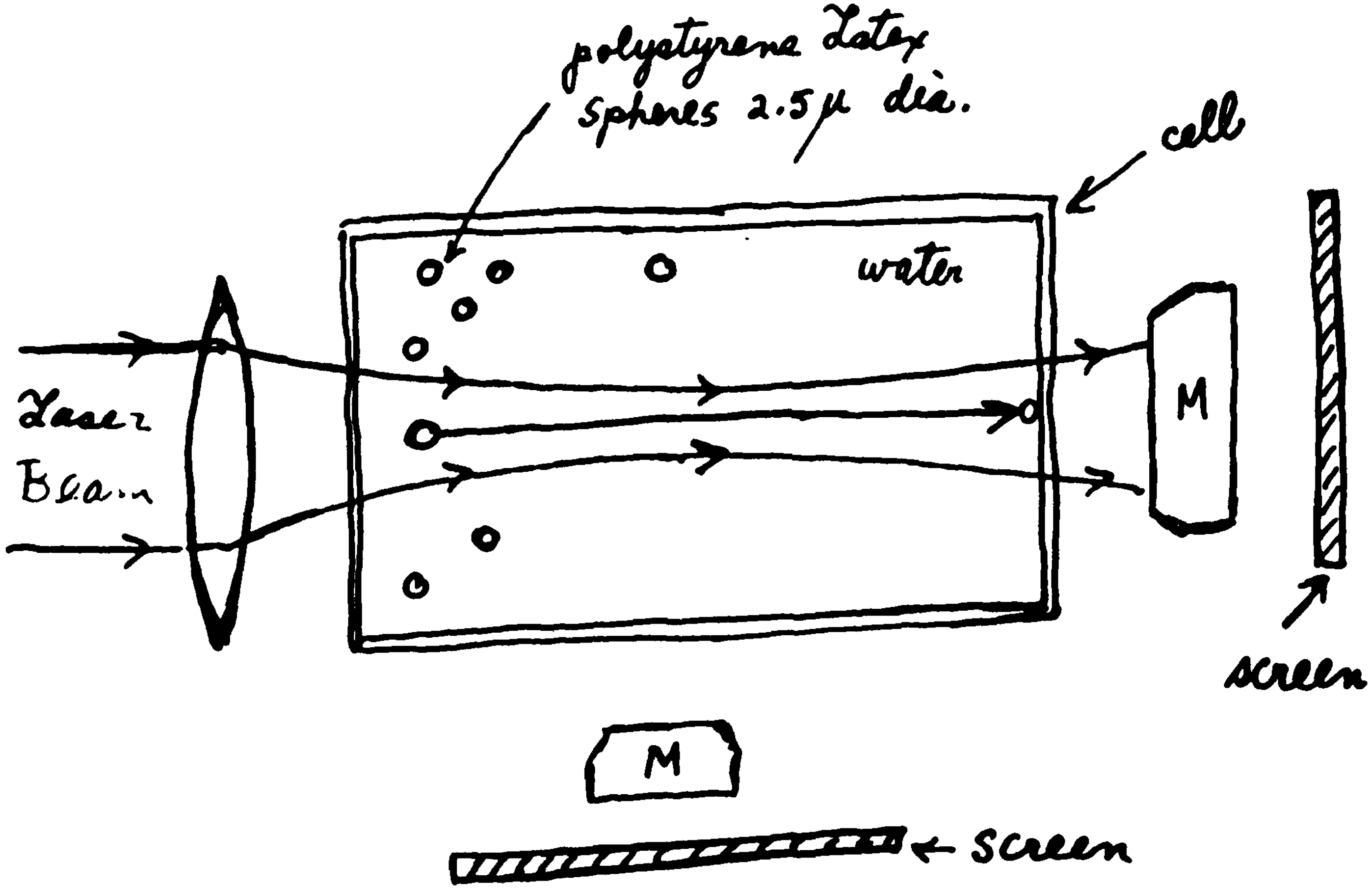
polystyrene latex spheres 2.5μ dia.
cell
water
Laser Beam
M
screen
M
screen

3

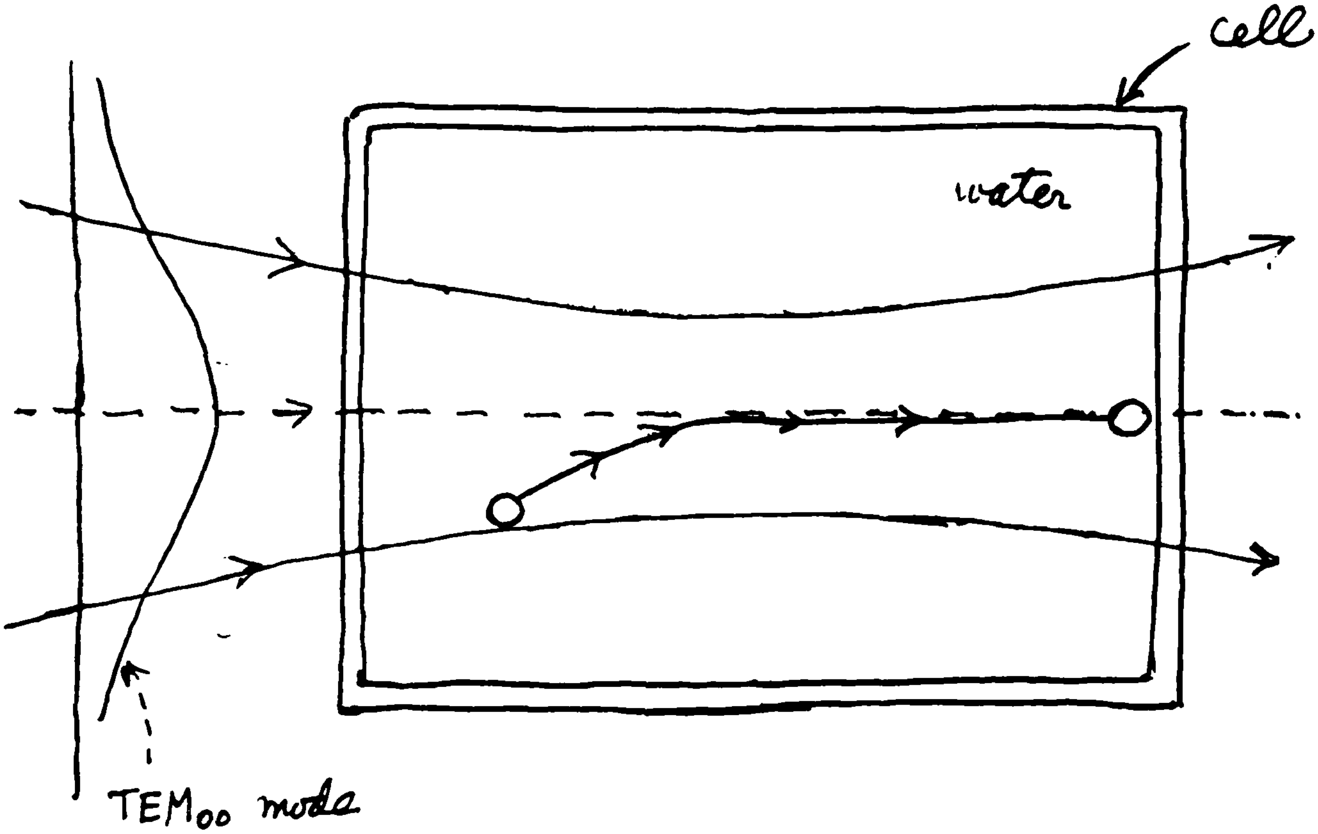
cell
water
TEM$_{00}$ mode

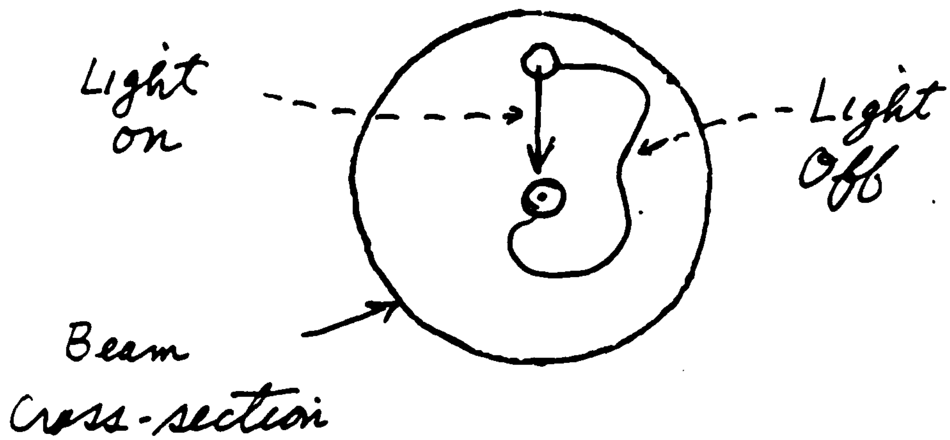
Light on
Light Off
Beam Cross-section

Mie Particles - $d \gg \lambda$

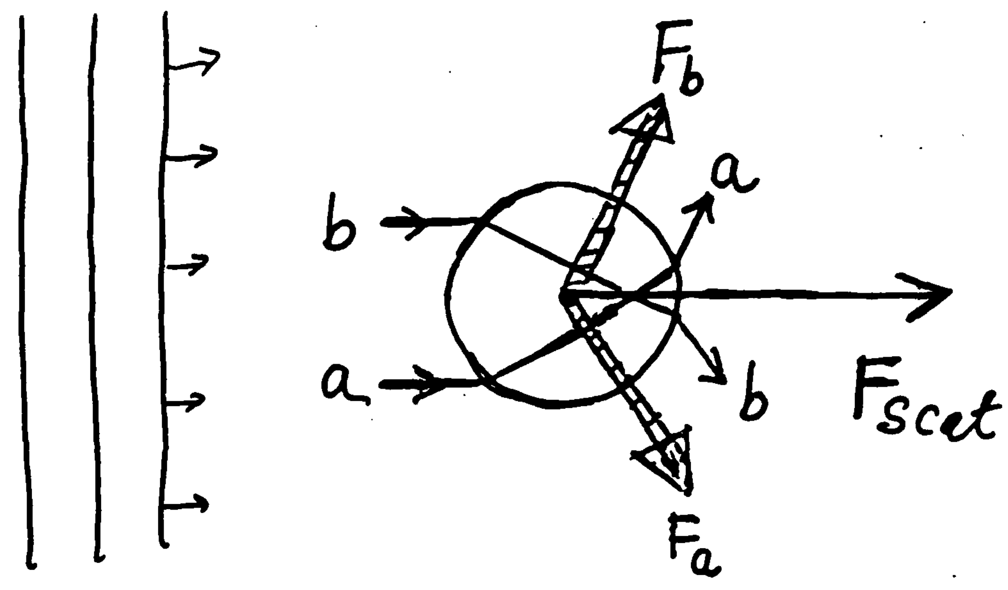

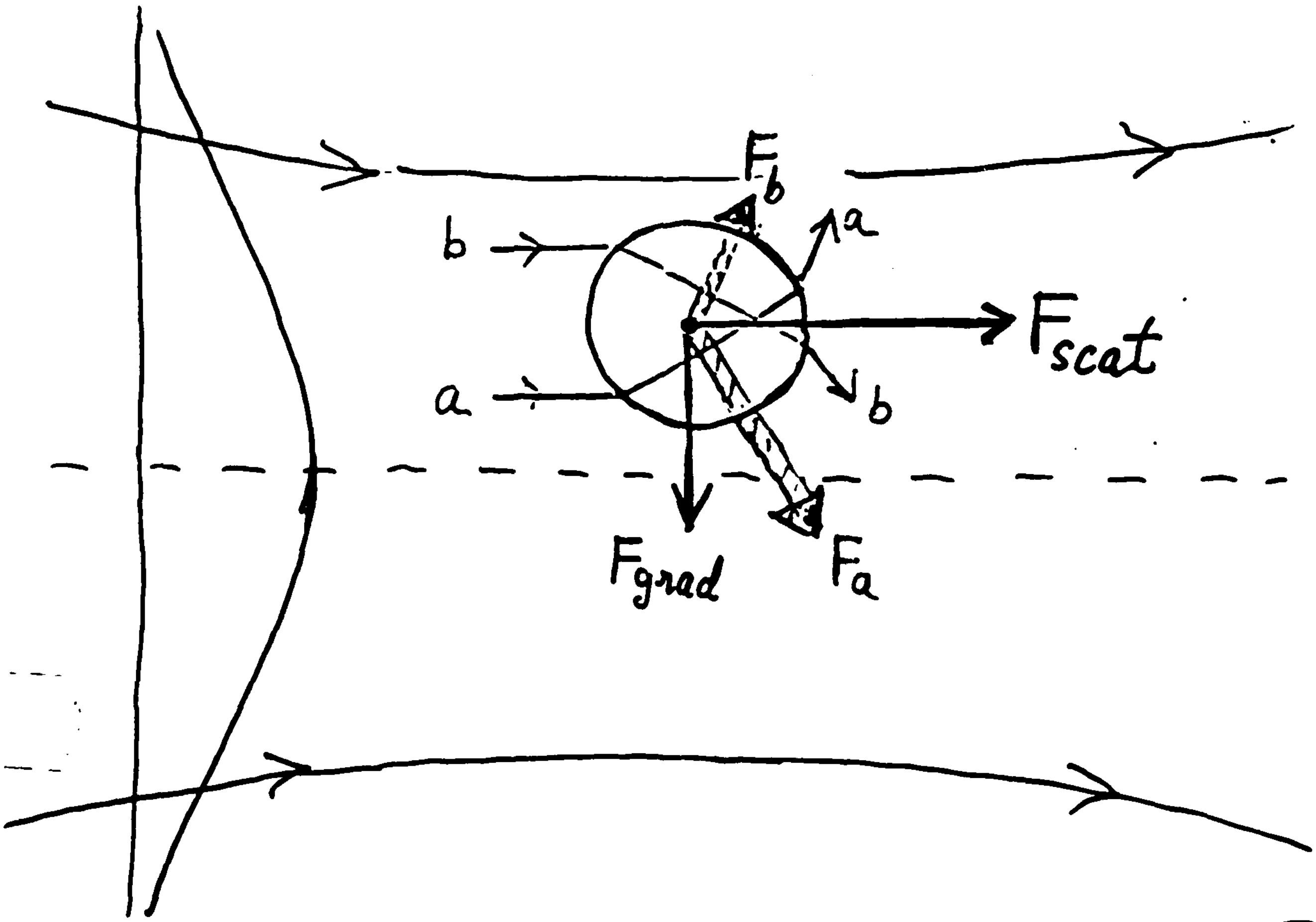

GRADIENT FORCE

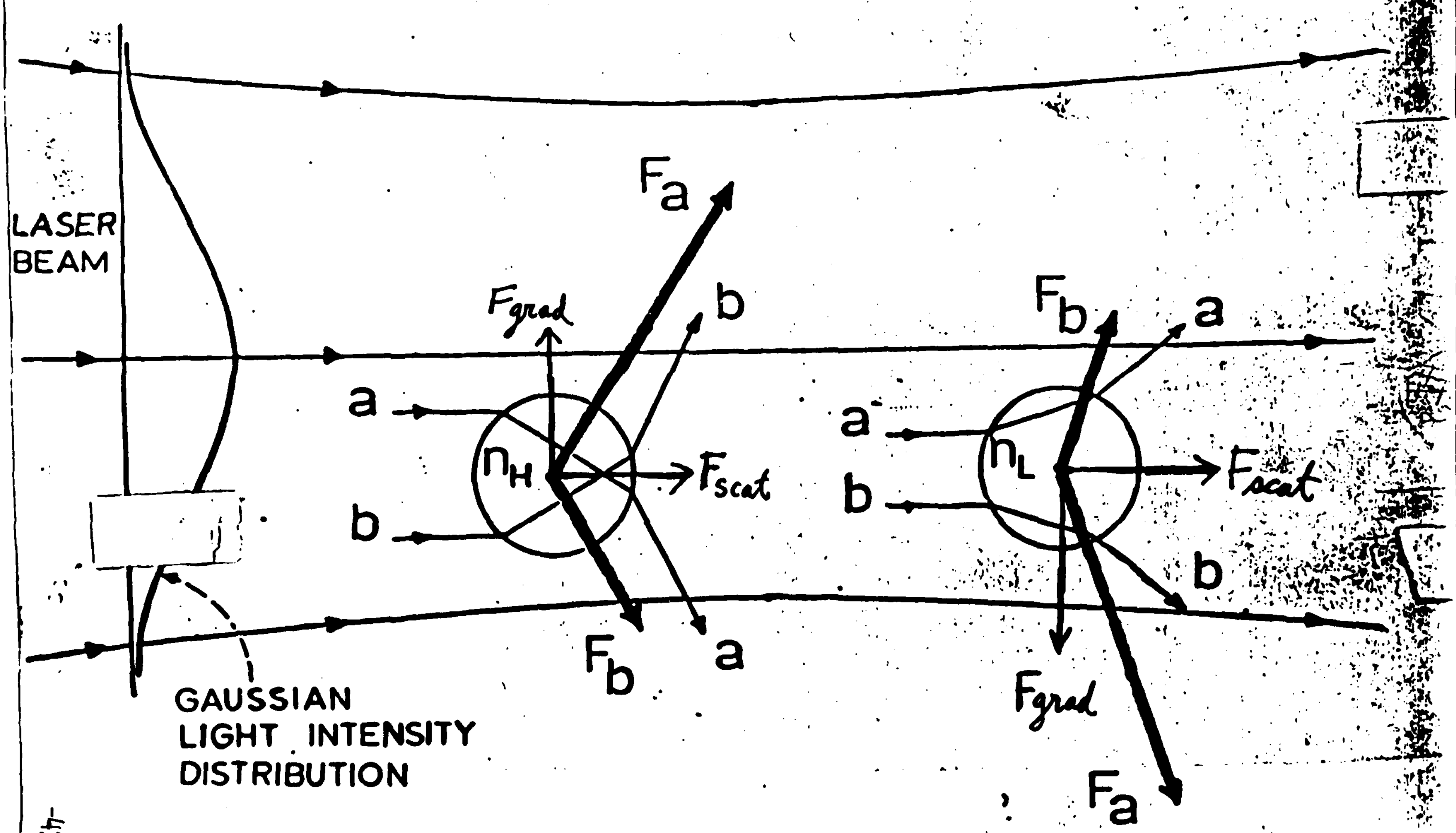

6

Just Optical Trap

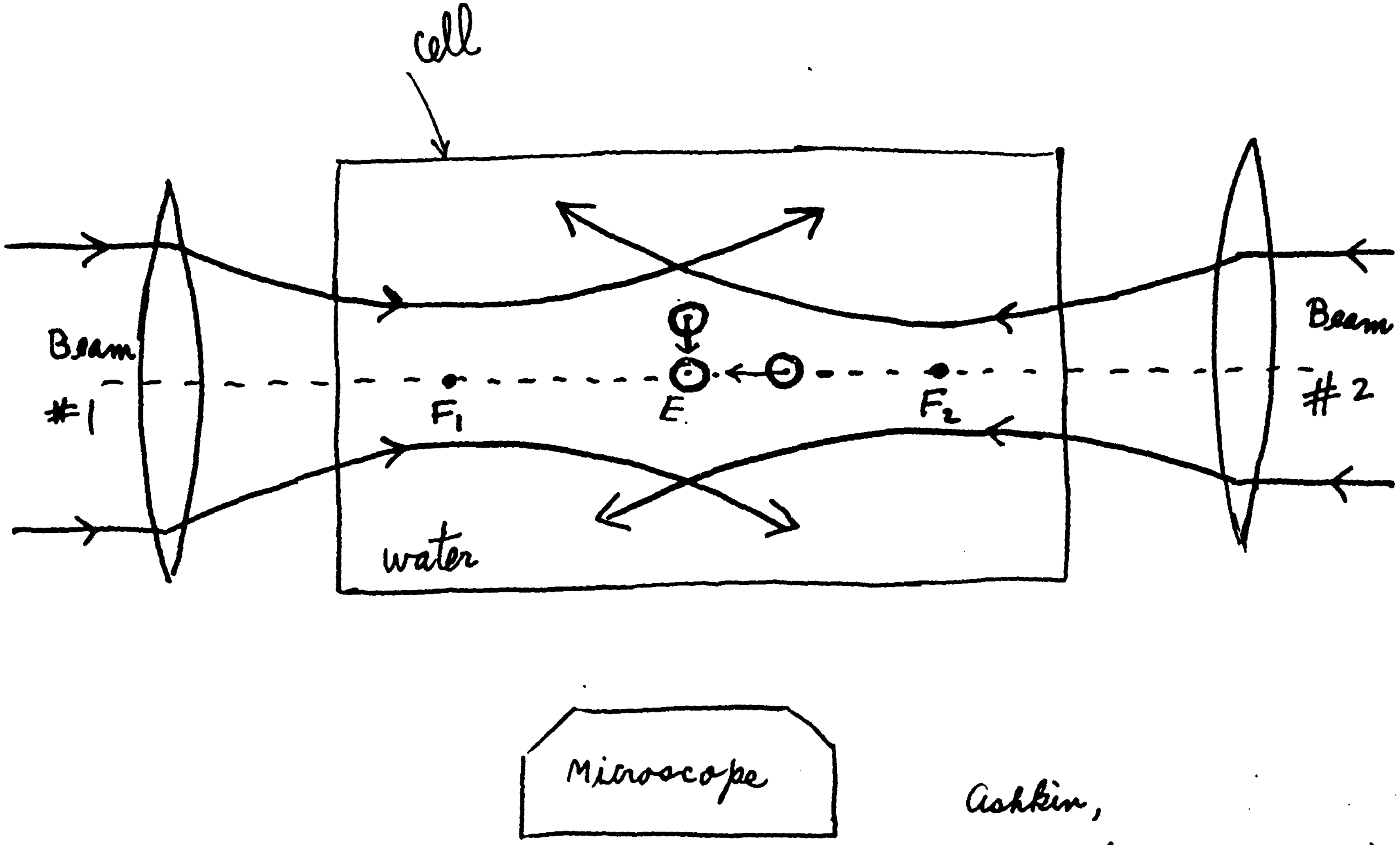

Ashkin,
Phys. Rev. Lett. 24, 156 (1970).

7

Optical Levitation Trap -

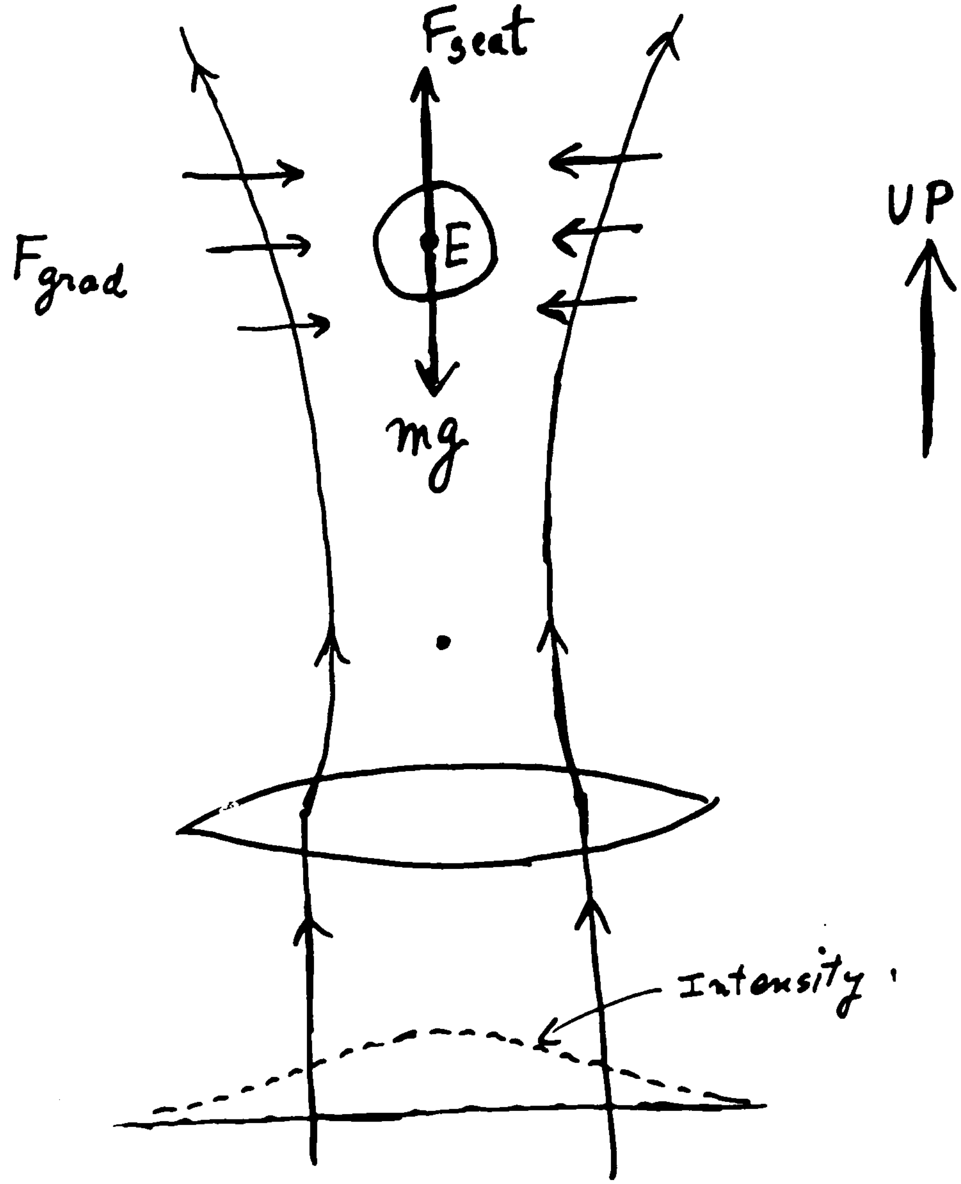

Ashkin and Dziedzic, Appl. Phys. Lett. 25, 283 (1971)

Photo of Levitated Glass Sphere

25 µm in diameter

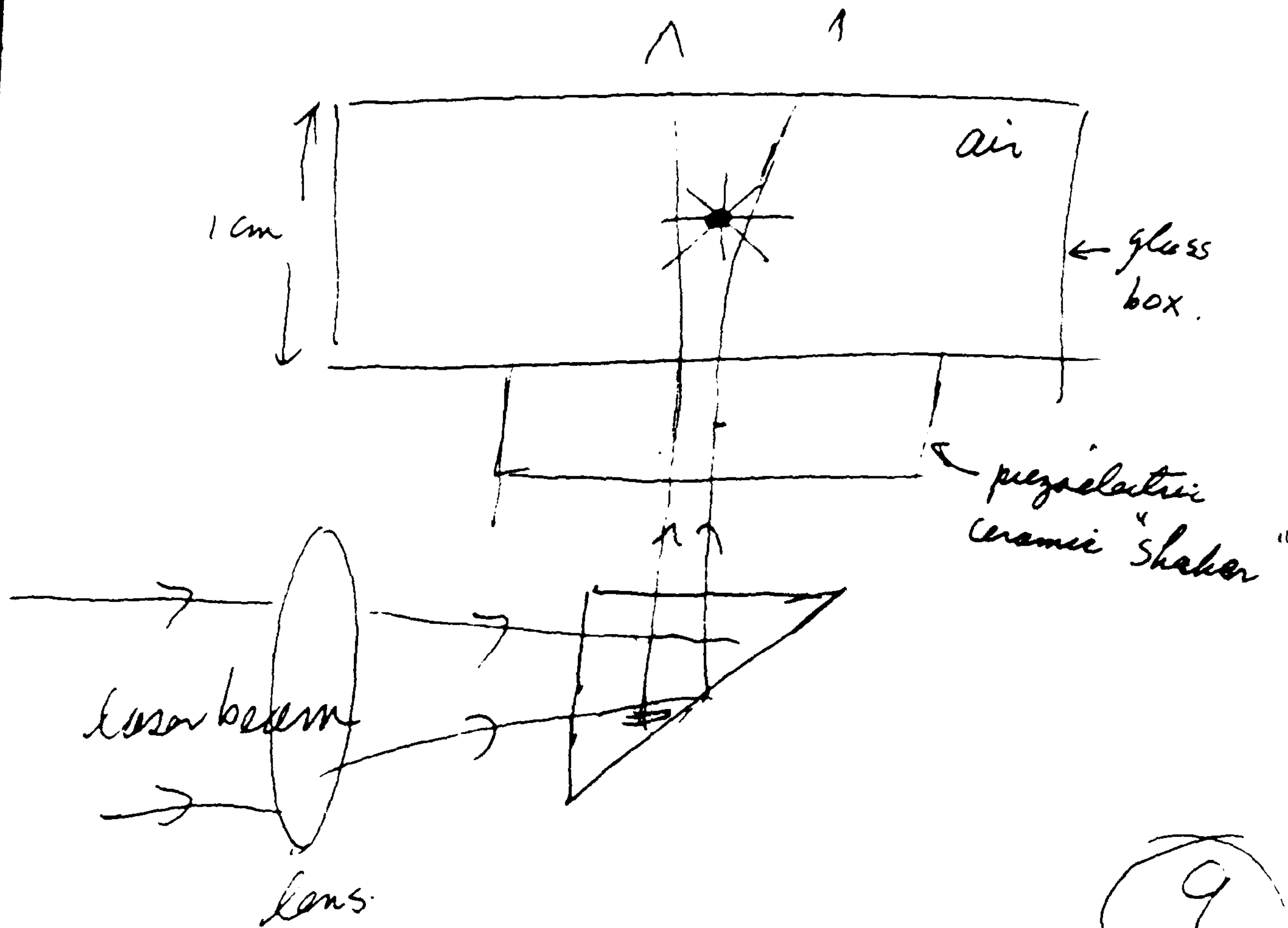

9

From Scientific American 226, 63 (1972)
"The Pressure of Laser Light" A. Ashkin

Photo of "Mie" Scattering Rings from levitated sphere.

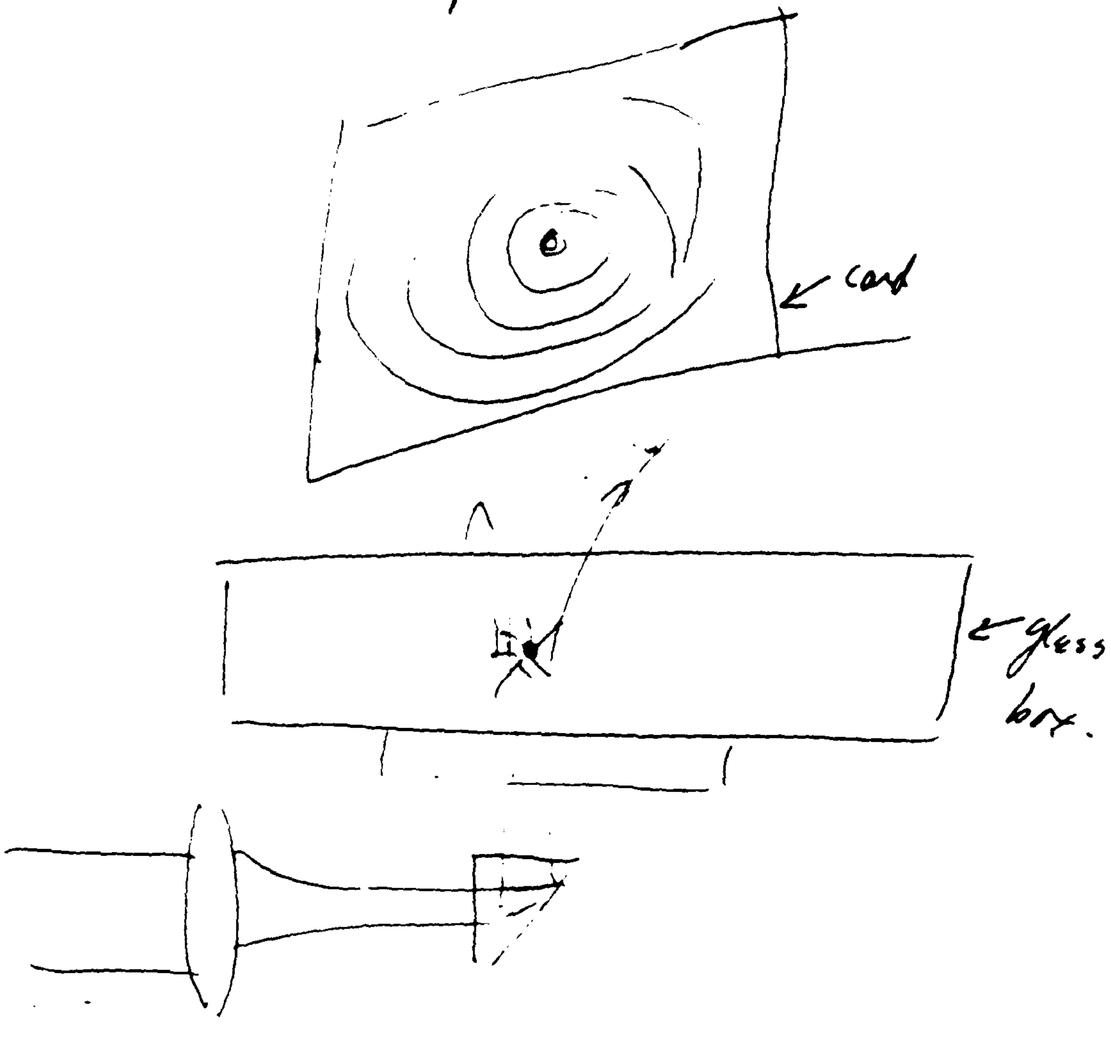

10

ISSUE	ENGR	TITLE	-46-
	DRAWN		BELL LABORATORIES
			NO. OF SHEETS PER SET

Levitation + Manipulation of Mie Particles

- Assembly of New Particles – Ashkin + Dziedzic Appl. Opt. 19, 660 (1980)
  using 2 beams

- Levitation in Vacuum – Ashkin + Dziedzic Appl. Phys. Lett. 28, 333 (19
  using optical feedback damping & Appl. Phys. Lett. 30, 202 (197

- Spectroscopy on Single Particles

  λ dependence of Force + Scattering

  (First Observation of hi Q Mie Surface-Wave Resonances)

  Ashkin + Dziedzic
  Phys. Rev. Lett. 38, 1331 (1977).

Ashkin, Science 210, 1031 (1980) Review Article

11

Optical Feedback Apparatus

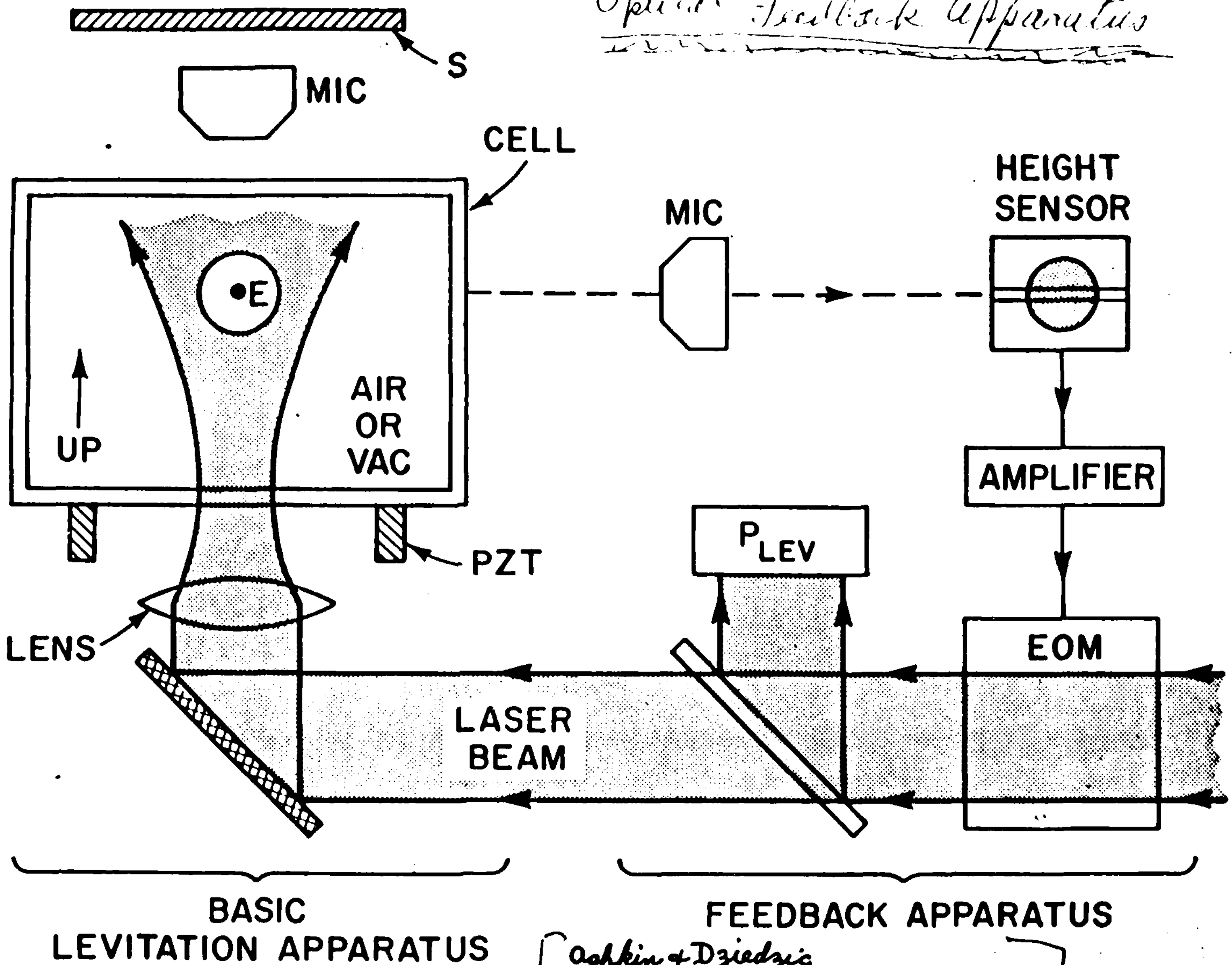

Ashkin + Dziedzic
Appl. Phys. Lett. 30, 202 (1977).

12

Radiation Pressure Forces on Atom In "Parallel" Gaussian Laser Beam

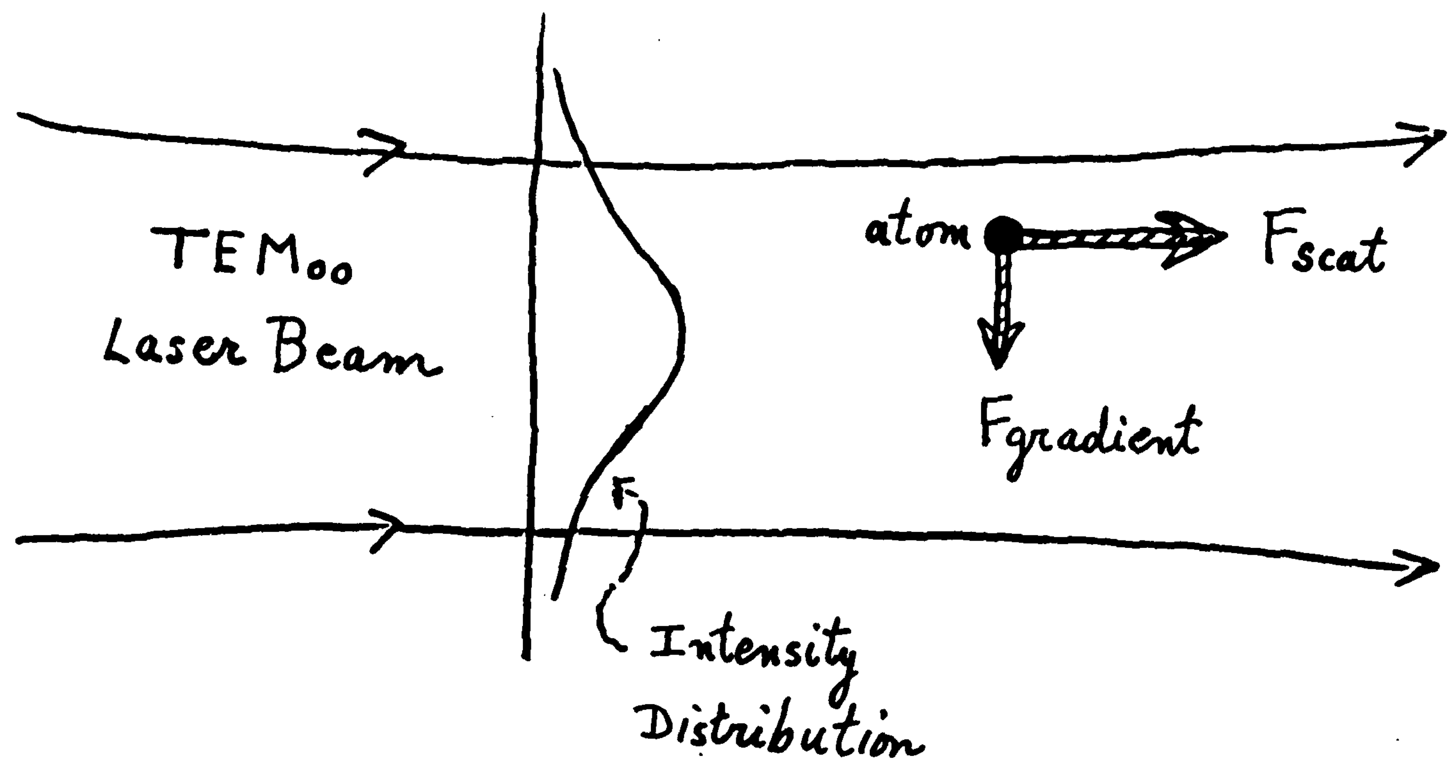

13

Atoms – Scattering Force

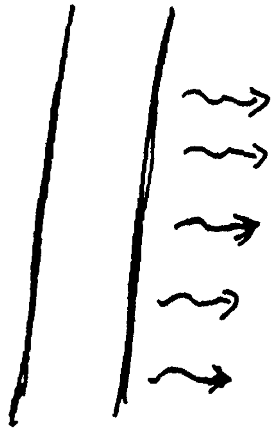

plane wave
resonant light

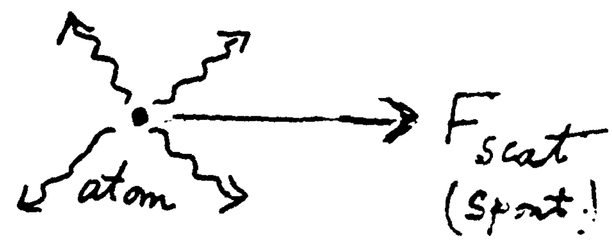

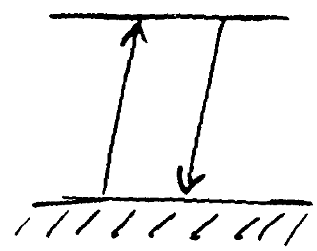

2-level atom

$$F_{scat} = \left(\frac{h}{\lambda}\right)\left(\frac{1}{\tau_N}\, f\right)$$

mom. photon   # phot/sec scattered

f = fraction of time spent in excited state

low power $f \propto I$

high power $f \to 1/2$ saturation

Ashkin, Phys. Rev. Lett. **25**, 1321 (1970).

Saturation – Use rate equations

$$F_{sat} = \frac{h}{\lambda} \frac{1}{\tau_N} f$$

$$f = \frac{1}{2} \frac{p}{1+p}$$

$$p \equiv \text{Sat. parameter} = \frac{I}{I_{sat}} \frac{(\gamma_N/2)^2}{(\nu-\nu_0)^2 + (\gamma_N/2)^2}$$

↳ line shape.

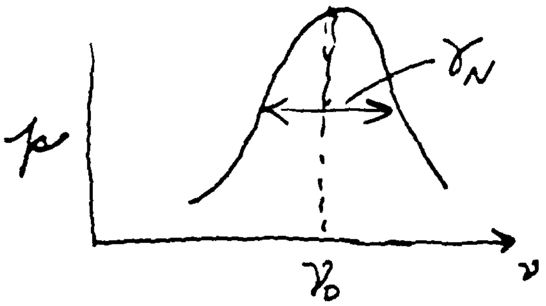

$$\left.\begin{aligned} \gamma_n &= 10 \text{ MHz}. \\ I_{sat} &= 20 \frac{\text{mW}}{\text{cm}^2} \end{aligned}\right\} \text{Na}$$

$p = 1$ $\quad I = I_{sat}$ $\quad f = \frac{1}{4}$

$p = \infty$ $\quad f = 1/2$

$$\boxed{A_{sat} = \frac{F_{sat}}{m} \cong 10^8 \text{ cm/sec}^2.}$$

Ashkin, Phys. Rev. Lett **25**, 1321 (1970).

15

Gradient Force
or Dipole Force

induced dipole moment $d = \alpha E$

α = polarizability of atom

$$\vec{F}_{dip} = -\frac{1}{2}\alpha \vec{\nabla} E^2$$

$$\alpha = \alpha_0 \frac{\nu - \nu_0}{(\nu-\nu_0)^2 + \gamma_n^2/4}\left(\frac{1}{1+p}\right)$$

saturates to zero

dispersive

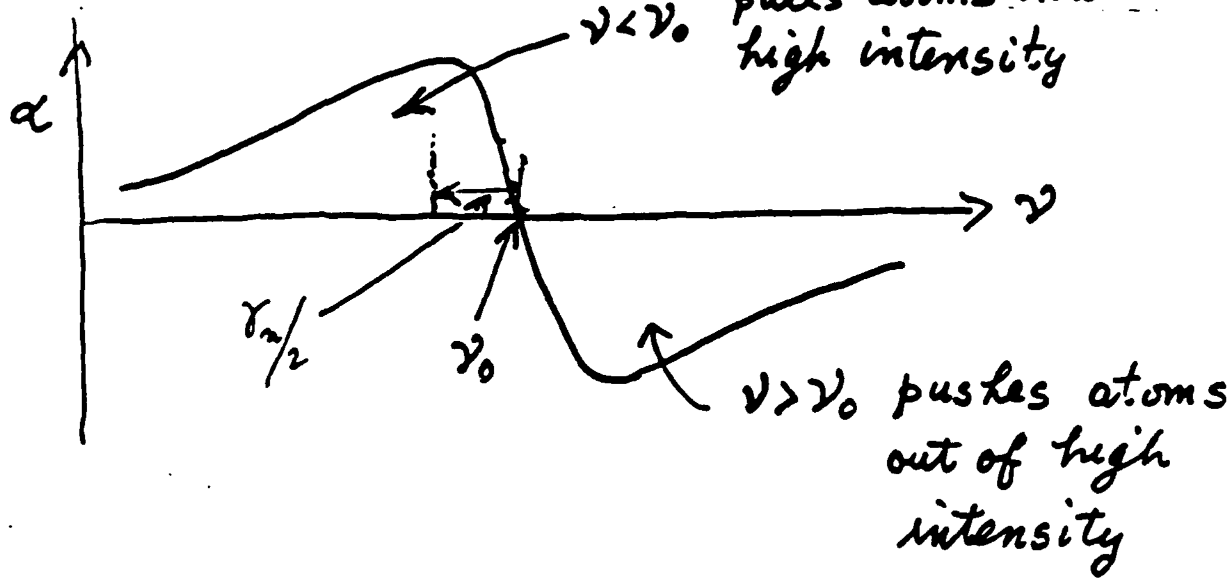

16

Saturation of F_{dip}

$$\vec{F}_{dip} = -\frac{\alpha}{2}\vec{\nabla}E^2 = -\vec{\nabla}U$$

$$U = \frac{h}{2}(\nu-\nu_0)\ln(1+p)$$

$$\text{same power}\begin{cases} \nu-\nu_0 = \frac{\gamma_n}{2}, & p = 5\times10^{-7}, \quad U \approx 4h\gamma_n \\ \nu-\nu_0 = 5\times10^{3}\gamma_N, & p = 1, \quad \underbrace{U \approx 1.7\times10^{3}h\gamma_n}_{\sim 400\times \text{ larger!}} \end{cases}$$

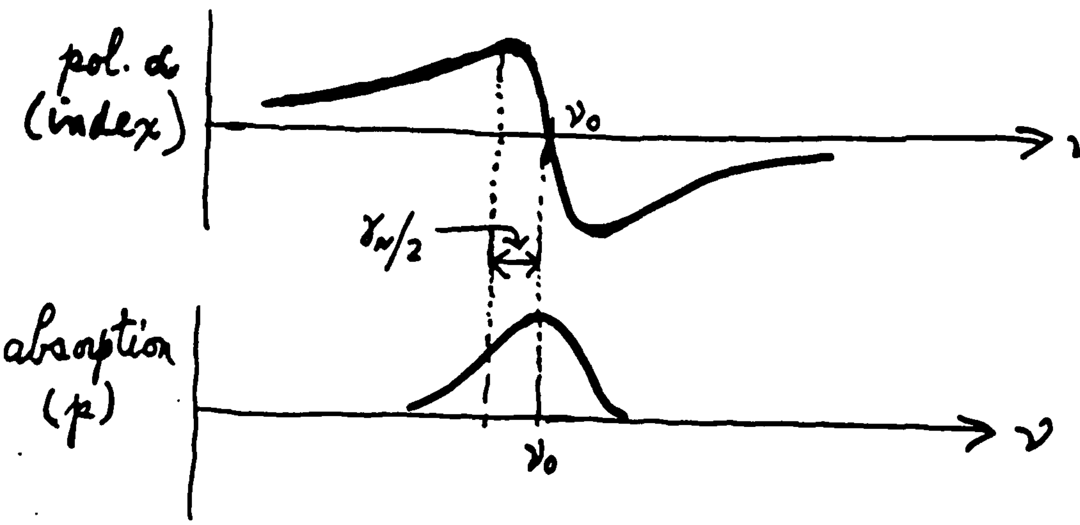

Ashkin, Phys. Rev. Lett. 40, 729 (1978).

Atomic Beam Deflection

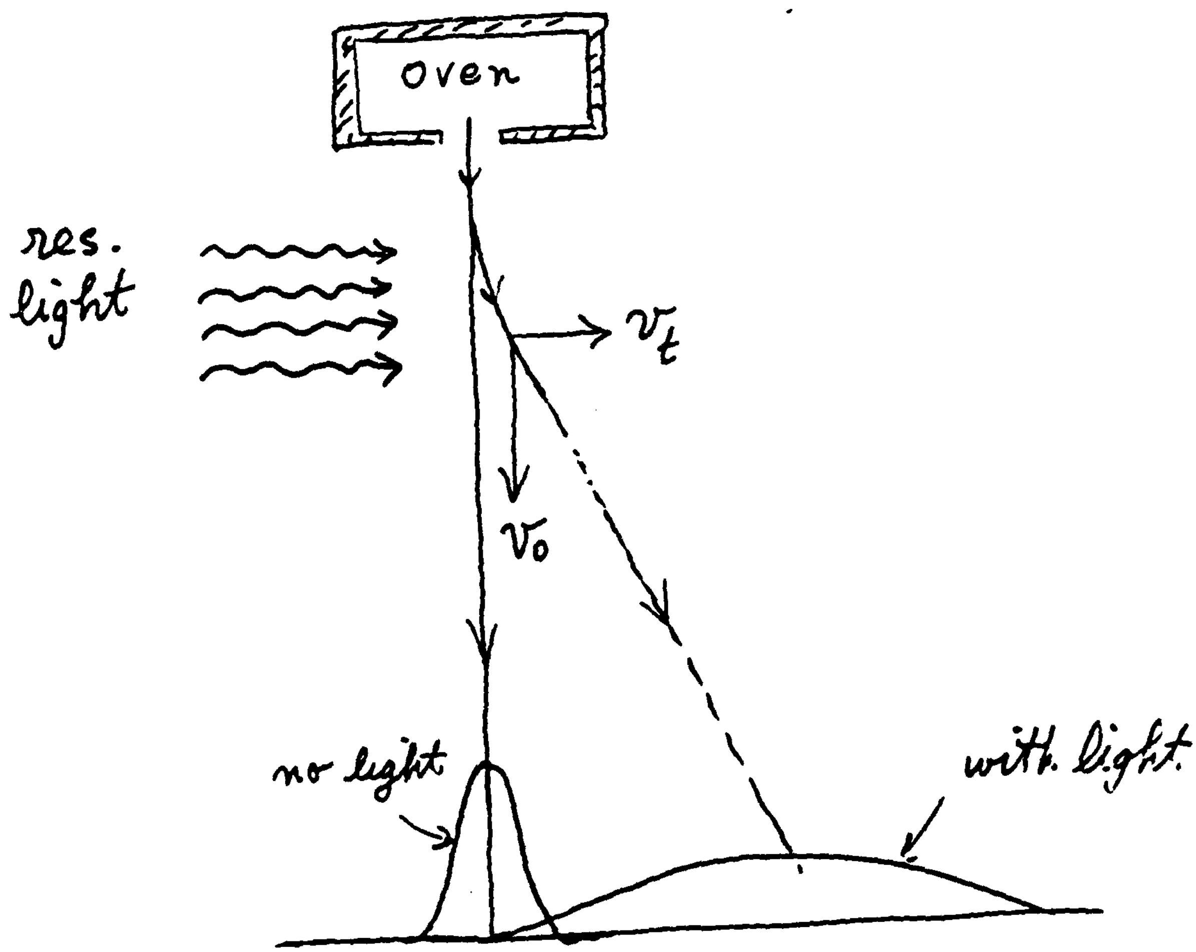

Bjorkholm et. al. Phys. Rev. A. **23**, 491 (1981).

18

Stopping Atoms –

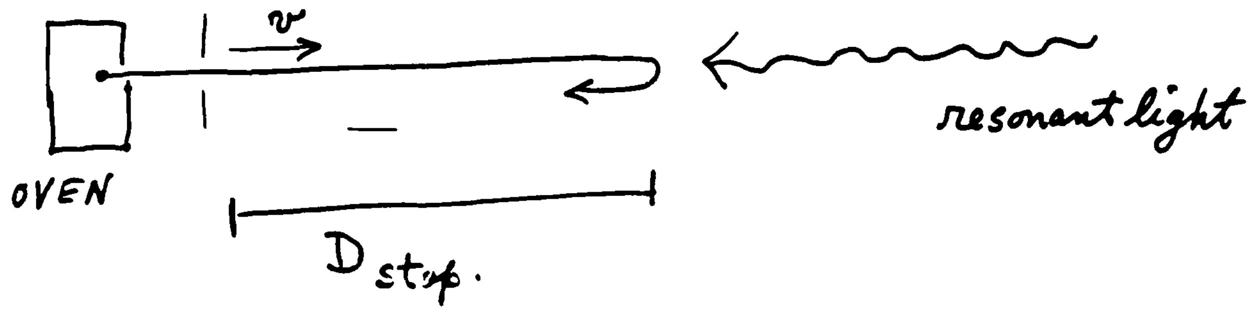

If $v \sim 2 \times 10^4$ cm/sec $\qquad D_{stop} \sim 5$ cm.

If continuously applied

- Doppler Shift –
- Chirp –

Prodan et. al., Phys. Rev. Lett. 54, 992 (1985).

Ertmer et. al., Phys. Rev. Lett. 54, 996 (1985).

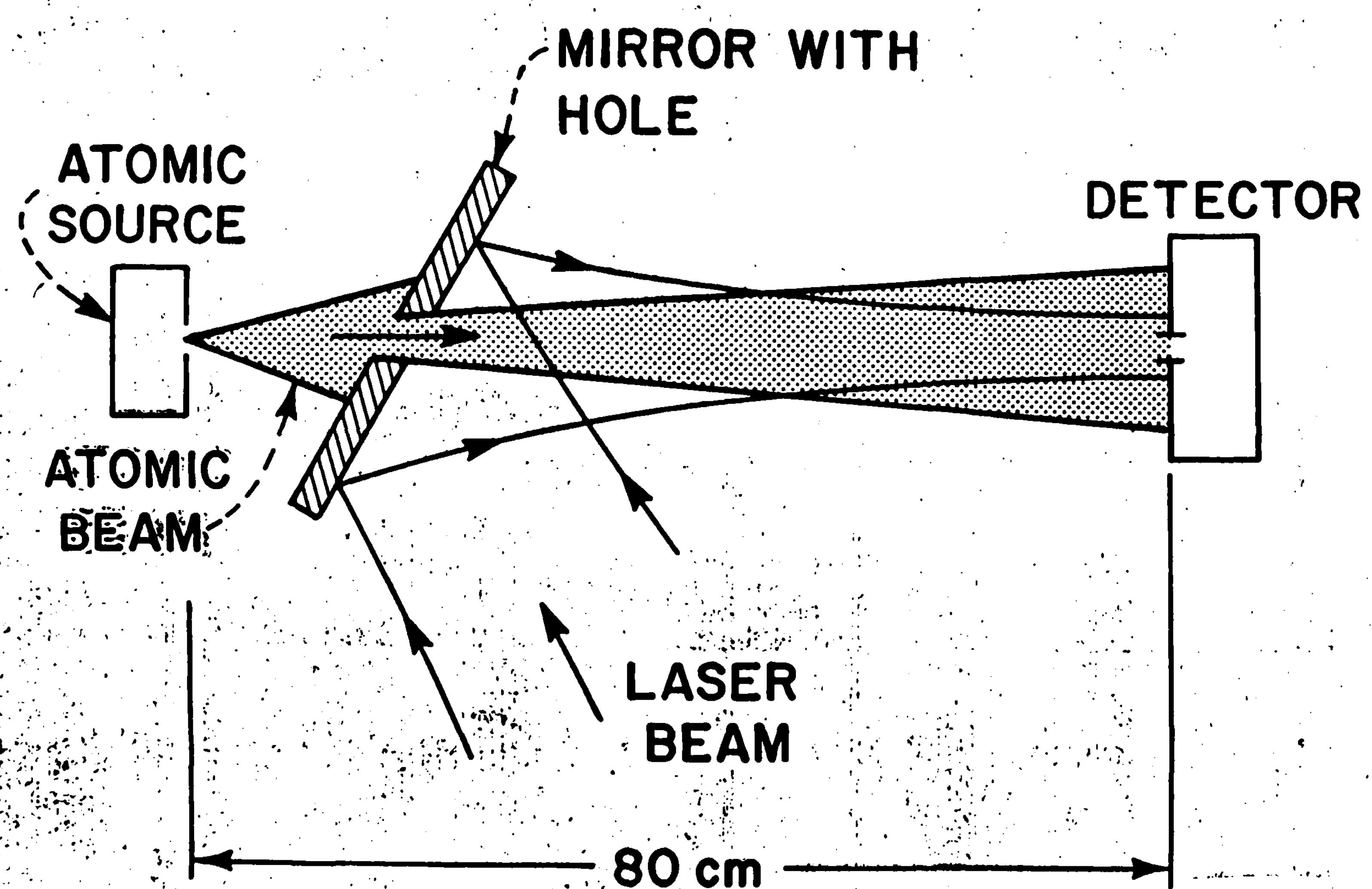

Bjorkholm, Freeman, Ashkin, Pearson,
Phys. Rev. Lett. 41, 1361 (1978).

20

21

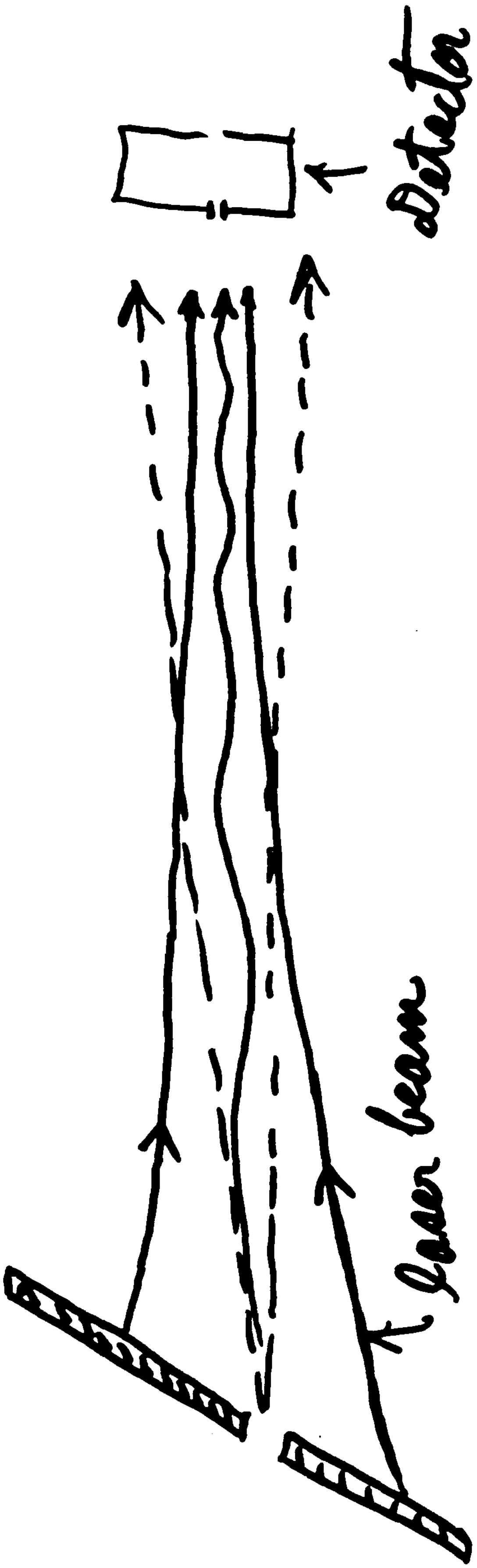

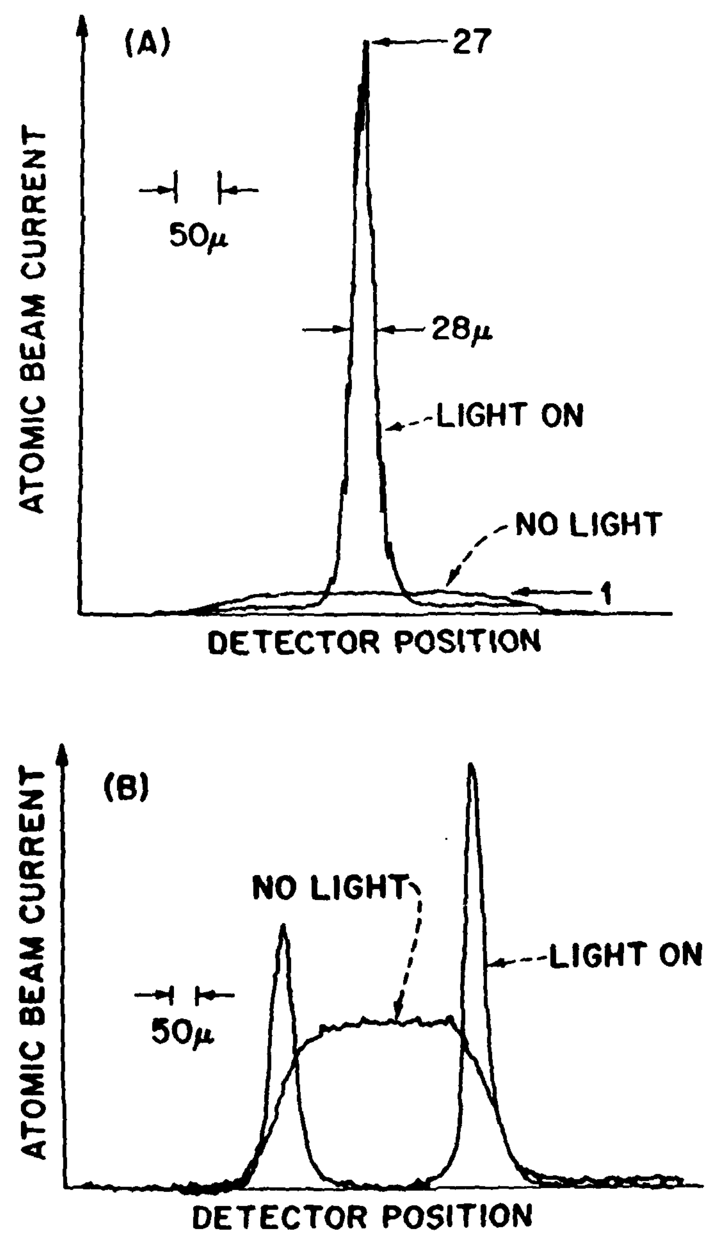

$\nu < \nu_0$

$\nu > \nu_0$

22

Bell Laboratories

SEQUENCE NO.

Single-Beam Gradient Trap

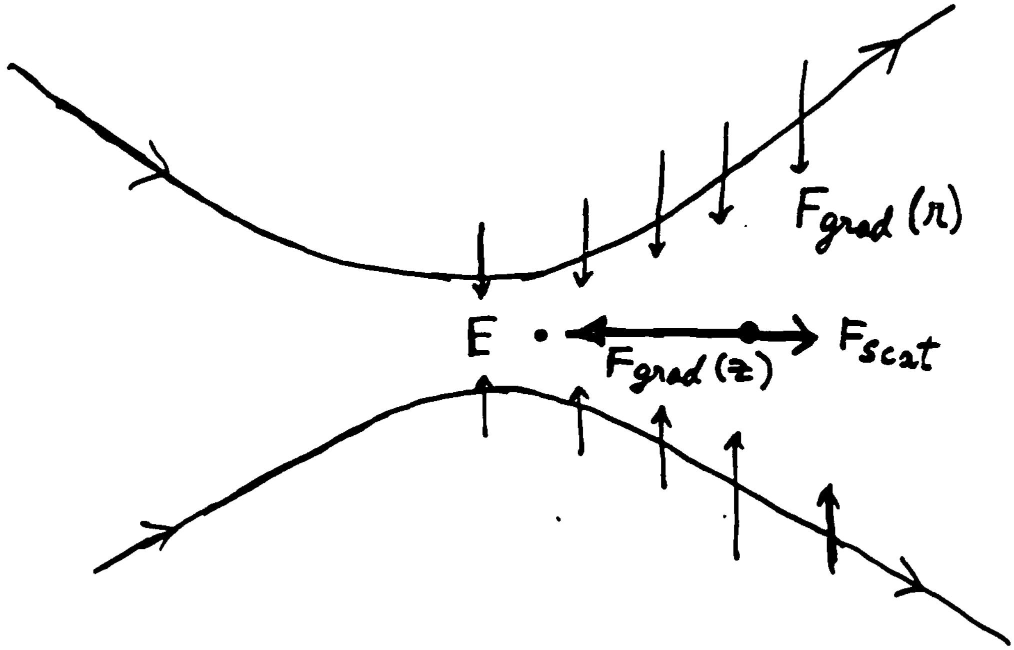

$$\underline{U \cong 10^3 \hbar \gamma_N \sim 0.3 \text{ K}}$$

$$v_{escape} \sim 2 \times 10^3 \text{ cm/sec.}$$

<u>Trapping Volume ~ 200 μ^3</u>

$$\begin{pmatrix} P = 100 \text{ mW} & \\ w_0 = 1.2\,\mu & p \simeq 0.2 \end{pmatrix}$$

Ashkin, Phys. Rev. Lett. 40, 729 (1978).

23

Trapping of Submicron Rayleigh Particles.

Apparatus -

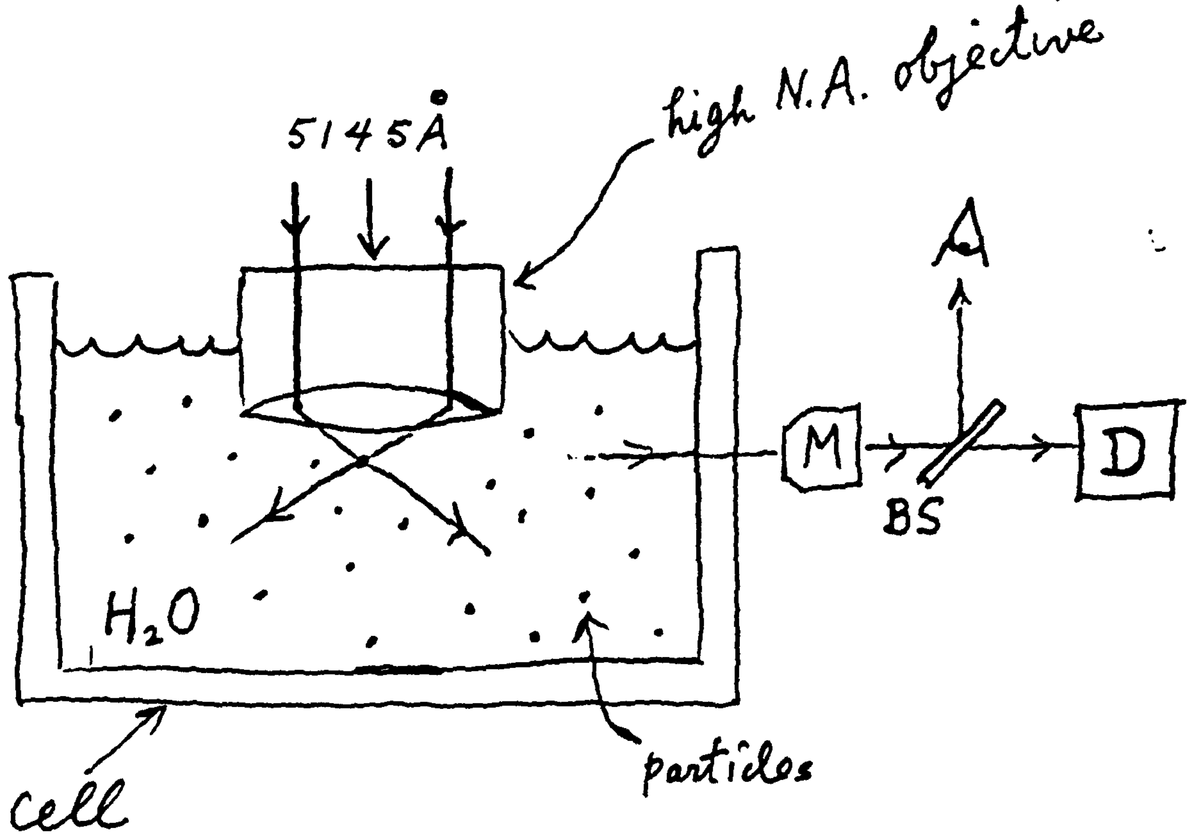

Ashkin, Dziedzic, Bjorkholm, Chu

Opt. Lett. 11, 288 (1986).

24

Optical Damping of Atomic Motion

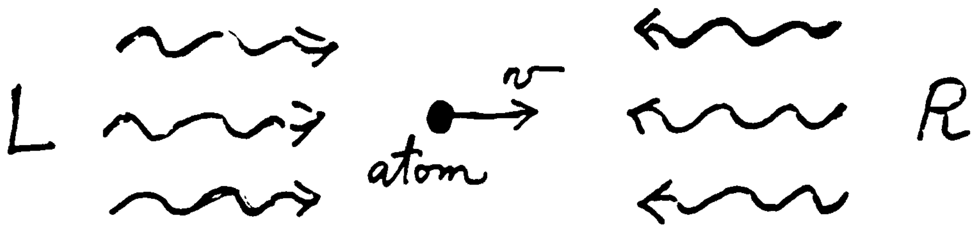

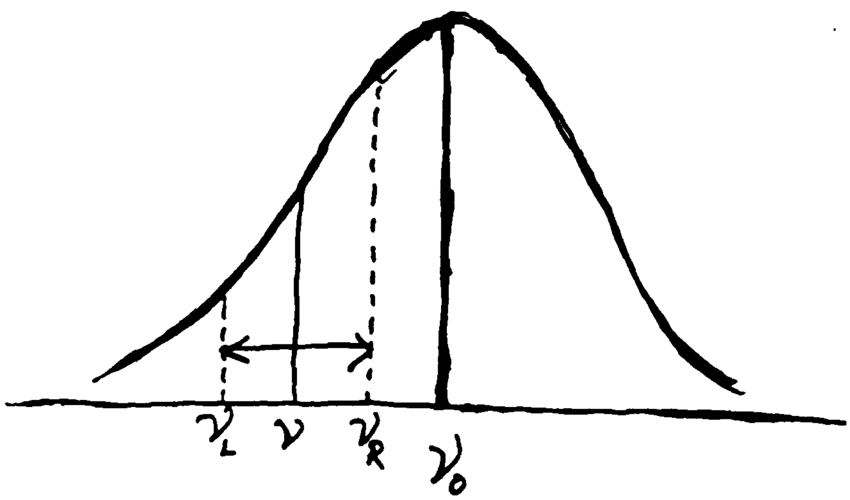

$\nu < \nu_0$ $\qquad$ $F = -\gamma v$

In 3 dimensions $\longrightarrow$ Optical Molasses

Hänsch & Schawlow, Opt. Comm. 13, 68 (1975)

Heating

Quantum Fluctuations in F_{scat}

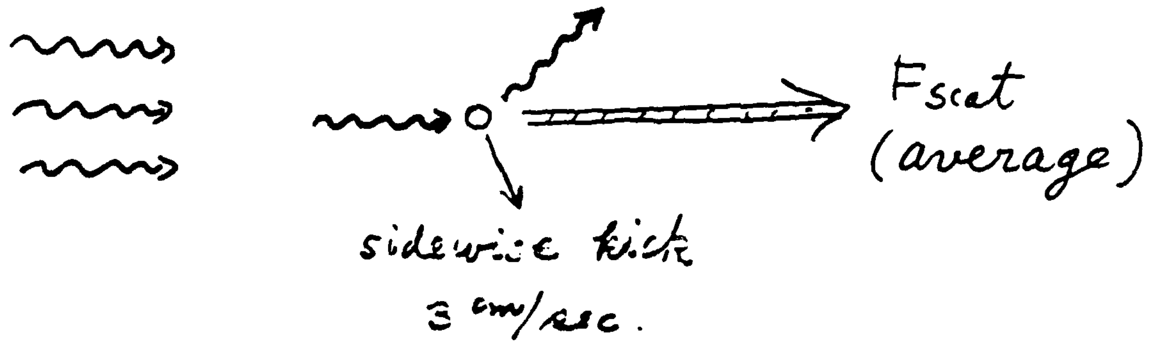

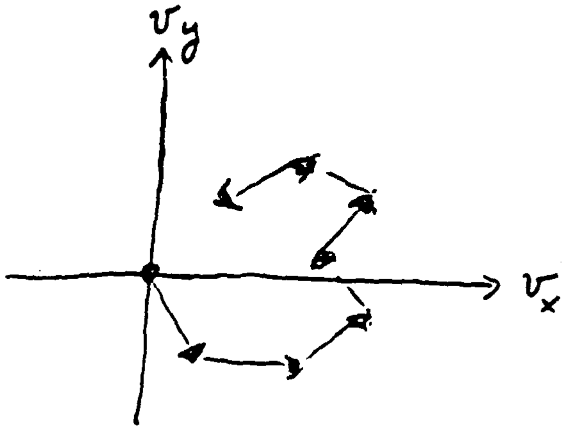

Random Walk in Velocity space –

$\langle \Delta v \rangle = 0$ in molasses.

$\langle \Delta v^2 \rangle \sim t$

$\overline{KE}_{random} \sim \langle \Delta v \rangle^2 \sim t$

linear heating rate –

Letokhov et. al. JETP 39, 698 (1977).

Ashkin + Gordon, Opt. Lett. 4, 161 (1979).

$KE_{equilib}$ – Balance of Heating & Cooling –

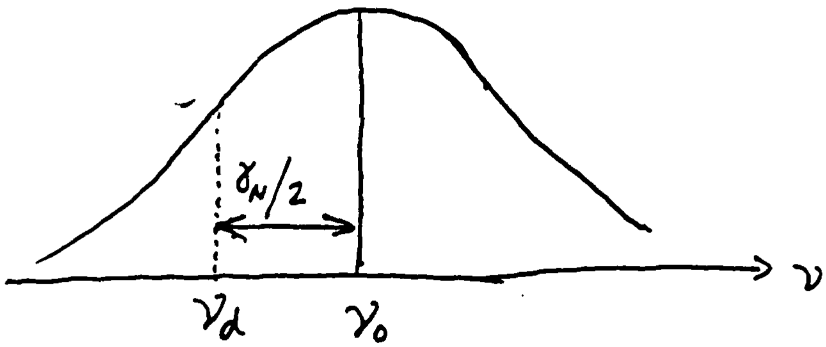

For optimum damping $\quad \nu_d = \nu_0 - \gamma_N/2$

$$KE_{min} = \underbrace{\frac{h\gamma_N}{4}}_{\text{From Scat Force}} + \frac{h\gamma_N}{4}$$ — From Dipole Force

$$\boxed{\begin{array}{l} KE_{min} = \dfrac{h\gamma_N}{2} \\ T_{min} \cong 240\,\mu K. \\ v_{av} \cong 60 \text{ cm/sec} \end{array}}$$

Gordon & Ashkin

Phys. Rev. A $\underline{21}$, 1606 (1980).

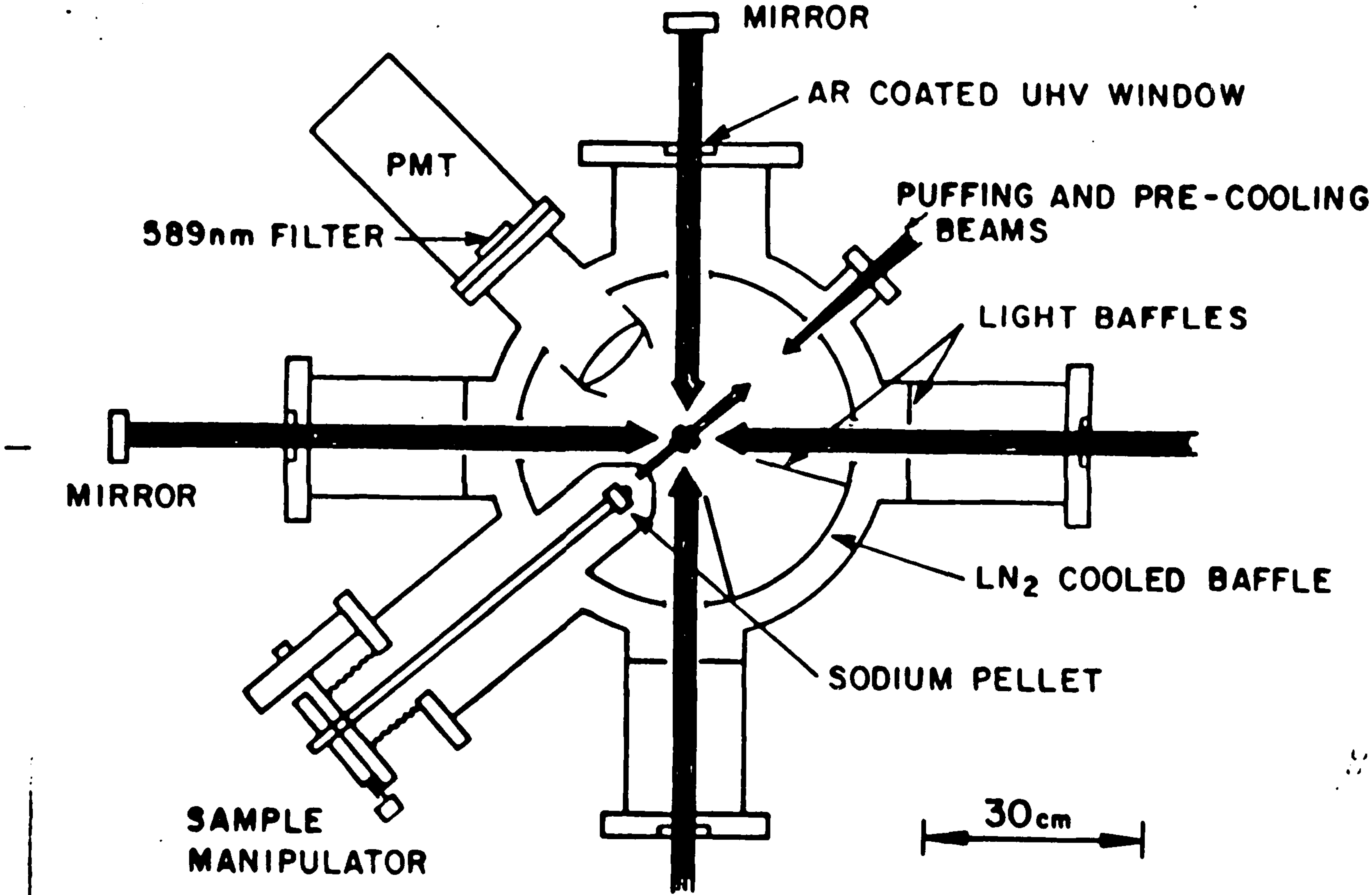

[~~Chu, Hollberg, Bjorkholm, Cable, Ashkin~~
Phys. Rev. Lett. 55, 48 (1985).]

E-9148 (10-83)

AT&T Bell Laboratories

28

TOP
DO NOT AFFIX OVERLAYS ALONG THIS SURFACE

VG. NO.________

Photo of Apparatus for [illegible]

29

E-9148 (6-85)
AT&T BELL LABORATORIES

AT&T

TOP
DO NOT AFFIX OVERLAYS ALONG THIS SURFACE

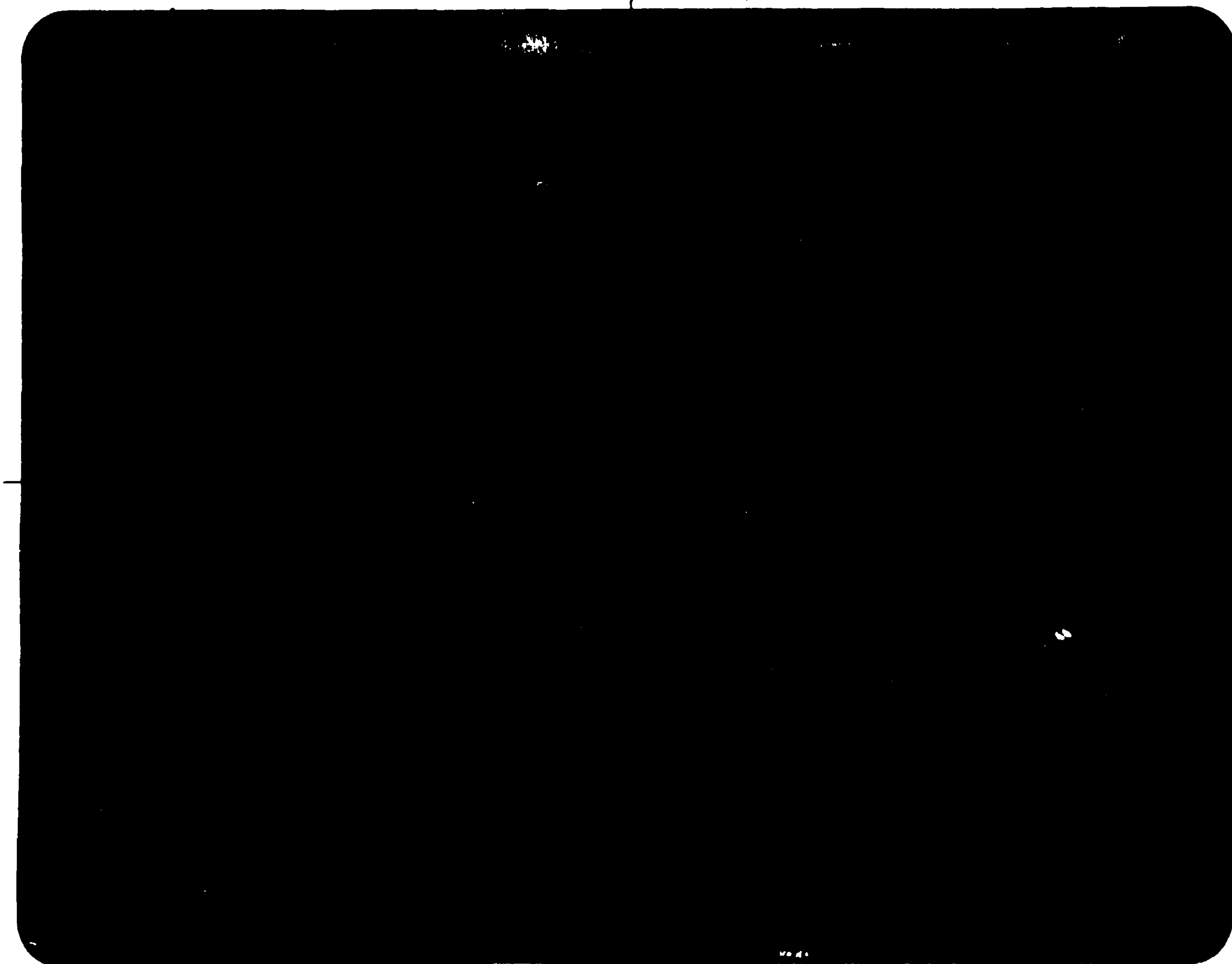

30

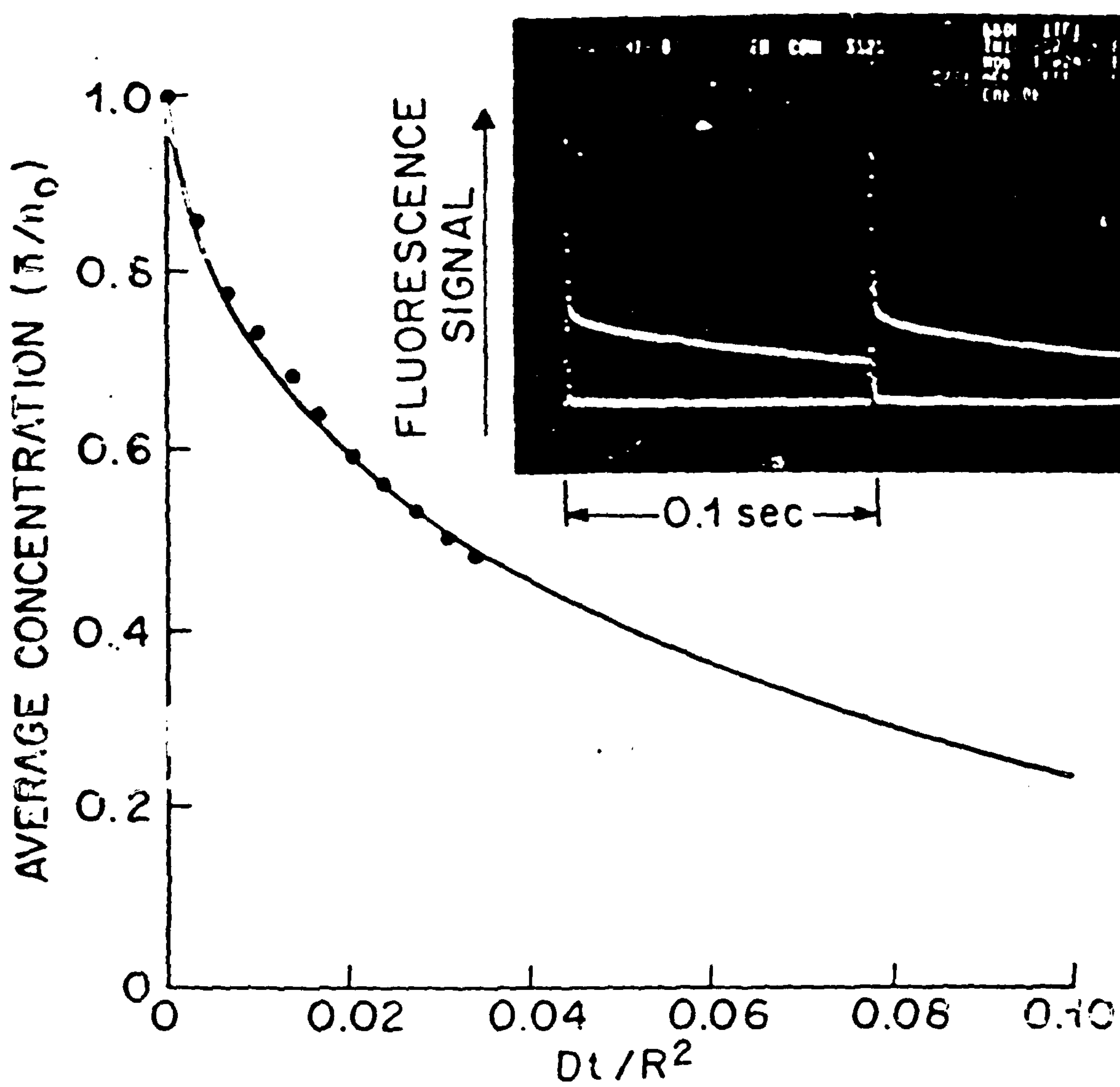

AVERAGE CONCENTRATION ($\bar{n}/n_0$)
1.0
0.8
0.6
0.4
0.2
0
0
0.02
0.04
0.06
0.08
0.10
Dt/R^2
FLUORESCENCE SIGNAL
0.1 sec

Fig 2.

Time of Flight Temperature Measurement

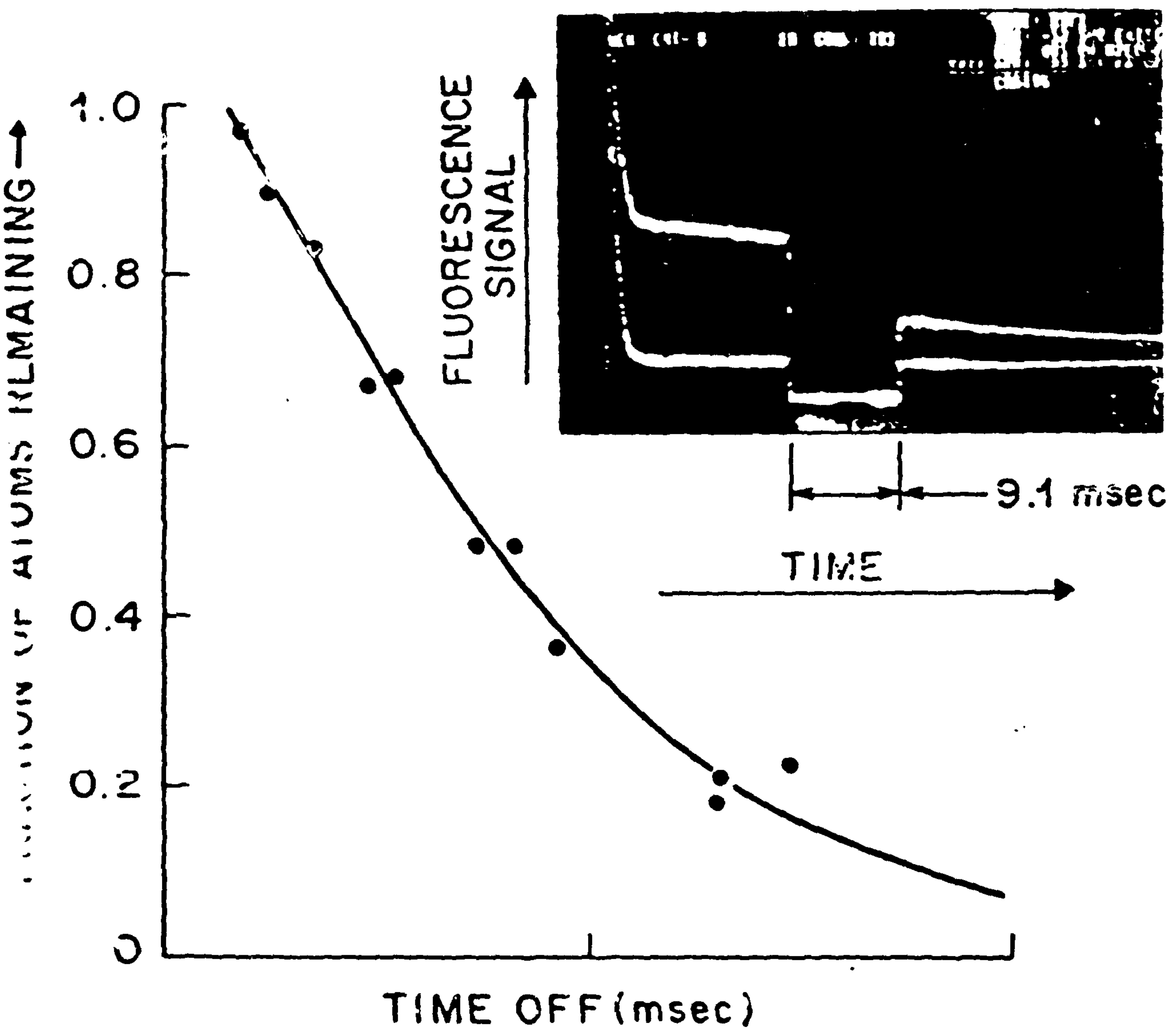

Fig 3.

Photo of Atom Trap in Molasses –

(33)

-69-

E-8814 (6-85)

AT&T

SEQUENCE NO.________

VG. NO.________

AT&T BELL LABORATORIES

MACROSCOPIC QUANTUM JUMPS IN A SINGLE ATOM

Axel Schenzle

University of Essen
4300 Essen
West Germany

Richard G. Brewer

IBM Almaden Research Center
650 Harry Road
San Jose, California 95120-6099

ABSTRACT: A single atom optical clock proposed over 10 years ago utilizes an amplification scheme which only recently was recognized as a novel problem in quantum statistics. The atom, a three state system, has two coupled transitions that are driven continuously by two external fields, one being an allowed transition ($1 \leftrightarrow 3$) and the other a forbidden transition ($2 \leftrightarrow 3$) where $|3>$ is the lowest state. It has been argued that the weak transition, which is difficult to detect, could be monitored by the presence or absence of spontaneous emission of the strong transition. Thus, when the atom is shelved in the metastable state $|2>$, the strong transition is extinguished, but when the atom executes a single quantum jump ($2 \rightarrow 3$), it triggers a succession of perhaps a million quantum jumps (macroscopic quantum jumps) in the strong transition, an amplification that can be detected easily. This intuitive argument for alternating bright and dark intervals assumes, however, that the atom is always in an eigenstate. Should the atom be in a superposition state, because of coherent excitation, one could imagine that the weak transition would merely reduce the intensity of the strong transition slightly. This issue is resolved, in favor of the first intuitive argument, by calculating the photon counting statistics, the probability W(n,T) of observing precisely n photon counting events in a collection T in a quantum mechanically consistent way. The results cannot

be described by classical statistics. A compact analytic form is obtained for $W(n,T)$ by considering the entire hierarchy of correlation functions where the emission interval peaks sharply about a particular n with a Poisson distribution and can be comparable in length to the darkness interval ($n = 0$) while the other values of n display vanishingly small probabilities.

The British Journal for the Philosophy of Science

VOLUME III | AUGUST, 1952 | No. 10

ARE THERE QUANTUM JUMPS?

PART I*

E. SCHRÖDINGER

"... cominciai a credere, che uno, che lascia un'opinione imbevuta col latte, e seguita da infiniti, per venire in un' altra da pochissimi seguita, e negata da tutte le scuole, e che veramente sembra un paradosso grandissimo, bisognasse per necessità, che fusse mosso, per non dir forzato, da ragioni più efficaci." Galileo, *Dialogue on the Two Greatest World Systems*, 2nd Day.

1 *The Cultural Background*

PHYSICAL science, which aims not only at devising fascinating new experiments, but at obtaining a rational understanding of the results of observations, incurs at present, so I believe, the grave danger of getting severed from its historical background. The innovations of thought in the last 50 years, great and momentous and unavoidable as they were, are usually overrated compared with those of the preceding century; and the disproportionate foreshortening by time-perspective, of previous achievements on which all our enlightenment in modern times depends, reaches a disconcerting degree according as earlier and earlier centuries are considered. Along with this disregard for historical linkage there is a tendency to forget that all science is bound up with human culture in general, and that scientific findings, even those which at the moment appear the most advanced and esoteric and difficult to grasp, are meaningless outside their cultural context. A theoretical science, unaware that those of its constructs considered relevant and momentous are destined eventually to be

* Received 28.iv.52

EUROPEAN ORGANIZATION FOR NUCLEAR RESEARCH

Are there quantum jumps?

J.S.Bell[1]

Geneva, 19 June 1986

If we have to go on with these damned quantum jumps, then I'm sorry that I ever got involved. E.Schrödinger.

1. Introduction

I have borrowed the title of a characteristic paper by Schrödinger (Schrödinger, 1952). In it he contrasts the smooth evolution of the Schrödinger wavefunction with the erratic behaviour of the picture by which the wavefunction is usually supplemented, or 'interpreted', in the minds of most physicists. He objects in particular to the notion of 'stationary states', and above all to 'quantum jumping' between those states. He regards these concepts as hangovers from the old Bohr quantum theory, of 1913, and entirely unmotivated by anything in the mathematics of the new theory of 1926. He would like to regard the wavefunction itself as the complete picture, and completely determined by the Schrödinger equation, and so evolving smoothly with-

---

[1] CERN - TH, 1211 Geneva 23, Switzerland

Trapping and Cooling a Single Ba^+ Ion

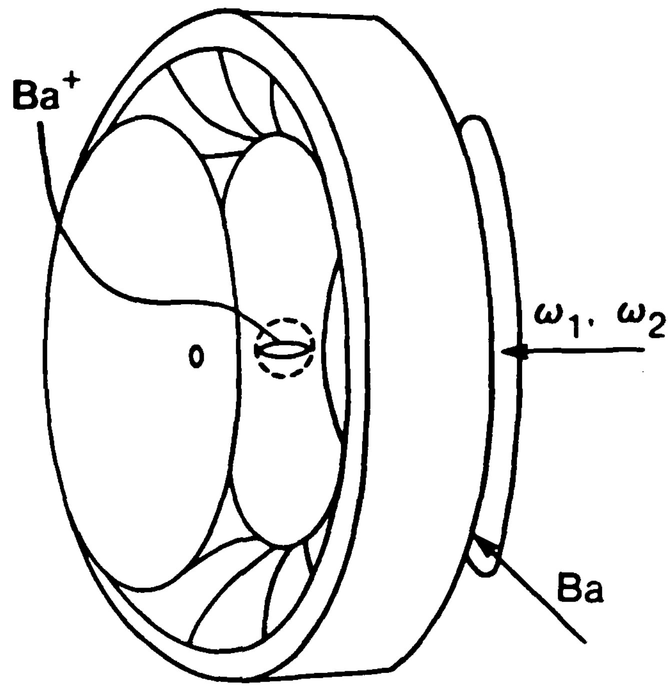

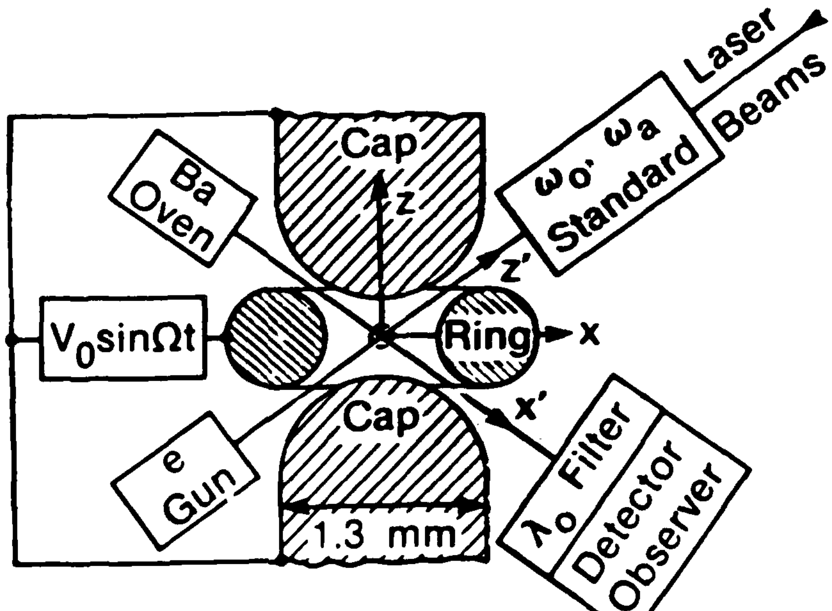

W. Neuhauser, H. Hohenstatt, P.E. Toschek
and H.G. Dehmelt, Phys. Rev. Lett. 41, 233 (1978)

Dehmelt proposal: single atom clock - $1/10^{18}$

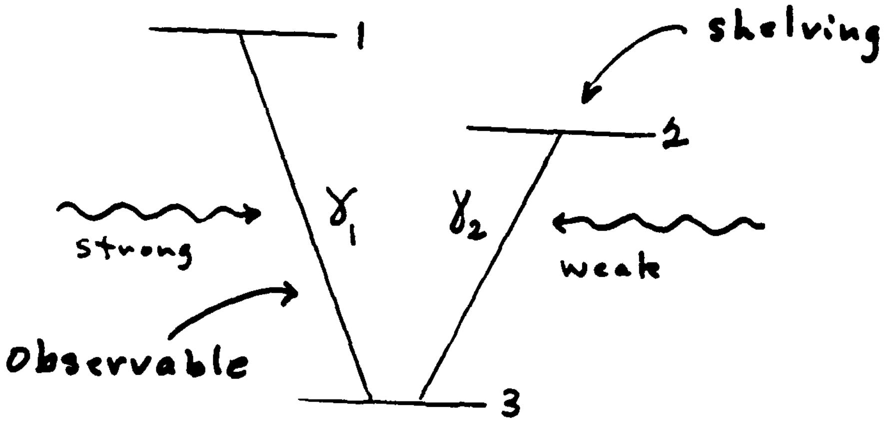

$\gamma_1 \gg \gamma_2$

"Macroscopic Quantum Jumps"?

Does weak transition switch strong transition on and off?

Or is intensity of strong transition just slightly reduced?

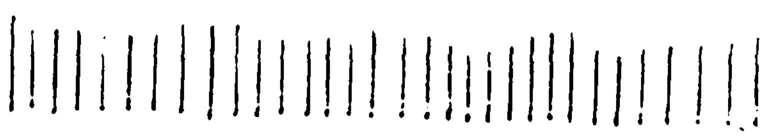

Macroscopic Quantum Jumps in a Single Atom

Proposal

H.G. Dehmelt, Bull. Am. Phys. Soc. 20, 60 (1975)

Theory

R.J. Cook and H.J. Kimble, Phys. Rev. Lett. 54, 1023 (1985)

F.T. Arecchi, A. Schenzle, R.G. DeVoe, K. Jungmann and R.G. Brewer, Phys. Rev. A 33, 2124 (1986)

A. Schenzle, R.G. DeVoe, and R.G. Brewer, Phys. Rev. A 33, 2127 (1986)

A. Schenzle and R.G. Brewer, Phys. Rev. A 34, 3127 (1986)

J. Javanainen, Phys. Rev. A 33, 2121 (1986)

C. Cohen-Tannoudji and J. Dalibard, Europhysics Letters 1, 441 (1986)

D.T. Pegg, R. London and P.L. Knight, Phys. Rev. A 33, 4085 (1986)

P. Zoller, M. Marte and D.F. Walls, Phys. Rev. A 35, 198 (1987)

Experiments

W. Nagourney, J. Sandberg and H. Dehmelt,
Phys. Rev. Lett. 56, 2727 (1986)

R.G. Hulet, J.G. Bergquist, W.M. Itano and
D.J. Wineland, Phys. Rev. Lett. 57, 1699 (1986)

Th. Sauter, W. Neuhauser, R. Blatt and
P.E. Toschek, Phys. Rev. Lett. 57, 1696 (1986)

M.A. Finn, G.W. Greenlees and D.A. Lewis
(to be published)

Object of this Talk

Describe a quantum statistical theory which predicts the existence of "macroscopic quantum jumps" and other details of a 3 state atom beginning with

(1) the Heisenberg equation of motion

(2) modeling spontaneous emission as a Markov process

Intuitive Arguments

Assume single atom, saturation and steady state

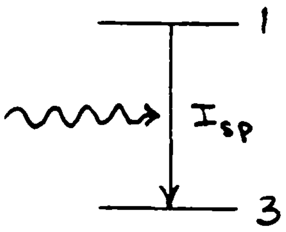

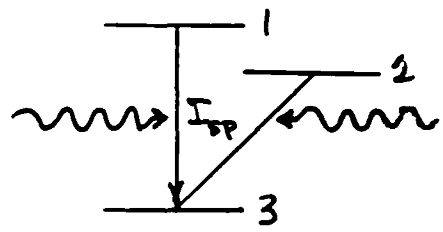

$I_{sp}^{ss}\rangle = \gamma_1 \rho_{11}^{ss}$ $\qquad \langle I_{sp}^{ss}\rangle = \frac{1}{2}\gamma_1$ $\qquad \langle I_{sp}^{ss}\rangle = \frac{1}{3}\gamma_1$

Assume atom is always in an eigenstate in 3-level case

- 2/3 probability of occupying $|1\rangle$ and $|3\rangle$ $\Rightarrow$ bright period
- 1/3 Probability of being shelved in $|2\rangle$ $\Rightarrow$ dark period
- $\tau_B / \tau_D = 2$
- During bright period, $I_{sp} = \frac{1}{2}\gamma_1$ as in two-level problem, but time average $\langle I_{sp}^{ss}\rangle = \frac{1}{3}\gamma_1 = \frac{1}{2}\gamma_1 \frac{\tau_B}{\tau_D + \tau_B}$

Assume 3 levels in superposition

Intensity is constant in time with $\langle I_{sp}^{ss}\rangle = \frac{1}{3}\gamma_1 - \epsilon$

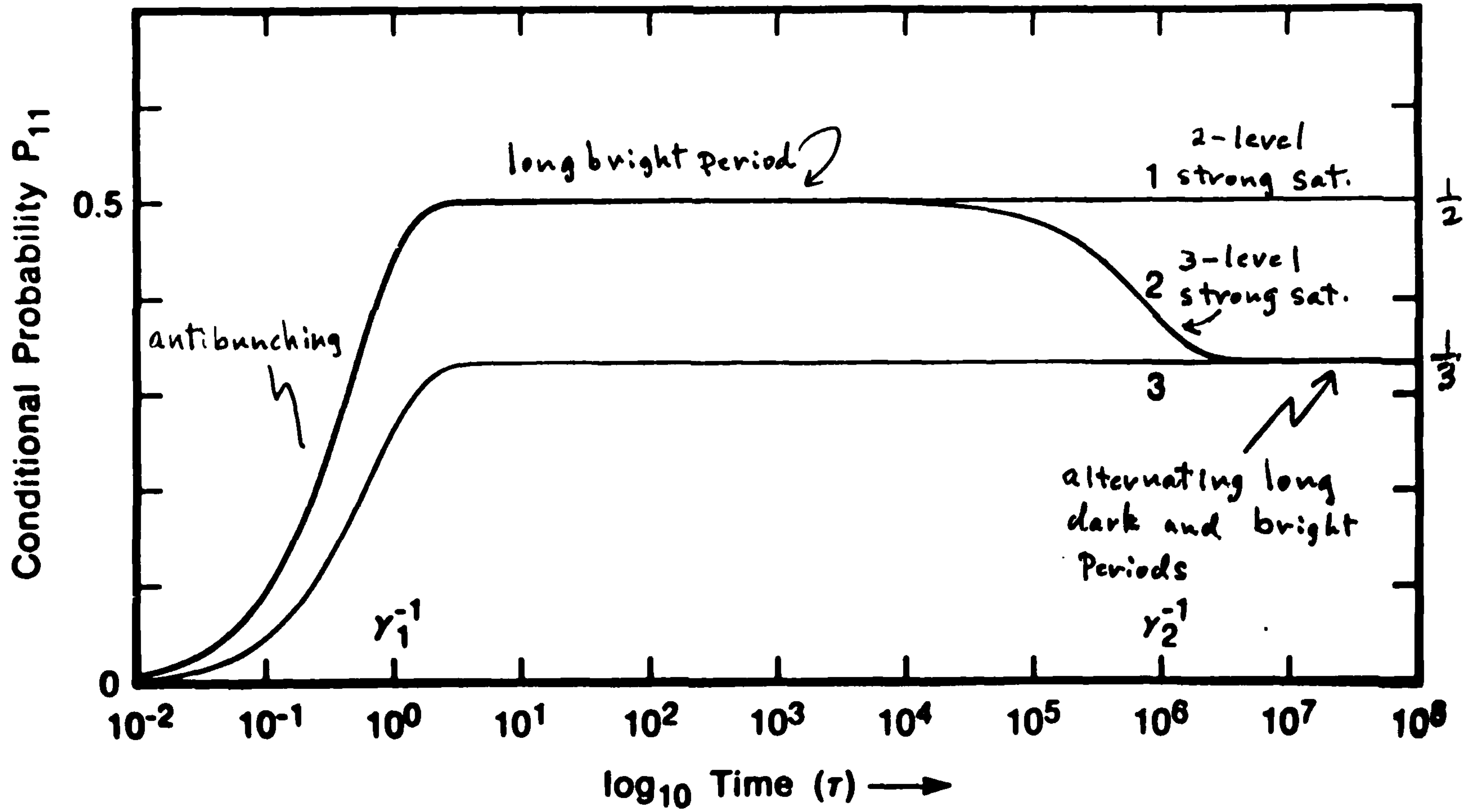
Conditional Probability P_{11}
0.5
0
long bright period
antibunching
2-level
1 strong sat.
$\frac{1}{2}$
3-level
2 strong sat.
3
$\frac{1}{3}$
alternating long
dark and bright
Periods
γ_1^{-1}
γ_2^{-1}
10^{-2} 10^{-1} 10^{0} 10^{1} 10^{2} 10^{3} 10^{4} 10^{5} 10^{6} 10^{7} 10^{8}
$\log_{10}$ Time (τ) →

More general treatment

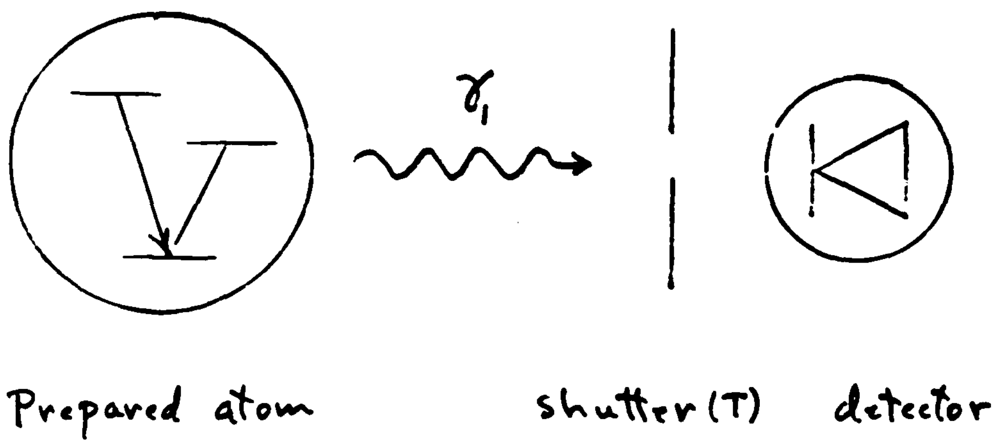

What is the probability $W(n,T)$ of detecting n photons in a collection time T?

Classical Photon Statistics

$$W(n,T) = \left\langle \frac{1}{n!}\left(\eta\int_0^T I(t)\,dt\right)^n e^{-\eta\int_0^T I(t)\,dt} \right\rangle$$

η: detector quantum efficiency

$\int_0^T I(t)\,dt \sim$ Probability of detecting 1 photon in time T

$W(0,T) \rightarrow 0 \qquad$ for $I = \frac{1}{2}\gamma_1$ and $T \approx \gamma_2^{-1}$

$\neq \frac{1}{3}$

Quantum Statistics

$$W(n,T) = \mathrm{tr}\,\rho\left\{\hat{T}\frac{1}{n!}\left(\gamma_1\eta\int_0^T b^\dagger(t)b(t)\,dt\right)^n e^{-\gamma_1\eta\int_0^T b^\dagger b\,dt}\right\} \quad *$$

$$= \sum_{\ell=0}^{\infty}(-1)^\ell(\gamma_1\eta)^{n+\ell}\binom{n+\ell}{\ell}\int_0^T dt_1\int_0^{t_1}dt_2\cdots\cdots\int_0^{t_{n+\ell-1}}dt_{n+\ell}$$

$$\times\ G_{n+\ell}(t_{n+\ell}-t_{n+\ell-1},\ \cdots\cdots,\ t_2-t_1)$$

Photon correlation function

* P.L. Kelley and W.H. Kleiner, Phys. Rev. 136, A316 (1964)

$$\boxed{\begin{aligned} W(0,T) &= \frac{1}{S+2}\left\{ S\, e^{-(R_2+\gamma_2)T} + 2e^{-\frac{1}{2}\eta\gamma_1 T} \right\} \\ W(n,T) &= \frac{2}{S+2}\, \frac{\left(\frac{1}{2}\gamma_1 \eta T\right)^n}{n!}\, e^{-\frac{1}{2}\gamma_1 \eta T}, \quad n = 1,2,3\ldots \end{aligned}}$$

$$S = R_2/(R_2+\gamma_2)$$

$$\left.\begin{aligned} \tau_D &= \frac{1}{R_2+\gamma_2} \\ \tau_B &= \frac{2}{R_2} \end{aligned}\right\}$$

$S = 1 \Rightarrow$

$\frac{1}{3}$ of the time dark

$\frac{2}{3}$ of the time bright

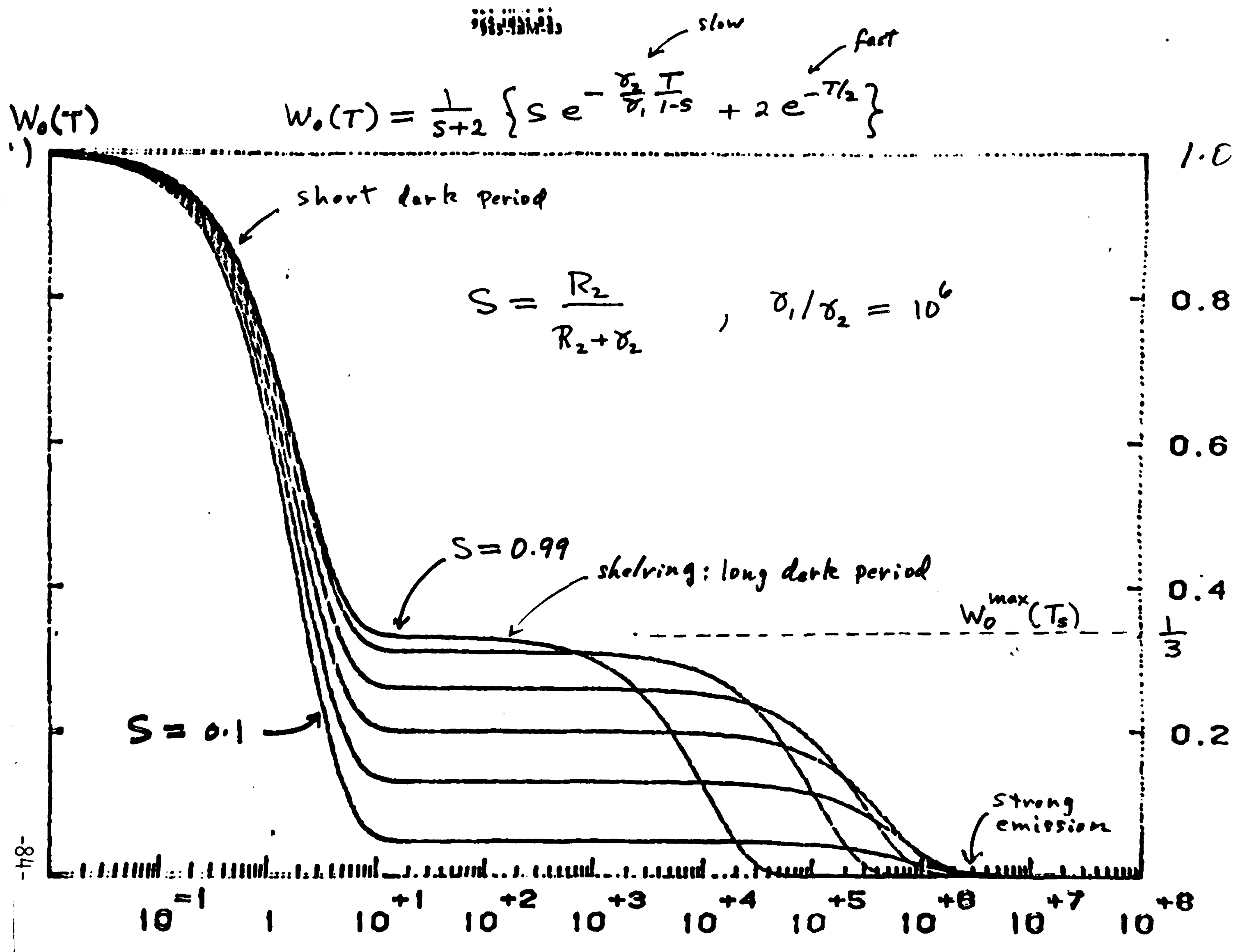

slow
fast
$W_0(T) = \frac{1}{s+2}\left\{ s\, e^{-\frac{\gamma_2}{\gamma_1}\frac{T}{1-s}} + 2\, e^{-T/2} \right\}$
$W_0(T)$
short dark period
$S = \frac{R_2}{R_2+\gamma_2}$, $\gamma_1/\gamma_2 = 10^6$
$S = 0.99$
shelving: long dark period
$W_0^{max}(T_s)$
$S = 0.1$
strong emission
1.0
0.8
0.6
0.4
$\frac{1}{3}$
0.2
10^{-1}
1
10^{+1}
10^{+2}
10^{+3}
10^{+4}
10^{+5}
10^{+6}
10^{+7}
10^{+8}

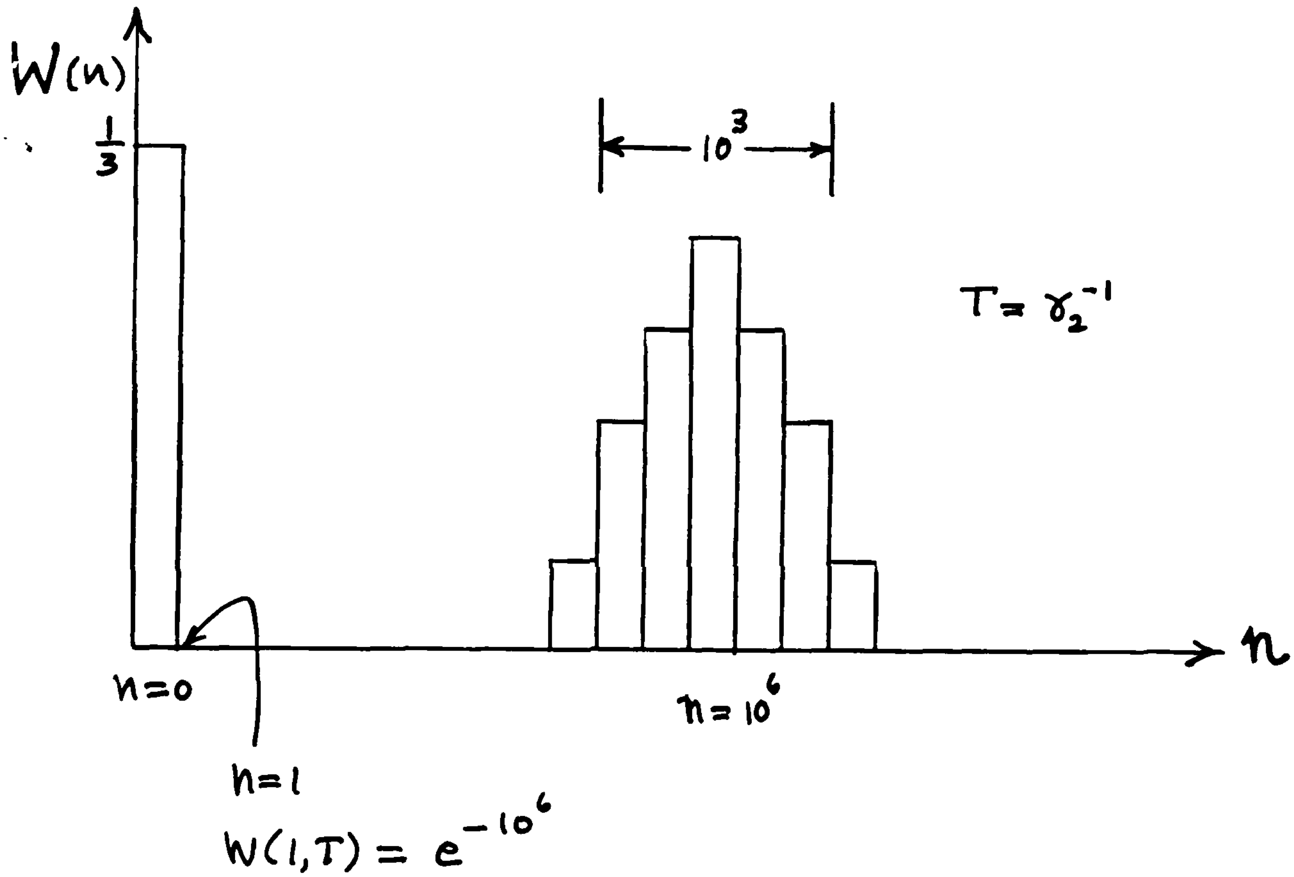

Thus, for an observation time $T \approx \gamma_2^{-1}$,
we have either

$$n = 0 \quad \text{or} \quad n = 10^6$$

but not $n = 1, 2, 3 \ldots\ldots$!

Many Atoms

Joint probability for n atoms not radiating in an interval T:

$$W(0,T)_n = W(0,T)^n$$

Average darkness interval:

$$\langle T \rangle_n \cong \frac{1}{n(R_2+\gamma_2)} \quad , \text{ slowly varying part}$$

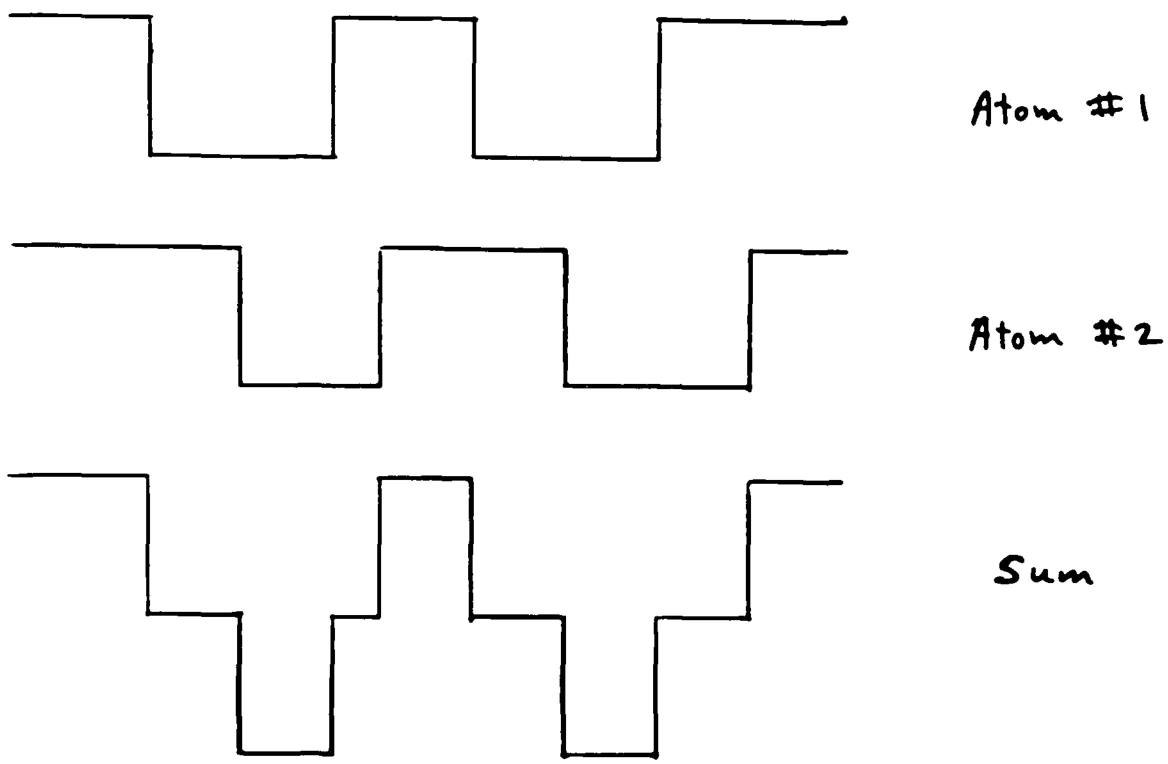

For an ensemble

$$\lim_{n\to\infty} \langle T \rangle_n = 0$$

W. Nagourney, J. Sandberg,
H. Dehmelt ~~[illegible]~~
PRL 56, 2727 (1986)

Ba^+

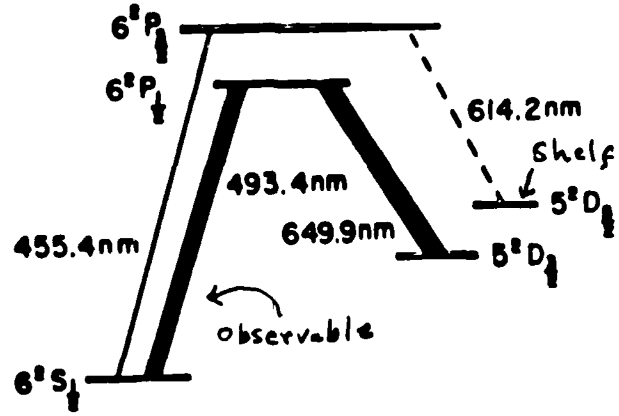

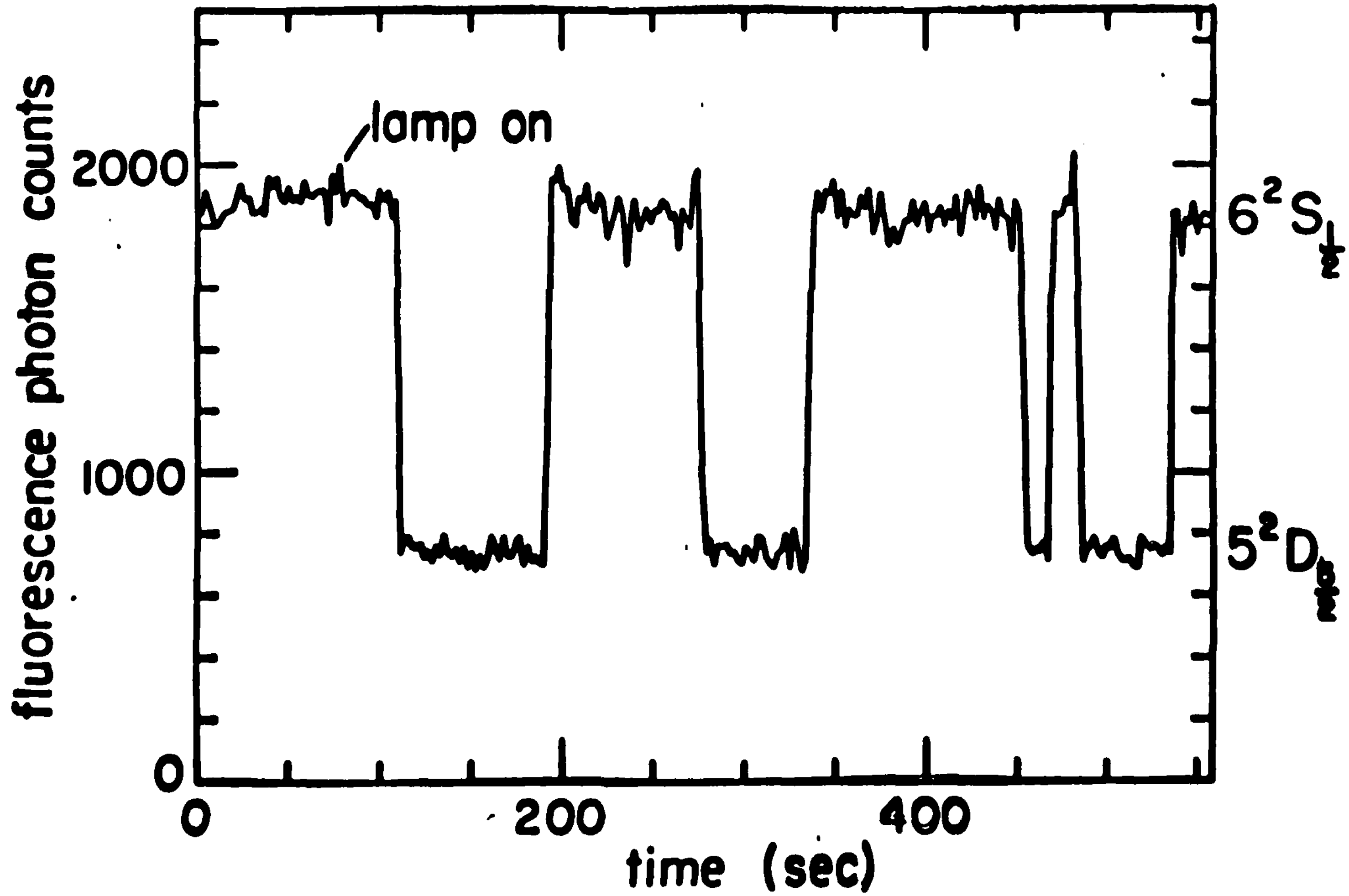

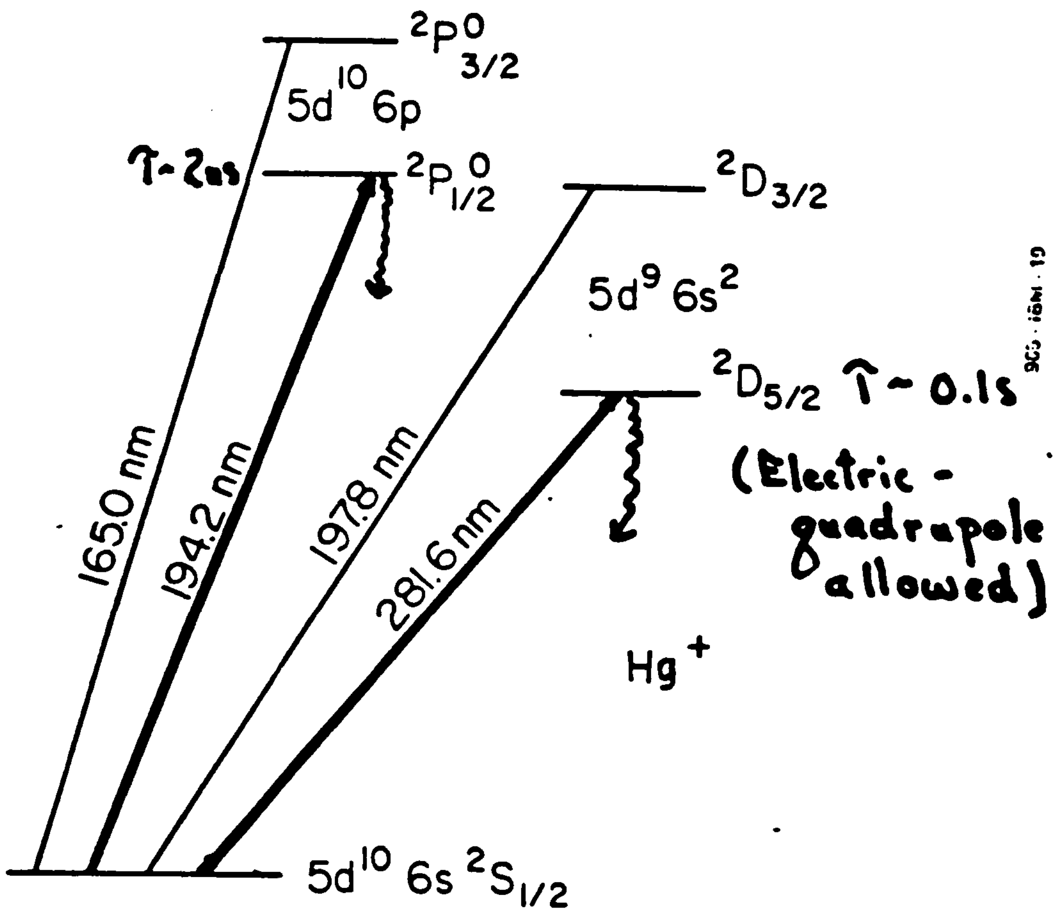

$^2P^0_{3/2}$
$5d^{10}\,6p$
τ~2ns
$^2P^0_{1/2}$
$^2D_{3/2}$
$5d^9\,6s^2$
$^2D_{5/2}$ τ~0.1s
(Electric-quadrupole allowed)
165.0 nm
194.2 nm
197.8 nm
281.6 nm
Hg$^+$
$5d^{10}\,6s\,^2S_{1/2}$

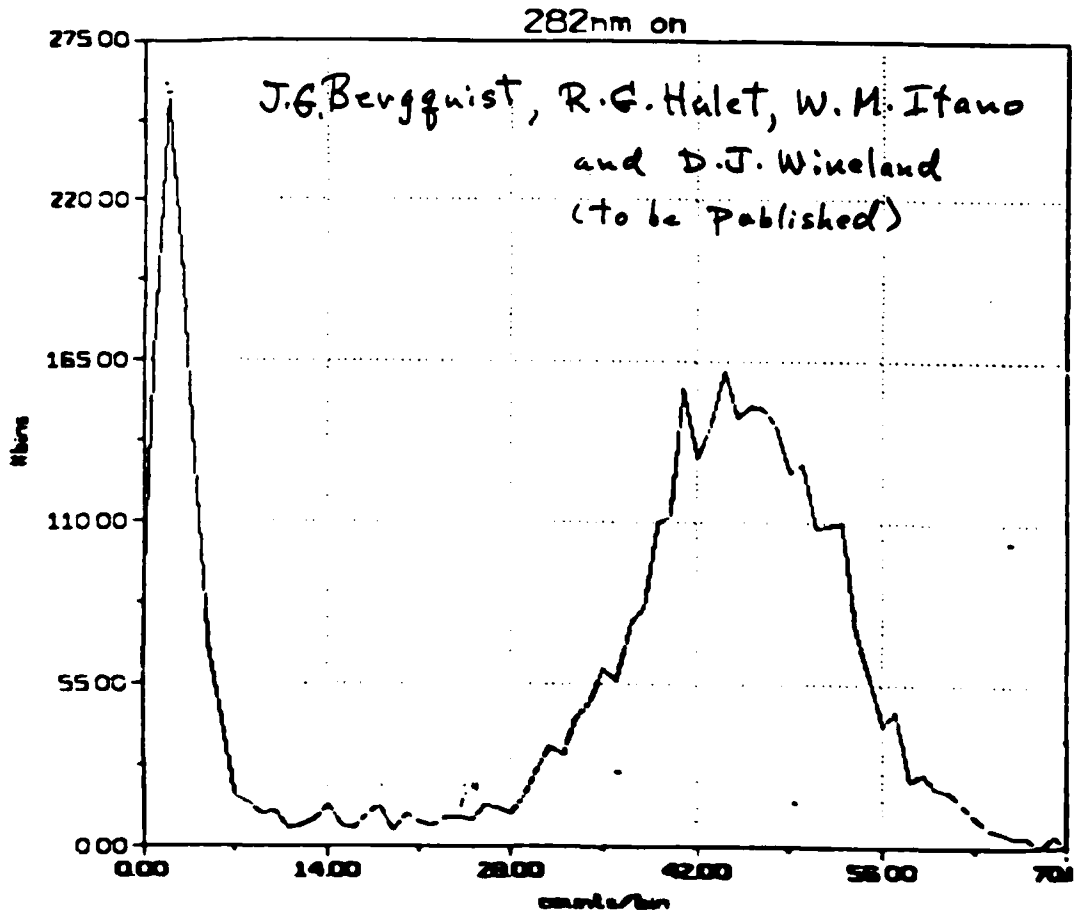

282nm on
J.G. Bergquist, R.G. Hulet, W.M. Itano and D.J. Wineland (to be published)
275.00
220.00
165.00
110.00
55.00
0.00
0.00
14.00
28.00
42.00
56.00

Conclusions

- A quantum statistical theory of a single three-state atom shows that quantum jumps of a macroscopic kind occur where the strong transition fluctuates between a state of strong spontaneous emission to a state of no emission when the electron is shelved in the metastable state. Thus, eventhough the atom is excited continuously, the emission is not continuous.

- Remarkably, this single atom quantum evolution can be seen by the naked eye.

- Like a Stern-Gerlach experiment, the three-level problem demonstrates how quantum measurements work.

Laser cooling of neon metastable states

Fujio Shimizu, Kazuko Shimizu and Hiroshi Takuma

We report the first demonstration of the laser cooling of a neutral atomic beam other than alkali atoms. A neon beam was cooled by using the 640nm transition between the metastable state $1s_5$ (J=2) and $2p_9$ (J=3). We further transfered this cooled $1s_5$ metastable atoms to another metastable state $1s_3$ (J=0). The population in $2p_9$ can decay only to the metastable state $1s_5$. Therefore, this metastable atoms can be cooled by the same technique as used for the cooling of alkali beams. The cooled atoms can be transfered to another metastable state $1s_5$, or to the ground state, by pumping $1s_9$ population to one of four J=1 levels of 2p state followed by spontaneous decay to 1s state, then to the ground state by emitting 70nm VUV photon. The heating in this process is very small, because the kinetic energy gain by the recoil momentum is very small even for the VUV photon.

The experimental setup is basically the same as the sodium cooling by Phillips et al. The metastable atoms are created by a dc discharge, and are extracted through a pinhole on the anode. The beam passes through a solenoid , which produces a nonuniform axial field. The deceleration laser with 640nm is sent from the opposite direction towards the Ne beam source. It is usually circularly polarized, and its frequency is 100 to 200MHz below the resonance without magnetic field. The velocity distribution of the decelerated atom emerging from the solenoid is monitored through the Doppler profile of $1s_5$-$2p_7$ and $1s_3$-$2p_5$ transitions, by detecting 70nm spontaneous photon by an electron multiplier. To transfer the cooled $1s_5$ atoms, to $1s_3$ level, a 588nm laser is crossed perpendicular to the Ne beam approximately 1cm upstream of the Doppler analysis point.

The result shows that a large fraction of the $1s_5$ atoms can be slowed 100m/s suitable for the further deceleration and trapping by standing wave lasers or by magnetic field. Neon atoms in the beam is expected in either one of $1s_5$, $1s_3$ and ground states. Because J=2 for $1s_5$ while for others J=0, one can separate $1s_5$ atoms by nonuniform magnetic field. It is also possible to produce pure $1s_3$ or ground state atoms from $1s_5$ atoms by various laser pumping schemes. Therefore, by combining the above cooling technique, we can produce cooled atoms in single metastable or ground state. Those cooled atoms are of interest for studying lifetime and dynamics of metastable states.

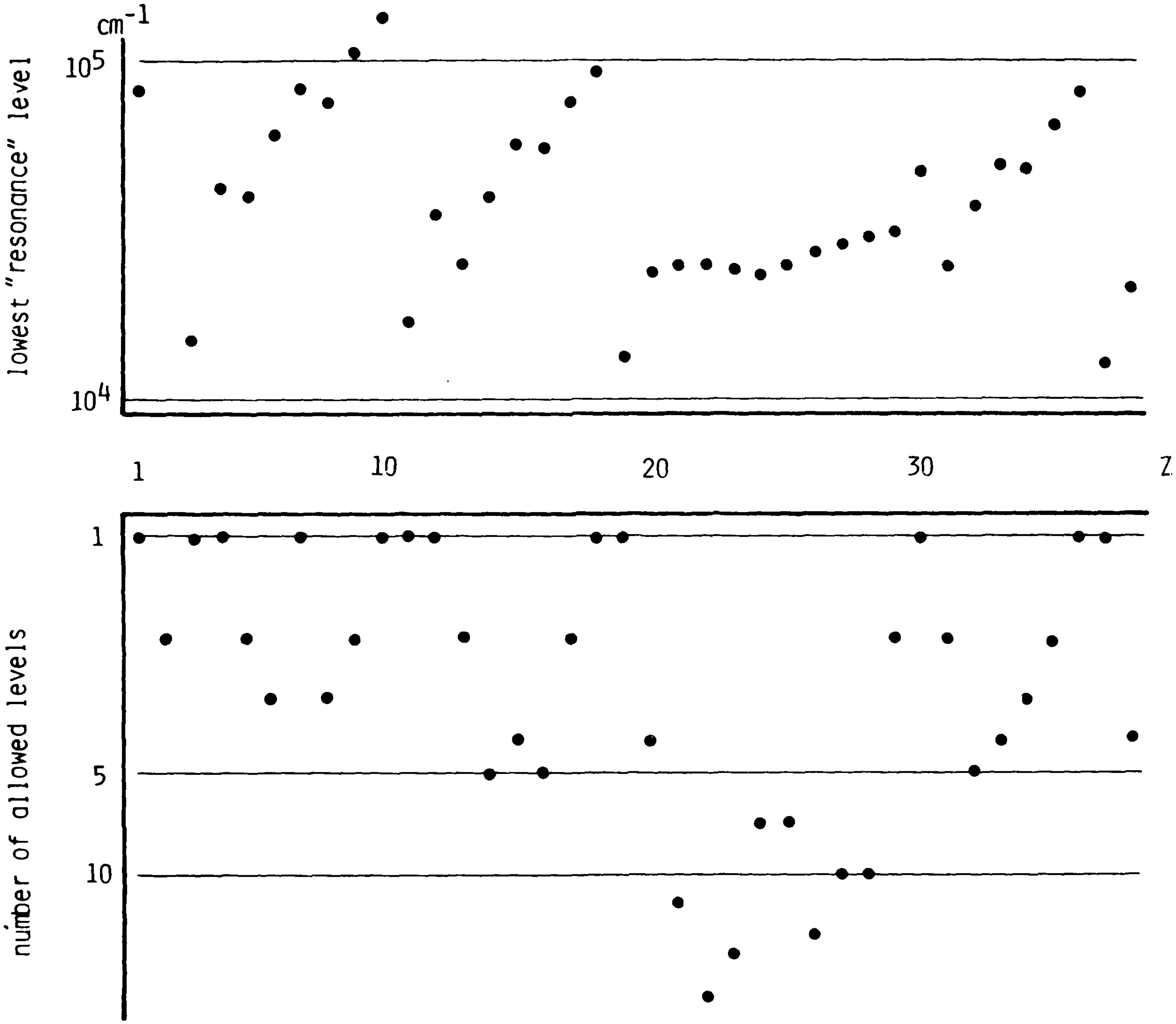
cm-1
10^5
10^4
lowest "resonance" level
1
10
20
30
Z
1
5
10
number of allowed levels

Silicon energy levels

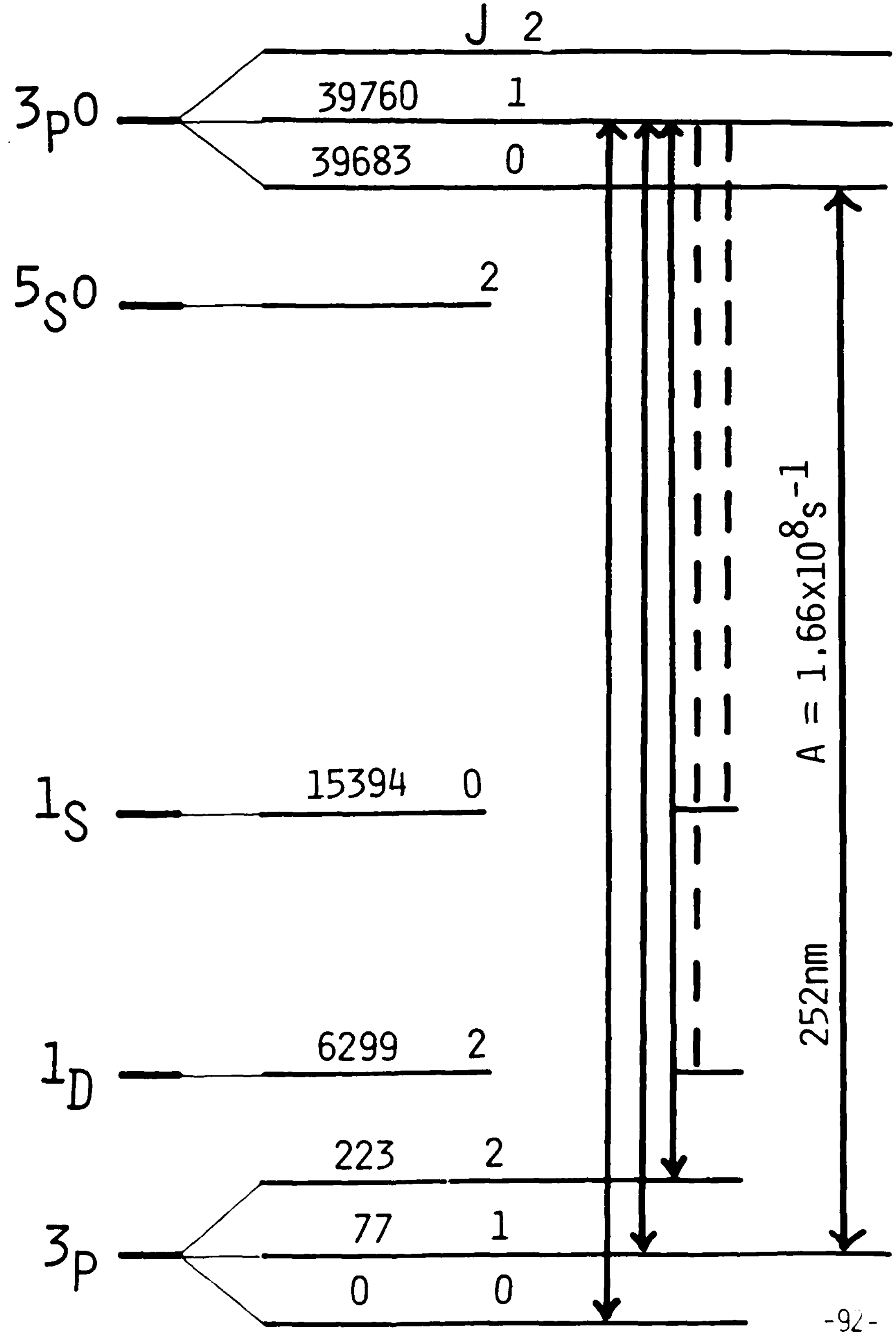

Oxygen energy levels

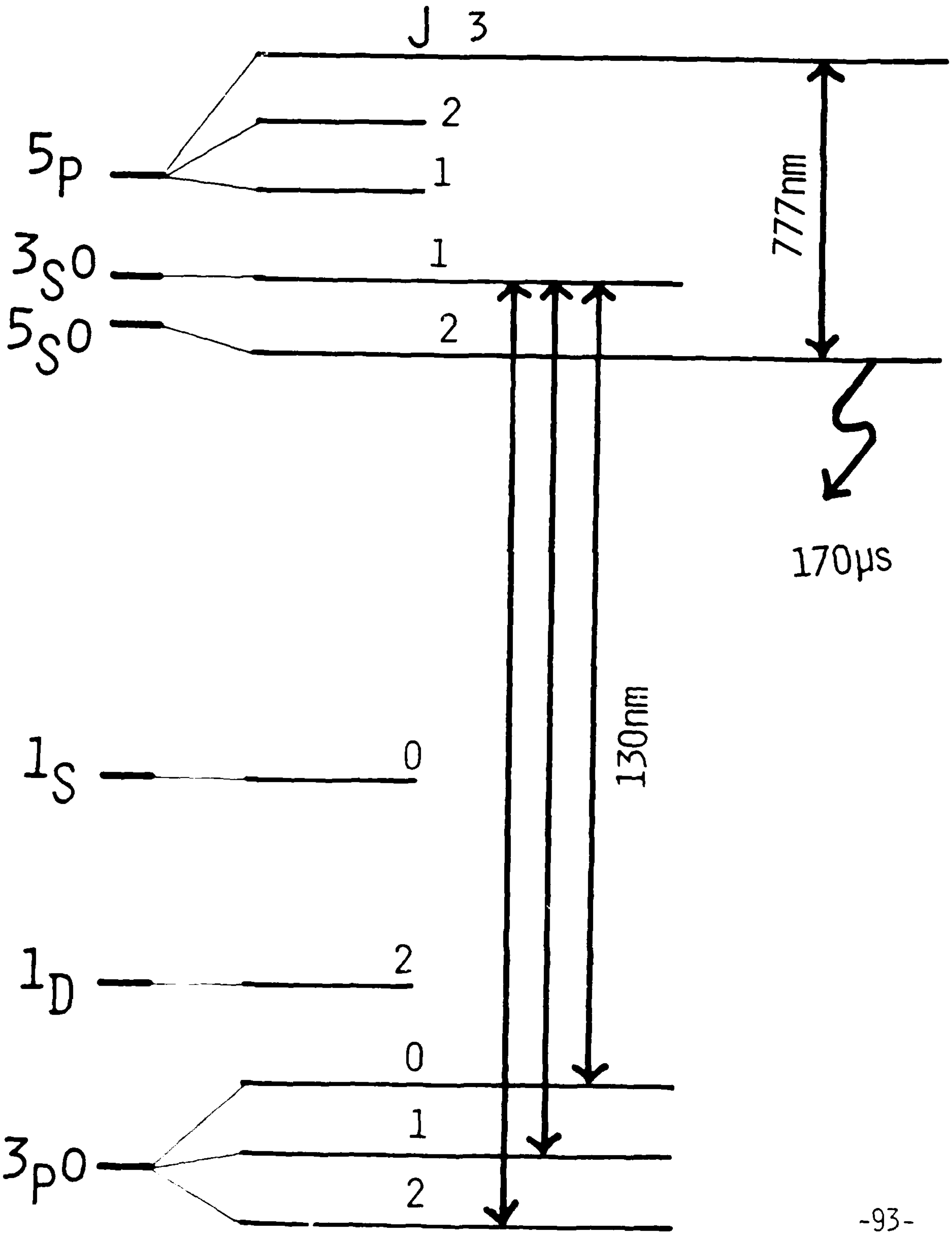

AD-A186 938 UNITED STATES - JAPAN SEMINAR ON QUANTUM MECHANICAL ASPECTS OF QUANTUM EL (U) MASSACHUSETTS INST OF TECH CAMBRIDGE RESEARCH LAB OF ELECTRON 2/7

UNCLASSIFIED J H SHAPIRO ET AL OCT 87 N00014-87-G-0198 F/G 20/3 NL

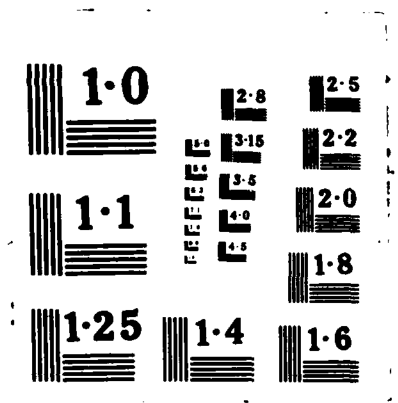
1·0
2·8
2·5
3·15
2·2
3·5
1·1
4·0
2·0
4·5
1·8
1·25
1·4
1·6

Neon energy levels

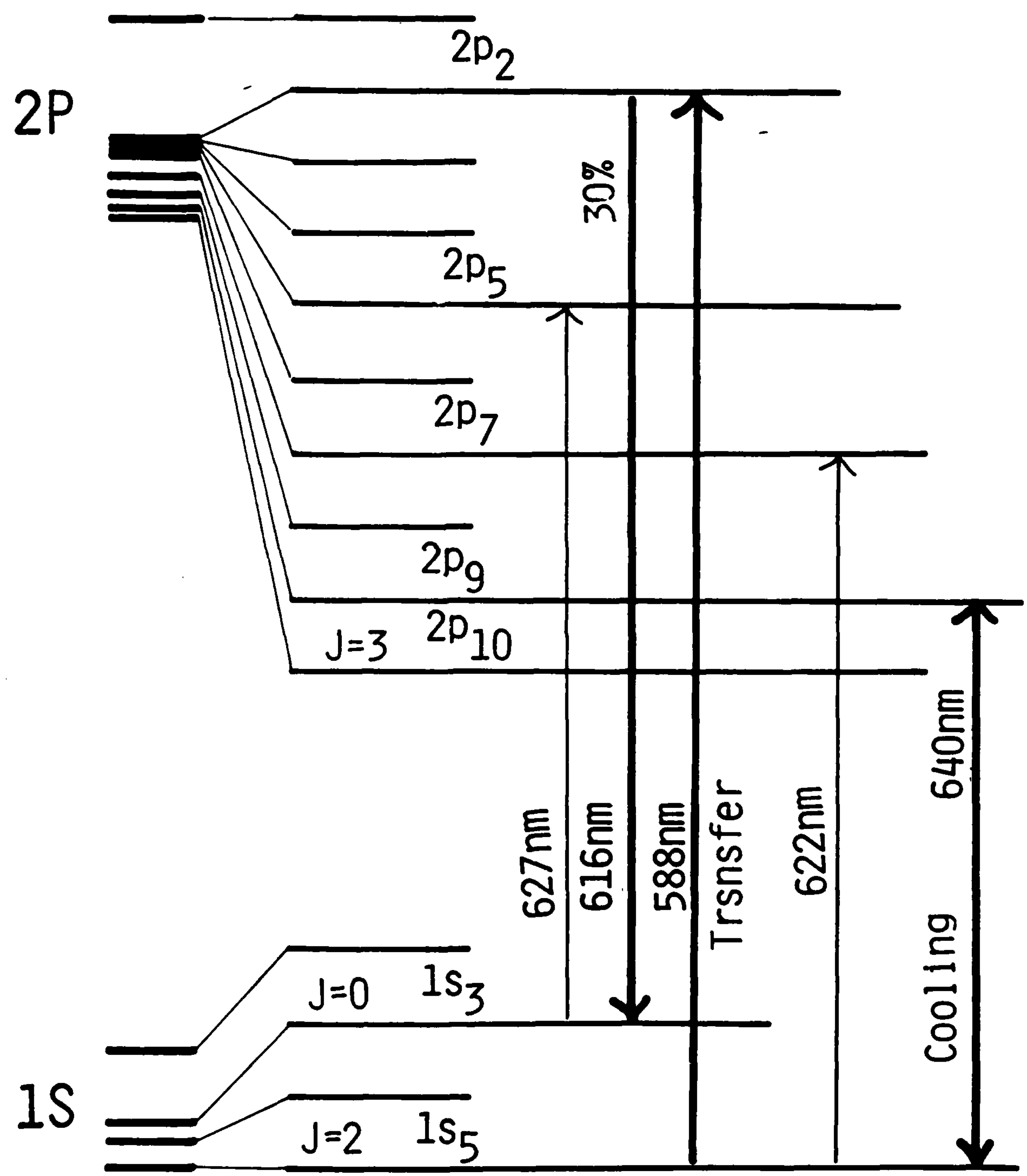

Experimental configuration

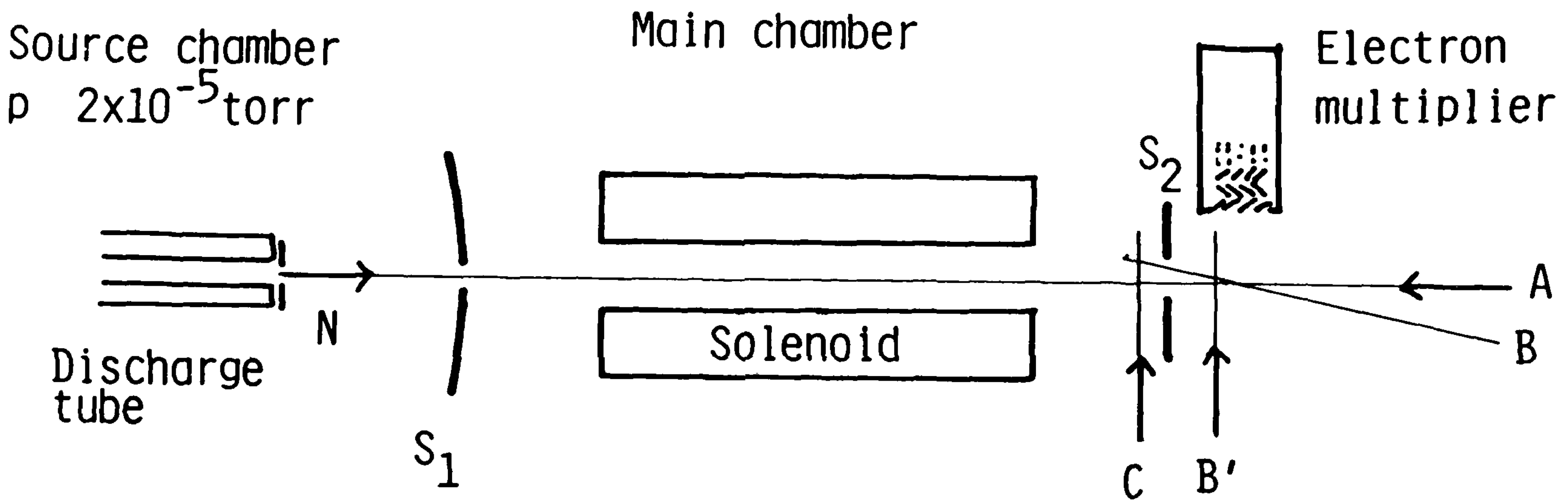

A: Deceleration laser

C: Transfer laser

B : Laser for velocity analysis

B': Laser for v≐0 marker

N: Neon beam

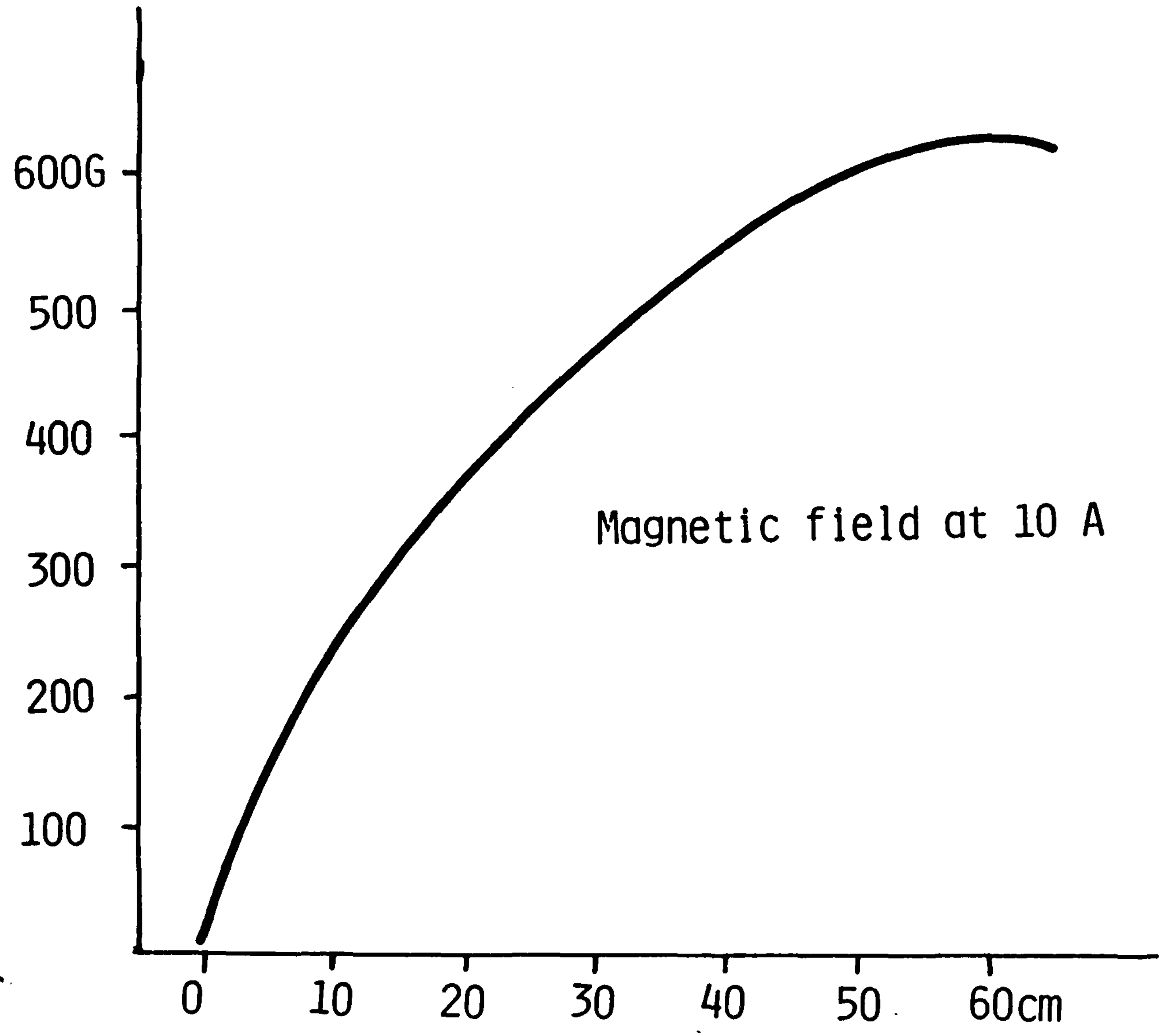
600G
500
400
300
200
100
0
10
20
30
40
50
60cm
Magnetic field at 10 A

Optical pumping scheme

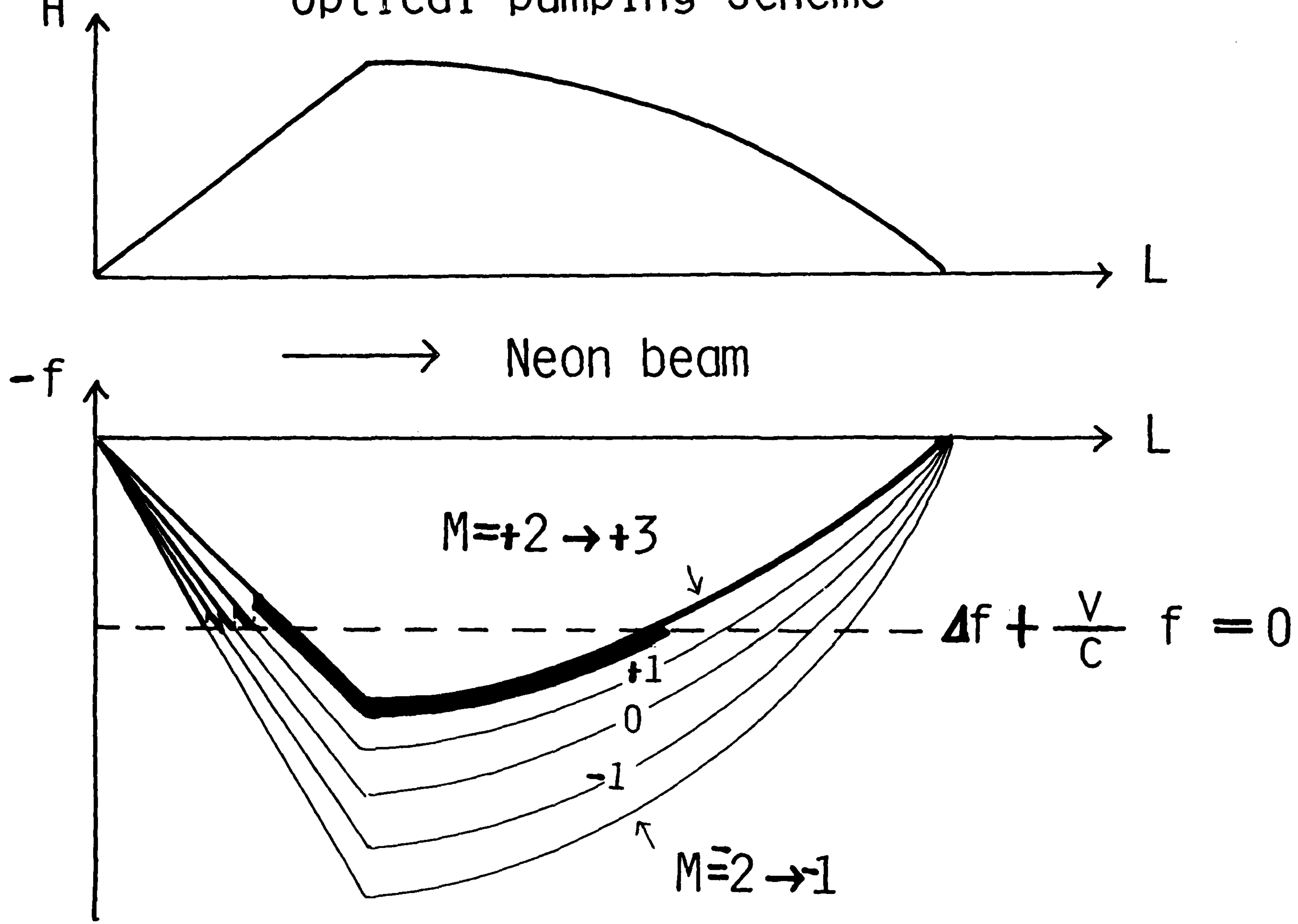

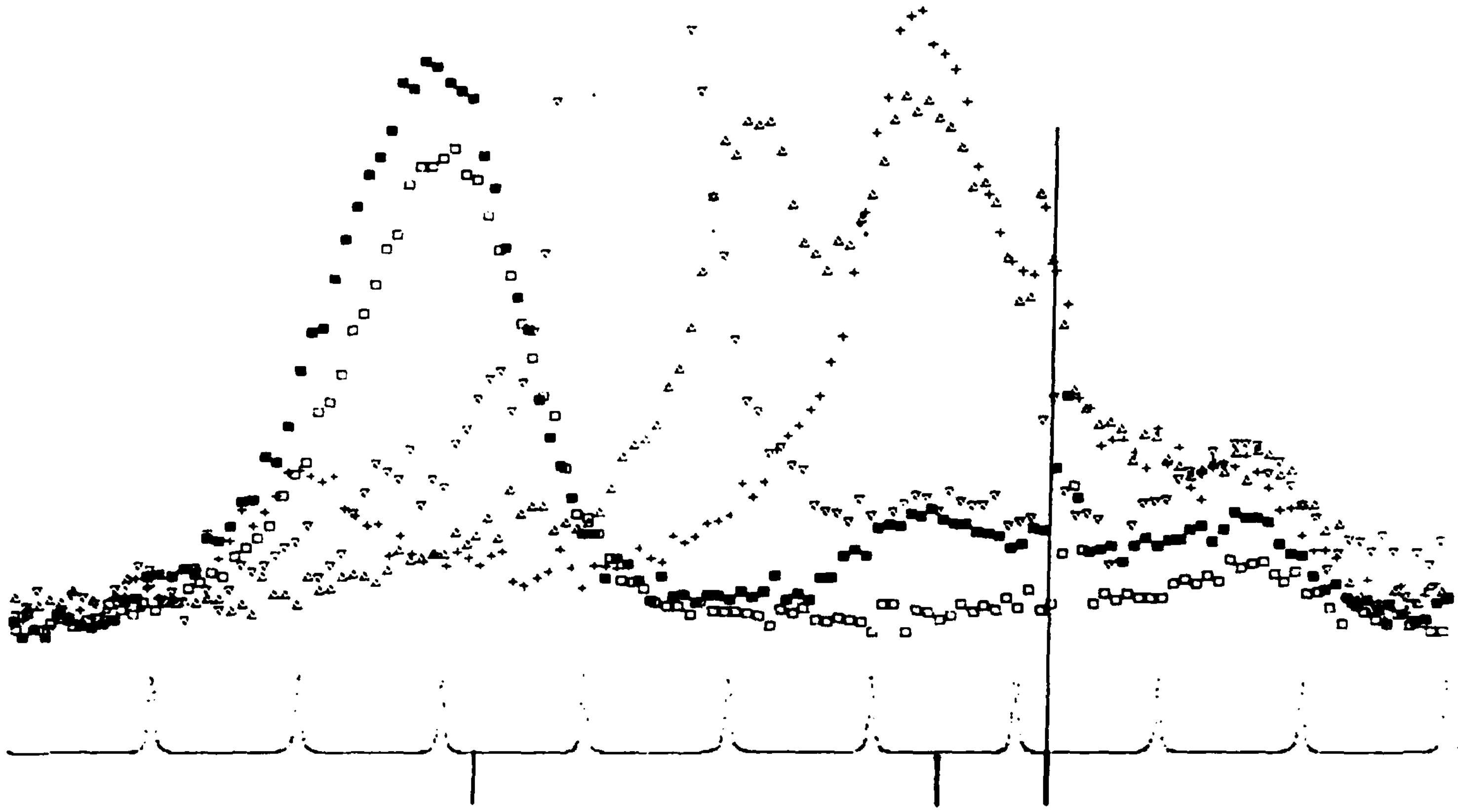

Circular polarization

Δ f=-150MHz

- □ No deceleration laser
- ■ H=260G
- + 460G
- ▵ 610G
- ▿ 790G

Magnetic field dependance

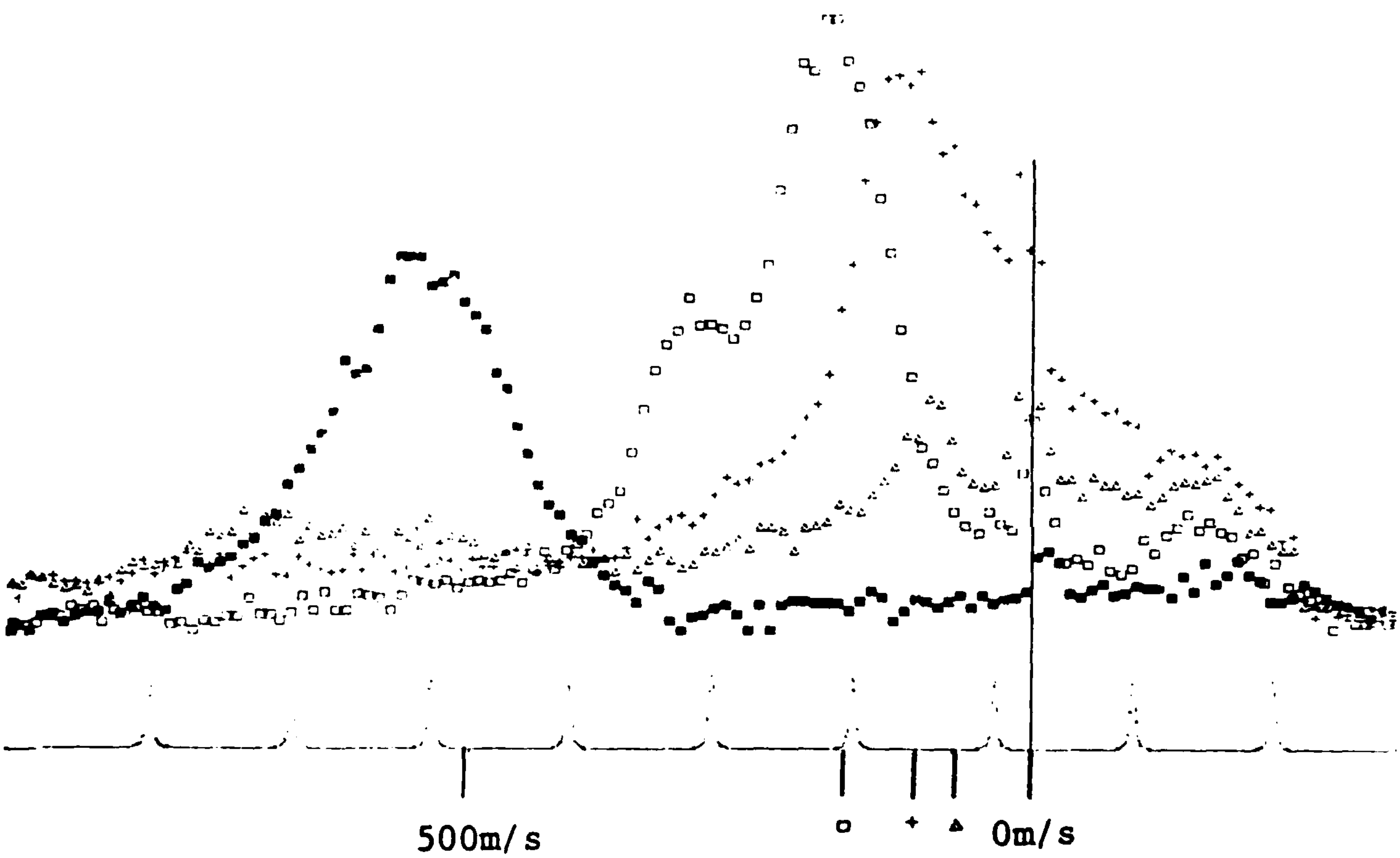

Circular polarization

H=470G

■ No deceleration laser
▲ Δ f=-100MHz
\+ -150MHz
□ -250MHz

Detuning dependence

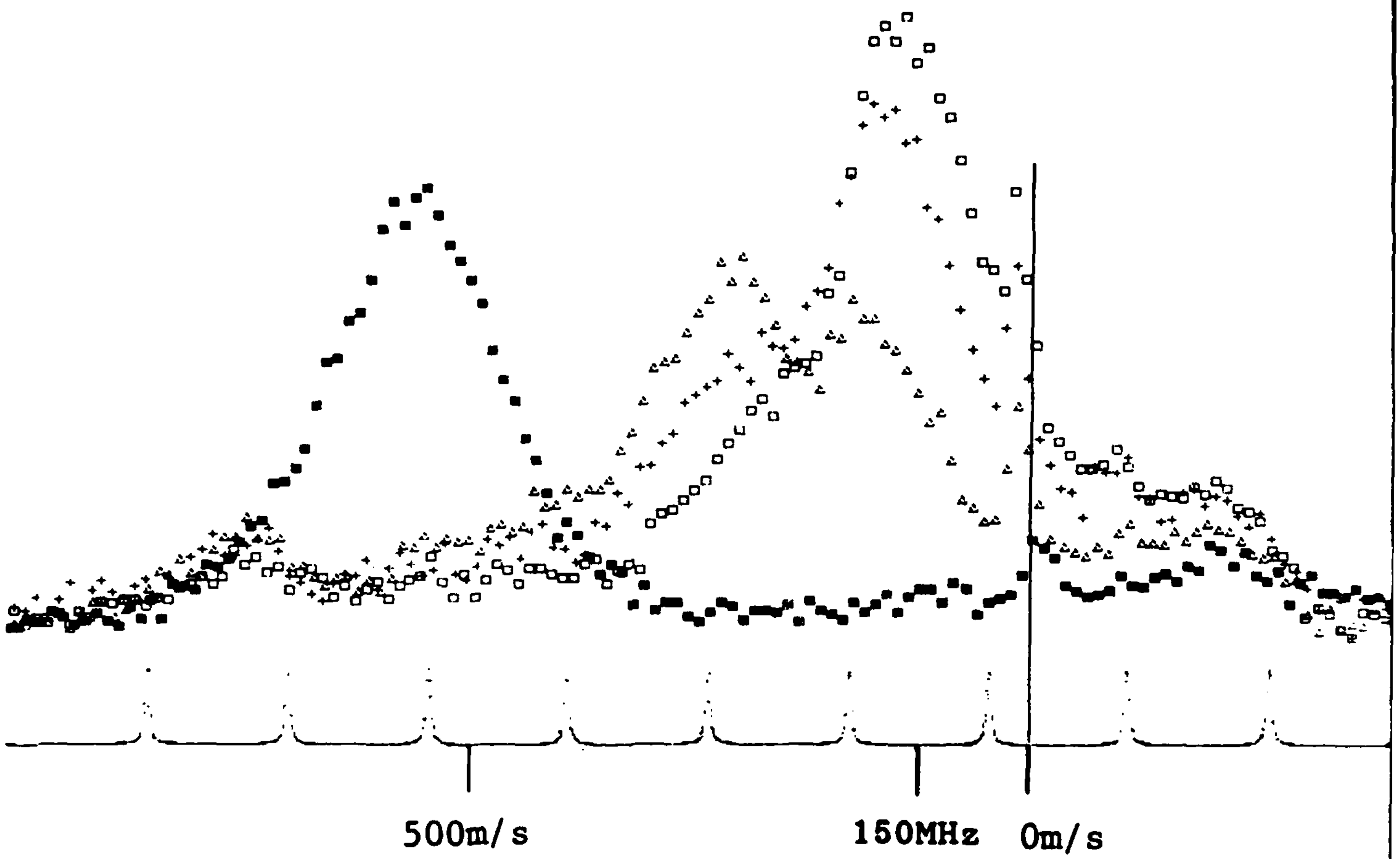

Circular polarization
H=470G
Δ f=-150MHz

■ No deceleration lase
□ 35mW
\+ 15mW
▲ 5mW

Power dependence

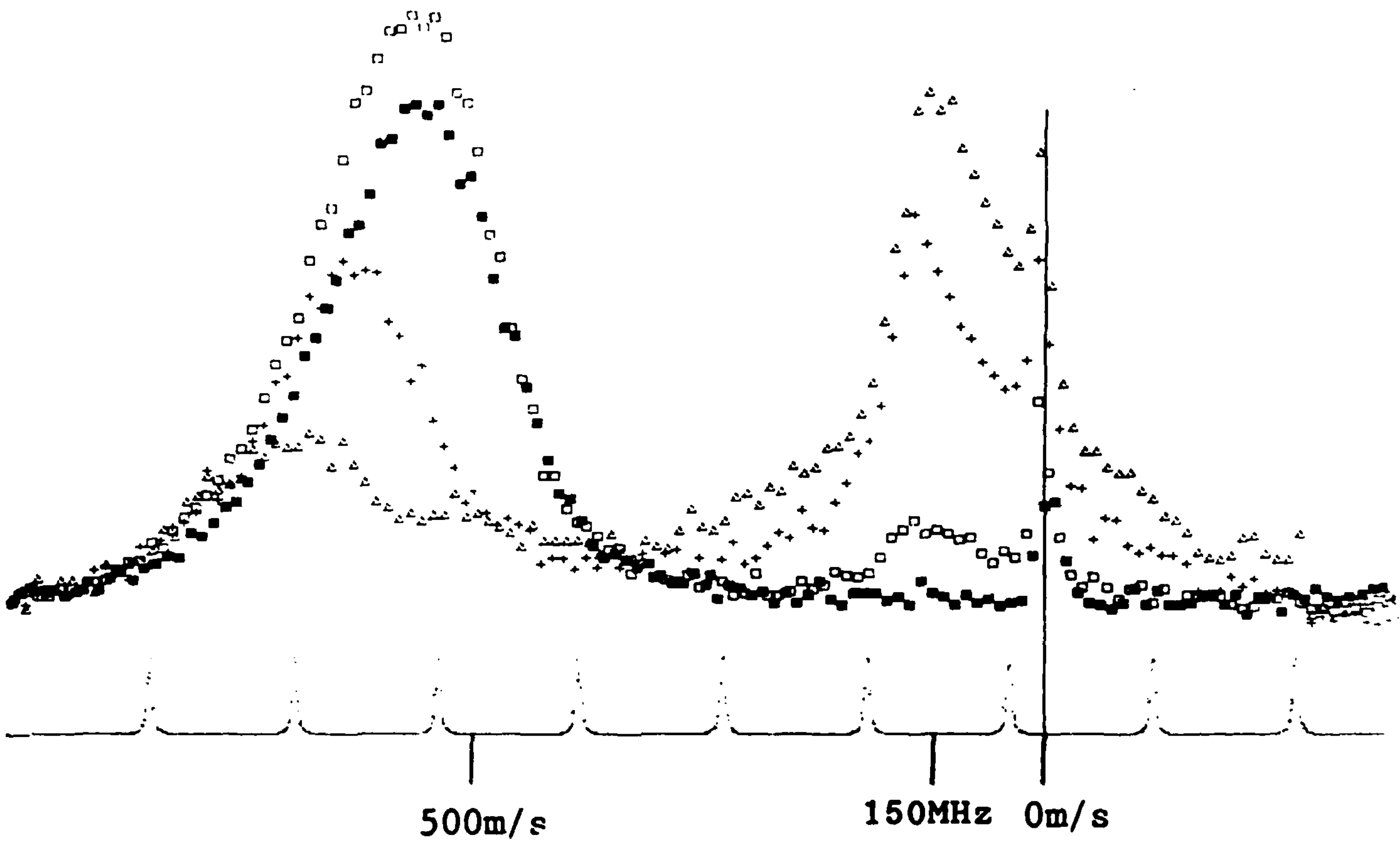

Linear polarization

Δ f=-150MHz

- ■ No deceleration laser
- □ H=260G
- + 350G
- ▲ 440G

Magnetic field dependance

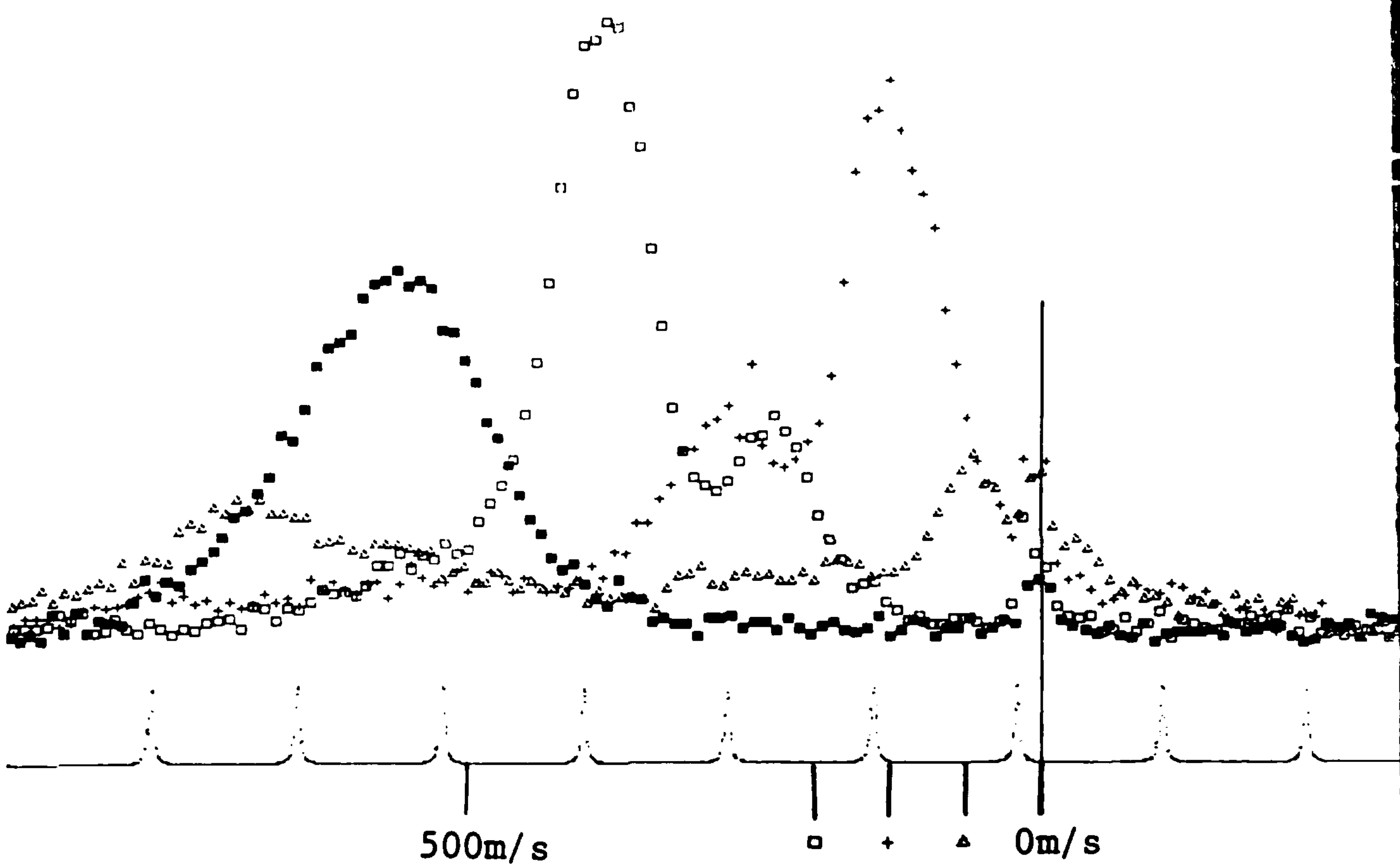

Linear polarization

H=470G

■ No deceleration laser
▲ Δ f=-100MHz
\+ -200MHz
□ -300MHz

Detuning dependence

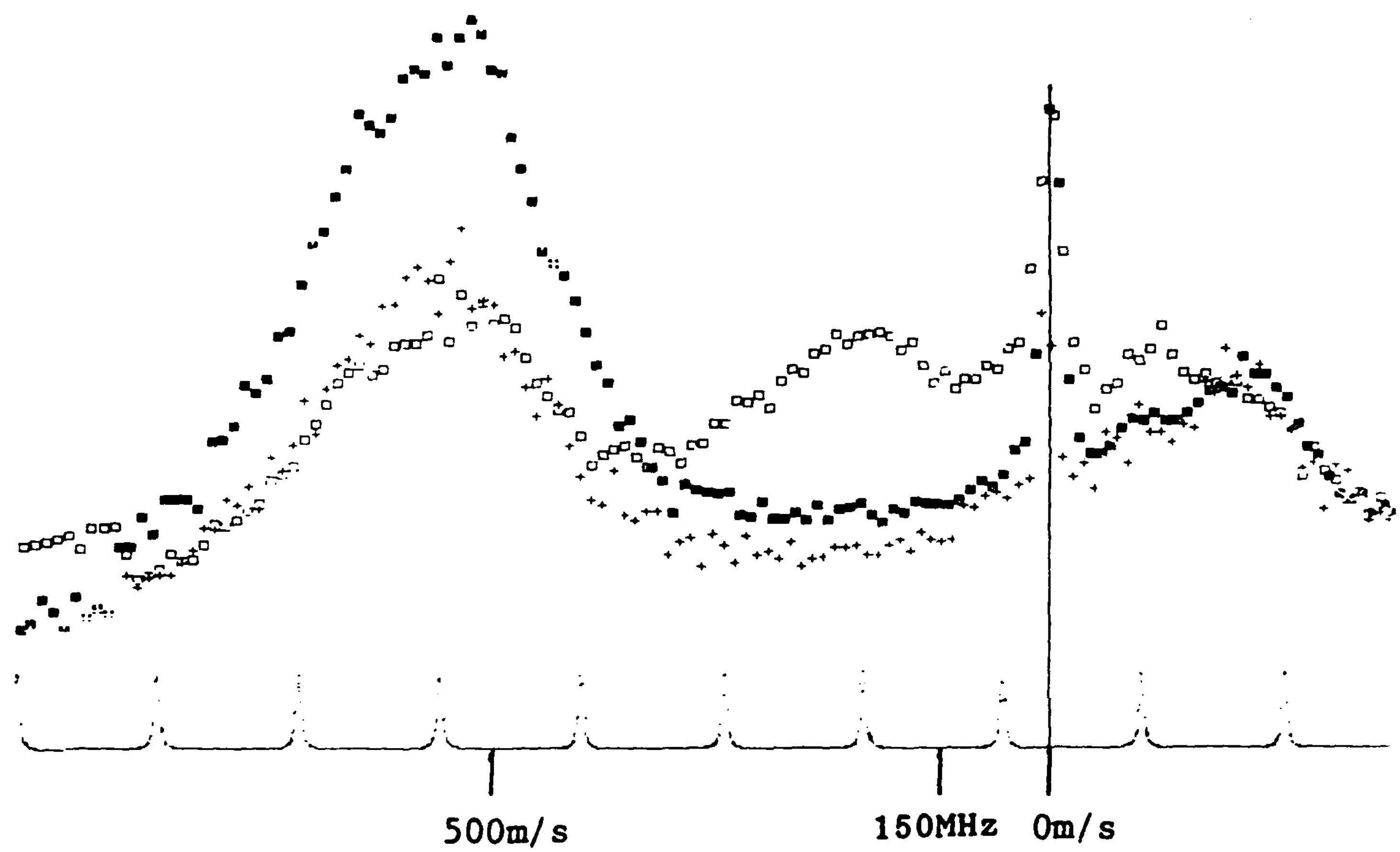

Transfer 150MHz

H=470G

+ No transfer, no deceleration laser
■ With transfer, but no deceleration lase
□ With transfer and deceleration lasers

Transfer of cooled atoms from J=2 to J=0 metastable state

Gigantic Optical Nonlinearity

in Low Dimensional Systems

Eiichi Hanamura

Department of Applied Physics, University of Tokyo,

Hongo, Bunkyo-ku, Tokyo 113, Japan

Artificial as well as natural low-dimensional materials are now available in addition to bulk crystals. The material system with larger nonlinear optical susceptibility, e.g., $\chi^{(3)}(\omega;-\omega,\omega,-\omega)$ the third order optical susceptibility, is being looked for to realized more effective optical information processor.

First, we discuss the dimensional effects on $\chi^{(3)}$ and how $\chi^{(3)}$ increases when we proceed from the bulk system of 3-dimension into the 2- and 1-dimensional systems. Here the larger $\chi^{(3)}$ comes from the enhanced oscillator strengths due to the stronger confinements of particles and the stronger exciton effect in lower dimensional system.

Second, the nonlinear optical susceptibility is shown to be extremely enhanced for an assembly of microcrystallites as 0-dimensional systems. This is because the exciton is quantized due to the confinement effect and the excitons in a single microcrystallite interact enough strongly to make the excitons deviate drom ideal harmonic oscillators.

Gigantic Optical Nonlinearity in Low Dimensional Systems

E. HANAMURA

3-D : bulk crystal

2-D : quantum well
layered-structure semiconductor (GaSe, ···)

1-D : quantum wire
polydiacetylene crystal ····

0-D : quantum box
semiconductor microcrystallites in glass
colloid particles of semiconductors

$\Downarrow$

large $\chi^{(3)}(\omega;-\omega,\omega,-\omega)$

$\Downarrow$

optical information processor

$$P^{(3)} = \chi^{(3)}(\omega_4; -\omega_1, \omega_2, -\omega_3)\, E_1 E_2^* E_3$$

$\omega_1 = \omega_2 = \omega_3 = \omega_4$: *degenerate 4-wave mixing*

$$\chi^{(3)}(\omega; -\omega, \omega, -\omega)$$

$$= \sum_{\alpha,\beta,\gamma} \frac{P_{g\gamma} P_{\gamma\beta} P_{\beta\alpha} P_{\alpha g}}{\hbar^3 (\omega_{\gamma g} - \omega)(\omega_{\beta g} - 2\omega)(\omega_{\alpha g} - \omega)}$$

α, γ : *lowest Wannier exciton*

$$P_{\alpha g} = P_{g\gamma} = \sqrt{\frac{N u^3}{\pi a_\alpha^3}}\, P_{cv}$$

u^3: unit cell volume

a_α : exciton Bohr radius

N : number of unit cells in the crystal

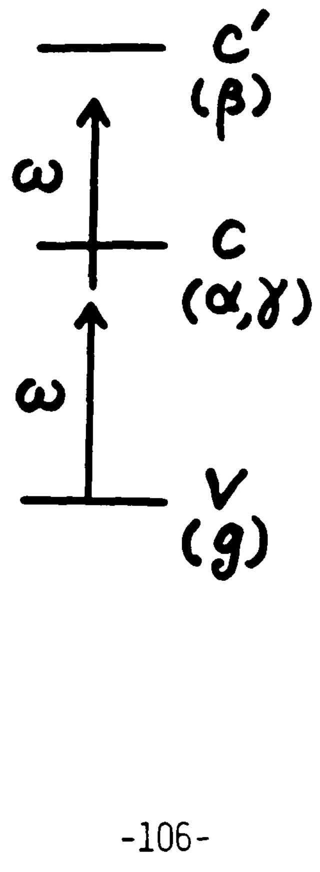

$$P_{\beta\alpha} = 8\left(\frac{\sqrt{a_\alpha a_\beta}}{a_\alpha + a_\beta}\right)^3 P_{c'c}$$

Dimensional Effects

3D-oscillator strength per unit cell

$$f_\alpha^{(3)} = \frac{2m\omega_\alpha}{\hbar e^2}\left|P_{\alpha g}\right|^2 \frac{1}{N}$$

$$= \frac{2m\omega_{exc}}{\hbar e^2}\left|P_{cv}\right|^2 \frac{u^3}{\pi a_\alpha^3}$$

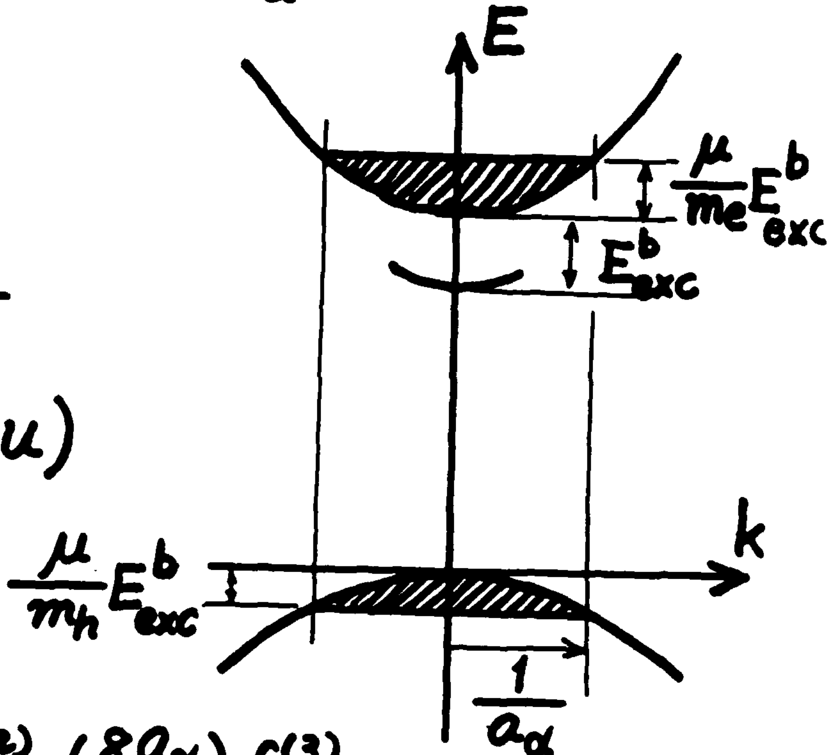

$$E^b_{exc} = \frac{\mu e^4}{2\hbar^2\epsilon_0^2}$$

$$a_\alpha (\gg u)$$

2D: $4E^b_{exc}$, $a_\alpha/2$

$$f_\alpha^{(2)} = \left(\frac{8a_\alpha}{u}\right) f_\alpha^{(3)}$$

1D: ∞ , 0 in the effective mass appr.

polydiacetylene crystal (1-D)

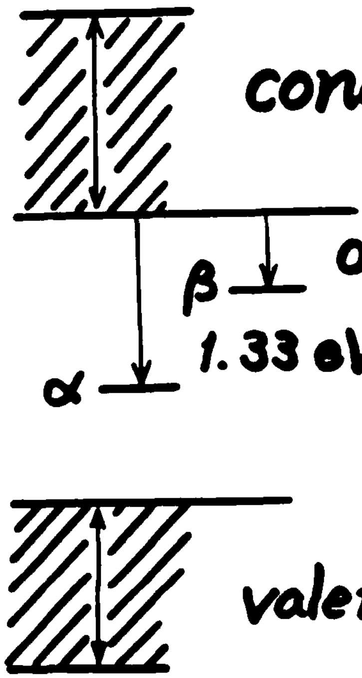

conduction band width 3.5 eV

β 0.55 eV A_{1g} exciton $f_{\beta\alpha} = 3.88$ (3.2)

α 1.33 eV B_{1u} exciton $f_{\alpha g} = 2.44$ (1.5)

c.f. $f_{\alpha g} = 10^{-4}$ GaAs (3-D)

$= 3.2 \times 10^{-3}$ CdS (3-D)

valence band width 3.1 eV

sum rule : $\sum_{\alpha} f_{\alpha g} = 4$

$\chi^{(3)} \sim 10^{-8}$ esu for $\hbar\omega = 1.33$ eV —

2-photon resonant to A_{1g} exciton

$\hbar\Gamma = 0.01$ eV

Size Effects

larger $\chi^{(3)}(\omega; -\omega, \omega, -\omega)$

① enhanced transition dipolemoments

② resonant energy denominators

under nearly resonant condition to the free exciton, ① and ② are satisfied.

excitons as almost ideal bosons
→ no nonlinear optical response

Reducing the size of microcrystallites the transition dipolemoment is reduced but the exciton interactions make excitons deviate from ideal bosons.

⟹ optimum size for largest $\chi^{(3)}$

two excitons are bound → excitonic molecule

$$P_{\beta\alpha} = p_{cv} \frac{u^3}{\pi a_\alpha^3} \sum_R G(R)$$

R: separation between two excitons

$\sqrt{N_m}$ → giant oscillator strength

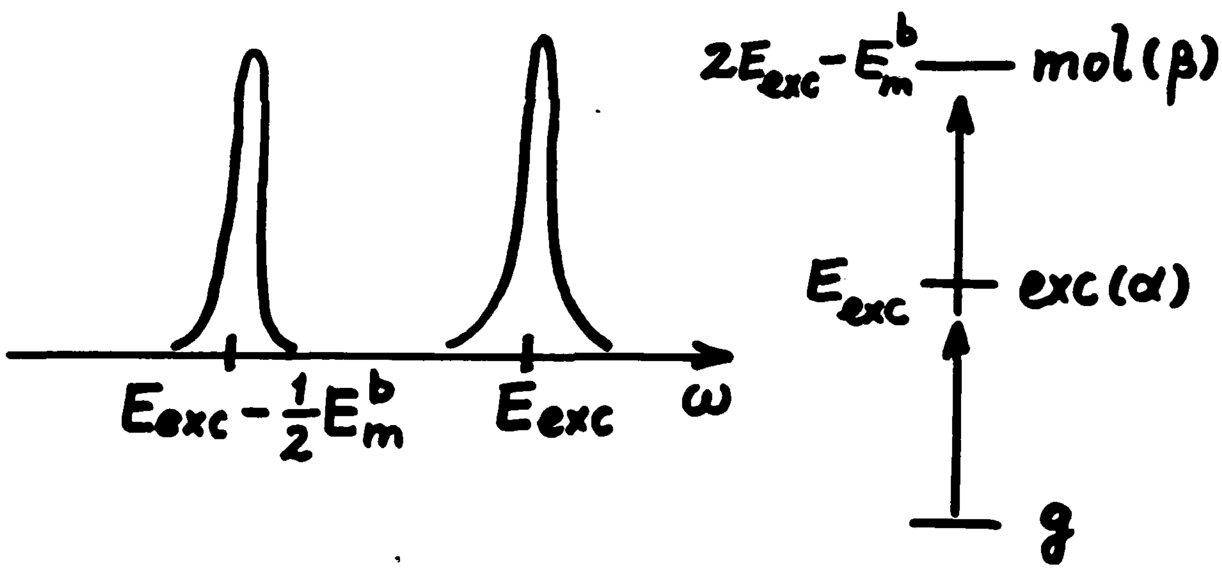

$$\chi^{(3)} \sim 4\times 10^{-8}\,\text{esu}\ (\text{for } 2E_{exc}-E_m^b-2\hbar\omega = 3\,\text{meV})$$

When the bound state of two excitons is not relevant and under resonant excitation,

$$\langle P^{(3)}(t) \rangle = \left(\frac{-i}{\hbar}\right)^3 \int_{-\infty}^{t} dt_1 \int_{-\infty}^{t_1} dt_2 \int_{-\infty}^{t_2} dt_3$$
$$\times \langle P(r,t)[H'(t_1),[H'(t_2),[H'(t_3),\rho_0]]] \rangle$$

$$H'(t) = -P\cdot E(t)$$

$$P^{(3)} e^{-i\omega t} = \chi^{(3)}(\omega;-\omega,\omega,-\omega)\, E(t)\, E(t)^{*}\, E(t)$$

$$E(t) = E e^{-i\omega t}$$

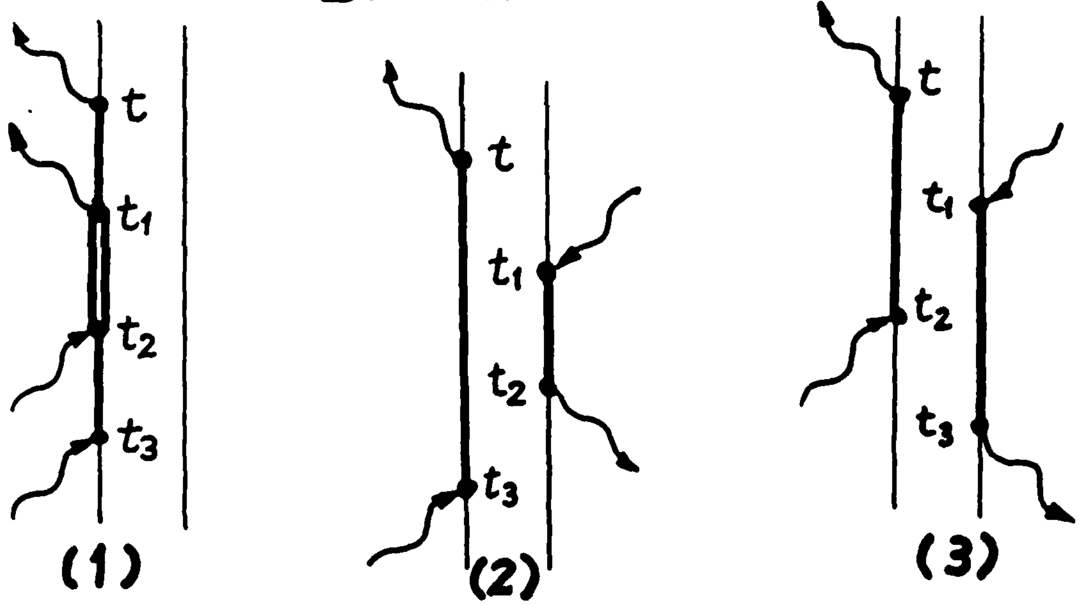

$$\gamma, \gamma' \ll |\omega - \omega_{exc}|, \quad \omega_{int} \ll |\omega - \omega_{exc}|$$

$\Longrightarrow$ excitons as harmonic oscillators

$\Longrightarrow$ $\chi^{(3)}(\omega; -\omega, \omega, -\omega) = 0$.

- under near resonance to the lowest exciton ω_0 in the
- microcrystallites $L, R \gg a_\alpha$

$$\chi^{(3)} = \frac{N_c|P|^4}{\hbar^3(\omega-\omega_0+i\Gamma)^2(\omega-\omega_0-i\Gamma)}\cdot\frac{\gamma'}{\gamma} + \frac{N_c|P|^4}{\hbar^3(\omega-\omega_0+i\Gamma)^2(\omega-\omega_0-i\Gamma)}\,\frac{\omega_{int}-2i\Gamma}{(\omega_0-\omega+\omega_{int}-i\Gamma)}$$

$$\Gamma = \gamma+\gamma'$$

$$P_n = \left(\frac{2\sqrt{2}}{\pi}\right)^3 P_{cv}\sqrt{\frac{u^3}{\pi a_\alpha^3}}\;\frac{N^{3/2}}{n_x n_y n_z}$$

for a cubic box with $L = uN$.

$$1 \le n_x, n_y, n_z \le N$$

$$P_{n00} = 2\sqrt{\frac{2}{\pi}}\,P_{cv}\sqrt{\frac{u^3}{\pi a_\alpha^3}}\;\frac{N^{3/2}}{n}$$

for a sphere with $R = uN$

$$1 \le n\ ,\ l=0,\ m=0$$

$$\gamma = \gamma_0 N^3 \longrightarrow \gamma'/\gamma \ll 1 \quad (N \gg 1)$$

$\omega_{int} \gg |\omega-\omega_0|$:

$$\chi^{(3)} \sim \frac{N_c|P|^4}{\hbar^3(\omega-\omega_0)^3} \sim N^3$$

$$N_c \sim \frac{1}{N^3}, \quad |P| \sim N^{3/2}$$

Conditions for gigantic $\chi^{(3)}$

(1) Exciton binding energy $\gg$ ele. & hole quantization energies

a_α(exciton Bohr radius) $\ll$ L, R (size)

(2) Exciton interaction energy $\hbar\omega_{int} \equiv 8\pi E^b_{exc} \frac{m_e m_h}{(m_e+m_h)^2} \frac{a^2 f_0}{L^3} \gg \hbar|\omega-\omega_0$

(3) Exciton quantization energy $\equiv \frac{3\pi^2\hbar^2}{2(m_e+m_h)L^2} \gg \hbar|\omega-\omega_0|$

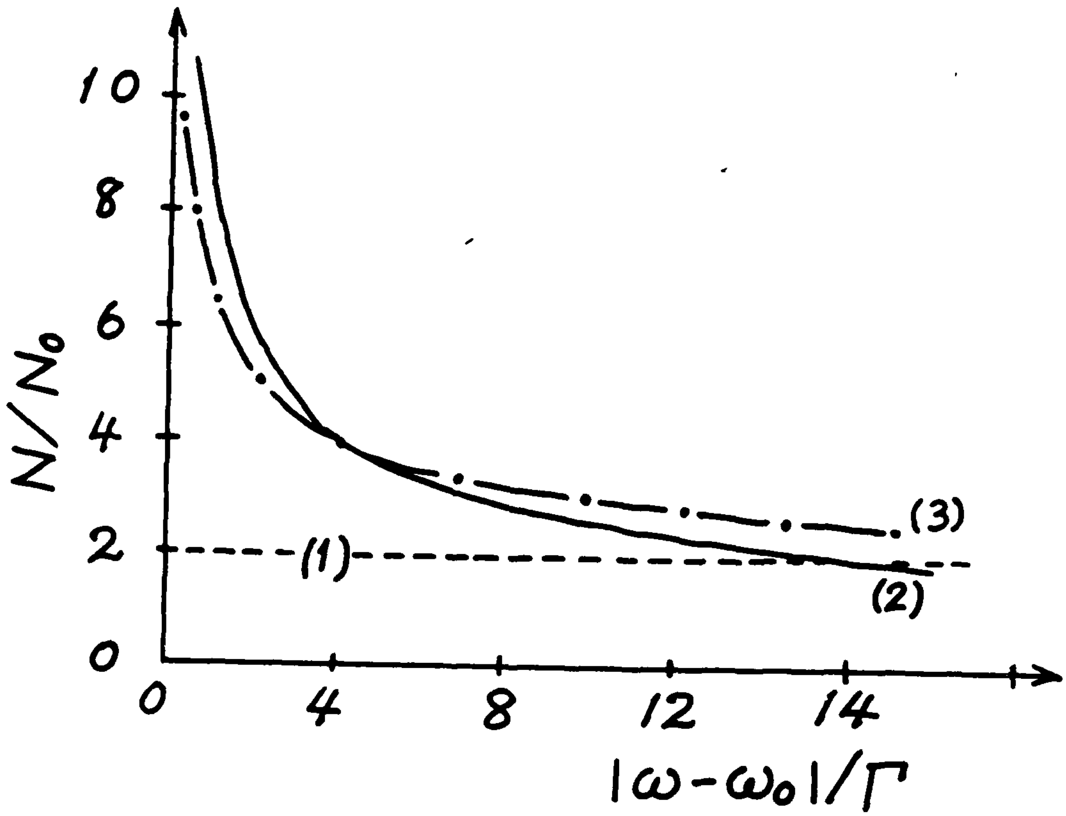

(1) CuCl microcrystallites

$E^{b}_{exc} = 213$ meV , $m_h = 2m$, $m_e = 0.5m$

$\hbar\omega^{l}_{exc} = 3.2079$ eV , $\hbar\omega_{exc} = 3.2022$ eV

$$\begin{matrix} 3.6\ (1\text{-}h) \\ 7.2\ (1\text{-}e) \end{matrix} \ll N \le \left[\frac{4.4\,\text{eV}}{\hbar|\omega-\omega_0|}\right]^{1/2} \sim 30\ (3)$$

$$\left[\frac{24.8\,\text{eV}}{\hbar|\omega-\omega_0|}\right]^{1/3} \sim 17\ (2)$$

$$\chi^{(3)} = 7\times10^{-7}N^3\,\text{esu} \longleftarrow \hbar|\omega-\omega_0| = 5\,\text{meV}$$

$\sim 4\times10^{-4}$ esu for $N = 17$,

(4900 unit cells)

(2) CdS and II-VI semiconductors

$E^b_{exc} = 30$ meV , $m_h = 1.6\,m$, $m_e = 0.25\,m$

$\hbar\omega^{\ell}_{exc} = 2.5546$ eV , $\hbar\omega_{exc} = 2.5546$ eV

$$\begin{matrix} 10 & (1-h) \\ 25 & (1-e) \end{matrix} \ll N \leq \sqrt{\frac{4.96\,\mathrm{eV}}{\hbar|\omega-\omega_0|}} \sim 32 \qquad (3)$$

$$\left[\frac{183\,\mathrm{eV}}{\hbar|\omega-\omega_0|}\right]^{1/3} \sim 33 \qquad (2)$$

$$\Uparrow$$

$$\hbar|\omega-\omega_0| = 5\,\mathrm{meV}$$

$$\chi^{(3)} = 1.2\times10^{-10} N^3 \,\mathrm{esu}. \leftarrow$$

$$\sim 3.2\times10^{-6}\,\mathrm{esu} \quad (N\sim30)$$

(3) GaAs and III-V semiconductors

$E^{b}_{exc} = 5.1$ meV, $m_h = 0.475m$, $m_e = 0.0665m$

$u = 3.56$ Å , $a_d = 107$ Å

$\epsilon_0 = 12.53$

$$\begin{matrix} 114 \ (1\text{-}e) \\ 43 \ (1\text{-}h) \end{matrix} \ll N < \sqrt{\frac{16.4\,\mathrm{eV}}{\hbar|\omega-\omega_0|}} \sim 57 \quad (3)$$

$$10\left[\frac{72.4\,\mathrm{eV}}{\hbar|\omega-\omega_0|}\right]^{1/3} \sim 200 \quad (2)$$

$\uparrow$

$\hbar|\omega-\omega_0| = 5$ meV

MEASUREMENTS OF OPTICAL NONLINEARITIES
IN MOCVD-GROWN GaAs/GaAlAs MULTIPLE QUANTUM WELLS

E. Garmire
Center for Laser Studies
University of Southern California
Los Angeles, CA 90089-1112

This paper reports on measurements of nonlinear absorption made by A. Kost and M. Kawase in material provided by H. C. Lee, A. Hariz and P. D. Dapkus. The work was supported by AFOSR, ARO and NSF. Five samples with differing well thicknesses were compared. By fitting measurements of saturable absorption at particular wavelengths to excitonic bleaching (at low intensity levels) and background absorption saturation (at higher intensity levels), we are able to infer the separate contributions to the absorption. The well dependence of the height of the absorption contributions and also of the saturation intensities were measured.

From measurements of the wavelength dependence of the saturable absorption, calculations were made of the wavelength dependence of the change in refractive index. The dependence of the change in index with intensity on or near resonance is sublinear.

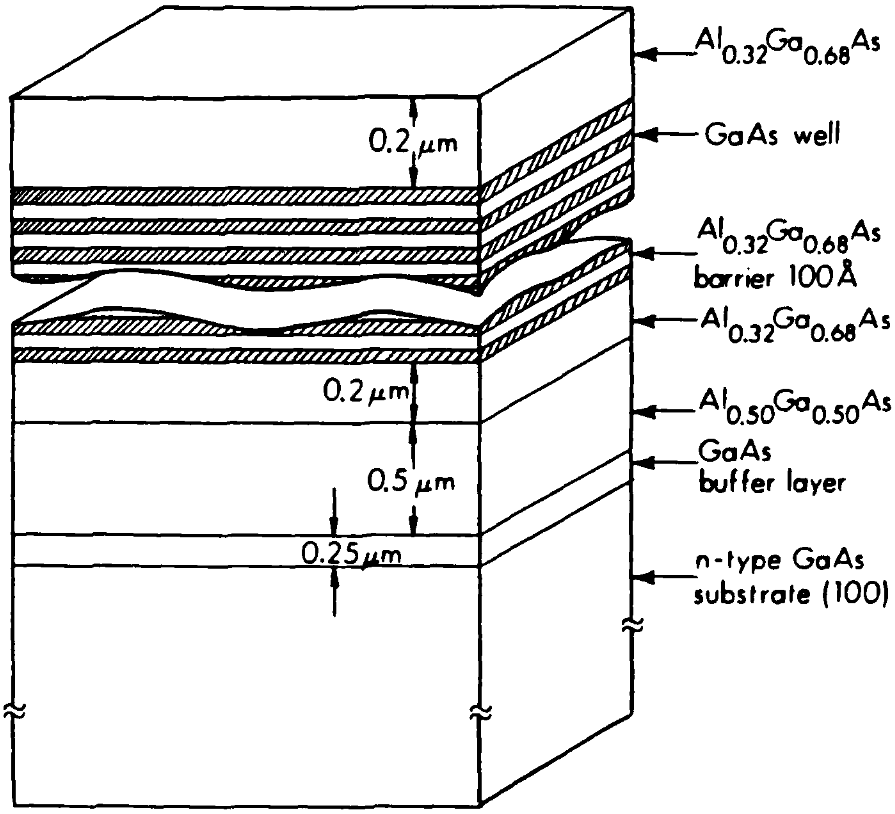
$Al_{0.32}Ga_{0.68}As$
GaAs well
$Al_{0.32}Ga_{0.68}As$ barrier 100Å
$Al_{0.32}Ga_{0.68}As$
$Al_{0.50}Ga_{0.50}As$
GaAs buffer layer
n-type GaAs substrate (100)
0.2 μm
0.2 μm
0.5 μm
0.25 μm

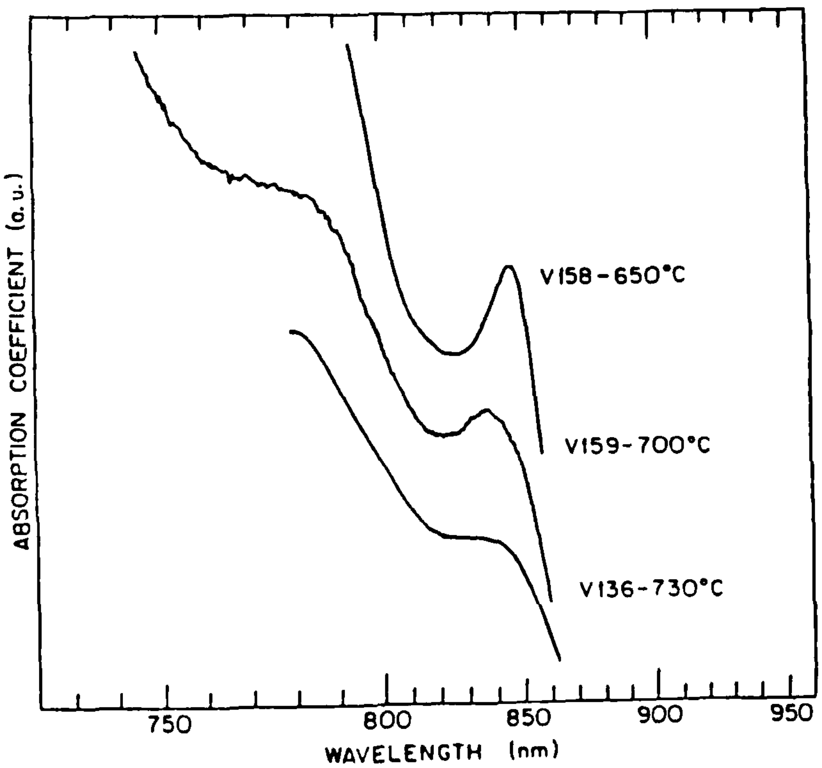
ABSORPTION COEFFICIENT (a.u.)
V158-650°C
V159-700°C
V136-730°C
750
800
850
900
950
WAVELENGTH (nm)

GAR MI

2

$$\alpha = \frac{\alpha_E}{1 + I/I_{SE}} + \frac{\alpha_{BG}}{1 + I/I_{SBG}}$$

INTENSITY-DEPENDENT ABSORPTION

MQW 238 - 54 Å (825nm, hh) CW

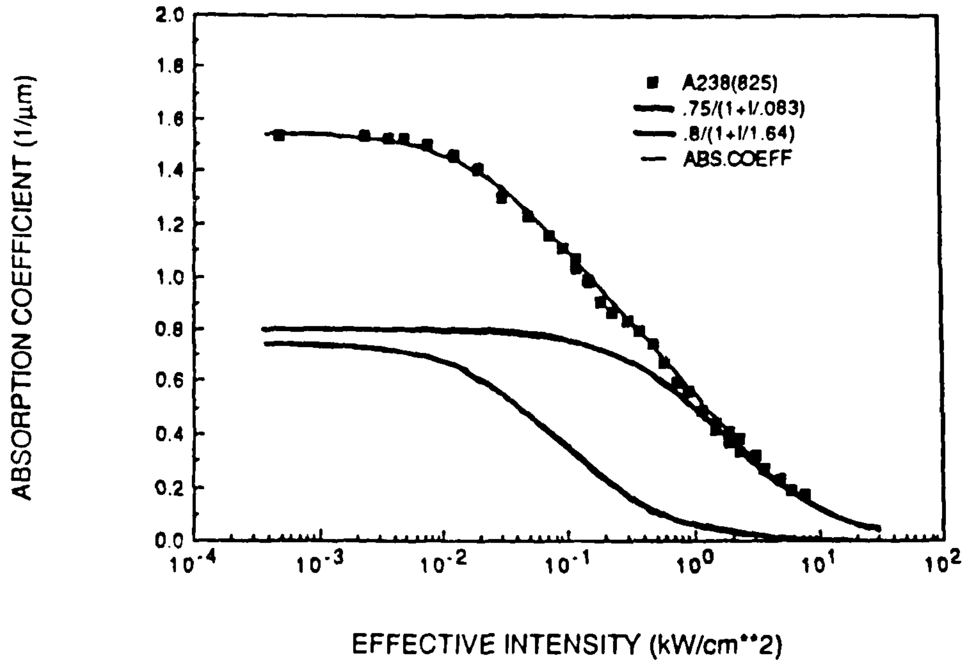

ABSORPTION

EXCITON (n,m) n = Qu. Nu (e)
m = Qu. Nu (h)

$$a_{n,m} = \frac{4\pi^2 e^2 \hbar f_{n,m}}{n m^* c \, L_z} \mathcal{L}(\hbar\omega - E_{n,m})$$

↳ LORENTZIAN

↳ WELL WIDTH

BAND-TO-BAND

$$E_B = \frac{\hbar^2}{2m^*}\left(\frac{\pi n}{L_z}\right)^2$$

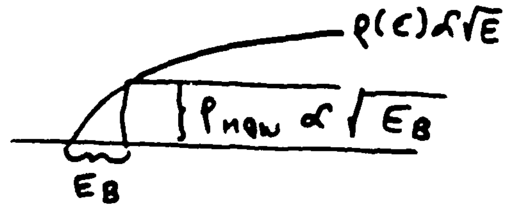

$$a(E) \propto \rho_{MQW}(E) \propto \frac{\hbar}{\sqrt{2m^*}}\left(\frac{\pi n}{L_z}\right)$$

GARMIRE 3

GaAs / GaAlAs MQW's GROWN
BY MOCVD; DAPKUS et. al.

ABSORPTION OF MQW'S

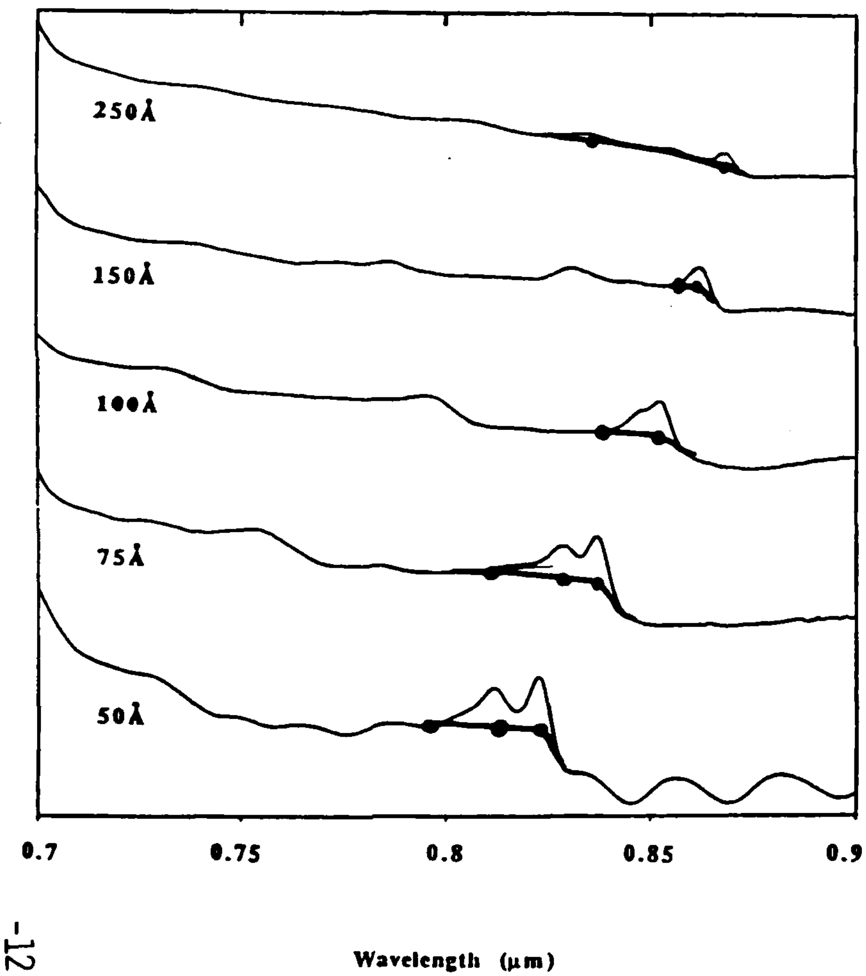

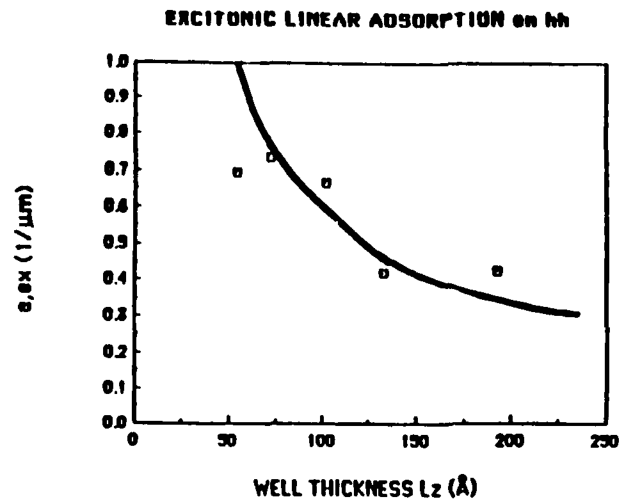

$a_e \propto \frac{1}{L_z}$

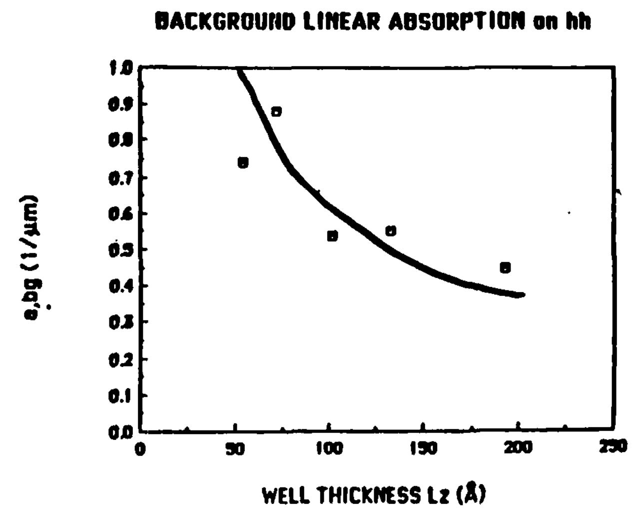

$a_B \propto \frac{1}{L_z}$

GARM 4

SATURATION INTENSITY

EXCITON

$$I_s \tau \approx \frac{\hbar\omega}{2}\left(\frac{1}{a_{n,m} L_z}\right)\left(\frac{1}{A_x}\right)$$

EXCITON AREA

CARRIER DIFFUSION

$$I = \frac{P_{cw}}{\pi(4D\tau + w_0^2)}$$

WHEN $2\sqrt{D\tau} \gg w_0$

$I\tau \propto P_{cw}$

ALSO

$$a_{n,m} \propto \frac{1}{L_z}$$

THUS

$$\rightarrow P_{s,cw} \propto \frac{1}{A_x} \propto \frac{1}{r_B^2}$$ INDEP. OF L_z

$$r_B = \frac{\hbar^2 \epsilon}{e^2 \mu^*} \qquad \frac{1}{\mu^*} = \frac{1}{m_e^*} + \frac{1}{m_h^*}$$

$$\frac{P_s(lh)}{P_s(hh)} = \left(\frac{\mu^*_{hh}}{\mu^*_{lh}}\right)^2 = 2.3$$

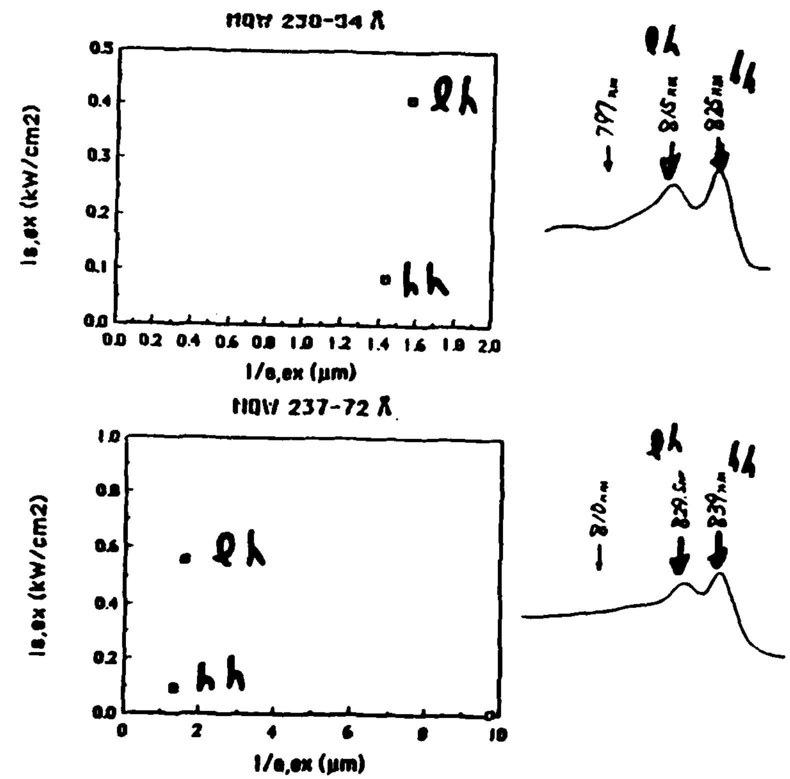

$$\frac{I_s(lh)}{I_s(hh)} = 5.42 \quad \text{EXPERIMENTALLY}$$

$$\sim\left(\frac{\mu^*_{hh}}{\mu^*_{lh}}\right)^4$$

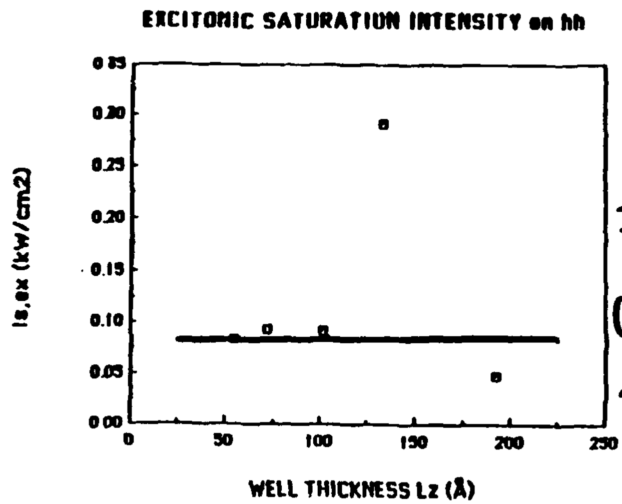

$I_{se} \tau \propto \frac{1}{(\alpha L) A_x}$

$\sim$ CONST.

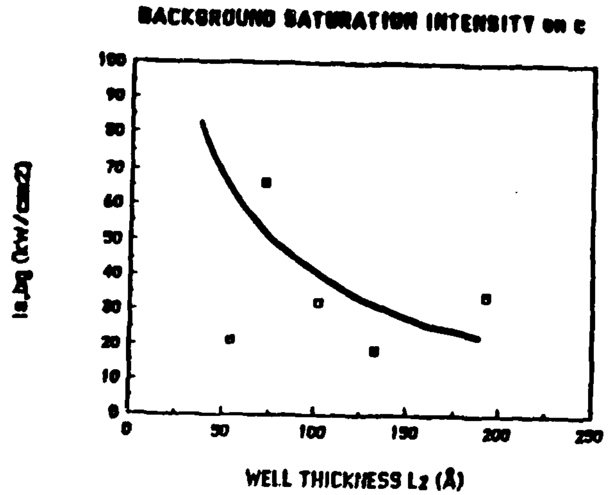

$\rho(\epsilon) \sim \sqrt{E_B}$

$\rho(\epsilon) \sim \frac{1}{L_z}$

$\rho(\epsilon)$

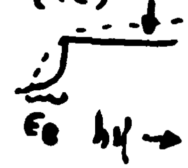

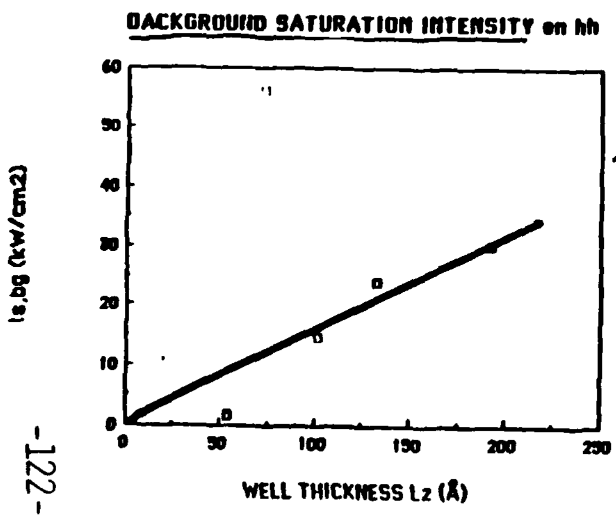

$I_{sB} \propto L_z$

$\rho(\epsilon)$ IN BAND TAIL

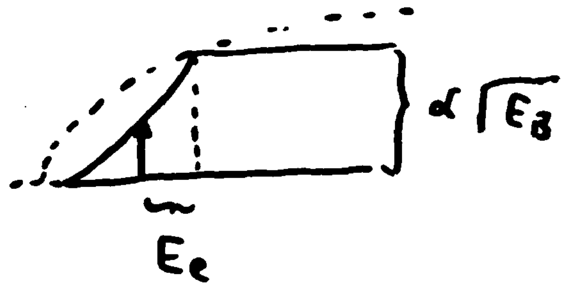

$\rho \sim \frac{1}{(\Delta E)^2}$ IN TAIL.

$$\rho_B \propto \frac{\sqrt{E_B}}{E_e^2} \propto \frac{1}{L_z} \cdot \frac{L_z^2}{1} \sim L_z^1$$

GARMIRE 6

WAVELENGTH DEPENDENCE OF SATURATION INTENSITY

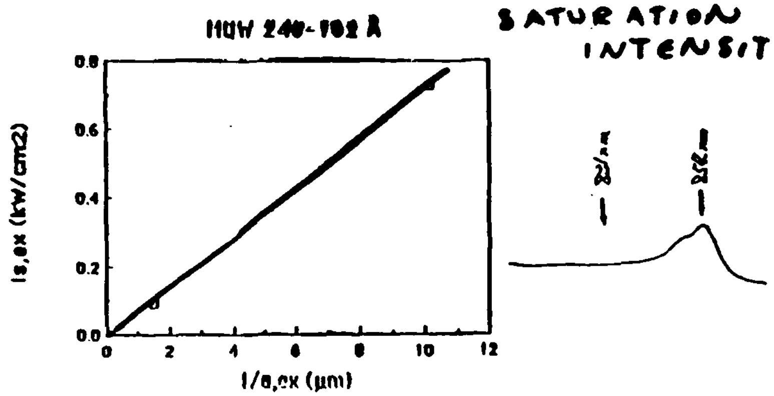

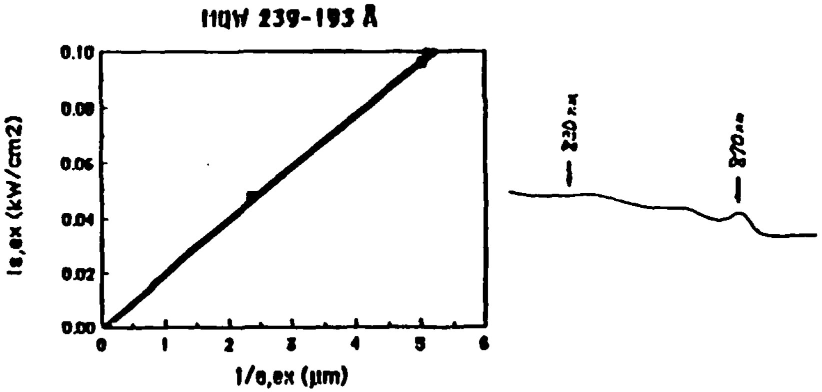

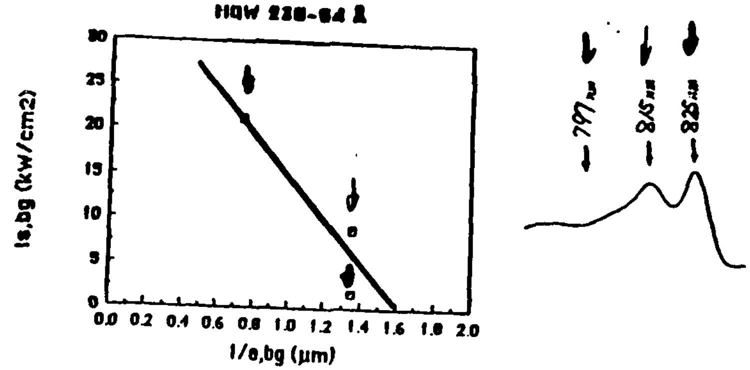

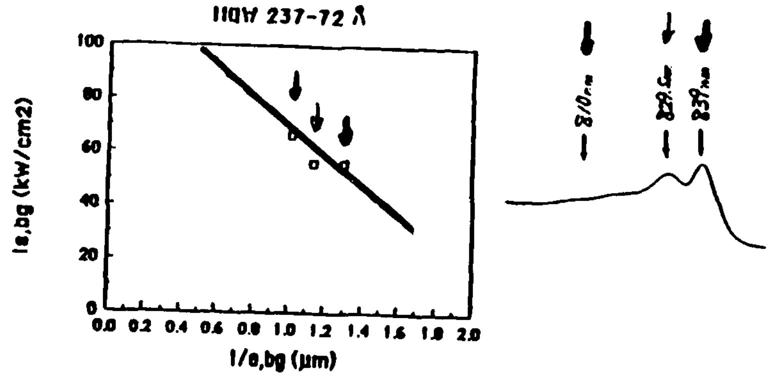

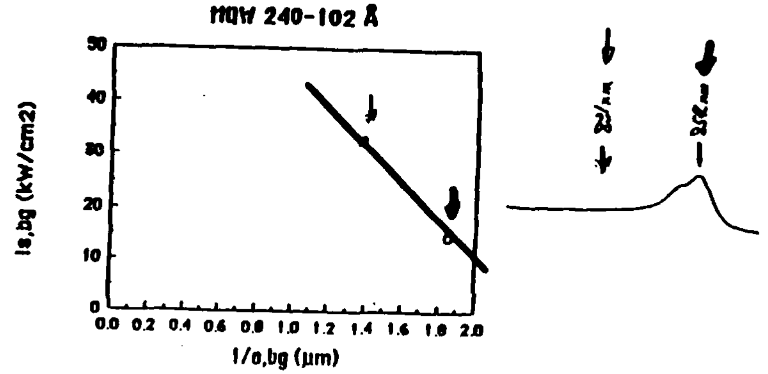

$I_{s,e} \propto \frac{1}{\alpha}$ FOR L CONSTANT

" τ "

absorption coefficient for various intensities

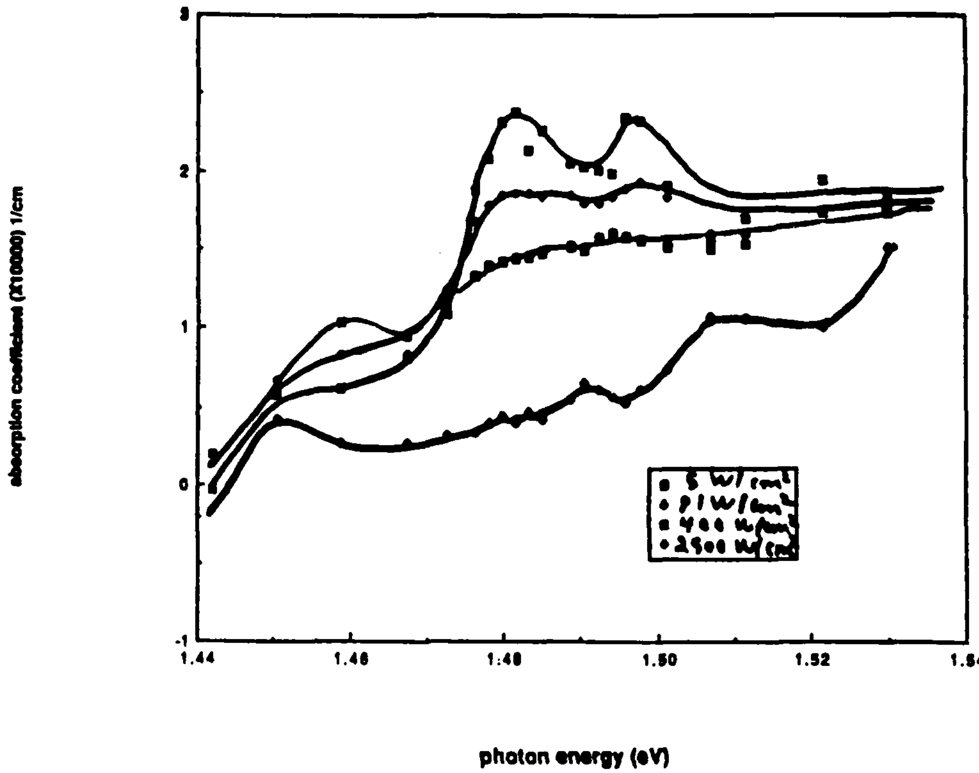

delta n for various intensities $\Delta n(E) = \frac{\hbar c}{\pi} P\int_0^\infty \frac{\Delta\alpha(E')\,dE'}{E'^2 - E^2}$
USING
NONLINEAR KRAMERS KRONIG

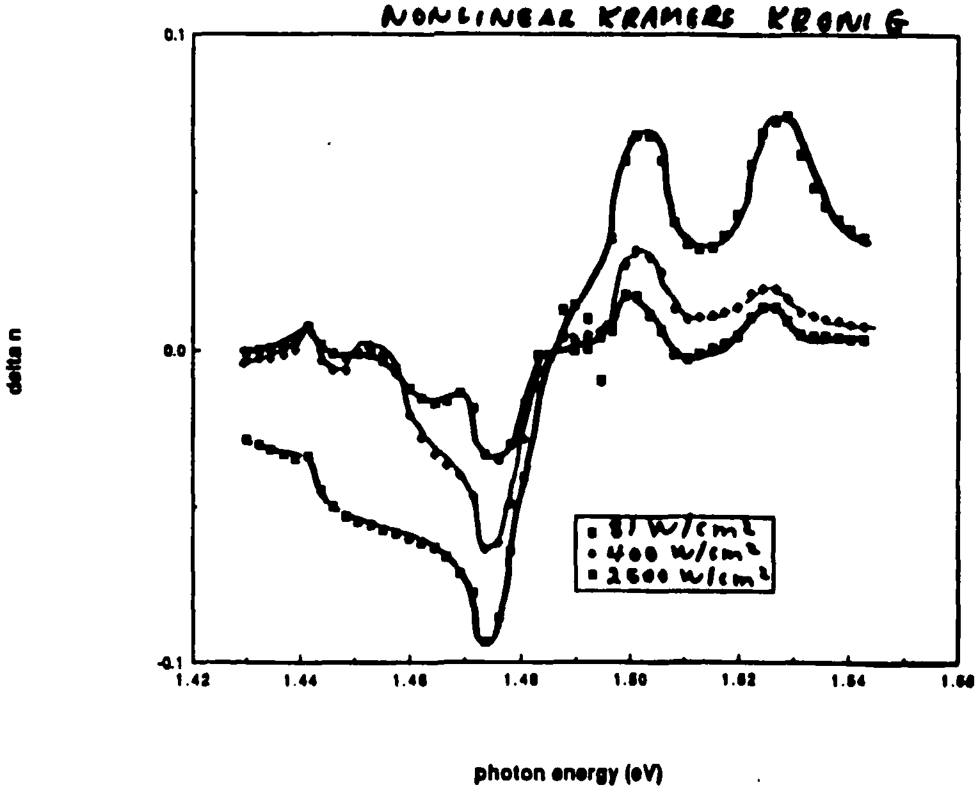

100 Å SAMPLE

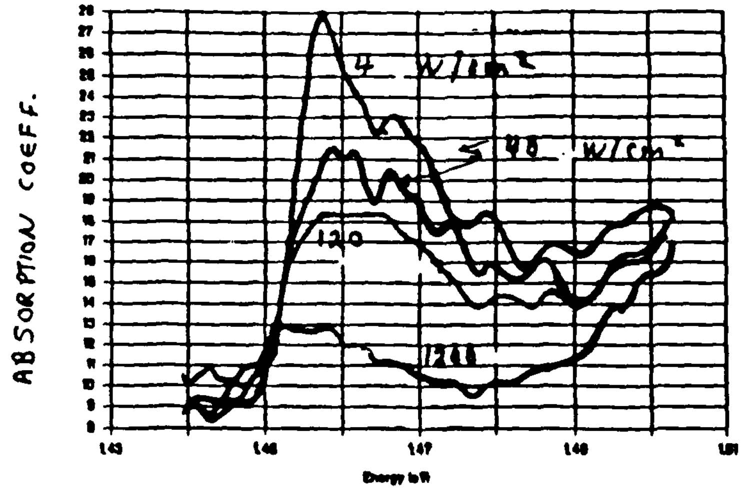

ABSORPTION COEFF.
4 W/cm²
40 W/cm²
120
1200
Energy (eV)

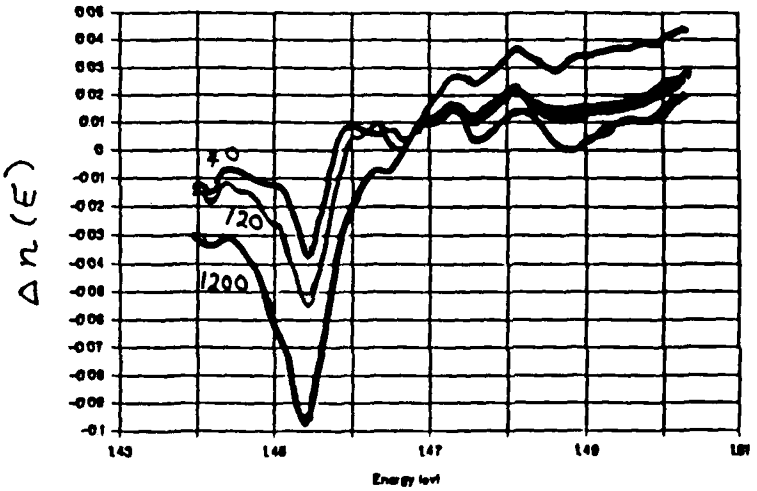

Δn (E)
40
120
1200
Energy (eV)

NONLINEAR INDEX
PROPORTIONAL TO $I^{1/3}$

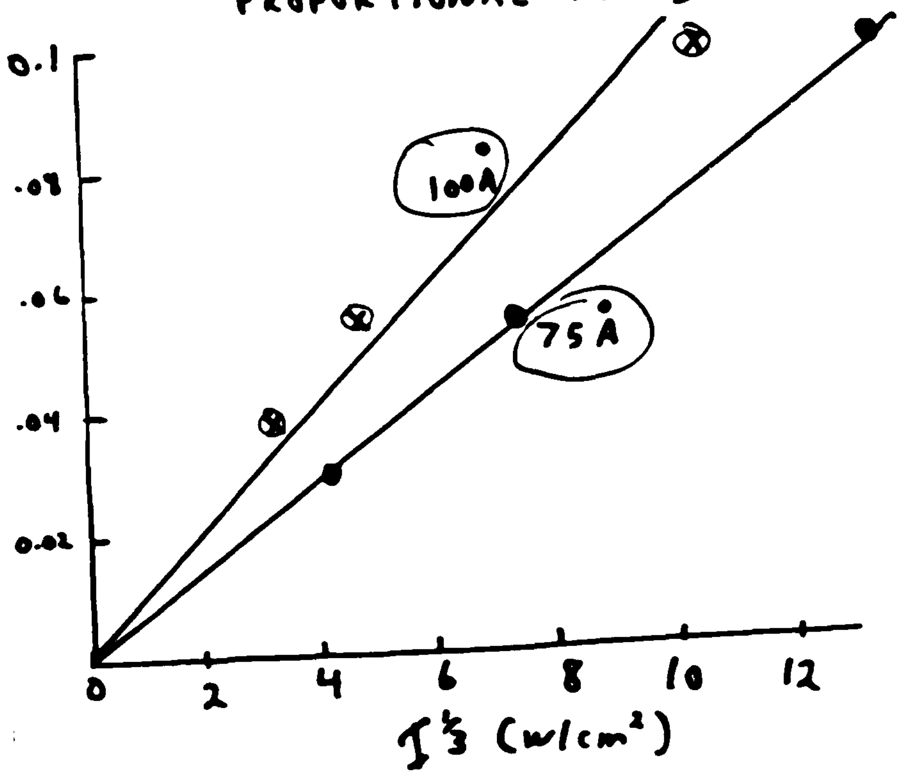

INTENSITY DEPENDENCE
OF THE NONLINEAR INDEX

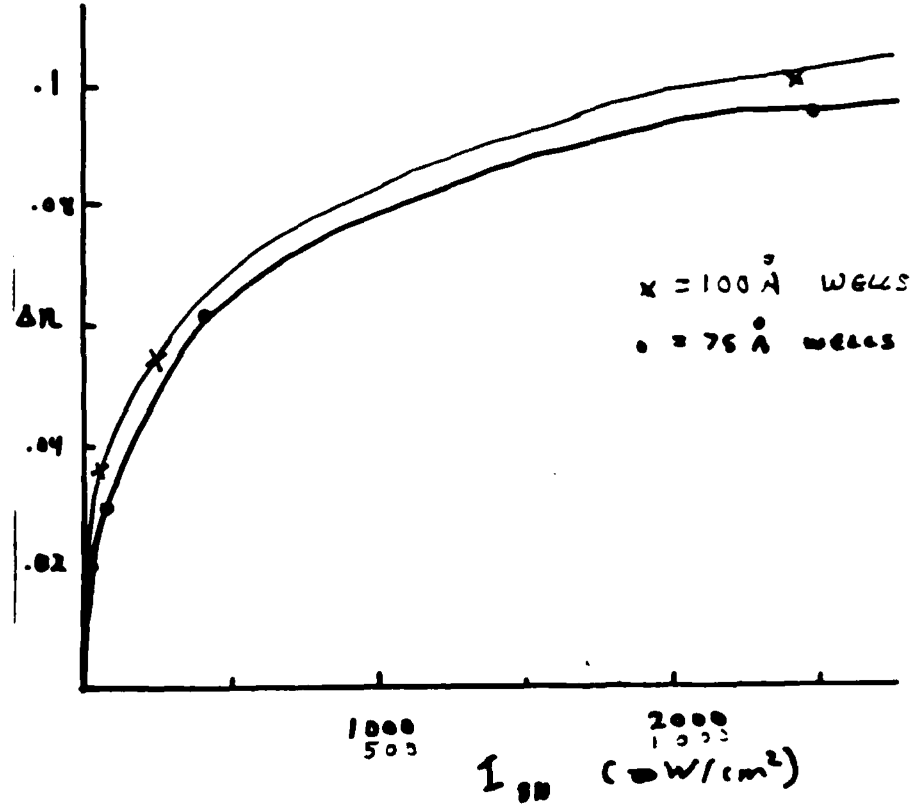

THIS IS NOT AN n_2 EFFECT

CONCLUSIONS

EXCITON AND BAND-TO-BAND NONLINEAR ABSORPTIONS HAVE BEEN SEPARATED

MEASUREMENTS OF ABSORPTION AGREE WITH THEORY

MEASUREMENTS OF SATURATION INTENSITIES ARE REASONABLE

CALCULATIONS OF THE NONLINEAR INDEX FROM KRAMERS-KRONIG SHOW LARGE DEVIATIONS FROM $n_2 I$

Progress in Stabilized Lasers

John L. Hall
Dieter Hils
Christophe Salomon
Jean-Marie Chartier
Franco Wong

SubDoppler Optical Multiplex Spectroscopy, with Stochastic Excitation

Klaus-Peter Dinse
Mike Winters
John L. Hall

Joint Institute for
Laboratory Astrophysics
Boulder, Colorado

Slow Atoms and Stable Lasers

j hall, d hils
JILA
University of Colorado
National Bureau of Standards

Some Interesting experiments REQUIRE a laser's frequency to be stable for a long time (seconds – years)

- Rydberg constant
- QED Tests - positronium vs hydrogen
- operational frequency/wavelength standards
- sources for long baseline interferometry
  - space gravity-wave antenna
  - space synthetic aperture astronomy
- tests of cherished fundamental ideas
  - ex - isotropy of c

$$g_1 = g_0 \quad \text{in} \quad ds^2 = g_1 dx^2 + g_2 (dy^2 + dz^2) - g_0 c^2 dt^2$$

Estimating the Laser Linewidth w̄ feedback

1. Residual FM of Laser – vibration

suppose $\delta\Omega_{laser} = a \cos \omega_v t$

linewidth is $\sim 2a$ if $a \gg \omega_v$

large excursions at low freq ~ Gaussian shape

<u>Many</u> sidebands

Apply servo control. Gain $(\omega_v) = G$

then $\delta\Omega_s \simeq \dfrac{\delta\Omega_{laser}}{1+G} \sim \dfrac{2a}{1+G}$

→ linewidth less by factor $G+1$

At high Gain, phase modulation index → 0

sidebands disappear for $\dfrac{a}{\omega_v} \lesssim 1$

ie for $G > \dfrac{a}{\omega_v}$

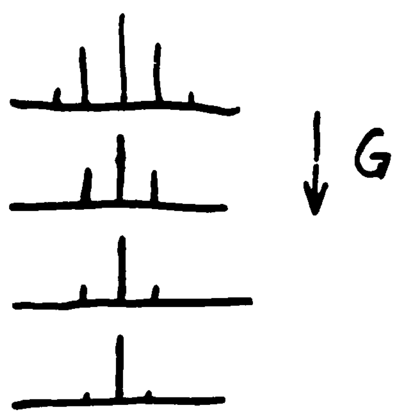

Conclusion: if servo feedback gain is high enough, INTRINSIC laser FM → 0 effectively

→ What new effect keeps real linewidth non-zero?

Shot-Noise-Induced Laser FM

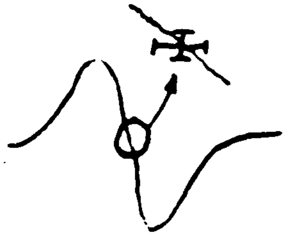

$$i_{\substack{Shot\\Noise}} = \sqrt{2 e i B}$$

$\rightarrow| \quad |\leftarrow \Delta$

$$\frac{Sig}{Noise} \sim \frac{i}{i_{shot\ noise}}$$

$$\delta\Omega_S \simeq \frac{\Delta}{Sig/Noise} \sim \Delta \cdot \frac{\sqrt{2eiB}}{i}$$

→ Residual Frequency Excursion ←

What is the laser linewidth?

$$\delta\Omega_{1/2} = \pi \frac{(\delta\Omega_S)^2}{B} = \pi \Delta^2 \frac{2e}{i}$$

$$= \pi \cdot (\text{frequency noise spectral density})^2$$

D Elliott et al
PR A ('82)

valid in High S/N limit : $B \gg \delta\Omega_S$

---

ex: $\delta\Omega_S \approx 100\ Hz$ in 3 MHz BW

$\delta\Omega_{1/2} \approx 100$ milli Hertz

Sig/Noise grows $\propto \sqrt{T}$
\# cycles grows $\propto T$
} we run out of S/N at long times

High Performance Frequency Servo

A frequency Servo system using a Reflection-mode phase/frequency optical discriminator and an "outside - the-laser" frequency transducer can achieve excellent closed loop performance. Here an Argon laser is stabilized tightly above 200 kHz so that measurement shot-noise is converted into a corresponding FM excursion, ie the servo null point goes 6 dB below the shot-noise level. The remaining FM noise at 100 kHz is near the shot-noise level and can be drastically reduced with additional low frequency gain.

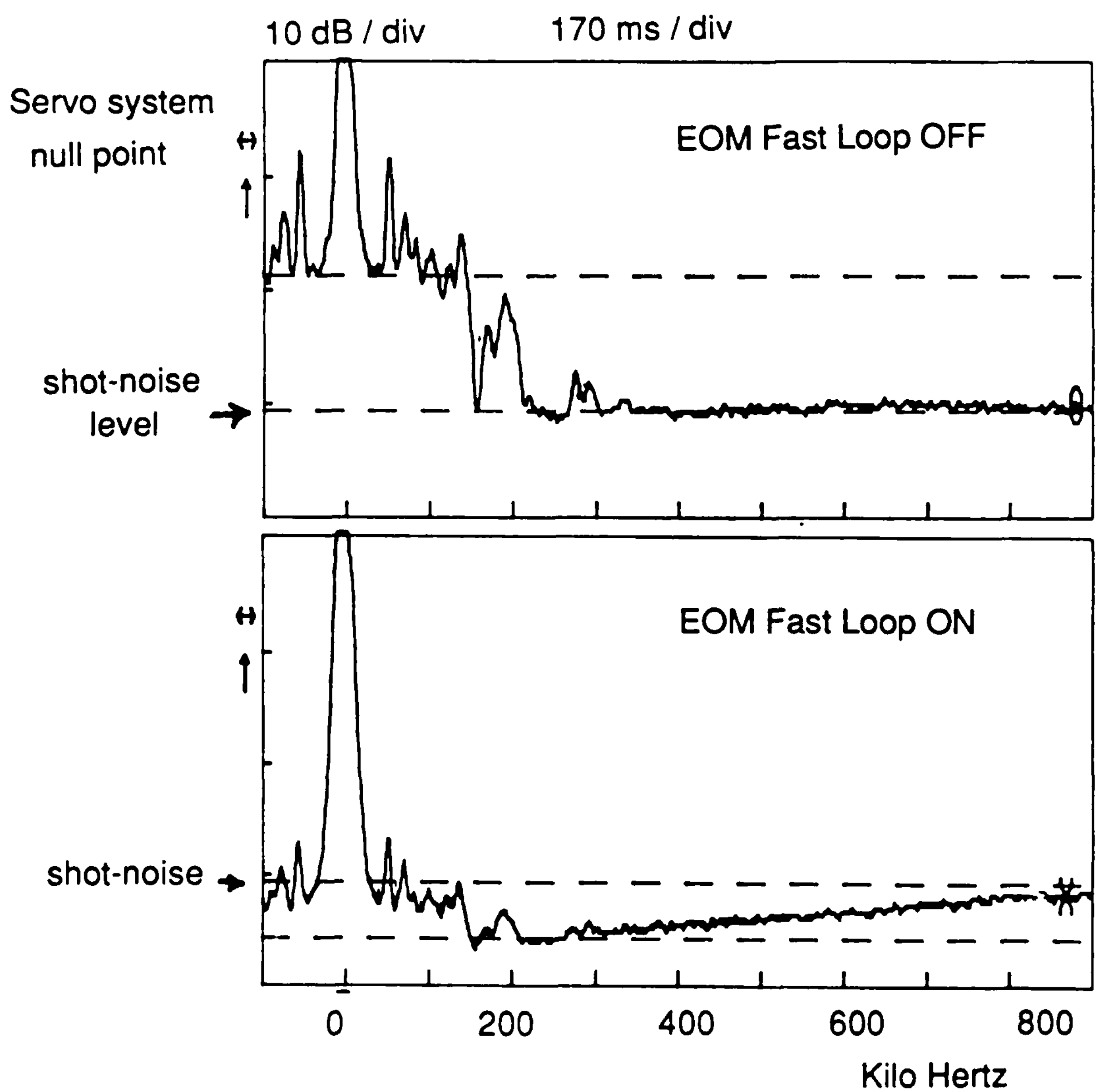

Limiting Narrow Laser Linewidth

Servo Gain is very large → laser intrinsic noise totally suppressed
only measurement noise important

$$\frac{\partial I}{\partial \nu} \times \delta\nu \quad + \quad \text{shot noise} \quad \simeq 0 \qquad \text{Servo Eq.}$$

gives a frequency excursion density

$$\frac{\Delta}{\sqrt{B}} = \frac{\sqrt{2e\, i_{dc}}}{i_{sig}} \times \Delta\nu_c \qquad \propto \qquad \frac{\text{Hz deviation}}{\sqrt{\text{Hz}}\ \text{bandwidth}}$$

Lorentz linewidth $\delta f = \pi \Delta^2$ — Elliott '82

Ex: $F = 6500$ $\quad c/2L = 500\,MHz$ $\quad \Delta\nu_c = 80\,kHz$

$\frac{\text{noise}}{\text{signal}} \sim 0.2$ ppm in 1Hz BW

$$\rightarrow \Delta = 15\ \text{milli}\,Hz/\sqrt{Hz} \times \sqrt{5\,kHz} \simeq 1\,Hz$$

$$\text{so} \quad \delta f = \pi\Delta^2 = \pi \cdot \left(.015\ \frac{Hz}{\sqrt{Hz}}\right)^2 = 700\,\mu Hz$$

coherence time $1/(2\pi\,\delta f) = 225$ sec !

"typical" time for ±1 radian now ~ 15–20 sec

$$\frac{10^{-2}\,Hz}{5\times10^{14}} \sim 2\times10^{-17} \quad \text{at 15 sec !}$$

D. Hils, Ch. Salomon, JH

Distinguishing a Spectral Line from Filtered Noise

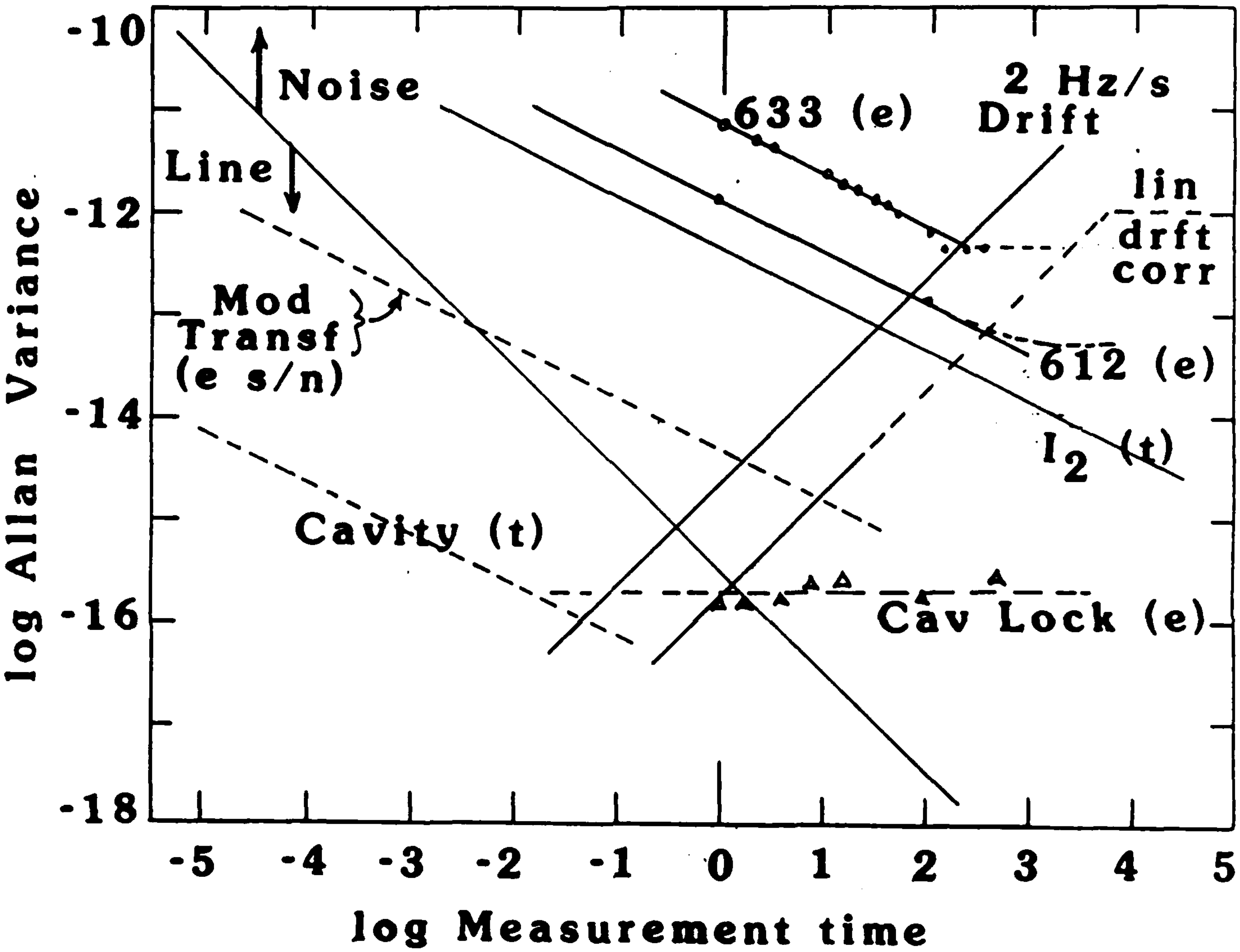

In the lower-left sector the fast laser phase-noise is below one radian, so the source looks like a spectral line which is (slowly) drifting in frequency. In the upper-right triangle, the phase noise exceeds one radian, and so no appreciable sharp carrier component is left. Thus the field has only a short time-coherence and looks like white noise which has been spectrally filtered, in our case by the resonance filter represented by the frequency servo loop. Note that the present cavity-locked results offer a line spectrum out to a few seconds, while the Iodine resonances are too broad and / or too weak to give good short-term locking.

Cavity Mirrors: $R = 575$ cm
$R = \infty$

are optically contacted to End Faces of

Zerodur Spacers : 15×30 cm^2

$\mathcal{F} \sim 6{,}600$

$FSR = 480$ MHz

$\Delta \nu_c = 72$ kHz

Cavity is located in sealed Aluminum Can.

Alu-Walls are temperature controlled

Vac Pressure $< 8 \times 10^{-8}$ Torr

Optical Set up is located inside Q-House

for Acoustic Isolation (~40 dB) and

Temperature Isolation (~mK).

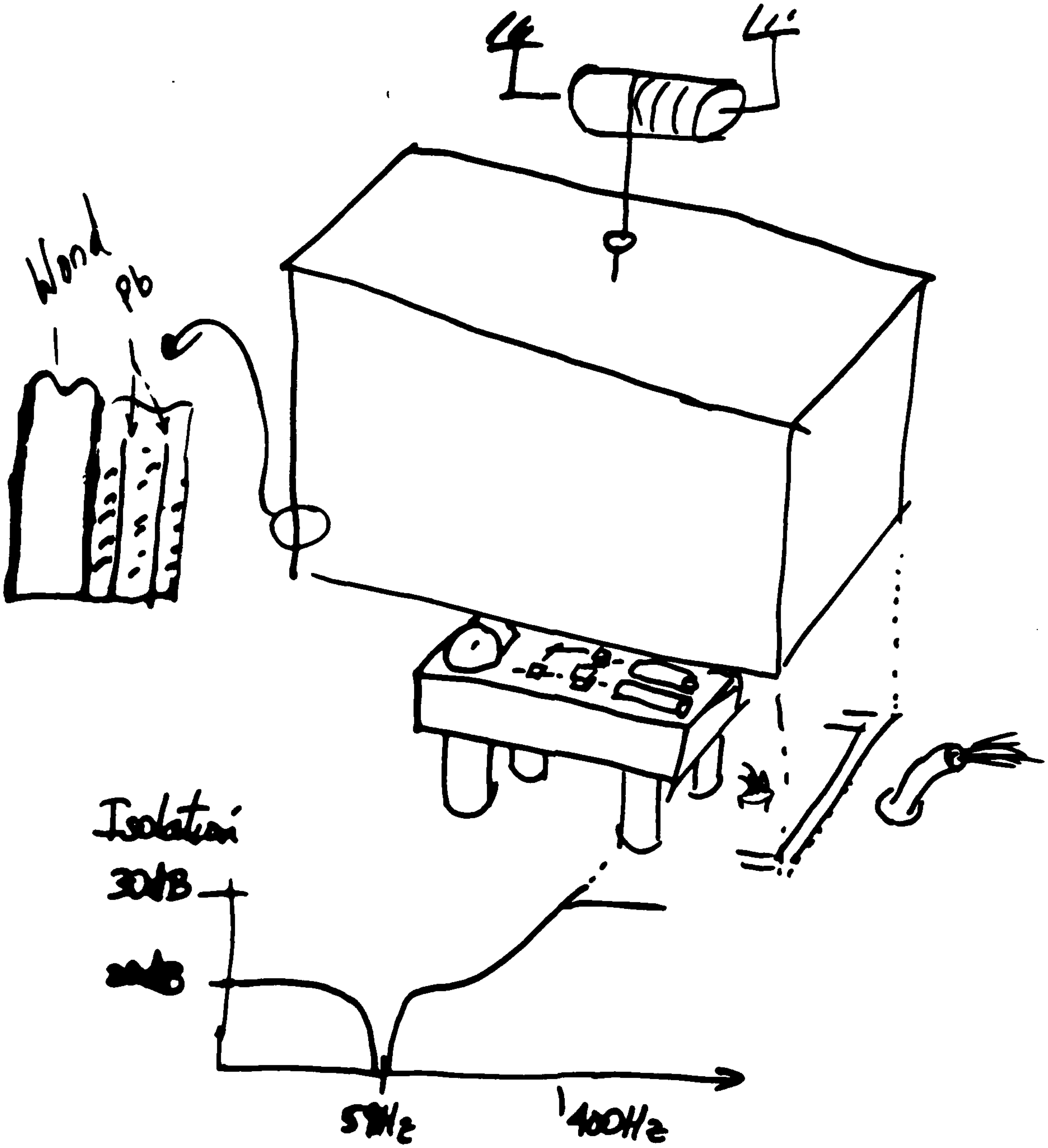

the JILA << QUIET HOUSE >>

d hils, j faller, j. hall RSI subm 1986

 57 2532 (1986)

Spectral Distribution of Phase (16.5 sec sample)

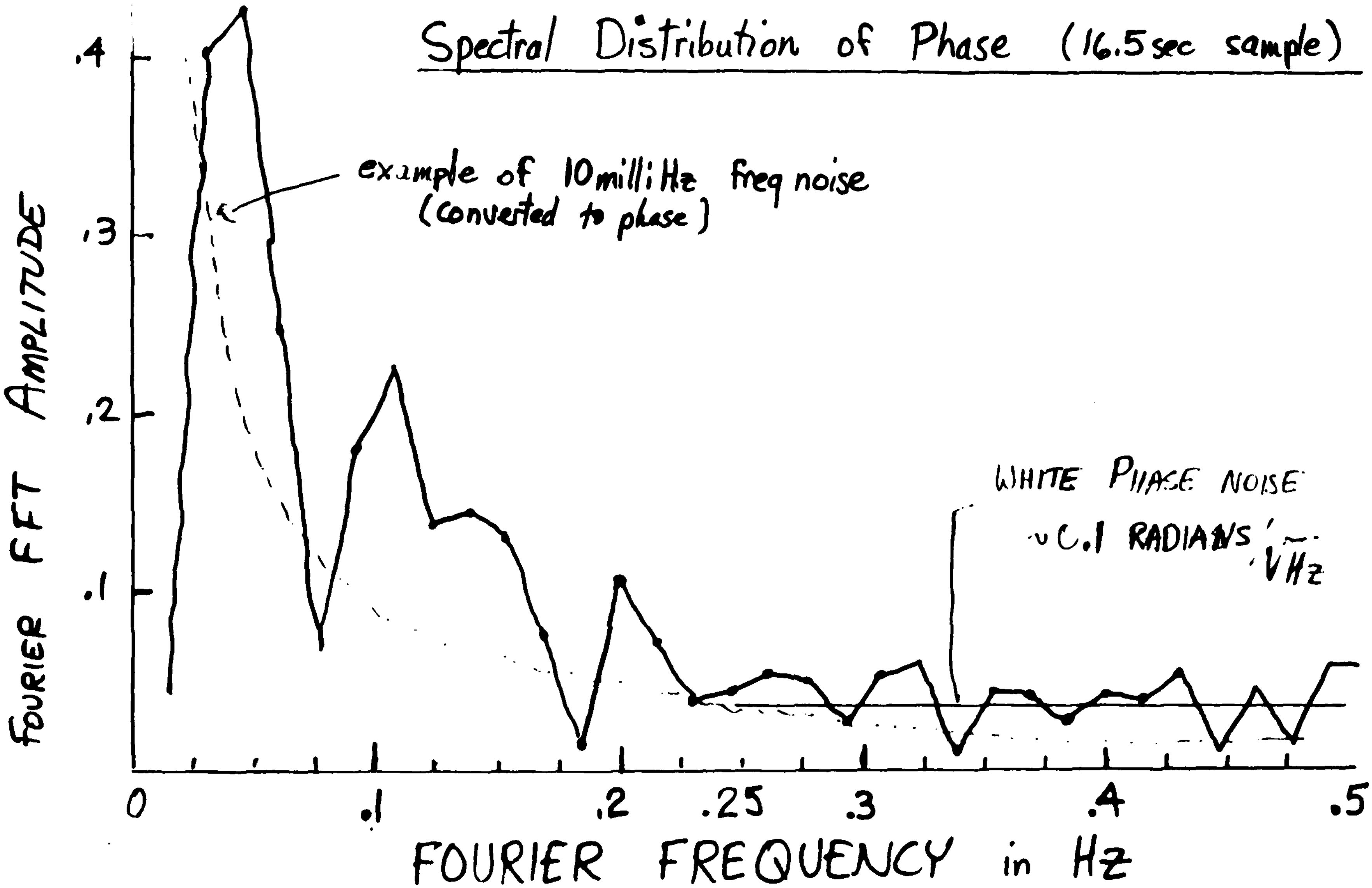

Hils & HALL Summer 87

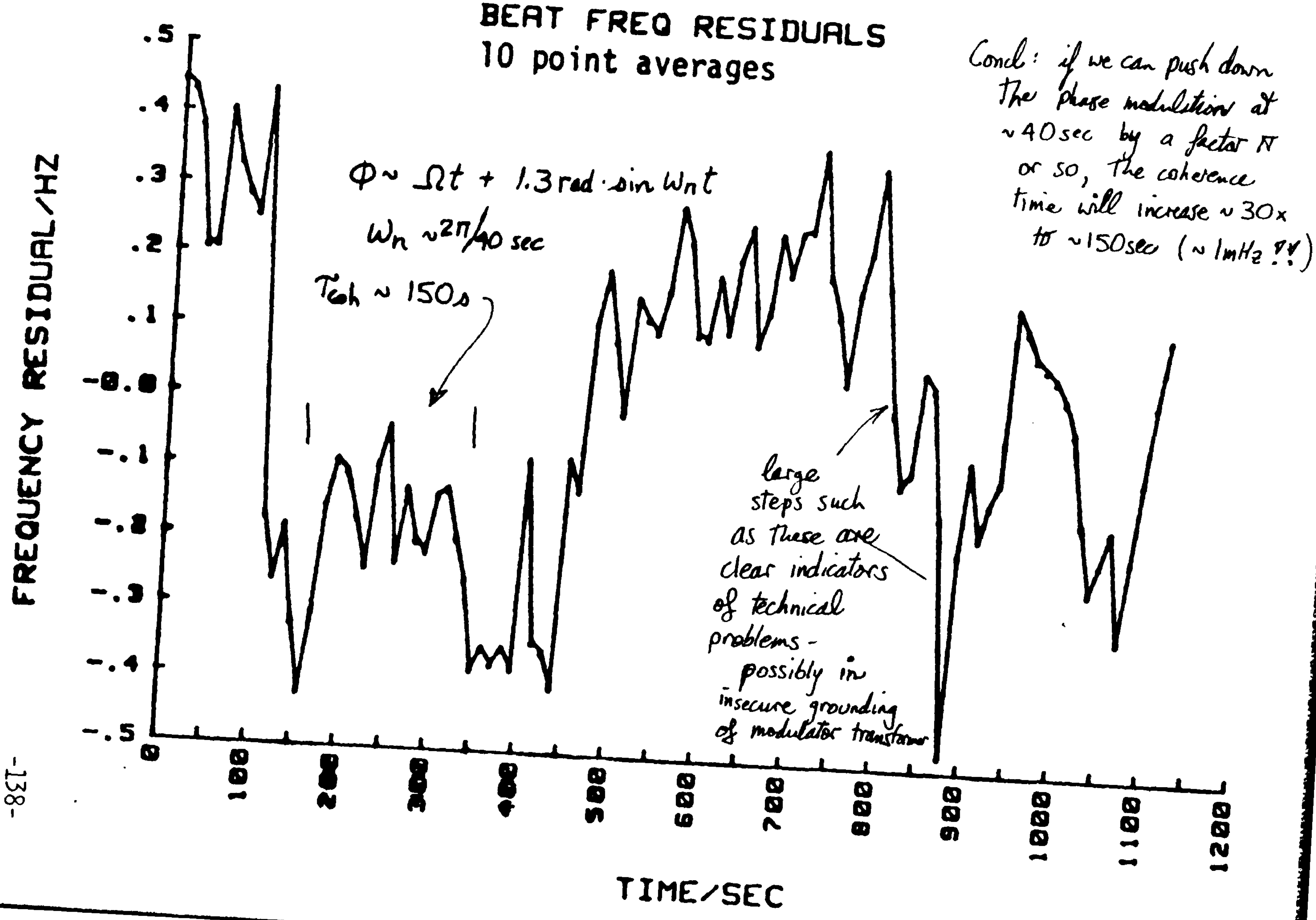

ALLAN VARIANCE OF CAVITY LOCKED HENE LASER

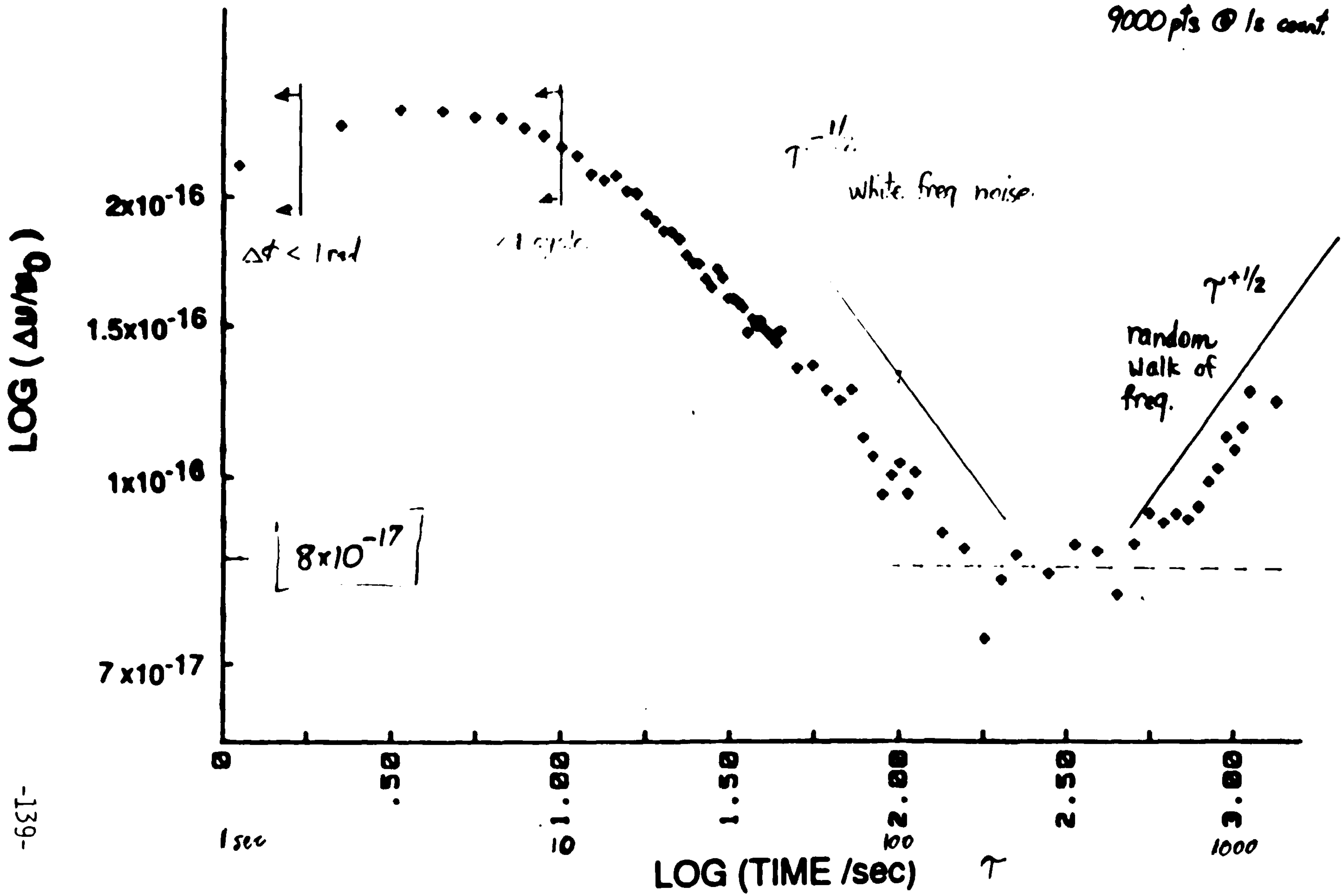

LONG-TERM STABILITY (CAVITY)

Cavity-Stabilized He/Ne vs I_2-Stabilized He/Ne

BEAT FREQUENCY [REF IS h-PEAK]

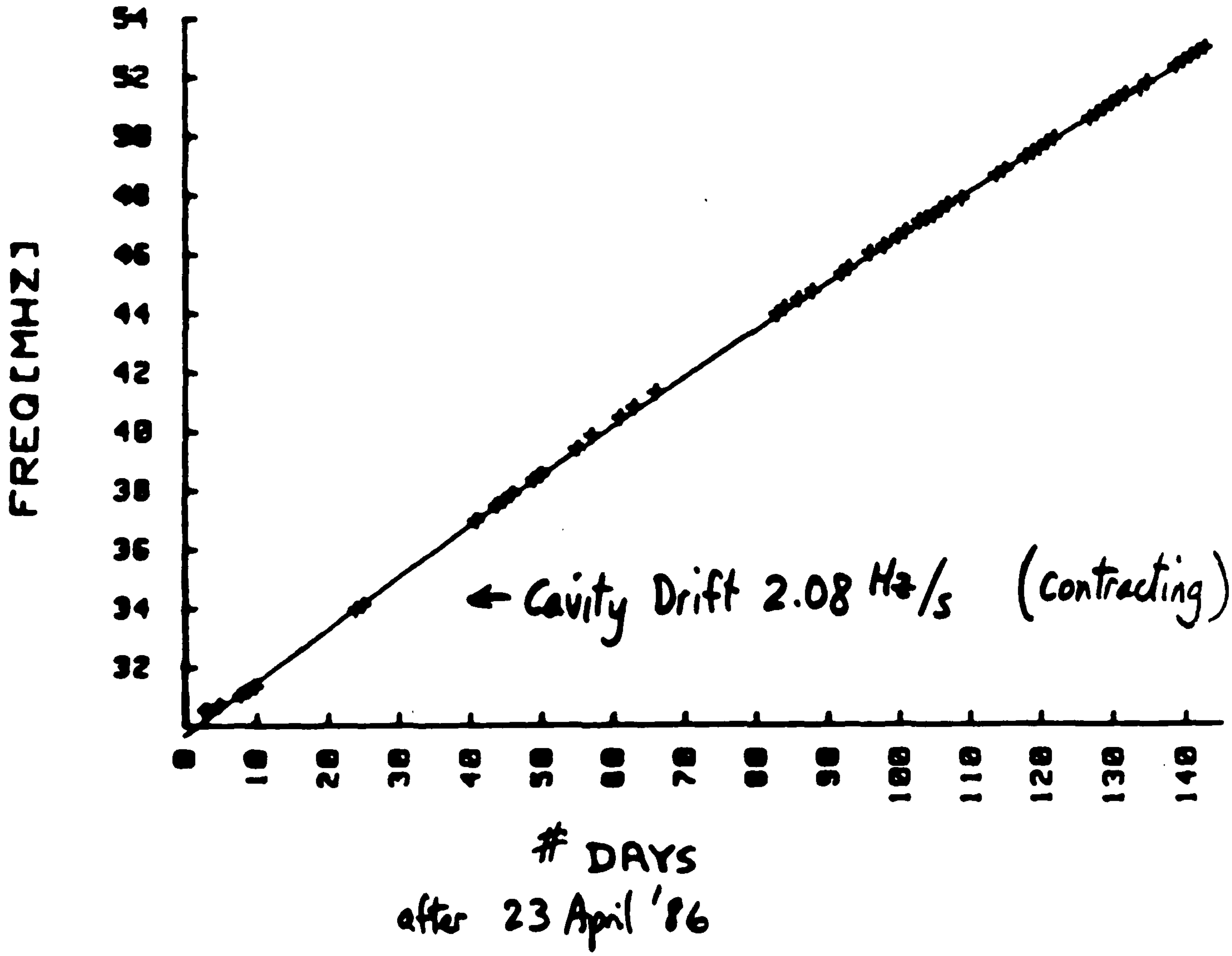

Strategy for Laser Locking

Tight lock to good cavity
\+ SLOW lock to atoms

assume 30cm cavity, $\mathcal{F} = 10{,}000$
$\eta = 10\%$
} → $\delta\nu$ < 1 milliHertz due to shot noise (theory)

exp't'l $\delta\nu < 0.1$ Hz
limit was drifting of cavity - thermal?

Compare I_2 - stabilized laser vs cavity-stabilized
drift rate +2.08 Hz/sec
rms deviations ~ 100 Hz in 24 hours

→ ready for ATOMS! (with sub-Hz linewidths)

$\delta\nu_{FW} = 50$ mHz
drift predictable to 0.1 Hz for 30 sec

Doppler-free Optical Multiplex Spectros. with Stochastic Excitation

P. DINSE, M. WINTERS, j hall

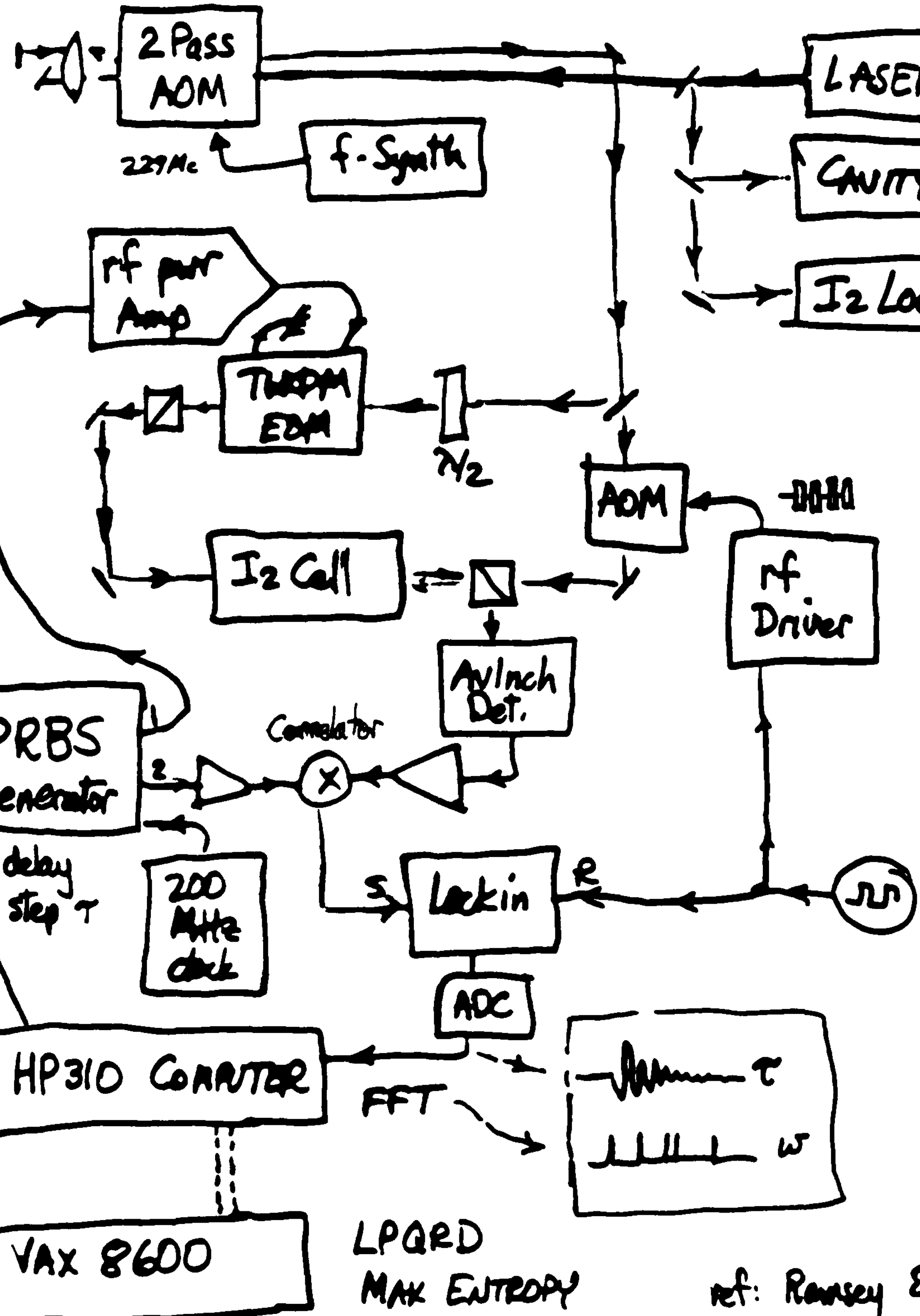

ref: Ramsey & Whitten RSI 57 1329 (1986

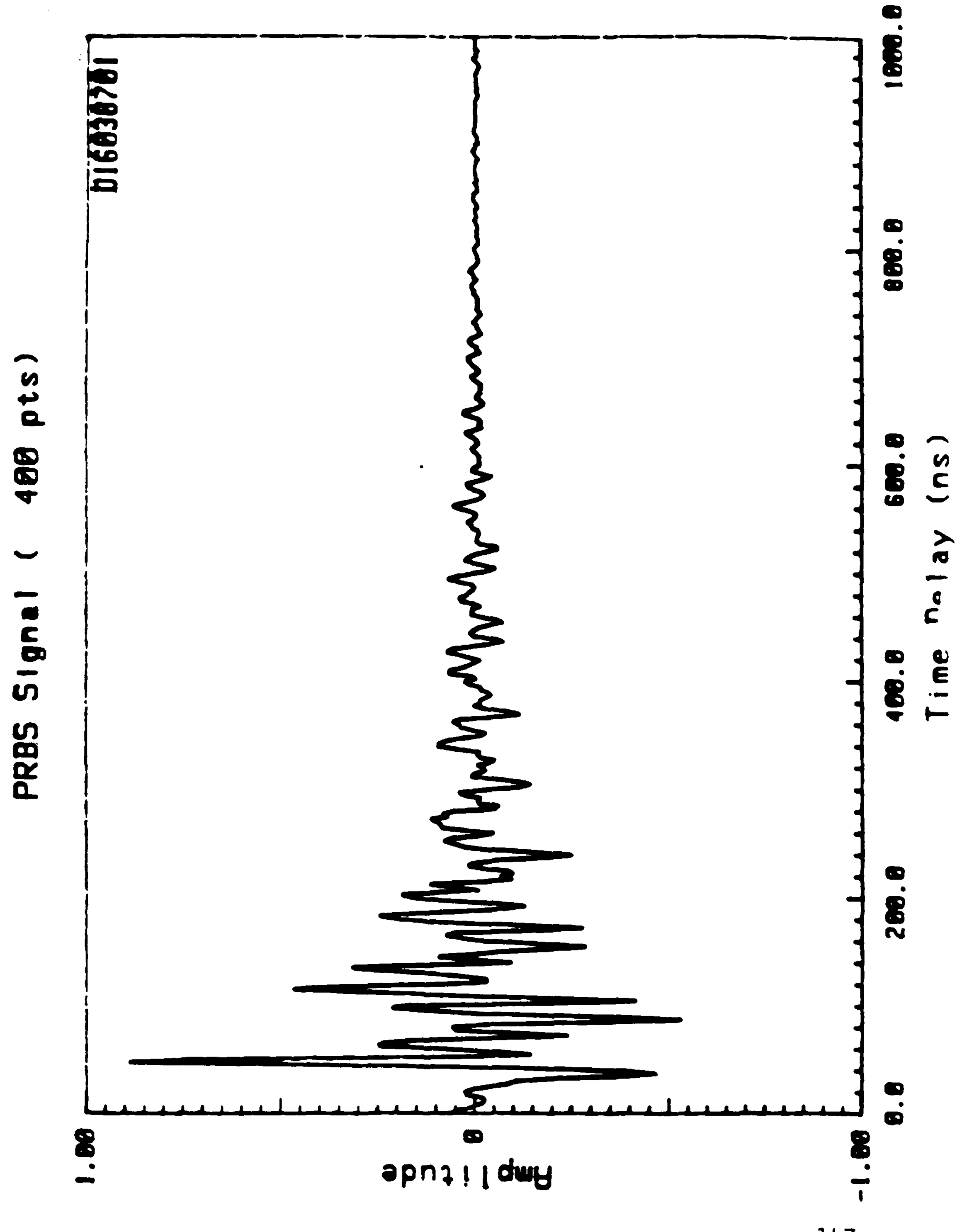
PRBS Signal (400 pts)
1.00
0
-1.00
Amplitude
0.0
200.0
400.0
600.0
800.0
1000.0
Time Delay (ns)

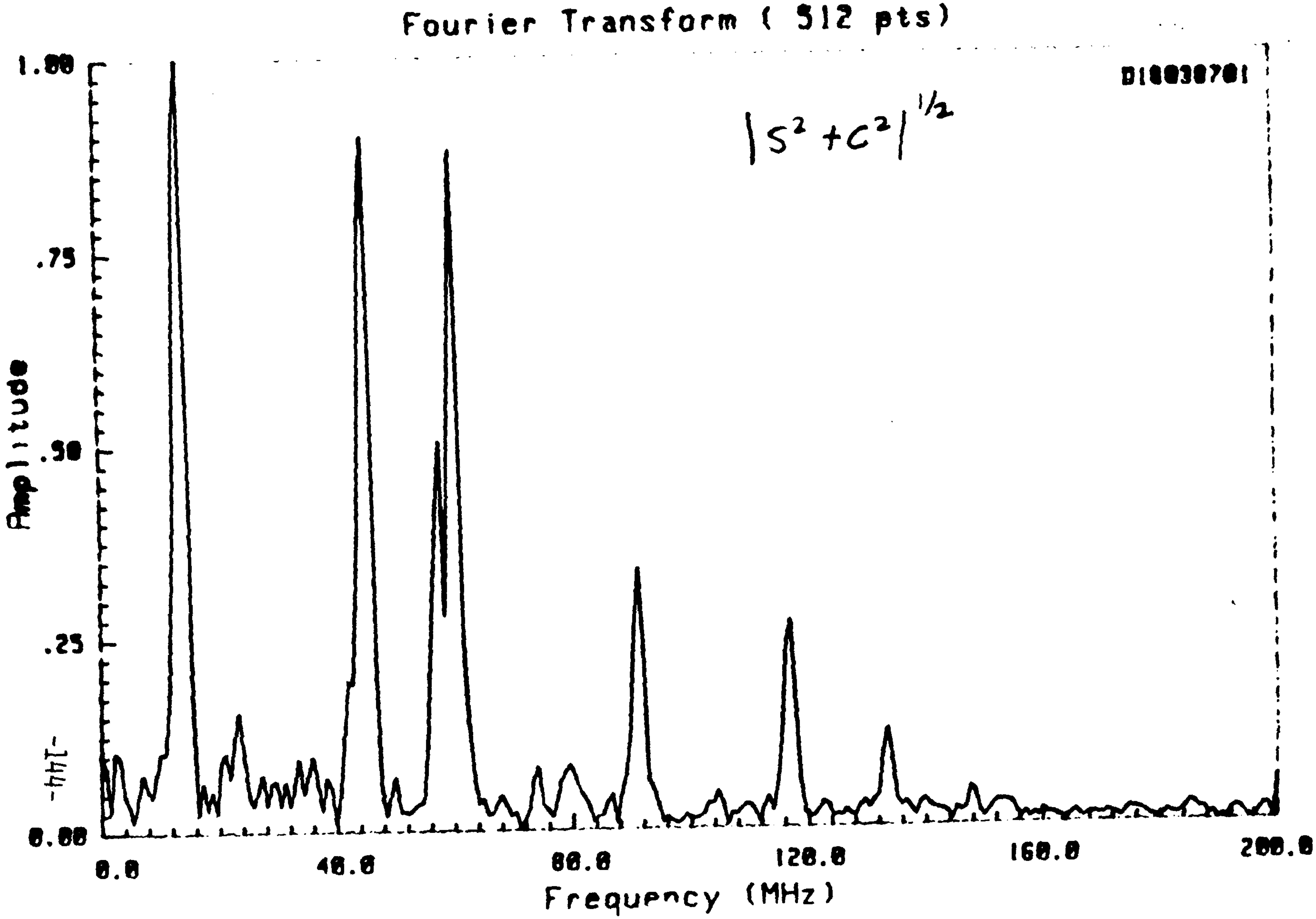
Fourier Transform (512 pts)
D18030701
$|S^2+C^2|^{1/2}$
Amplitude
1.00
.75
.50
.25
0.00
0.0
40.0
80.0
120.0
160.0
200.0
Frequency (MHz)

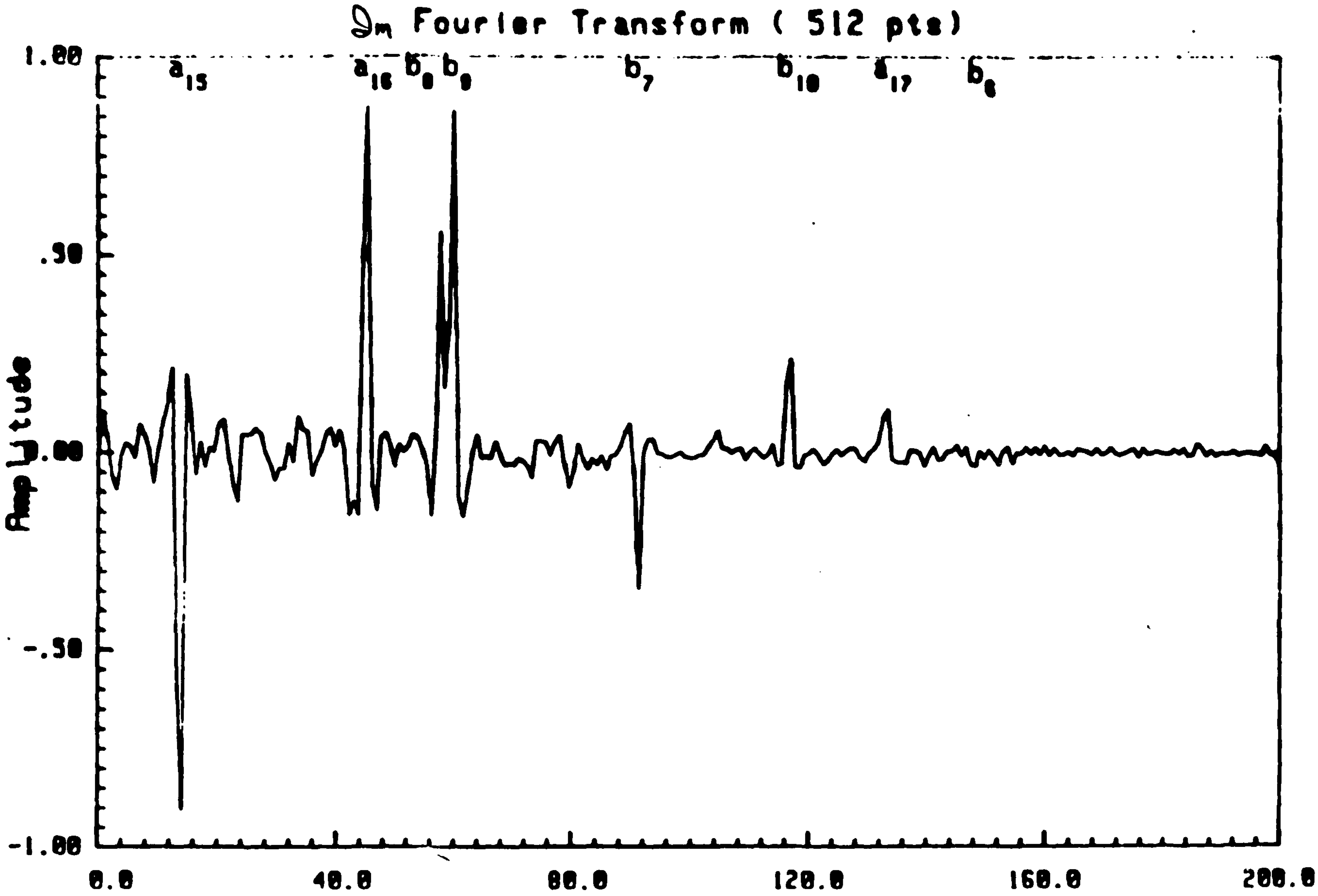
Im Fourier Transform (512 pts)
1.00
.50
0.00
-.50
-1.00
Amplitude
a_{15}
a_{16}
b_6
b_9
b_7
b_{10}
a_{17}
b_8
0.0
40.0
80.0
120.0
160.0
200.0
Frequency (MHz)

Figure 4.

Doppler-Free Spectroscopy with Multiplex Detection & Stochastic Ex

The present: idea demonstrated
paper ready for JOSA-B
K.P. Dinse, M. Winters, jl hall

the future:

1. Servo-control phase modulator to produce pure FM
   → correlation at $t=0$ vanishes
   → only molecules give signal

2. Digital filtering to whiten $\sin x/x$ modulation
   → flat to $\sim .9 \times f_c$

3. Try bigger beams for I_2 at 5017 Å
   $20\,\mu s = \tau_n$ → < 20 kHz linewidth
   with 200 MHz excitation width
   $N \approx 10^4$ multiplex factor $\sqrt{10^4}$ S/N

4. GaAs chips - 1 GHz BW covers most Dopplers

the A[illegible]:

1. S/N win by $\sqrt{N}$
2. freq. axis is accurate
3. lineshape involves single intense field → calculable

Dynamic and Spectral Properties of Semiconductor Lasers with Quantum Well, Quantum Wire, and Quantum Box Structures

Yasuhiko Arakawa

University of Tokyo, Roppongi, Minato-ku, Tokyo 106 Japan

Abstract

Effects of reduced dimensionality of electron motion alter various properties of semiconductor lasers. In fact, quantum well structures have brought significant improvements in semiconductor laser characteristics. In 1982, Arakawa et. al. proposed the concept of the quantum box laser as well as the quantum wire lasers. In an ideal quantum box structures, electrons and holes have highly localized wavefunctions and the state space in each box is discrete as opposed to the quasi continuum of the bulk. The contribution to gain from each ideal quantum box arises from a pair of two level systems. In this case, the overall active layer would much like a gas laser in which the quantum boxes are analogous to the atoms in the gas.

In this paper, we discuss dynamic and spectral properties of semiconductor lasers having such quantum-mechanical micro-structures, with emphasis on the quantum box lasers. The theoretical analysis indicates that laser characteristics are significantly improved in low-dimensional electronic gas systems. In order to demonstrate the quantum box effects experimentally, we place a quantum well laser in a high magnetic fields, in which zero-dimensional electronic systems are formed by both Lorentz force and the quantum well potential effects. In addition, recent progresses of picosecond pulse generation in quantum well lasers are also discussed.

DYNAMIC AND SPECTRAL PROPERTIES OF SEMICONDUCTOR LASERS WITH QUANTUM WELL, QUANTUM WIRE, AND QUANTUM BOX STRUCTURES

Y.ARAKAWA

UNIVERSITY OF TOKYO, TOKYO, JAPAN

---

1. BASIC PROPERTIES OF ELECTRONS IN QUANTUM-WELL(2D) STRUCTURES, QUANTUM-WIRE(1D) STRUCTURES, AND QUANTUM-BOX STRUCTURES(0D)
2. MODULATION DYNAMICS
3. FIELD SPECTRAL PROPERTIES
4. EXPERIMENTAL DEMONSTRATION USING HIGH MAGNETIC FIELD
5. PICOSECOND PULSE GENERATION IN QUANTUM WELL LASERS

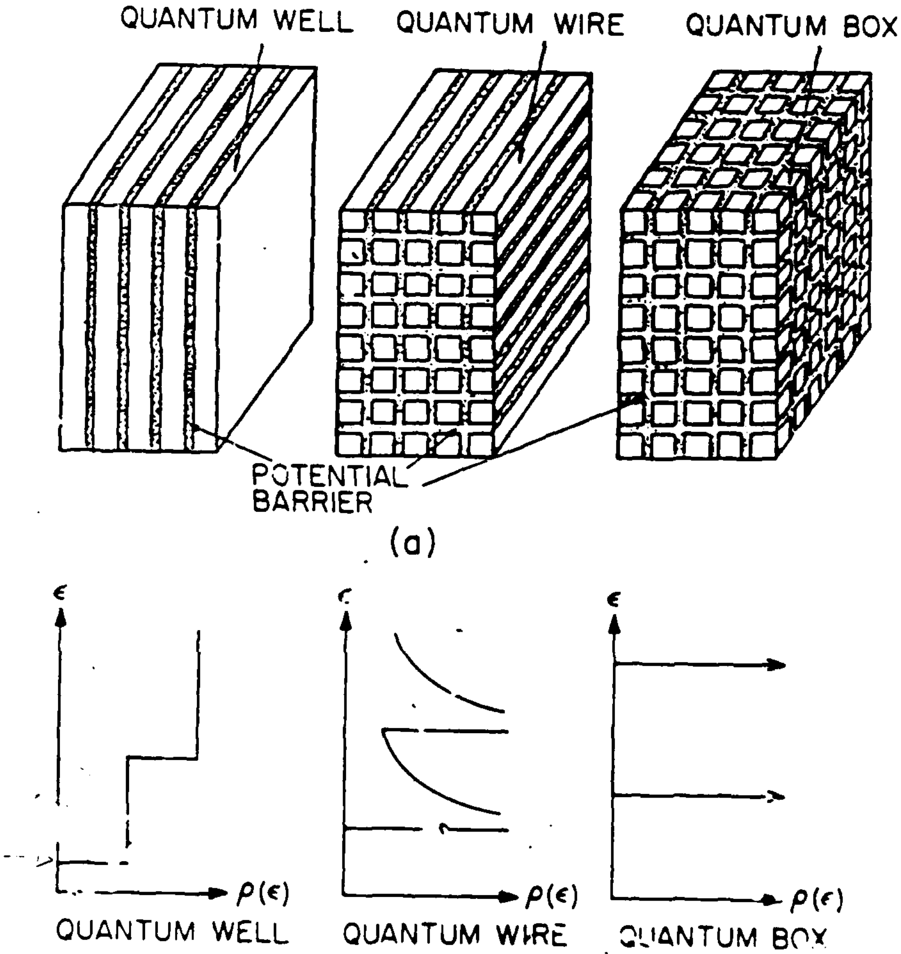

(b) DENSITY OF STATES

FABRICATION OF QUANTUM-WIRE AND QUANTUM-BOX STRUCTURES

(GaAs/AlGaAs and InP/InGaAs)

ELECTRON BEAM LITHOGRAPHY
(1986 Worlock et al., 1987 Temkin et al.)

ETCHING THROUGH THE USE OF ANISOTROPIC PROPERTIES OF CRYST
(1982 Petroff)

USE OF DISORDERING EFFECTS IN QUANTUM-WELL STRUCTURES
(1986 Petroff et al., 1986 Hirayama et al.)

GROWTH ON VICINAL SURFACES
(1984 Petroff)

(HIGH MAGNETIC FIELDS
(1982 Arakawa et al.))

DEVICE PHYSICS

ANALYSIS OF ELECTRON TRANSPORT IN QUANTUM-WIRE STRUCTURES
(1980 Sakaki)

PROPOSAL OF QUANTUM-WIRE LASERS AND QUANTUM-BOX LASERS
(1982 Arakawa et al.)

....

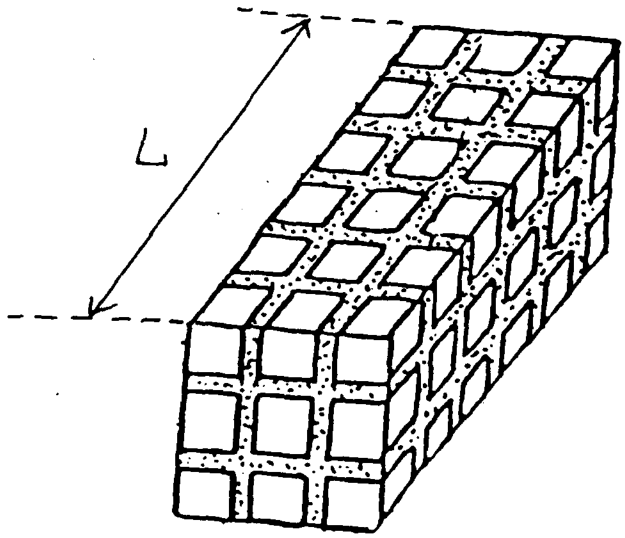

N = 9

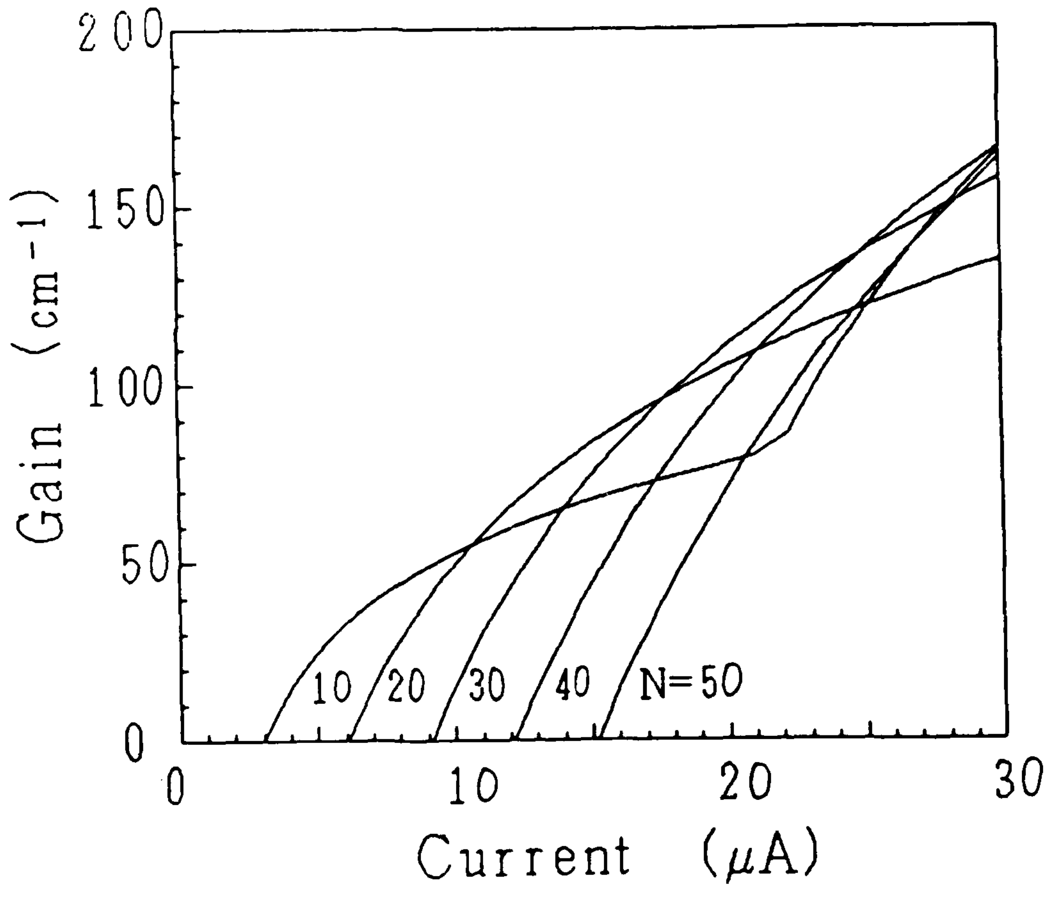
200
150
100
50
0
Gain (cm-1)
10
20
30
40
N=50
0
10
20
30
Current (μA)

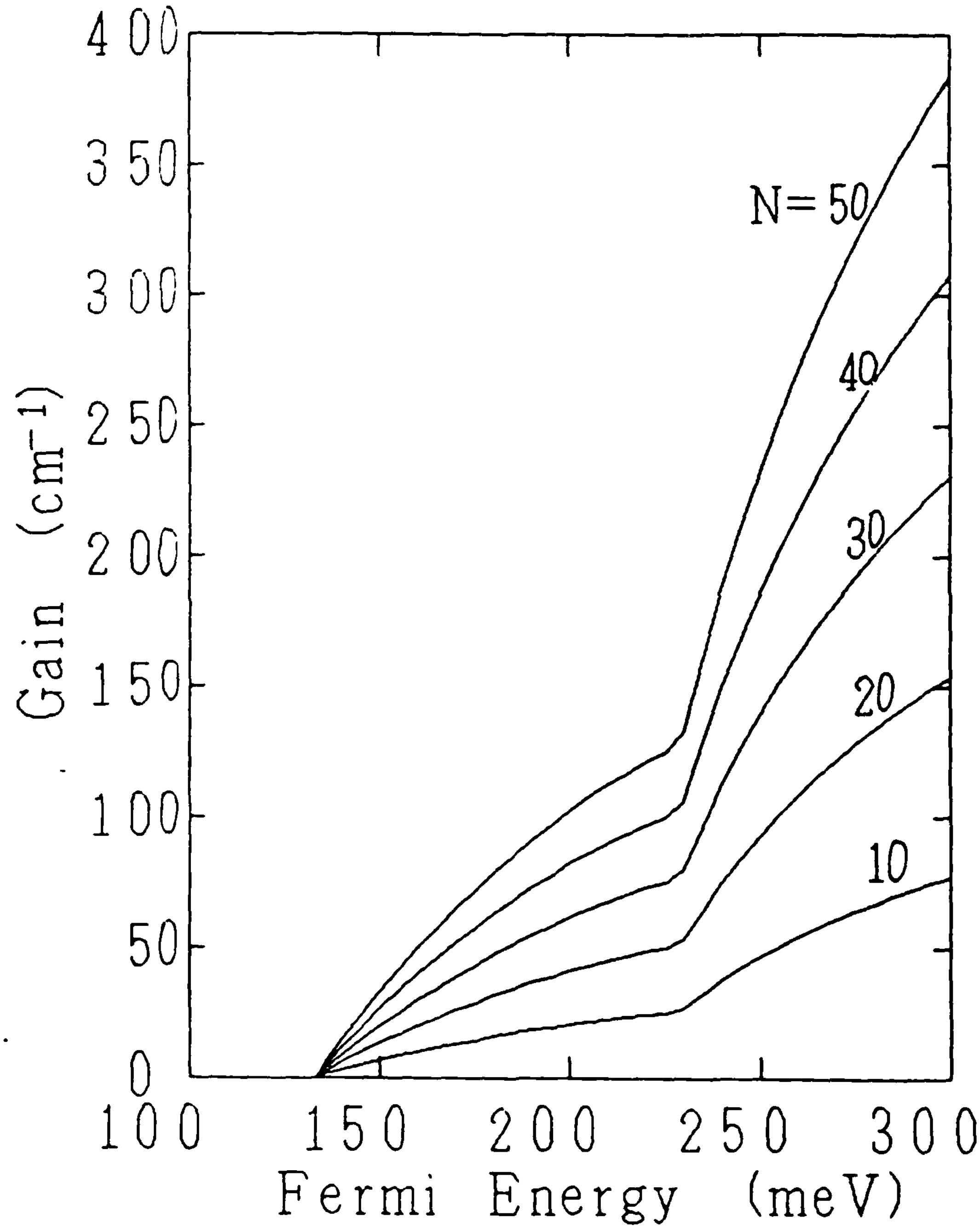

Gain (cm^{-1})
0
50
100
150
200
250
300
350
400
N=50
40
30
20
10
100
150
200
250
300
Fermi Energy (meV)

GAIN

$$\chi = \chi_R + j\,\chi_I$$

0D SYSTEM

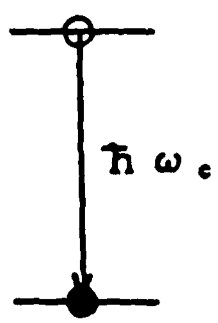

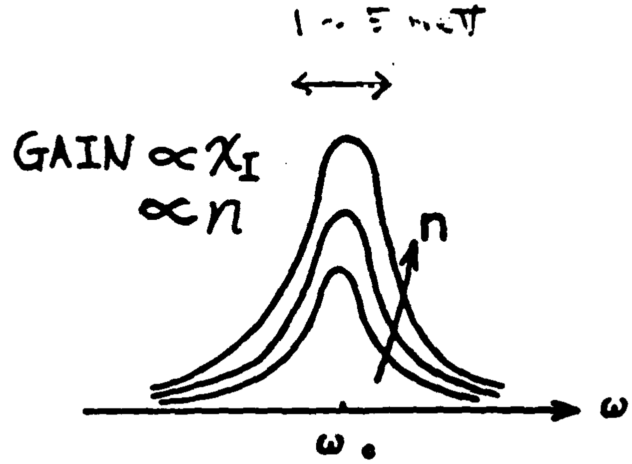

3D SYSTEM

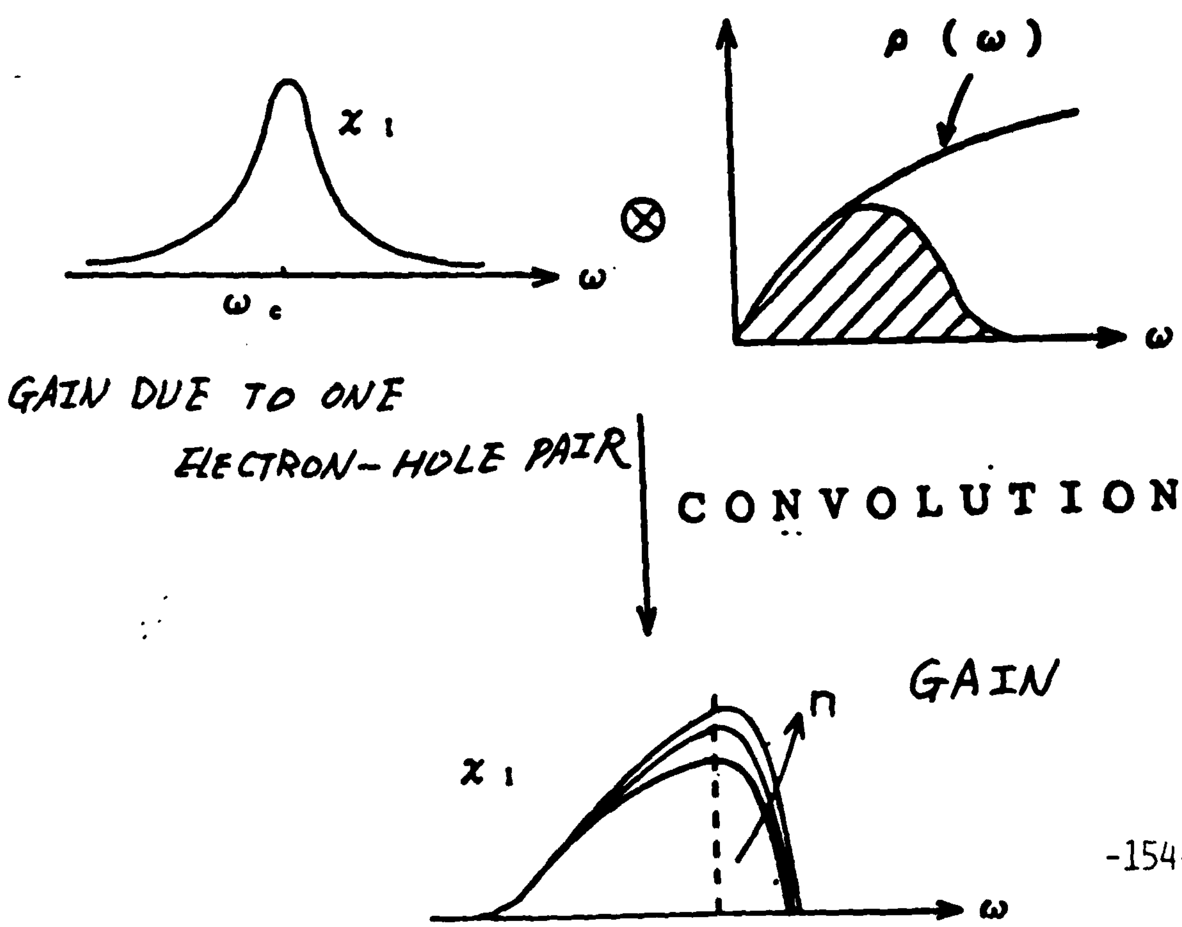

TEMPERATURE DEPENDENCE OF THRESHOLD CURRENT

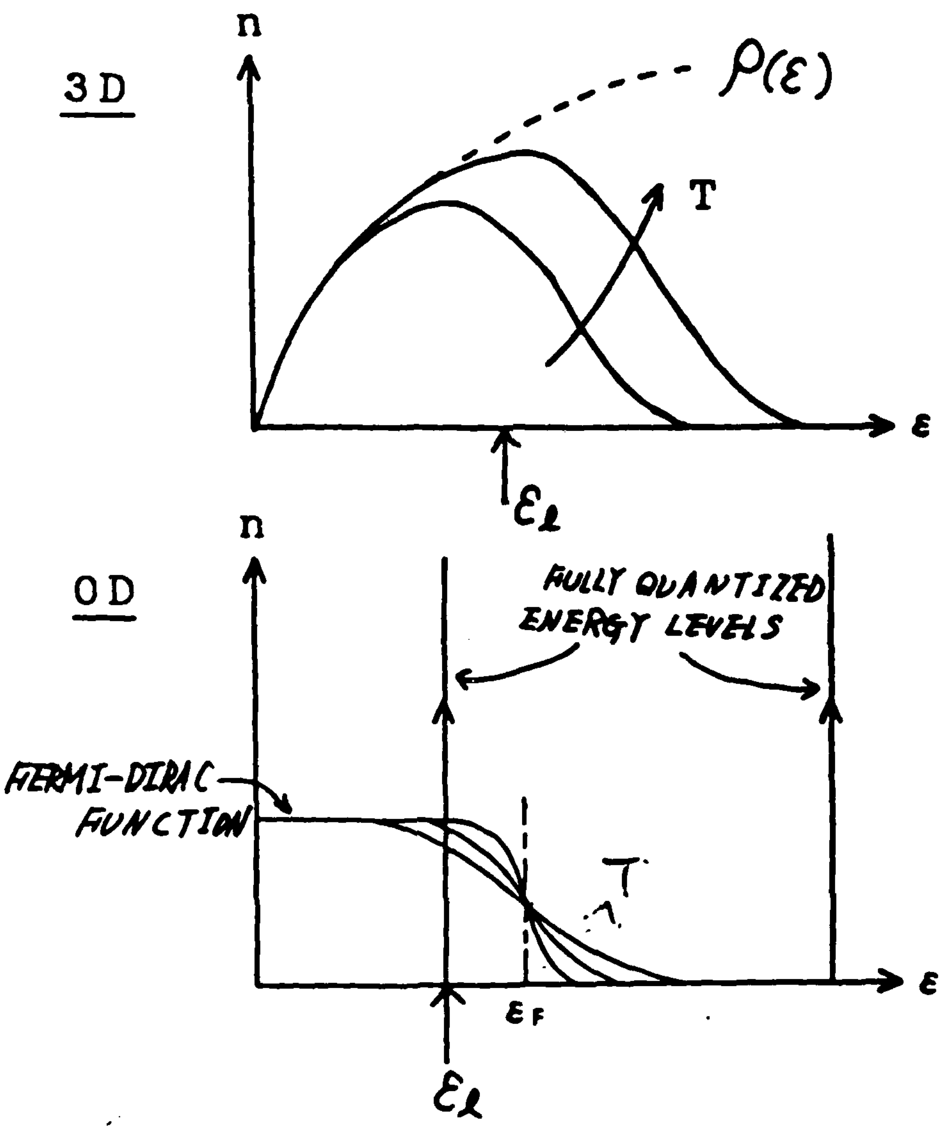

Resonance Frequency f_r

$$\frac{dn}{dt} = \frac{J(t)}{eL_z} - \frac{c}{n_r} g(n)P - \frac{n}{\tau_s}$$

$$\frac{dP}{dt} = \Gamma \frac{c}{n_r} g(n)P + \beta \frac{n}{\tau_s} - \frac{P}{\tau_p}$$

Small Signal Analysis

$$n = n_0 + \Delta n; \quad P = P_0 + \Delta P$$

$$\boxed{f_r = \frac{1}{2\pi}\sqrt{\frac{c}{n_r}\frac{g' P_0}{\tau_p}}}$$

$$g'(n, E) = dg(n, E)/dn$$

$: Differential \quad Gain$

$P_0 : PhotonDensity$

$\tau_p : PhtonLifetime$

$$f_r \uparrow \leftrightarrow \begin{cases} g' \uparrow & \text{Low Temperatu} \\ P_0 \uparrow & \text{Window Type} \\ \tau_p \downarrow & \text{Short Cavity} \end{cases}$$

RELAXATION RESONANT FREQUENCY

$f_r(L) / f_r(L \to \infty)$

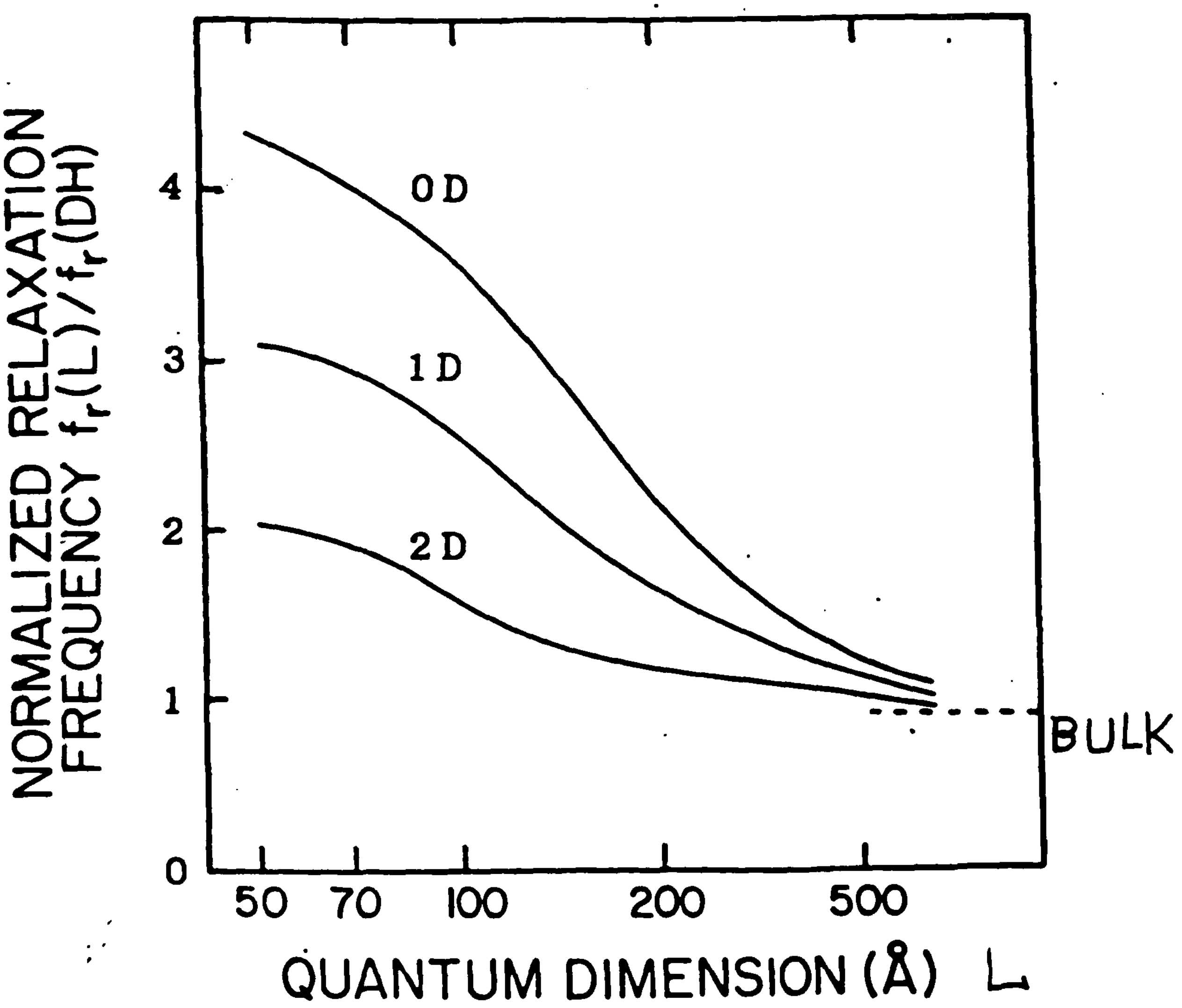

DIFFERENTIAL GAIN

$$g' = \Delta g / \Delta n$$

0D SYSTEM

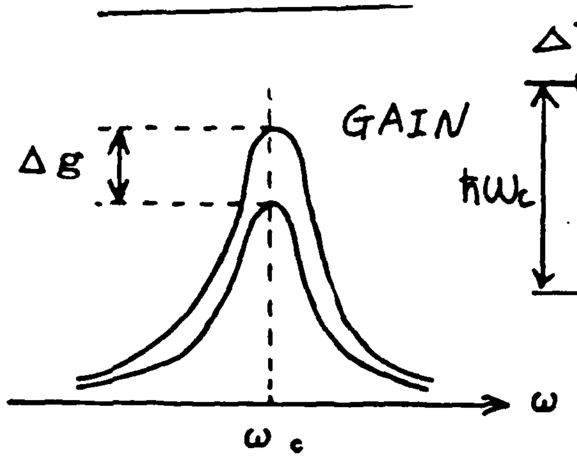

3D SYSTEM

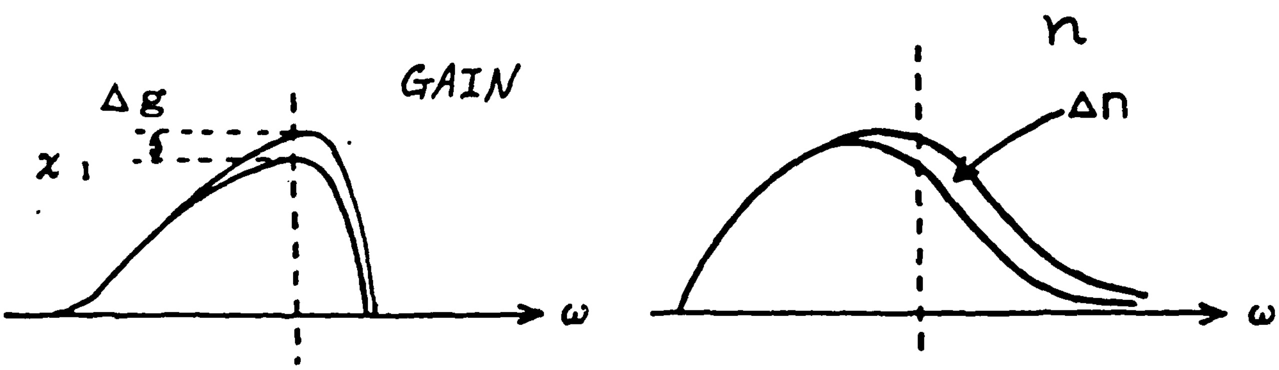

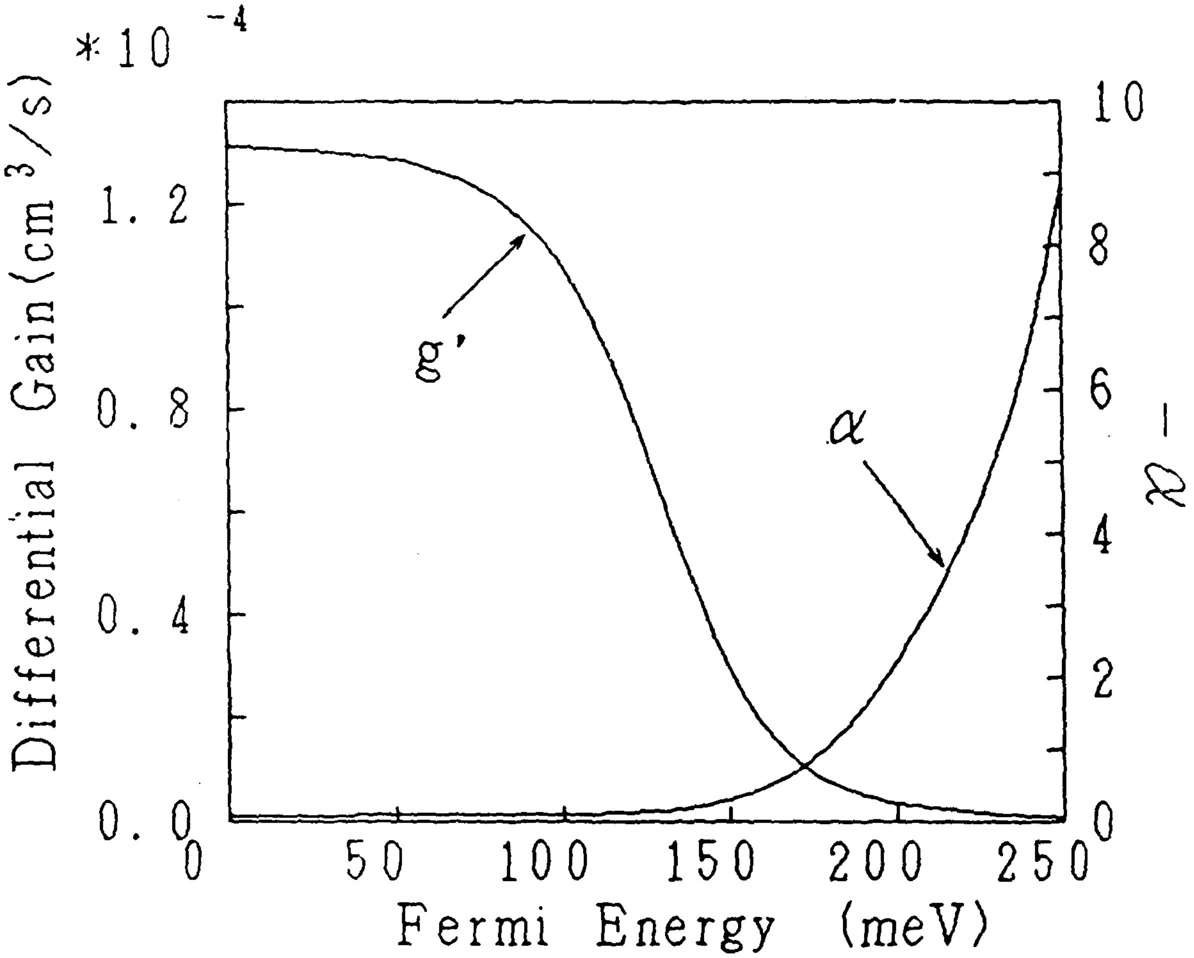

*10 -4
Differential Gain (cm 3/s)
1.2
0.8
0.4
0.0
0
50
100
150
200
250
Fermi Energy (meV)
10
8
6
4
2
0
g'
α

$$\Delta\nu = \Delta\nu_{ST} + \Delta\nu_{AF}$$

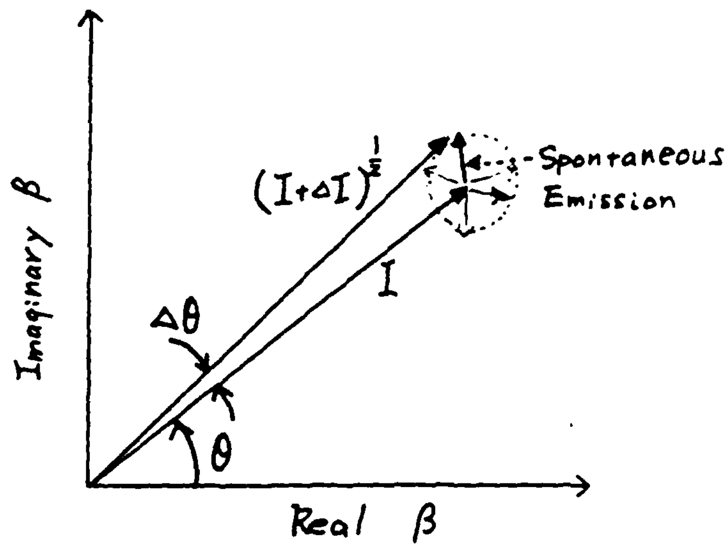

$\Delta\nu_{ST}$: Shawlow-Townes Linewidth

Spontaneous Emission $\rightarrow \Delta\theta \rightarrow \Delta\nu_{ST} \propto 1/I$

$\Delta\nu_{AF}$: Phase Noise due to AM/FM Coupling

Spontaneous Emission $\rightarrow \Delta I \rightarrow \Delta n \rightarrow \Delta n_r$

$\rightarrow \Delta\theta_{AF} \rightarrow \Delta\nu_{AF}$

$$\Delta\nu_{AF} = \alpha^2 \Delta\nu_{ST} ; \quad \alpha = \frac{d\chi_R/dn}{d\chi_I/dn} ; \quad \chi = \chi_R + i\chi_I$$

$$\boxed{\Delta\nu = (1+\alpha^2)\Delta\nu_{ST}}$$

χ depends on ρ

$\rightarrow$ α is improved by the use of quantum well and quantum wire structures

LINEWIDTH ENHANCEMENT FACTOR

$|\alpha|$

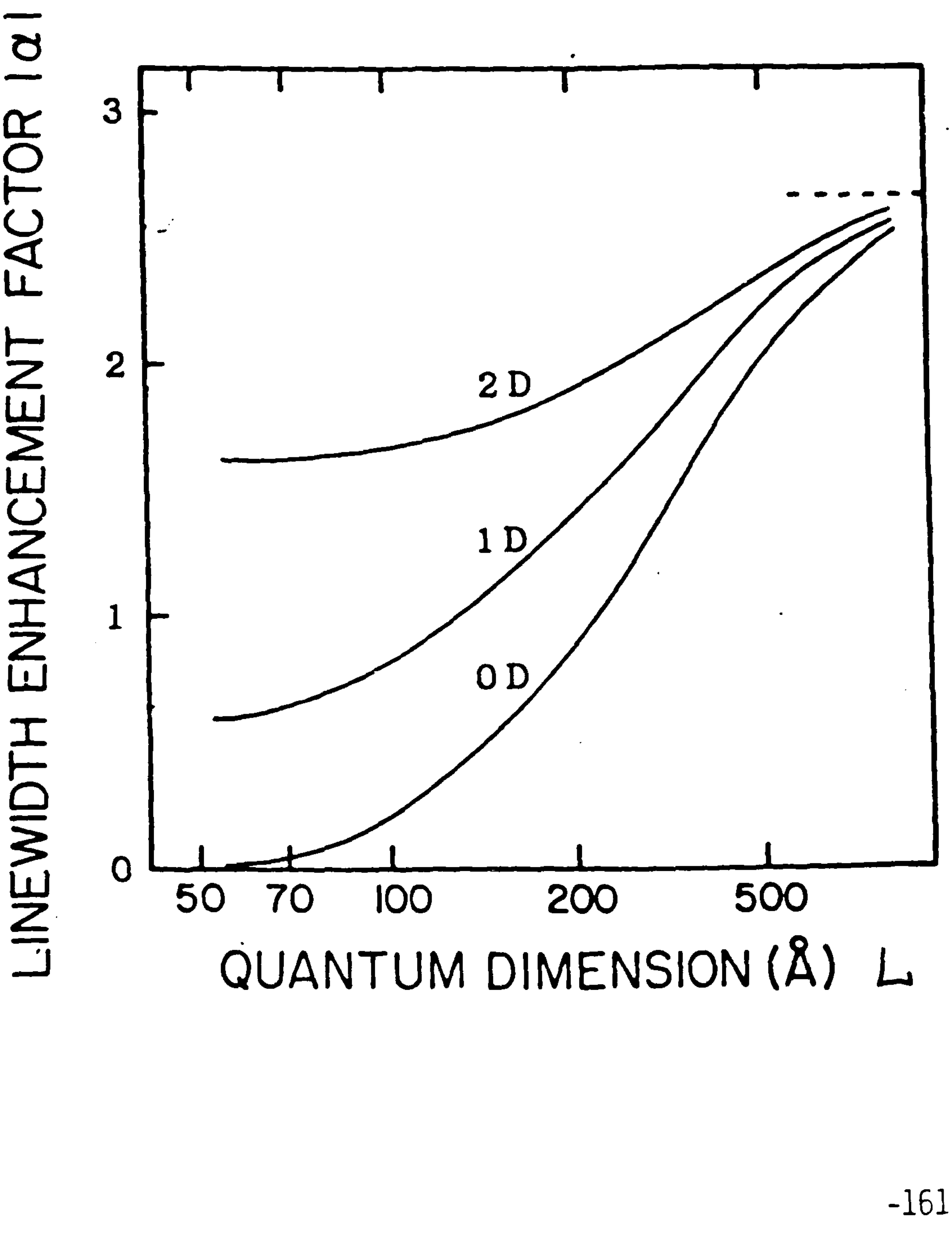

OD SYSTEM

$$\chi = \chi_R + j\,\chi_I$$

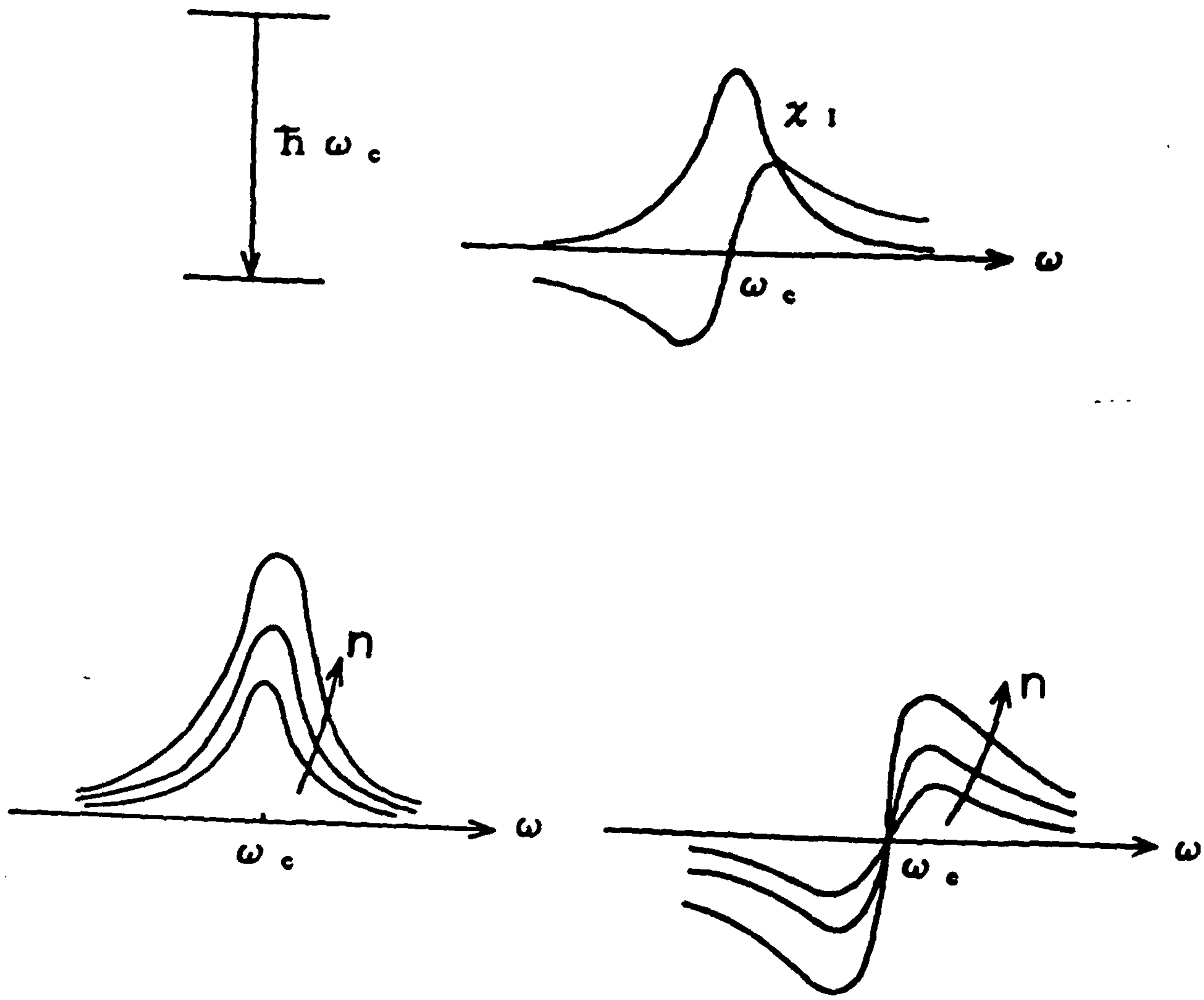

3D SYSTEM

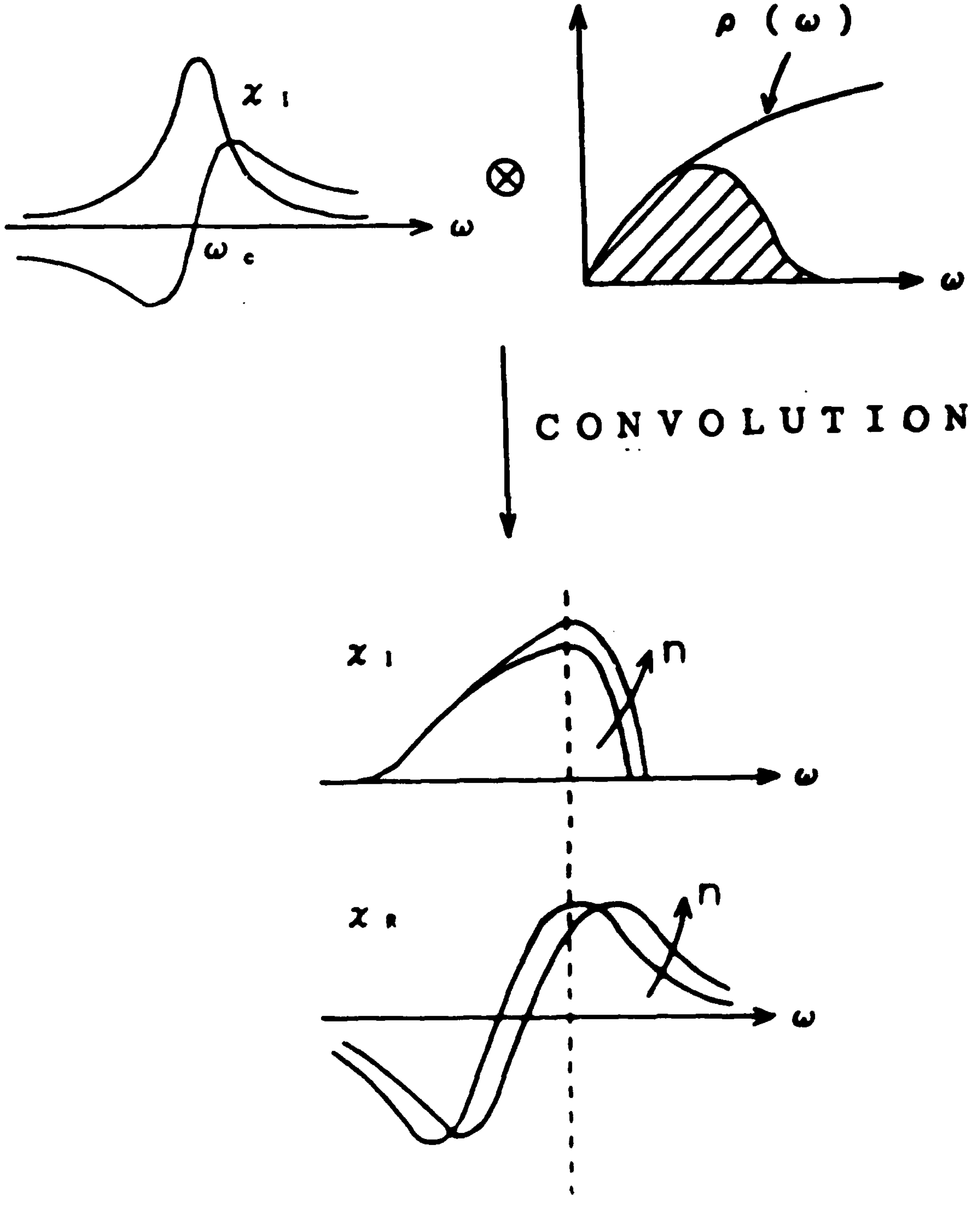

χ_I
ω
ω_c
$\rho(\omega)$
ω
CONVOLUTION
χ_I
n
ω
χ_R
n
ω

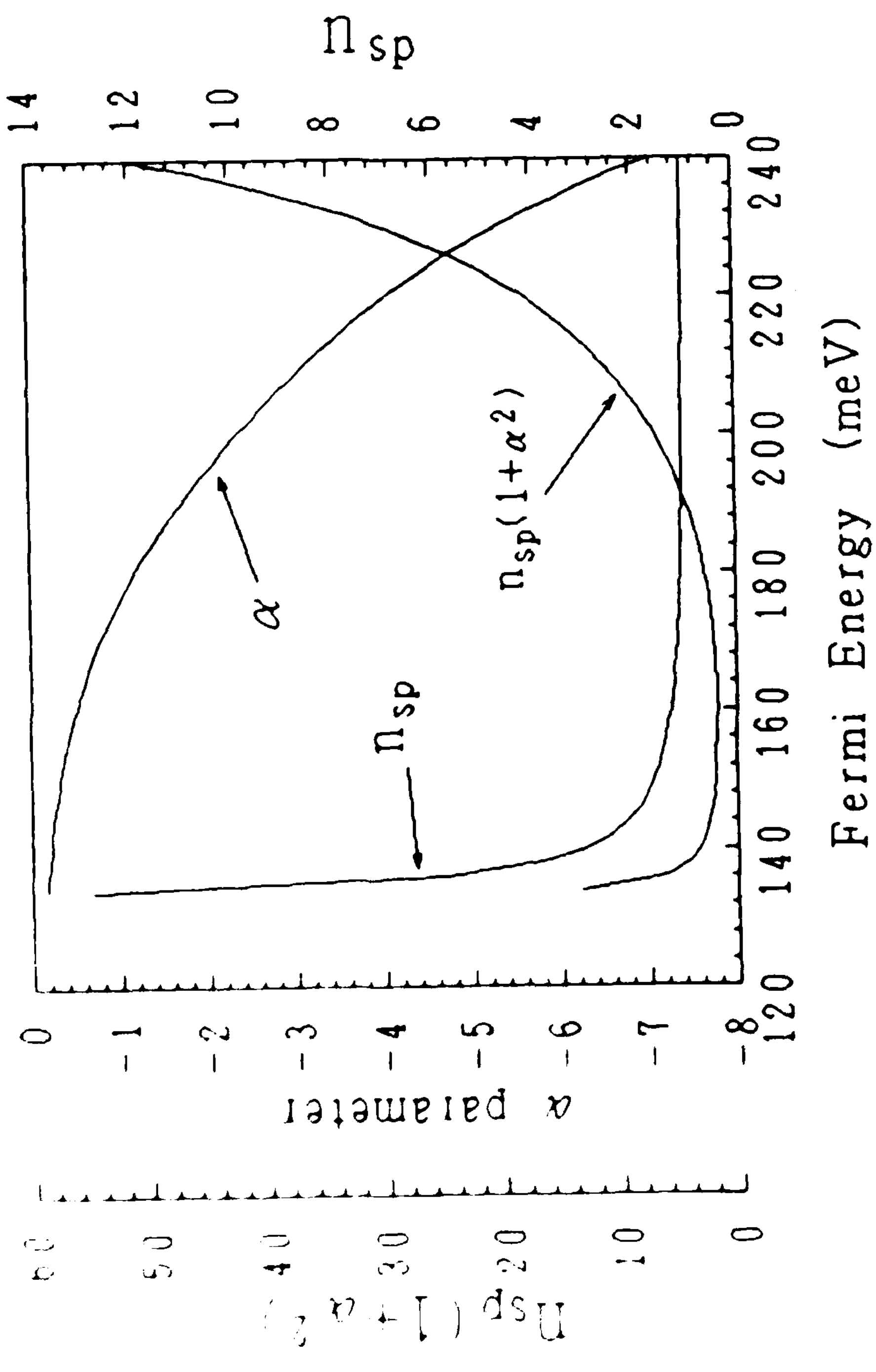

n sp
α
n sp(1+α²)
Fermi Energy (meV)
α parameter
n sp (1+α²)

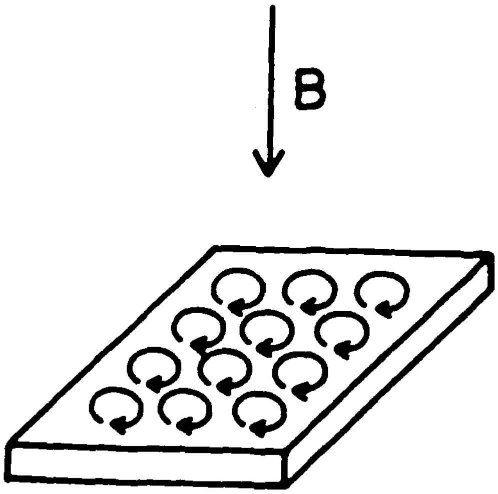

B ⊥ QW plane

$2D - 2D = 0D$

QW EFFECT

MAGNETIC FIELD

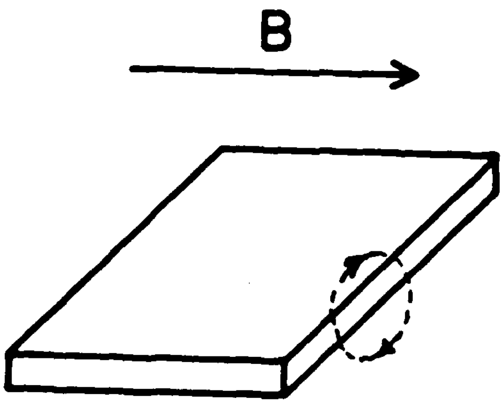

$2D$

B // QW plane

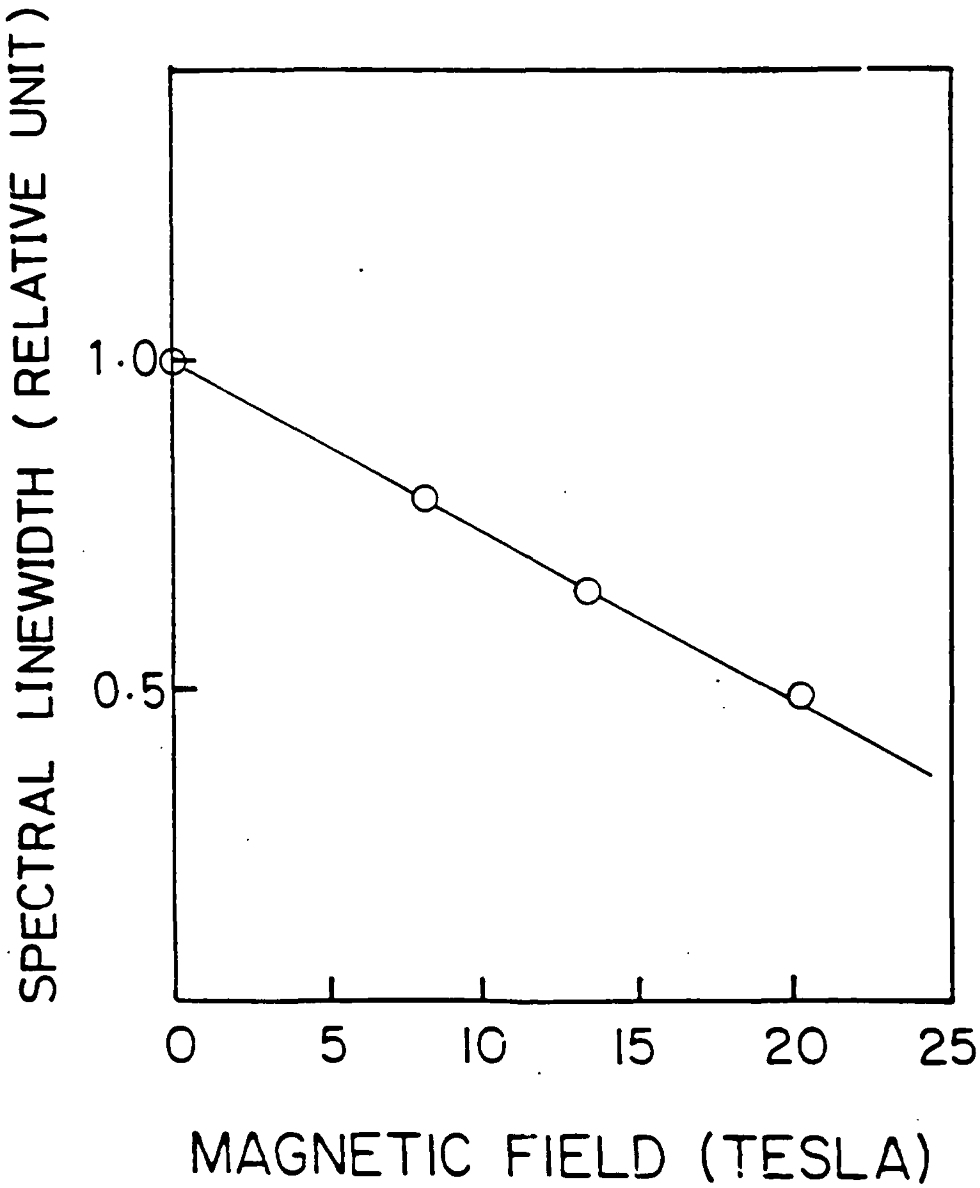
SPECTRAL LINEWIDTH (RELATIVE UNIT)
1.0
0.5
0
5
10
15
20
25
MAGNETIC FIELD (TESLA)

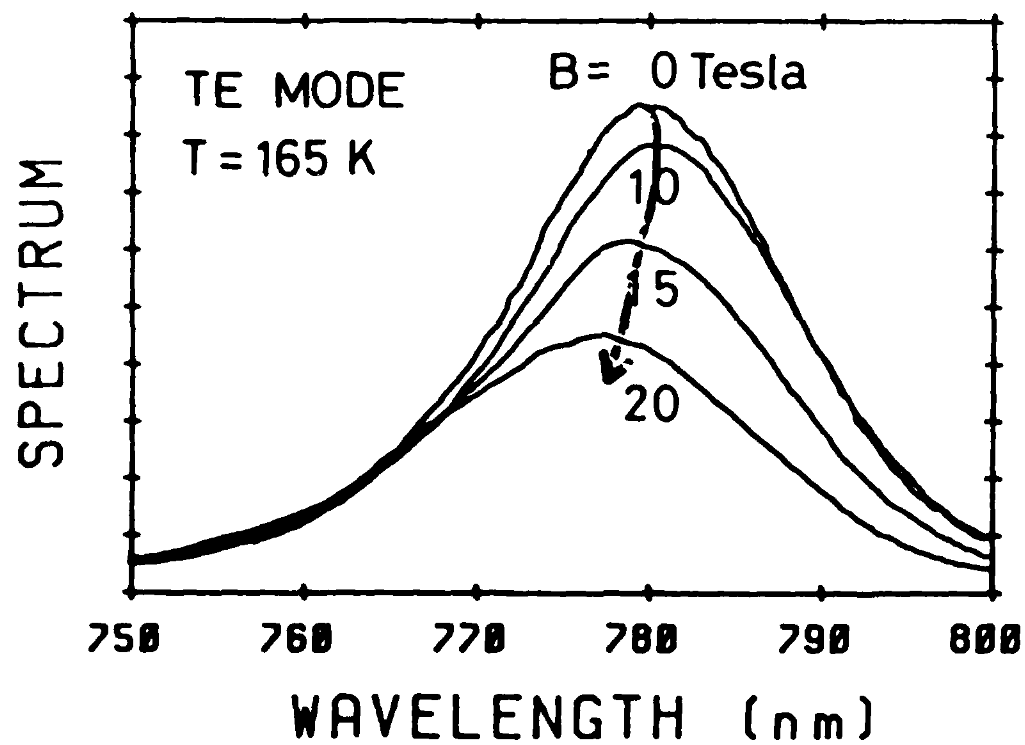
TE MODE
T = 165 K
B = 0 Tesla
10
15
20
SPECTRUM
750
760
770
780
790
800
WAVELENGTH (nm)

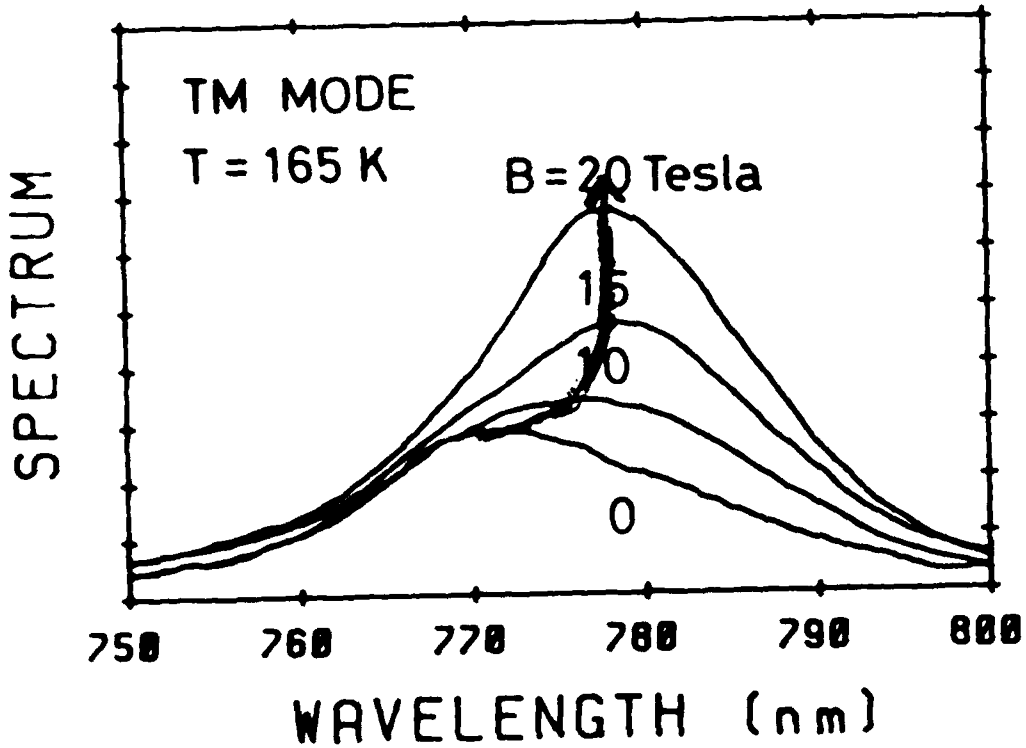
TM MODE
T = 165 K
B = 20 Tesla
15
10
0
SPECTRUM
750
760
770
780
790
800
WAVELENGTH (nm)

SUMMARY

1. BASIC PROPERTIES OF ELECTRONS IN QUANTUM-WIRE (1D) STRUCTURES AND QUANTUM-BOX (0D) STRUCTURES

2. MODULATION DYNAMICS

   $4 \times f_R$(QUANTUM-BOX) $3 \times f_R$(QUANTUM-WIRE)

3. FIELD SPECTRAL PROPERTIES

   $\alpha \sim 0$(QUANTUM-BOX) $\alpha \sim 0.8$(QUANTUM-WIRE)

4. EXPERIMENTAL DEMONSTRATION USING HIGH MAGNETIC FIELD

   B~20TESLA

   SIGNIFICANT IMPROVEMENTS IN MODULATION DYNAMICS AND SPECTRAL PROPERTIES ARE OBSERVED

PICOSECOND PULSE GENERATION IN QUANTUM WELL LASERS

GAIN SWITCHING METHOD

PULSE CURRENT INJECTION
MATRIX ELEMNT MODULATION

MODE LOCKING METHOD

ACTIVE
PASSIVE

Q-SWITCHING METHOD

ACTIVE
PASSIVE

IN THIS TALK

ACTIVE Q-SWITCHING IN MULTI-QUANTUM WELL LASERS WITH INTRACAVITY MONOLITHIC LOSS MODULATOR (18.6psec)

GAIN SWITCING IN MULTI-QUANTUM WELL LASERS (1.8psec)

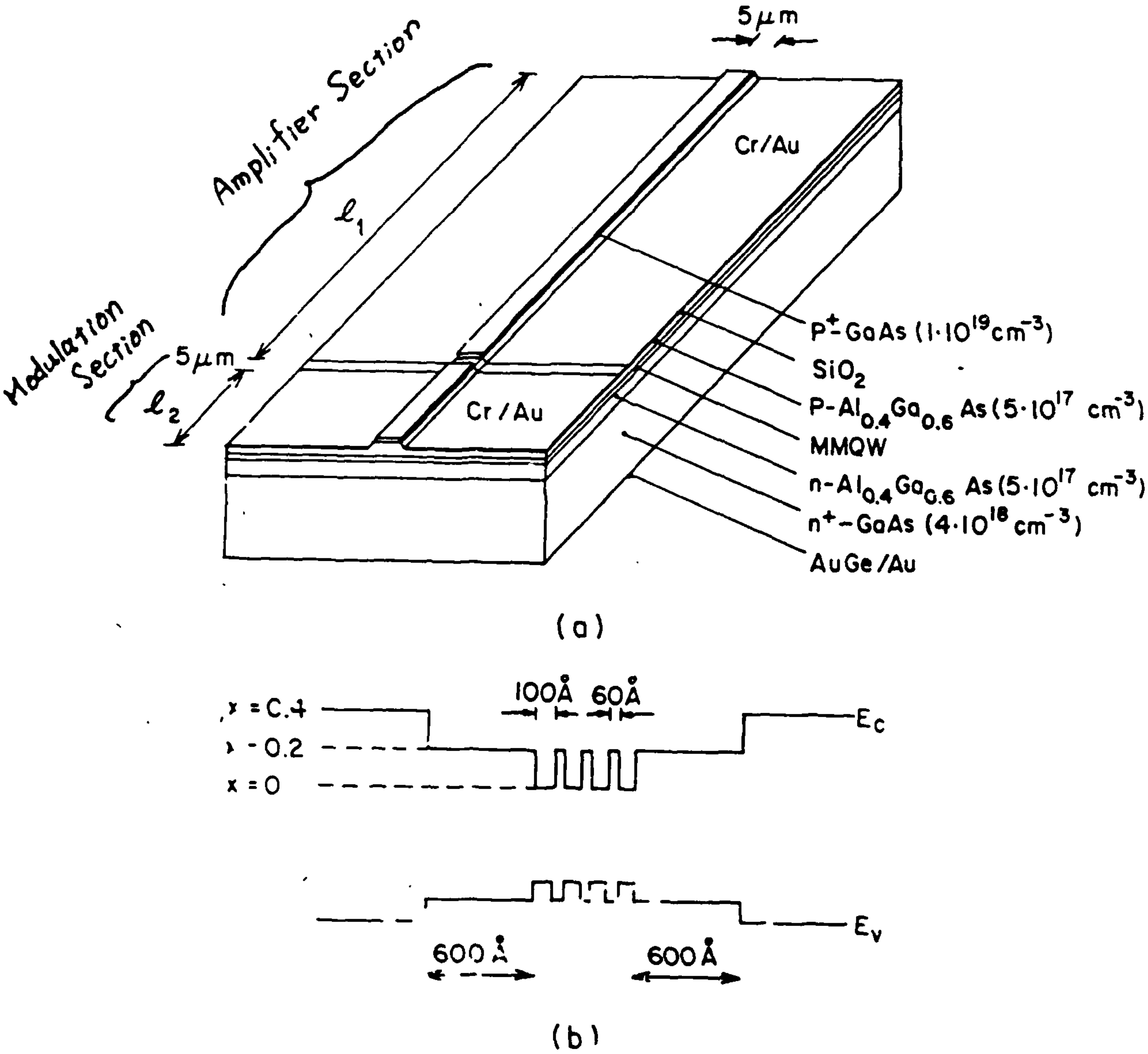

5μm
Amplifier Section
Cr/Au
ℓ_1
Modulation Section
5μm
ℓ_2
Cr / Au
P+-GaAs (1·10^19 cm^-3)
SiO2
P-Al0.4Ga0.6 As (5·10^17 cm^-3)
MMQW
n-Al0.4Ga0.6 As (5·10^17 cm^-3)
n+-GaAs (4·10^18 cm^-3)
AuGe/Au
(a)
100Å
60Å
x = 0.4
x = 0.2
x = 0
Ec
Ev
600 Å
600 Å
(b)

ENHANCED BAND SHRINKAGE EFFECTS

QUANTUM CONFINED STARK EFFECTS

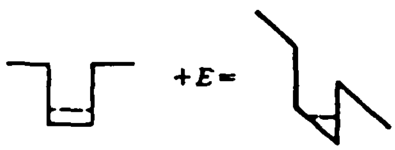
+E=

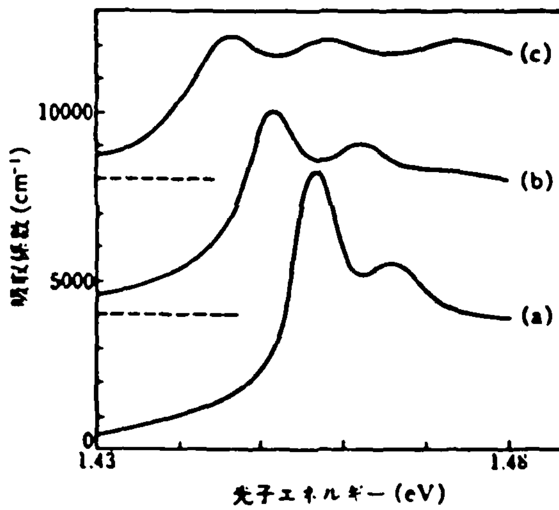
10000
5000
0
(c)
(b)
(a)
1.43
1.48
吸収係数 (cm⁻¹)
光子エネルギー (eV)

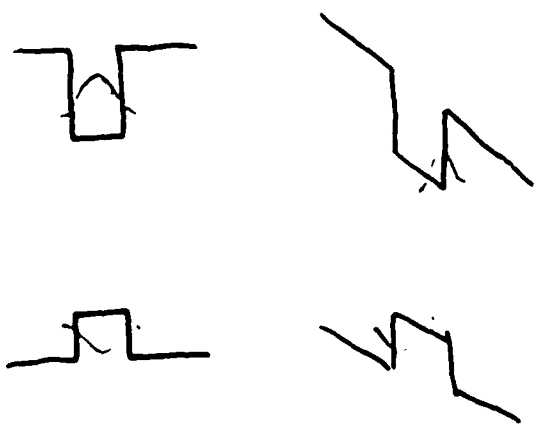

Without Electric Field

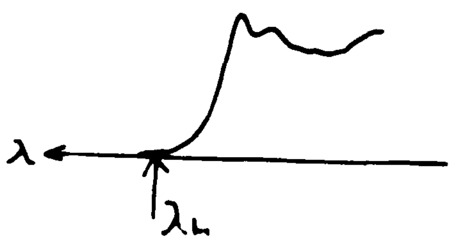

With Electric Field

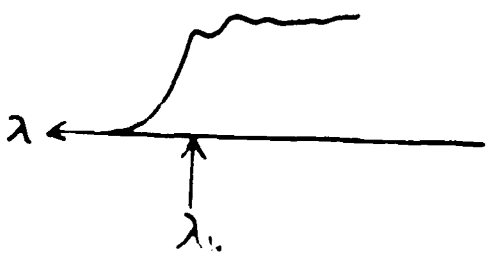

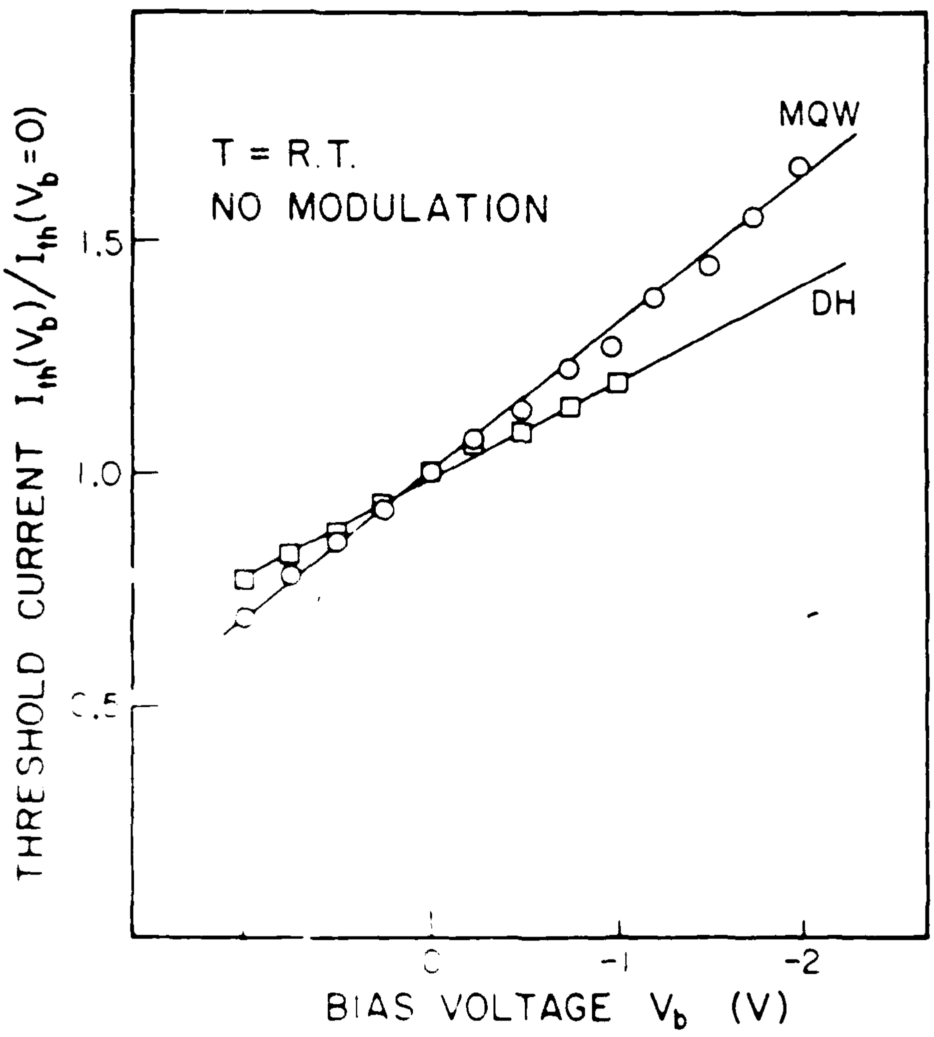
T = R.T.
NO MODULATION
MQW
DH
1.5
1.0
0.5
0
-1
-2
THRESHOLD CURRENT $I_{th}(V_b)/I_{th}(V_b=0)$
BIAS VOLTAGE V_b (V)

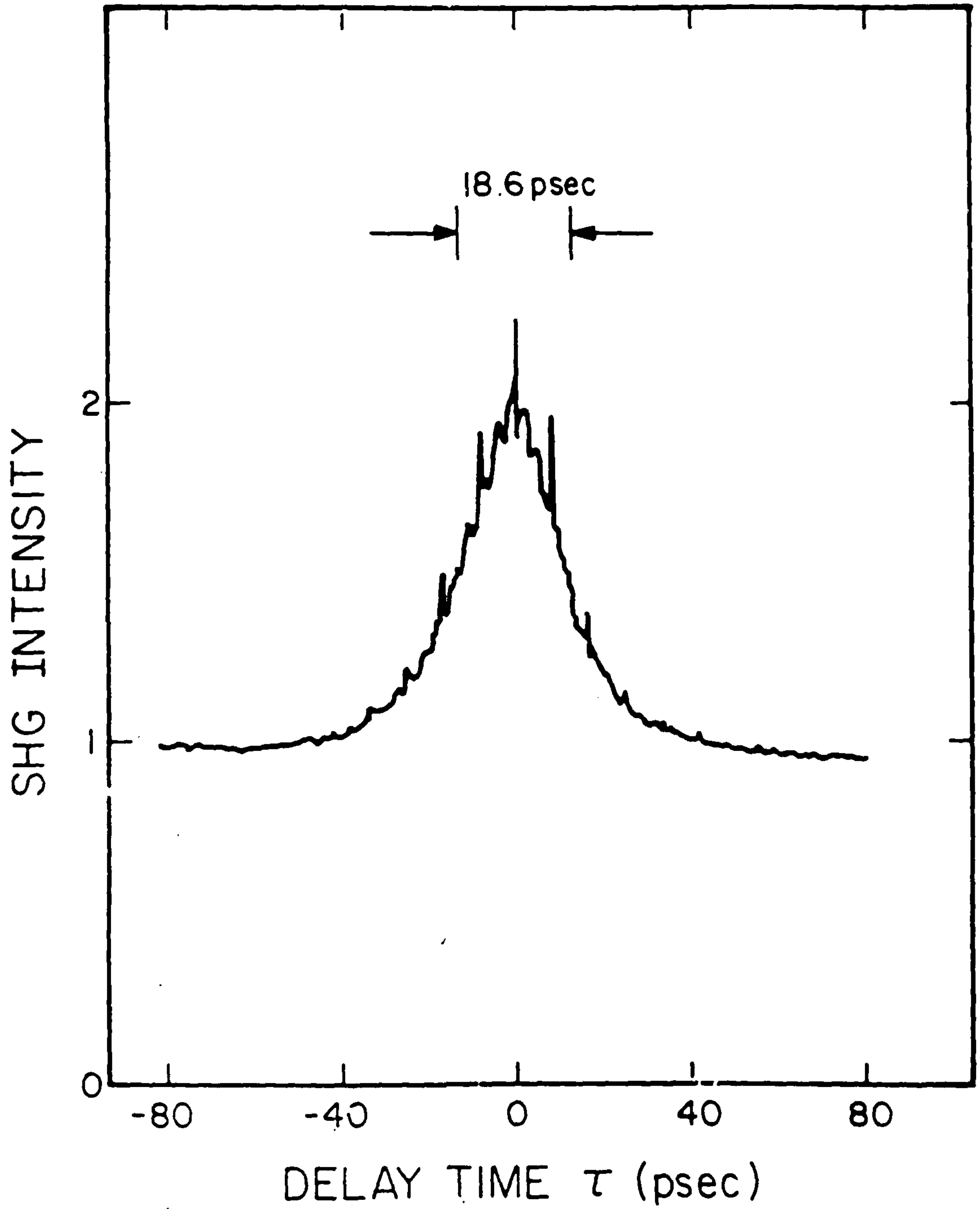

18.6 psec
SHG INTENSITY
2
1
0
-80
-40
0
40
80
DELAY TIME τ (psec)

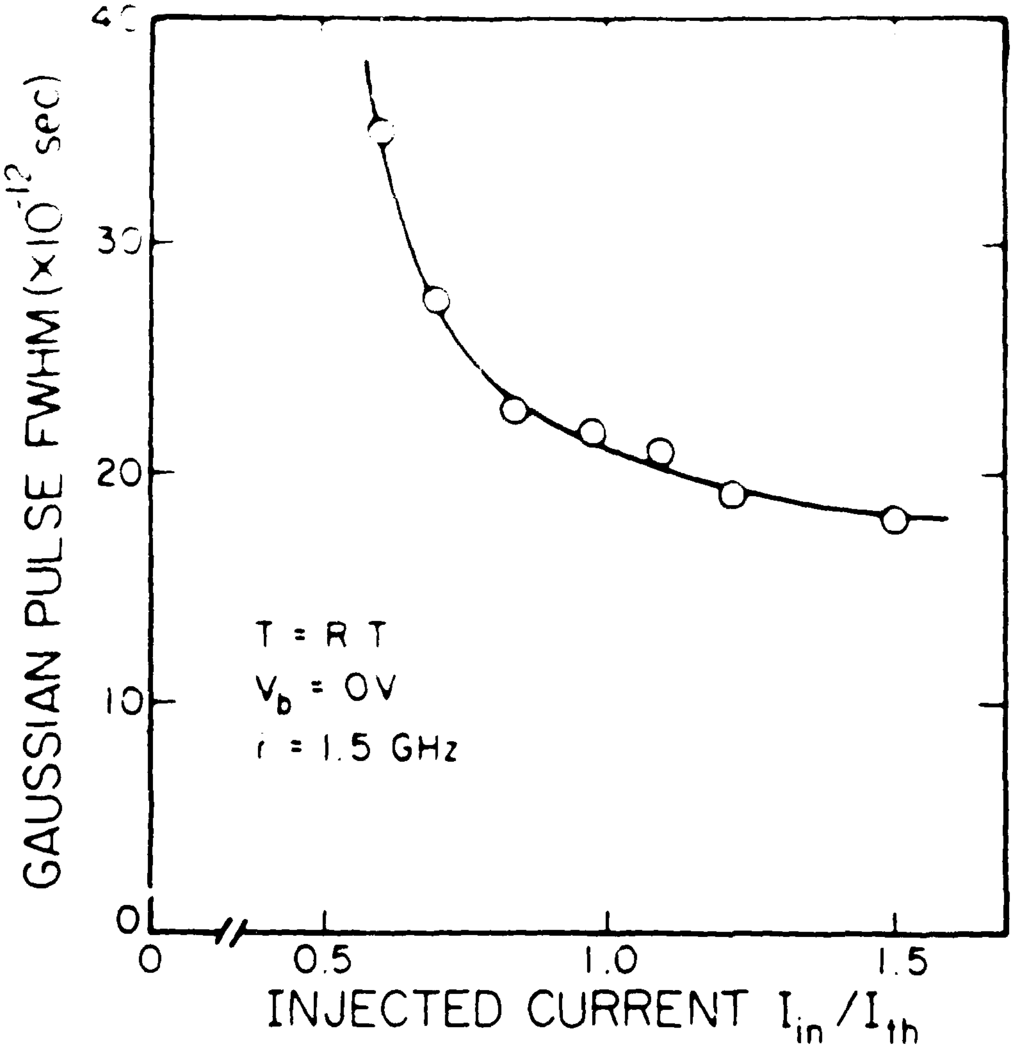
GAUSSIAN PULSE FWHM (×10⁻¹² sec)
T = R T
V_b = 0V
f = 1.5 GHz
0
10
20
30
40
0
0.5
1.0
1.5
INJECTED CURRENT I_{in}/I_{th}

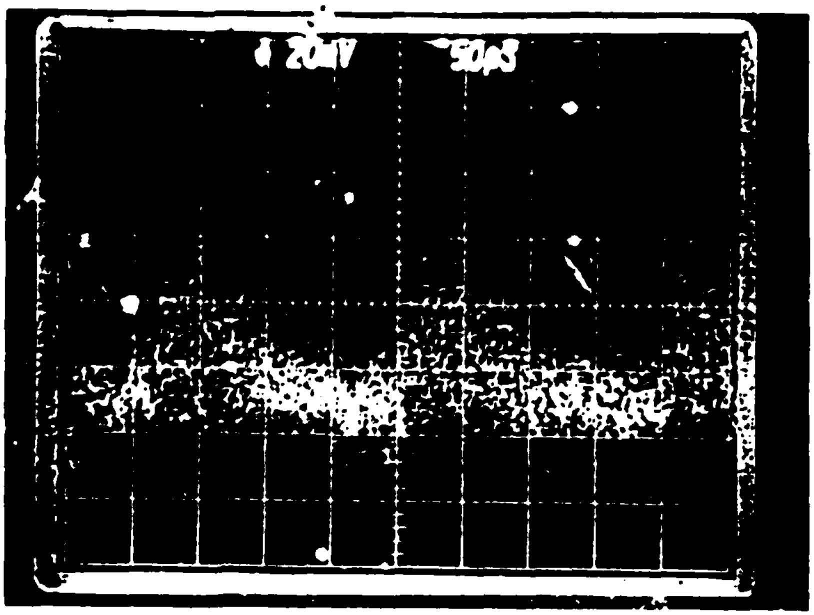
20mV
50μS

GAIN SWITCHING IN QUANTUM WELL LASERS

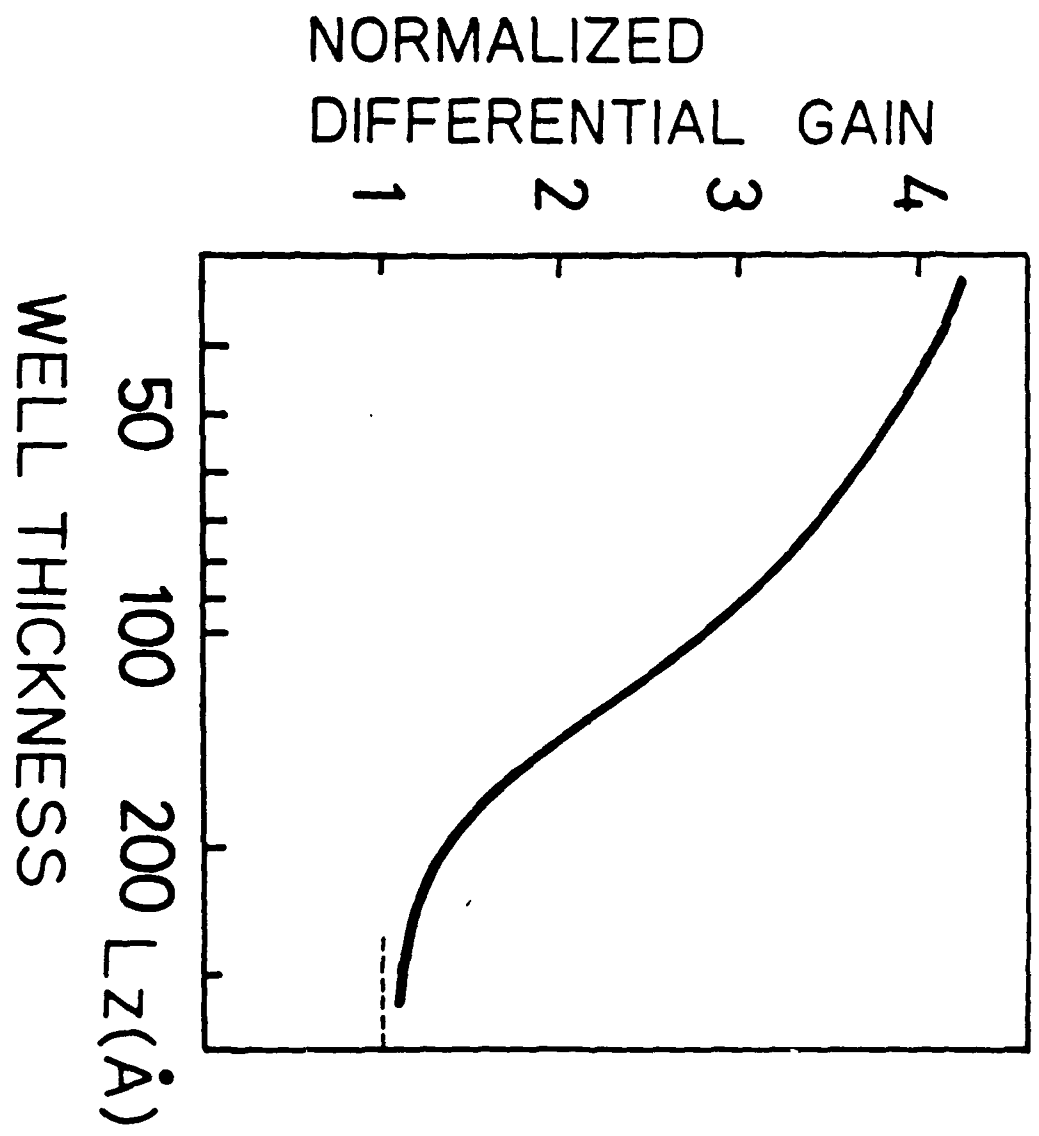

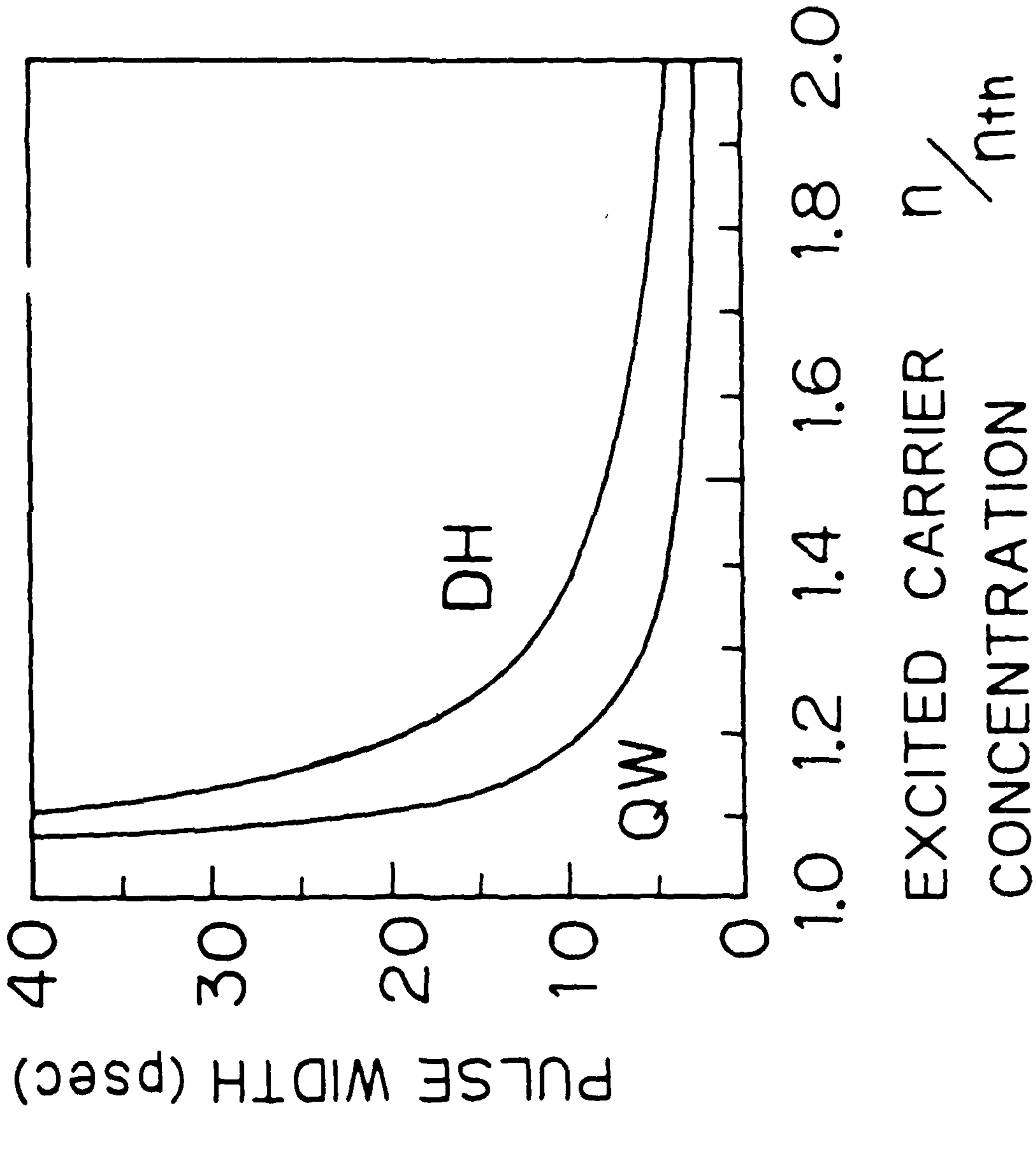
PULSE WIDTH (psec)
40
30
20
10
0
1.0
1.2
1.4
1.6
1.8
2.0
EXCITED CARRIER CONCENTRATION n/n_{th}
DH
QW

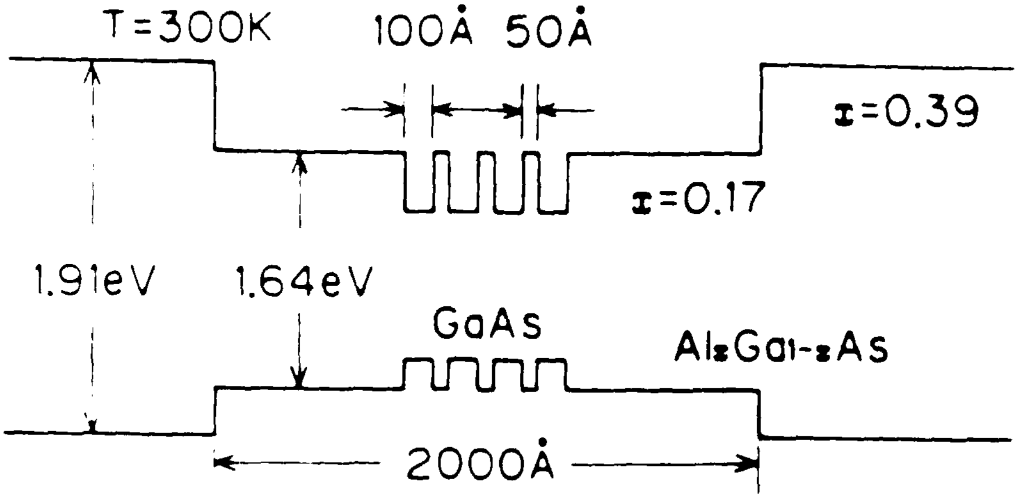
T=300K
100Å
50Å
x=0.39
x=0.17
1.91eV
1.64eV
GaAs
AlxGa1-xAs
2000Å

(a)

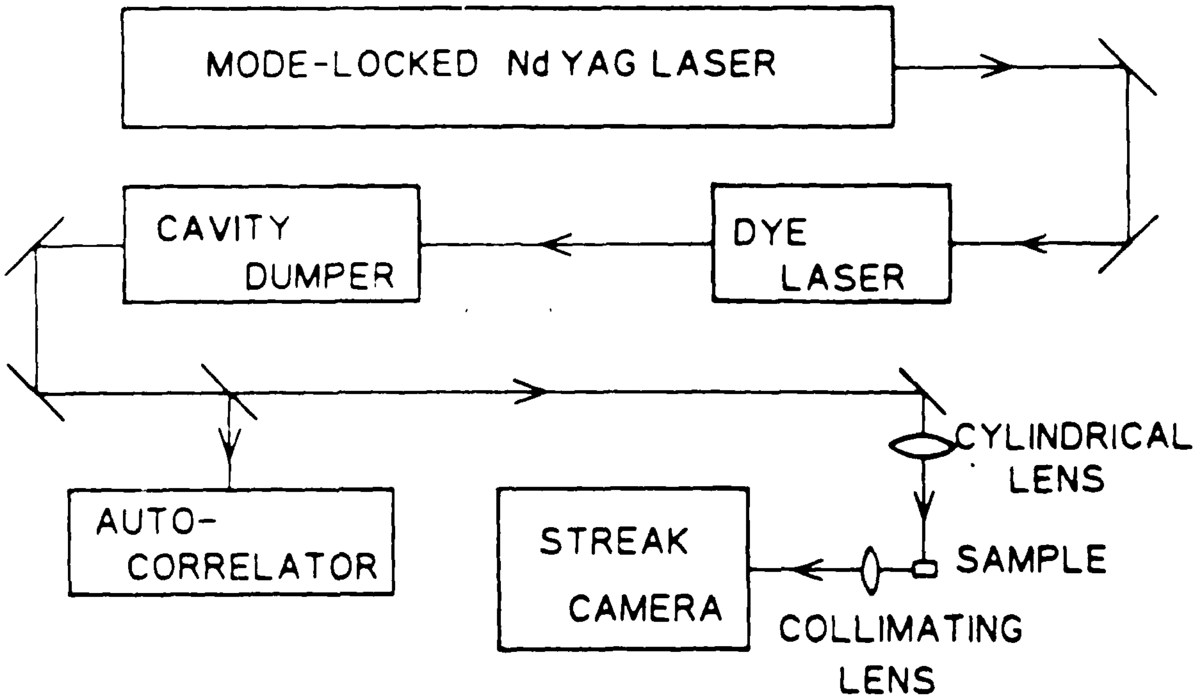
MODE-LOCKED Nd YAG LASER
CAVITY DUMPER
DYE LASER
CYLINDRICAL LENS
AUTO-CORRELATOR
STREAK CAMERA
SAMPLE
COLLIMATING LENS

(b)

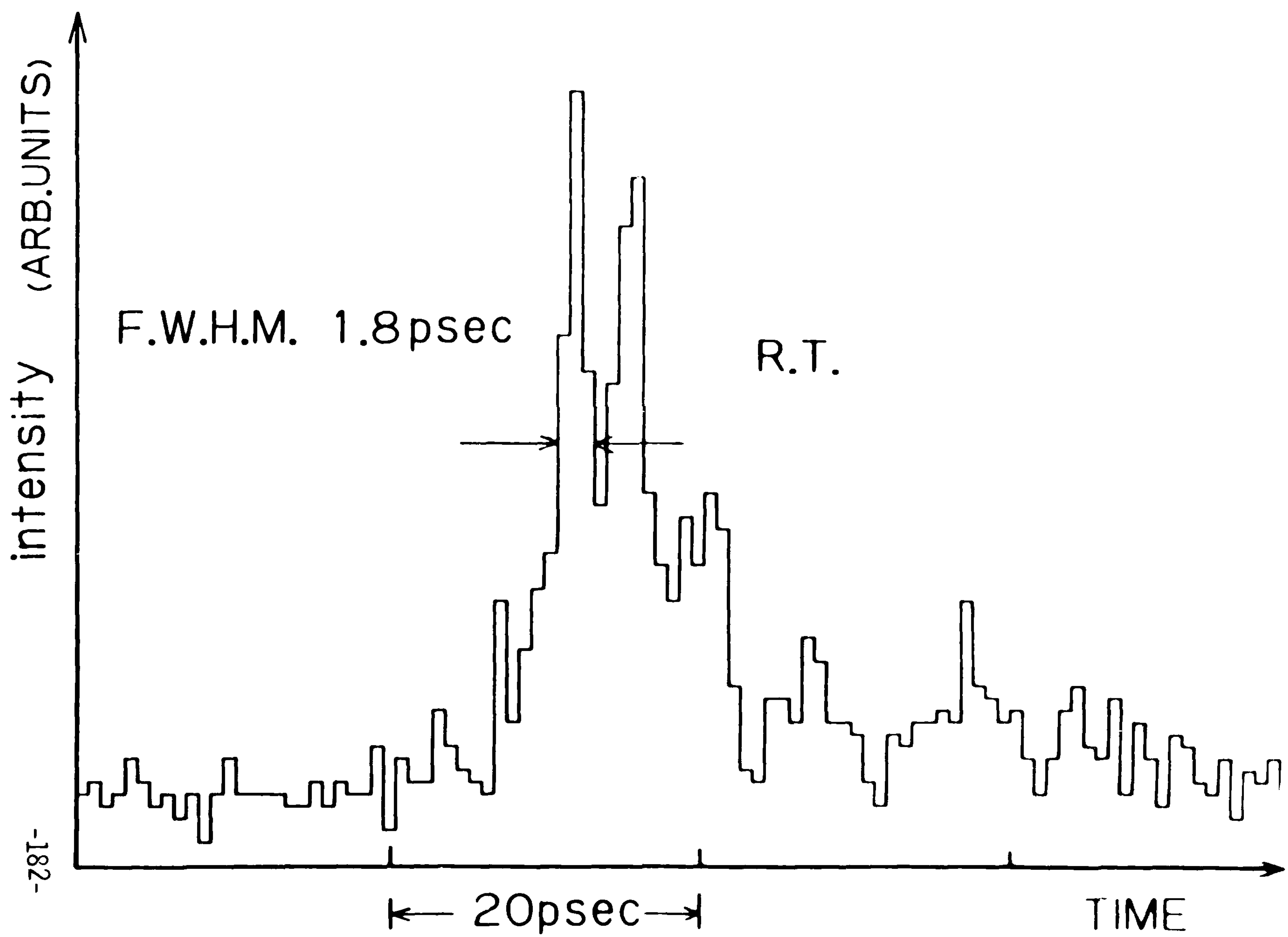
intensity (ARB.UNITS)
F.W.H.M. 1.8psec
R.T.
20psec
TIME

[illegible] Semi[illegible] Lasers
[illegible] Rb Atomic [illegible]

[illegible]*, K. K[illegible] and M. Hashimoto

[illegible] Institute of Technology
[illegible] Yokohama, Kanagawa 227 Japan

*Present [illegible] AT&T Bell Laboratories
[illegible] NJ 07733 USA

ABSTRACT

We [illegible] FM noise in semiconductor lasers can be reduced to a value lower than the quantum noise limit by using negative electrical feedback. A synthesized method of [illegible] feedback (Fig 1) is proposed to realize such ultrahigh temporal coherence of semiconductor lasers. The center frequency fluctuations of the field spectrum are reduced as low as $2\times10^{-[illegible]}$ by this feedback. The linewidth of the field spectrum is reduced to 100 kHz, which is narrower than the value given by the quantum noise limit of the free-running laser (Fig 2). Optical phase-locked loop realizes a frequency tracking accuracy of 3×10^{-4}, capture range of 1.2 GHz, and locking range of 5.3 GHz.

As an alternative scheme to realize ultrahigh coherence in semiconductor lasers, we present a novel experimental method for accurate frequency tracking using the correlated spontaneous emission between the two longitudinal modes (1,2). We employ a method of resonant coupling between the two optical transitions via optical sidebands produced by parametric modulation of the laser gain. By this modulation, the linewidth of the heterodyned signal was reduced to 25 kHz (Fig 3). (The minimum of the linewidth obtained is limited by resolution of our linewidth measurement system.) This value corresponds to suppression of the relative phase noise between the two modes to less than one-twentieth of the quantum noise limit of the free-running laser.

As an application of these ultrahigh coherent lasers, we have used them as optical pumping sources for Rb atomic clock of 6.8 GHz frequency. A novel optical-microwave double resonance spectral shape with the linewidth as narrow as 20 Hz is demonstrated by utilizing FM sidebands of the laser induced by nonlinear susceptibility of the three-level Rb atoms (Fig 4). Theoretical analysis shows that by optimizing the modulation parameters one can realize ultra-sensitive microwave frequency discrimination, which is about 7500 times more sensitive than a conventional Rb atomic clocks.

REFERENCES

(1) M. O. Scully, Phys. Rev. Lett. 55, 2802 (1980)

(2) P. E. Toschek and J. L. Hall, Technical Digest of 15th International Quantum Electronics Conference, April 1987, Baltimore, WDD2

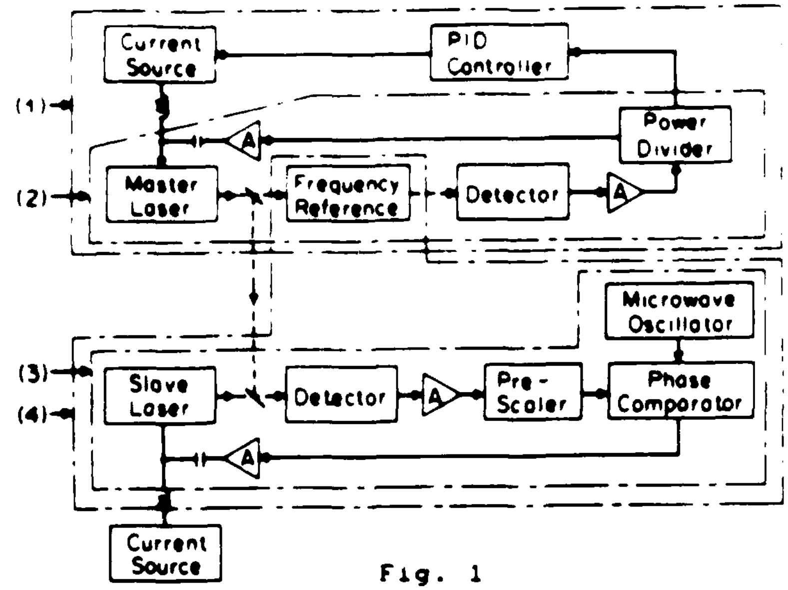

Fig. 1

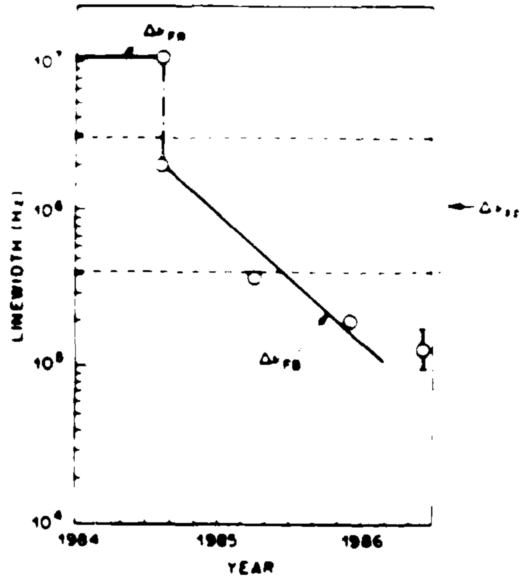

Fig. 2

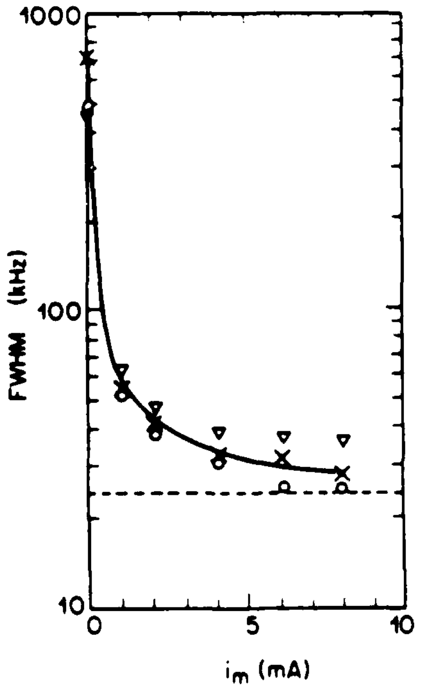

Fig. 3

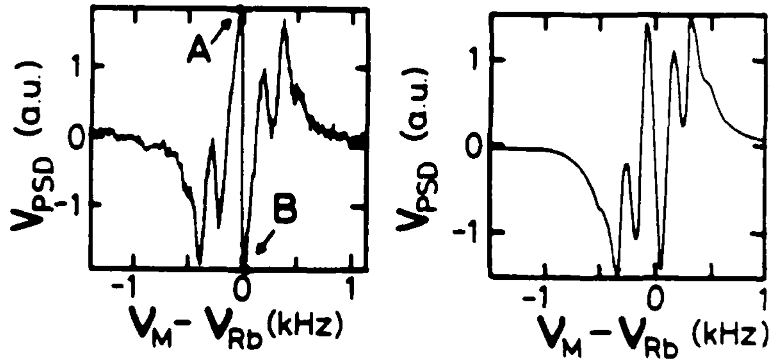

Experimental Theoretical

Fig. 4

Ultrahigh Coherent Semiconductor Lasers, and Their Application to Rubidium Atomic Clock

M. OHTSU*, K. KUBOKI, & M. HASHIMOTO

Tokyo Institute of Technology

* Presently, AT&T Bell Laboratories
Crawford Hill Laboratory

(1) Reduction of FM noise to a value lower than quantum noise limit by

(a) negative electrical feedback

(b) correlated spontaneous emission

(2) Application to optical pumping of a Rb atomic clock

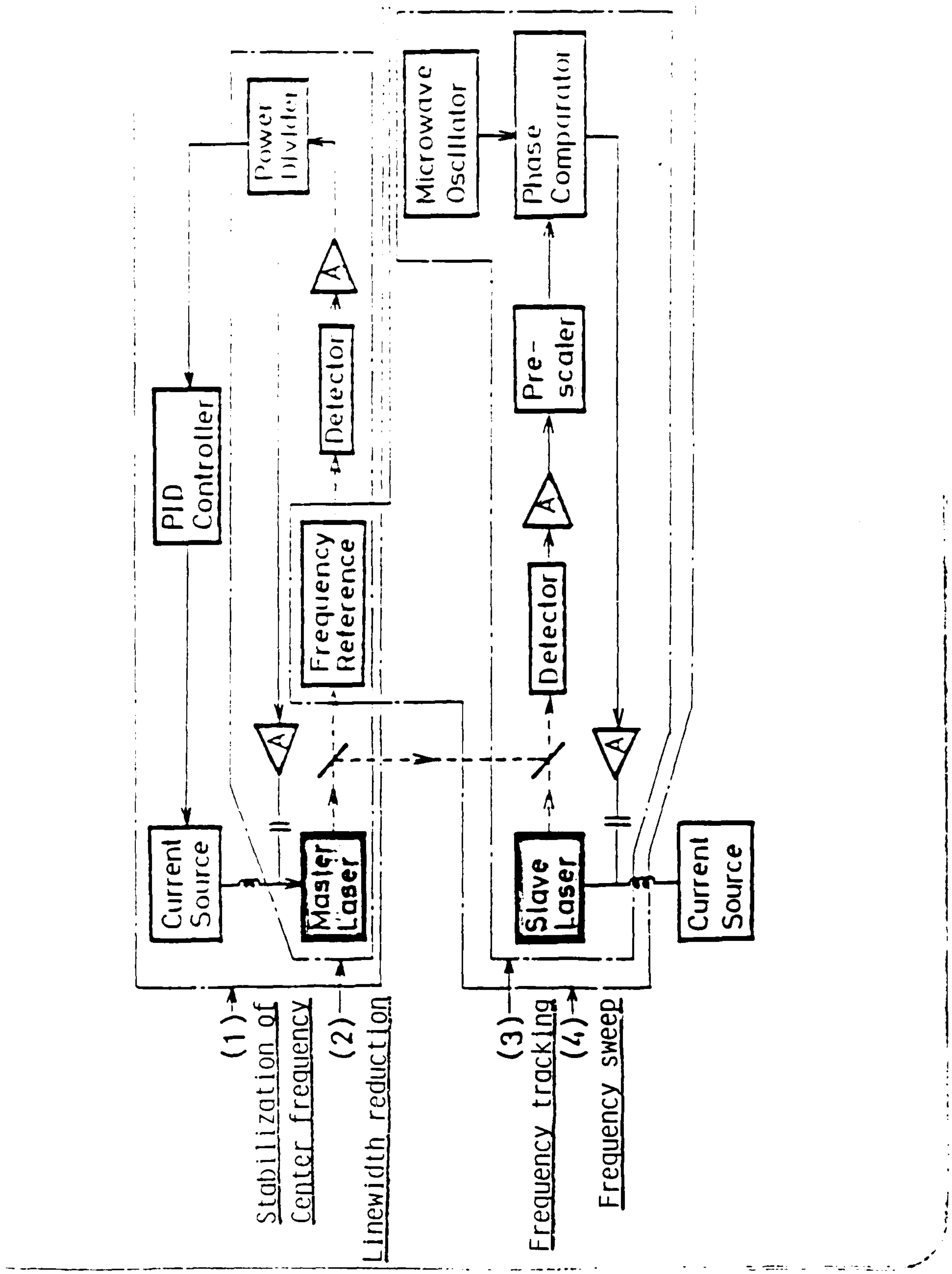
PID Controller
Power Divider
Current Source
Master Laser
Frequency Reference
Detector
A
Microwave Oscillator
Phase Comparator
Pre-scaler
Detector
A
Slave Laser
Current Source
(1) Stabilization of Center frequency
(2) Linewidth reduction
(3) Frequency tracking
(4) Frequency sweep

[Assumptions]

(1) Quantum FM noise can be measured by classical electro-optical techniques.

(2) Frequency can be countermodulated by modulating a macroscopic quantity.

(3) Infinite Feedback Bandwidth

[Y. Yamamoto, et. al.: IEEE J. Quantum Electron., QE-21 (1985) p.1919]

spontaneous emission

carrier

$$\delta\nu(t) = \frac{1}{2\pi}\frac{d}{dt}(\delta\phi) = \Gamma_s(t) + \Gamma_c(t) \quad (\alpha\text{-parameter})$$

$$- \int_0^\infty h_f(\tau)\,[\,\delta\nu(t-\tau) + \Gamma_n(t-\tau)\,]\,d\tau$$

inpulse response

noise in feedback loop

Fourier transform

$$F(f) = \frac{W_s(f)}{1 + H(f)} + \frac{W_c(f)}{1 + H(f)} - \frac{H(f)}{1 + H(f)} W_n(f)$$

$$(\ |H| \rightarrow \infty\ ) \qquad \underline{0} \qquad \underline{0} \qquad \underline{W_n(f)}$$

Real quantities		Fourier transform
$\delta\nu(t)$	$\longrightarrow$	$F(f)$
$h_f(t)$	$\longrightarrow$	$H(f)$
$\Gamma_i(t)$	$\longrightarrow$	$W_i(f)$

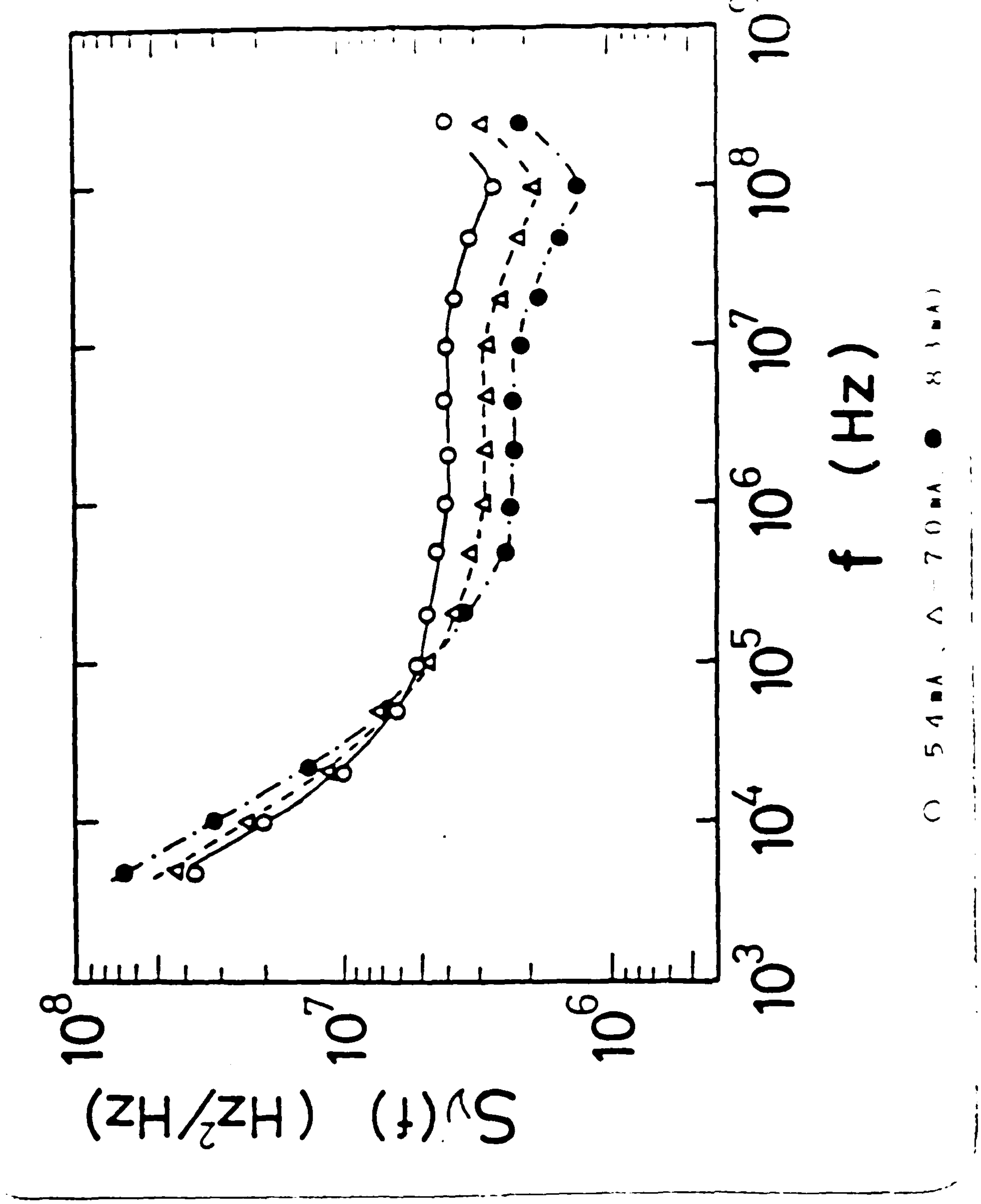

$S_\nu(f)$ (Hz^2/Hz)
f (Hz)

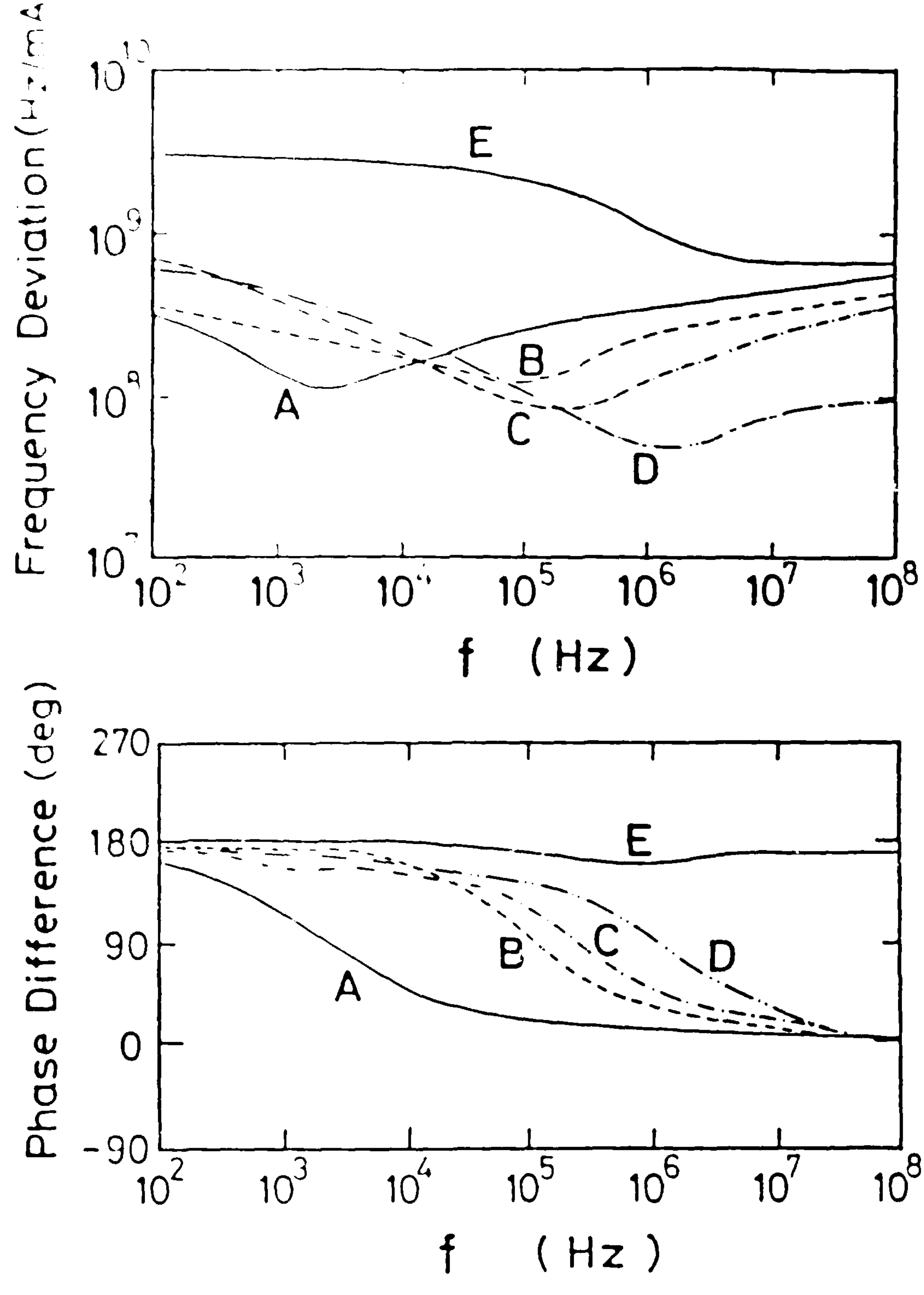

Frequency Deviation (Hz/mA)
10^{10}
10^{9}
10^{8}
10^{7}
E
A
B
C
D
10^{2} 10^{3} 10^{4} 10^{5} 10^{6} 10^{7} 10^{8}
f (Hz)
Phase Difference (deg)
270
180
90
0
-90
E
A
B
C
D
10^{2} 10^{3} 10^{4} 10^{5} 10^{6} 10^{7} 10^{8}
f (Hz)

AD-A186 938 UNITED STATES - JAPAN SEMINAR ON QUANTUM MECHANICAL ASPECTS OF QUANTUM EL (U) MASSACHUSETTS INST OF TECH CAMBRIDGE RESEARCH LAB OF ELECTRON 3/7

UNCLASSIFIED J H SHAPIRO ET AL OCT 87 N00014-87-G-0198 F/G 20/3 NL

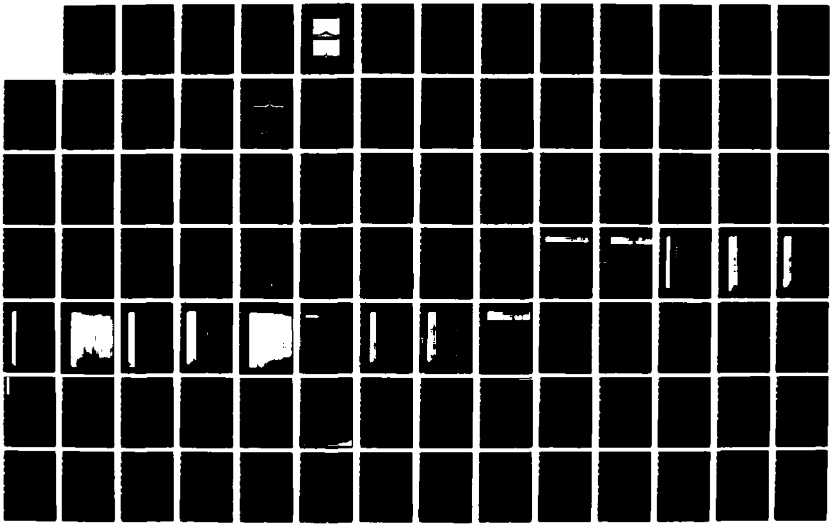

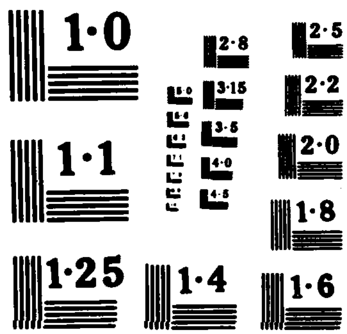
1·0
2·8
2·5
3·15
2·2
3·5
2·0
1·1
4·0
4·5
1·8
1·25
1·4
1·6

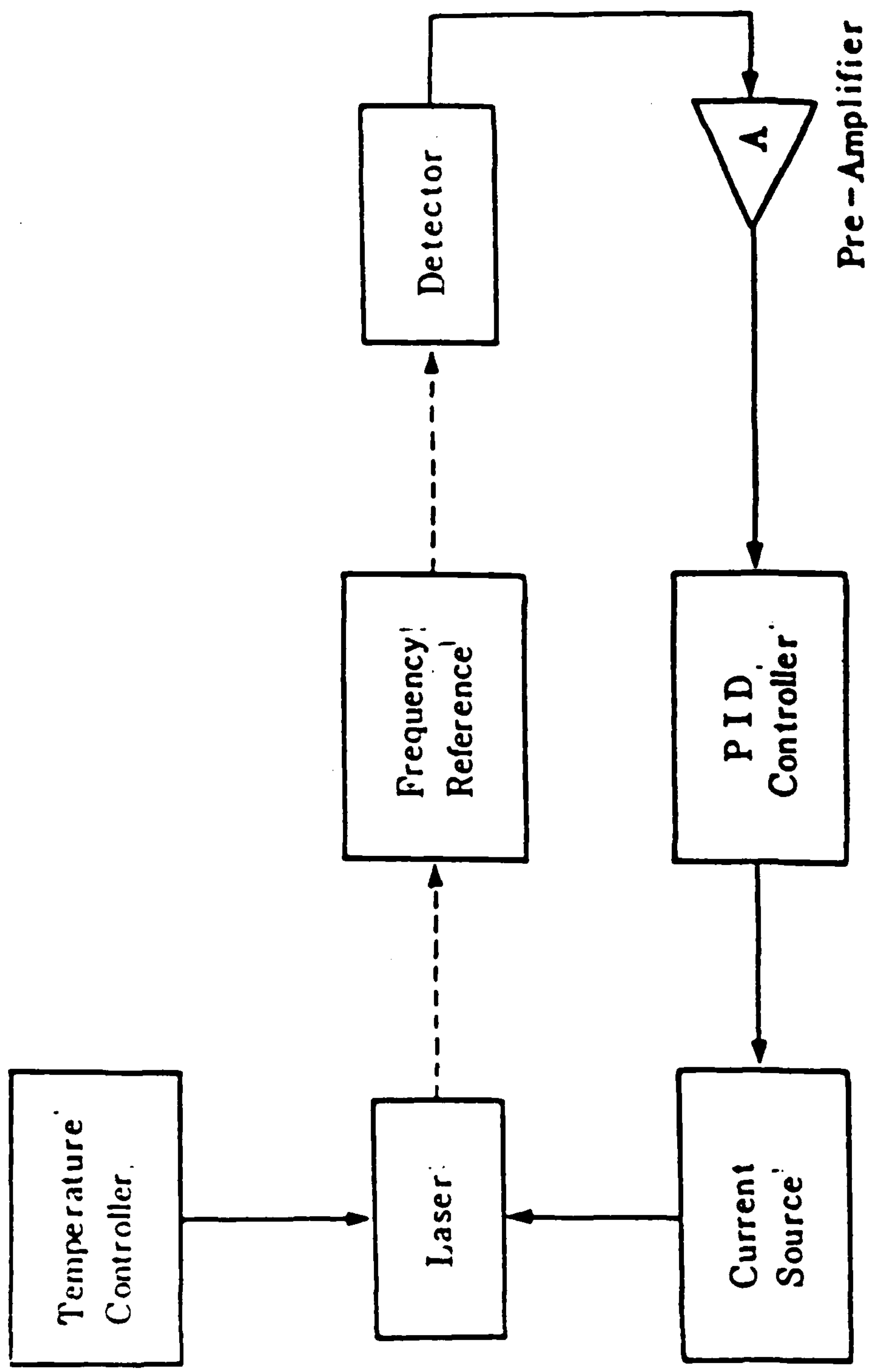
Detector
Pre-Amplifier
A
Frequency Reference
P I D Controller
Temperature Controller
Laser
Current Source

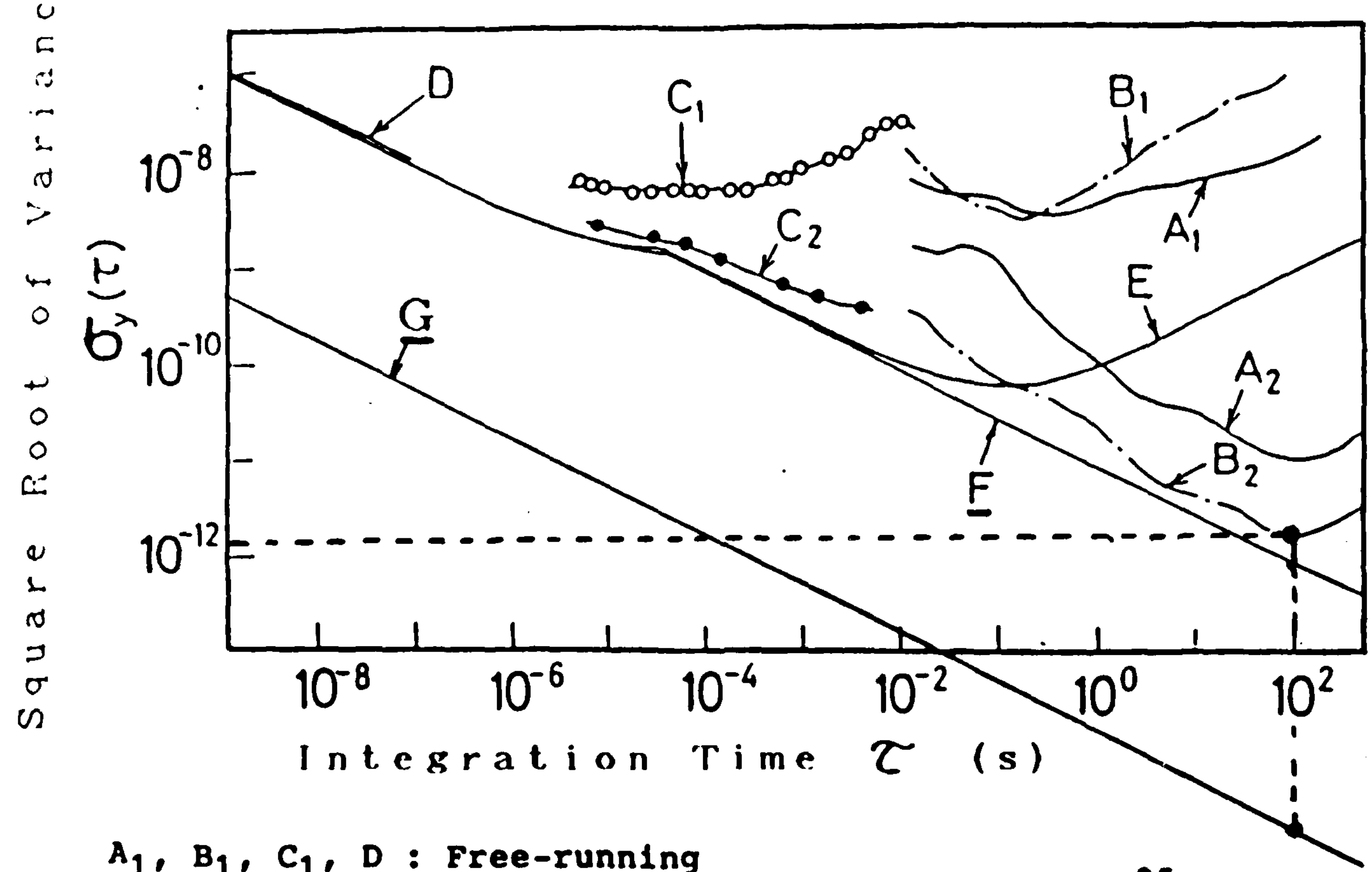

A_1, B_1, C_1, D : Free-running
A_2 : Stabilized by H_2O B_2 : Stabilized by ^{85}Rb
C_2 : Stabilized by a rigid Fabry-Perot interferometer
E : Free-running laser including external noises
F : Quantum noises in free-running laser
[M. Ohtsu, et. al. : Jpn. J. Appl. Phys., 22 (1983) p.1157]
G : Detector noise limited

[2] Linewidth reduction

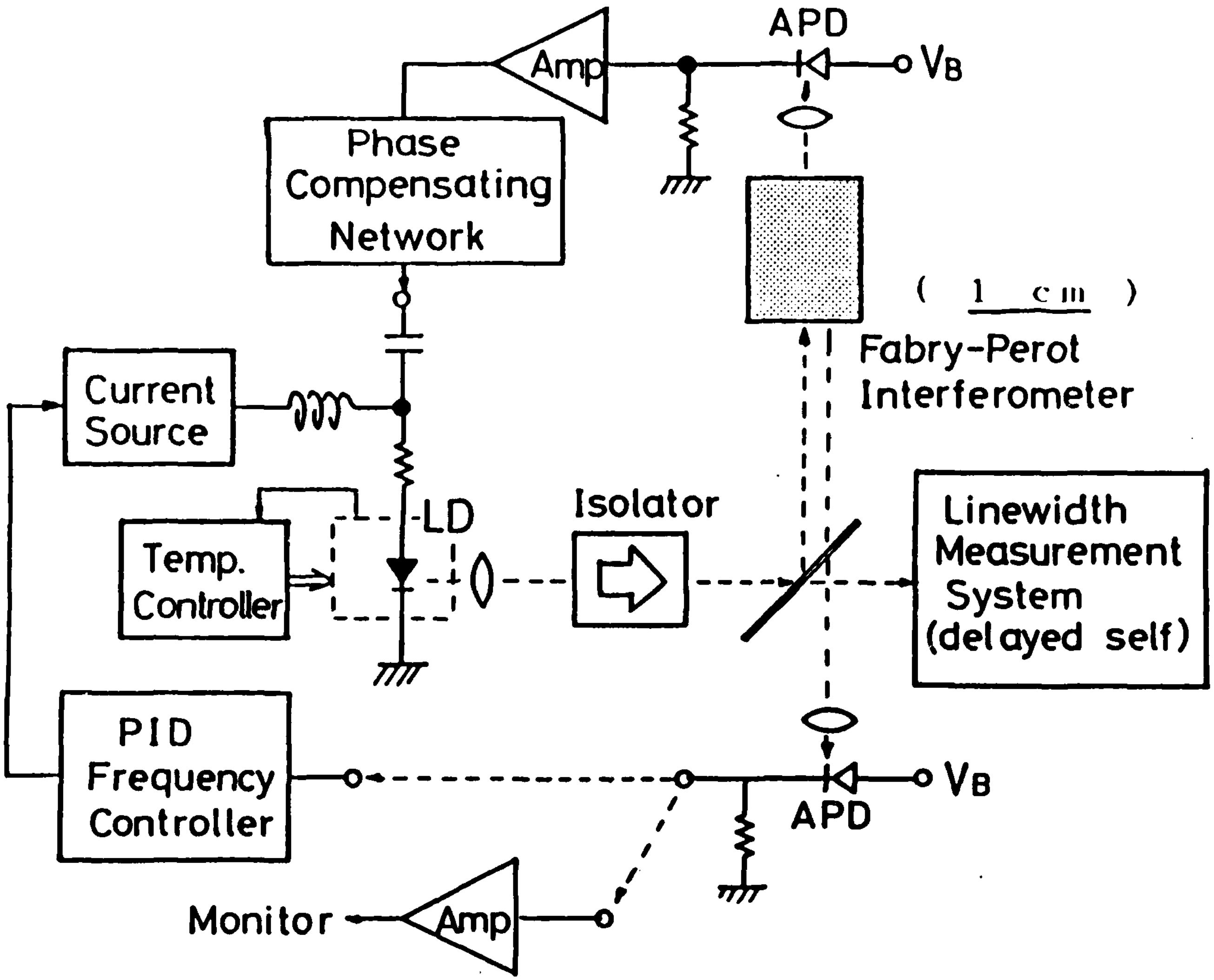

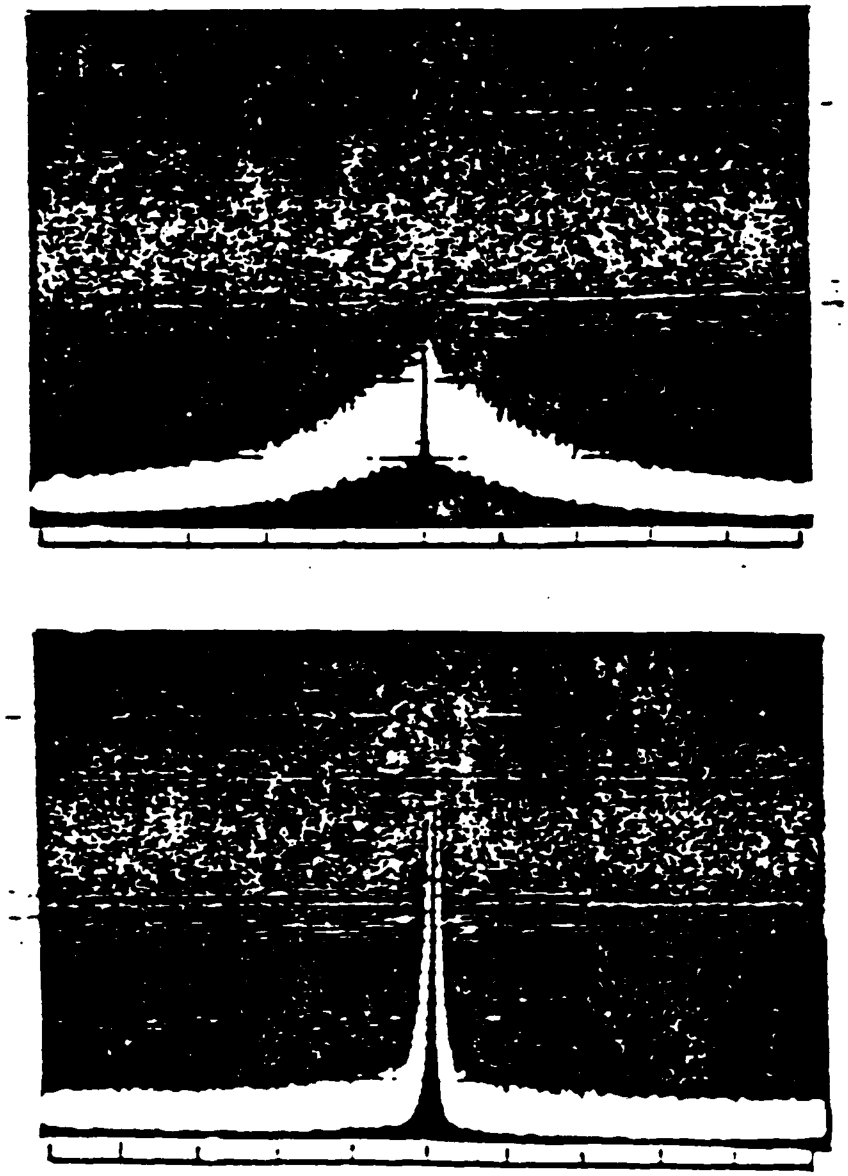

10MHz/div

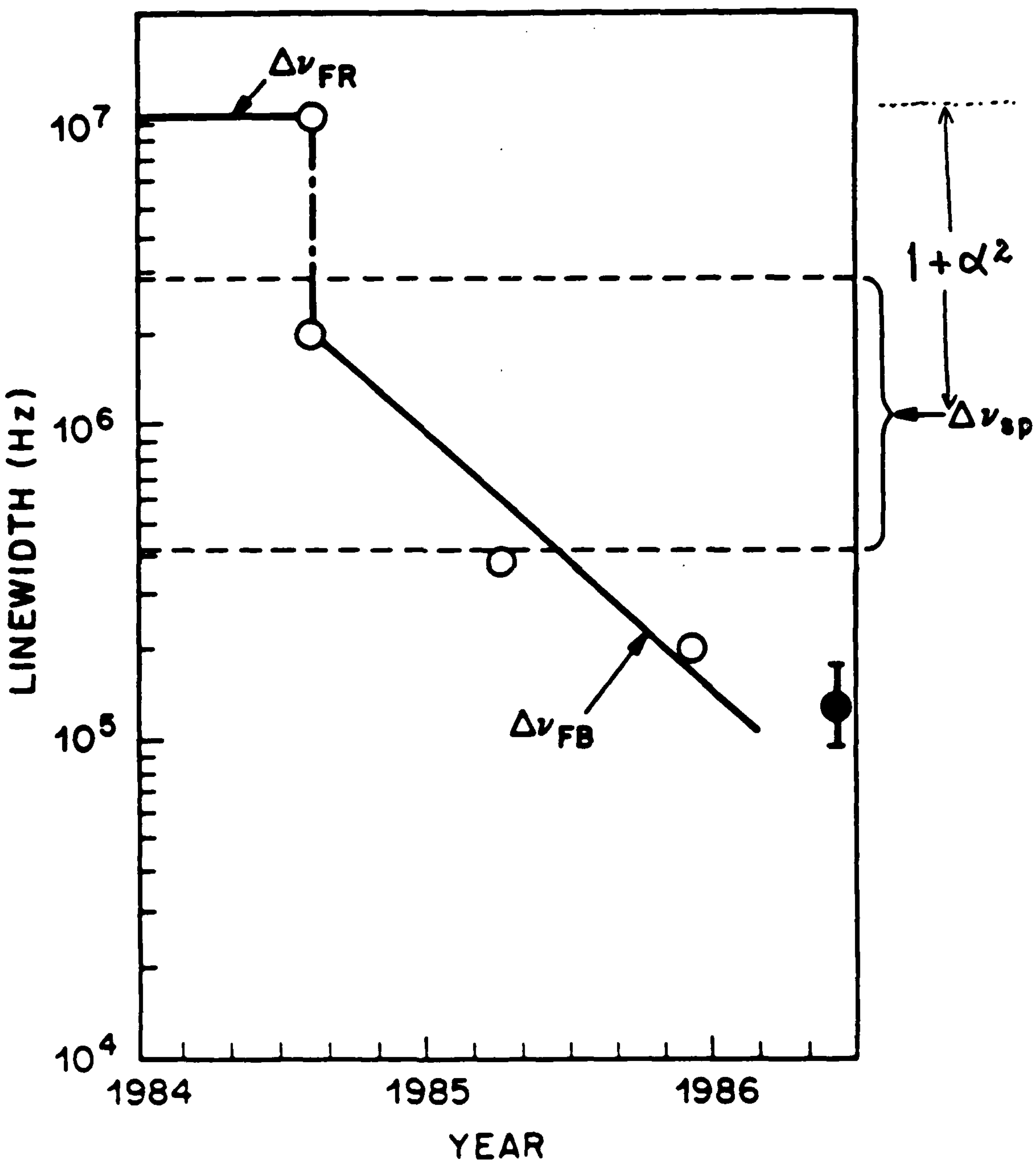

$\Delta\nu_{FR}$
10^7
$1+\alpha^2$
10^6
$\Delta\nu_{sp}$
LINEWIDTH (Hz)
10^5
$\Delta\nu_{FB}$
10^4
1984
1985
1986
YEAR

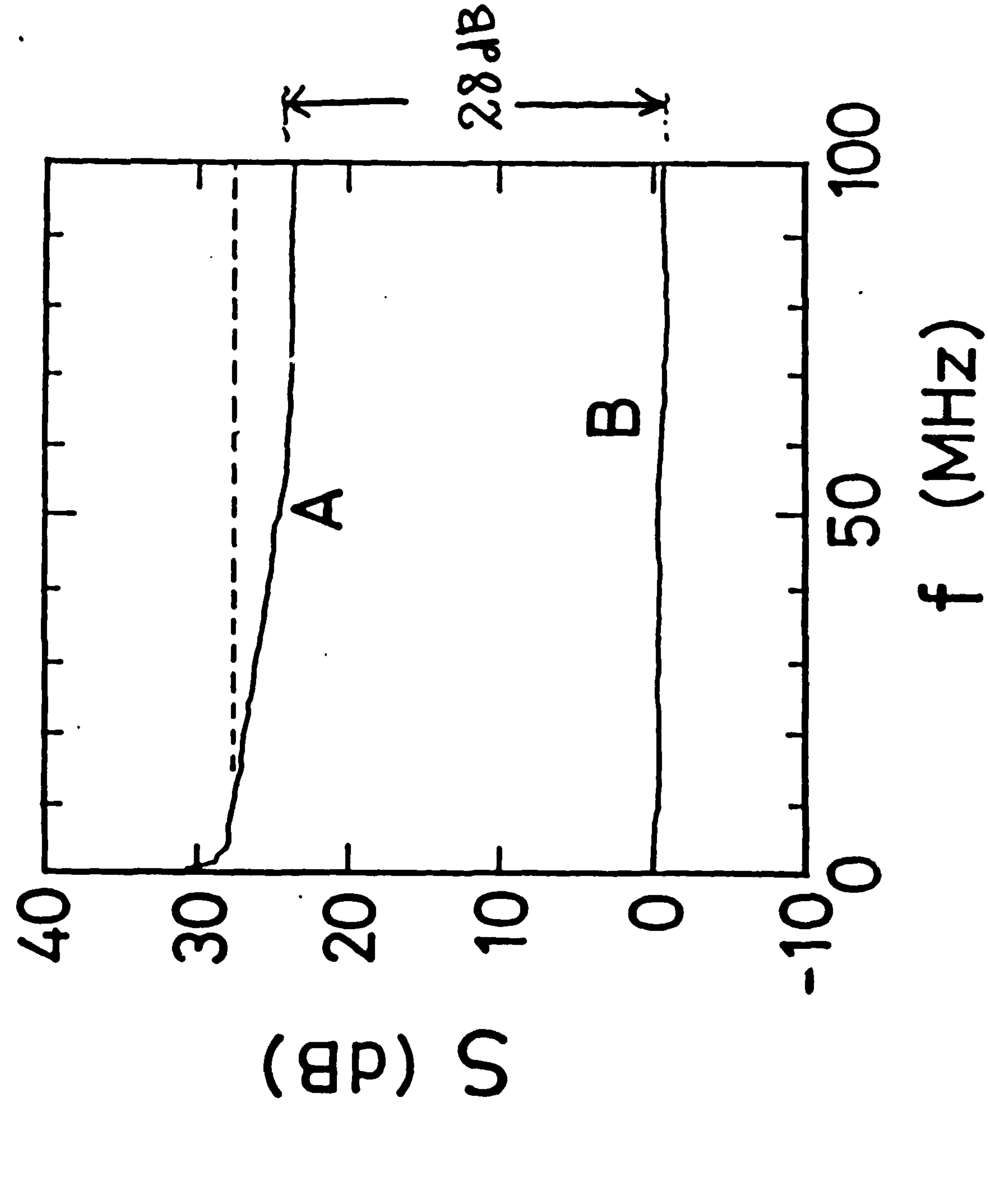
28 dB
A
B
S (dB)
f (MHz)
40
30
20
10
0
-10
0
50
100

Network Analysis

$\downarrow$ Delay Time $\tau_d \lesssim 0.6$ ns

- 0.2ns : GaAs IC Servo-amplifier
- 0.4ns : Optical & electrical path length $\lesssim 12$ cm

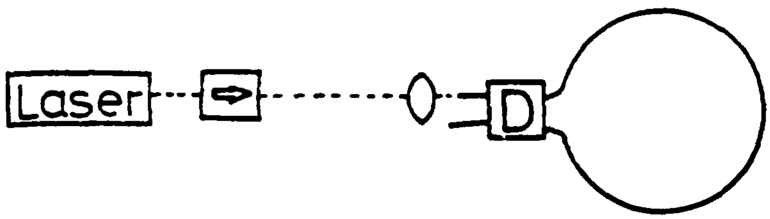

Fiber Ring Cavity

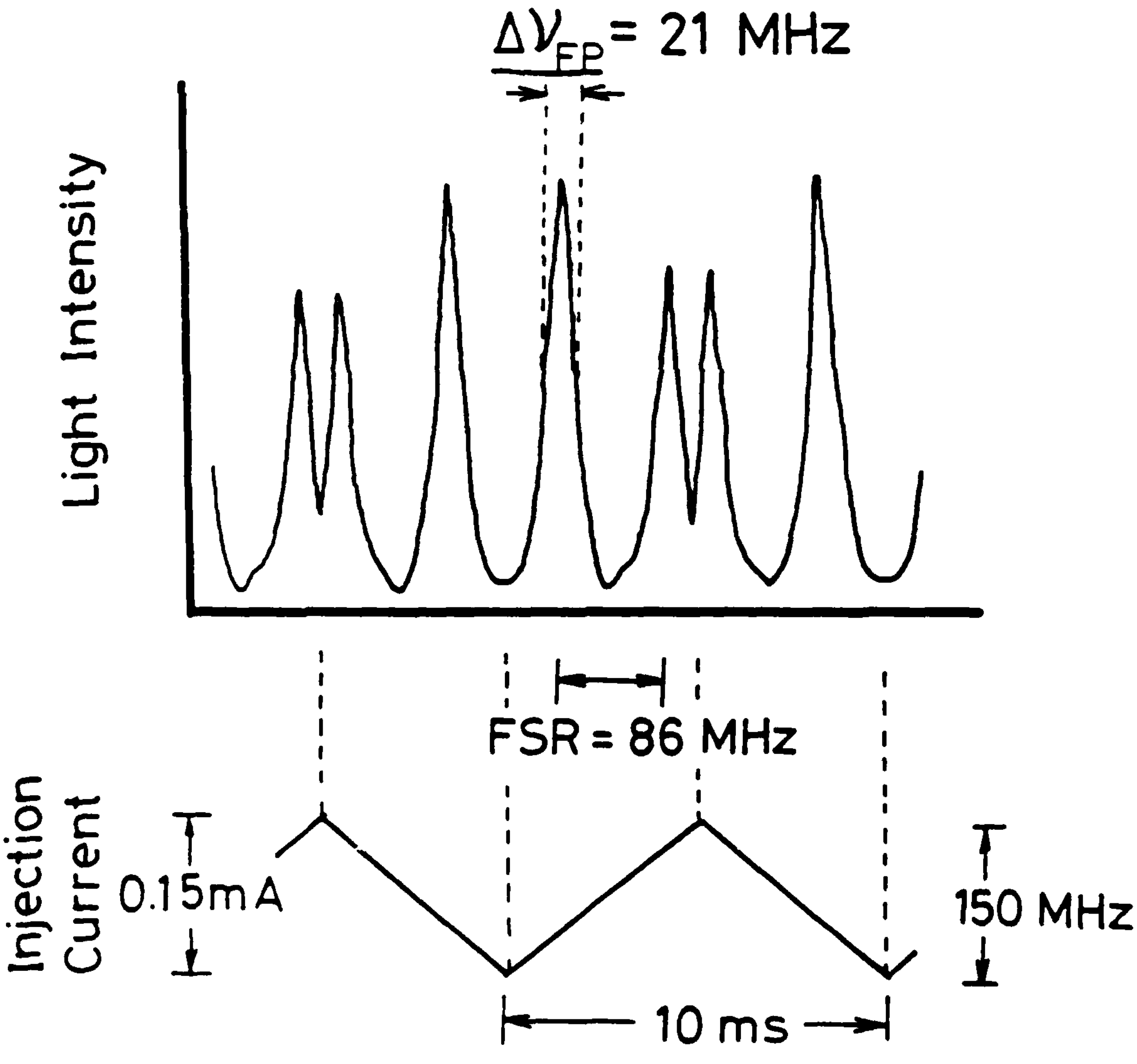

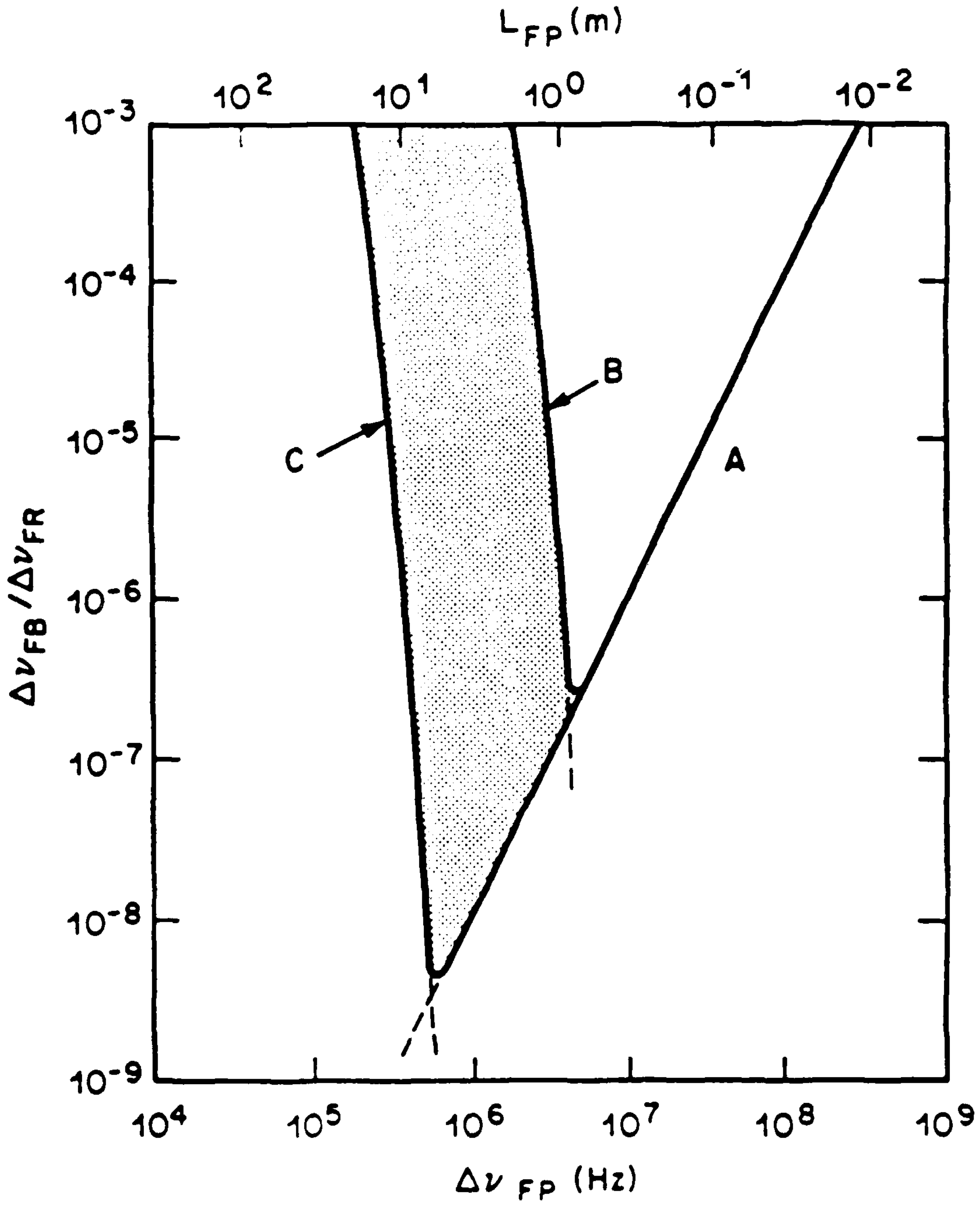

L_{FP} (m)
10^2
10^1
10^0
10^{-1}
10^{-2}
10^{-3}
10^{-4}
10^{-5}
10^{-6}
10^{-7}
10^{-8}
10^{-9}
$\Delta\nu_{FB}/\Delta\nu_{FR}$
A
B
C
10^4
10^5
10^6
10^7
10^8
10^9
$\Delta\nu_{FP}$ (Hz)

[Summary]

	Experimental Results	Theoretical Limits	
(1) Frequency Stabilization	2×10^{-12}	1×10^{-15}	(at τ = 100 s)
(2) Linewidth Reduction	100kHz	1 Hz	
(3) Frequency Tracking	3×10^{-14}	2.7×10^{-16}	(at τ = 100 s)
(4) Frequency Sweep	53.4GHz	1 THz	

(1) High stability and reproducibility
(2) Degree of coherence is varied by varying the feedback gain, without modifying laser cavity structure
(3) Analogy with electronic circuits is employed for design of feedback system
(4) Compatible with opto-electronic IC
(5) Applicable to sensing, low~medium bit rate coherent optical communication

Correlated Spontaneous Emission Between the Two Longitudinal Modes in a Semiconductor Laser

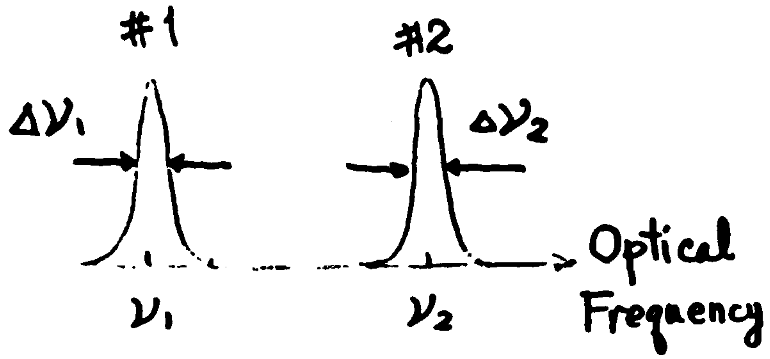

Two-Mode Laser

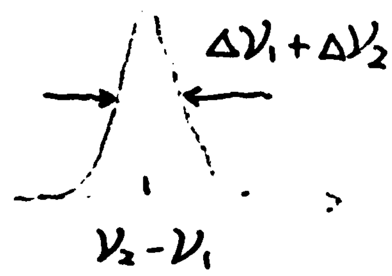

Heterodyned Signal

◎ M.O. Scully : Phys. Rev. Lett., 55 pp 2802-2805 (1985)

《 Hanle Effect Laser 》

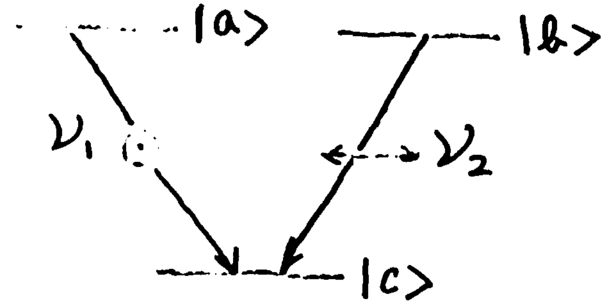

Polarization Induced Coherence

《 Quantum Beat Laser 》

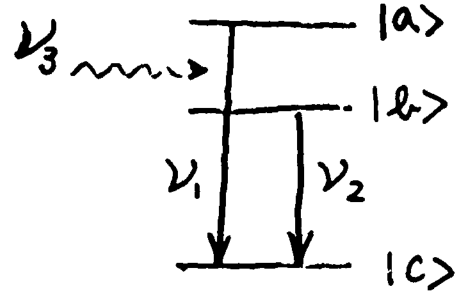

Microwave Induced Coherence

◎ Toschek & Hall : IQEC'87 , Baltimore, WDD2

He - Ne Zeeman Laser

$\Delta\nu \rightarrow$ (Schawlow - Townes Limit) $\times$ 1/10

The state vector of the three-level atoms :

$$|\psi\rangle = \alpha e^{-i\underline{\phi_a}}|a\rangle + \beta e^{-i\underline{\phi_b}}|b\rangle + \gamma e^{-i\underline{\phi_c}}|c\rangle \quad (1)$$

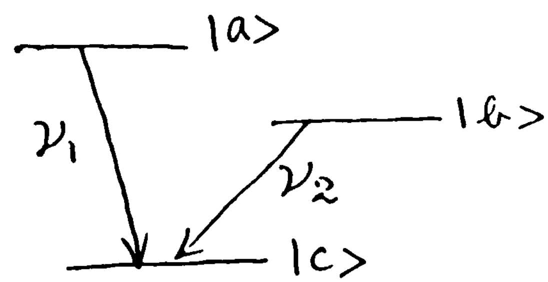

Spontaneously emitted fields :

$$\left.\begin{aligned} E_{1s} &= \mathcal{E}_1 e^{-i(\underline{\phi_a-\phi_c})-i\nu_1 t} \\ E_{2s} &= \mathcal{E}_2 e^{-i(\underline{\phi_b-\phi_c})-i\nu_2 t} \end{aligned}\right\} \quad (2)$$

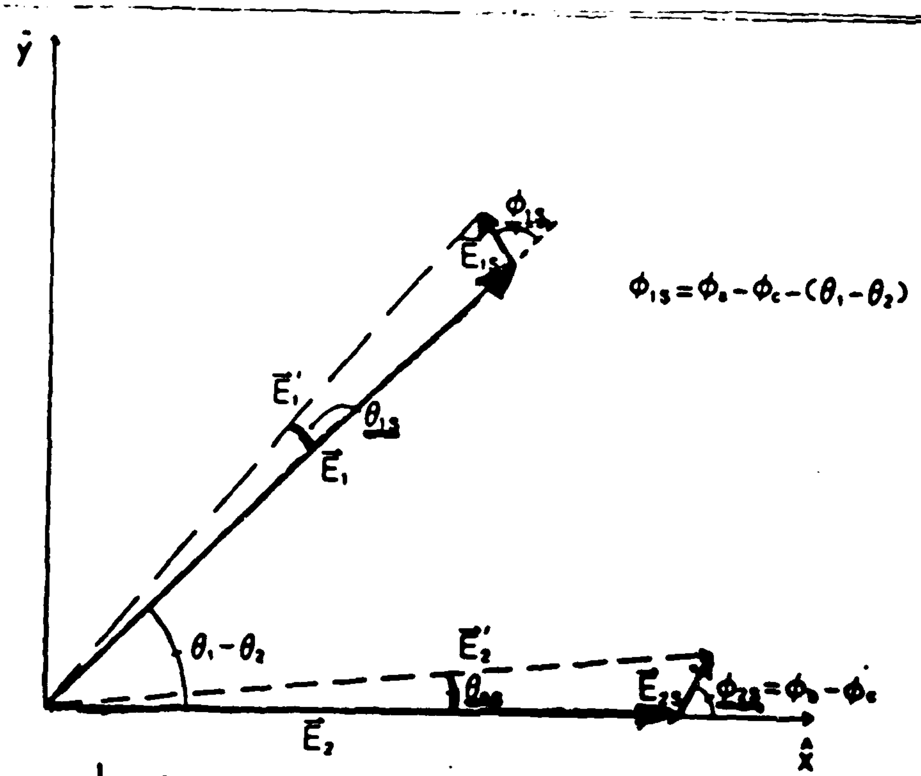

Phase difference between the laser field and spontaneously emitted field :

$$\left.\begin{aligned} \underline{\phi_{1s}} &= \phi_a - \phi_c - (\theta_1 - \theta_2) \\ \underline{\phi_{2s}} &= \phi_b - \phi_c \end{aligned}\right\} \quad (3)$$

Fluctuations in the phase of laser field :

$$\left.\begin{aligned} \underline{\theta_{1s}} &= \frac{|\vec{E}_{1s}|}{|\vec{E}_1|} \cdot \sin \underline{\phi_{1s}} \\ \underline{\theta_{2s}} &= \frac{|\vec{E}_{2s}|}{|\vec{E}_2|} \cdot \sin \underline{\phi_{2s}} \end{aligned}\right\} \quad (4)$$

For quenching the phase noise in heterodyned signal :

$$\theta_{1s} = \theta_{2s} \qquad (5)$$

From eqs. (3),(4), this is met if

$$\theta_1 - \theta_2 - (\Phi_a - \Phi_b) = 0 \qquad (6)$$

By applying microwave, $\Phi_a - \Phi_b = \Phi_\mu$, then the condition to be satisfied is

$$\underline{\theta_1 - \theta_2 = \Phi_\mu} \qquad (7)$$

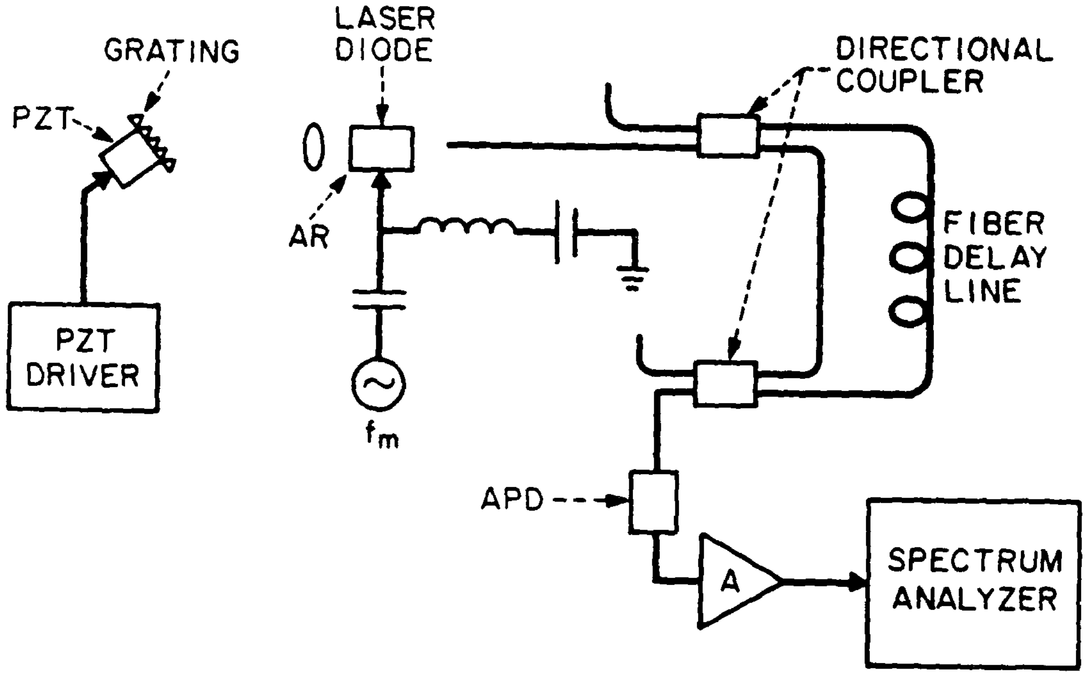
GRATING
PZT
LASER DIODE
DIRECTIONAL COUPLER
AR
FIBER DELAY LINE
PZT DRIVER
f_m
APD
A
SPECTRUM ANALYZER

(a)

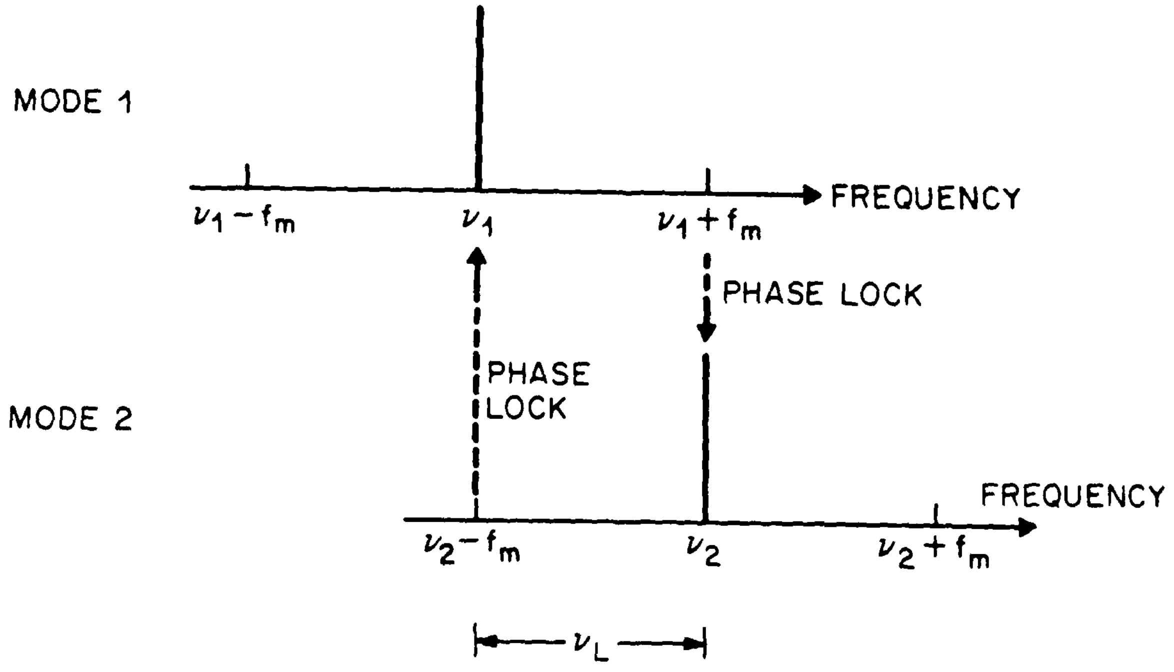
MODE 1
FREQUENCY
$\nu_1 - f_m$
ν_1
$\nu_1 + f_m$
PHASE LOCK
PHASE LOCK
MODE 2
FREQUENCY
$\nu_2 - f_m$
ν_2
$\nu_2 + f_m$
ν_L

(b)

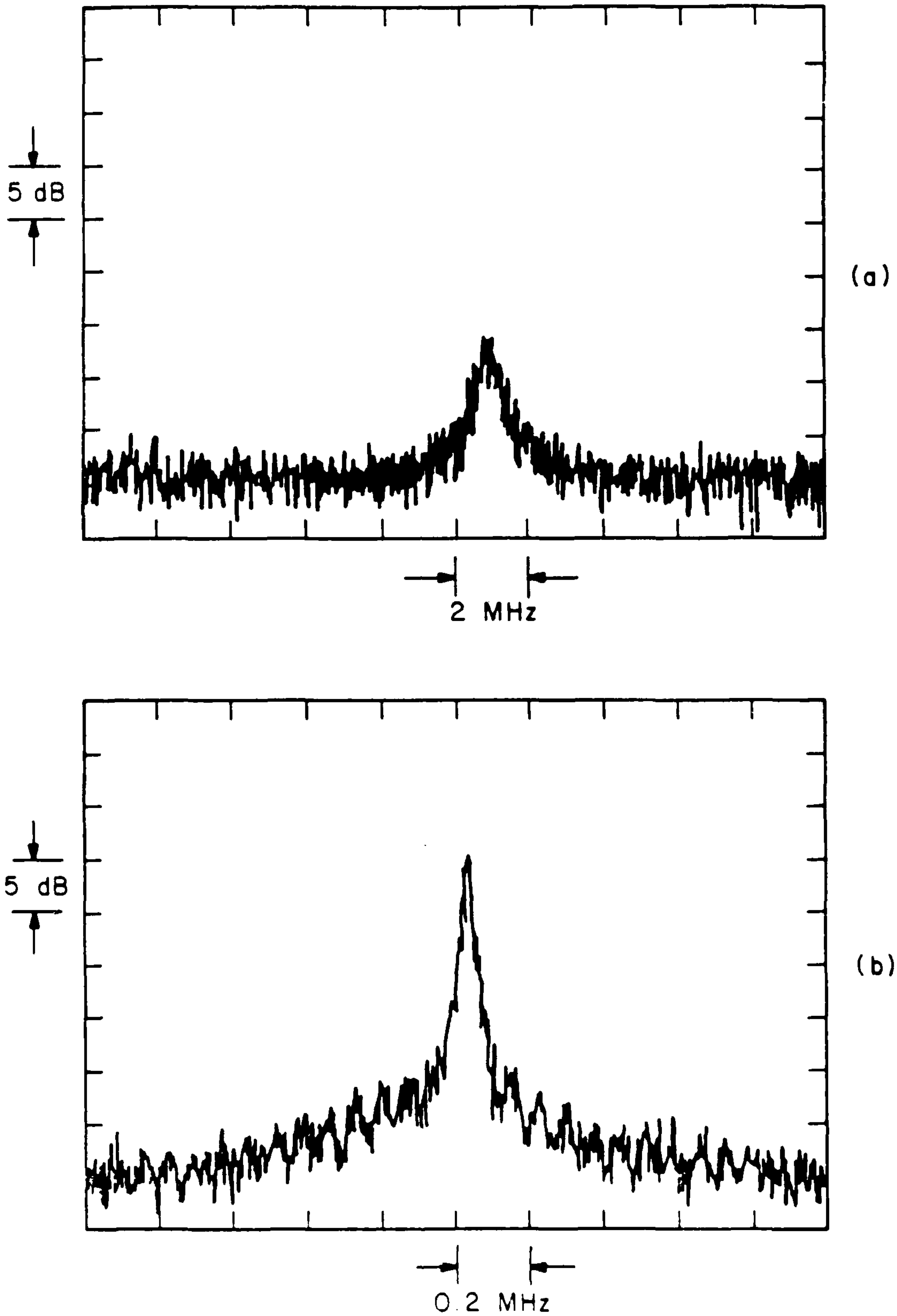
5 dB
(a)
2 MHz
5 dB
(b)
0.2 MHz

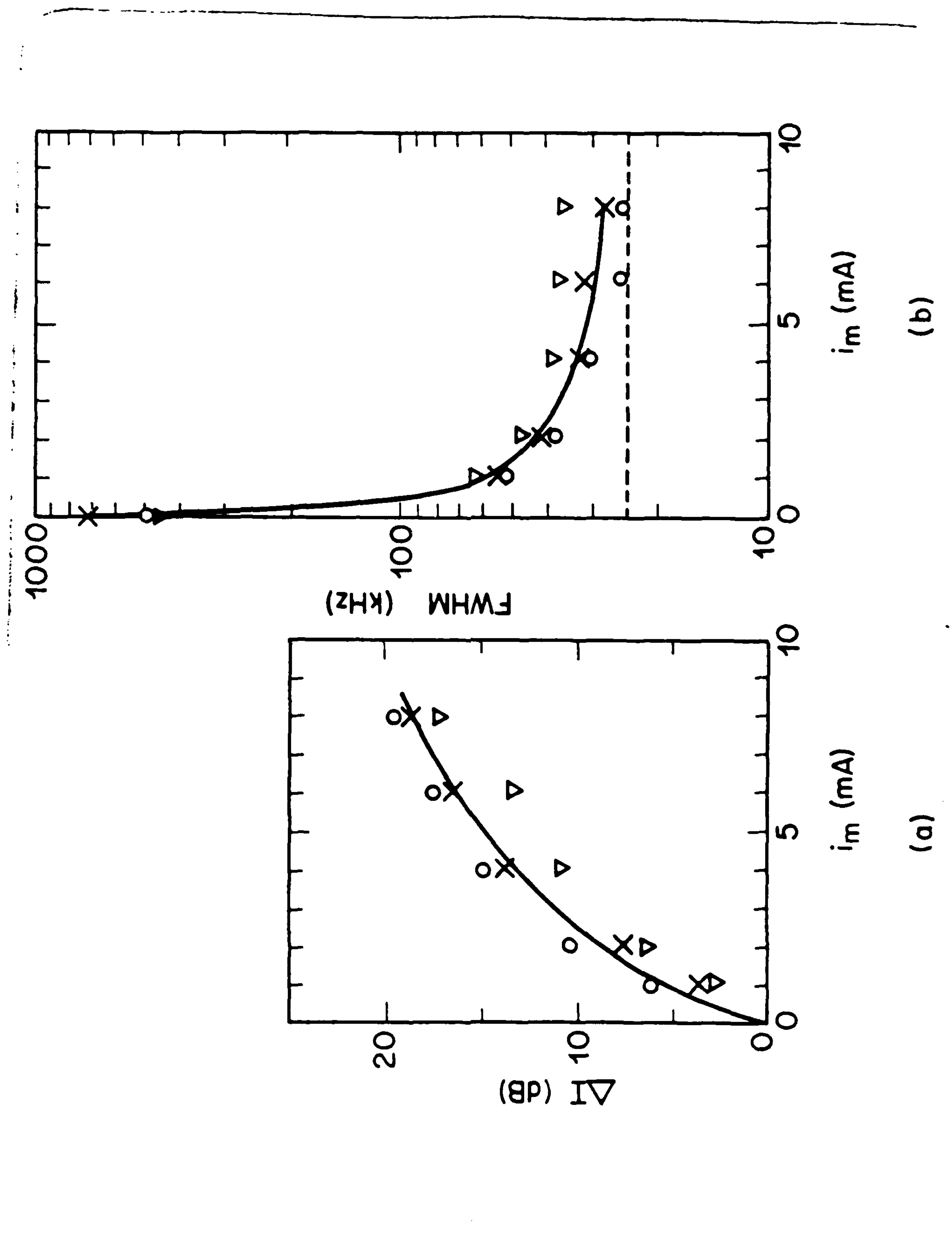
1000
100
10
FWHM (kHz)
0
5
10
i_m (mA)
(b)
20
10
0
ΔI (dB)
0
5
10
i_m (mA)
(a)

^{87}Rb Atomic Clock

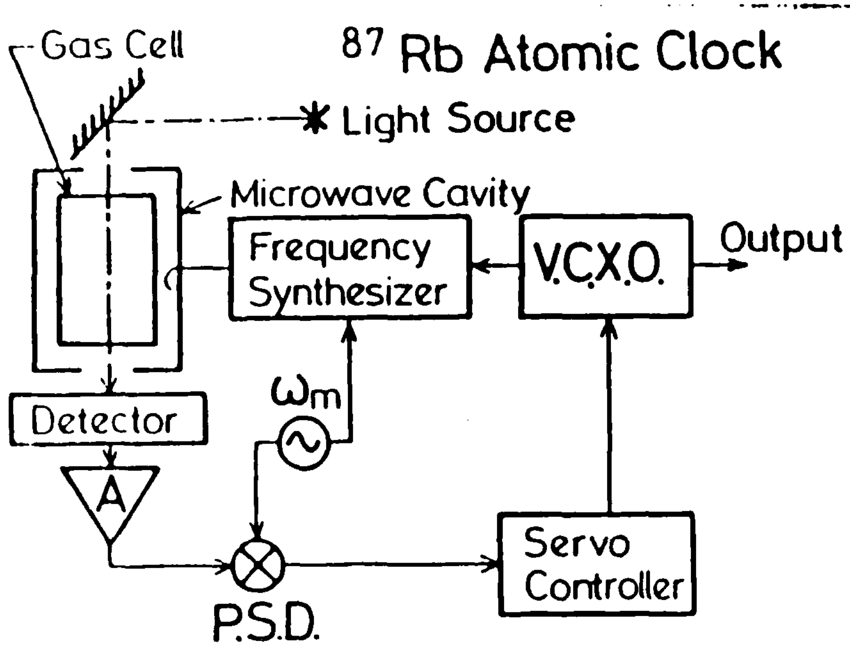

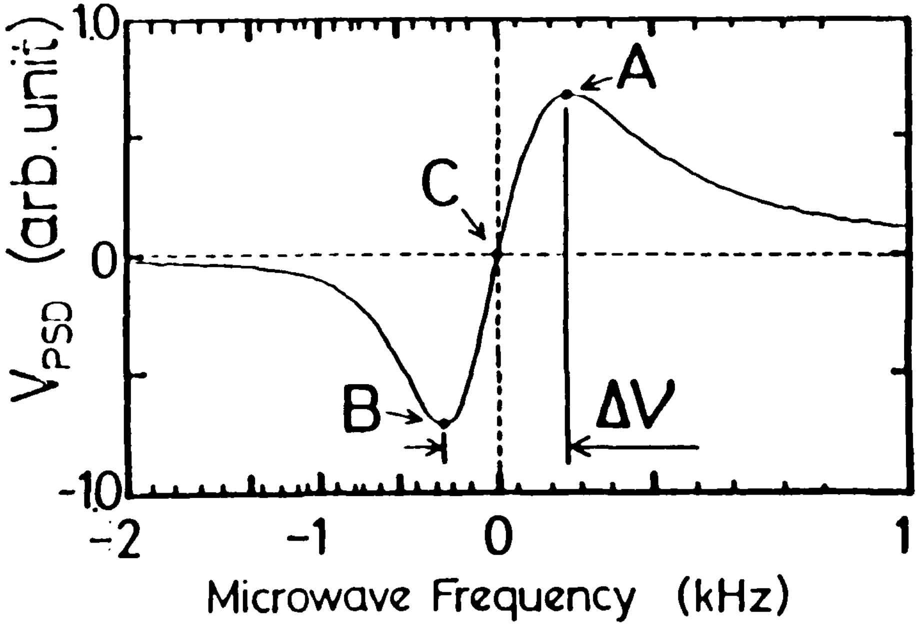

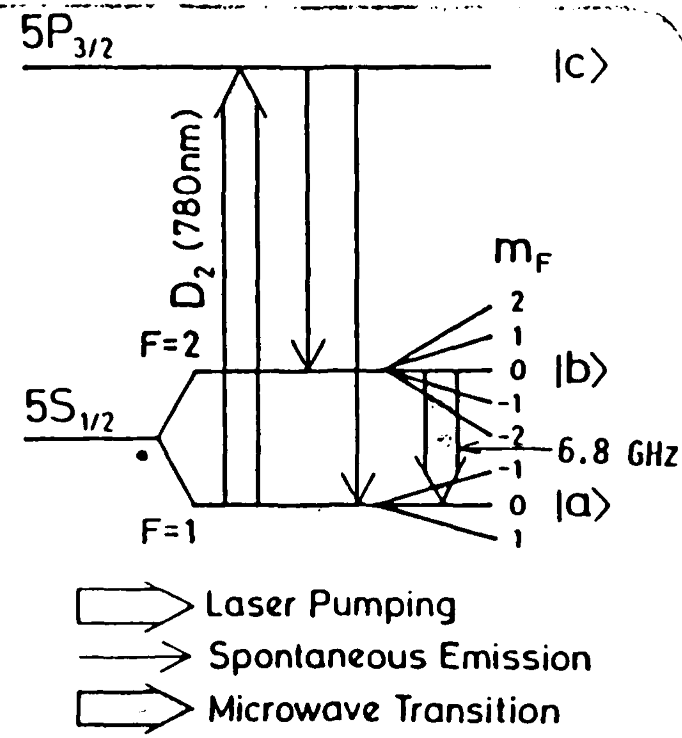

Frequency Stability

$$\sigma_y(\tau) = \frac{1}{\sqrt{2}\pi(\nu_M/\Delta\nu)(S/N)}\tau^{-1/2}$$

$$= \frac{N}{\sqrt{2}\pi\nu_M \underline{(S/\Delta\nu)}}\tau^{-1/2}$$

Slope

Reference Signal $\cos(\omega_m t-\theta)$

PSD Output $V_{PSD} = V_0[(B/2)\cos\theta + (C/2)\sin\theta]$

Experimental

$M = 1.8$
$f_m/\gamma_{ab}' = 2.3$
$\theta = 234°$

$M = 1.6$
$f_m/\gamma_{ab}' = 2.9$
$\theta = 270°$

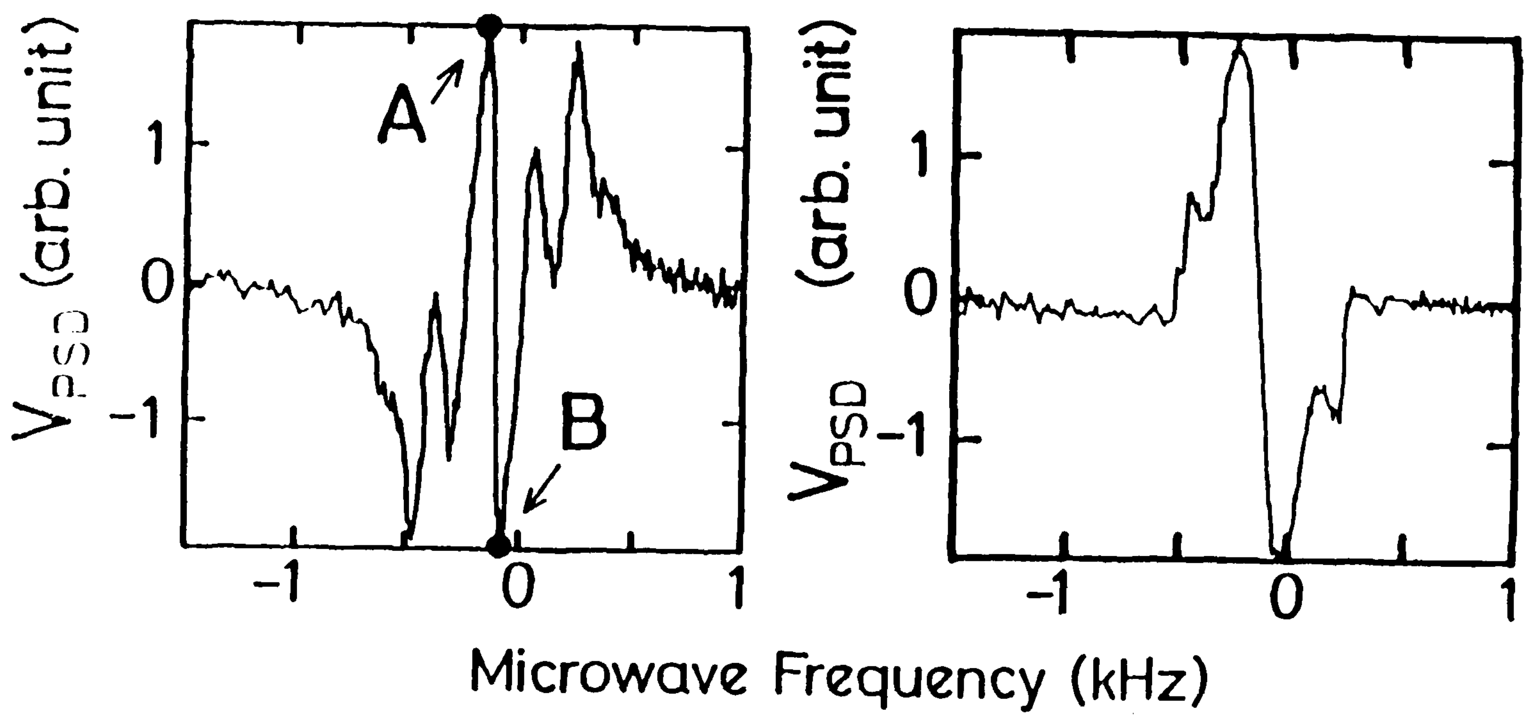

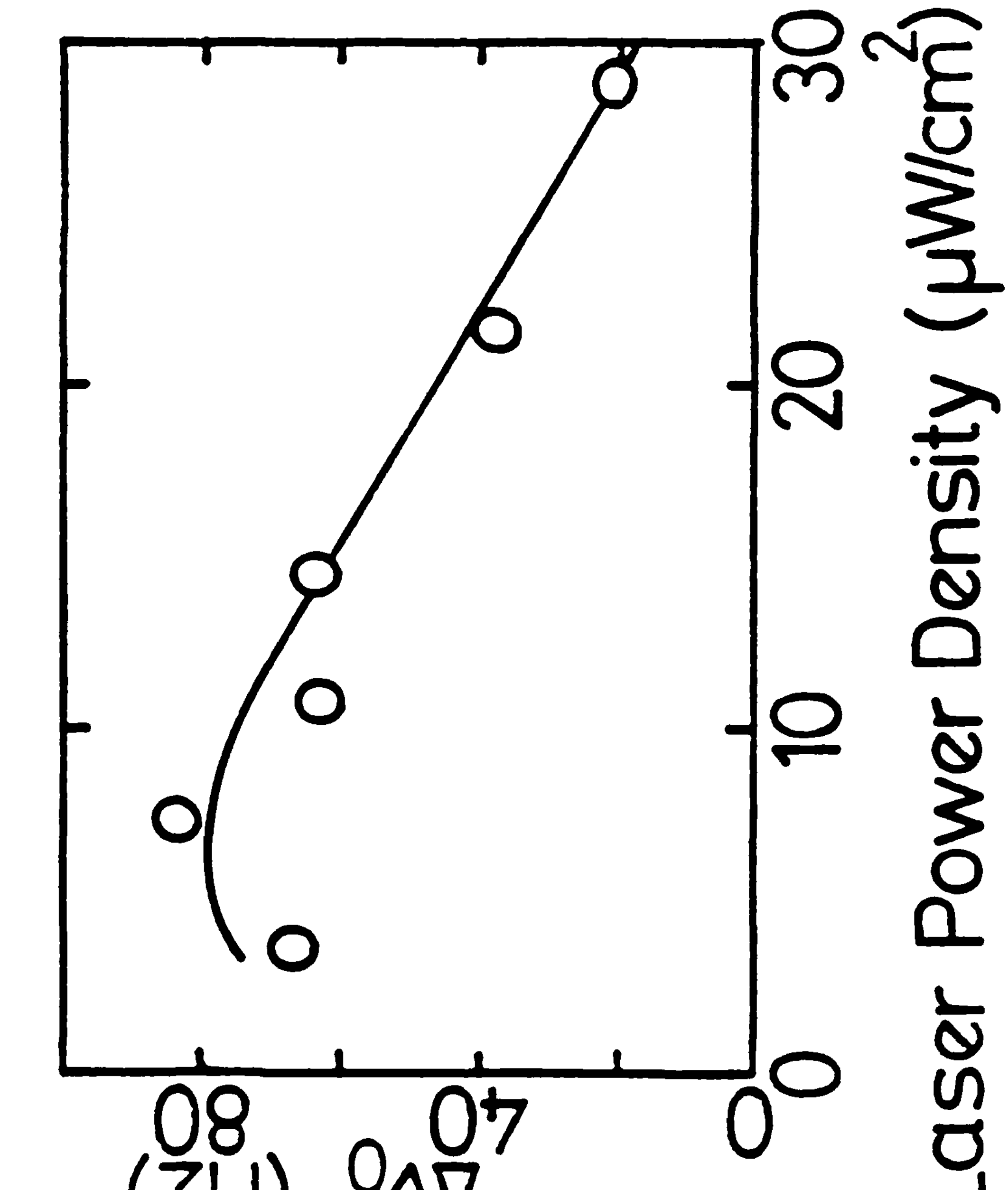
Δν₀ (Hz)
0
40
80
0
10
20
30
Laser Power Density (μW/cm²)

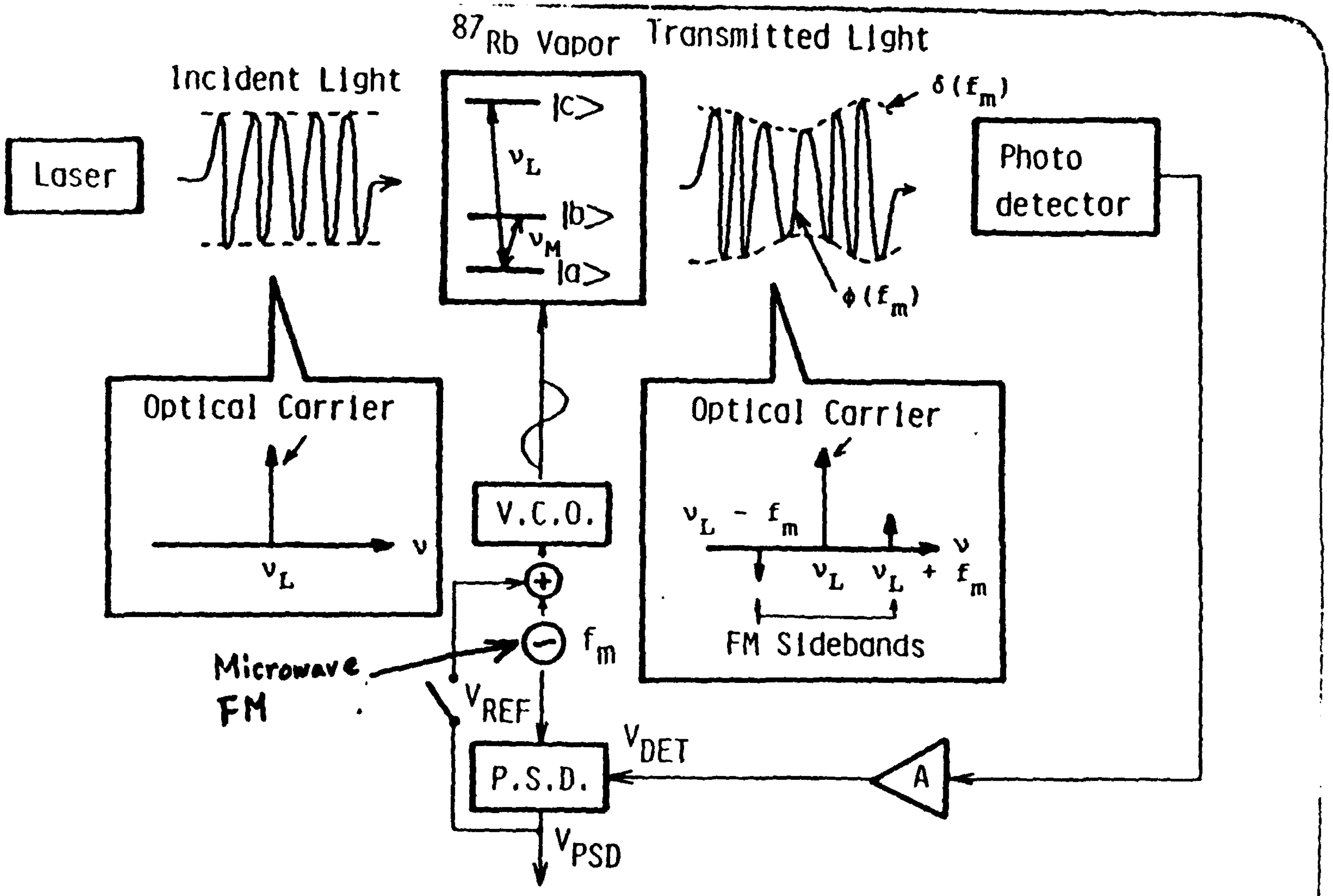

Detector Ouptput $V_{DET} = V_0[A + B\cos(2\pi f_m t) + C\sin(2\pi f_m t)]$

Reference Signal $V_{REF} = \cos(2\pi f_m t - \theta)$

PSD Output $V_{PSD} = (B/2)\cos\theta + (C/2)\sin\theta$

Reference Signal $\cos(\omega_m t-\theta)$

PSD Output $V_{PSD} = \underline{V_0}[(\underline{B}/2)\cos\underline{\theta} + (\underline{C}/2)\sin\underline{\theta}]$

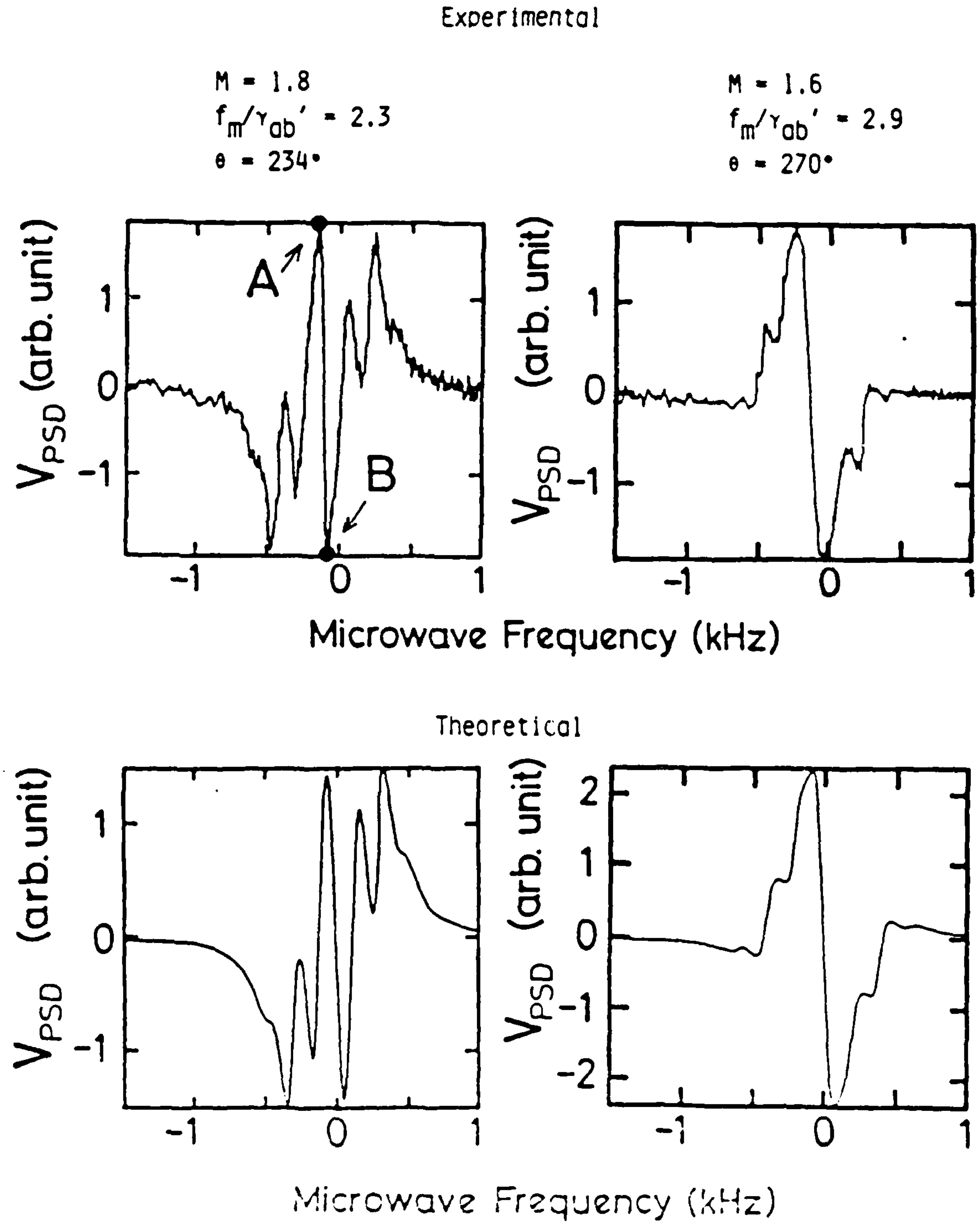

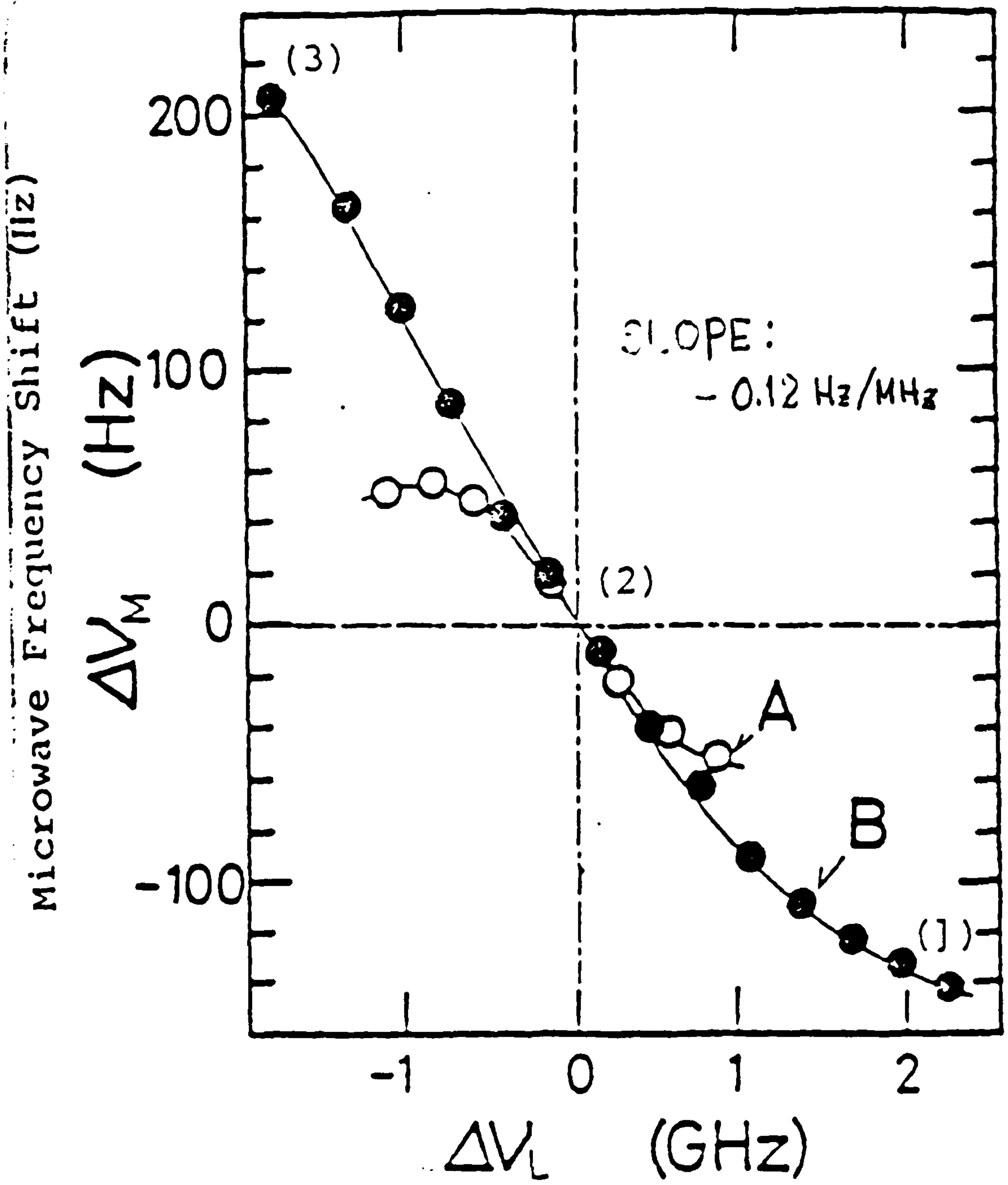

Laser Frequency Detuning (GHz)

A: Laser Power Density 57.6 $\mu W/cm^2$

B: Laser Power Density 2880 $\mu W/cm^2$

$$V_{PSD} = V_0[(B/2)\cos\theta + (C/2)\sin\theta]$$

<u>Slope</u>

Pumped by Incoherent Lamp (Experiment)

x 25 — Linewidth Reduction (1/25)

Pumped by Coherent Laser (Experiment)

Estimation

x 3 — Optimization of Modulation and PSD parameters

x 4 — Increases in Laser Power Density (x 7) (Increases in γ_{ab}' is also counted)

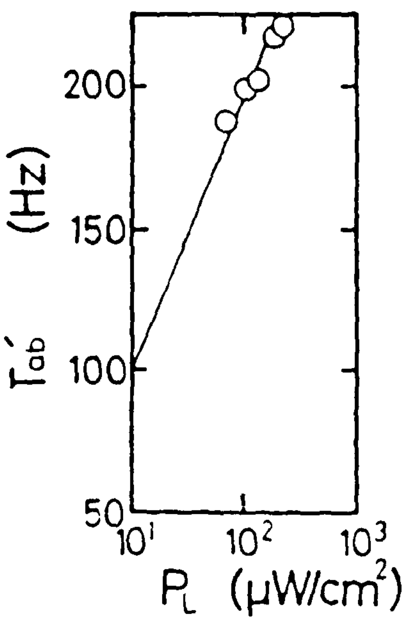

x 25 — Laser Beam Expansion (x 25) (Increases in Number of Rb Atoms Used)

Total : x 7500

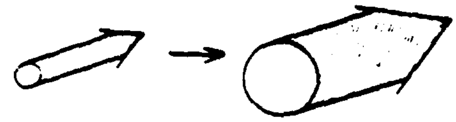

4 mm² 20 mm²

[Summary]

(1) Novel FM detection technique for double resonance spectral shape

(2) Sensitivity of frequency discriminator : x 7500 (under optimum condition)

(3) Improve the frequency accuracy

Squeezed State in Degenerate Parametric Amplification Discussed by H. Takahasi in 1963

Koichi Shimoda
Department of Physics, Keio University
3-14-1 Hiyoshi, Kohokuku, Yokohama 223

Professor Hidetosi Takahasi who died in 1985 had developed a theory of quantum noise in 1963 by appropriately applying the quantum mechanics to a general theory of communication channels.

He discussed the quantum-mechanical coherent state of a harmonic oscillator, and subsequently developed a quantum theory of parametric amplifiers, in which the squeezed state in degenerate parametric conversion was particularly emphasized.

§1. Introduction

On January 14, 1963 Professor Hidetosi Takahasi, who died on June 30, 1985, gave a talk on "Semiclassical theory and quantum theory of photon noise" at a colloquium in the Department of Physics, University of Tokyo. He presented his conception of the coherent photon state and discussed that the "squeezed state" would be produced in parametric amplification. These works were first published in August, 1963 in Japanese.[1] His paper in English entitled "Information Theory of Quantum-Mechanical Channels" which included these considerations was published in 1965.[2]

It is the purpose of the present paper to reveal his early consideration of the squeezed state in degenerate parametric amplification. He developed the theory in a quite general way so that it could be applied to either mechanical, acoustic, electric, microwave, or optical systems. In particular, the Schrödinger equation of a parametric oscillator was treated with natural units. In the present paper, however, some of his terminologies and notations have been replaced by more familiar ones.

Although the full treatment in the present paper follow those in ref.1) and 2), almost faithful quotations from ref.2) will be accompanied by quotation marks.

§2. Quantum Noise in Linear Systems

Quantum noise is essentially different from classical noise.

Classical noise such as thermal noise is a definite physical quantity that varies stochastically with time. Quantum noise, on the other hand, is the result of uncertainties in quantum-mechanical measurements which depend how we observe what in quantum-mechanical terms. Even without any classical noise in a system, we still have a statistical relation between transmitted and received signals, which arises from the intrisic nature of quantum-mechanical observations.

We consider a linear system, either an attenuator or an amplifier, with a black-box model. It is important to see that we deal exclusively with transmission of discrete samples of signals with angular frequency ω rather than a continually varying function of time.

A simple calssical relation between the input x and the output y of a linear system is

$$y = kx \tag{2.1}$$

where x and y represent the strength of oscillating fields, so that $|x|^2$ and $|y|^2$ give respectively the input and output energies of the observed mode. However, the relation (2.1) should be modified in order to take the effect of external systems into consideration.

Consider an attenuator for which $k < 1$. Then the absorbed power must be deposited to a heat reservoir, external space, or elsewhere. Likewise many external systems are coupled to the attenuator so that they may bring in noise. A number of such external systems are represented in our black-box treat-

ment as shown in Fig. 1, where a lossless channel (a beam splitter, for example) is coupled with four external systems.

Here the classical input-output relations should be

$$y = kx + k'x'$$
$$y' = -k'x + kx' \tag{2.2}$$

where the coefficients have been made real by adjusting the time origins of x, x', y, and y'. The energy conservation requests that

$$k^2 + k'^2 = 1 \text{ or } k' = \sqrt{1 - k^2}, \tag{2.3}$$

In quantum-mechanical measurements, x' includes zero-point fluctuations even in the ground state of the lowest energy.

"If we further assume that x' and y' are coördinates of harmonic oscillators having the same natural frequency, the pair of coordinates (x, x') may be thought of as representing a two-dimensional (isotropic) oscillator. Likewise (y, y') may represent the coordinates of a two-dimensional oscillator. We now see that actually these two two-dimensional oscillators are identical and that (2.2) is a coordinate transformation relating these two pairs of coordinates."

In quantum mechanics x, x', y, and y' are regarded as annihilation operators, while their hermitian conjugates are creation operators. They satisfy commutation relations:

$$[x, x^\dagger] = 1, \quad [x', x'^\dagger] = 1, \quad [x', x^\dagger] = 0$$

and similar commutation relations for y, and y'. These relations are inconsistent with (2.1) except when $k = 1$, so that we should use (2.2) and (2.3).

Now an amplifier is represented by assuming that k is larger than 1. Thus k' must be imaginary from (2.3), since $k^2 > 1$. If we shift time origins for x and y by $\pi/4\omega$ and those of x' and y' by $-\pi/4\omega$, the relations for an amplifier can be written with real coefficients k and k' in the form

$$\begin{aligned} y &= kx + k'x' \\ y' &= k'x + kx' \end{aligned} \qquad (2.4)$$

and

$$k^2 - k'^2 = 1, \text{or } k' = \sqrt{k^2 - 1}. \qquad (2.5)$$

Quantum-mechanical interpretation for (2.4) requires that, while x and y are annihilation operators, x' and y' are not annihilation but creation operators. This situation is related to the negative temperature in the laser and the effective negative energy quanta in the amplifier.

§3. Wave Packet for a Parametric Oscillator

"The characteristic property of a degenerate parametric amplifier is its phase-locking property. In other words, it amplifies one vector component, say, the cosine component of a sinusoidal input signal, while it attenuates the quadrature (sine) component. This unique property of degenerate parametric amplification will be discussed from a quantum-mechanical standpoint.

Instead of employing the more customary approach using a molecular model of the nonlinear optical system based on the higher-order perturbation theory, we will take a simple classi-

cal model of a harmonic oscillator having a time-varying force constant and to try to solve the corresponding Schrödinger equation. While such a model seems to have little resembrance to the multiple quantum transition scheme of parametric action, the property of wave equations obtained for such a variable parameter system would be an interesting problem in quantum mechanics which can be solved rigorously."

The Schrödinger equation for a harmonic oscillator with an effective mass m is expressed as

$$i\hbar \frac{\partial \psi}{\partial t} = -\frac{\hbar^2}{2m}\frac{\partial^2 \psi}{\partial x^2} + \frac{K}{2}x^2\psi \qquad (3.1)$$

where $K = m\omega^2$ will be modulated in a parametric oscillator. Equation (3.1) is known to have a solution which represents a wave packet in the form

$$\psi = \exp(-ax^2 + bx + c) \qquad (3.2)$$

where $a, b,$ and c are functions of time. We find

$$|\psi|^2 = \exp[-2(\mathrm{Re}\ a)x^2 + 2(\mathrm{Re}\ b)x + 2(\mathrm{Re}\ c)] \qquad (3.3)$$

so that the width of this Gaussian distribution is

$$\Delta x = (4\mathrm{Re}\ a)^{-\frac{1}{2}} \qquad (3.4)$$

and the position of the maximum probability is given by

$$x_m = \frac{\mathrm{Re}\ b}{2\ \mathrm{Re}\ a} \qquad (3.5)$$

Let us put (3.2) into the Schrödinger equation (3.1). Then we obtain

$$2i\hbar m(-\dot{a}x^2 + \dot{b}x + \dot{c}) = -\hbar^2(4a^2x^2 - 4abx + b^2 - 2a) + mKx^2.$$

Since both sides are polynomials of the second order in x, we obtain a set of equations as follows:

$$2i\hbar m\dot{a} = 4\hbar^2 a^2 - mK \tag{3.6}$$

$$2im\dot{b} = 4\hbar ab \tag{3.7}$$

$$2im\dot{c} = \hbar(2a - b^2) \tag{3.8}$$

Now if we write

$$a = -\frac{im}{2\hbar} \cdot \frac{\dot{\xi}}{\xi} \tag{3.9}$$

we obtain

$$m\ddot{\xi} = -K\xi \tag{3.10}$$

which is exactly the classical equation of harmonic oscillation when K is constant.

To obtain x_m and δx, we have to calculate Re a and Re b. We find

$$\text{Re } \dot{a} = \frac{\hbar}{im}a^2 + \text{c.c.} = \frac{4\hbar}{m}(\text{Re } a)(\text{Im } a) \tag{3.11}$$

from (3.6), and

$$\frac{d}{dt}|\xi|^2 = \dot{\xi}\xi^* + \text{c.c.} = \frac{2i\hbar a}{m}|\xi|^2 + \text{c.c.} = -\frac{4\hbar}{m}|\xi|^2 \text{Im } a \tag{3.12}$$

from (3.9). Equations (3.11) and (3.12) give

$$\frac{d}{dt}(|\xi|^2 \text{ Re } a) = 0$$

so that

$$|\xi|^2 \text{Re } a = C_1 \tag{3.13}$$

where C_1 is a constant.

Equation (3.7) is solved by using (3.9)

$$\frac{\dot{b}}{b} = -\frac{\dot{\xi}}{\xi}$$

to give

$$b = C_2/\dot{\xi}. \tag{3.14}$$

Here the integration constant C_2 is related to the unit for measuring the magnitude of $\dot{\xi}$.

Equation (3.5) is then written as

$$x_m = \frac{C_1 \operatorname{Re}\xi}{|\xi|^2 \operatorname{Re} a} = \frac{C_2}{2C_1} \operatorname{Re} \xi .$$

If we take $2C_1 = C_2$ for convenience, the center of the oscillating wave packet is given by

$$x_m = \operatorname{Re} \xi . \tag{3.15}$$

Now a parametric oscillator can be represented by using

$$K(t) = m\omega^2[1 + 2q\cos 2\omega' t] \tag{3.16}$$

where ω is the natural frequency of oscillation for $q = 0$. We will treat the simplest case of resonant excitation from $t = 0$ to t_1, when $\omega' = \omega$ and $q \ll 1$. The general solution of (3.10) for $q = 0$, when $t < 0$ or $t_1 < t$, is written in the form

$$\xi = A_1 e^{i\omega t} + A_2 e^{-i\omega t}. \tag{3.17}$$

We obtain

$$(\Delta x)^2 = \frac{\hbar}{m}\left(\frac{\dot{\xi}}{\xi} - c.c.\right)^{-1}$$

$$= \frac{\hbar}{2m\omega} \frac{|A_1|^2 + |A_2|^2 + A_1 A_2^* e^{2i\omega t} + A_1^* A_2 e^{-2i\omega t}}{|A_1|^2 - |A_2|^2} \tag{3.18}$$

from (3.4) and (3.9).

We see that harmonic oscillation of a wave packet with a constant width corresponds to the case $A_2 = 0$ and

$$\xi = A_1 e^{-i\omega t} \tag{3.19}$$

so that the locus of ξ becomes a circle.

"The form (3.17) obviously applies to the part $t < 0$ as well as to the part $t > t_1$. If we use A_1, A_2 to denote the coefficient values valid before amplification (i.e., $t \leq 0$) and B_1, B_2 to denote the values valid after amplification ($t \geq t_1$), then we must have a linear relation

$$\begin{aligned} B_1 &= k_{11}A_1 + k_{12}A_2 \\ B_2 &= k_{21}A_1 + k_{22}A_2 \end{aligned} \tag{3.20}$$

which completely describes the characteristics of the amplification. Here we note that the relation (3.20) must give real final values of ξ if we give real initial values for ξ, since the differential equation has only real coefficients. Since real values of ξ correspod to the conditions $A_1^* = A_2$ and $B_1^* = B_2$, we put these in (3.20) and get the conditions

$$k_{22} = k_{11}^*, \quad k_{21} = k_{12}^* \tag{3.21}$$

for the transformation coefficients.

By properly shifting the time origins in both input and output independently, we can make the coefficients real and positive, so that (3.20) may become

$$\begin{aligned} B_1 &= kA_1 + k'A_2 \\ B_2 &= k'A_1 + kA_2. \end{aligned} \tag{3.22}$$

-224-

Invariance of the Wronskian, $|B_1|^2 - |B_2|^2 = |A_1|^2 - |A_2|^2$, requires that condition

$$k^2 - k'^2 = 1 , \qquad (3.23)$$

The relation (3.22) can be thought of as a canonical form of the input-output relation for a degenerate parametric amplifier. It is not only gives the relation for the center of distribution (mean value) but also gives the relation for the width (or variance)."

Let us apply (3.22) to an input wave packet corresponding to the coherent state of an optical signal as given by

$$\xi_0 = A_0 e^{i\omega t} . \qquad (3.24)$$

From (3.18) its width is

$$\Delta x_0 = \sqrt{\frac{\hbar}{2m\omega}} . \qquad (3.25)$$

Then the output is given from (3.22) by

$$\xi = kA_0 e^{i\omega t} + k' A_0 e^{-i\omega t} \qquad (3.26)$$

and the width of the output wave packet is calculated from (3.18) to be

$$\Delta x = \Delta x_0 \sqrt{k^2 + k'^2 + 2kk'\cos 2\omega t} . \qquad (3.27)$$

This shows how the width varies with time. Since $k' = \sqrt{k^2 - 1}$, we find that

$$\Delta x_{max} / \Delta x_0 = k + \sqrt{k^2 - 1}$$

$$\Delta x_{min} / \Delta x_0 = k - \sqrt{k^2 - 1} = \Delta x_0 / \Delta x_{max}$$

The center position of the wave packet is obtained from

(3.15) to become

$$x_m = |\xi| \cos \phi \qquad (3.28)$$

where ϕ is the phase angle of $\xi = |\xi| e^{i\phi}$. From (3.26) we obtain

$$|\xi|^2 = |A_0|^2 (k^2 + k'^2 + 2kk' \cos 2\omega t) \qquad (3.29)$$

The signal-to-noise ratio of the output is hence written in the form

$$(S/N) = \frac{x_m}{\Delta x} = \frac{|A_0|}{\Delta x_0} \cos\phi \qquad (3.30)$$

from (3.27, 28, and 29). Since $|A_0| = |\mathrm{Re}\,\xi|$ is the amplitude of the input signal and Δx_0 the input noise, the S/N of the output is equal to that of the input signal, provided that the output is observed at an instant when ξ becomes real ($\phi = 0$). It is [redacted] noted that the instant for the maximum value of S/N does not in general coincide with the instant of maximum deviation (maximum of Re ξ).

"If we take a limit $\xi \to 0$, we obtain a pulsating wave packet whose center is at rest. In classical oscillators, parametric excitation has no effect whatever if it is initially at rest. In quantum-mechanical oscillators, on the contrary, the wave function can make a natural pulsating oscillation at a frequency twice the natural frequency of translatory oscillation, and application of parametric excitation at the frequency of this natural pulsating oscillation results in the

building-up of the pulsation, quite independently of the existence of translatory oscillation. The pulsation of wave packet may somehow be regarded as amplification of the zero-point fluctuation.

If there is a translatory oscillation, this will also build up (Fig. 2), and the ratio of the amplification of this translatory oscillation is just equal to the amplification of zero-point fluctuation if it has a proper phase, as we have shown.

If we use q_0 and p_0 instead of A_1 and A_2 , and q and p instead of B_1 and B_1, using the relations

$$q_0 = A_1 + A_2, \quad p_0 = i\omega m(A_1 - A_2)$$
$$q = B_1 + B_2, \quad p = i\omega m(B_1 - B_2). \tag{3.31}$$

then (3.22) are transformed to

$$q = (k + k')q_0$$
$$p = (k - k')p_0. \tag{3.32}$$

Obviously, q_0 and q have the meaning of the coordinates, and p_o and p the velocities or momenta, at the specified instant.

It would be appropriate at this point to make some remarks from the standpoint of quantum-mechanical measurement.

In quantum mechanics, measurements of the cosine and sine components of oscillation may be regarded as the measurement of coordinate q and the momentum p, respectively. In fact a harmonic oscillator is a system in which the roles of q and p are constantly being interchanged, but we can define a measurement of q and p by specifying a fixed time point to make the

measurement.

Our results are in good accord with the uncertainty principle. The input-output relations (3.22) satisfy

$$\Delta q \, \Delta p = \Delta q_0 \, \Delta p_0 \tag{3.33}$$

since $k^2 - k'^2 = 1$. In the absense of input signal we have $\Delta q_o = \Delta x_0$ and $\Delta p_0 = \omega m \Delta x_0$, where Δx_0 is given by (3.25) so that we can find

$$\Delta q \, \Delta p \geq \omega m (\Delta x_0)^2 = \hbar/2 \tag{3.34}$$

which is exactly the uncertainty relation.

From what has been said, we may regard the degenerate parametric amplifier as a practical method of observing either q or p with arbitrary accuracy. We have seen that, in the degenerate parametric amplifier, the minimum noise just equals the zero-point fluctuation multiplied by the amplification factor, so that no deterioration of S/N ratio results. This is in contrast to the case of an ordinary amplifier where noise was $\sqrt{2k^2 - 1}$ times the zero-point fluctuation, and for large k we have a 3-dB deterioration of the S/N ratio, and it is of some interest to study this point in some detail.

Apparently, this 3-dB difference may be regarded as a compensation for the loss of information on the quadrature component in the degenerate parametric amplifier. In order to make the argument convincing we take the follwing model (Fig. 3).

We have two degenerate parametric amplifiers, the q-amplifier and p-amplifier, which will be used for amplifying the two com-

ponents separately. The input signal coming into a waveguide is divided using an ideal branch and is fed into these amplifiers. Their outputs are again combined using another branch, so that we have an output which would appear as if an output of an ordinary amplifier. What would be the overall S/N ratio of this whole system?

Let the input power S/N be a^2 (with respect to quantum noise). At the input of each amplifier, we would have an S/N ratio of $a^2/2$, since the signal power is halved by the branching, while the noise remains the same. Or we can say that noise power is also halved, but the same amount of noise power is added that comes from the blind guide. The output branch would also cause a minimum power loss of 3dB, but this is immaterial for the S/N consideration since we now have a sufficiently strong signal. Hence we see that over-all S/N ratio is 3dB less than a single phase-locking amplifier, that is, just equal to an ordinary amplifier."

§4. Conclusion

We have seen that the degenerate parametric oscillator allows us to measure either the cosine component q or the sine component p of a coherent wave with any accuracy within the limit of the uncertainty relation $\Delta q \Delta p = \hbar/2$.

Furthermore, photon interpretation of parametric excitation and the probability distribution of photon numbers in the case of a degenerate parametric amplifier were discussed in detail in ref. 1), pp. 284-291.

At the time when Professor Takahasi proposed in 1963 that the quantum noise could be squeezed in degenerate parametric oscillation, no optical parametric oscillation had been achieved. Although the optical parametric oscillator was believed to be realizable, the required driving power was believed to be too high at that time to consider any application to low-noise measurements.

References

1) H. Takahasi: Kagaku 33(1963)434-439. (in Japanese)

2) H. Takahasi: *Advances in Communication Systems*, vol. 1 (1965) pp. 227-310.

Figure Captions

Fig.1 Schematic diagram of an attenuator or a linear amplifier

Fig.2 Parametric amplification of a wave packet. Note that S/N ratio is unchanged at the peak points.

Fig.3 Combination of two phase-locking amplifiers; equivalent to an ordinary amplifier.

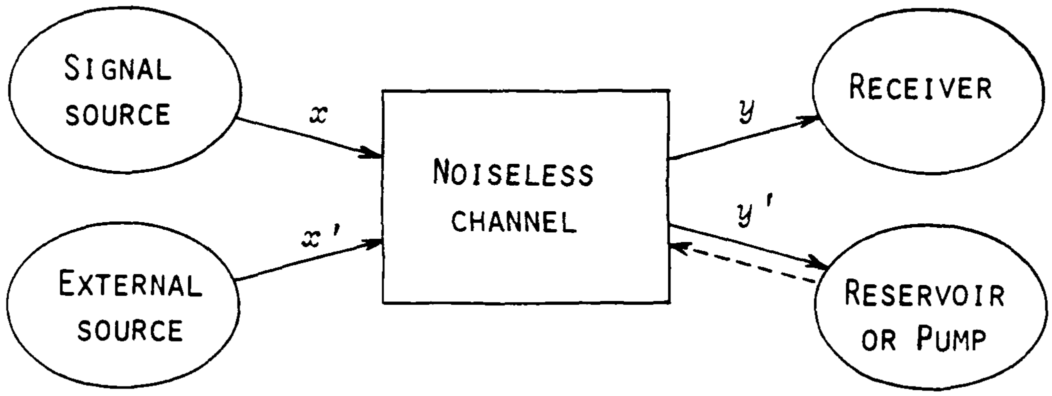

Fig.1 Schematic diagram of an attenuator or a linear amplifier

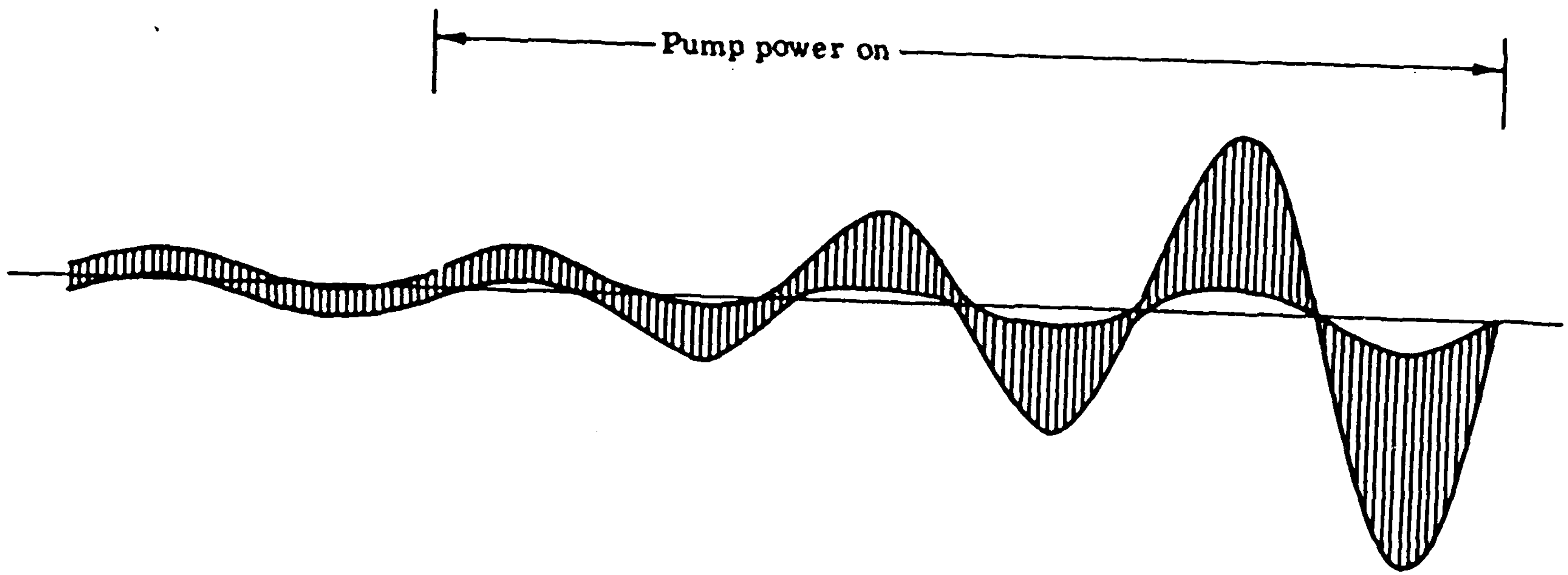

Fig.2 Parametric amplification of a wave packet. Note that S/N ratio is unchanged at the peak points.

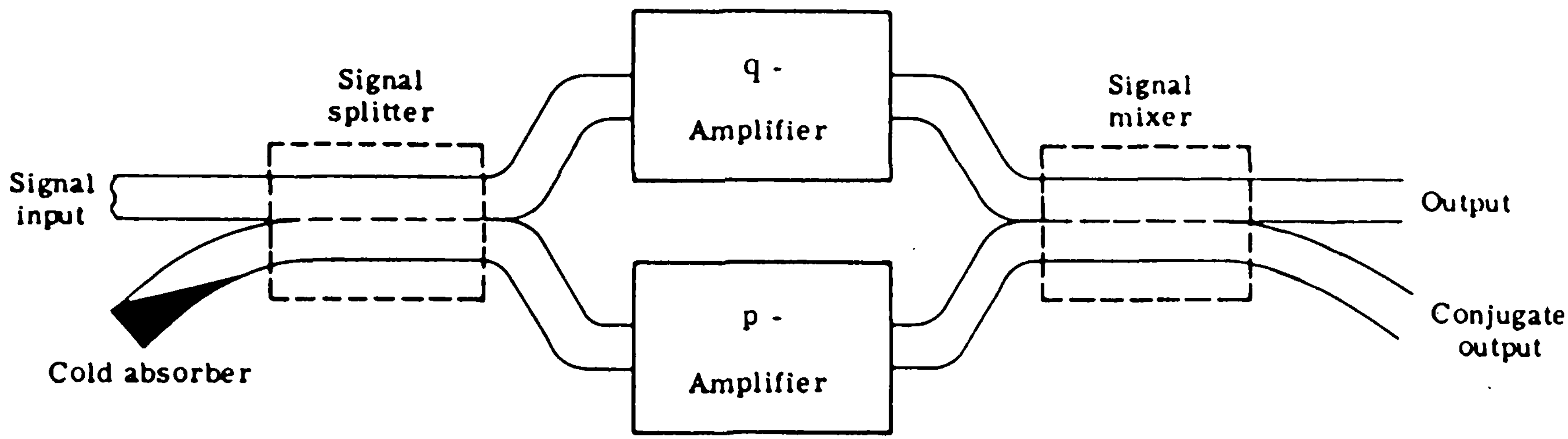

Fig.3 Combination of two phase-locking amplifiers; equivalent to an ordinary amplifier.

Squeezed States of Light

H.J. Kimble, R.J. Brecha, L.A. Orozco, M.G. Raizen,
L.A. Wu, and M. Xiao
Department of Physics
University of Texas at Austin
Austin, Texas 78712

Summary

In our laboratory squeezed states of light have been generated in two distinct physical systems. The first experiment investigates squeezing for two-level atoms coupled to the intracavity field of a high quality optical resonator. For large coupling of the atoms to the cavity field, there is a mode splitting in the eigenvalue structure of the system analogous to the splitting found when two otherwise independent pendulums are coupled by a spring. We employ the coupling-induced structure of the composite system to generate squeezing (1-3). The second experiment involves the process of degenerate parametric down conversion in which a photon of frequency 2ω is split into a correlated pair of photons at the subharmonic frequency ω. While we have observed noise reductions of greater than 60% relative to the vacuum-state limit, a quantitative analysis of the various propagation and detection losses in the current apparatus indicates that the field would in fact be squeezed more than ten-fold in the absence of these losses. Quite recently we have made use of the squeezed light to demonstrate that precision measurements can be made with a sensitivity greater than that given by the vacuum-state or shot-noise limit.

References

1. M.G. Raizen, L.A. Orozco, Min Xiao, T.L. Boyd, and H.J. Kimble, "Squeezed-state Generation by the Normal Modes of a Coupled System", Phys. Rev. Letter 59, 198 (1987).

2. L.A. Orozco, M.G. Raizen, Min Xiao, R.J. Brecha, and H.J. Kimble, "Squeezed State Generation in Optical Bistability", J. Opt. Soc. Am. B (October, 1987).

3. Min Xiao, H.J. Kimble and H.J. Carmichael, "Squeezed State Generation for Two-Level Atoms in a Spatially Varying Field Mode", J. Opt. Soc. Am. B (October, 1987).

4. L.A. Wu, H.J. Kimble, J.L. Hall, and Huifa Wu, "Generation of Squeezed States by Parametric Down Conversion", Phys. Rev. Lett. 57, 2520 (1986).

5. L.A. Wu, Min Xiao, and H.J. Kimble, "Squeezed States of Light from an Optical Parametric Oscillator", J. Opt. Soc. Am. B (October, 1987).

6. Min Xiao, L.A. Wu, and H.J. Kimble, "Precision Measurement Beyond the Shot-Noise Limit", Phys. Rev. Lett. 59, 278 (1987).

PULSED SQUEEZED LIGHT

Talk by R. E. Slusher
U.S./Japan Conference
7/22/87

Generation of interesting quantum states of light, including squeezed states and number states, requires a large nonlinear interaction (or nonlinear phase shift $\Delta\phi_{NL}$). At the same time, the length of the nonlinear generating medium must be short enough so that there is very small loss, $\alpha\ell << 1$ where α is the linear absorption constant and ℓ is the effective length of the nonlinear medium. A pulsed pump field can be used in many nonlinear systems to obtain high peak powers and the nonlinear phase shifts $\Delta\phi_{NL} \sim 1$ required for quantum light states in media which are sufficiently short to obtain $\alpha\ell << 1$. There is also a broader range of high-intensity laser pump sources available in a pulsed mode. This talk describes an extension of standard generation and homodyne detection experimental techniques to the pulsed case. An earlier paper referenced in VG-1 described the theory upon which these experiments are based. It is expected that by using mode-locked pulse trains as the pump laser and a portion of the pulse train as the local oscillator for the homodyne detector that squeezing can be observed which is comparable to the CW case but which corresponds to generation by the **peak** laser pump intensity in the pulse train. No cavity is required in cases where the peak pump intensity is sufficiently large. This allows squeezing over very large bandwidths limited only by phase-matching conditions in the nonlinear medium.

A number of interesting quantum phenomena may be associated with pulsed conditions including quantum noise on soliton pulses propagating in optical fibers, free electron nonlinearities, pulsed communications or data processing systems and short time scale measurements. An example of short time scale measurements is interferometry where the shot noise limit will be a dominant limitation at very short times ($\sim$ ps or fs) when there are very few photons per pulse.

Viewgraphs 3 through 6 describe the analysis of pulsed squeezing. As shown in VG-6, the optimum noise reduction in the Gaussian pulse envelope approximation is only slightly reduced from the CW case or the case when the local oscillator pulse length $\tau_{LO} << \tau_P$ the pump pulse length.

Viewgraphs 7 and 8 describe a pulsed LO homodyne detector which is working at present. Limits due to amplifier and photodiode saturation restrict the dynamic range of this detector. A balancing network between the photodiodes and the amplifier reduces the amplifier saturation problem.

Experiments in progress are described in VU 9-12. GAWBS noise in the glass fiber experiment is still a problem in the pulse case, since this extra phase modulation noise scales with the peak pump power. A parametric down-conversion experiment using KTP will probably allow a demonstration of pulsed squeezing but the noise reduction is not expected to be spectacular.

The talk concludes with a short discussion of pulsed measurement of interference in phase space (VU 13) and a summary. A paper on this topic is in preparation and will be available this fall.

PULSED SQUEEZING

I. Why Pulsed?

II. Generation of Pulsed Squeezed Light

III. Homodyne Detection

IV. Experiments

- A. Detector
- B. Glass Fiber
- C. Bananas
- D. KTP

Collaborators: Experiment – Philippe Grangier
Arthur LaPorta

Theory – Bernard Yurke
Mary Potasek

PRA 35, 3586 (1987)

VU-1

WHY PULSED SQUEEZING?

I. Nonlinear-Gain/Linear-Loss Increased

→ More Squeezers

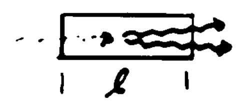

$\alpha \ell \ll 1$

$\Delta\phi_{NL} \sim \frac{2\pi \ell}{\lambda} \Delta n$

$\propto E_p$

II. More Laser Pumps Achieve

$\Delta\phi_{NL} \sim 1$

III. No Cavity Required

→ Broad Band Squeezing

IV. Interesting Pulsed Phenomena

— Quantum Noise on Solitons in Optical Fibers

— FEL, TOK, etc.

— Atomic Radiation

— Communications Systems & Data Processing

— Short Time Scale Measurements

TOP
DO NOT AFFIX OVERLAYS ALONG THIS SURFACE

GENERATION OF PULSED SQUEEZED LIGHT

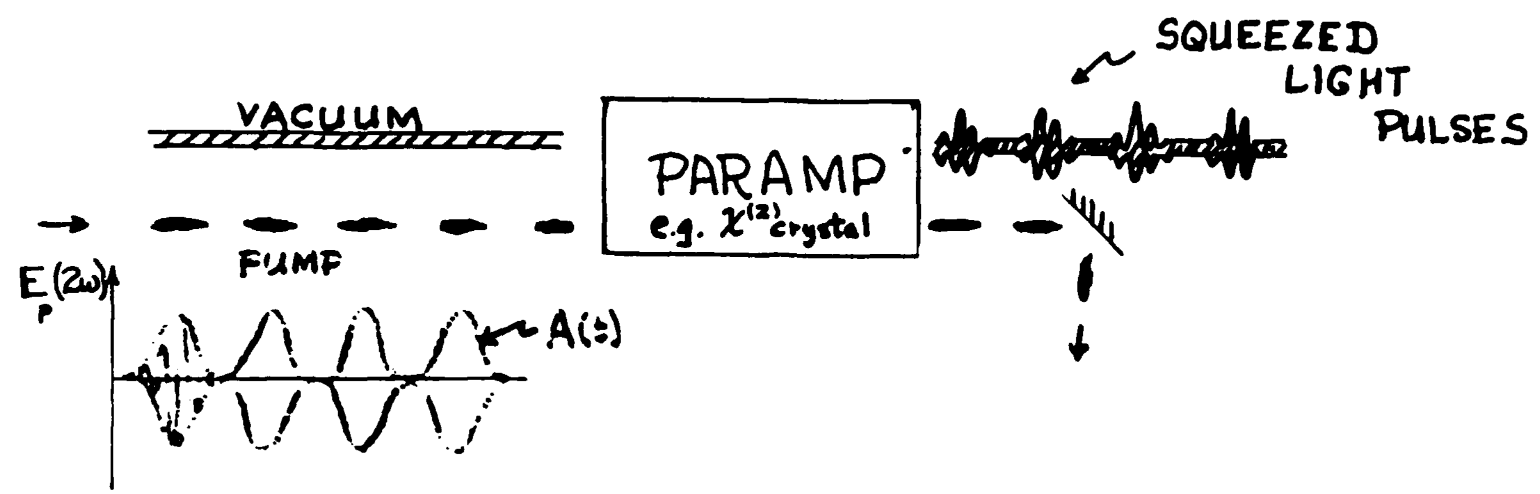

VII-3

SQUEEZED FIELD: $E_s^{(+)}(0,t) = \mathcal{E}_0 \int a(\omega)\, e^{-i\omega t}\, d\omega$

$$E_s^{(+)}(x,t) = \cosh\left[\frac{2K(t-x/v)\,x}{v}\right] E_s^{(+)}(0,t-x/v) - e^{-i\theta}\sinh\left[\frac{2K(t-x/v)\,x}{v}\right] E_s^{(-)}(0,t-x/v)$$

WHERE NONLINEAR PHASE SHIFT:

$$\Delta\phi_{NL}(t) \sim \omega_0 K(t) \sim \chi_{NL} A(t)$$

$\sim 1 \Rightarrow$ LARGE SQUEEZING

TOP
DO NOT AFFIX OVERLAYS ALONG THIS SURFACE

HOMODYNE DETECTION FOR PULSED SQUEEZED LIGHT

— "Strobe" detect squeezed pulses with pulsed local oscillator

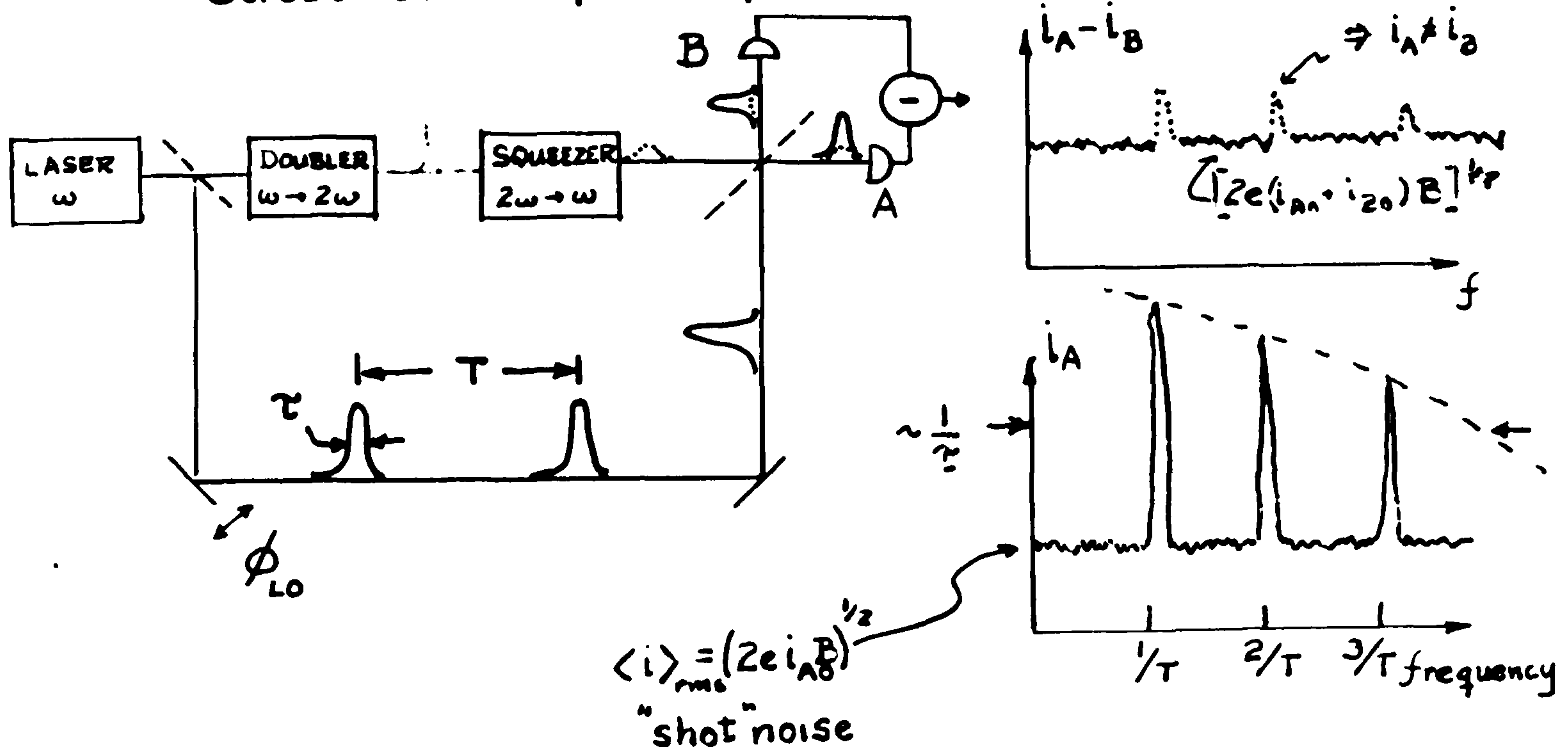

VII-4

NOISE POWER SPECTRUM FOR PULSED SQUEEZED LIGHT

$$S_n(\omega)_{\substack{Max\\Min}} = \frac{\int_{-T/2}^{+T/2} F_{LO}^2(t)\exp[\pm 2\Delta\phi_{NL}(t)]\,dt}{\int_{-T/2}^{+T/2} F_{LO}^2(t)\,dt}$$

$$\Delta\phi_{NL}(t) = \Delta\phi_{NLO}\, A_p(t)/A_{po}$$

PUMP AMPL. ENVELOPE

e.g.

$$F_{LO}(t) = F_{LO}(0)\exp(-t^2/2\sigma^2)$$

Double for Pump

$$A_p(t) = A_{po}\exp(-t^2/\sigma^2)$$

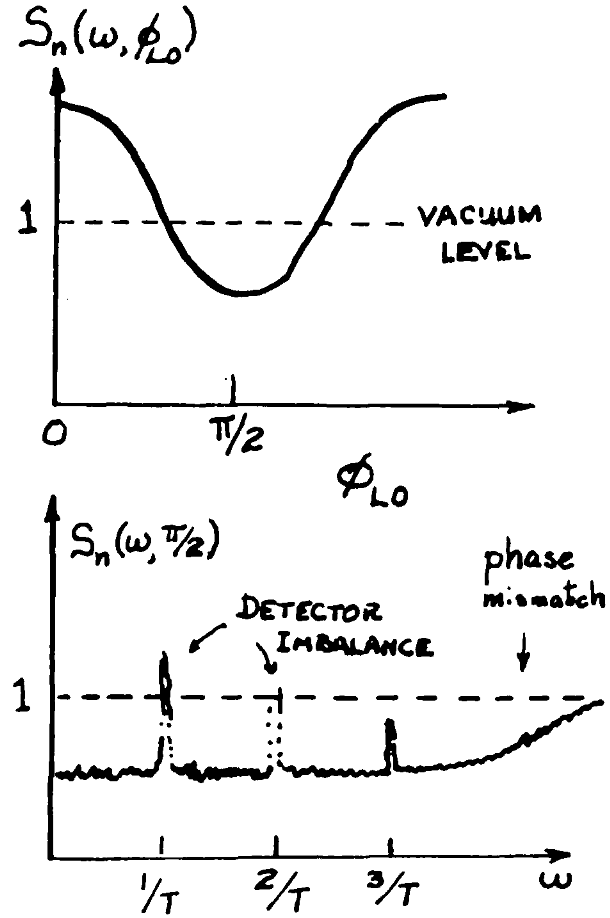

VU-5

TOP
DO NOT AFFIX OVERLAYS ALONG THIS SURFACE

SQUEEZED NOISE

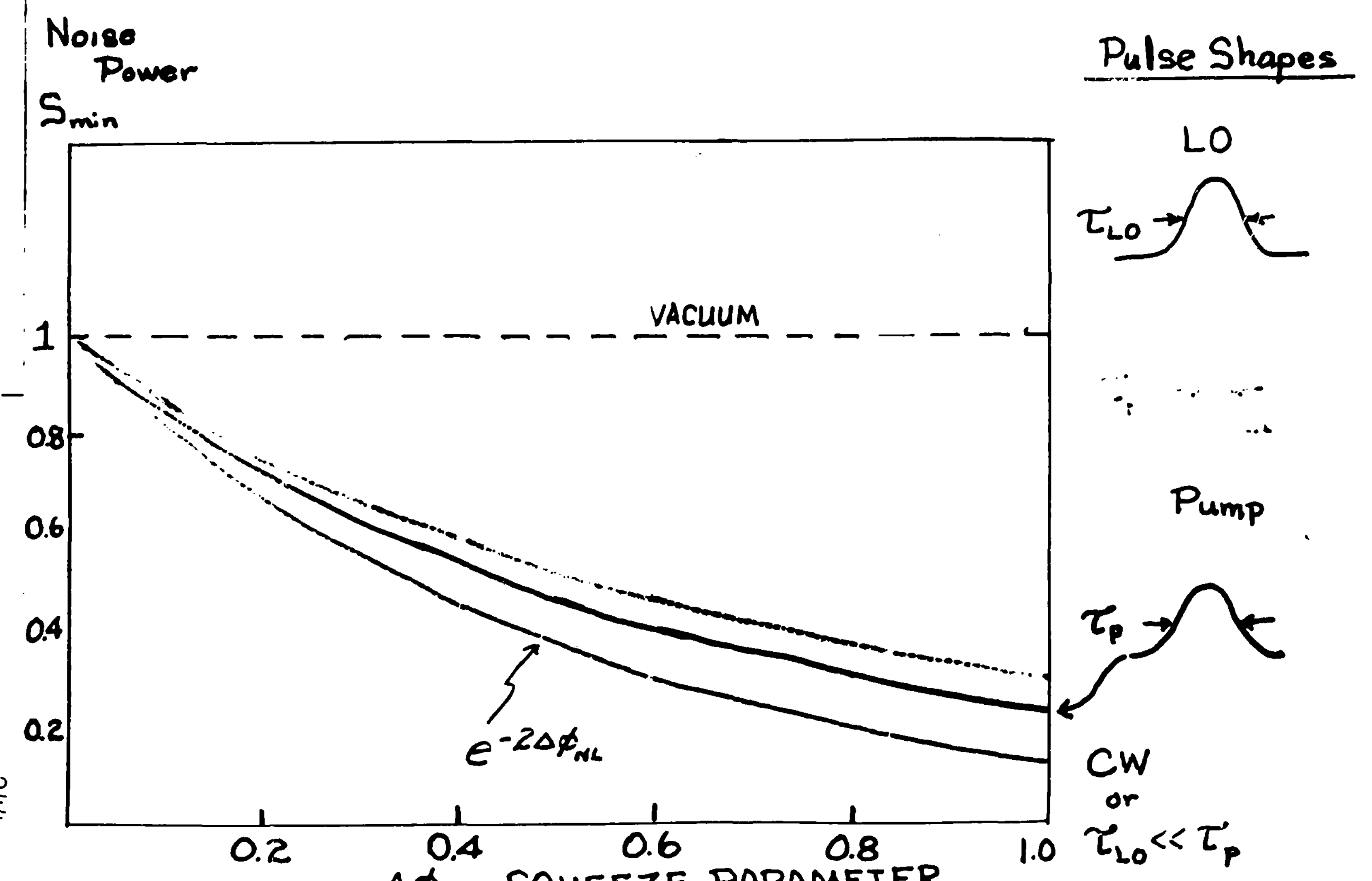

VU-6

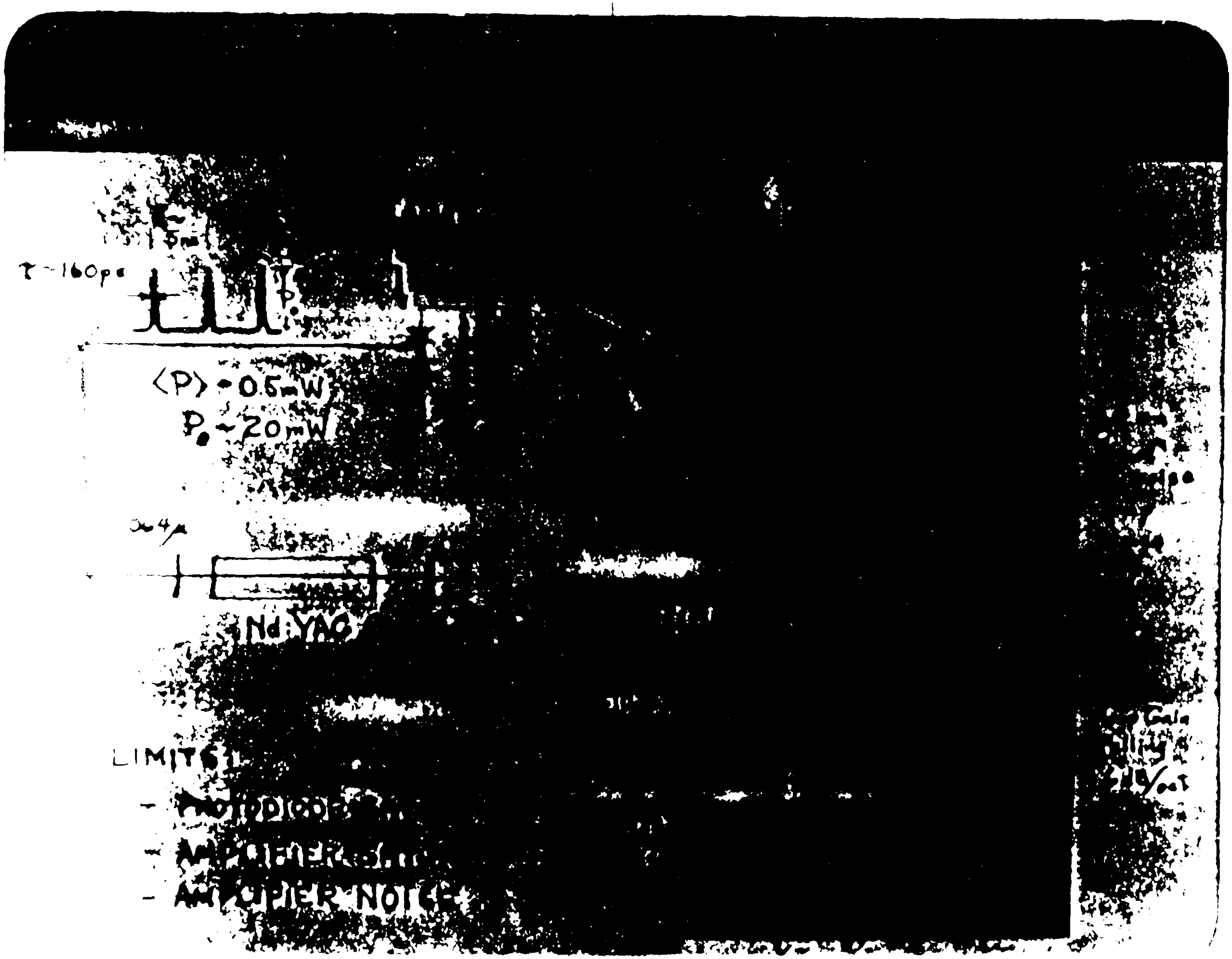
τ ~ 160ps
⟨P⟩ ~ 0.5mW
P0 ~ 20mW
Nd:YAG
LIMITS

TOP
DO NOT AFFIX OVERLAYS ALONG THIS SURFACE

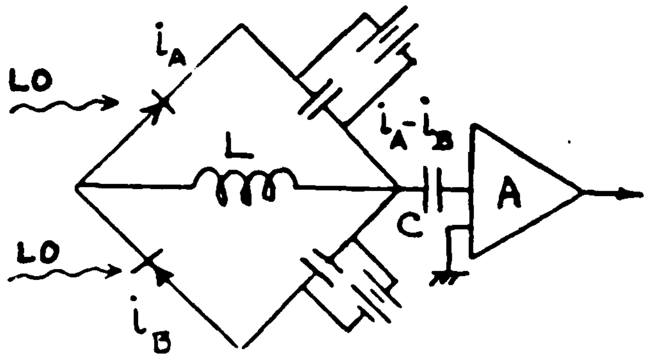

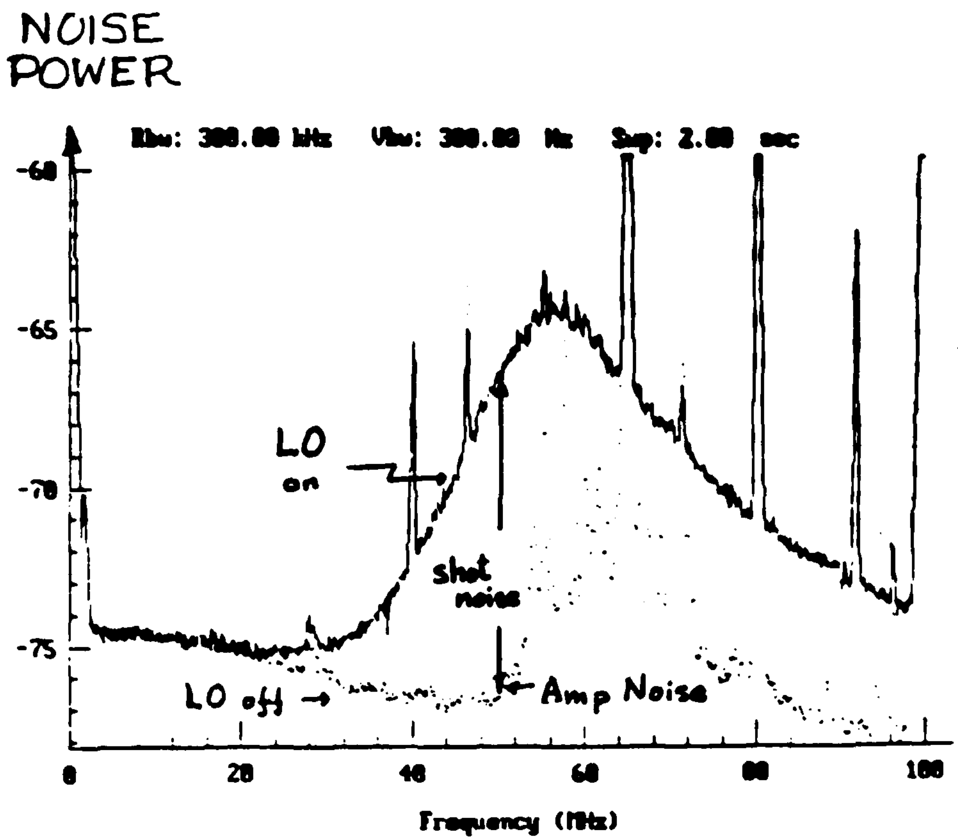

$$\frac{\omega_r}{2\pi} \sim \frac{1}{\sqrt{LC}} \sim 50 \pm 10\,\mathrm{MHz}$$

200 MHz pulse train suppressed

VU-8

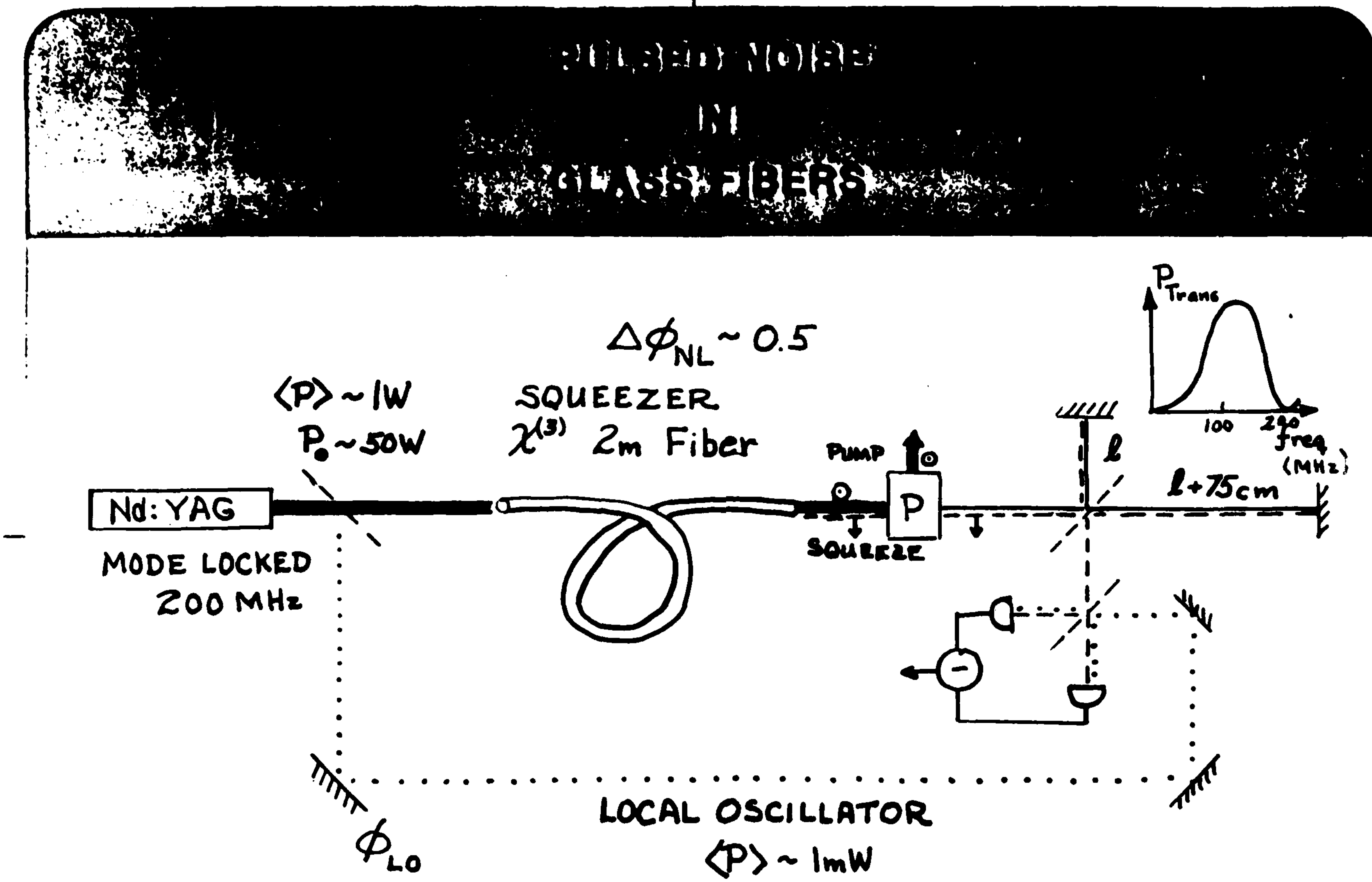
$\Delta\phi_{NL} \sim 0.5$
$\langle P \rangle \sim 1W$
$P_o \sim 50W$
SQUEEZER
$\chi^{(3)}$ 2m Fiber
PUMP
SQUEEZE
P
P_{Trans}
100
200
freq (MHz)
ℓ
$\ell + 75cm$
Nd: YAG
MODE LOCKED
200 MHz
LOCAL OSCILLATOR
$\langle P \rangle \sim 1mW$
ϕ_{LO}

VU-9

TOP
DO NOT AFFIX OVERLAYS ALONG THIS SURFACE

(VII-10)

GLASS FIBER NOISE

PULSED

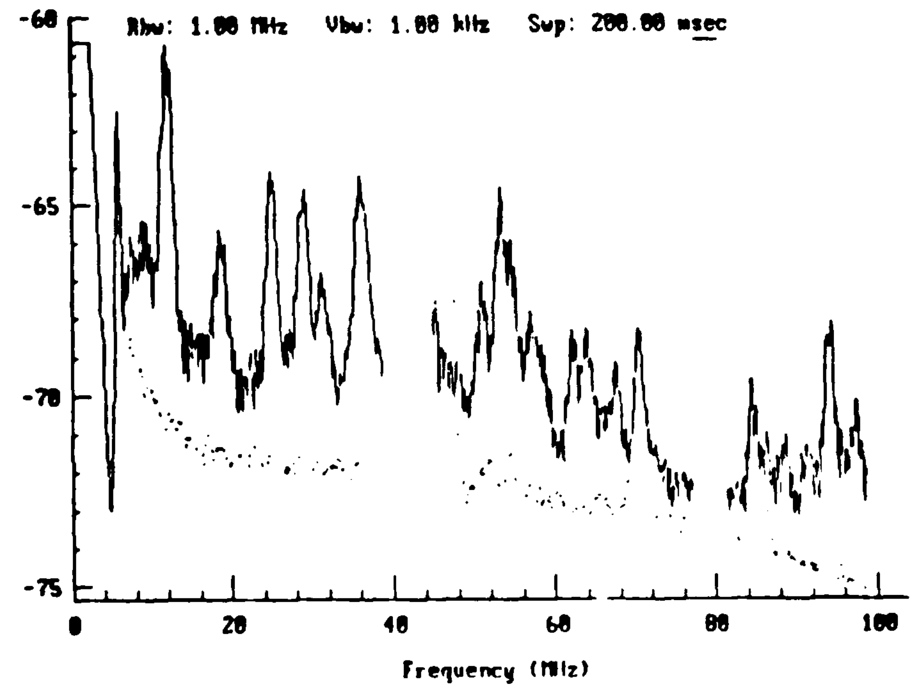

"CW"

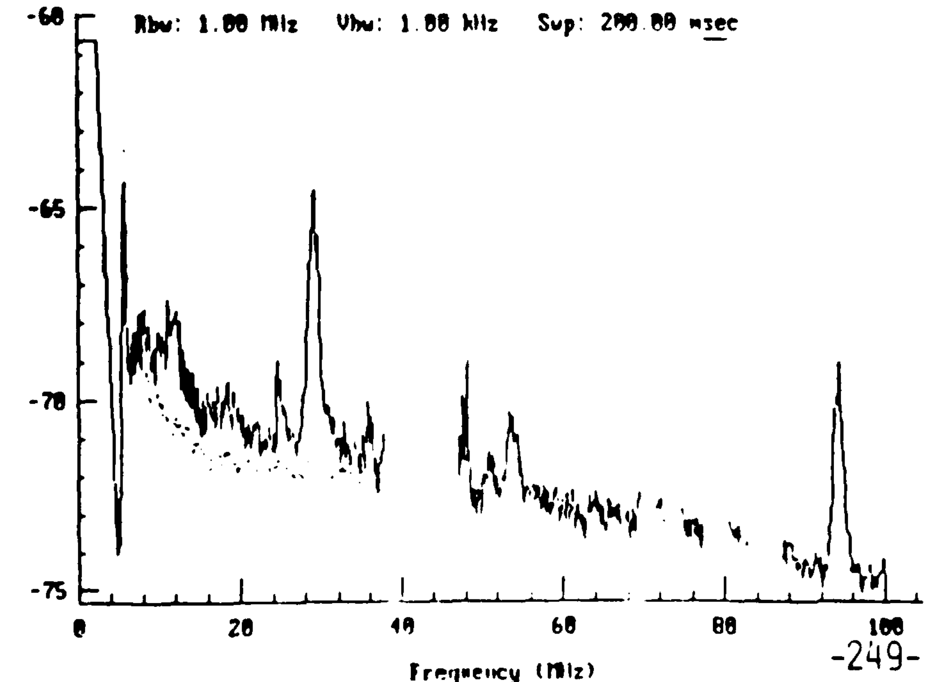

TOP
DO NOT AFFIX OVERLAYS ALONG THIS SURFACE

PRESENT EXPERIMENT

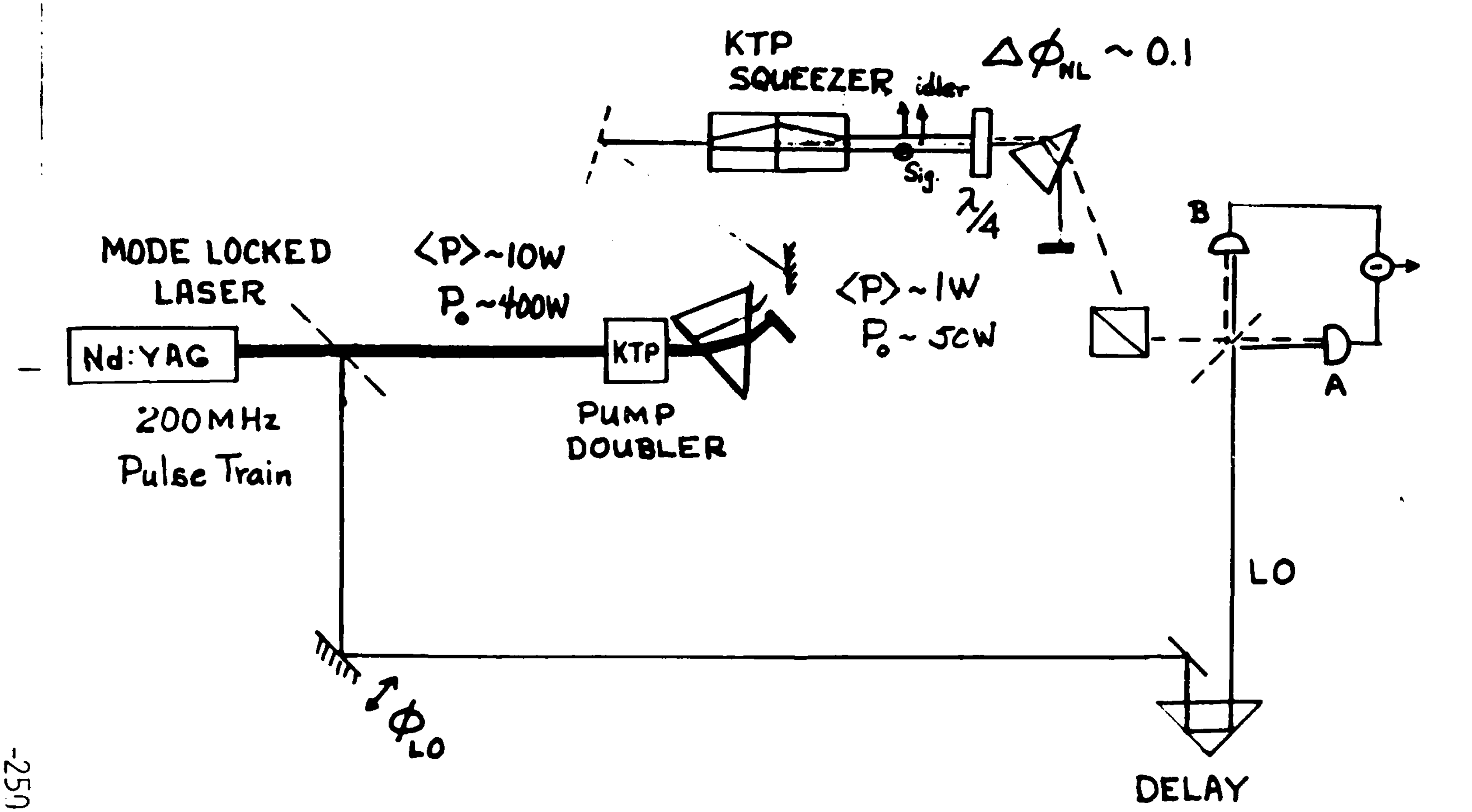

10-20% SQUEEZED NOISE REDUCTION
"POSSIBLE"

VU-12

DIRECT DETECTION PULSED SQUEEZED LIGHT

VU-13

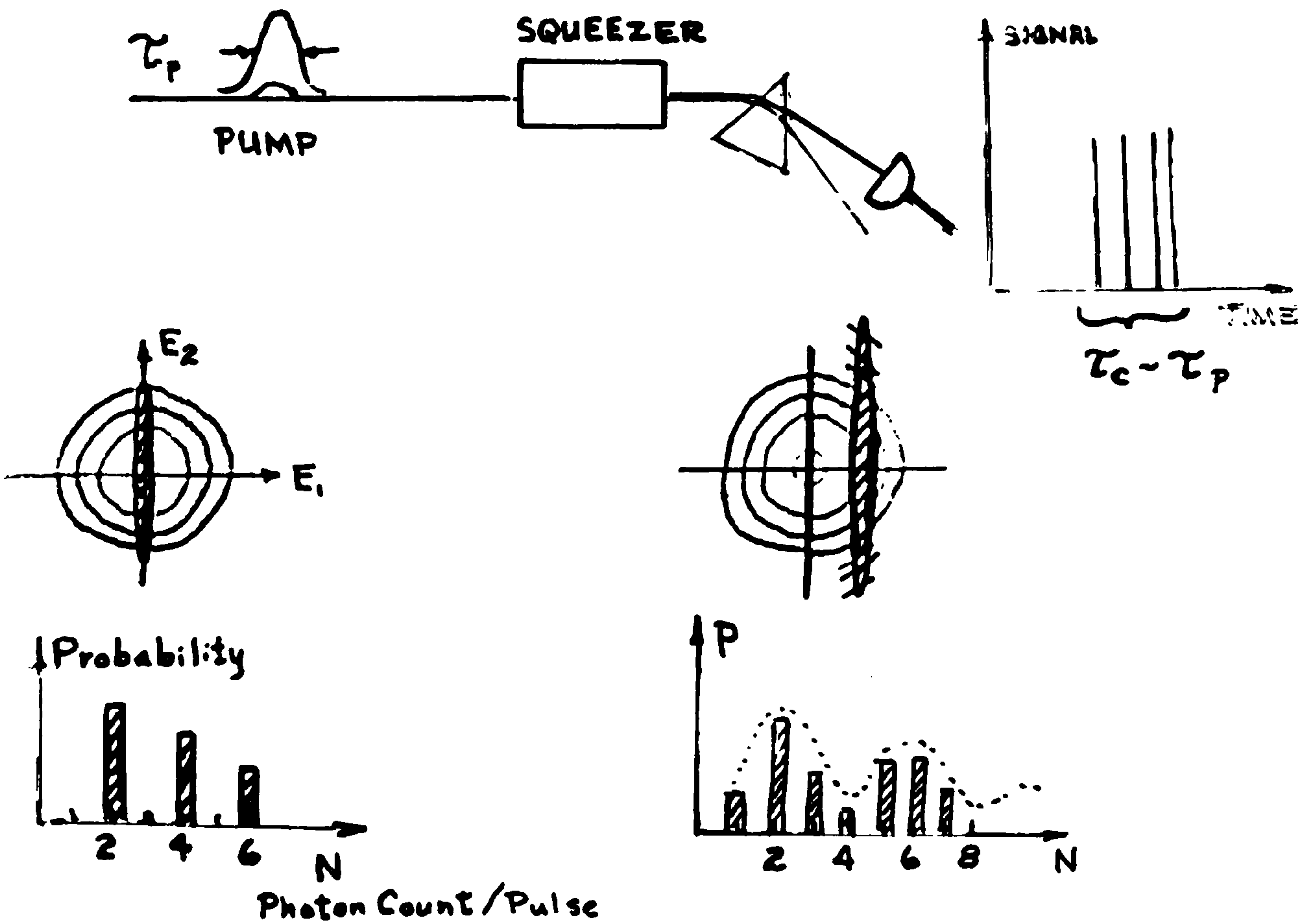

PULSED SQUEEZING
SUMMARY

I. Broader Spectral & Materials Range
Accessible for Squeezed Light

II. Homodyne Detection Works

III. No Cavity ⟶ Broadband Squeezing

IV. Applications

A. Quantum Noise on Solitons

B. Relativistic Electron Squeezing

C. Pulsed Atomic Excitation

D. Pulse Trains in Data Storage or Communications

E. Short Time Scale Precision Measurement

Quantum Nondemolition Detection and Squeezing in Optical Fibers

M.D. Levenson, R.M. Shelby, and S.H. Perlmutter

IBM Almaden Research Center
650 Harry Road
San Jose, CA 95120

The nonlinear optical interactions in an optical fiber permit the amplitude of one wave to be inferred from the phase of a coupled wave, and the partial suppression of quantum noise.

Conventional light detectors must destroy the quantum state of the electromagnetic field in order to measure its amplitude. They are Quantum Demolition detectors. The nonlinear index of refraction of an optical fiber permits one to infer the amplitude of one wave by measuring the light induced phase shift of a nonlinearly coupled wave. This process has been termed Quantum Nondemolition Detection or Back Action Evading Measurement. The amplitude of the first wave is unchanged by the interaction. That amplitude is the QND variable; the phase of the second wave is the QND readout. The uncertainty which quantum mechanics requires to be added to a system being measured appears in the phase of the first beam, not its amplitude, thus the back action is evaded.

We have demonstrated this effect by correlating the QND readout with a subsequent QDD measurement of the QND variable (1). We have demonstrated back action evasion by showing that the QND variable at the output of the detector has no greater noise than at the input - which was at the vacuum noise level.

When the correlated noise on two coupled laser beams is made to subtract coherently, the net noise level can be below the vacuum noise level. This effect has been termed "four-mode squeezing" since the fluctuations involve two sidebands of each of two strong pump waves (2). The noise on each beam can separately be above the vacuum noise level, but strong four mode correlations can lower the sum of the noise at two detectors to a value below the vacuum. Indeed, the correlations can be so strong that the noise on the two detectors can be less than that on one of them (3).

It is necessary to cool the optical fiber to 2K to suppress phase noise caused by light scattering in the optical fiber. The stimulated Brillouin effect must be suppressed by phase modulating the light to broaden the spectrum. The modulation frequency must be exactly equal to the mode spacing of the Fabry Perot interferometer needed to phase shift the carrier wave. Other experimental innovations are necessary to accurately measure the vacuum level and to maximize the effective quantum efficiency.

The same nonlinear interactions in an optical fiber give rise to conventional two-mode squeezing (4). The fluctuations in the amplitude of the beam cause correlated phase fluctuations of that beam. The nonlinear index of refraction cannot alter the amplitude of a wave. The correct superposition of amplitude and phase quadratures has been shown to have a noise level 12.5% below the vacuum level.

Squeezed light has the property that the ratio of noise to intensity rises as the light is attenuated (5). The squeezed light generated in an optical fiber is not a minimum uncertainty state as light scattering adds phase noise.

References:

1. M.D. Levenson, R.M. Shelby, M. Reid, and D.F. Walls, Quantum Nondemolition Detection of Optical Quadrature Amplitudes, Phys. Rev. Lett. 57, 2473 (1986).

2. B.L. Schumaker, S.H. Perlmutter, R.M. Shelby and M.D. Levenson, Four-Mode Squeezing, Phys. Rev. Lett 58, 357 (1987).

3. M.D. Levenson and R.M. Shelby, Four-Mode Squeezing and Applications, Optica Acta (to be published).

4. R.M. Shelby, M.D. Levenson, S.H. Perlmutter, R.G. DeVoe, and D.F. Walls, Broad-Band Parametric Deamplification of Quantum Noise in an Optical Fiber, Phys. Rev. Lett 57, 691 (1986).

5. G.J. Milburn, M.D. Levenson, R.M. Shelby, and D.F. Walls, On Optical Media for Squeezed State Generation, J. Opt. Soc. Am (to be published).

2 Conventional light detectors measure the amplitude of a light beam by absorbing photons and thus destroying the quantum state. They are QUANTUM DEMOLITION devices.

Quantum Demolition Detector (QDD)

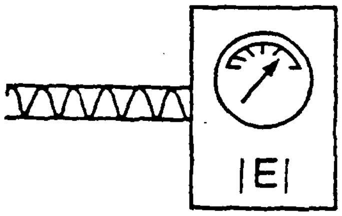

Light Absorbed

Quantum Nondemolition Detectors (QND)

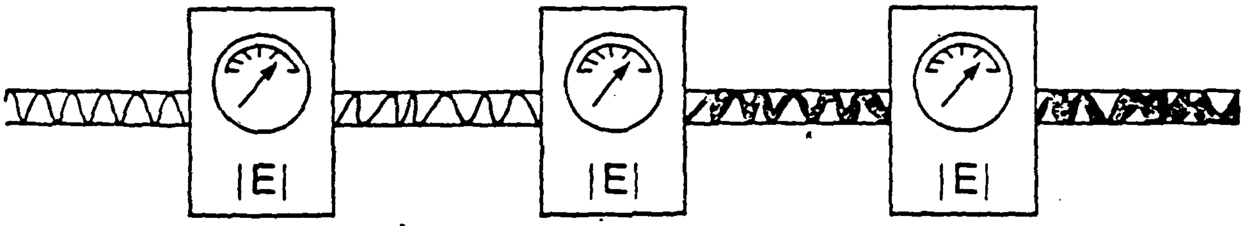

No Absorption. Phase becomes more uncertain after each measurement.

Quantum Nondemolition Measurement System

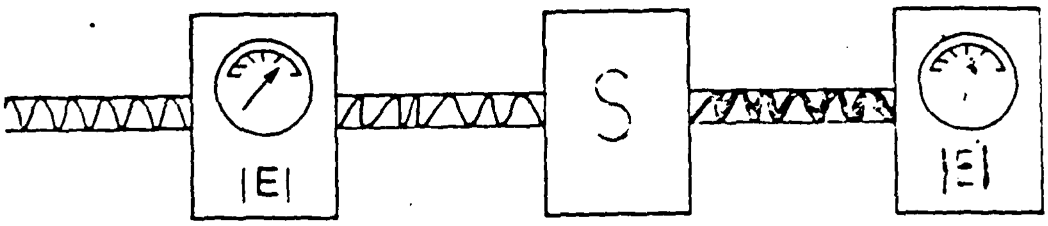

A QND measurement system would allow small amplitude changes due to a sample to be determined by comparing before and after amplitudes. Such measurements can be more accurate than the shot noise limit.

3

Nonlinearity:

$$n(E) = n_o + n_2|E|^2$$

Phase:

$$\Phi(\ell) = 2\pi n(E)\ell/\lambda$$

Some Phase Fluctuations are Correlated With Amplitude Fluctuations

$$\delta\Phi_x(\ell) = \delta\Phi(0) + 4\pi n_2|E_x|\delta E_x\ell/\lambda$$

QND Experiments - There is Another Term

$$\delta\Phi_{xy}(\ell) = \delta\Phi_x(\ell) + 8\pi n_2|E_y|\delta E_y\ell/\lambda$$

This Last Term is QND Readout

4

Quantum Nondemolition detector measures an optical power induced phase shift interferometrically.

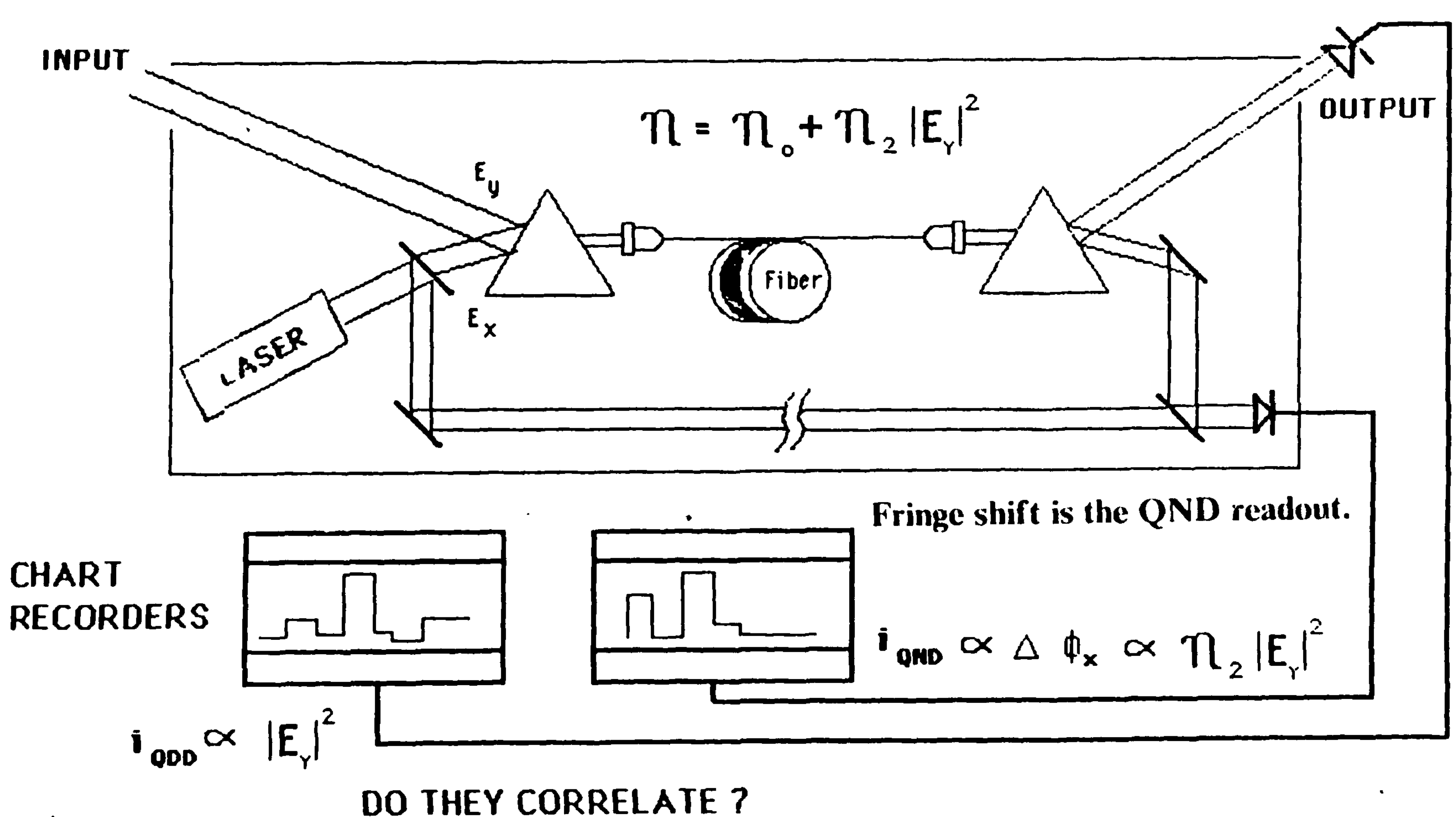

To verify that a QND measurement is valid, one must prove that it correlates with a quantum demolition measurement. To prove back action evasion, one must show that the fluctuations of the QND variable are no larger at the output of the QND meter than at the input. We have done both

5

The actual apparatus uses a coil of optical fiber as the nonlinear medium. It must be cooled to 2K to suppress phase noise caused by light scattering. The inputs must be phase modulated to suppress the stimulated Brillouin effect. At the output, the phase fluctuations of one beam are converted to amplitude fluctuations by a phase shifting cavity. Summing the delayed output of the QND readout detector DX with that of a QDD detector DY produces a signal level that varies sinusoidally with frequency - if the two signals correlate. The results are shown in the next figure.

Actual QND Apparatus.

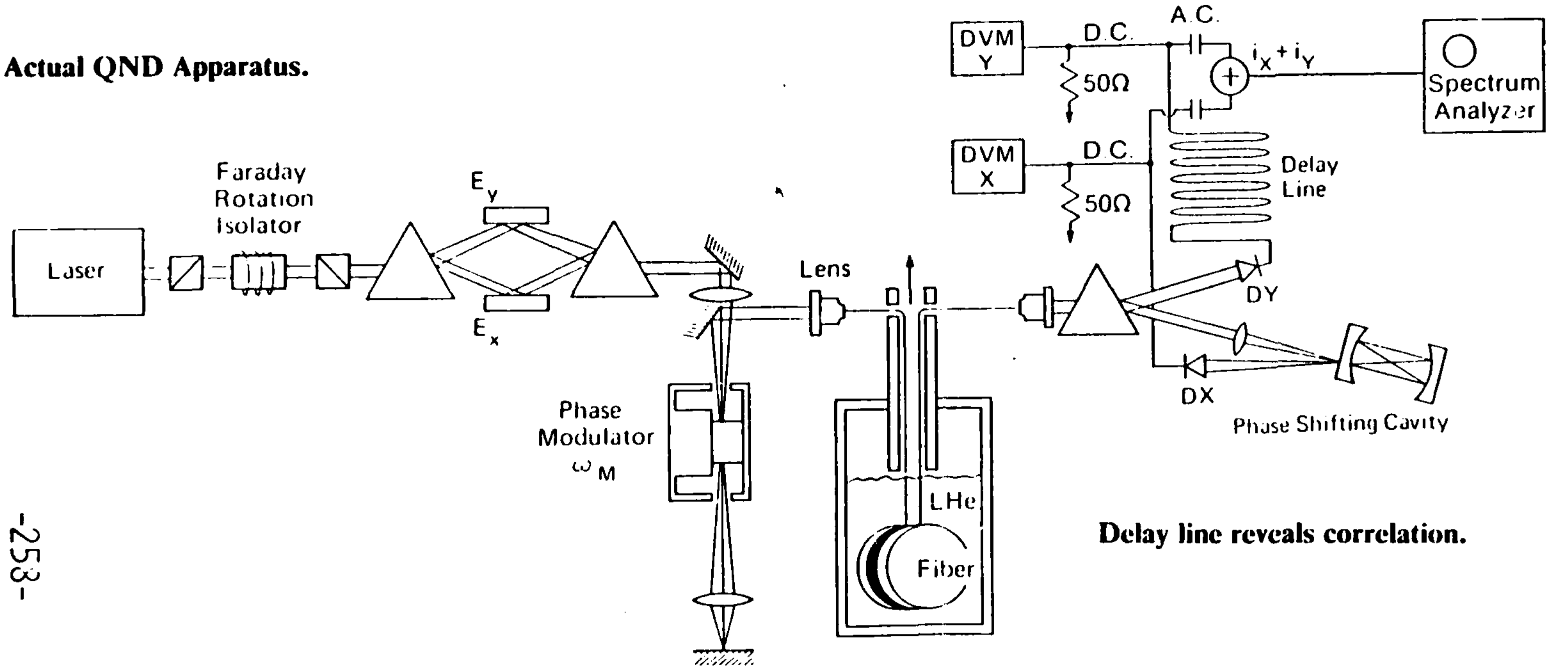

Delay line reveals correlation.

6 Sinusoidal Power Level shows interference between DX and DY signals.

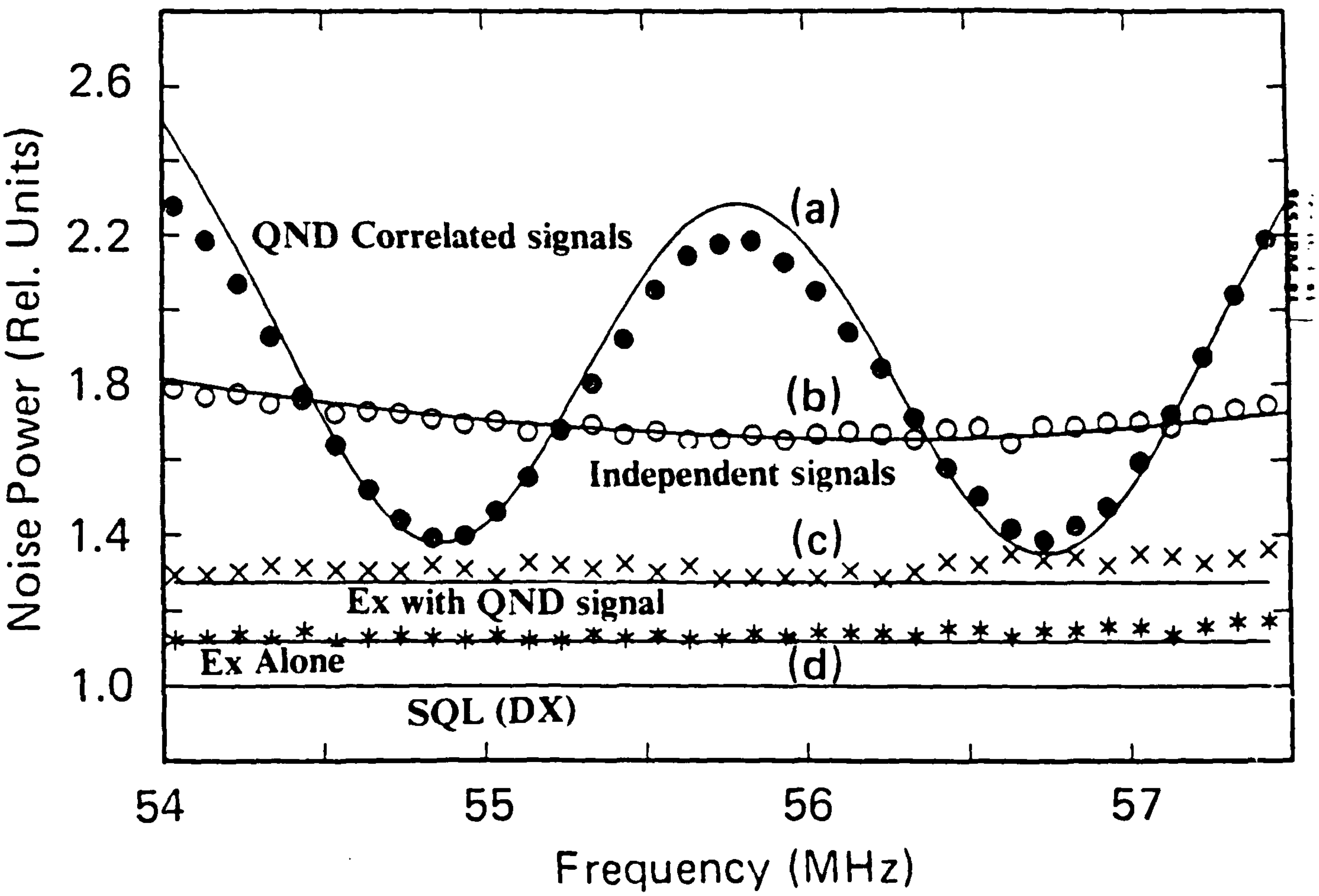

Noise below the sum of independent noises at two detectors shows quantum correlations in the QND signal.

Difference between traces (b) and (d) is the standard quantum limit noise level on detector DY.

7 Minima of sinusoid is 1 dB below sum of vacuum noise levels on two detectors.

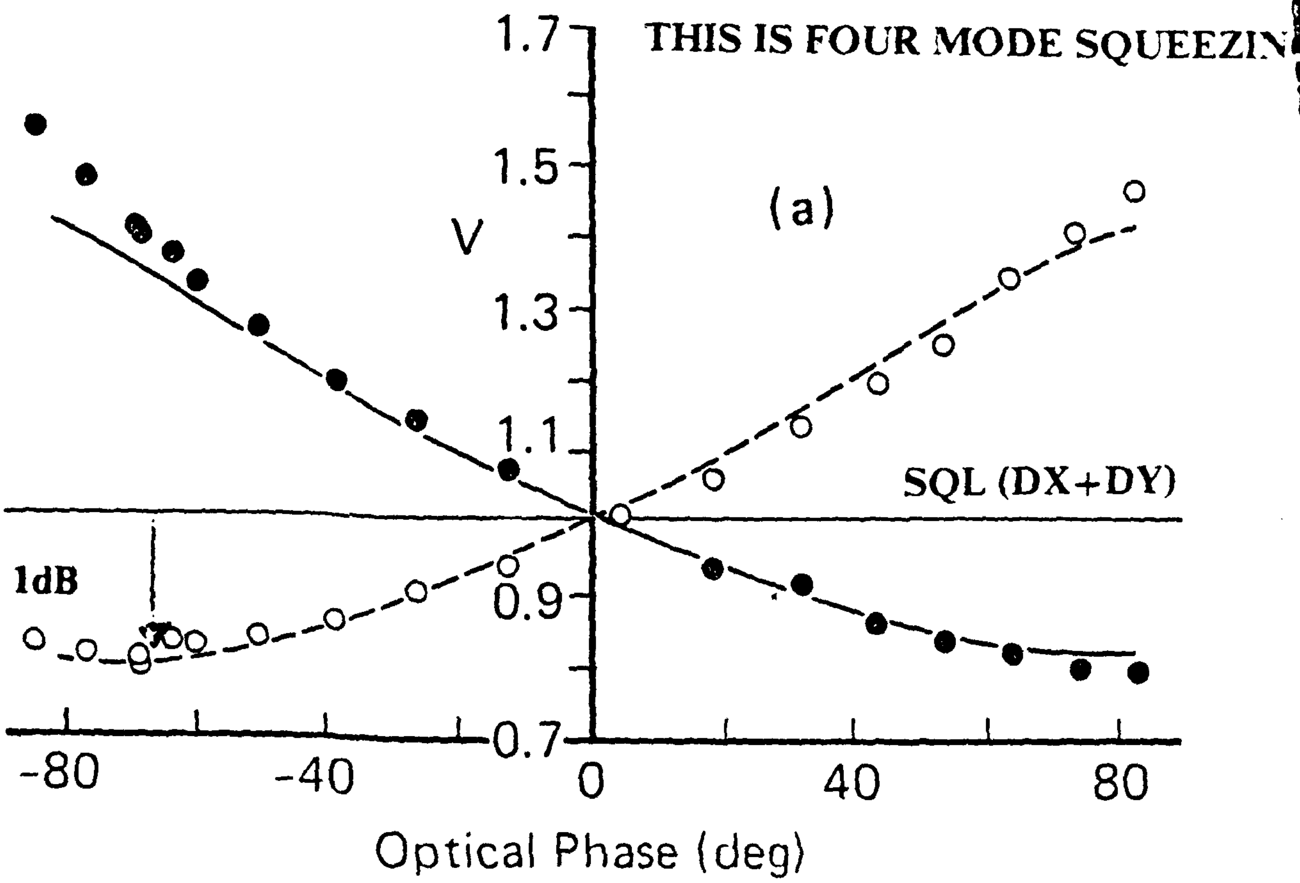

965-IBM-81

8

DY noise is at the Standard Quantum Limit, DX noise level is above, BUT with correct gains, the sum of the noise is below the quantum level on detector DY.

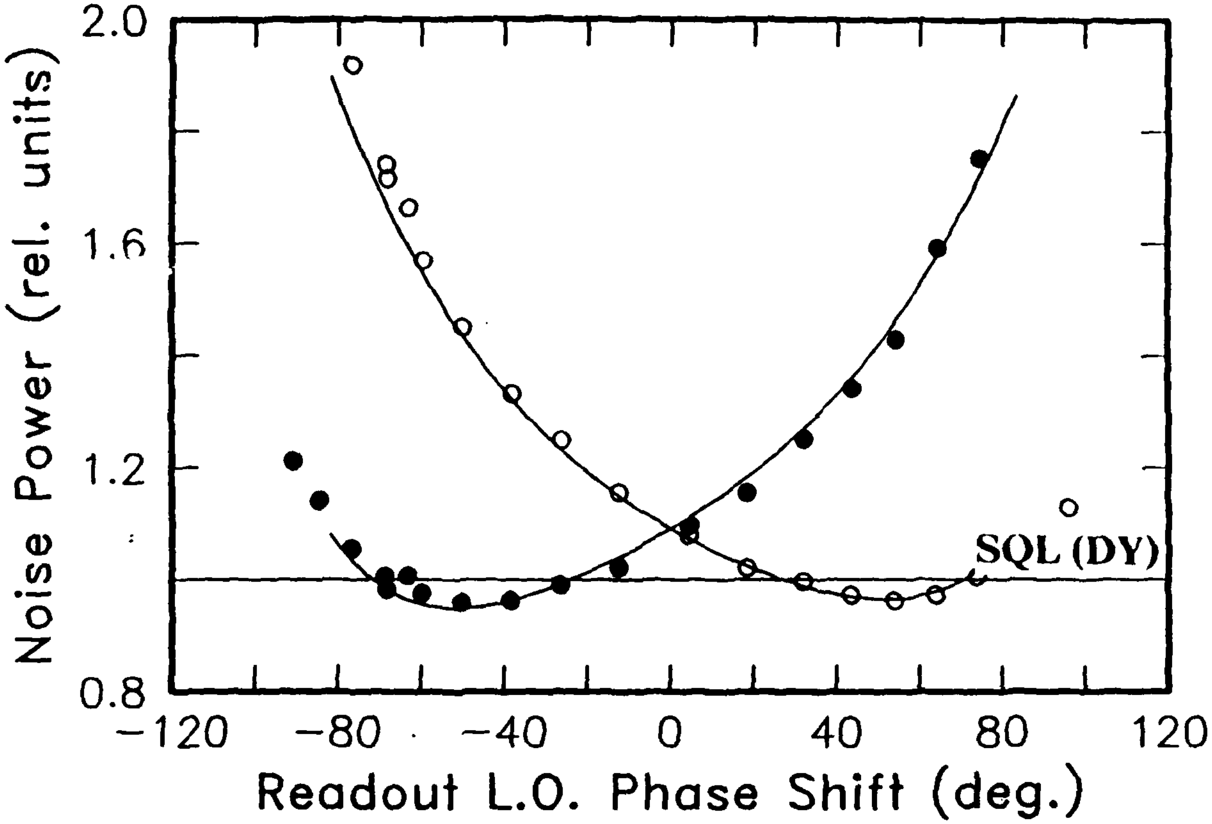

9 Quantum Cary 14 Dual Beam Spectrometer

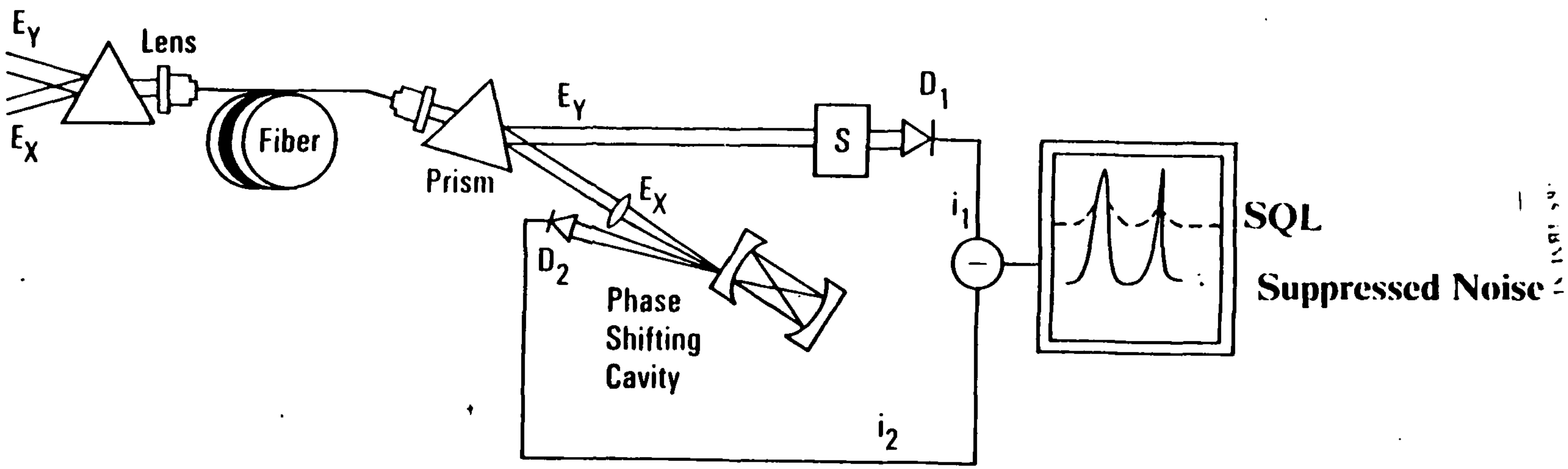

A QND detector can measure the amplitude fluctuations of a tuneable beam. That beam could then pass through a sample that absorbs weakly. A QDD detector then records the output. The fluctuations of the input can be subtracted off, resulting in an absorption spectrometer with the sensitivity of fluorescence spectroscopy.

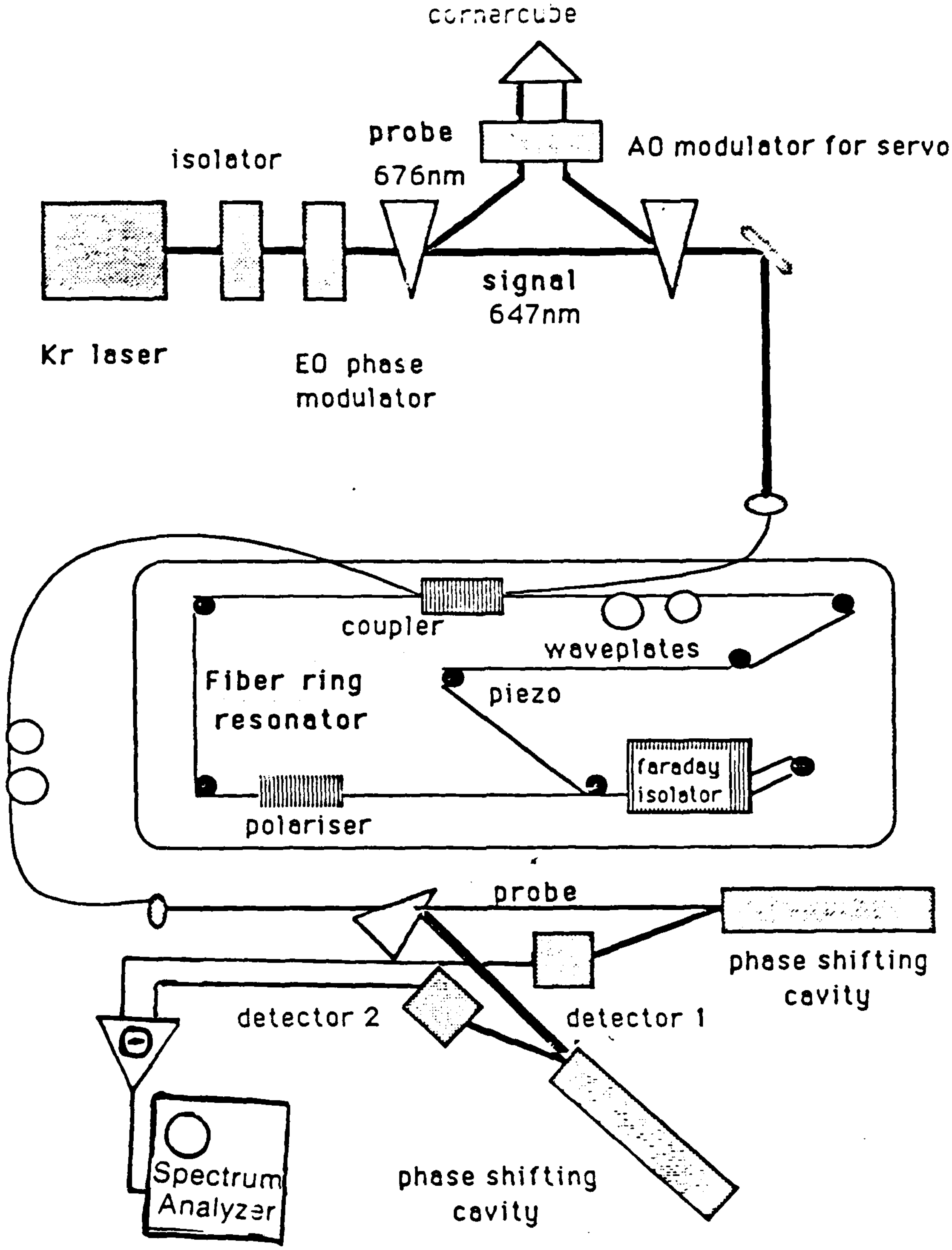

Ring Cavity 4 Mode Squeezing Experiment

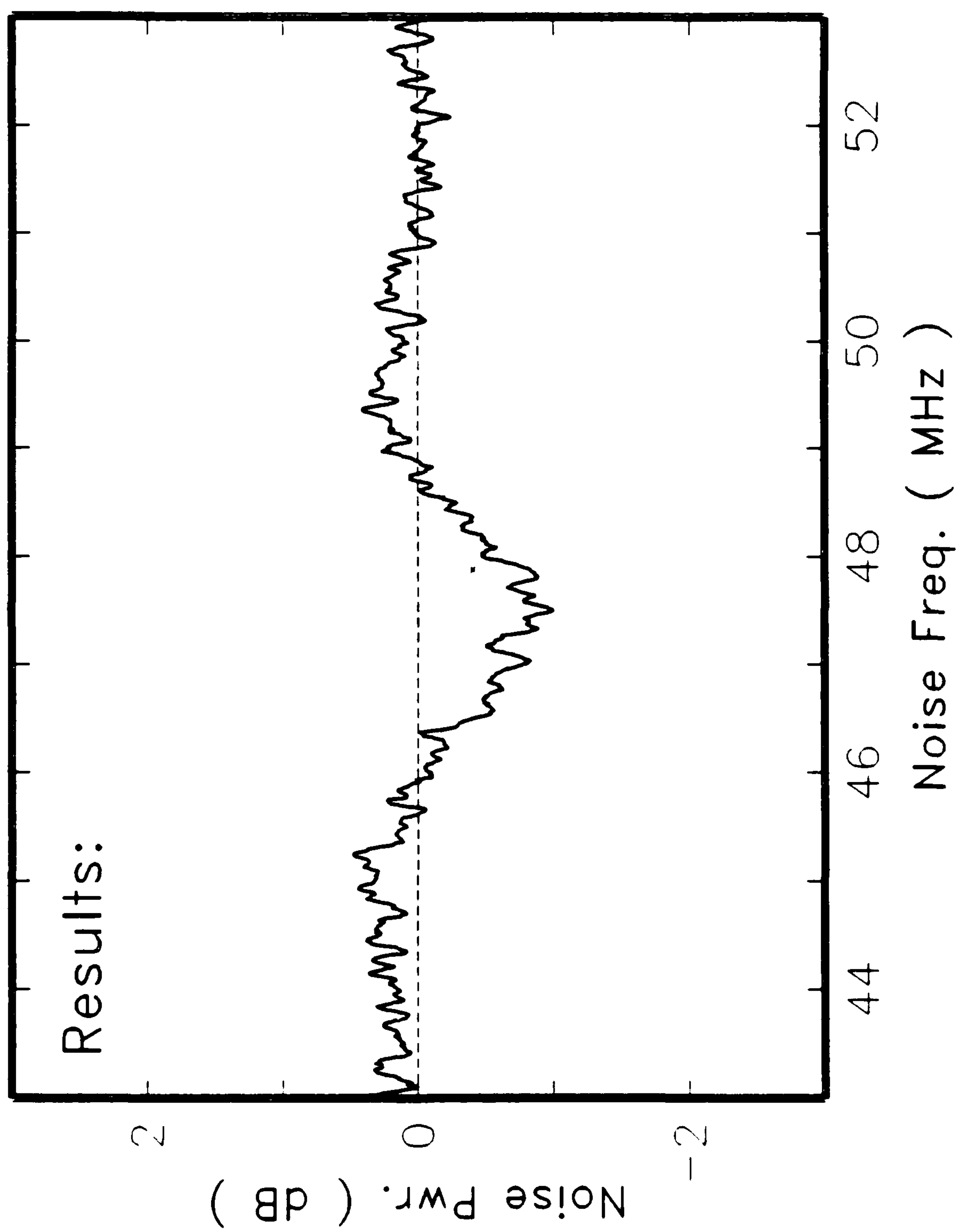
Results:
Noise Pwr. (dB)
2
0
-2
Noise Freq. (MHz)
44
46
48
50
52

10

The same nonlinearity can give rise to a squeezed state of light. The amplitude fluctuations of the beam cause correlated fluctuations of the phase of that wave. The amplitude fluctuations are unaffected. The uncertainty circle characteristic of a coherent state is converted to the ellipse of a squeezed state. Phase shifting the average amplitude permits the creation of a strong beam with suppressed amplitude or phase noise.

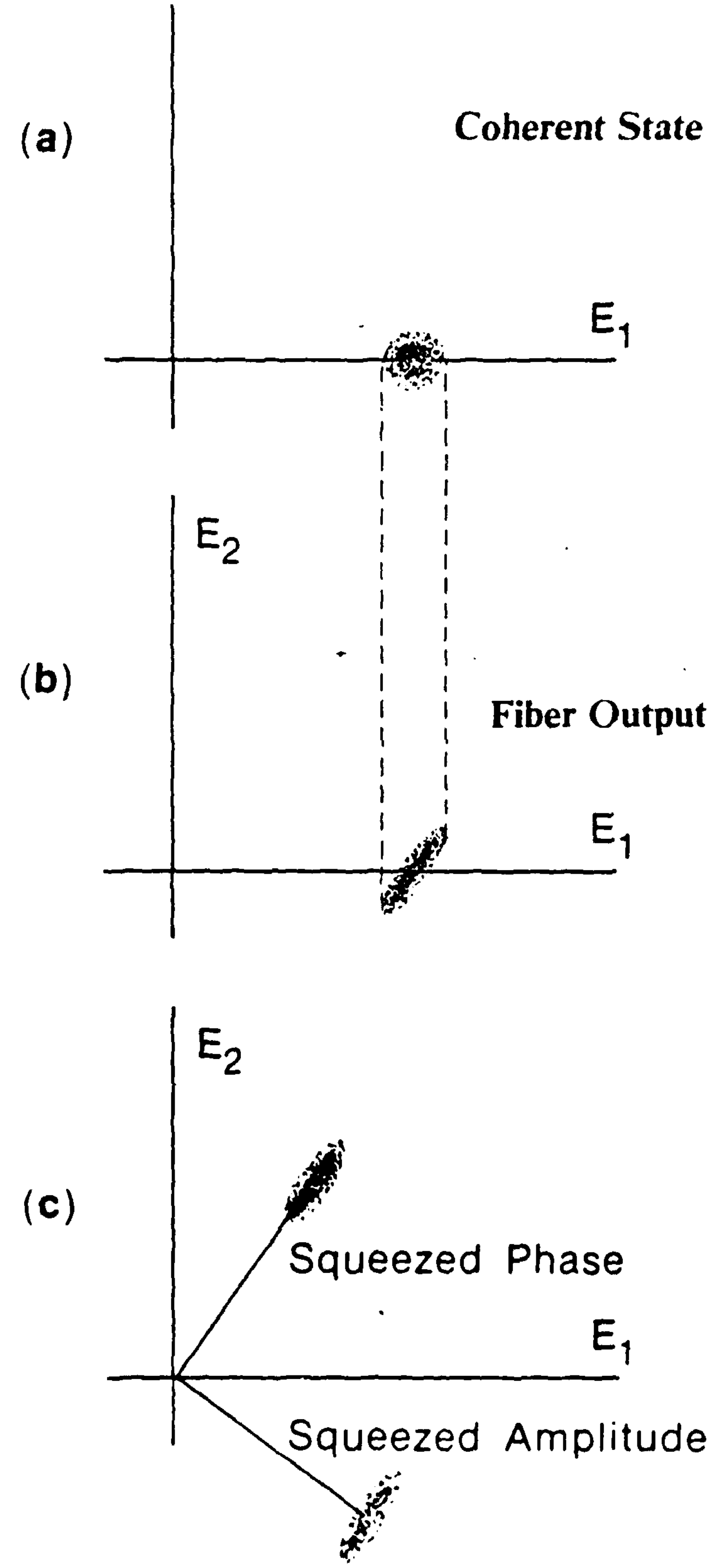

965-IBM-81

11 The apparatus is very similar to that used for QND, but only one beam is necessary.

Apparatus for Squeezing

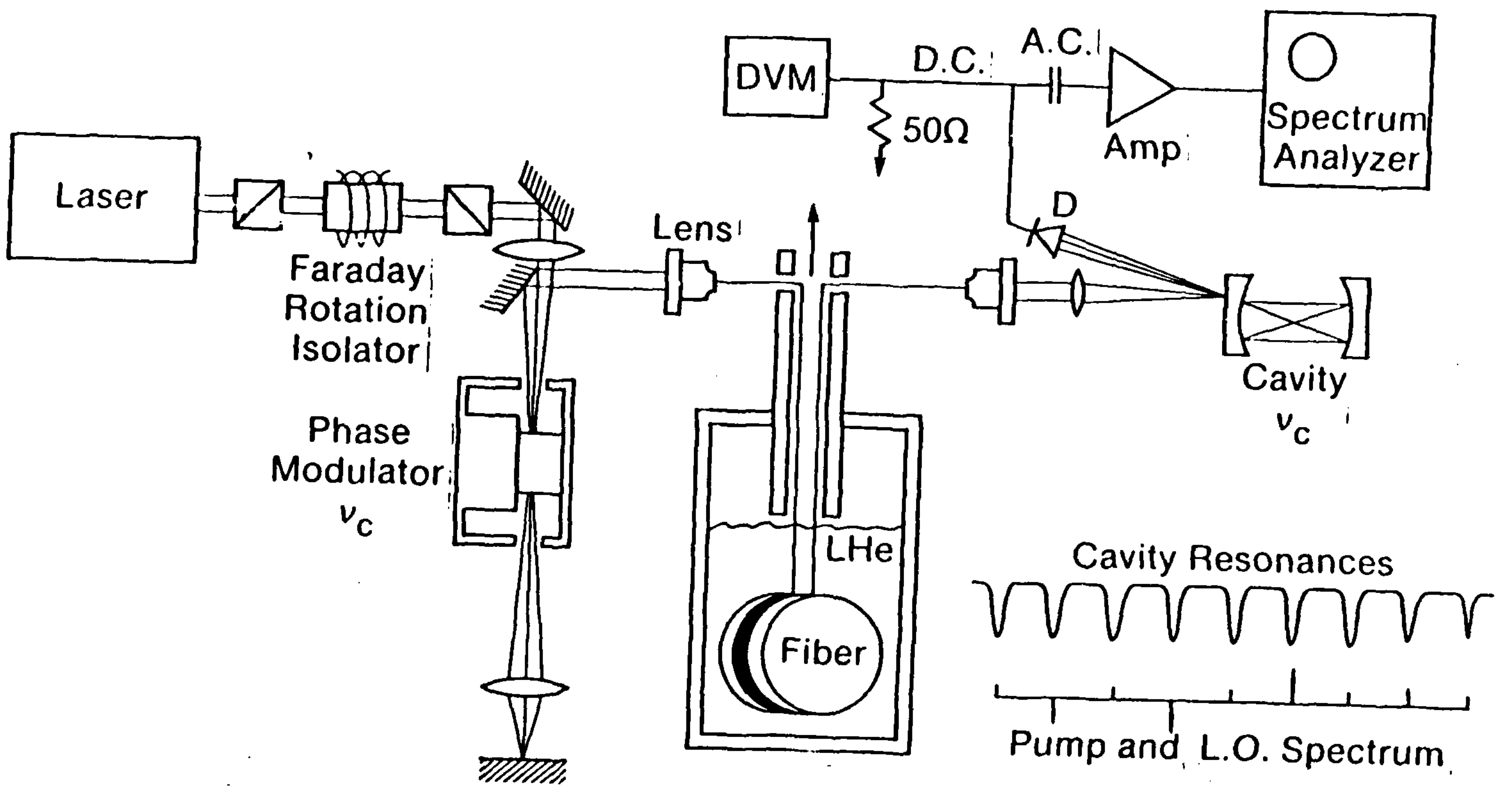

The phase modulation is at the cavity mode separation frequency.

12

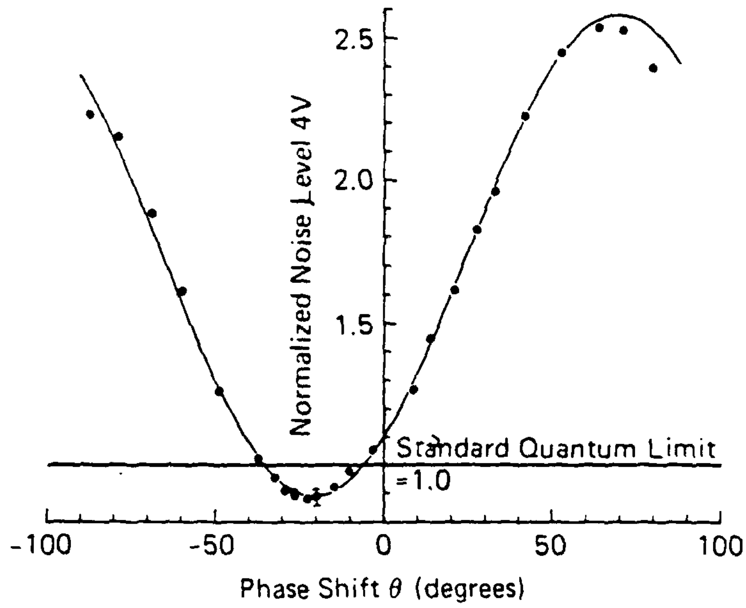

The noise level depends upon phase and falls 12.5% below the vacuum noise level or SQL. This beam is not a minimum uncertainty state because of excess phase noise added by light scattering in the fiber - even at 2K.

When the squeezed beam is attenuated, the noise level rises towards the noise level characteristic of coherent light.

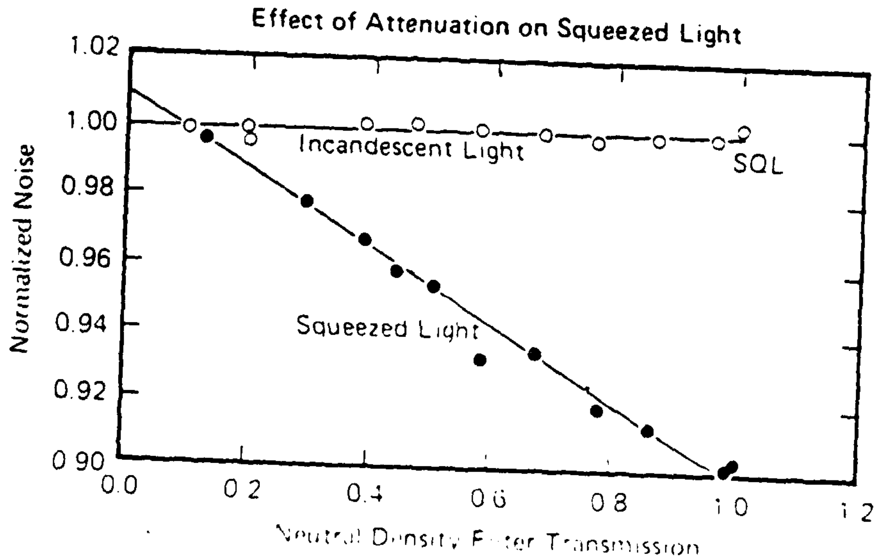

Optical Properties of Quantum Well Structures with Electric Field : Life Time Free Switching of Luminescence Intensity and Virtual Charge-Induced Ultrafast Optical Nonlinearity

Masamichi Yamanishi

Department of Physical Electronics,
Hiroshima University
Saijocho, Higashi-Hiroshima, 724 Japan

New modulation schemes for luminescence intensity and for attaining an ultrafast optical nonlinearity are discussed, pointing out possibilities of field controlled light emitters and of ultrafast control of quantum states.

(a) Dynamics of field control of luminescence intensities in GaAs/AlGaAs quantum well structures.

High speed photoluminescence (PL) switching by electric field-induced carrier separation inside the Quantum Well (QW), combined with carrier escaping out from the well to the barrier layer is demonstrated to be free from carrier life time limitation. A new technique for evaluating radiative life time is also shown.

Figure 1 shows the PL response for a short pulsed voltage applied to a p-i-n diode with a GaAs(100Å)/AlAs(300Å) multi-QW

structure. The 300psec delay of PL from the pulsed voltage was observed to be much shorter than the life time (30nsec). However, for a consecutive input pulse train, the PL response was degraded with the increasing number of the input pulses as shown in Fig.2(a) as long as the radiative recombination dominates over nonradiative processes under the condition of a constant generation rate. In order to solve this problem, we examined a modulation scheme in which a field-induced increase in radiative life time is combined with a field-induced decrease in nonradiative life time due to the carrier leakage at a high field. One of the examples of such a modulation is shown in Fig.2(b), indicating a significant improvement of the PL responses for the consecutive pulses. Figure 3 shows overall life time and radiative life time of the carriers obtained with the transient response of PL for pulsed electric field, as functions of the applied field. The new technique will be, in more detail, discussed at the presentation.

The obtained result can convince us of the realization of the proposed light emitter.[1)]

b) Ultrafast optical nonlinearity by virtual charge polarization in DC biased quantum well structures

A new concept on field-induced optical nonlinearity due to virtual transitions in QW structures[2)] will be proposed, showing some examples of theoretical result on the nonlinearity. In a QW structure subjected to DC electric field E_0, negative and posi-

tive electric charges of which spatial profile are given by wave function at the subbands (1e, 2e,···, and 1hh, 2hh,···, 1ℓh, 2ℓh,···) induced by the virtual transitions due to an intense pump light with a photon energy $\hbar\omega_p$ far below the band gap may produce a screening field E_s, cancelling out, to some extent, the external bias field E_0 (see Fig.4). As a result, one may expect a blue shift of the energy gap and changes in oscillator strengths for a weak signal light with a photon energy $\hbar\omega_s$. The switching times of the nonlinearity should be very short, ~100 femtosec., both for the ON- and OFF-processes because the electric charges are induced by the virtual processes and the field cancellation results from the internal charges inside the QWs. In other words, the switching characteristic is free from life time limitation, in a contrast with those due to real excitation processes, and from C·R-time constant limitation.

As a consequence of numerical estimations, the following result is obtained for a $Ga_{1-x}Al_xAs$ graded gap ($x=0 \rightarrow 0.3$, $L_z=200\text{Å}$) QW structure. An increase in the 1e-1hh transition oscillator strength, 1.5%, and a blue shift of band gap, 0.05meV are expected for a pump power density of $10^7 W/cm^2$ with a photon energy, 50meV below the energy gap and for an electric field E_0 of $9\times10^4 V/cm$. Effective four-wave-mixing $\chi^{(3)}$ parameter was estimated to be 1×10^{-9}[esu] for the graded gap QW biased by the DC field, 90KV/cm and for the detuning energy, 35meV. The variation in the oscillator strength is significantly larger than that (bleaching) due to conventional phase space filling mechanism. The amount of blue shift is comparable to that due to dressed

exciton mechanism.[3] The field-induced optical nonlinearity seems to be observable and quite useful for designing an ultrafast optical gate.

References

1) M.Yamanishi and I.Suemune : Japan. J. Appl. Phys. 22 (1983) L22.

2) The basic idea of the proposed nonlinearity was discussed by the author and by D.S.Chemla et al., independently of each other.

M.Yamanishi, presented at technical meeting on Optics and Quantum Electronics of Inst. Electronic and Communication Engineers of Japan, paper No. OQE86-167, January 27, 1987 and at spring meeting of Japan Society of Applied Physics, abstract No.31p-ZH-7, March 31, 1987 : submitted to Phys. Rev. Letters, and, also, to be presented at 3rd Int. Conf. on Superlattices, Microstructures and Microdevices, Chicago, Aug.17-20, 1987.

D.S.Chemla, D.A.B.Miller and S.Schmitt-Rink, presented at a post dead line paper session, '87IQEC, paper No.PD-4, April 28,1987 : submitted to Phys. Rev. Letters.

3) S.Schmitt-Rink and D.S.Chemla, Phys. Rev. Letters, 57 (1986) 2752.

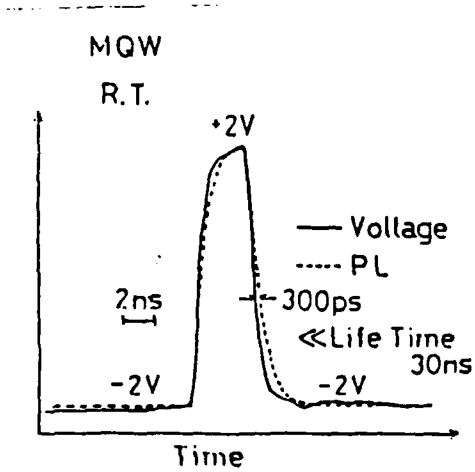

Fig. 1

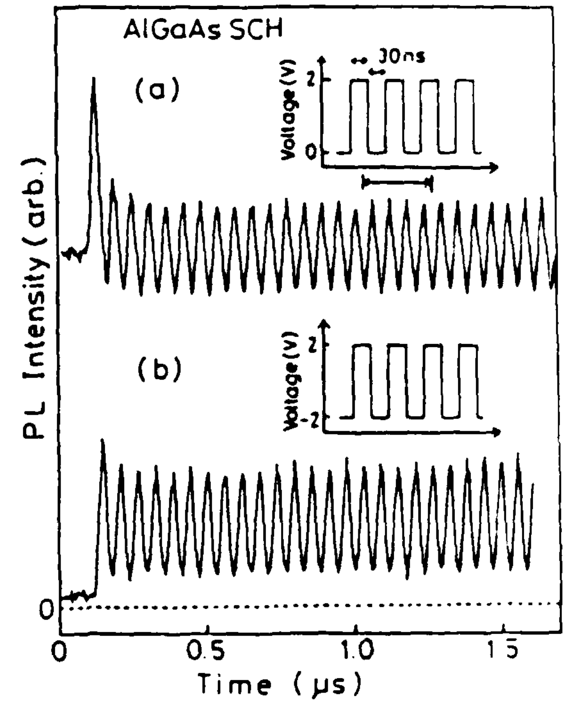

Fig. 2

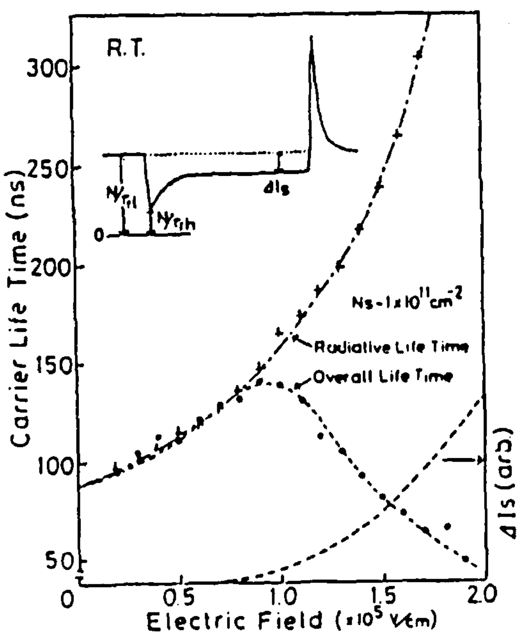

Fig. 3

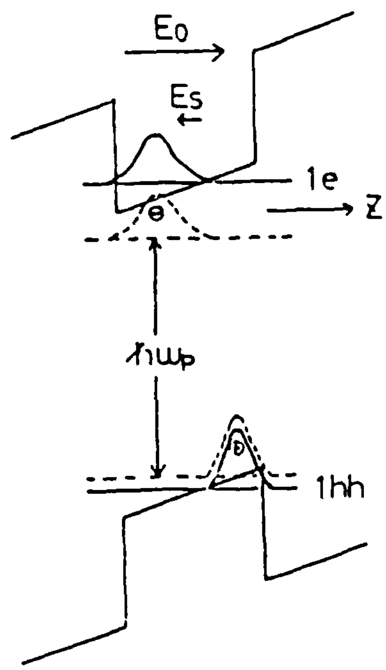

Fig. 4

Optical Properties of Quantum Well Structures biased by DC Electric Field

Masamichi Yamanishi
(Hiroshima University)

- Field effects on optical properties of QWs : High Speed Switching

- Life-Time-free switching of PL in AlGaAs QWs

- Proposal of Ultrafast optical nonlinearity

Outline of Presentation

1. Dynamics of field control of PL from AlGaAs QWs

   - Completely life-time-free switching of PL by field induced polarization of carriers, combined with carrier escapings.
   - Response time of PL ~ 300 psec, limitted by a C·R time constant

2. New mechanism for ultrafast optical nonlinearity in QWs biased by D.C. electric field

   - Response time, ~ 100 fsec
   - Virtual charge polarization, life-time free and free from C·R time constant

Field induced Optical Phenomena in QWs

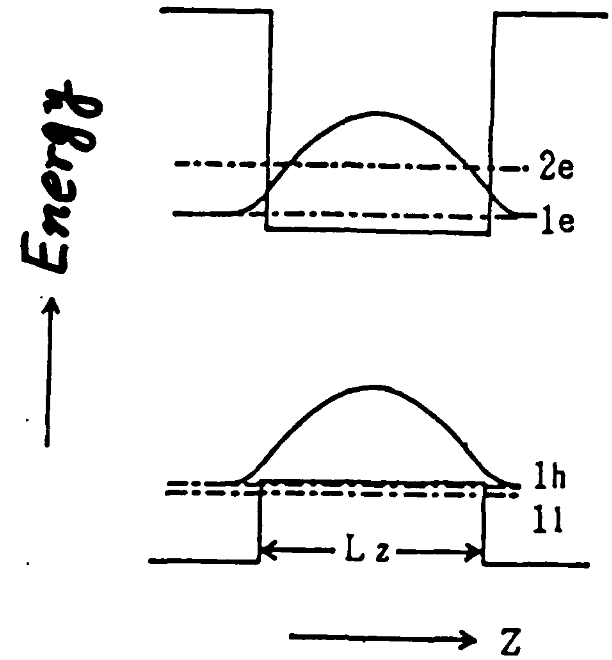

(a)

$E = 0$

Decreasing M^2 and $E_{g,eff.}$

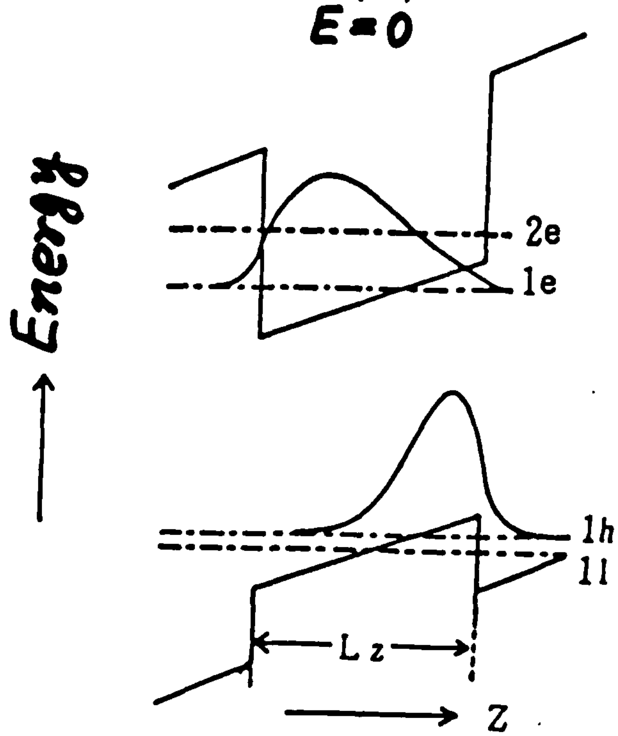

(b)

$E \neq 0$

For exciton,

decrease in E_{ex}

Changes in γ_B

⇒ Additional Changes in Oscillator Strength

<u>Q</u>uantum <u>C</u>onfined <u>S</u>tark <u>E</u>ffect

- Modulations of Light Output from Laser Diodes and LEDs

  by changes in injection current , i.e, changes in carrier density

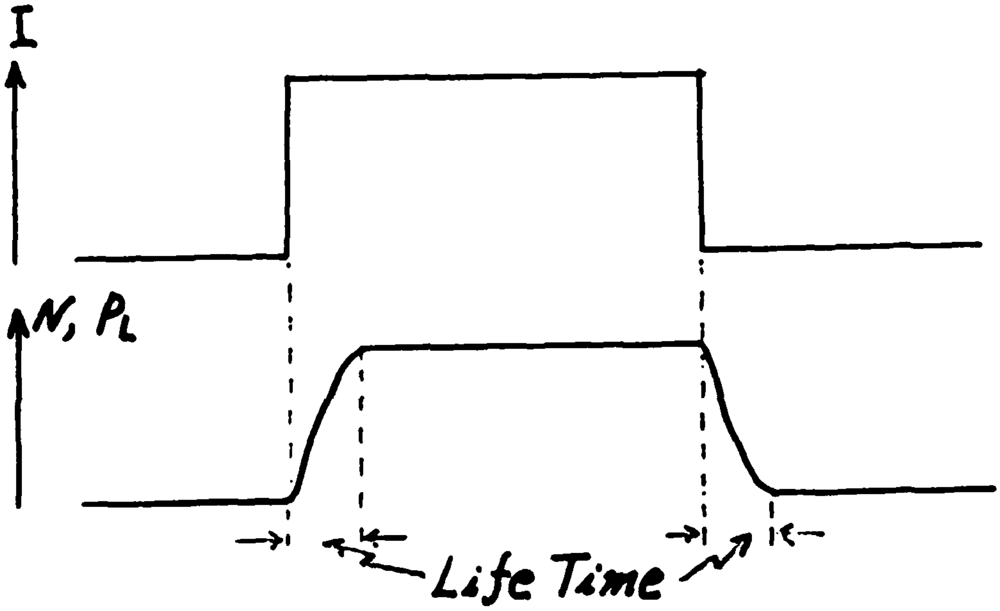

- Control of Oscillator Strength (Matrix Element) by Static Electric Field

  * not depend on changes in carrier density

  * fast switching, free from life time limitation

Field Control of Luminescence from QWs

$$\frac{\partial N}{\partial t} = G - N/\tau_r - N/\tau_{nr}$$

τ_r: Radiative life time controlled by E.

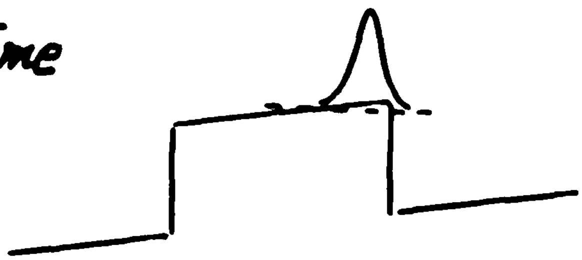

τ_{nr}: none-radiative life time

- For quick change in electric field, PL switching is free from life-time limitation.
- If $N/\tau_r \gg N/\tau_{nr}$ and unchanged G, emission rate $N/\tau_r = G$ (unchanged) under steady state condition

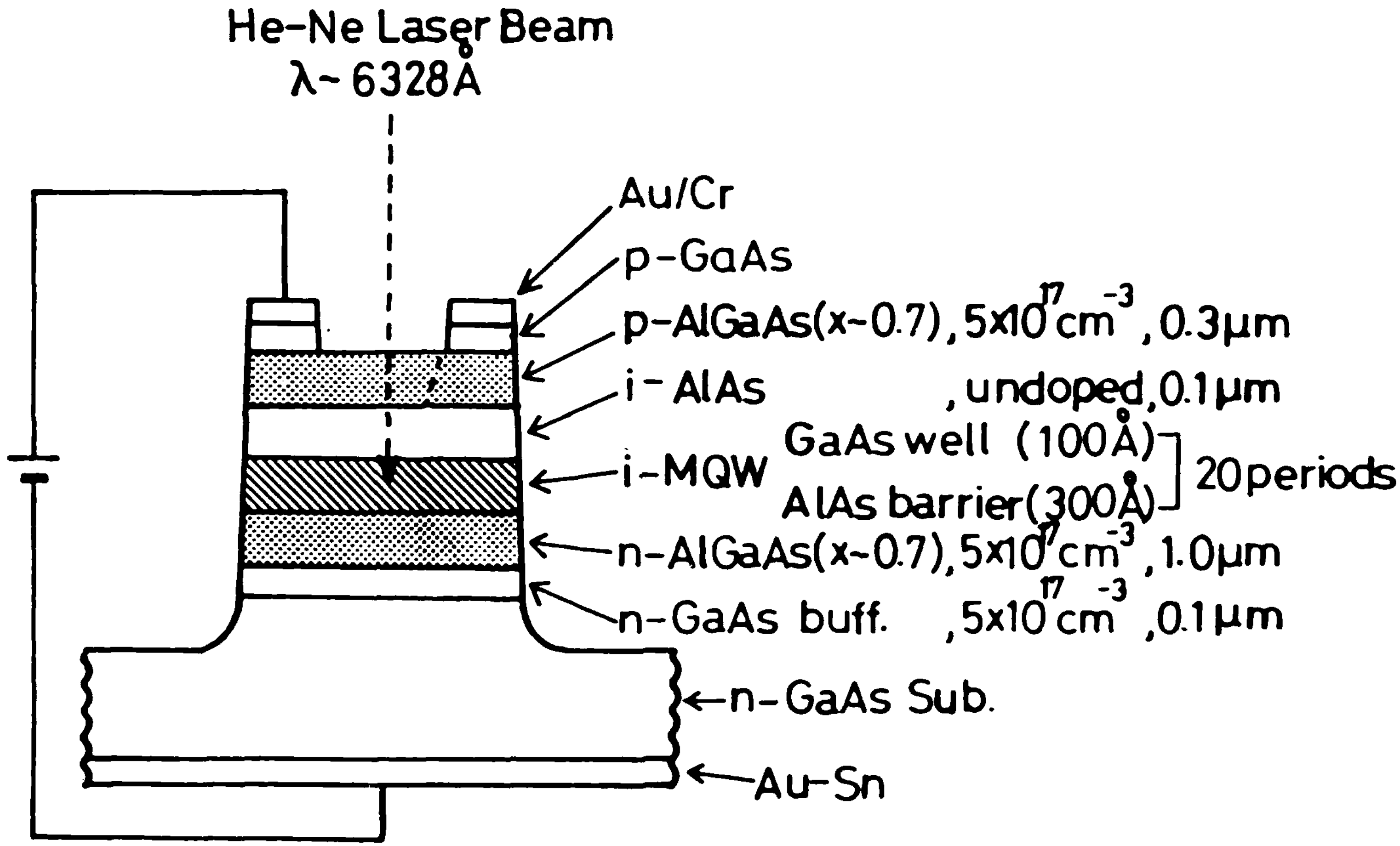
He-Ne Laser Beam
λ~ 6328Å
Au/Cr
p-GaAs
p-AlGaAs(x~0.7), 5x10¹⁷cm⁻³, 0.3μm
i-AlAs , undoped, 0.1μm
i-MQW
GaAs well (100Å)
AlAs barrier (300Å)
20periods
n-AlGaAs(x~0.7), 5x10¹⁷cm⁻³, 1.0μm
n-GaAs buff. , 5x10¹⁷cm⁻³, 0.1μm
n-GaAs Sub.
Au-Sn

20 periods MQW. GaAs(100Å)/AlAs(300Å)

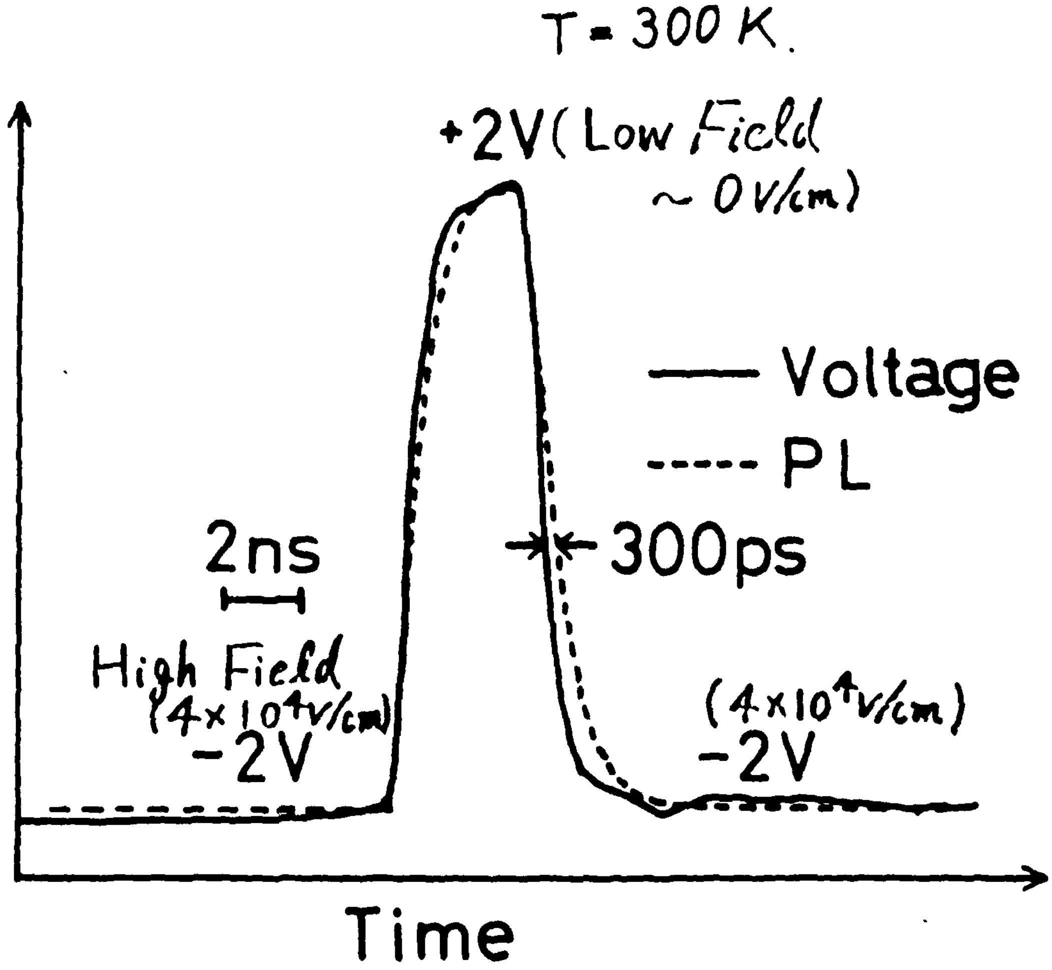

Switching time
300 psec ≪ Recombination life time ~30 nsec

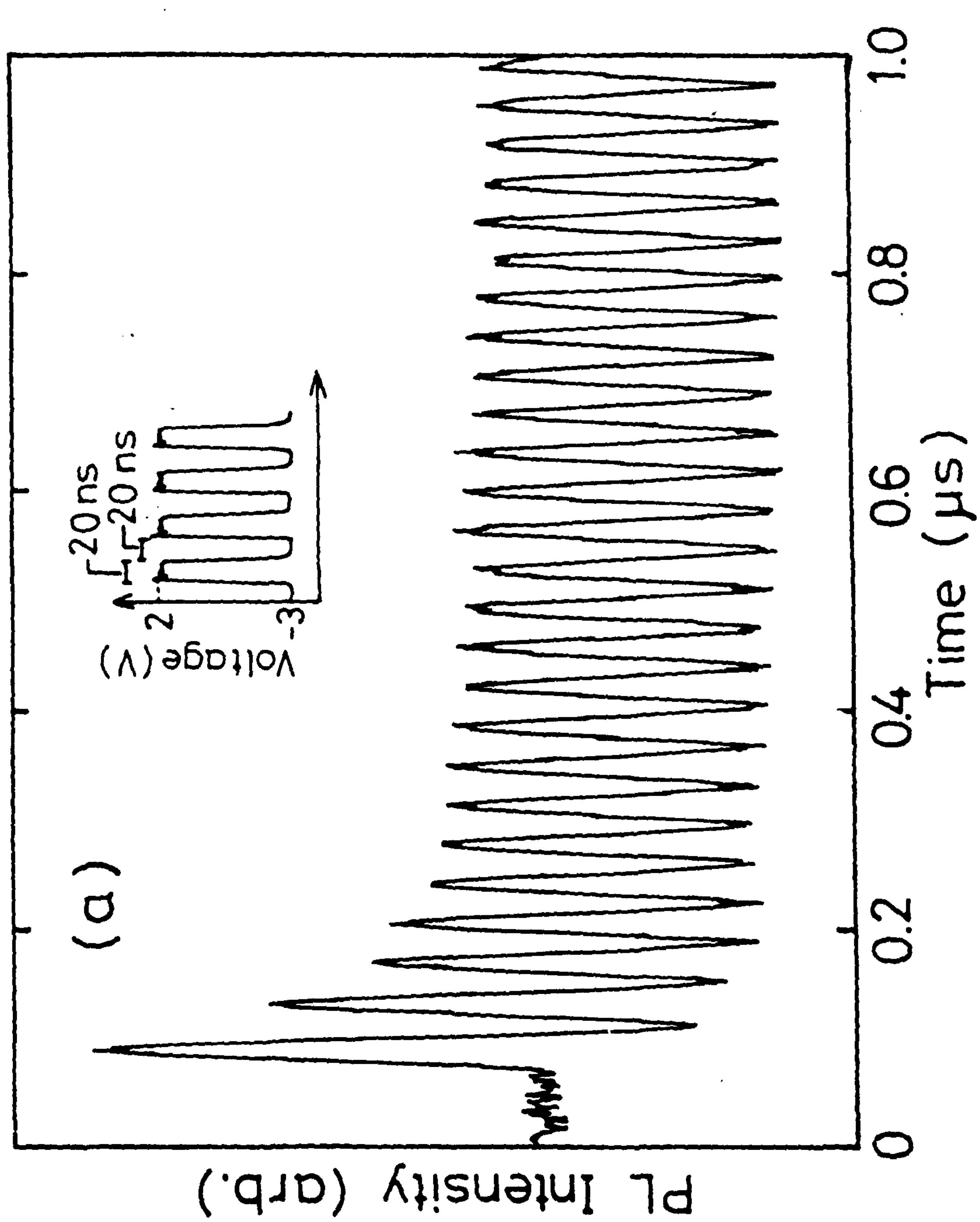
(a)
PL Intensity (arb.)
Time (μs)
0
0.2
0.4
0.6
0.8
1.0
Voltage (V)
2
-3
20 ns
20 ns

Problems

1. ON/OFF aspect ratio of PL intensities

modification of QW structure

=> SCH/QW

2. Unchanged PL intensity at steady state. i.e. degradation of PL response for consequtive input pulses

carrier leakage at high field

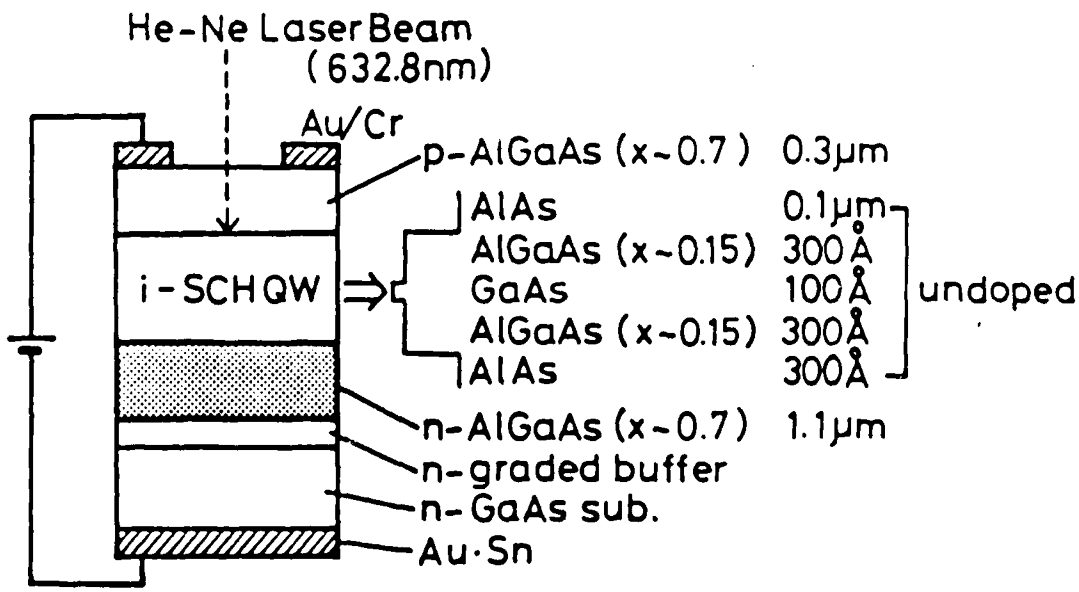

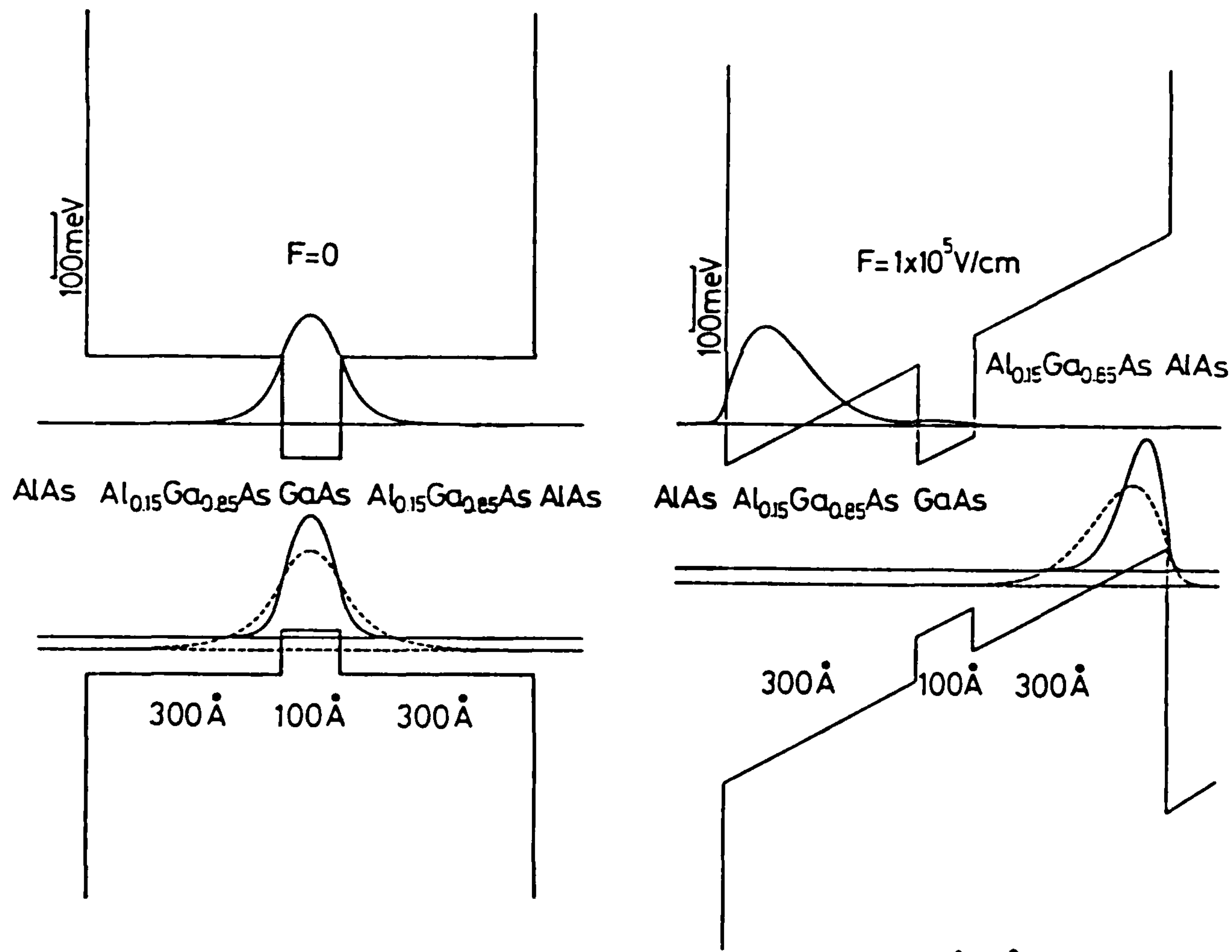

° Enough spatial separation

SCH/QW

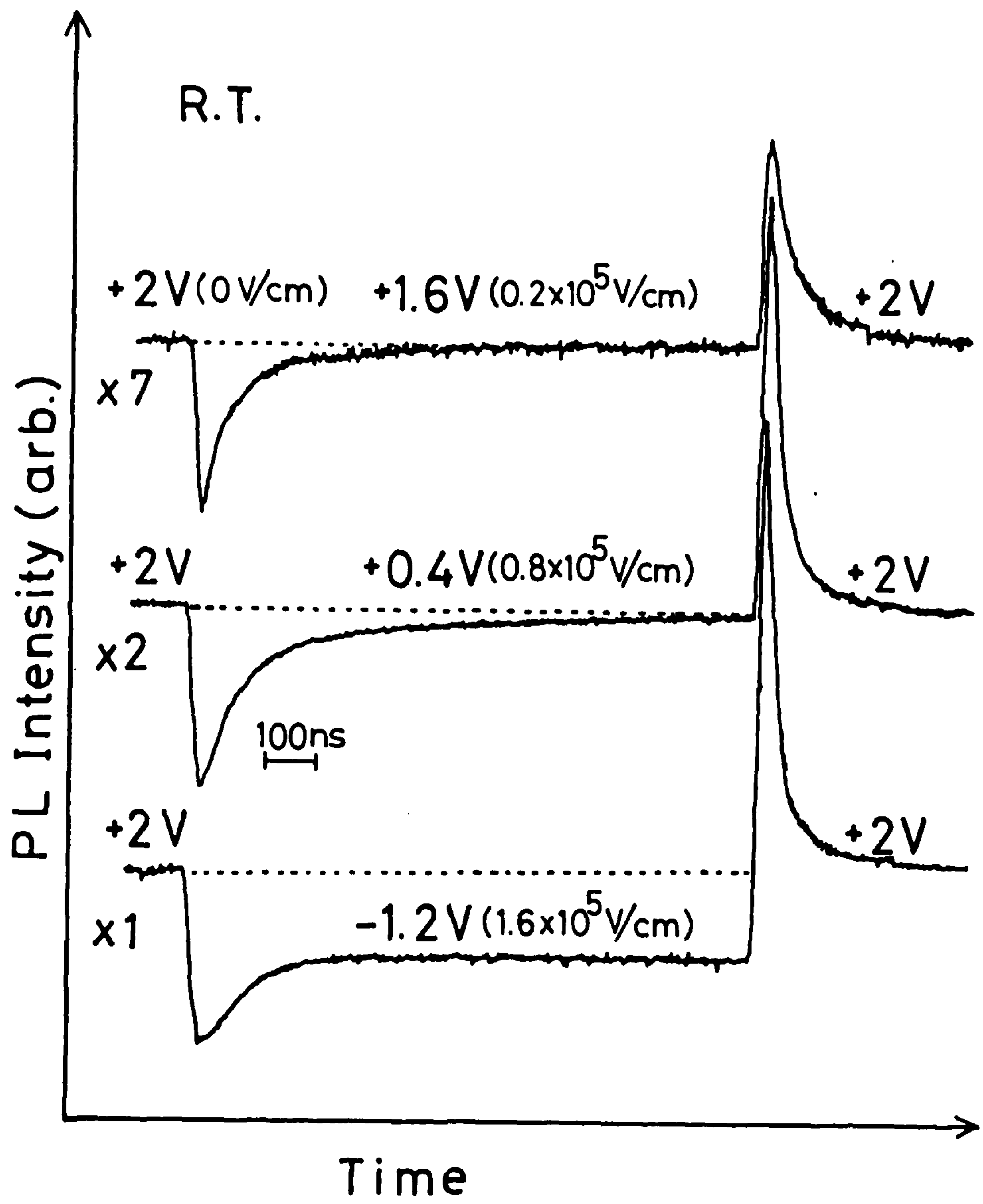

R.T.
+2V(0V/cm)
+1.6V(0.2x10^5V/cm)
+2V
x7
+2V
+0.4V(0.8x10^5V/cm)
+2V
x2
100ns
+2V
+2V
x1
-1.2V(1.6x10^5V/cm)
PL Intensity (arb.)
Time

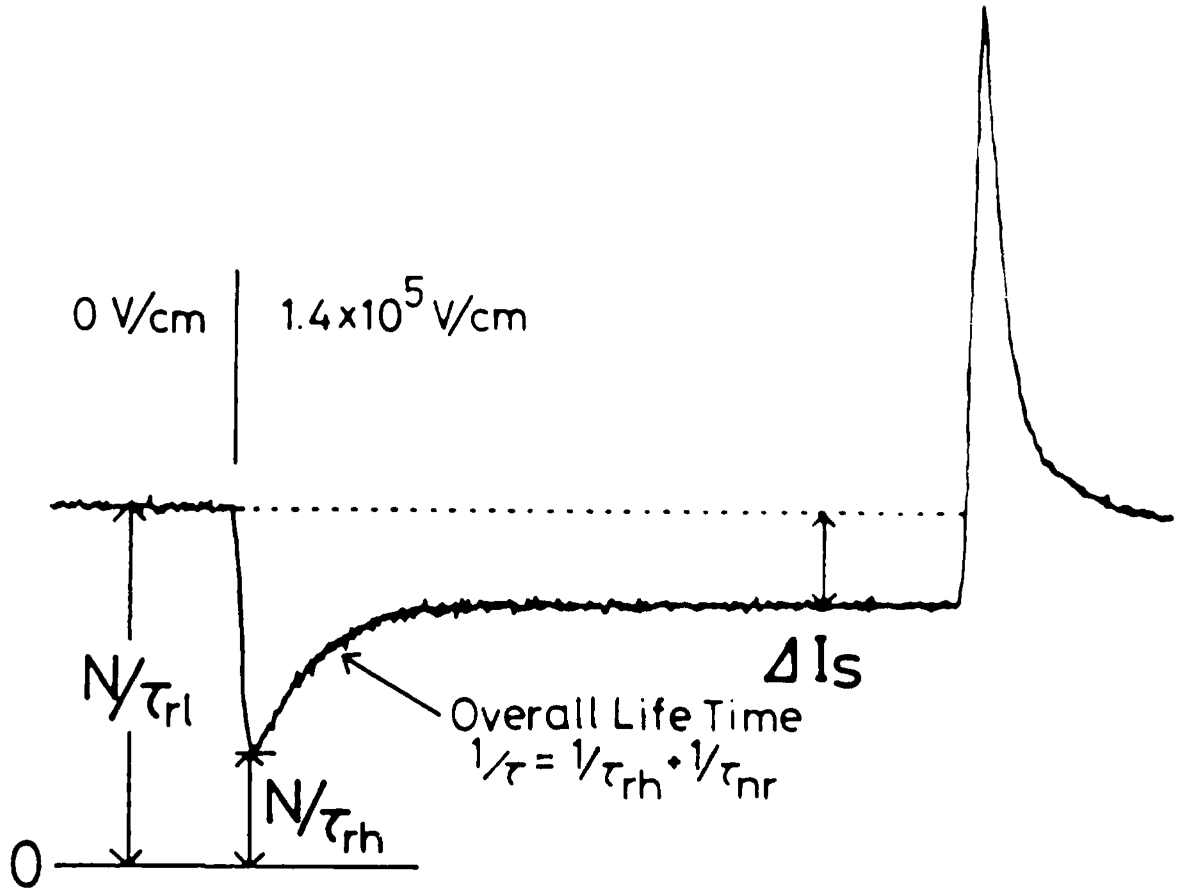

$$\frac{PL\ at\ E=0}{PL\ at\ E=1.4\times10^5\,V/cm} = \frac{N/\tau_{rl}}{N/\tau_{rh}} = \frac{\tau_{rh}}{\tau_{rl}}$$

- Carrier density is kept constant on a sudden change of life time.

SCH / QW

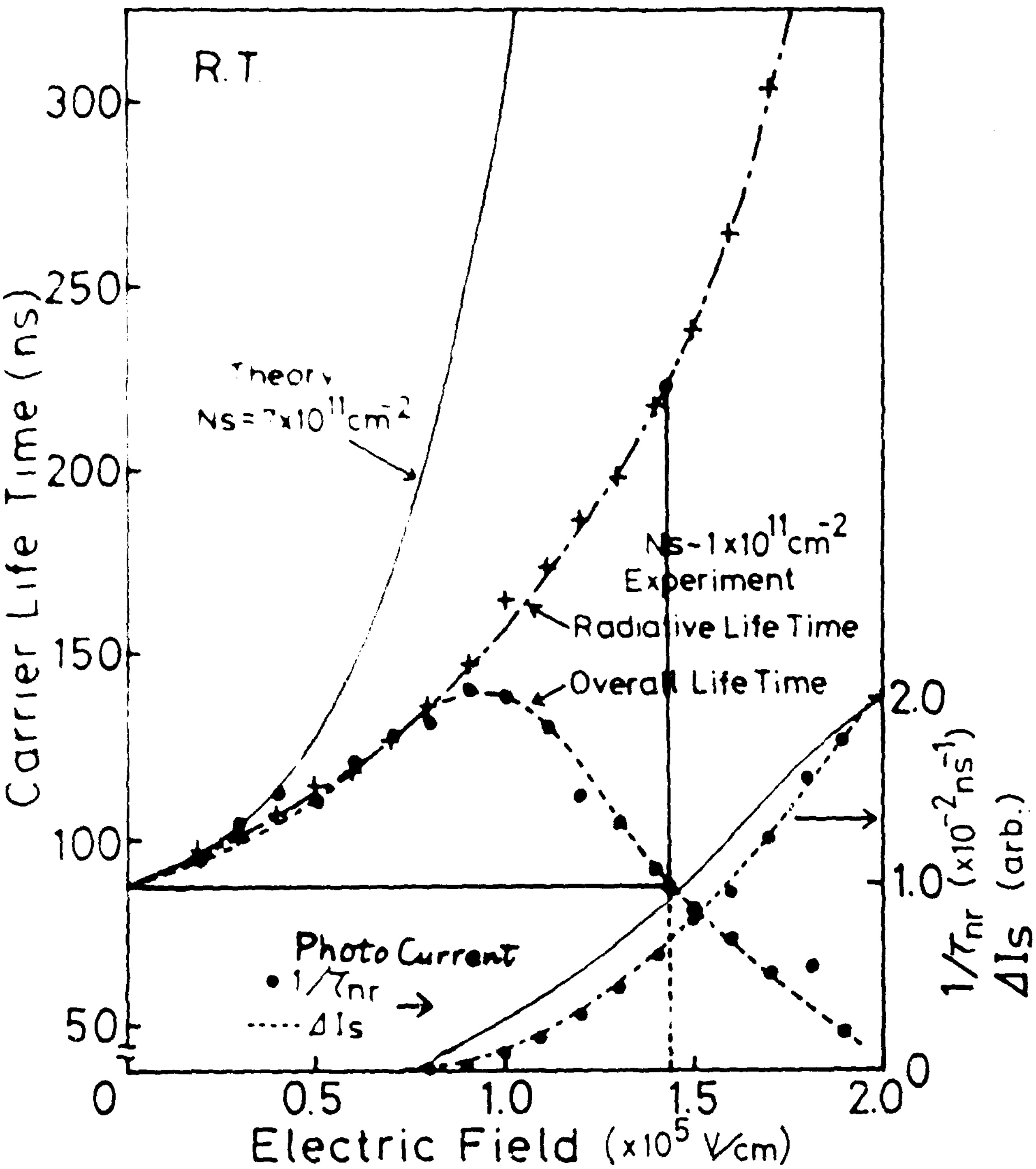

$1/\tau_{nr} = 1/\tau(\text{overall}) - 1/\tau_r$

AD-A186 938 UNITED STATES - JAPAN SEMINAR ON QUANTUM MECHANICAL ASPECTS OF QUANTUM EL (U) MASSACHUSETTS INST OF TECH CAMBRIDGE RESEARCH LAB OF ELECTRON 4/7

UNCLASSIFIED J H SHAPIRO ET AL OCT 87 N00014-87-G-0198 F/G 20/3 NL

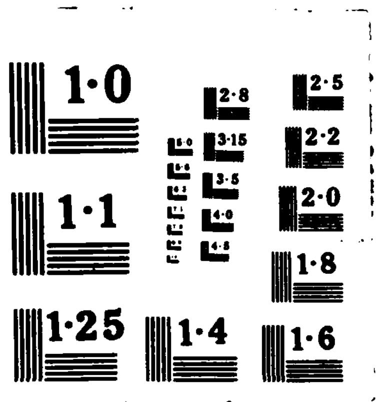
1·0
2·8
2·5
3·15
2·2
3·5
2·0
4·0
1·1
4·8
1·8
1·25
1·4
1·6

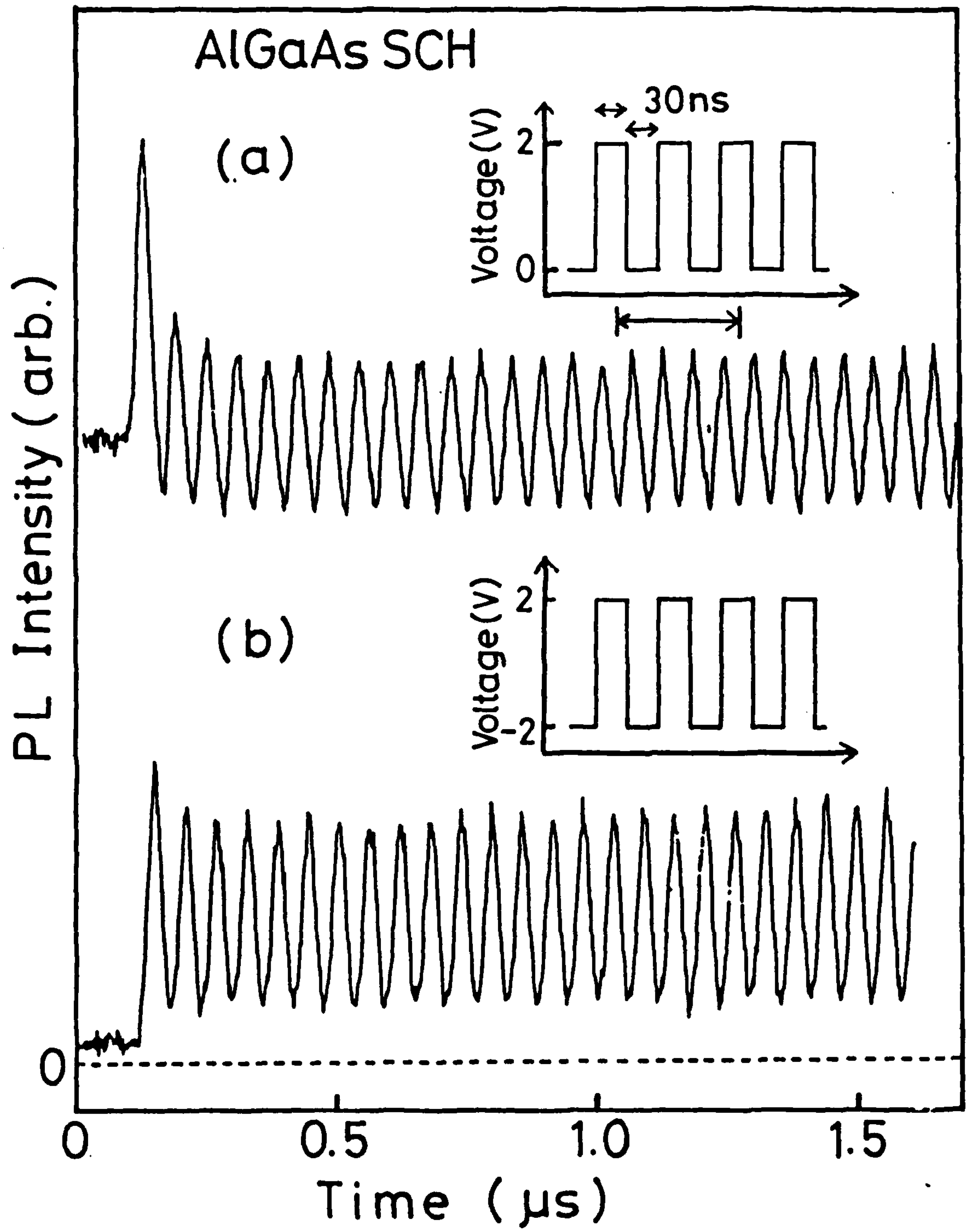
AlGaAs SCH
(a)
30ns
Voltage (V)
2
0
(b)
Voltage (V)
2
-2
PL Intensity (arb.)
0
0
0.5
1.0
1.5
Time (μs)

Possible device structure of field controlled light emitter

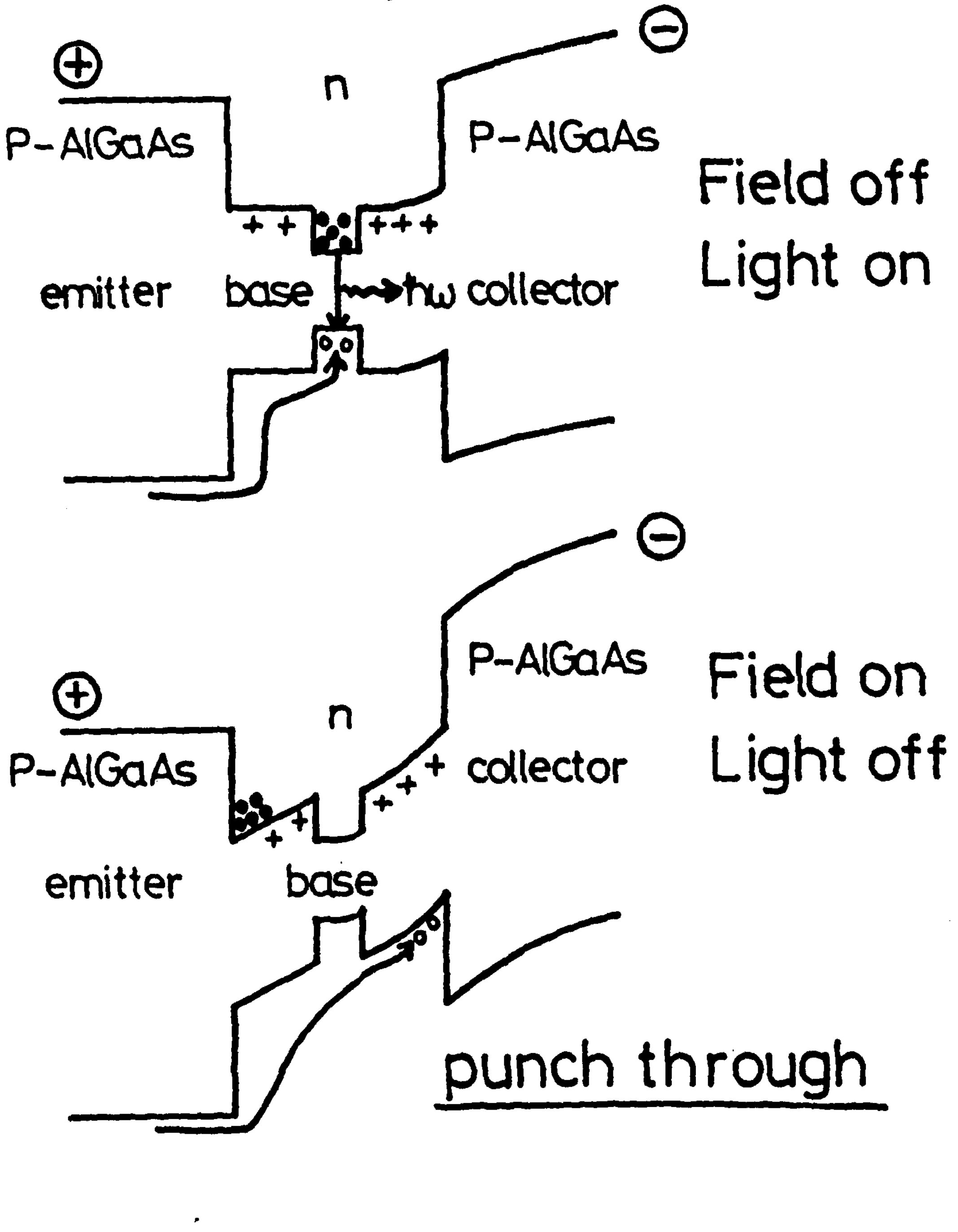

Hetero Bipolar Transistor

M. Yamanishi et al.

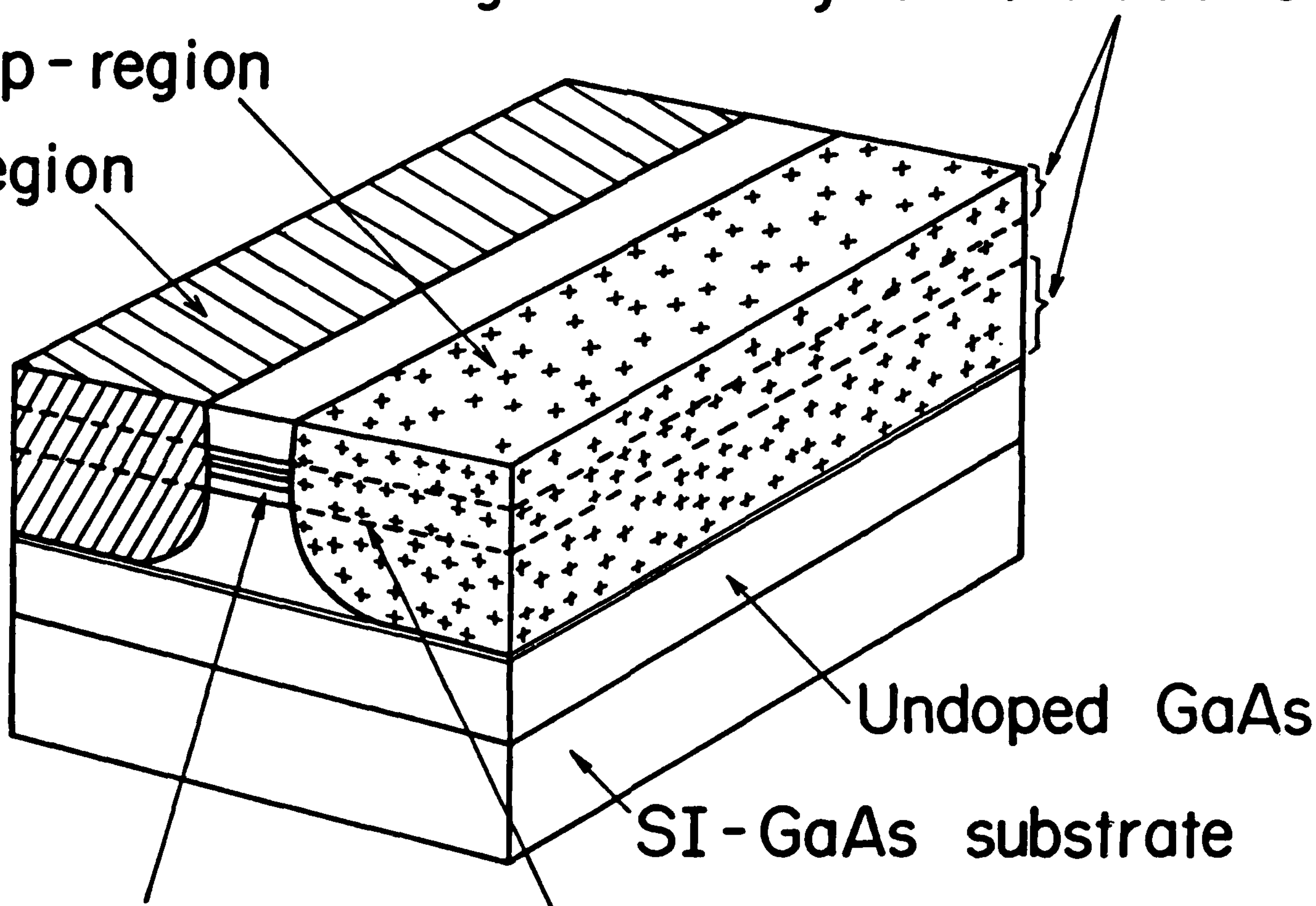

LCI MQW laser

Makiuchi et al.
Fujitsu Labs

Summary

1) Demonstration of field control of PL from AlGaAs QWs

- life time free switching of PL by field induced polarization of carriers. combined with carrier escapings
- response time of PL. ~300 psec ~C·R.

2) Proposed field controlled light emitters; quite possible

Ultrafast Optical Nonlinearity in Quantum Well Structures Biased by DC Electric Fields

M. Yamanishi
(Hiroshima University)

- Proposal of a new mehanism on ultrafast optical nonlinearity

  switching time ~ 100 femtosec.

Virtual Charge-induced Optical Nonlinearity : VCON

- A. Mysyrowicz. D. Hulin et al.

  A. Von Lehmen et al. (1986)

  discovery of AC Stark effects in AlGaAs QWs

- S. Schmidt-Rink and D. S. Chemla.

  Theory of nonlinear optical properties

  Virtual carriers behave as if real ones

- Proposal of virtual charge induced optical nonlinearity in DC biased QWs

  M. Yamanishi: presented at IECE. Japan. tech. meeting (Jan. 1987) and at spring meeting of JSAP (March. 1987)

  D.S. Chemla et al: presented at '87IQEC. post deadline paper (April. 1987).

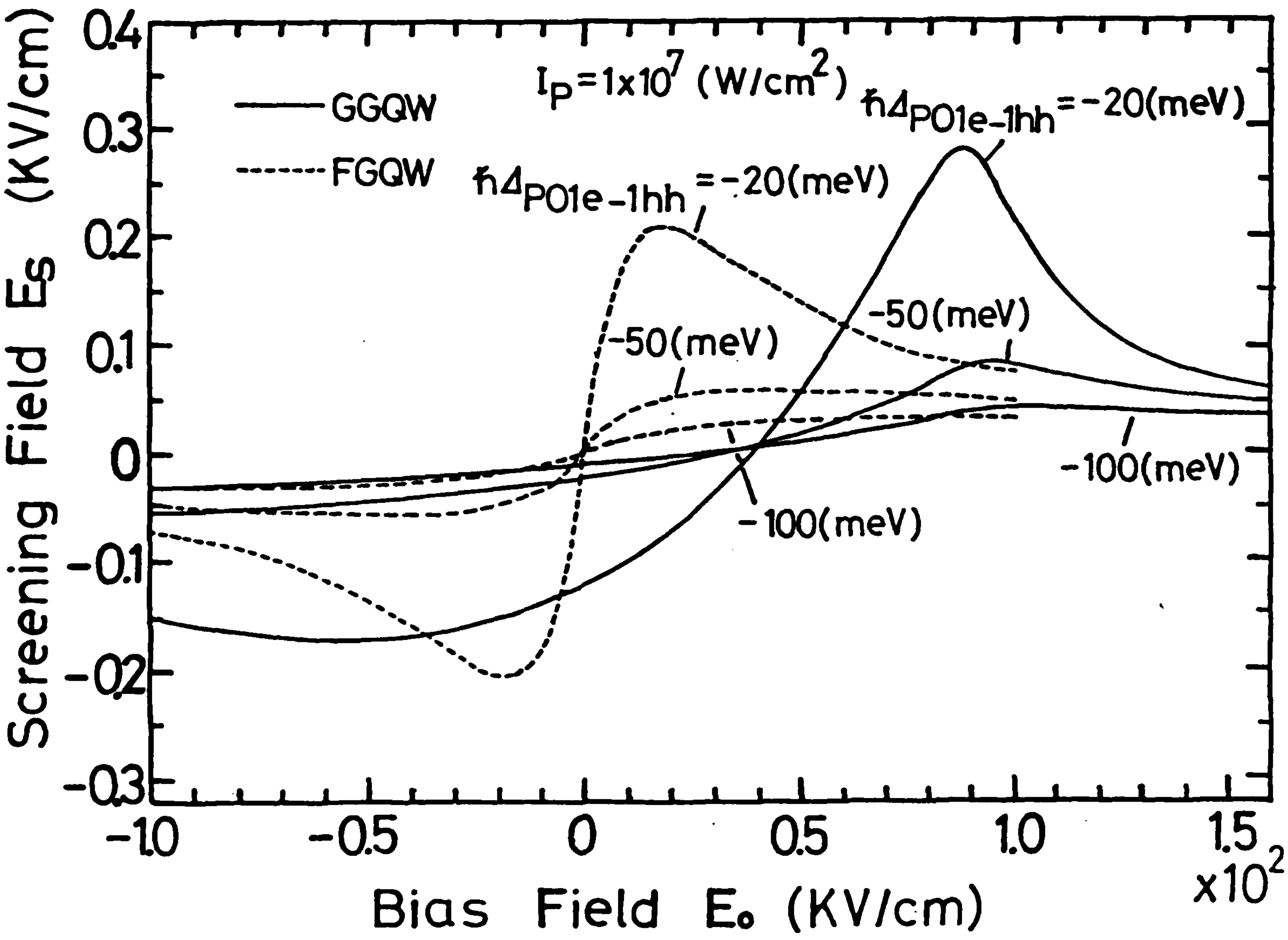

Screening Field Es (KV/cm)
0.4
0.3
0.2
0.1
0
-0.1
-0.2
-0.3
GGQW
FGQW
Ip=1x10^7 (W/cm^2)
ħΔP01e-1hh=-20(meV)
ħΔP01e-1hh=-20(meV)
-50(meV)
-50(meV)
-100(meV)
-100(meV)
-1.0
-0.5
0
0.5
1.0
1.5
x10^2
Bias Field E₀ (KV/cm)

Fig. 2 M. Y.

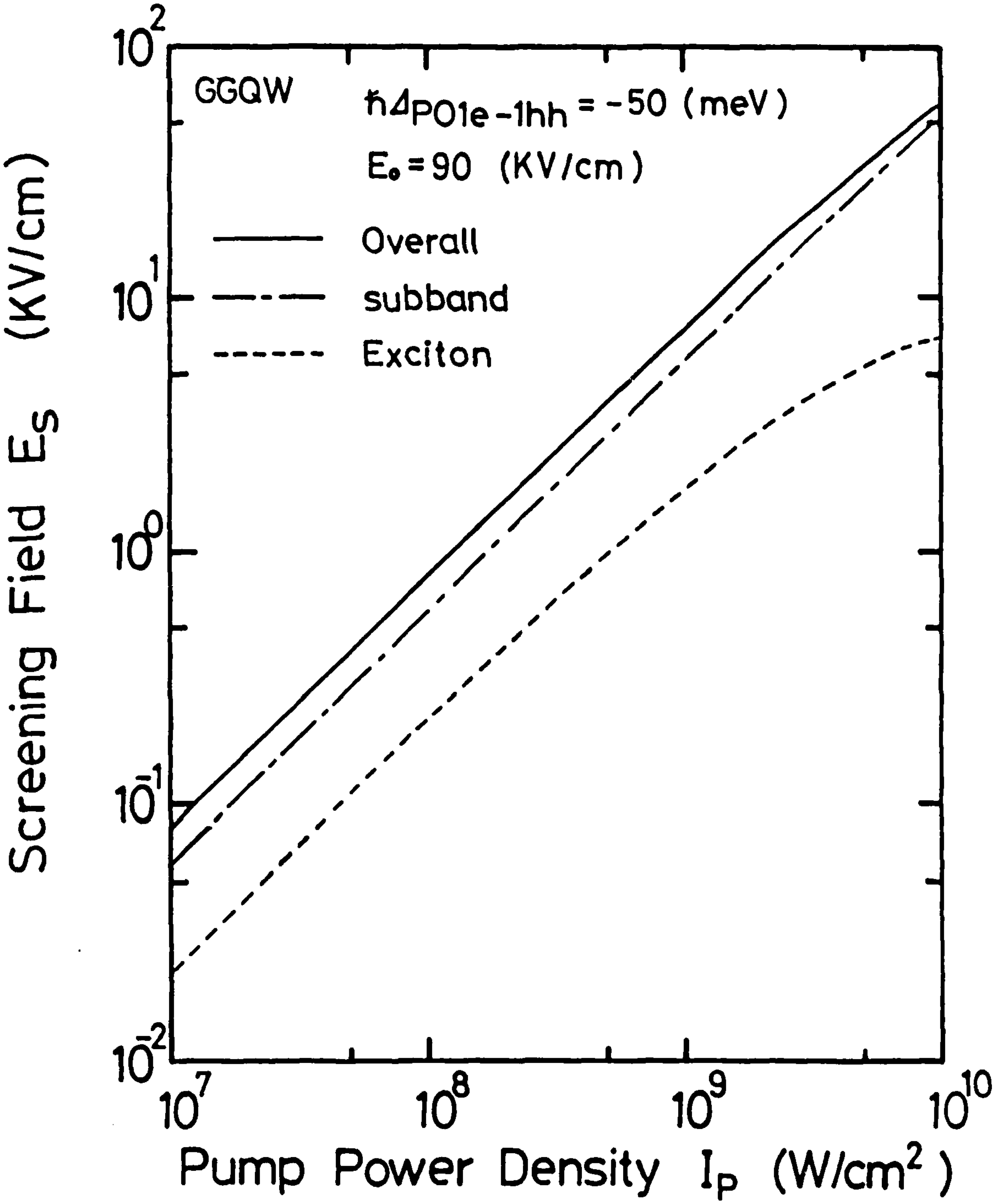

$E_s = 8$ KV/cm for $I_p = 10^4$ W/cm^2

$\Rightarrow V \sim 0.4V$ in a 25 period MQW

(Virtual pair density $\sim 5 \times 10^{16}$ cm^{-3})

GaAs/AlAs FGQW $L_z = 200Å$

$Ga_{1-x}Al_xAs$/AlAs GGQW $L_z = 200Å$

$(x = 0 \longrightarrow 0.3)$

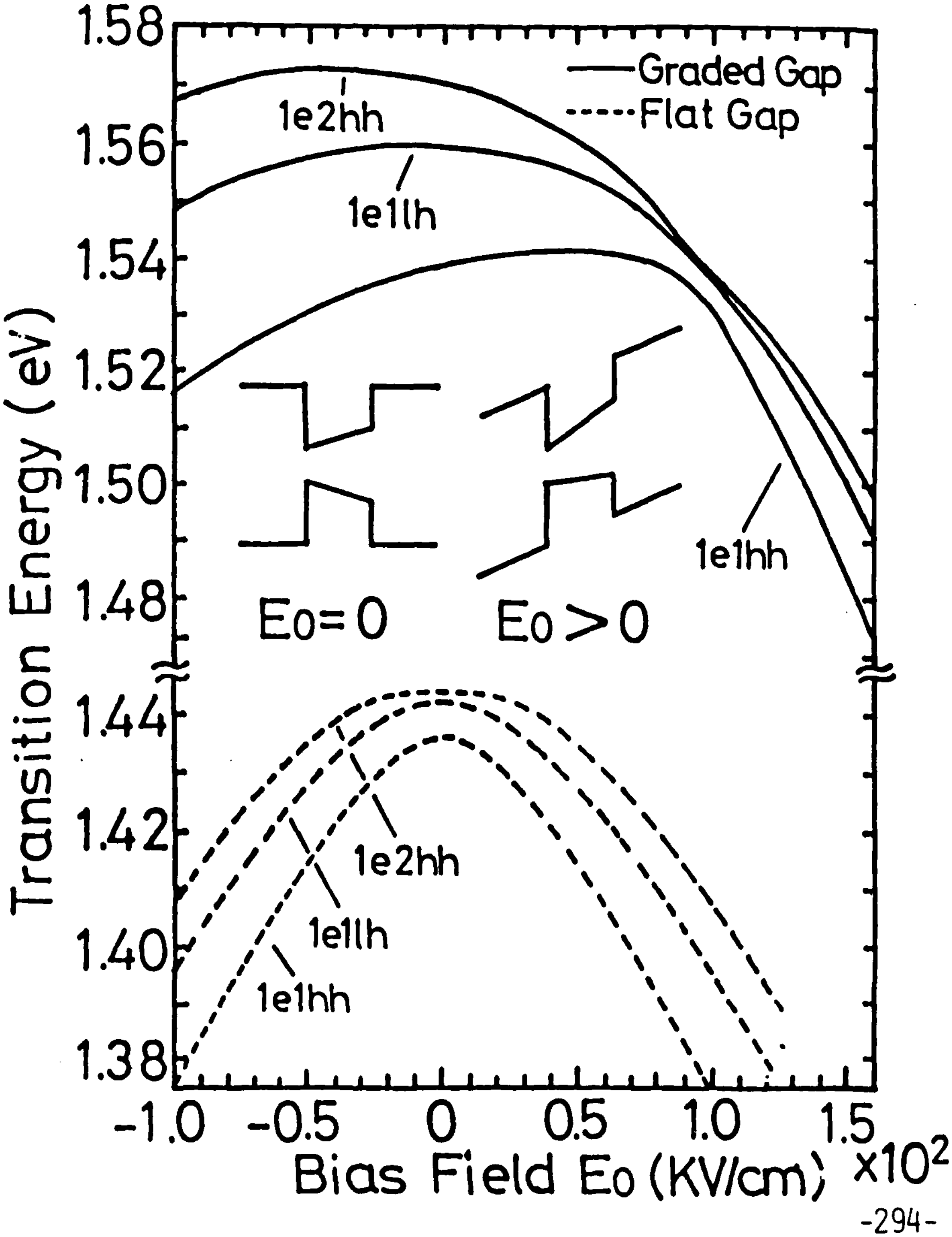

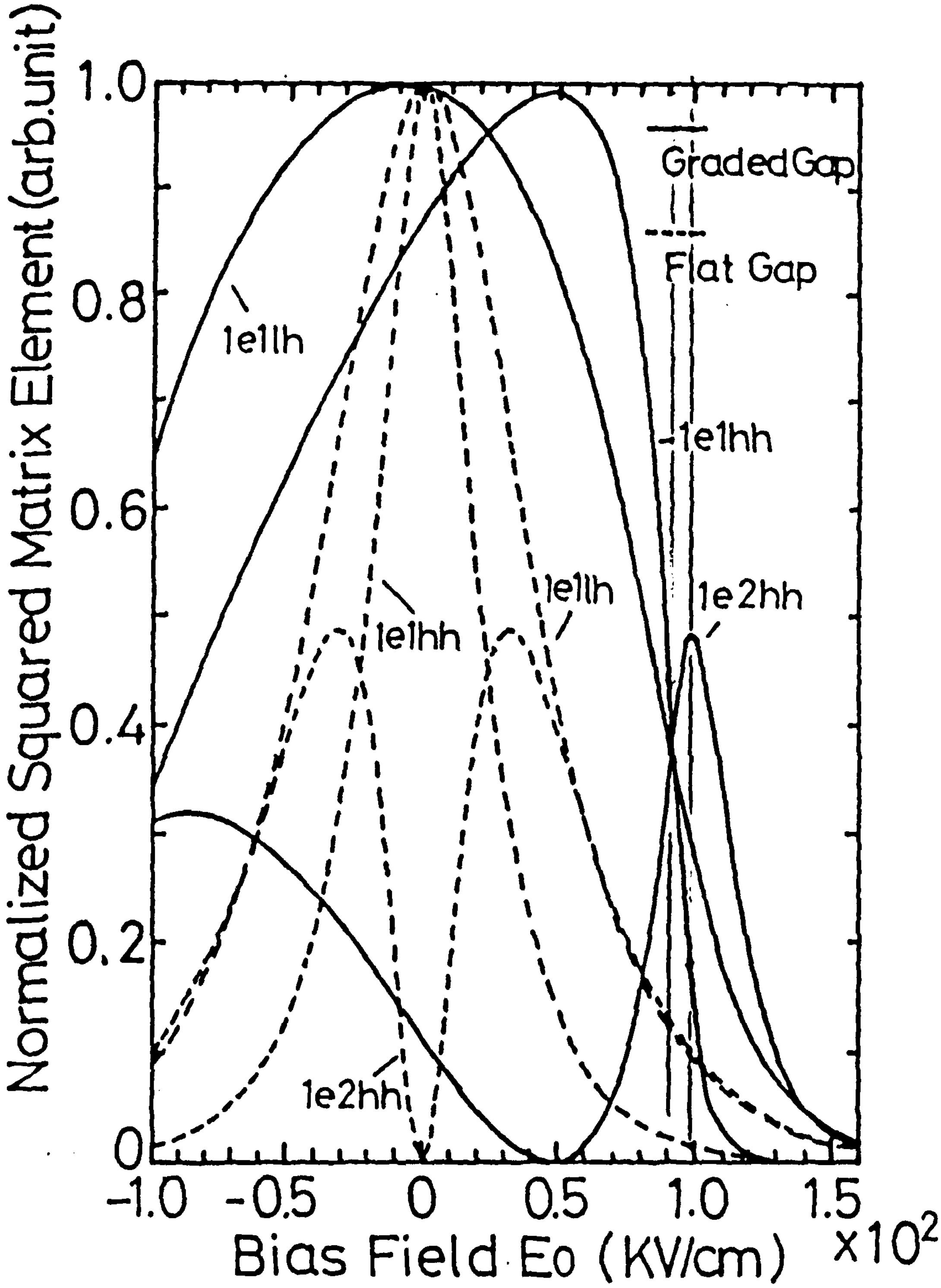
1.0
0.8
0.6
0.4
0.2
0
Normalized Squared Matrix Element (arb.unit)
-1.0
-0.5
0
0.5
1.0
1.5
x10²
Bias Field Eo (KV/cm)
Graded Gap
Flat Gap
1e1lh
1e1hh
1e1hh
1e1lh
1e2hh
1e2hh

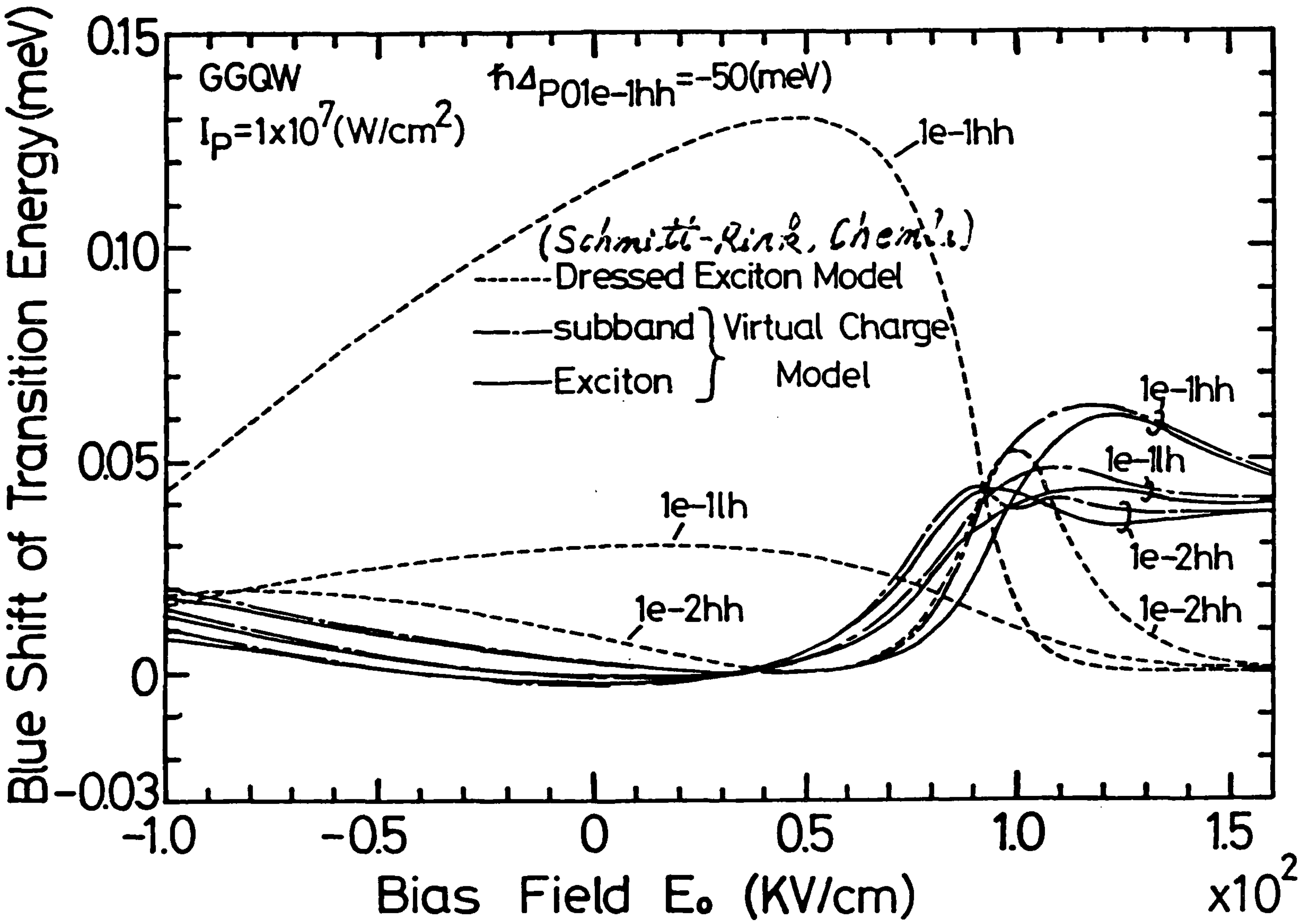
Blue Shift of Transition Energy (meV)
0.15
0.10
0.05
0
−0.03
−1.0
−0.5
0
0.5
1.0
1.5
Bias Field E₀ (KV/cm)
x10²
GGQW
$I_P=1x10^7 (W/cm^2)$
$\hbar\Delta_{P01e-1hh}=-50(meV)$
1e−1hh
(Schmitt-Rink, Chemla)
Dressed Exciton Model
subband
Virtual Charge
Exciton
Model
1e−1lh
1e−2hh
1e−1hh
1e−1lh
1e−2hh
1e−2hh

Virtual PSF : $4\Omega_{pij}^2/(\Delta_{poij}^2+4\Omega_{pij}^2)$

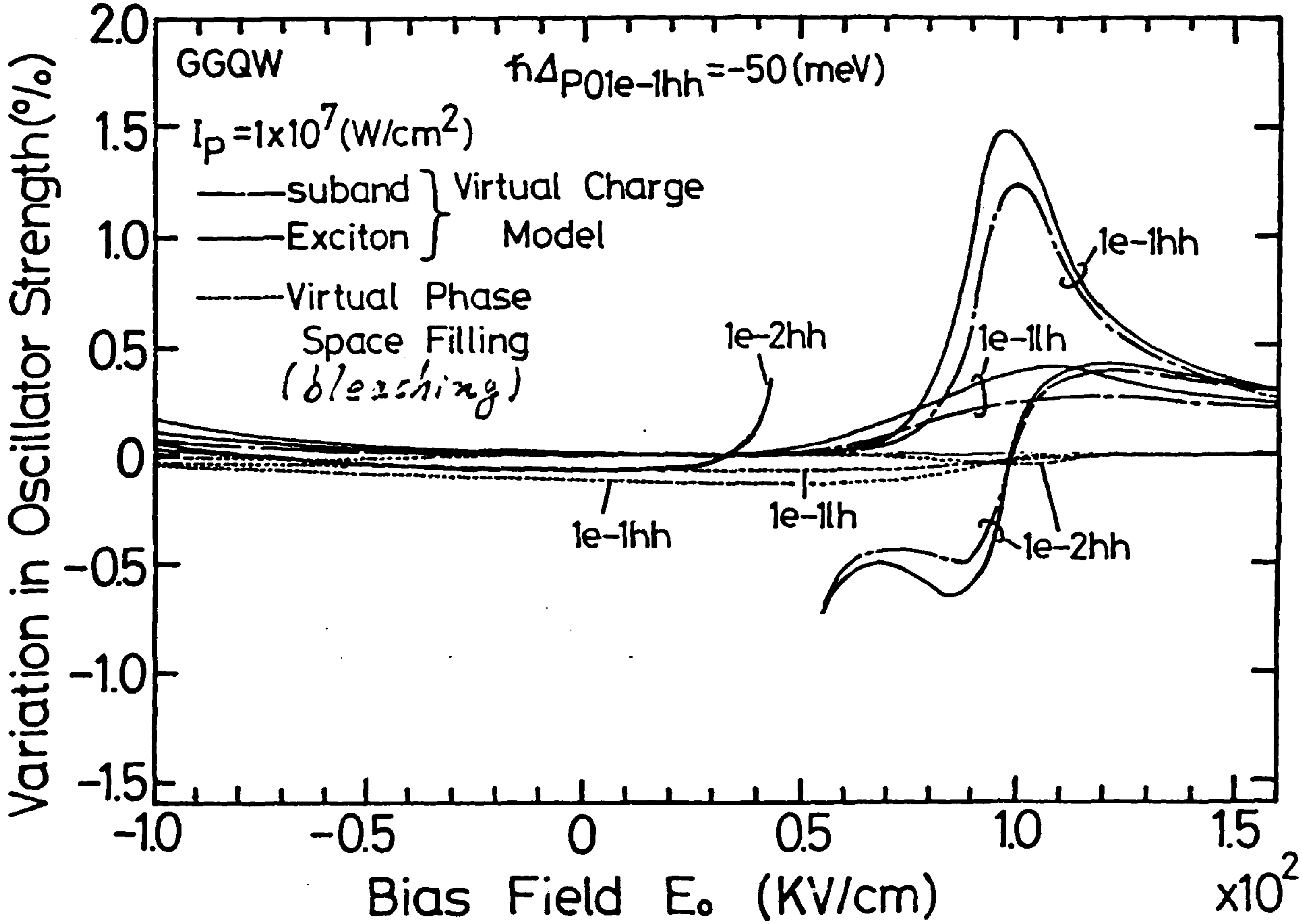

Fig. 6(b) M. Yamanishi +

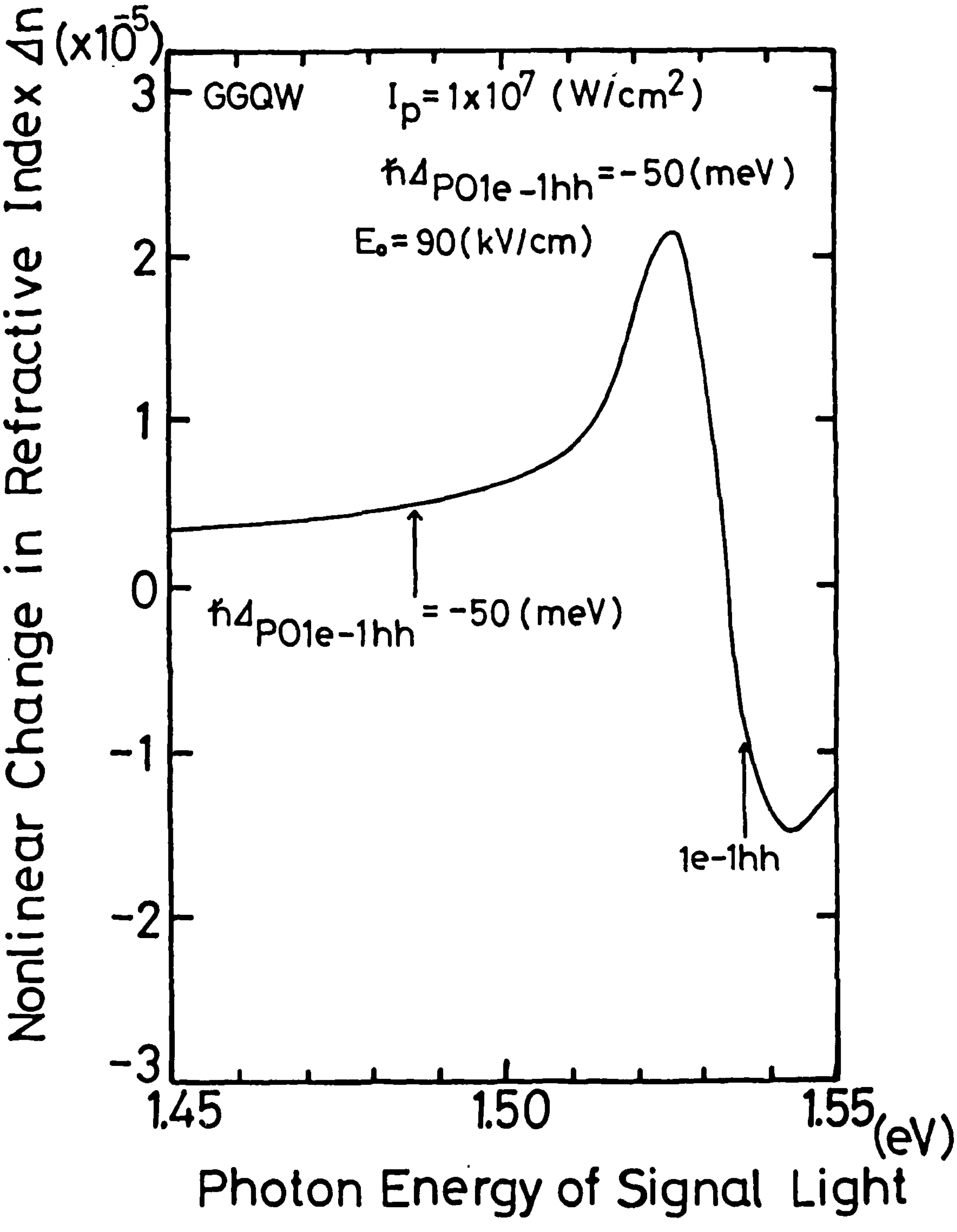

Fig. 7(b) M. Yamanishi

Table 1 Estimated nonlinear refraction coefficient n_2 and effective degenerate four-wave $\chi^{(3)}$s. The FGQW and GGQW were assumed to be biased by electric fields of 20KV/cm and 90KV/cm, respectively. The $\chi^{(3)}$s are the values for MQW samples with equal well and barrier thickness.

$$n = n_1 + n_2 I_p$$

$$\chi^{(3)}(-\omega_p, \omega_p, -\omega_p, \omega_p) = (1/3)(n_1^2 c_0 \varepsilon_0) n_2 \times (1/2)$$

QW (L_z = 200Å)	Detuning energy $\hbar\Delta_{p01e1hh}$	n_2 [cm^2/W]	$\chi^{(3)}$ [esu]
FGQW	-50 meV	8×10^{-14}	3.2×10^{-11}
GGQW	-50 meV	4.8×10^{-13}	1.9×10^{-10}
	-35 meV	2.6×10^{-12}	1.0×10^{-9}

cf. QW (L_z = 100Å) $\hbar\Delta_p$ = 42 meV. E_0 = 100KV/cm

$\chi^{(3)} \sim 7 \times 10^{-11}$ [esu] by D. S. Chemla et al.

$\chi^{(3)} \sim 10^{-12}$ [esu] CS_2 Kerr effect

$\sim 10^{-14}$ [esu] Silica Fiber

1) Off-resonant pump light

2) Virtual transitions

3) Virtual charges
< 100 f·s

4) Field screening
$\lesssim 10$ f·s

5) Blue shifts of band gap and changes in oscillator strength
~ 100 f·s

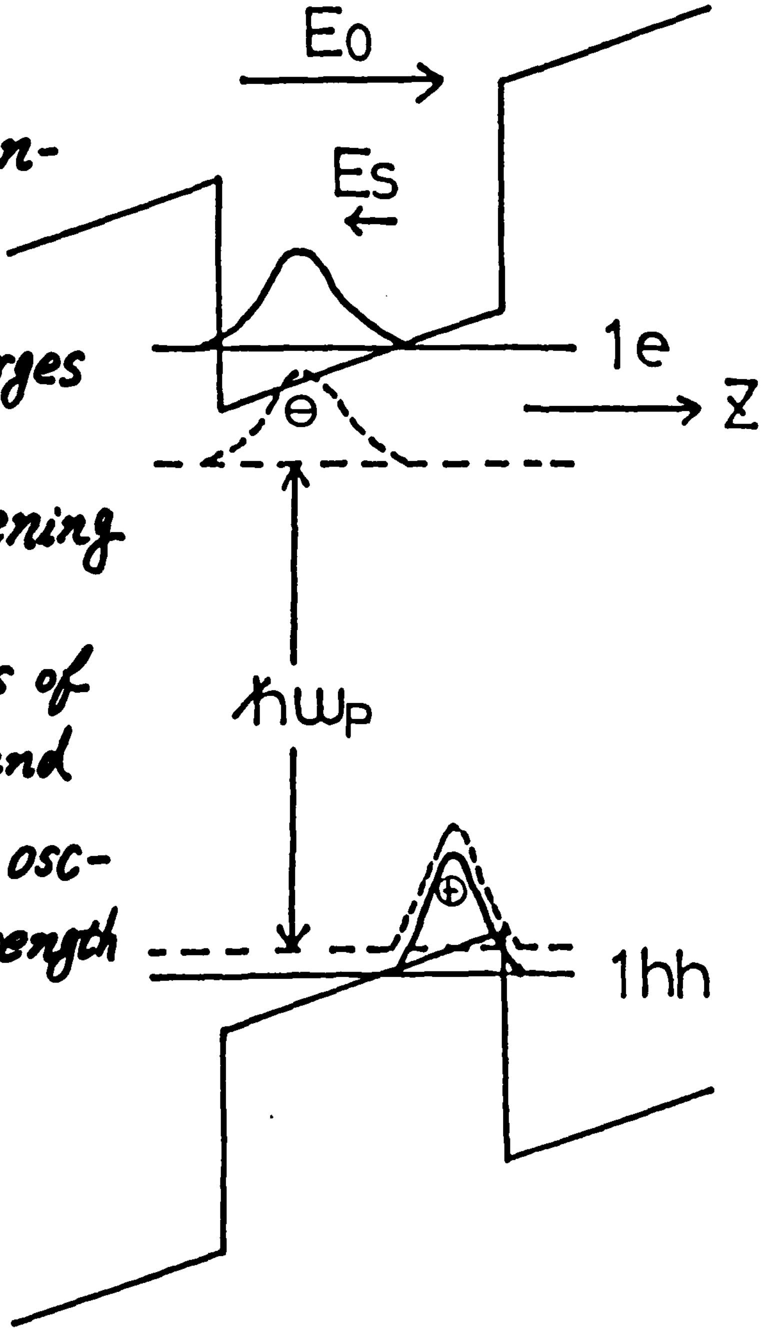

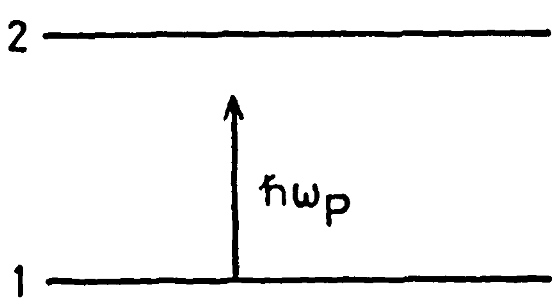

$E_p \cos(\omega_p t)$: pump light

$$\psi(\vec{r},t)=a_1(t)\phi_1(\vec{r})e^{-i\omega_1 t}+a_2(t)\phi_2(\vec{r})e^{-i\omega_2 t}$$

$$(\omega')^2=\Delta_p^2+4\Omega_p^2$$

$$\Delta_p=\omega_p-(\omega_2-\omega_1)$$

Detuning frequency

$$\Omega_p=\mu E_p/2\hbar$$

Rabi frequency

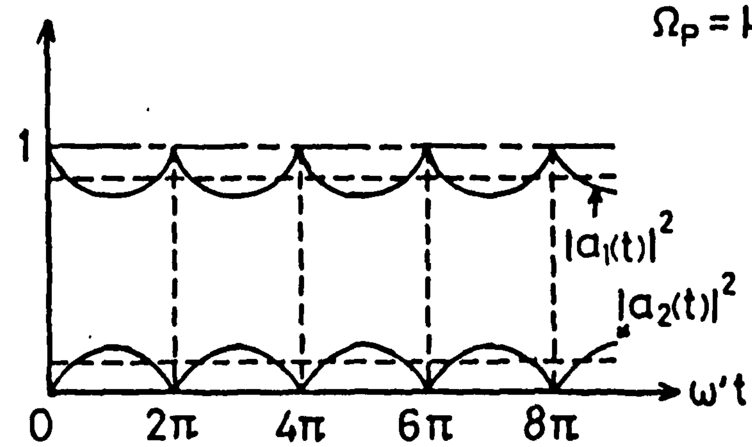

Polarization

$$P_{DC}=\langle\psi|-ez|\psi\rangle_{DC}$$
$$=\{1-\overline{|a_1(t)|}^2\}\langle\varphi_1|+ez|\varphi_1\rangle$$
$$+\overline{|a_2(t)|}^2\langle\varphi_2|-ez|\varphi_2\rangle$$

virtual hole

virtual electron

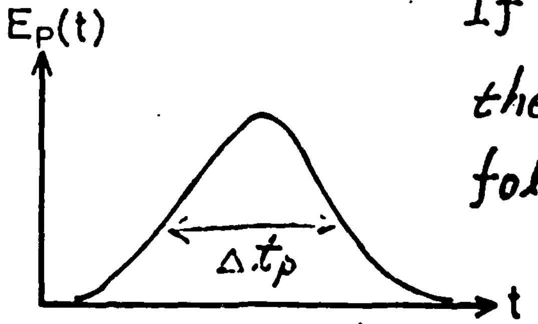

If $|1/\Delta_p| \ll \Delta t_p$,
the virtual charges can follow up the pump pulse.

$|\hbar\Delta_p| = 60\,\mathrm{meV} \Rightarrow |1/\Delta_p| = 10\,\mathrm{fs}$

virtual population

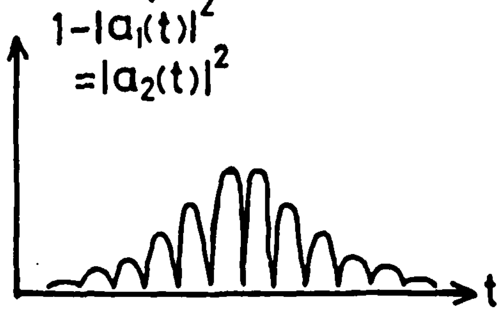

$$1-|a_1(t)|^2 = |a_2(t)|^2 = \left(\frac{2\Omega_p}{\omega'}\right)^2 \sin^2(\omega' t/2)$$

$$= \left(\frac{2\Omega_p}{\omega'}\right)^2 \sin^2(\Omega_p t)$$

$$\langle P_{DC}\rangle_{QW} = \sum_{\substack{i=1hh,2hh,\cdots\\ 1\ell h,2\ell h,\cdots}} \ \sum_{j=1e,2e,\cdots} \overbrace{\int (ez)(|\psi_i(z)|^2-|\psi_j(z)|^2)dz}^{\text{spatial polarization}}$$

$$\times\left[\left(\frac{2\Omega_{pij}^2}{\Delta_{pijex}^2+4\Omega_{pij}^2\cdot\alpha}\right) \frac{2|\phi_{exij}(0)|^2}{L_z} \ \text{exciton} + \int_0^\infty \left(\frac{2\Omega_{pij}^2}{\Delta_{pij}^2+4\Omega_{pij}^2}\right)\left(\frac{m_{rij}^*}{\pi\hbar^2 L_z}\right)dE \right] \qquad (4)$$

where $\Omega_{pij} = \left(\int \psi_i^*(z)\psi_j(z)dz\right)\langle u_1|er|u_2\rangle_c \cdot E_p/2\hbar$,

$\Delta_{pijex} = \omega_p - \omega_{exij}$

$\Delta_{pij} = \omega_p - (\omega_j - \omega_i) - E/\hbar$, $\alpha = 2|\phi_{exij}(0)|^2/N_s^{PSF} = \frac{32}{7}$

$E_s = \langle P_{DC}\rangle_{QW}/\varepsilon_0\varepsilon_s$

1e, ... 4e,
1hh ..... 8hh.
1lh ..... ~~8~~ 4 lh.

Summary

1) Proposal of Ultrafast Optical Nonlinearity in DC Biased QWs: VCON

over all switching time $\sim 100\,fs$
(ON. OFF)

2) For a GGQW ($L_z = 200\,\text{Å}$)

Blue shift of $E_g \sim 0.05\,meV$

Percentage change in
1e-1hh oscillator strength. $\sim 1.5\%$

for $I_p = 1\times10^7\,W/cm^2$. $\hbar\Delta_{p0\,1e\text{-}1hh} = -50\,meV$

and $E_0 = 90\,KV/cm$.

Effective degenerate four-wave mixing $\chi^{(3)}(-\omega_p, \omega_p, -\omega_p, \omega_p)$,
1×10^{-9} [esu]

3) Virtual charge polarization:
a key process in the nonlinearity
a new opportunity in OE devices

WHY LOSE SLEEP OVER II-VII COMPOUND SEMICONDUCTOR SUPERLATTICES ? : SELECTED EXAMPLES

S. Chang, Q. Fu, D. Lee, A. Mysyrowicz, A. Nurmikko (Brown)
J.-W. Wu (Indiana)
R. Gunshor, L. Kolodziejski (Purdue)

Outline

- Bandoffsets, Excitons, and Some Phonons in CdTe/(Cd,Mn)Te Quantum Wells
- Interfaces and the Magnetic Polaron Problem
- Excitonic Molecules in ZnSe Quantum Wells
- Dynamics of Nonequilibrium Carriers
- Magnetic Properties in Lower Dimensions ~ monolayer MnSe (MSS III)

'New' II-VI Superlattices (strained layer) 1985 –

CdTe/(Cd,Mn)Te CdTe/ZnTe

ZnSe/(Zn,Mn)Se ZnSe/ZnTe

ZnSe/Zn(S,Se) ZnS/ZnTe

* optical devices in blue wavelength region (ZnSe)
* strong exciton effects in optical spectra (quasi 2D ?)
* bandoffset questions (common anion vs. cation; polarity)
* magnetic properties in lower dimensions : 3D → 2D
* large electron-phonon coupling

→ doping still a problem

'Semimagnetic' (Diluted Magnetic) Semiconductors:

e.g.

$Cd_{1-x}Mn_xTe$

$Zn_{1-x}Mn_xSe$

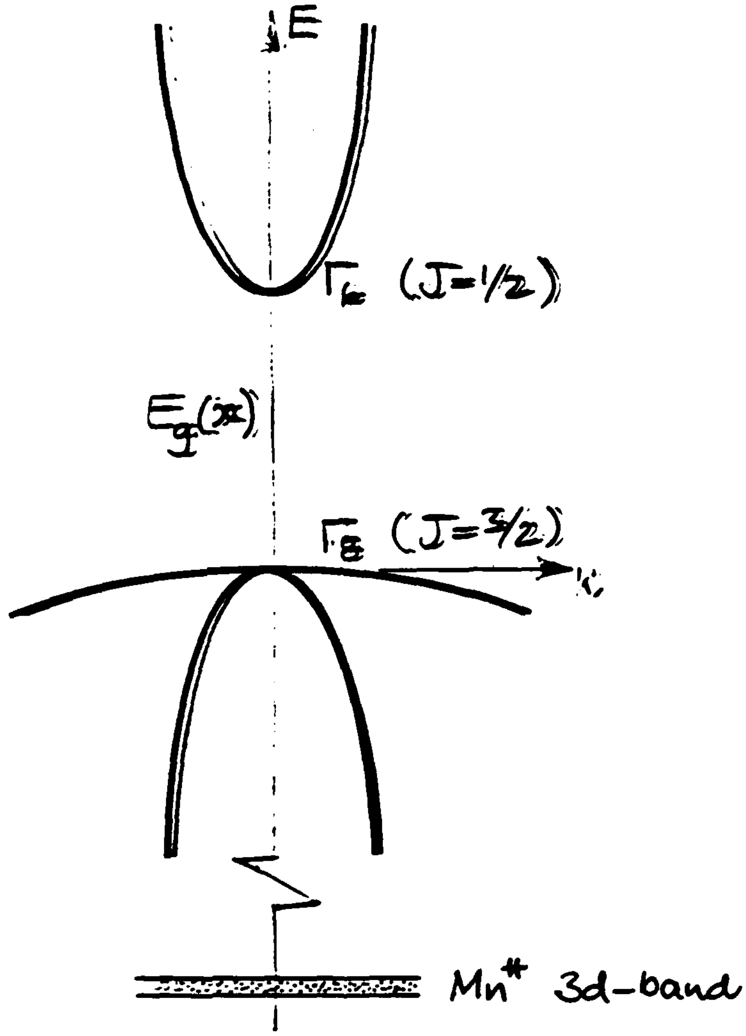

exchange interaction of s- and p-band electrons with Mn-ion d-electron states: short range (a_0)

$$\boxed{\mathcal{H}_{exch} \sim \sum_j J(\vec{r}_e - \vec{R}_j)\, \vec{s}_e \cdot \vec{S}_j}$$

e.g. external magnetic field (bulk material)

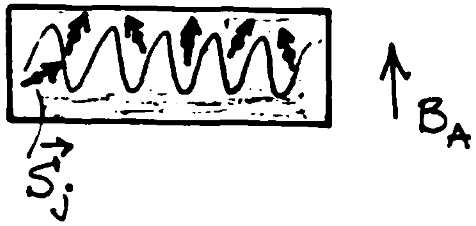

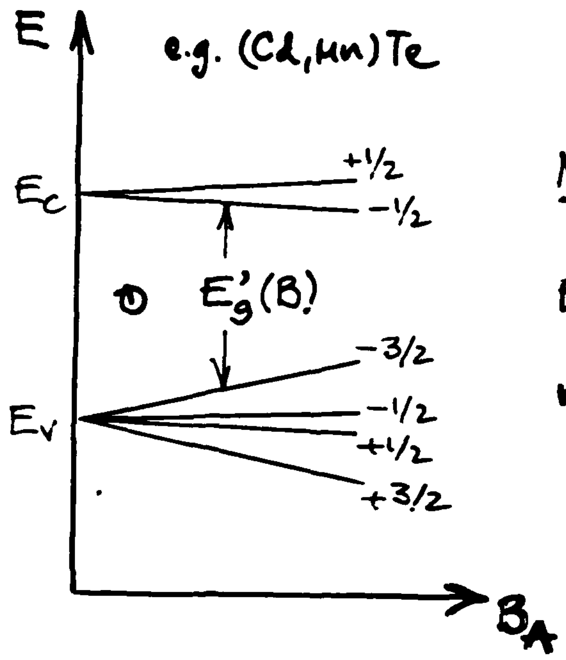

<u>MFA</u>:

$$E_g' = E_g^0 - N_0 x \cdot (\alpha - \beta) \cdot S_z(B_A)$$

where

$$S_z = \underset{5/2}{S_0}\, B_{5/2}\left(g\mu_B B_A / kT_L\right)$$

(paramagnetic limit)

← low x

→ 'giant' Zeeman effect (low T)

$$\Delta E_g \approx g_{eff}\, \mu_B\, B_A \;, \quad g_{eff} \gtrsim 100-200$$

Bandoffset Question in Wide-Gap II-VI Heterostructures

* sparse experimental information to date ↔ theory

* early indicators that ΔE_V is <u>small</u> for CdTe/(Cd,Mn)Te (also for CdTe/ZnTe)

* <u>exciton</u> effects strong e.g. for CdTe, ZnSe, ZnTe etc.

* <u>exploit the magnetic "tunability"</u> in a DMS quantum well

'Giant' Zeeman Effect : Bandoffset and Exciton Effects

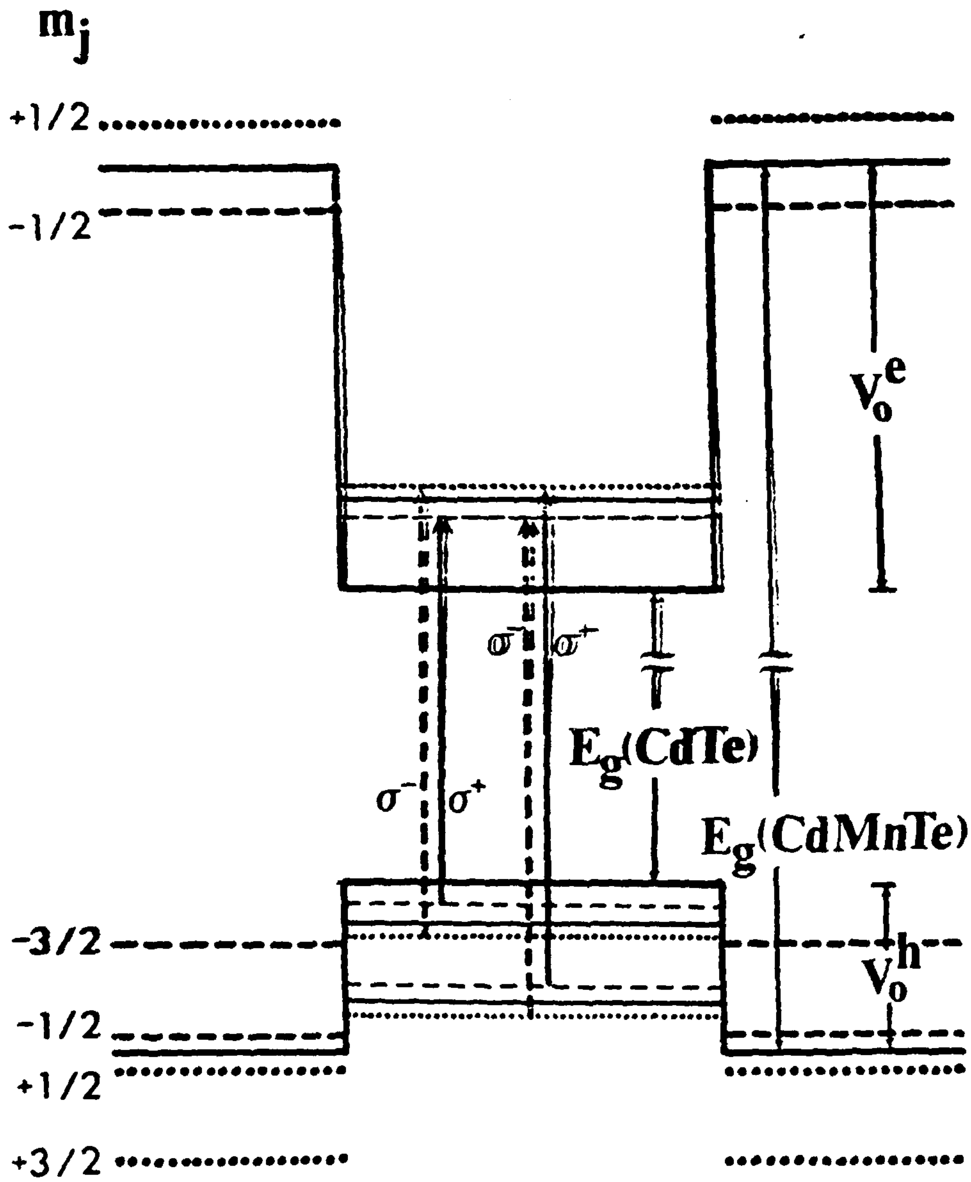

- e-h pair vs. exciton
- Faraday vs. Voigt
  → anisotropy in exchange interaction

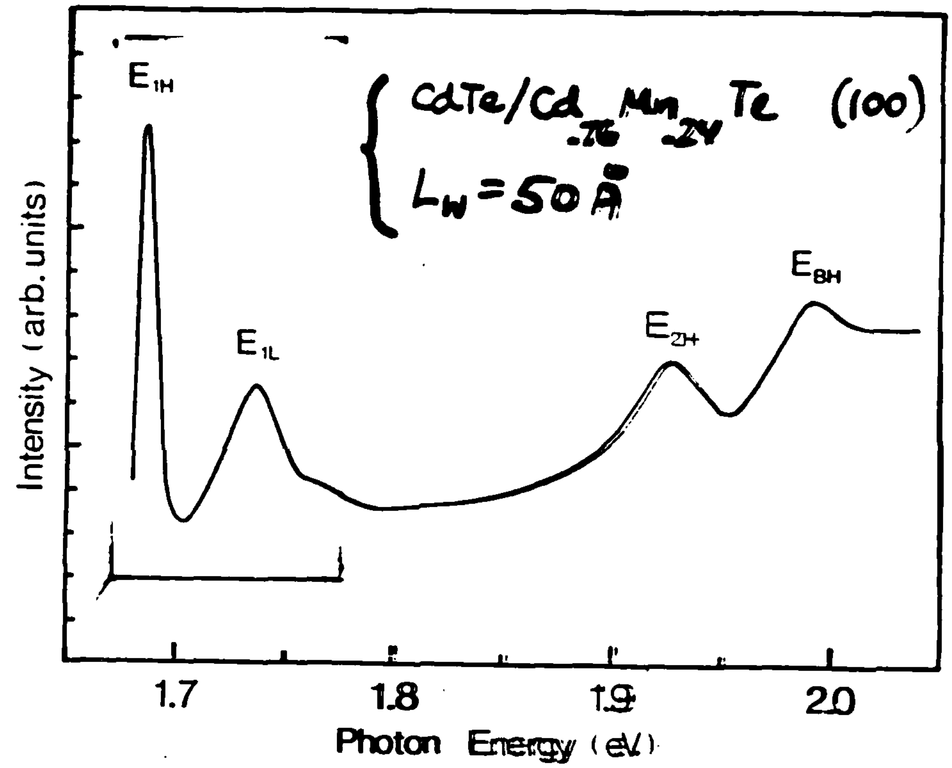

E1H
E1L
E2H
E8H
CdTe/Cd.76Mn.24Te (100)
Lw = 50 Å
Intensity (arb. units)
1.7
1.8
1.9
2.0
Photon Energy (eV)

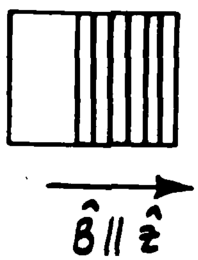

B || z

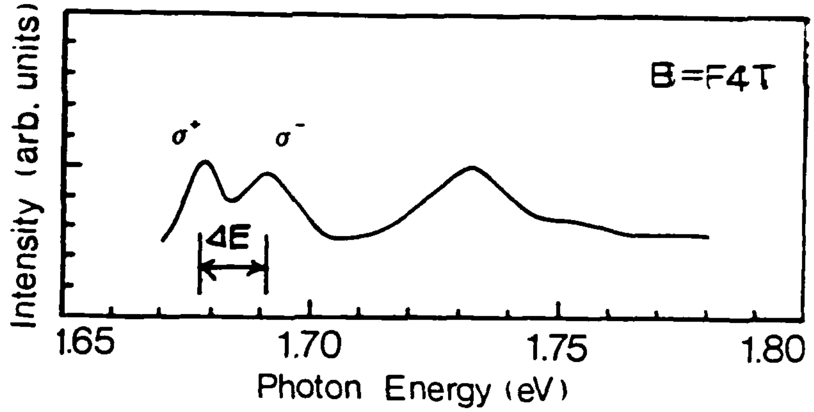

B = F4T
σ+
σ-
ΔE
Intensity (arb. units)
1.65
1.70
1.75
1.80
Photon Energy (eV)

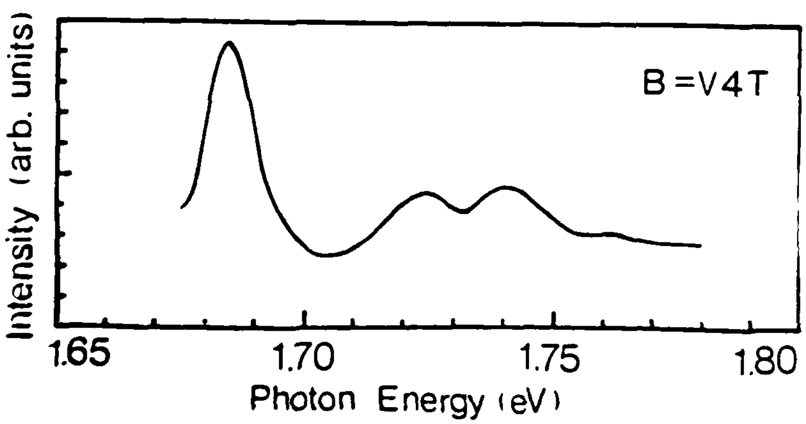

B = V4T
Intensity (arb. units)
1.65
1.70
1.75
1.80
Photon Energy (eV)

CdTe/$Cd_{.76}Mn_{.24}Te$ MQW, $L_W = 50\,\mathring{A}$ (100)

Zeeman splittings in $B_z = 4$ Tesla ($T = 2K$):

	n=1 HH	n=2 HH	n=1 LH	$barrier_{HH}$
ΔE	14 meV	44 meV	≤3 meV	80 meV
	≤4 meV		17 meV	

- Single particle ~~calculation~~ predicts large asymmetry in $\Delta E = \Delta E_1 + \Delta E_2$

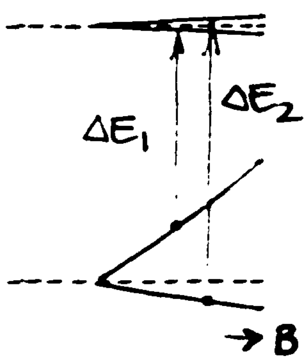

- with exciton contribution $\Delta E_1 \simeq \Delta E_2$ as observed

- Coulomb attraction adds 'extra depth' for hole potential

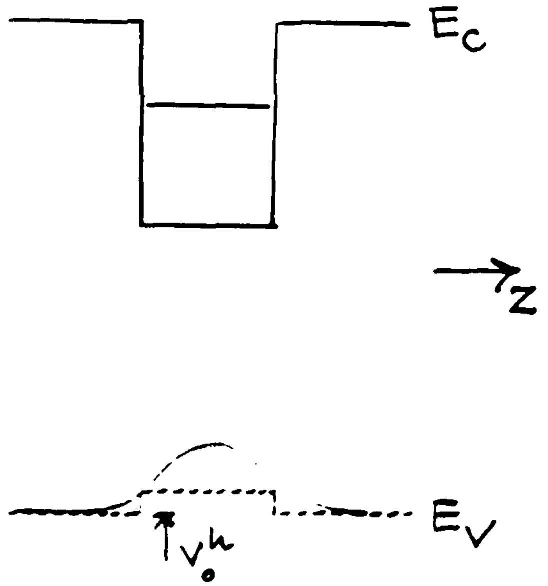

$V_o^{hx} > V_o^h$

J.W. Wu et. al.

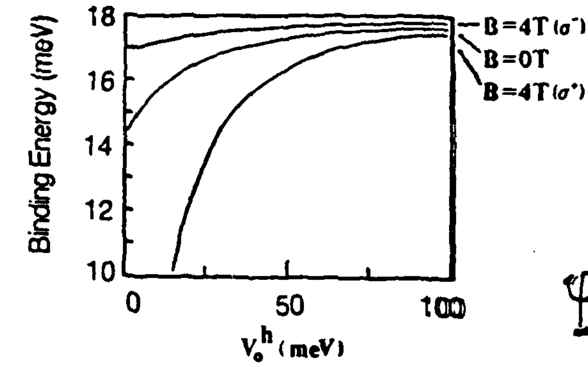

$$\Psi = \psi(z_e)\,\psi(z_h)\,\phi(r_\perp, z_e - z_h)$$

$$\phi(r_\perp) = \sqrt{\frac{2}{\pi}}\,\lambda^{-1}\,e^{-r_\perp/\lambda}$$

n=1
hh

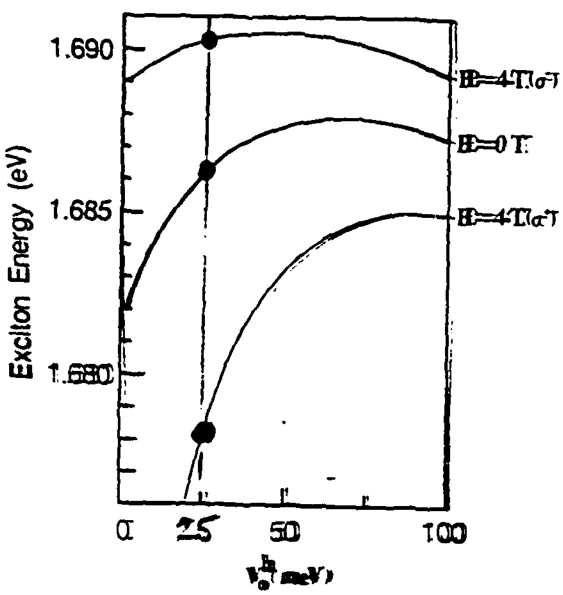

Coulomb interaction:

$\psi(z_e)$ and $\psi(z_h)$ no longer simple solutions in z-directions of the Hamiltonian.

$V_o^h = 25$ meV
$V_o^e \approx 360$ meV

subtract strain
$V_o^{hh} \simeq 0$ meV

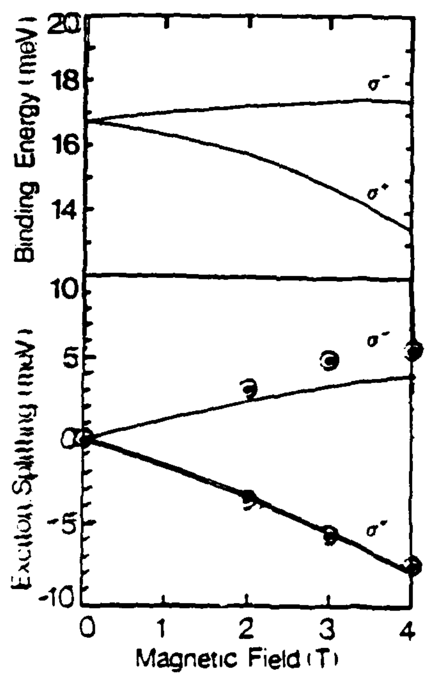

$E_B^{QW} \to 20$ meV

($E_B^{CdTe} \sim 9$ meV)

Summary: CdTe/(Cd,Mn)Te MQW

* Excitation spectroscopy in external magnetic fields at exciton transitions of the QW and barrier layers: 'tuning' of offsets

* Theory to account for the strong Coulomb effects in the case of a 2D-electron and a quasi 3D-hole

* Determination of conduction to valence band offset of 14:1 for a particular QW; when corrected for strain, the valence band offset is zero within 10 meV for the heavy hole

→ at variance with theory by Tersoff (interface dipoles)

→ devices (APD & vertical transport)

Recombining vs. Absorbing Exciton:

"Magnetic Relaxation" at an interface of a CdTe/(Cd,Mn)Te QW (Magnetic Polaron)

Goncalves da Silva
J. W. Wu et. al.
S. Jackson

bulk: Benoit et. al.
Spalek & Dietl
Wolff et. al

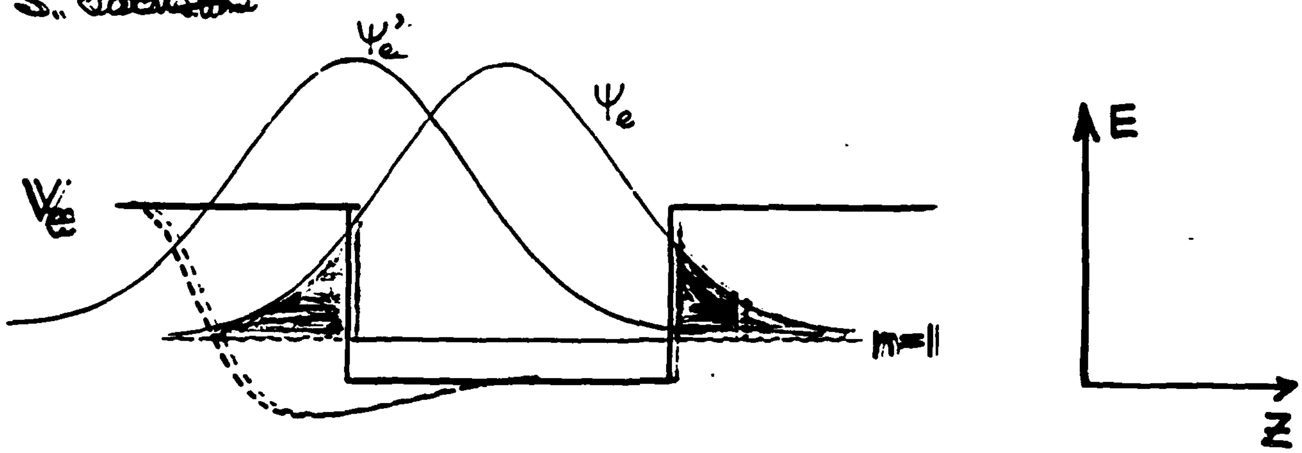

$$\mathcal{H} \sim p_e^2/2m_e^* + \theta(z_e - L/2)\cdot\left[V_0^e - V_m^e \, \mathcal{B}_{5/2}\left(g\mu_B \vec{B}_{eff}(\vec{r}_e)/kT\right)\right]$$

(MFA) $\hookrightarrow \alpha$ or β

- magnetically induced interface localization (spontaneous magnetization)

- MP effect enhanced for small bandoffset

$\hookrightarrow$ CdTe/$Cd_{1-x}Mn_xTe$

$V_0^h << V_0^e$; $\beta > \alpha$

not simple unif. strain → valenceband dispersion

Differences between (111) and (100) CdTe/(Cd,Mn)Te: photoluminescence excitation spectra

S-K. Chang et. al.

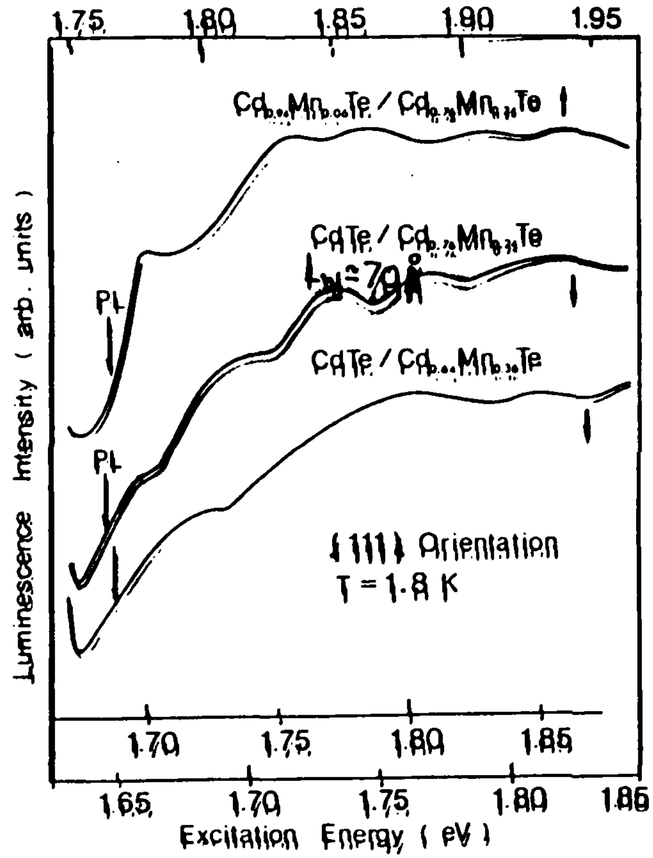

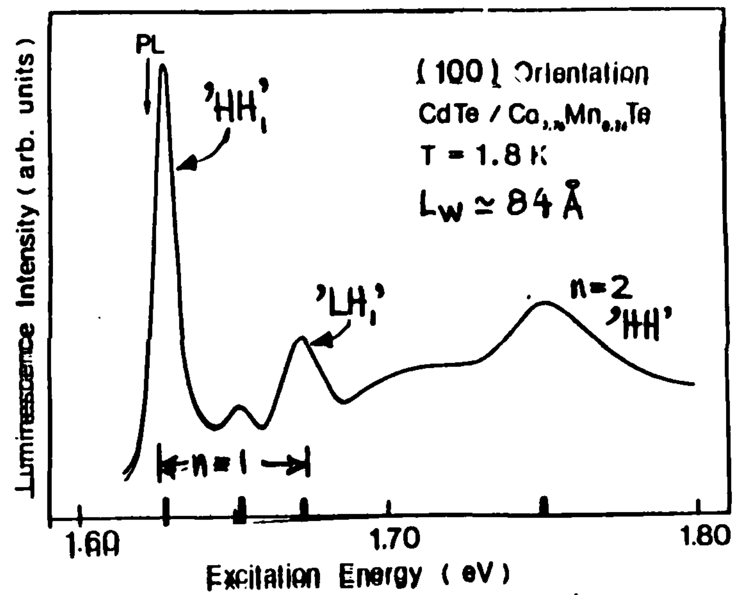

$\overline{\Delta E}_V \sim 30\,\text{meV} \lesssim 0.1\,\Delta E_c$?

but, a DMS quantum well !

- strain fluctuations ← 'disorder'
- microfield screening (Smith, Hailhiot)

exciton broadening

Q. Fu, Don Lee, André Mysyrowicz

Towards 2D H_2

Excitonic Molecules in ZnSe Quantum Wells

* well established in bulk (e.g. CuCl) + = +

Chem Phys

* quasi-2D enhancement for (i) exciton binding and (ii) molecular binding energy → overall $\gtrsim 10\times$ over 3D case

* II-VI vs. III-V heterostructures

→ GaAs/(Ga,Al)As, R. Miller et. al.

→ bulk ZnSe $E_{BX} \sim 2$–3 meV

$\frac{E_{BX}}{E_X}$

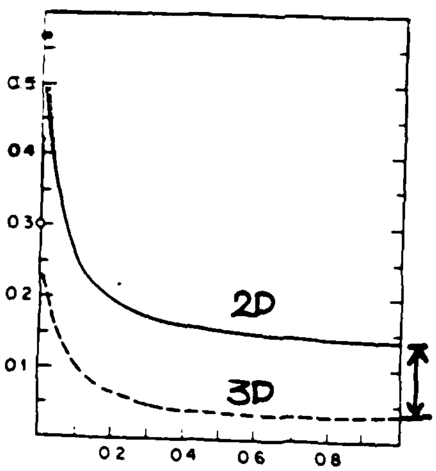

$\sigma = m_e / m_h^{\parallel}$

D.A. Kleinman (1983)

Biexc ≡ Exc. Mol.

$ZnSe/Zn_{.72}Mn_{.28}Se$ MQW

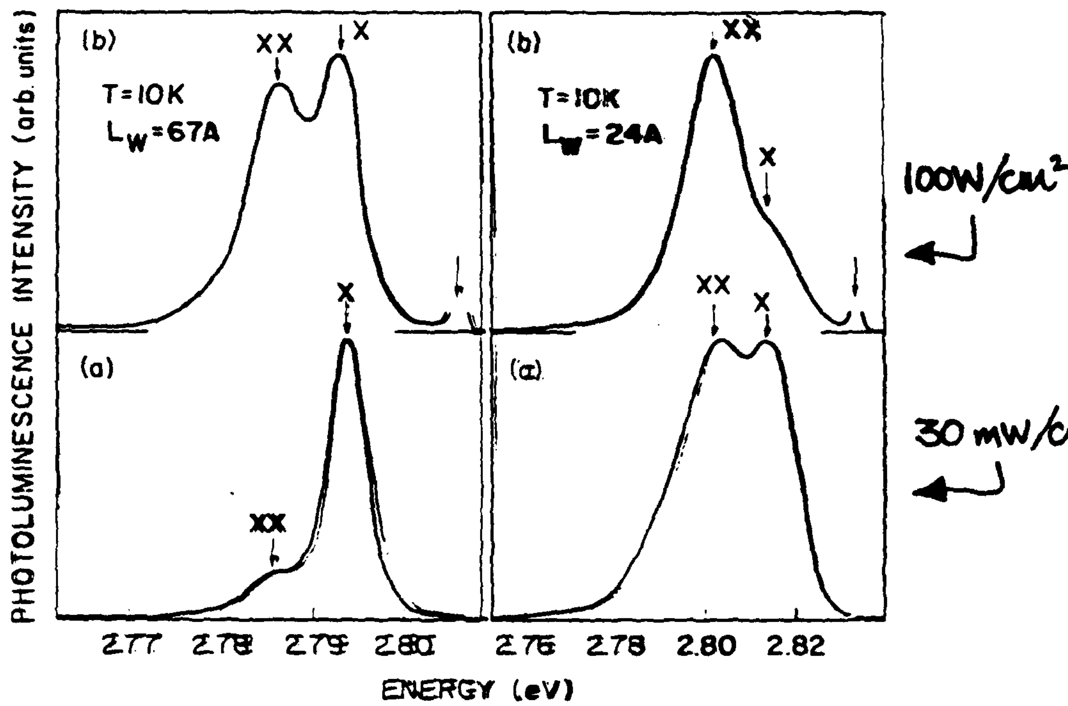

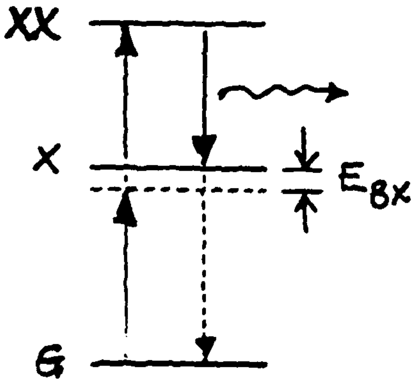

($k=0$)

$\rightarrow E_{BX}/2 = E_X - \hbar\omega$

- 'XX' gains over X with increasing excitation
- Kinetics complicated & difficult to quantify
- 'XX' prominent at low excitation levels

Excitation by circular vs. linear polarization:

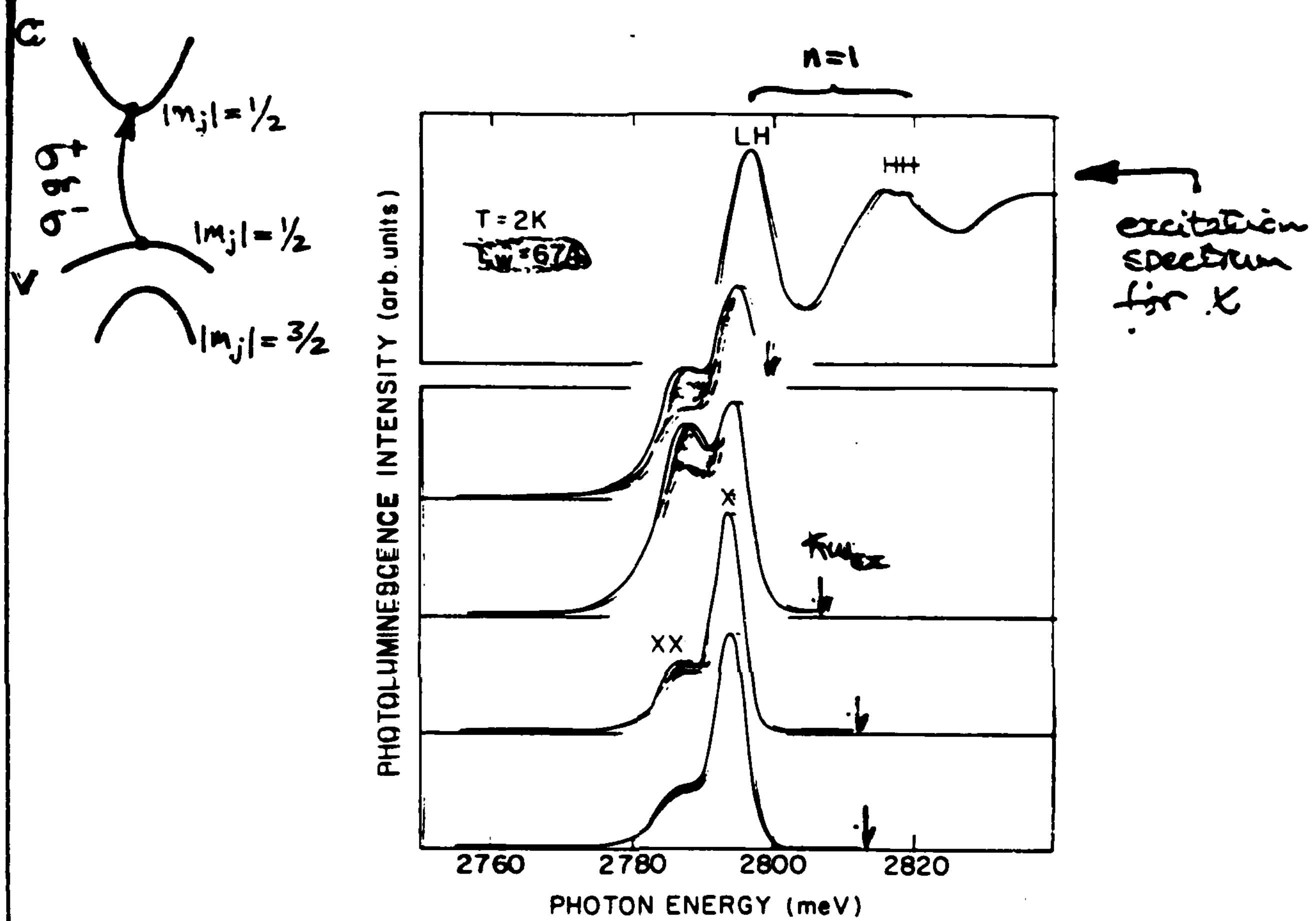

- large polarization contrast for XX and X (molecule in singlet state)

- spin relaxing collisions for $\hbar\omega_{ex} \gg E_x$

Giant Two-Photon Absorption

→ excitation spectrum of line 'XX'

intensity dep. polarization dep.

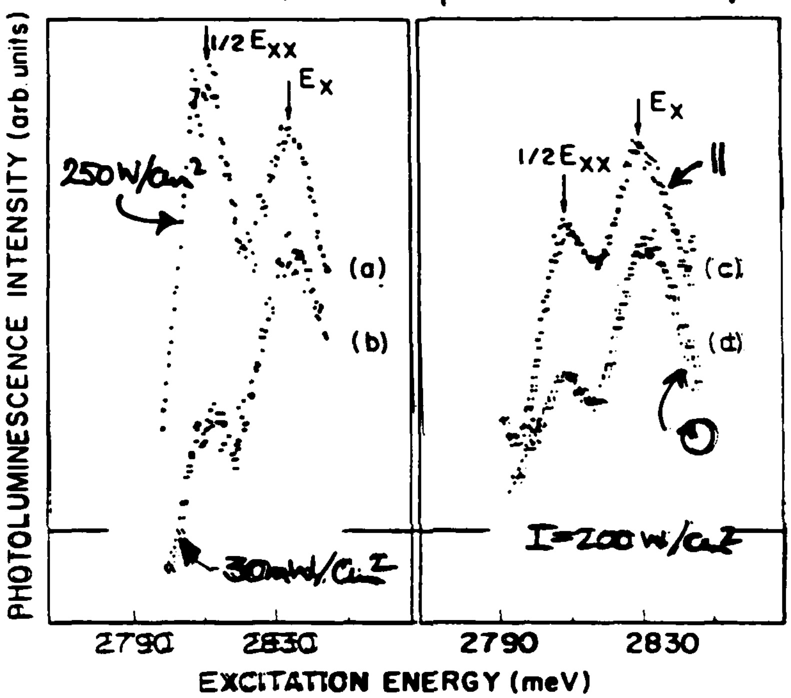

$ZnSe/Zn_{.72}Mn_{.28}Se$

$L_W = 24\,Å$

$T = 2K$

- $(k=0)$ $E_{BX}/2 = E_X - \hbar\omega$ at TPA resonance

  → $E_{BX} \sim 40$ meV for $L_W = 24\,Å$

  from PL $E_{BX} \sim 33$ meV → –

  $E_{BX} \sim 11$ meV $L_W = 67\,Å$

- note low intensities

Summary

* evidence for excitonic molecule in ZnSe/(Zn,Mn)Se quantum wells from luminescence, nonlinear absorption, polarization selection rules, and temperature dependence.

* scaling of E_{Bx} with well thickness roughly as predicted

* surprisingly stable molecular state $E_x^{3D}(\mathrm{ZnSe}) \sim 20\,\mathrm{meV}$

* microscopic details not yet known → QW profile
  → bandoffsets

Enhanced Excitonic Optical Nonlinearity and Exciton Dynamics in Semiconductor Microstructures

T. Takagahara

NTT Electrical Communications Laboratories, Musashino-shi,

Tokyo 180, Japan

The mechanisms of enhanced excitonic optical nonlinearity in semiconductor microstructures are clarified to be the easily attainable state filling of discretized levels due to the quantum size effect and the enhanced oscillator strength. The calculated third-order nonlinear susceptibility explains successfully the recent experimental results. A comprehensive interpretation of the exciton dynamics in semiconductor microcrystallites is presented to explain the fast and slow decay components in phase conjugation and luminescence measurements.

Recently the excitonic states in semiconductor microstructures have attracted much attention due to the enhanced excitonic optical nonlinearity and fast response time [1-7] . In semiconductor microstructures of lower dimensionality, the energy levels of carriers are discretized due to the quantum size effect. The oscillator strength becomes concentrated on the sharp transitions of the lower energy and the mechanism of excitonic optical nonlinearity is simply the state filling of these sharp excitonic transitions in contrast to the band filling of continuum states in the bulk material. As a consequence, the excitonic optical nonlinearity is enhanced while the saturation power is reduced, relative to the bulk semiconductor. The response time of the optical nonlinearity is determined by the build-up time and recombination lifetime of photo-generated carriers. The dynamics of photo-generated carriers in semiconductor-doped glasses have been studied extensively by the transient grating method [1,3-7] and photo-luminescence [3-5,8,9] . Some controversies

exist about the origins of the fast and slow components of the electron-hole recombination [1,3-9] .

First of all, the excitonic states in semiconductor quantum dots are discussed. The energy of the excitonic state measured from the bulk band gap energy consists of the kinetic energy of the electron and hole(E_k), the Coulomb energy between them(E_C) and the surface polarization energy(E_S) [10] . These are shown in Fig.1 as a function of the quantum dot radius normalized by the exciton Bohr radius a_B in bulk crystals. The exciton binding energy in a semiconductor quantum dot is obtained from the energy difference between the exciton state and a free electron-hole pair state. Figure 2 shows the dependence of the exciton binding energy on the normalized quantum dot radius. It is important to note that the rather small exciton binding energy implies the ionization of excitonic states at room temperature. In fact, for semiconductor(CdS) quantum dots with radii in the range shown in Fig.2, the excitonic state may be ionized to the free electron-hole pair state at room temperature.

The radiative recombination lifetime τ_R of excitons in a quantum dot can be estimated from the oscillator strength of the excitonic transition [11] . For a free electron-hole pair in a semiconductor(CdS) quantum dot, the oscillator strength f_0 is estimated to be 8.14 using the relevant parameters [12] and the corresponding radiative lifetime τ_R is 440 ps. These values are independent of quantum dot size. When the excitonic effect, namely the electron-hole correlation, is included, the oscillator strength f is enhanced since it is proportional to the probability of finding an electron and a hole at the same position. This enhancement factor and the corresponding radiative recombination lifetime are given in Fig.3 as a function of the normalized radius of the quantum dot. For a 100Å radius CdS quantum dot, the radiative recombination time is estimated to be 20 ps. This value is of the same order as the so-far-reported time constants of the fast decay component in transient grating measurements [3-7] .

The excitonic optical nonlinearity in semiconductor quantum dots can be enhanced due to the large oscillator strength of the exciton and the energy level discretization which leads to an easily attainable state filling. The calculated frequency dispersions of the linear susceptibility $\chi^{(1)}$ and the third-order nonlinear susceptibility $\chi^{(3)}$ for the degenerate case, i.e., $\omega_1=\omega_2$, are shown in Fig.4. The out-of-phase behavior between $\chi^{(3)}$ and $\chi^{(1)}$ for both real and imaginary parts explains the experimental results [2] very well. The absolute value of $\chi^{(3)}$ for CdS quantum dots is estimated to be about 3.8×10^{-8} esu for a number density N of 10^{14} cm^{-3} and for the Lifshitz-Slezov [13] distribution of quantum dot radius with an average of 100Å. This value is also in good agreement with the experimental value at room temperature [1]. In this calculation, the oscillator strength of the free electron-hole pair is employed in consideration of the aforementioned possibility that the excitonic state is ionized at room temperature. At low temperatures, the excitonic state is stable and its large oscillator strength is available to enhance the optical nonlinearity. In fact the excitonic optical nonlinearity at low temperatures is calculated to be as large as 10^{-4} esu.

Our comprehensive interpretation of the controversial exciton dynamics in semiconductor quantum dots is presented with respect to the exposure time dependence of the decay characteristics [5,7] and the darkening of the glass [5]. The slow decay component can be attributed to the radiative recombination of an electron and a hole trapped by a donor-acceptor pair, whose rate is dependent on the distance between the donor and the acceptor and which gives rise to a broad luminescence spectrum. This assignment is corroborated by the recent measurement of the donor-acceptor pair recombination rate in bulk CdS [14]. In the course of this recombination process, the emitted phonons induce some kind of structural change around the donor-acceptor pair and efficient non-radiative recombination centers will be formed. The temperature rise due to laser irradiation regarded as uniform in semiconductor microcrystallites is estimated to be rather small. This suggests the importance of local phonon

modes in inducing the structural change. After repeated exposure to laser irradiation, these non-radiative recombination centers are accumulated and the photo-generated carriers lose their energy via these centers. Thus the radiative recombination via a donor-acceptor pair becomes quenched leading to the disappearance of the broad luminescence spectrum [5] and also of the slow decay component in the transient grating measurements [5,7]. This accumulated structural change may be a cause of the permanent holographic grating and the darkening of the glass. This kind of photo-induced structural change is seen extensively in amorphous materials, such as a-Si [15], chalcogenide glasses [16] and Eu-doped glasses [17]. On the other hand, the fast decay component can be considered as arising from the radiative recombination of free excitons as calculated above. This interpretation is consistent with the experimental result [5] that the narrow luminescence line attributed to the excitonic recombination shows a very rapid decay. However, we have to keep in mind the possibility that the fast decay component arises from the nonradiative recombination of an electron-hole pair via defect states or surface states. Thus it is crucial to examine the size dependence of the decay time constant in identifying the origin of the fast decay component.

References:

[1] R.K. Jain and R.C. Lind, J. Opt. Soc. Am. 73, 647(1983).

[2] G.R. Olbright and N. Peyghambarian, Appl. Phys. Lett. 48, 1184(1986).

[3] S.S. Yao, C. Karaguleff, A. Gabel, R. Fortenberry, C.T. Seaton, and G.I. Stegeman, Appl. Phys. Lett. 46, 801(1985).

[4] P. Roussignol, D. Ricard, K.C. Rustagi, and C. Flytzanis, Opt. Commun. 55, 1431(1985).

[5] P. Roussignol, D. Ricard, J. Lukasik, and C. Flytzanis, J. Opt. Soc. Am. B4, 5(1987).

[6] D. Cotter, Technical Digest of XIV International Quantum Electronics Conference, San Francisco, June 1986, PD19.

[7] H. Shinojima, M. Mitsunaga, and K. Kubodera, presented at the Spring

Meeting of the Physical Society of Japan, March 1987(in Japanese).

[8] J. Warnock and D.D. Awschalom, Phys. Rev. B32, 5529(1985).

[9] N. Chestnoy, T.D. Harris, R. Hull, and L.E. Brus, J. Phys. Chem. 90, 3393 (1986).

[10] L.E. Brus, J. Chem. Phys. 80, 4403(1984).

[11] C.H. Henry and K. Nassau, Phys. Rev. B1, 1628(1970).

[12] C. Weisbuch and R.G. Ulbrich, in Light Scattering in Solids III, ed. M. Cardona and G. Guntherodt(Springer, Berlin 1982), p.218.

[13] I.M. Lifshitz and V.V. Slezov, J. Exptl. Theoret. Phys.(U.S.S.R) 35, 479 (1958) [Sov. Phys. J.E.T.P. 35, 331(1959)] .

[14] R.T. Cox and J.J. Davies, Phys. Rev. B34, 8591(1986).

[15] R.A. Street, Adv. Phys. 30, 593(1981).

[16] K. Tanaka, in Fundamental Physics of Amorphous Semiconductors, ed. F. Yonezawa(Springer, Berlin 1981), p.104.

[17] F.M. Durville, E.G. Behrens, and R.C. Powell, Phys. Rev. B35, 4109(1987).

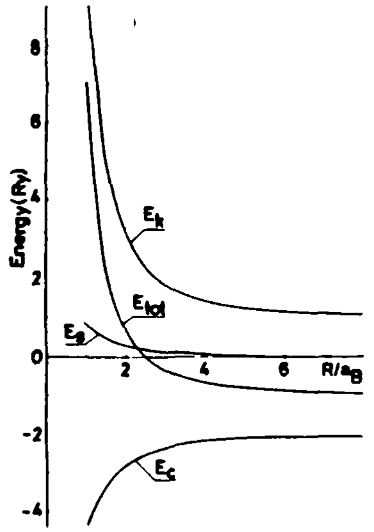

Fig.1:Exciton energy(E_{tot}) versus radius of spherical semiconductor particles (quantum dots). E_k denotes the kinetic energy, E_C, the Coulomb energy and E_S is the surface polarization energy, respectively. a_B is the exciton Bohr radius in bulk semiconductors.

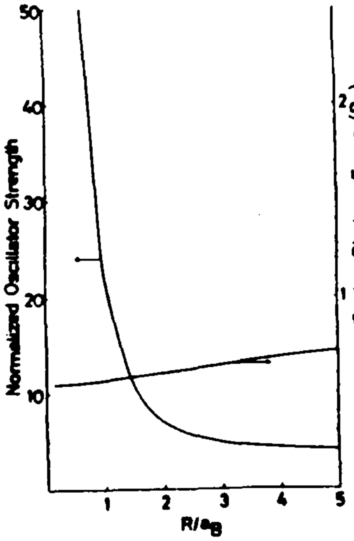

Fig.2:Exciton binding energy in units of Rydberg(Ry) and normalized oscillator strength in spherical semiconductor particles plotted as a function of particle radius.

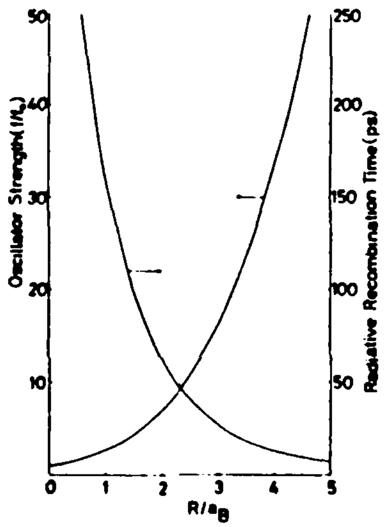

Fig.3:Enhancement factor of the oscillator strength of exciton relative to that of free (uncorrelated) electron-hole pair and the radiative recombination time in spherical semiconductor particles plotted as a function of particle radius.

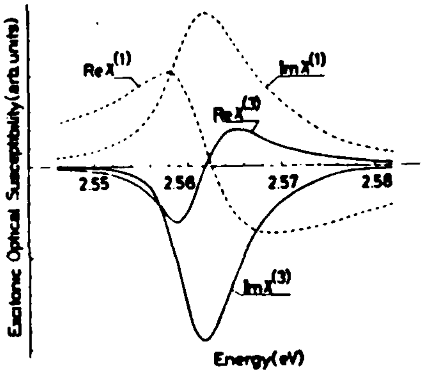

Fig.4:Frequency dispersion of $\chi^{(1)}$ and $\chi^{(3)}$ of spherical semiconductor(CdS) particles. Particle size distribution is taken into account by the Lifshitz-Slezov distribution function for an average radius of 100Å.

FREE CARRIER NONLINEAR OPTICS

P. A. WOLFF
Francis Bitter National Magnet Laboratory
MIT, Cambridge, MA 02139

Free carriers in semiconductors cause optical nonlinearity in two ways. In some cases it arises from the inherent nonlinearity of electron dynamics in crystals; in others it is caused by scattering. Such processes are interesting because they can be used to study carrier dynamics and kinetics in semiconductors. In particular, the large frequency dispersion of these nonlinearities determines carrier relaxation times. These times, which are generally in the picosecond range, also characterize the speed of the nonlinearity.

Until lately, all known free-carrier-induced optical nonlinearities were weak. We have recently investigated two crystals, HgTe and HgCdSe:Fe, in which large, fast, free-carrier-induced $\chi^{(3)}$'s may be attainable. These materials will be used as examples to illustrate the mechanisms and features of free-carrier-induced optical nonlinearity.

Large, room temperature, third order nonlinear optic susceptibilities are observed in HgTe and HgMnTe at 10.6μ. These materials have the largest known third order optical nonlinearities with response times in the picosecond range. In HgTe, $\chi^{(3)} = 1.6 \times 10^{-4}$ esu at 300K; this value is twenty times the previous record.

The nonlinear susceptibilities were measured by four wave mixing experiments performed with a pair of Q-switched CO_2 lasers. The nonlinear signal varied as $P_3 \sim P_1P_2$ to the highest laser intensities, $P_1 = P_2 = 500\text{kW}/\text{cm}^2$, used in these experiments. The absence of saturation is striking. We attribute the optical nonlinearity to interband population modulation between the heavy mass Γ_8 valence band and the light mass Γ_8 conduction band. A plasma density modulation exceeding 10^{17} electron-hole pairs/cc is required to produce the observed effect. Calculations suggest that this oscillating plasma could also radiate efficiently in the far infrared.

The figure of merit, $\chi^{(3)}/\alpha T$, for HgTe is comparable to that of other semiconductors. However, the product $\chi^{(3)}P_{sat}$ for HgTe far exceeds that of other semiconductors. Further enhancement of the HgTe nonlineary is anticipated with appropriate doping or alloying.

We have observed a novel free carrier nonlinear optical effect due to scattering by the resonant $Fe^{2+}(3d^6)$ donor states in HgCdSe:Fe. The effect is only seen if the Fe states are located inside the conduction band. For a HgCdSe sample with energy bandgap of 303 meV and free electron concentration of 1.7×10^{18} cm^{-3} at 80K, a third order optical susceptibility of 1×10^{-6} esu was measured by four wave mixing experiments with CO_2 lasers. This value is twenty times larger than that induced by the energy band nonparabolicity, and can be explained by a theory taking into account the strong energy dependence of the scattering rate due to the presence of the resonant scattering level. The theory assumes that the pump lasers modulate the electronic temperature via free carrier absorption, which in turn modulates the dielectric constant through the energy dependent scattering mechanism, leading to large optical nonlinearity. The nonlinear optical effect can be further increased if the resonant scattering level is located closer to the Fermi energy. The theory can also be used to infer the Fe level width from the optical data; in our sample Δ = 20 meV.

1. # OPTICAL NONLINEARITIES OF SEMICONDUCTORS 1.

Four Wave Mixing :

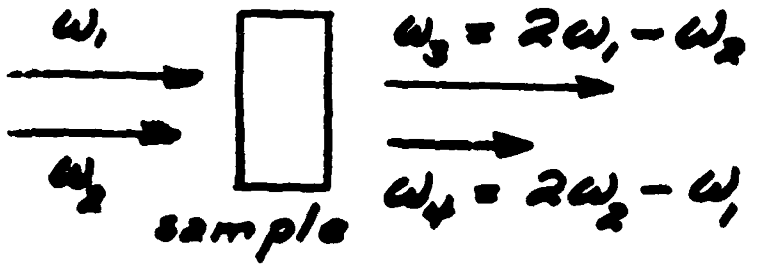

$$P_3 \sim |\chi^{(3)}|^2 P_1^2 P_2$$

$\epsilon(\omega)$ modulated at $\Delta\omega = \omega_1 - \omega_2$.
Beams acquire sidebands at
$\omega_1 + \Delta\omega = 2\omega_1 - \omega_2$; $\omega_2 - \Delta\omega = 2\omega_2 - \omega_1$

Here

$$\epsilon(\omega) = \epsilon_0(\omega) - \frac{4\pi n e^2}{m^* \omega(\omega + i/\tau)}$$

for a doped, single-valley semiconductor.

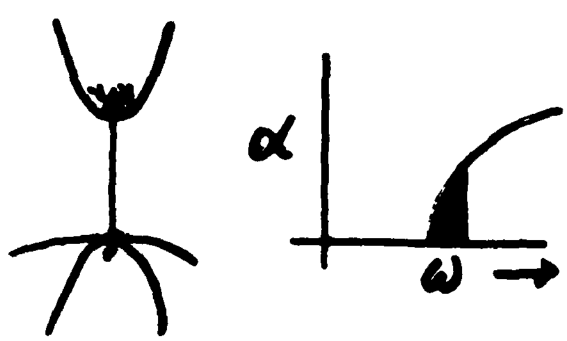

modulate :
i) m^*
ii) τ
iii) n (in multi-valley crystals)

2. FREE CARRIER NONLINEARITIES

Nonparabolicity (e.g. n-InSb)

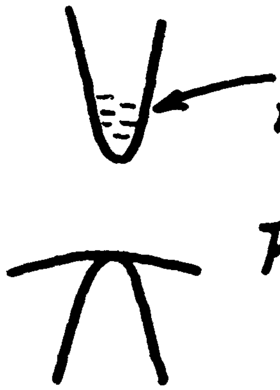

$$\frac{1}{m^*(E)} = \frac{1}{m^*}\left(1 - \frac{2E}{E_G}\right)$$

$$P \propto \left[|\mathcal{E}_1|^2 + |\mathcal{E}_2|^2 + 2\mathcal{E}_1\cdot\mathcal{E}_2^* + 2\mathcal{E}_1^*\cdot\mathcal{E}_2\right]$$

Intervalence Band (e.g. p-GaAs)

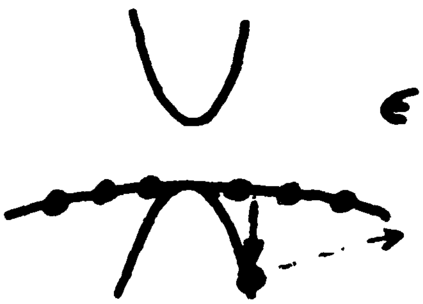

$$\epsilon = \epsilon_0 - \frac{4\pi n_1 e^2}{m_1^* \omega^2} - \frac{4\pi n_2 e^2}{m_2^* \omega^2}$$

Valley Transfer (e.g. n-GaAs)

$$\epsilon = \epsilon_0 - \frac{4\pi n_\Gamma e^2}{m_\Gamma^* \omega^2} - \frac{4\pi n_L e^2}{m_L^* \omega^2}$$

(requires $T \simeq 800K$)

3. FEATURES OF FREE CARRIER NONLINEARITIES

1.) Broadband.

2.) Fast - response is usually in picosecond range.

3.) Dispersive - $\chi^{(3)}$ varies rapidly with $\Delta\omega$. Why? Consider nonparabolicity:

$$\frac{dT_e}{dt} + \frac{T_e - T_L}{\tau_{th}} = \frac{c\sqrt{\epsilon}\,\alpha(\mathcal{E}_1 \cdot \mathcal{E}_2^*)e^{-i\Delta\omega t}}{8\pi C_v}$$

$$\Delta T_e = \frac{c\sqrt{\epsilon}\,\alpha(\mathcal{E}_1 \cdot \mathcal{E}_2^*)e^{-i\Delta\omega \tau_{th}}}{8\pi C_v\left[1 - i(\Delta\omega)\tau_{th}\right]}$$

4.) Strong frequency variation

$$\chi^{(3)} \approx \frac{ne^4}{(m^*)^2 E_G \omega^4}\left(\frac{2\tau_{th}}{\tau_M}\right)$$

5.) Relatively weak:

$\chi^{(3)} \approx 10^{-8}$ esu in n-InSb with $n = 10^{16}$ electrons/cc.

4.

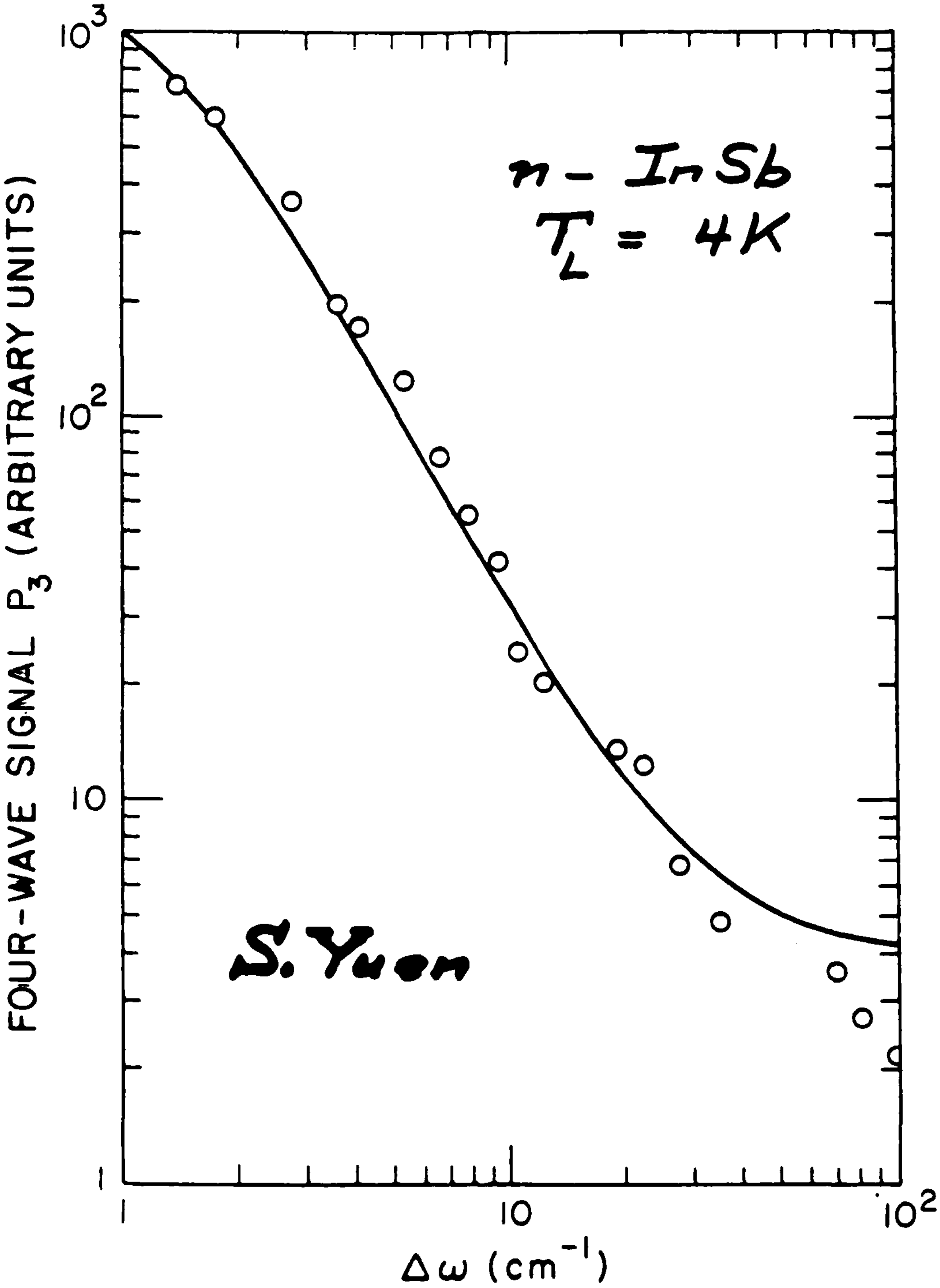

$\Delta\omega = (\omega_1 - \omega_2)$

4.

5. HgTe EPILAYERS VS HgCdTe

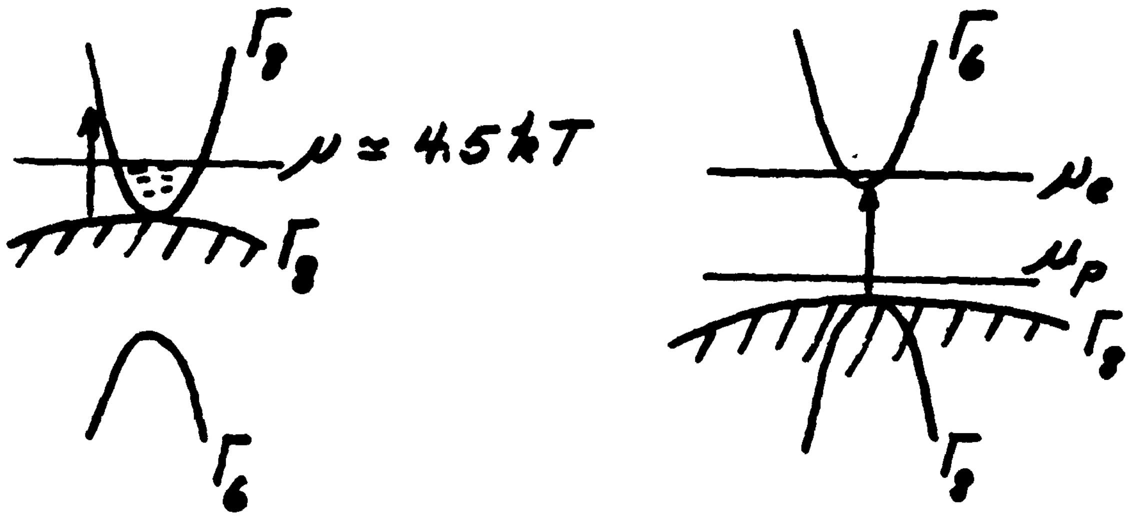

<u>HgTe</u>	<u>HgCdTe</u>
$\chi^{(3)} \simeq 2\times10^{-4}$ esu	$\chi^{(3)} \simeq 5\times10^{-2}$ esu
$\tau = 5$ psec. (thermal relaxation)	
$\tau_r = 0.1$ psec. D'yakonov *et al*	$\tau_r = 30$ nsec.
$\alpha = 3400\ cm^{-1}$	$\alpha = 8\ cm^{-1}$
$\chi^{(3)}/\alpha\tau \simeq 10^4$	$\chi^{(3)}/\alpha\tau \simeq 2\times10^5$
$\mu_e \simeq \mu_p \simeq \mu$	$\mu_e \neq \mu_p$

6.

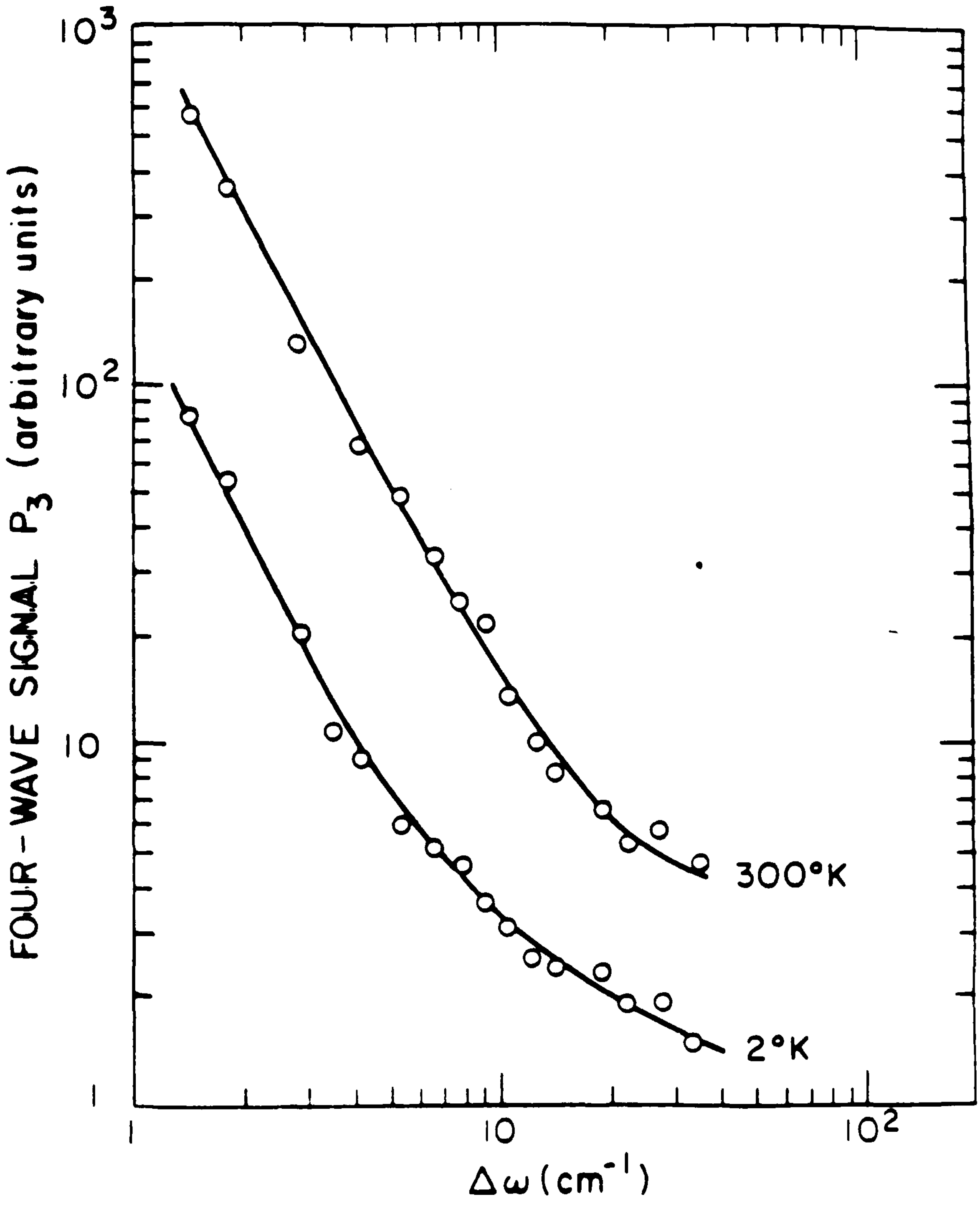

Wolff, Yuen, Harris, Cook,
and Schatzina

7. MODEL FOR HgTe NONLINEARITY

1.) τ_r for HgTe ~ 0.1 psec.

2.) Electrons and holes in thermal equilibrium $\longrightarrow \mu_e \simeq \mu_p \simeq \mu$. But $T_e > T_L$

3.) Carrier density strongly dependent on T_e.

4.) For undoped samples $n = p \sim T_e^{3/2}$

These assumptions imply:

$$\chi^{(3)} = \frac{f}{160\pi}\left(\frac{e^2}{m_e^* \omega^2}\right) \frac{c\sqrt{\epsilon}\,\alpha \tau_{th}}{kT_e\,(1 + i\Delta\omega\tau_{th})}$$

where

$$f = \frac{E_G + \mu/2}{E_G + \mu/2 - \hbar\omega}$$

HgTe: $T_L = 300K$, $E_G \simeq 150\,meV$

$\chi^{(3)}_{exp.} = \underline{1.6 \times 10^{-4}\,esu}$; $\chi^{(3)}_{th.} = \underline{2.1 \times 10^{-4}\,esu}$

8. HgTe NONLINEARITY

1.) High saturation power. $\chi^{(3)}P_{sat.}$ exceeds that of other fast optical nonlinearities.

2.) Large, oscillating plasma densitie. $n \approx 10^{17}$ electron-holes/cc. ; $\Delta\epsilon \approx 10\%\,\epsilon_0$

3.) Further enhancement possible:

i) By matching $E_G + \mu/2 \approx \hbar\omega$.

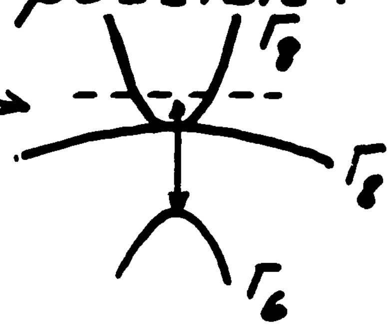

ii) By doping $E_F \approx \hbar\omega$

(Genkin et al)

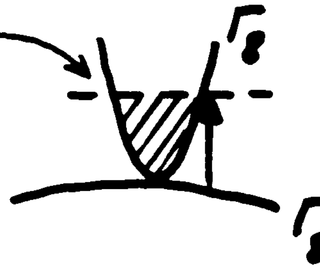

4.) Weak frequency dependence. For a forbidden optical transitio $\alpha(\omega) \sim \omega^{3/2} \longrightarrow \chi^{(3)} \sim \omega^{-1/2}$.

5.) Tailor semimetal band structur to give large $\chi^{(3)}$ at 3ν?

i) Semimetals with larger E_G?

ii) Pump above E_G?

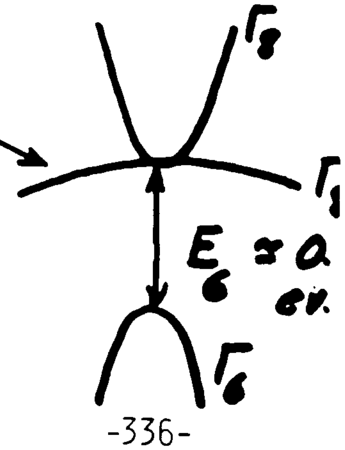

6.) Why is τ_{th} so long?

9.

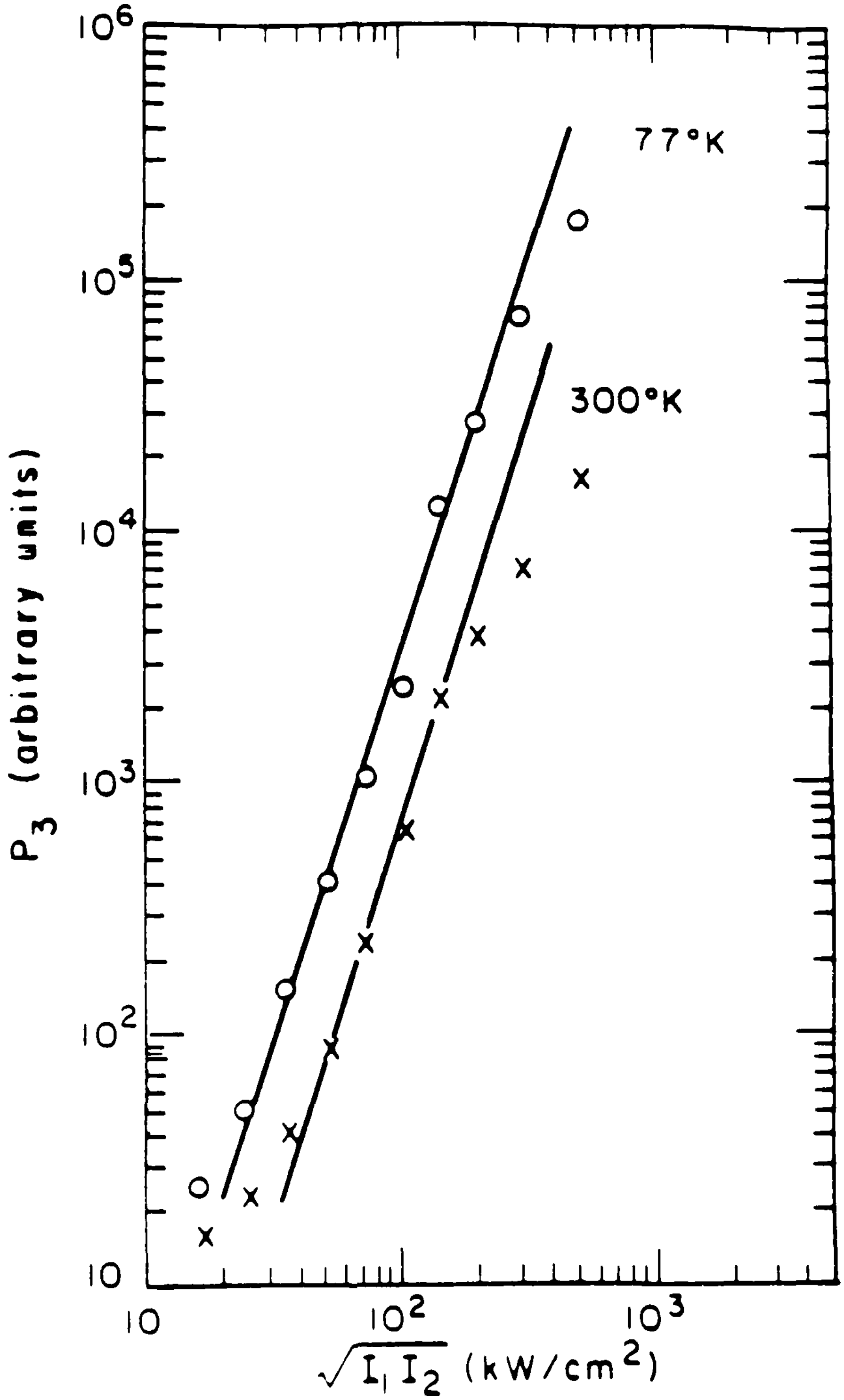

Wolff, Yuen, Harris, Cook, and Schatzina

10. WHAT TO DO WITH HgTE OPTICAL NONLINEARITY ?

FIR Generation

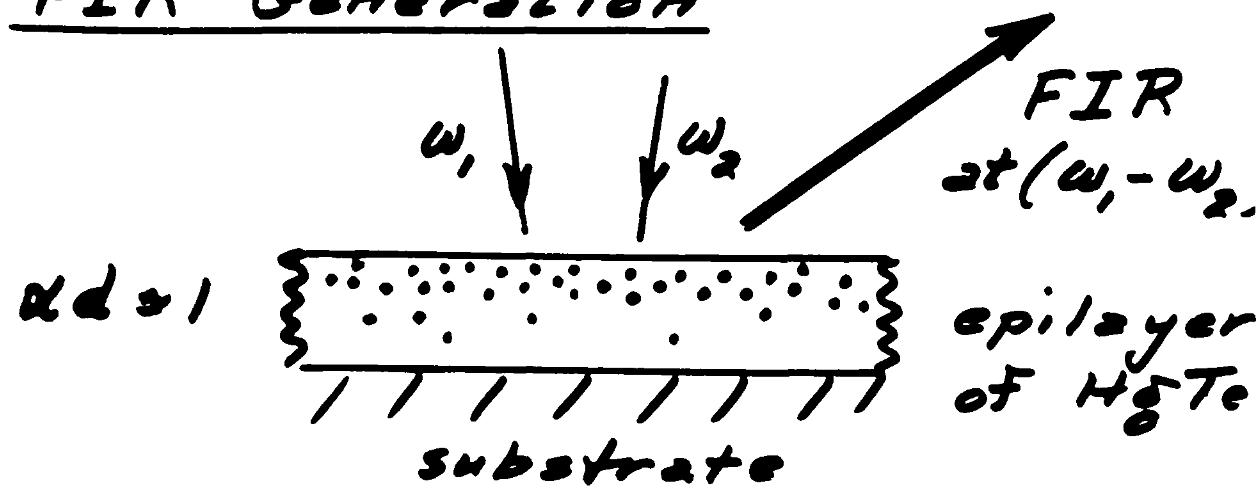

Ambipolar diffusion requires charge separation, coupling to plasma modes, radiation.

Stimulated Plasmon Emission

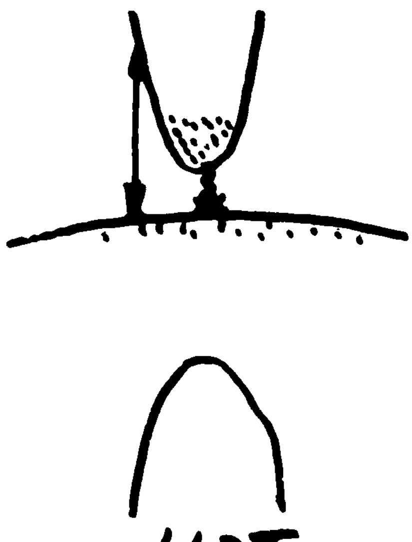

HgTe

Field induced gap
$E_c \approx$ 10 - 20 meV.
When pumped hard get
$n = p \approx 10^{17}$ carriers/c

Calculations predict stimulated plasmon recombination

11. OPTICAL NONLINEARITY DUE TO RESONANT DONOR LEVELS

Fe^{2+} level in $Hg_{1-x}Cd_xSe:Fe$ (Mycielski *et al*)

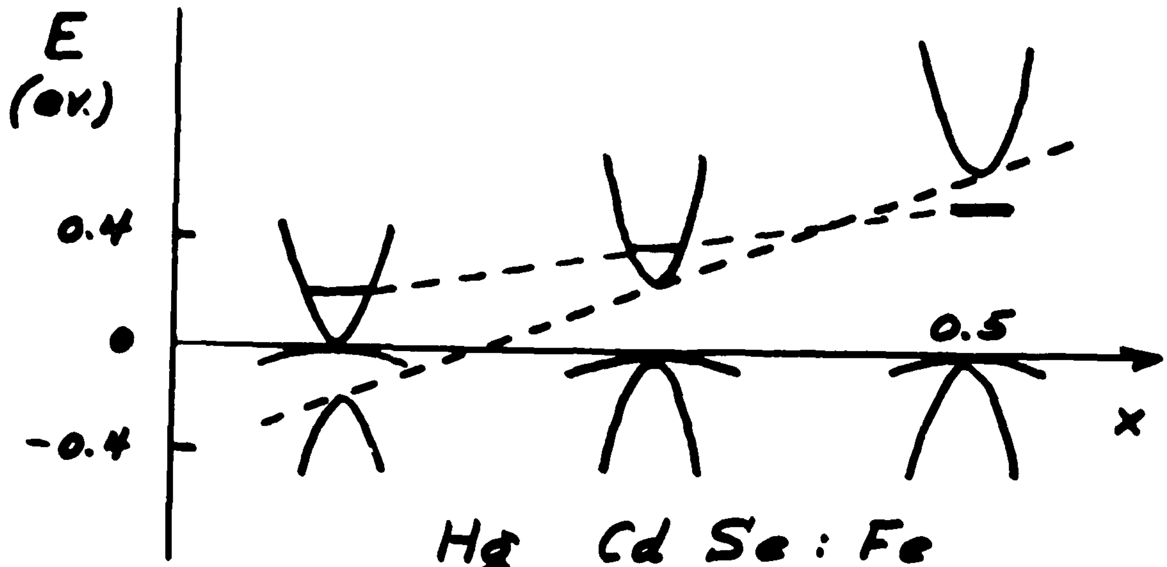

$Hg_{1-x}Cd_xSe:Fe$

$Hg_{1-x}Cd_xSe:Fe$ Samples

$T = 80K$ $n = 1\text{-}2 \times 10^{18}/cc.$

E_g	E_{Fe}	$\chi^{(3)}_{exp}$	$\chi^{(3)}_{nonp}$	$\chi^{(3)}_{Fe}$
670	420	5×10^{-8}	3×10^{-8}	
330	380	1×10^{-6}	6×10^{-8}	7×10^{-7}

12. MODEL OF [illegible] NONLINEARITY

Laser beams modulate electron temperature, promoting carriers

$$\chi^{(3)} \propto \frac{d\chi^{(1)}}{dT_e} \frac{(\delta T_e)_{NL}}{\mathcal{E}_1 \mathcal{E}_2^*}$$

$$\chi^{(3)} \simeq -i\left(\frac{d\sigma_1}{dT_e}\right) \frac{c\sqrt{\epsilon_0}\,\alpha\,\tau_{th}}{8\pi\omega C_v\left[1 + i(\Delta\omega)\tau_{th}\right]}$$

Here, from the Anderson model:

$$\sigma_1(\omega) = \frac{2\pi e^2 N_i |V|^2}{3m^* \hbar^2 \omega^3} \int \Big\{ \rho(E)\rho(E+\hbar\omega) \cdot$$

$$\left[f(E) - f(E+\hbar\omega)\right]\left[\frac{E}{|\mathcal{D}(E+\hbar\omega)|^2} + \frac{(E+\hbar\omega)}{|\mathcal{D}(E)|^2}\right]\Big\}$$

with $|\mathcal{D}(E)|^2 = \left[(E-E_0)^2 + \Delta^2\right]$

Fit to experiment gives:

$\alpha = 90\,cm^{-1}$; $\chi^{(3)} \simeq 10^{-6}$ esu

with

$\Delta = 20$ meV.

13.

NONLINEAR MECHANISM	MEDIUM	$\chi^{(3)}$ (esu)	τ (sec)	α (cm^{-1})	$\chi^{(3)}/\alpha\tau$ (esu-cm/s)
band filling	HgCdTe	5×10^{-2}	3×10^{-8}	8	2×10^{5}
*interband	HgTe	2×10^{-4}	5×10^{-12}	3400	9×10^{3}
inter-valence	p-HgCdTe	8×10^{-6}	2×10^{-13}	48	8×10^{5}
*resonant-scattering	HgCdSe:Fe	1×10^{-6}	5×10^{-12}	100	2×10^{3}
*impurity	Si:P	3×10^{-7}	1×10^{-12}	700	430
nonparabolicity	InSb	2×10^{-7}	4×10^{-12}	2	3×10^{4}
intervalley	GaSb	1×10^{-7}	2×10^{-12}	30	2×10^{3}
free exciton	GaAs/GaAlAs	4×10^{-2}	2×10^{-8}	12000	170

14.

RELAXATION MECHANISMS	MEDIUM	N (cm^{-3})	T (K)	τ_{exp} (ps)	τ_{th} (ps)
LH → HH Optical phonon emission	p-GaAs	4×10^{16}	300	0.09	0.15
	p-GaAs	4×10^{16}	80	0.23	0.20
	p-GaAs	2×10^{19}	300	0.46	0.52
	p-Ge	3×10^{16}	300	0.70	1.7
Γ ↔ L	n-GaSb	4×10^{17}	300	2	
thermalization	n-InSb	2×10^{16}	2	3	
	n-Si:P	2×10^{18}	300	1	
	n-GaAs	3×10^{17}	300	0.7	
	n-HgCdSe:Fe	2×10^{18}	300	0.7	

15. DIRECTIONS FOR FUTURE

1.) Free carrier induced optical nonlinearities can be fast and large:

i) Optimize $\chi^{(3)}$ of HgCdTe via alloying and doping. Expect $\chi^{(3)} \approx 10^{-3}-10^{-2}$ esu ; $\tau \sim 5$ ps.

ii) Study $\chi^{(3)}$ vs. ω in HgTe.

iii) Tailor band parameters in HgTe/CdTe superlattices.

2.) Enhanced optical nonlinearity at the threshold of <u>electrical instabilities</u>. Optical triggering of electrically <u>bistable</u> structures?

Berry's Phase in Fiber Optics

(A talk by R. Y. Chiao at the U. S. - Japan Seminar on Quantum Mechanical Aspects of Quantum Electronics at Monterey, July 21-24, 1987)

Abstract: Berry discovered in quantum mechanics a topological phase factor similar to the Aharonov-Bohm phase factor. This phase is acquired by a system when it is adiabatically transported around a closed circuit in the parameter space of the Hamiltonian. Several experiments have now confirmed the existence of this phase. I shall report on an optical experiment which observed a manifestation of Berry's phase as a topological optical activity in a helical optical fiber. The wavelength-independence of this new optical activity has also been verified. Recently, this phase has been generalized to nonadiabatic evolutions by Aharonov and Anandan. I shall report on another optical experiment to observe this nonadiabatic phase. Possible applications, e.g., to gyroscopes, will be discussed.

U.S. - Japan Seminar
July 21-24, 1987

Berry's Phase in Fiber Optics

Collaborators:

Y. S. Wu (Theory)

A. Tomita (Experiment)

Recent work:

A. Antaramian, K. Ganga, H. Jiao,
A. Landsberg (students at Berkeley)
Dr. H. Nathel (LLNL)

Outline

I. What is Berry's phase?

A. A Classical Analog: Hannay's angle

B. QM adiabatic theorem derivation

C. Relationship to Sagnac effect and Aharonov-Bohm effect: the twin paradoxes

D. Relationship to Dirac monopole

II. The Optical Fiber Experiment

A. Theory

B. Schematic of experiment

C. Data showing topological invariance

D. " " wavelength independence

III. The Three-Mirror Experiment.

A. Kitano-Yabuzaki-Ogawa Periscope

B. Aharonov-Anandan Phase

C. Interferometry

IV. Applications to gyroscopes

Hannay's Angle

J. H. Hannay, J.Phys. A18, 221 (19..
M.V. Berry, J.Phys. A18, 15 (1985)

1. Frictionless bead on a hoop:

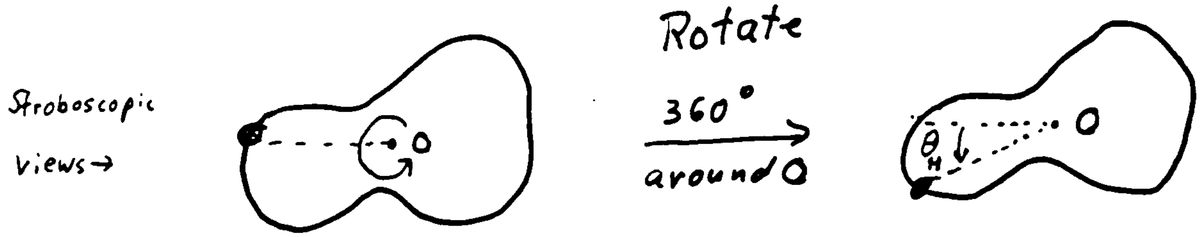

$$\theta_H \propto \frac{\text{area}}{(\text{Perimeter})^2}$$ ← SHIFT IN ANG. POSITION

2. Symmetric top forced around circuit

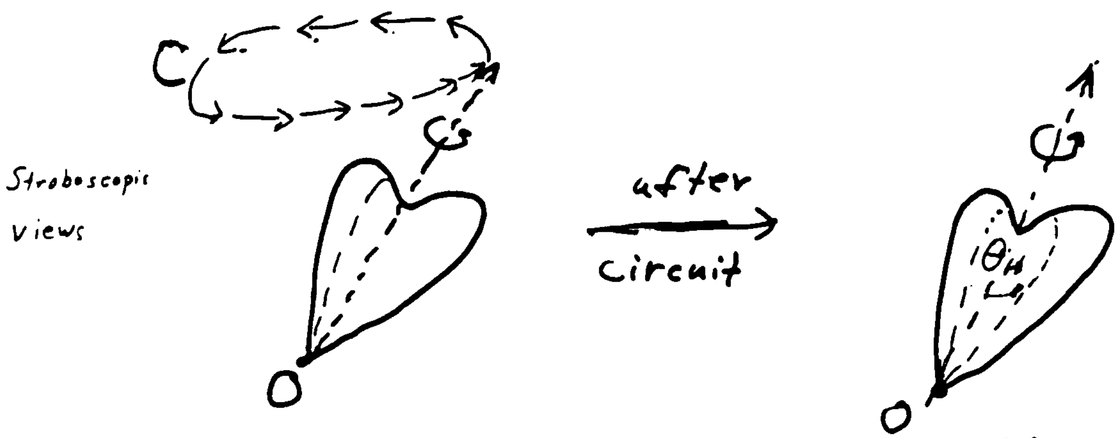

$\theta_H \propto$ Solid angle subtended by C w.r.t. O

$$\theta_H = \frac{d\gamma_n}{dn} \text{ as } n \to \infty$$

Berry's phase

M.V. Berry, Proc. Roy. Soc. A392, 45 (1984)

S.E. $\quad i\hbar \frac{d}{dt}|\psi(t)\rangle = H(\underset{\sim}{R}(t))|\psi(t)\rangle$

Adiabatic theorem

$$H(\underset{\sim}{R})|n(\underset{\sim}{R})\rangle = E_n(\underset{\sim}{R})|n(\underset{\sim}{R})\rangle$$

Berry's Ansatz

$$|\psi(t)\rangle = e^{-\frac{i}{\hbar}\int_0^t dt' E_n}\, e^{i\gamma_n(t)}\, |n(\underset{\sim}{R}(t))\rangle$$

$$i\hbar \frac{d}{dt}|\psi(t)\rangle = \cancel{i\hbar\left(-\frac{i}{\hbar}E_n\right)|\psi(t)\rangle}$$

$$-\hbar\dot{\gamma}_n\, e^{-\frac{i}{\hbar}\int_0^t dt' E_n}\, e^{i\gamma_n(t)}\, |n(\underset{\sim}{R}(t))\rangle$$

$$+\, e^{-\frac{i}{\hbar}\int_0^t dt' E_n}\, e^{i\gamma_n(t)}\, i\hbar\frac{d}{dt}|n(\underset{\sim}{R}(t))\rangle$$

$$= H|\psi(t)\rangle = \cancel{E_n|\psi(t)\rangle}$$

$$\therefore \quad \dot{\gamma}_n = i\langle n(\underset{\sim}{R}(t))|\frac{d}{dt}|n(\underset{\sim}{R}(t))\rangle$$

$$= i\langle n(\underset{\sim}{R}(t))|\nabla_R|n(\underset{\sim}{R}(t))\rangle\cdot\dot{\underset{\sim}{R}}(t)$$

Now let $t = T$ be cycle time, i.e. $\underset{\sim}{R}(T) = \underset{\sim}{R}(0)$

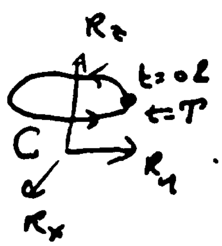

$$\therefore \boxed{\gamma_n(C) = i\oint_C \underbrace{\langle n(\underset{\sim}{R})|\nabla_R|n(\underset{\sim}{R})\rangle}_{\vec{A}}\cdot d\underset{\sim}{R}}$$

t drops out. cf. Aharonov-Bohm Phase.

Four Types of Twin Paradoxes (from Chiao's seminar at M.I.T., Oct. 28, 1986)

① Special relativistic twin paradox.

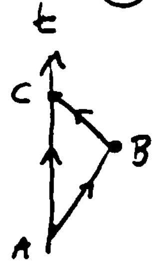

$$\Delta t = \underbrace{\oint \frac{ds}{c}}_{\text{proper time}} = \oint \sqrt{1-\frac{v^2(t)}{c^2}}\,dt$$

Checked by Hafele & Keating, Science, 177, 166 (1972)

② Sagnac-effect twin paradox.

$$\Delta t = \frac{1}{c^2}\oint \vec{v}_a \cdot d\vec{l} = -\frac{1}{c}\oint \frac{g_{0i}\,dx^i}{g_{00}} \quad (i=1,2,3)$$

Interferometers best way to measure Δt:

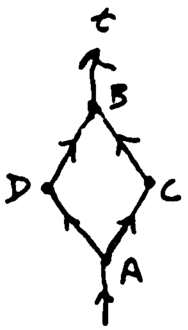

$$\Delta\varphi = \omega\Delta t = \frac{\omega}{c^2}\oint \vec{v}_a \cdot d\vec{l} = \frac{\omega}{c^2}\vec{S}\cdot\vec{\Omega}$$

For neutrons, $\omega = \frac{mc^2}{\hbar}$ (Werner et al, PRL 42, 1103 (1979))

For photons, ω = freq. of light $\Rightarrow$ LASER GYRO

③ Aharonov-Bohm twin paradox

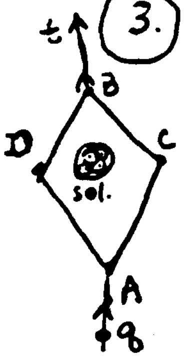

$$\Delta\varphi = \frac{q}{\hbar c}\oint \vec{A}\cdot d\vec{l}$$

NO FORCES!

(Tonomura et al, PRL 56, 792 (1986)

④ Berry's phase: Generalization of A-B effect

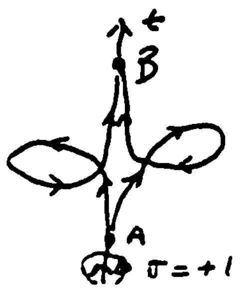

$$\Delta\varphi \equiv \gamma(C) = \frac{q}{\hbar c}\oint_C \vec{A}\cdot d\vec{l}$$

$d\vec{l}$ = line element in parameter space

$\vec{A}$ = effective vector potential $\equiv \langle n|\frac{d}{d\vec{l}}|n\rangle$

q = topological charge = σ, for example

(Chiao & Wu, PRL 57, 933 (1986); Tomita & Chiao, PRL 57, 937 (1986)).

Young's two-slit interference

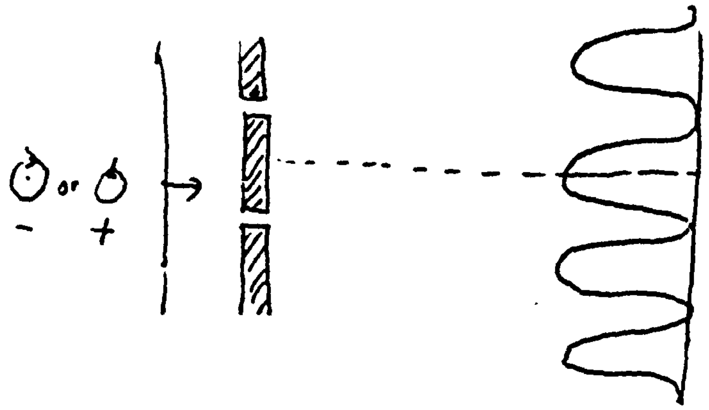

← Same pattern for + + − polarizations

Now replace two slits by two fibers

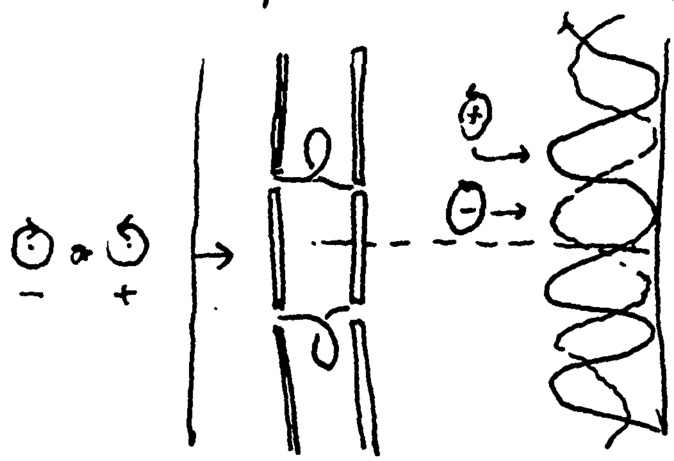

← Different patterns

Dirac Monopole + charge on sphere

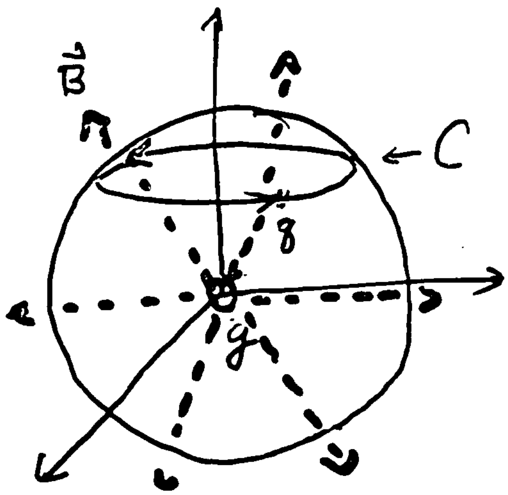

A - B phase shift around circle C

$$\Delta\phi = \frac{q\,\Phi}{\hbar}$$

$$\Phi = \frac{\Omega(C)}{4\pi} \cdot 4\pi g$$

$$\left(\oint \vec{B} \cdot d\vec{S} = 4\pi g \text{ Gauss's law} \right)$$

$$\therefore \quad \Delta\phi = \frac{qg\,\Omega(C)}{\hbar}$$

Quantization of charge

WITTEN

$$\Delta\phi = \frac{qg\,\Omega}{\hbar} = -\frac{qg\,(4\pi - \Omega)}{\hbar} \pm 2\pi n$$

$$\therefore \quad qg\,\frac{4\pi}{\hbar} = \pm 2\pi n$$

$$\boxed{qg = \pm n\,\frac{\hbar}{2}}$$

Topological result (can deform S & C)

global "

SPIN $\vec{S}$ IN ADIABATIC $\vec{B}(t)$

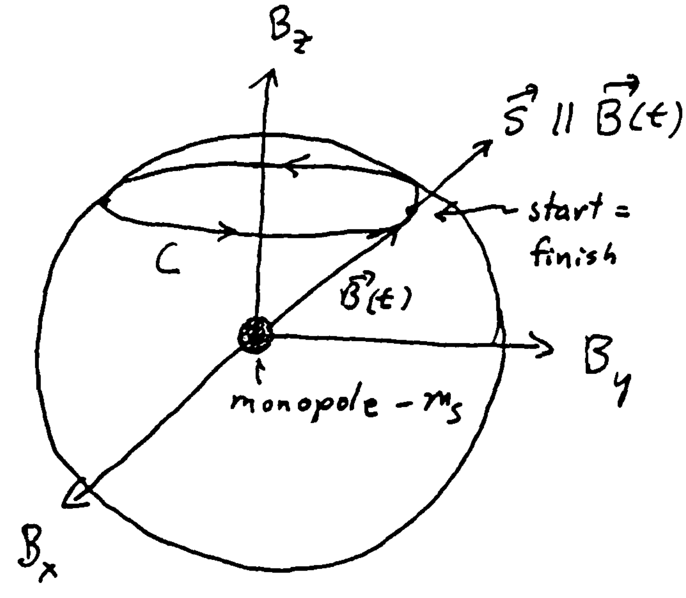

$\gamma(C) =$

$-m_s \, \Omega(C)$

cf.

$$\gamma(C) = \frac{q}{\hbar} \oint \vec{A} \cdot d\vec{\ell}$$

$$= \frac{q}{\hbar} \int \vec{\nabla} \times \vec{A} \cdot d\vec{S}$$

$$= \frac{q}{\hbar} \int \vec{B} \cdot d\vec{S}$$

$$= \frac{q}{\hbar} \cdot 4\pi g \cdot \frac{\Omega}{4\pi} = \frac{qg}{\hbar} \Omega$$

PHOTON SPINS $\vec{S}$ IN HELICAL WAVEGUIDE $\vec{k}(\tau)$

HELICITY $\vec{S} \cdot \vec{k}(\tau)$ IS ADIABATIC

INVARIANT : $\vec{S} \cdot \vec{k}(\tau) \, | \vec{k}(\tau), \sigma \rangle = \sigma \, | \vec{k}(\tau), \sigma \rangle$

σ = HELICITY IS EITHER $+1$ OR -1

PHOTON IN $\vec{k}$ - SPACE

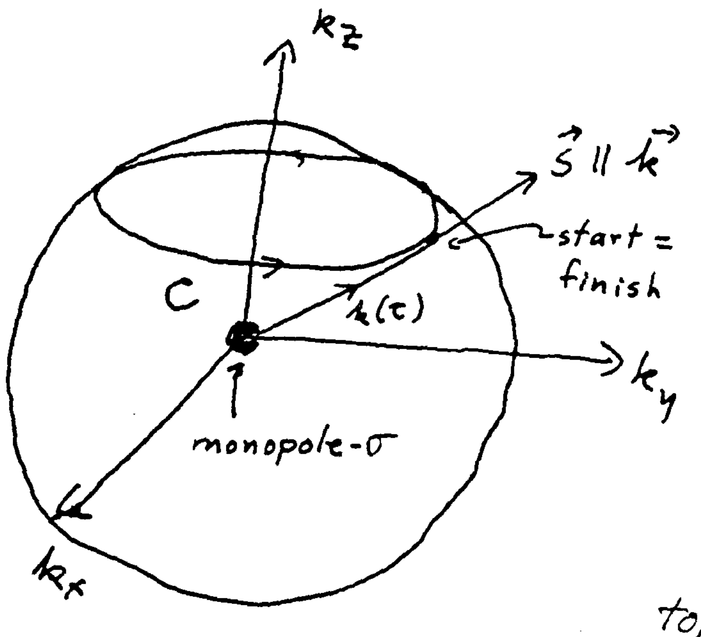

$\gamma(C) =$

$-\sigma\,\Omega(C)$

$\Rightarrow$

Dirac monopole of topological charge-σ

FOR LINEAR POLARIZATION, AND STANDARD EXAMPLE:

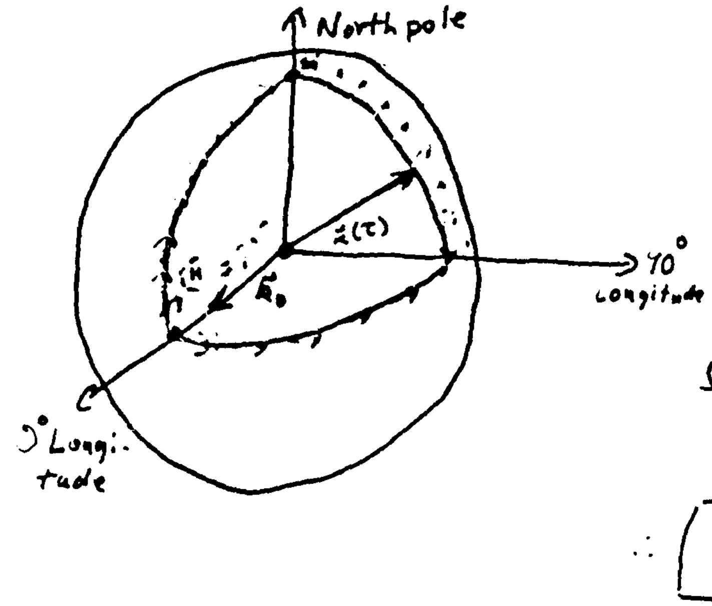

Our theory predicts

$-\gamma_+ = \Theta =$ angle of rotation of linear polarization

$\Omega = \underbrace{\frac{1}{8}}_{\text{one octant}} \times 4\pi = \frac{\pi}{2}$

$\therefore \boxed{\Theta = \frac{\pi}{2} = 90^\circ}$

Ordinary Optical Activity:

$$\Delta\varphi = 2\pi(n_+ - n_-)L/\lambda$$

$$\Theta = \Delta\varphi/2$$

Topological Optical Activity:

$$|x\rangle = (|+\rangle + |-\rangle)/\sqrt{2}$$

$$|x'\rangle = (e^{i\gamma}|+\rangle + e^{-i\gamma}|-\rangle)/\sqrt{2}$$

$\gamma = -\Omega$ is Berry's phase for $|+\rangle$

$$\langle x|x'\rangle = \cos\gamma$$

$|\langle x|x'\rangle|^2 = \cos^2\gamma$ is Malus's law

Therefore, $\Theta = \pm\Omega$.

The sign of effect is determined by interference with ordinary optical activity.

Answer: a left-handed helix is dextrorotatory.

Comparing

$$\Theta = \pi(n_+ - n_-)L/\lambda$$

and

$$\Theta = \Omega$$

we see that the topological optical activity is wavelength independent.

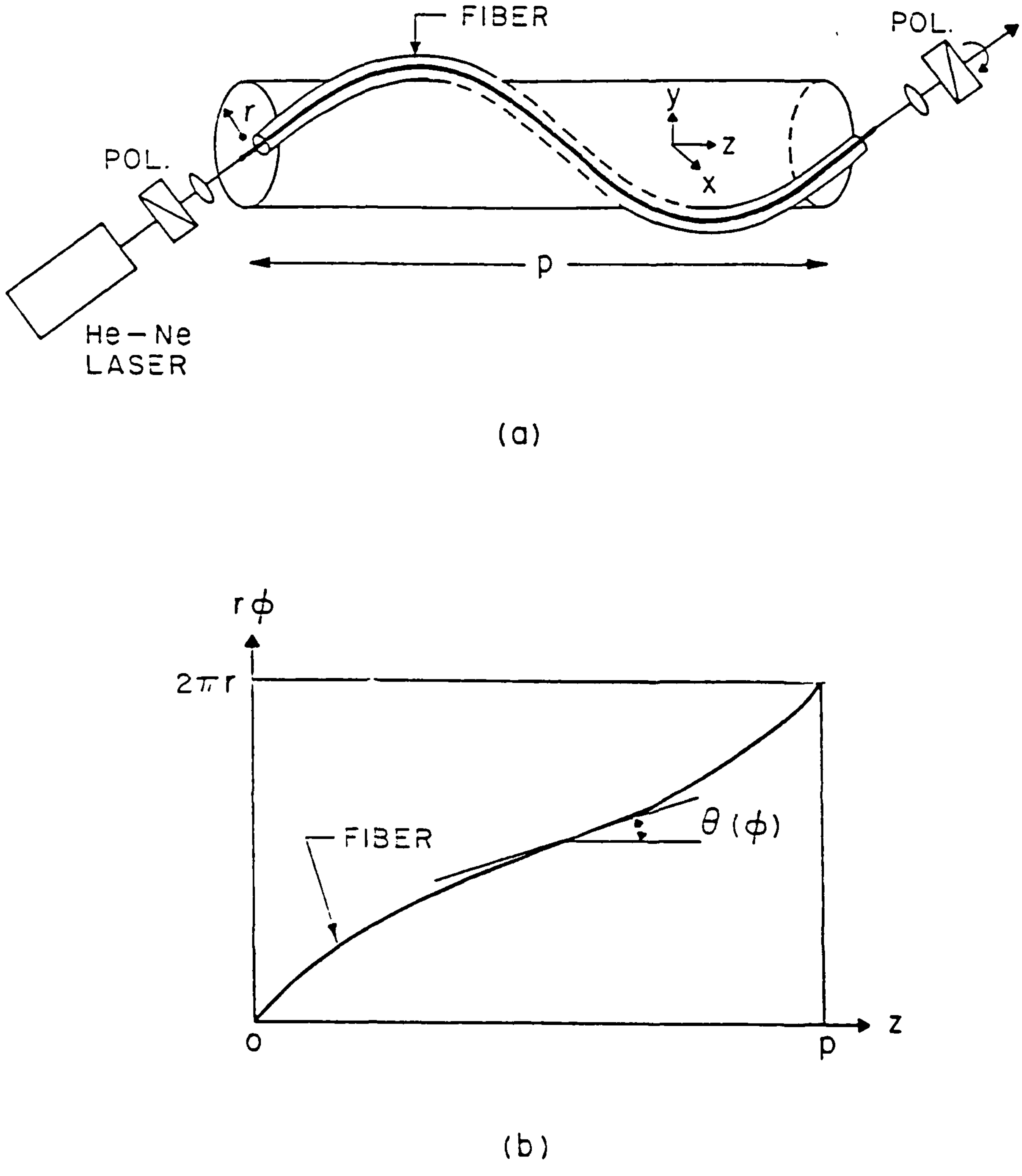

Fig. 1

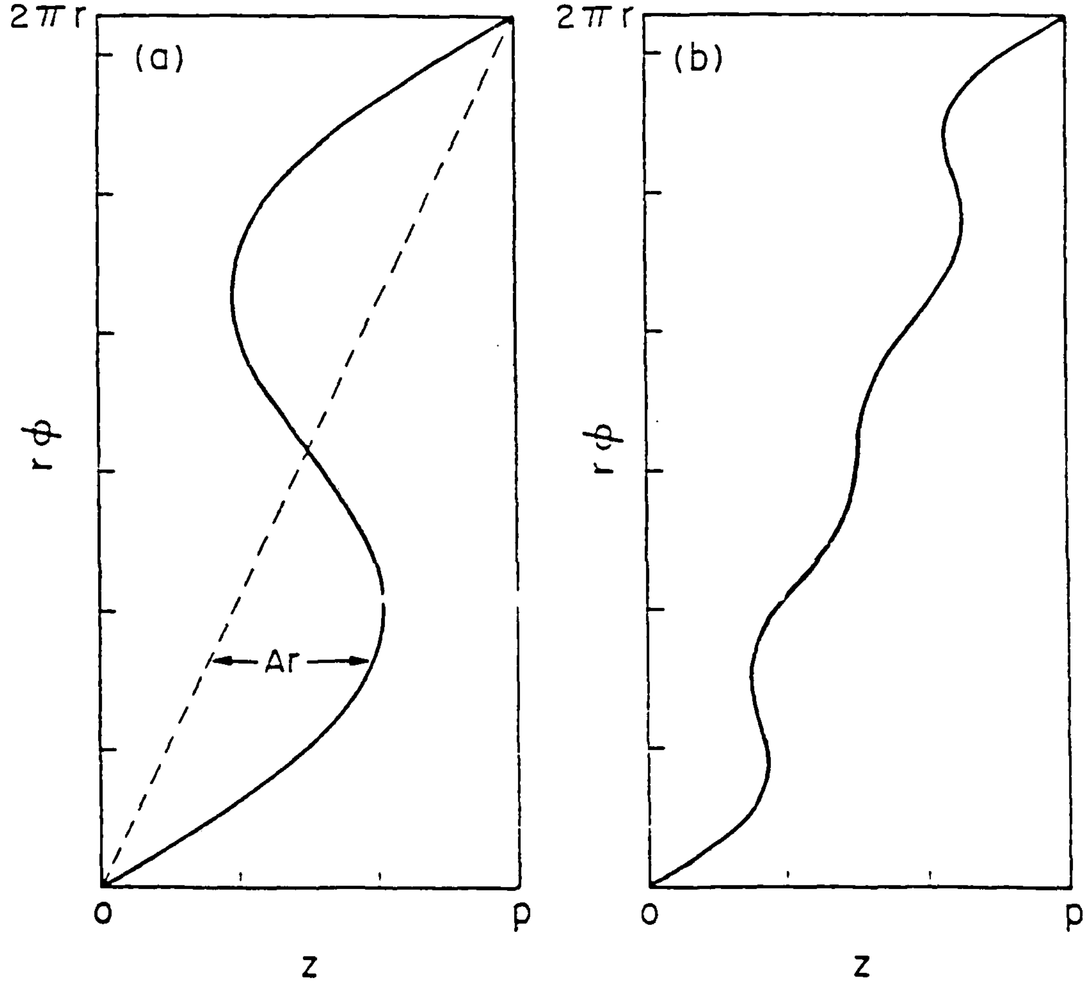

Fig. 3

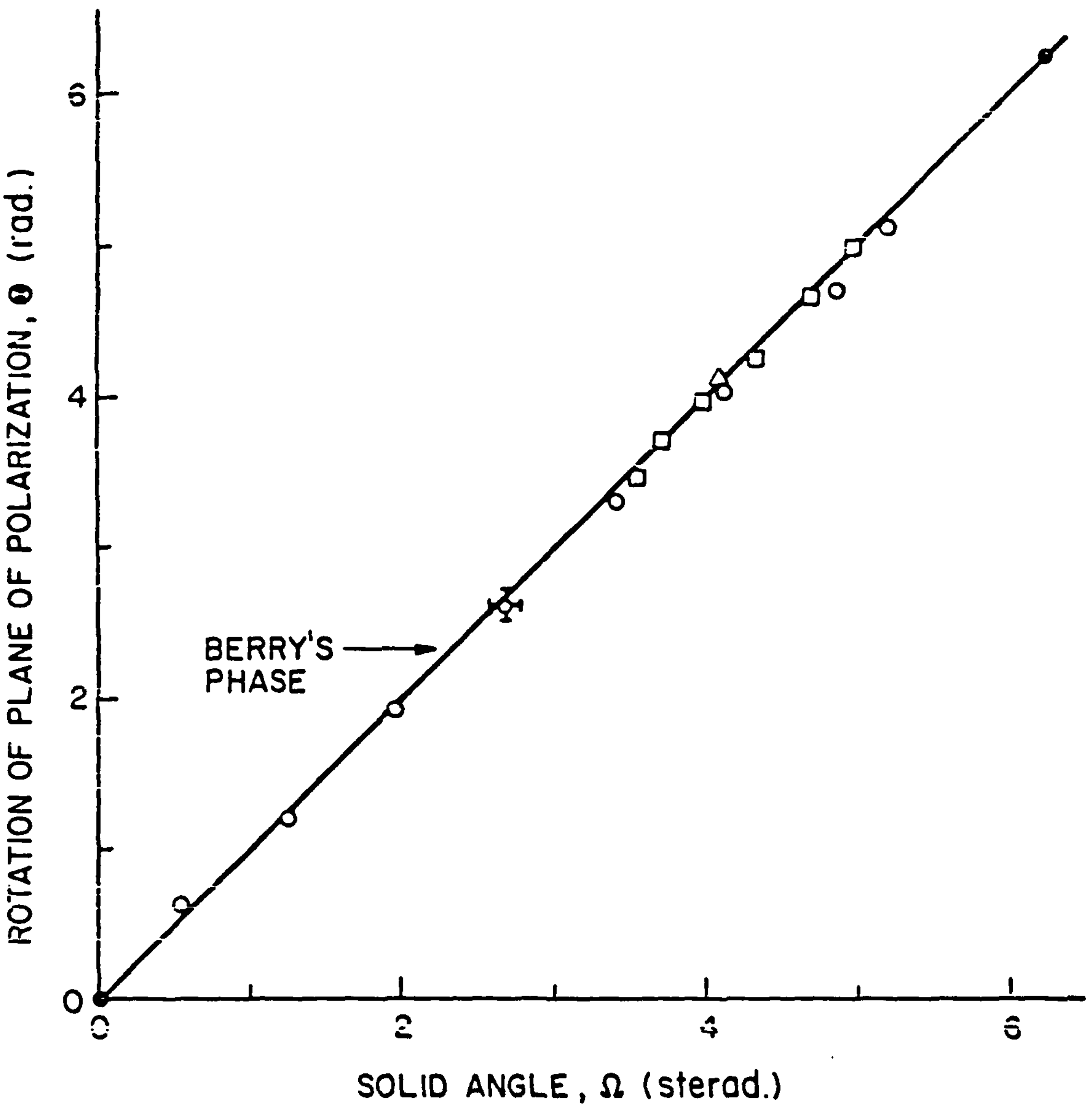
ROTATION OF PLANE OF POLARIZATION, Θ (rad.)
SOLID ANGLE, Ω (sterad.)
BERRY'S PHASE
0
2
4
6

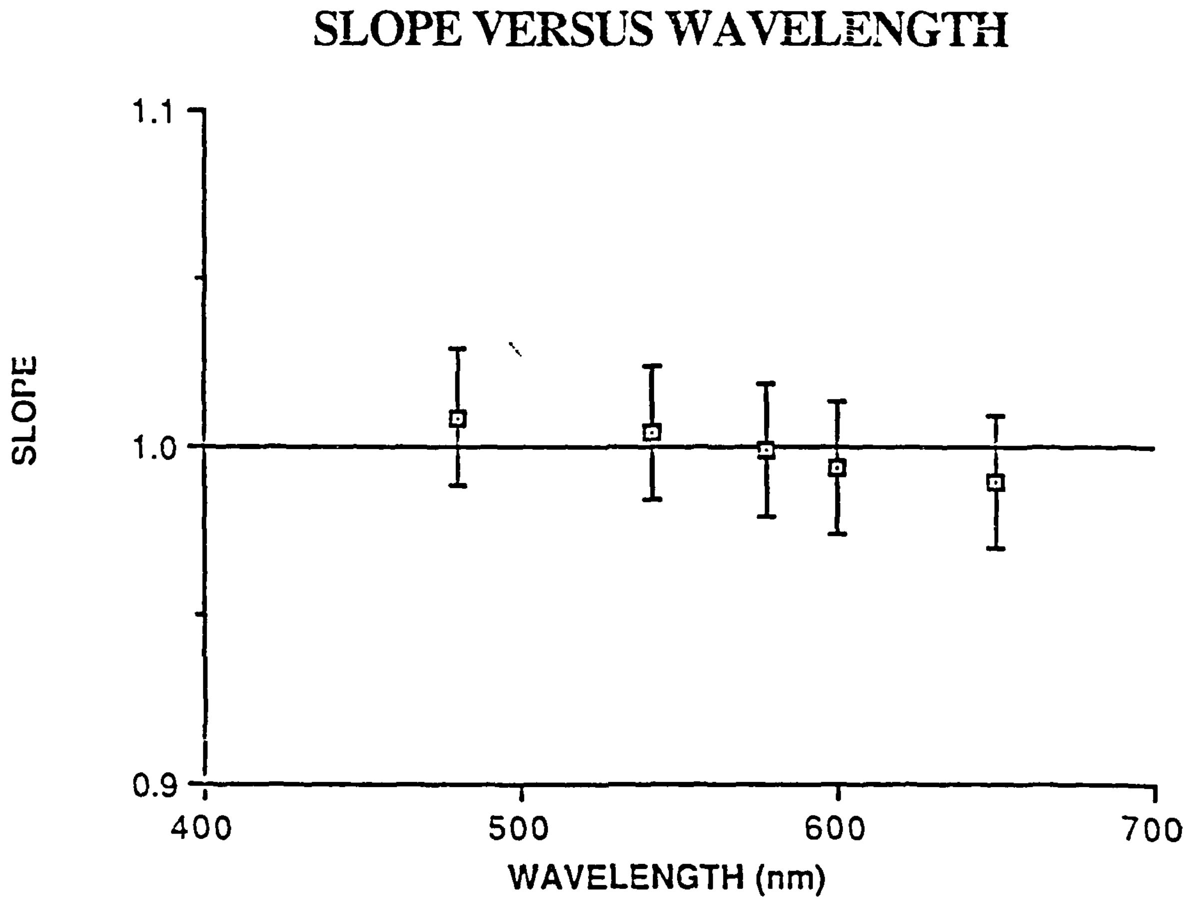
SLOPE VERSUS WAVELENGTH
1.1
1.0
0.9
SLOPE
400
500
600
700
WAVELENGTH (nm)

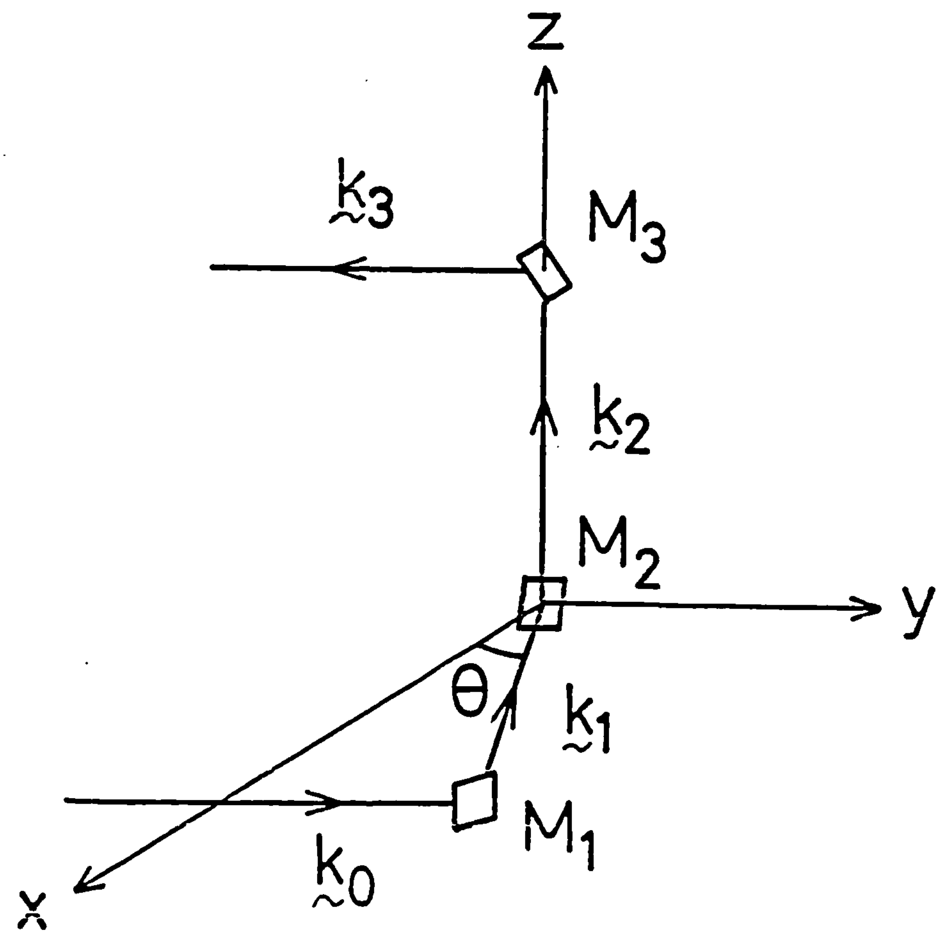

z
$\underset{\sim}{k}_3$
M_3
$\underset{\sim}{k}_2$
M_2
y
θ
$\underset{\sim}{k}_1$
M_1
x
$\underset{\sim}{k}_0$

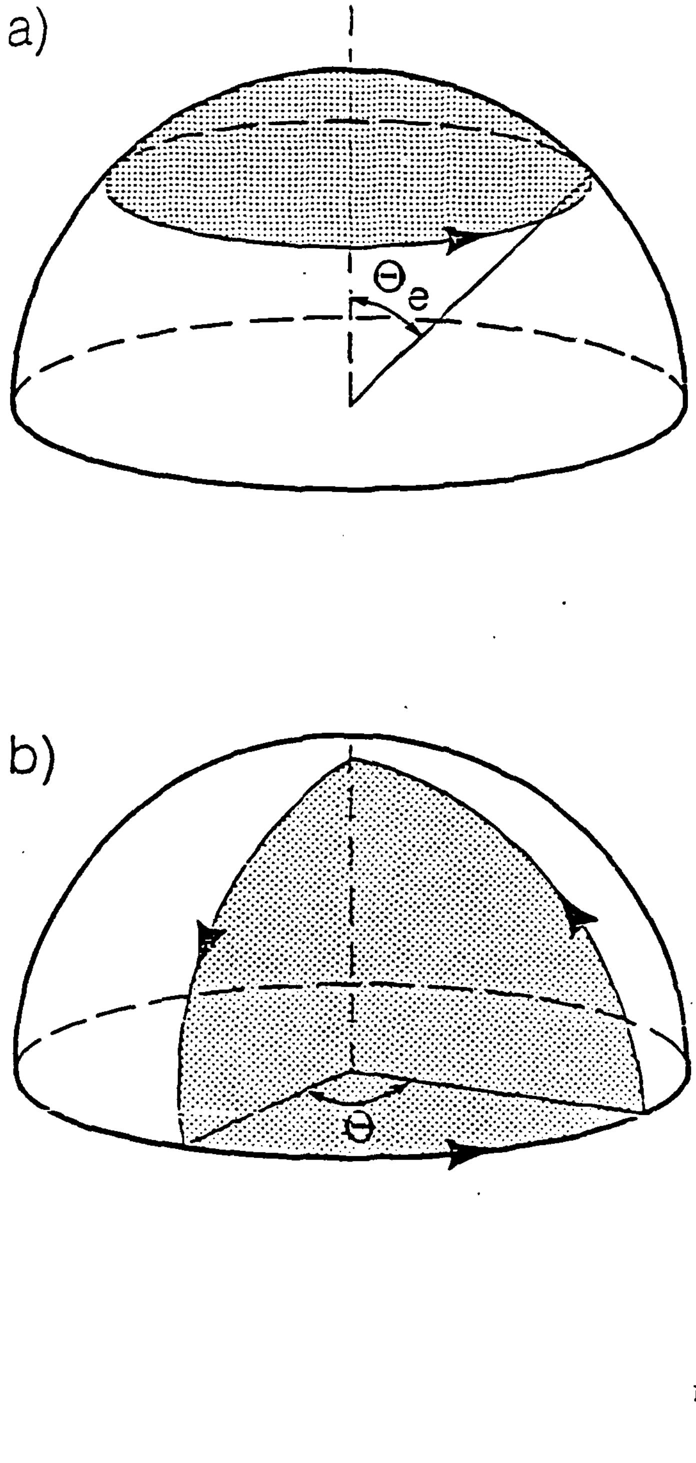

Figure 2

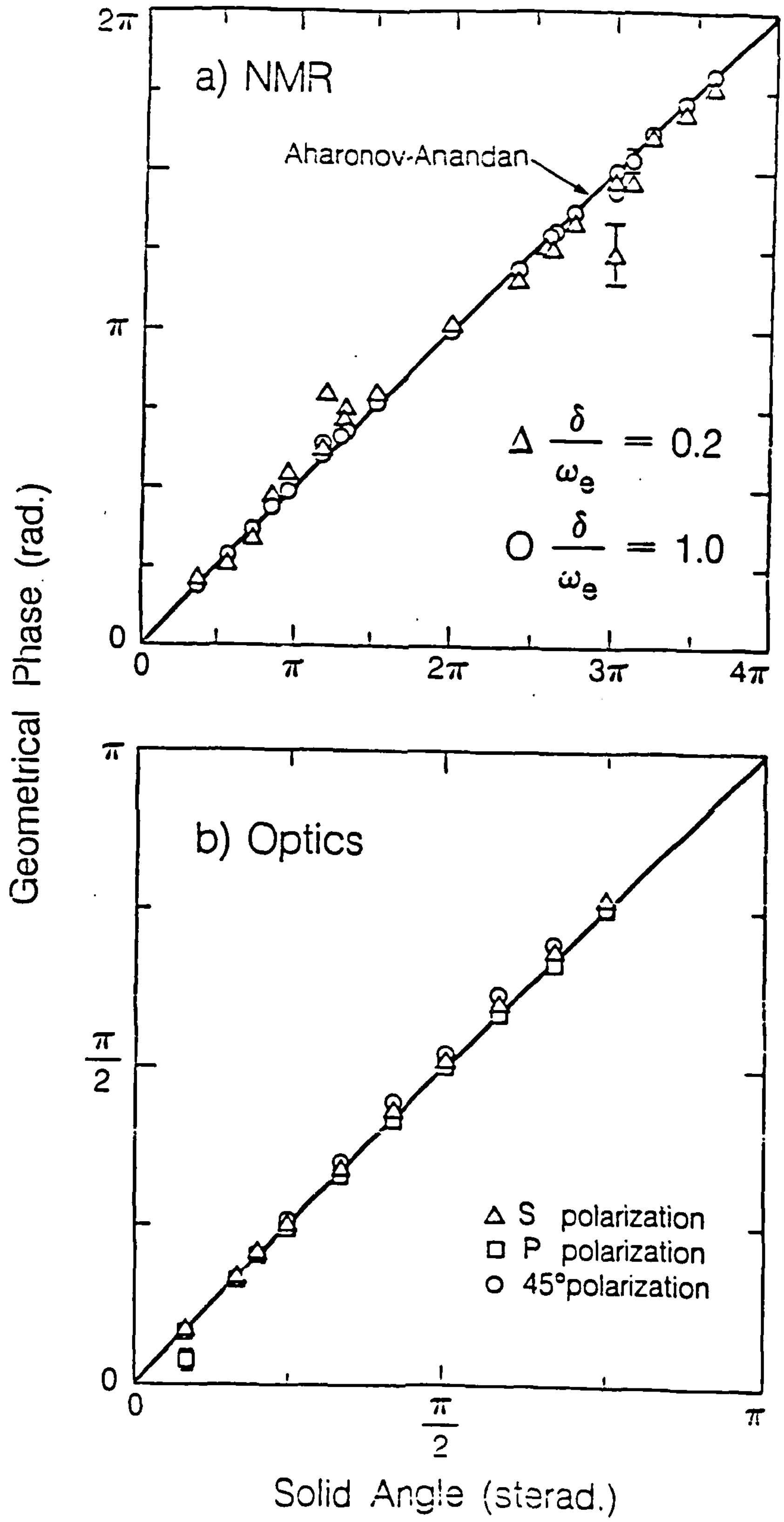
a) NMR
Aharonov-Anandan
$\Delta \ \frac{\delta}{\omega_e} = 0.2$
$O \ \frac{\delta}{\omega_e} = 1.0$
b) Optics
△ S polarization
□ P polarization
○ 45°polarization
Geometrical Phase (rad.)
Solid Angle (sterad.)
0
π
2π
3π
4π
π/2

Application to gyroscopes

Let us replace spin by persistent current ring in a superconductor

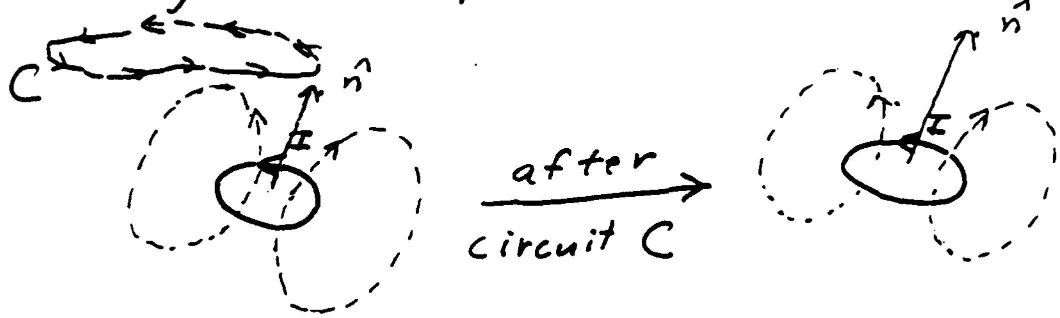

$$\Psi \longrightarrow \Psi \cdot e^{i\gamma(C)}$$

where $\gamma(C) = -n\,\Omega(C)$ ← detect with J.J

where n = flux quantum number

Alternatively, use unidirectional ring laser gyro

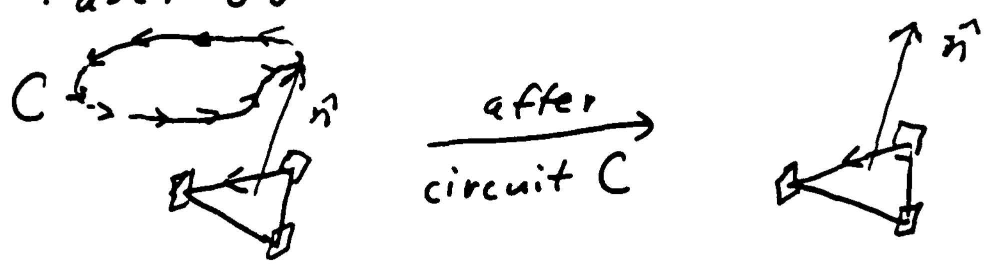

$$E \longrightarrow E \cdot e^{i\gamma(C)}$$

$\gamma = -n\Omega$, n = mode number (NOT SAGNAC EFFECT)

HIGH DENSITY FEMTOSECOND EXCITATION OF NONTHERMAL CARRIER DISTRIBUTIONS IN INTRINSIC AND MODULATION DOPED GaAs QUANTUM WELLS

Wayne H. Knox, Daniel S. Chemla and Gabriela Livescu
AT&T Bell Laboratories
Holmdel, N.J. 07733

We investigate the dynamics of non-thermal carrier distributions in undoped and modulation doped GaAs Quantum Well Structures (layer thickness $\approx 100\,A$*) with near bandgap-resonant intense femtosecond light pulses. We are able to study selectively the carrier-carrier scattering process up to very high densities and we carry out the first optical investigation of non-thermal carrier generation in the presence of a thermalized Fermi-sea of electrons. In undoped quantum wells we find a reduction of the thermalization time from about 100 fs to about 30fs as the photocarrier density increases from* $N_{eh} \approx 2\times10^{10}\ cm^{-2}$ *to* $\approx 10^{12}\ cm^{-2}$*. The thermalization time is found to be sensitive to background doping with excess electrons in modulation doped samples.*

Following absorption of light by a semiconductor, electrons and holes are placed into states of energy which are defined by the power spectrum of the exciting light and the band structure of the material. The very first relaxation process which the electrons and holes undergo is a scattering interaction, mediated by the Coulomb force between the particles. This process is only one of the many elementary interactions which may occur in semiconductors such as phonon absorption and emission, intervalley scattering, plasmon emission and radiative recombination.

We have designed experiments in which the carrier-carrier scattering process can be effectively isolated and studied under diverse conditions in order to learn more about this basic interaction mechanism which has been to date elusive by virtue of both its short time constants (10-100 fs) and its admixture with other processes. In particular, it is interesting to consider the separate roles of electron-electron scattering, electron-hole scattering and hole-hole scattering and to understand their various contributions in optical experiments. Of course, optical experiments in intrinsic semiconductors give little information about the distinction of these effects since equal numbers of electrons and holes are simultaneously created. We have begun investigations in modulation-doped samples which are designed to help us understand more clearly the effects of the electron and hole relaxations in the presence of both excess electrons and excess holes.

The first evidence of rapid thermalization of carriers in GaAs with high excess energy excitation was obtained by Tang and Erskine (1983) in single-wavelength experiments with femtosecond optical pulses at 625 nm. Oudar and coworkers (1985) later studied spectral hole burning in bulk GaAs with 500 fs pulses near the bandgap. Knox and coworkers (1986) then reported experiments in GaAs Multiple Quantum Well Structures (MQWS) wherein pulses of 80 fs duration near the bandgap were used to

probe the dynamics of thermalization of an initially non-thermal distribution. In this experiment, the excitation pulsewidth was less than the thermalization time, so the actual thermalization process was spectrally and temporally resolved. Excitation at 1.50 eV insured that the electrons and holes were excited only in the gamma valley and had insufficient energy to emit optical phonons. Under these conditions, carrier-carrier scattering is the dominant operable relaxation mechanism. The maximum excitation density in this experiment was about $N_{eh} \approx 2\times10^{10}\ cm^{-2}$, limited by optical pulse energy due to the weak infrared continuum which is available from a system which operates in the visible spectral range, since the continuum intensity decays exponentially with energy on both sides of the center wavelength. In the present experiments, we use a new laser system which has recently been developed which makes available for the first time intense femtosecond continuum pulses with a center wavelength in the near infrared at 805 nm at 6 kilohertz repetition rate (Knox 1987). This system now allows us to continue the study of non-thermal distributions to much higher densities than previously possible. In fact, we have been able to achieve carrier densities near the maximum theoretical carrier density, beyond which the sample has no optical absorption at the pump wavelength. The laser system has been discussed in detail (Knox 1987), and only the essential features will be mentioned here. Optical pulses of 100 fs duration are generated at 805 nm wavelength in a two-jet synchronously pumped dispersion-compensated dye laser and amplified to 1 microjoule energies at 6 kilohertz repetition rate in a six-pass jet amplifier (Knox and colleagues 1984). These pulses are focused into a 1 mm jet of ethylene glycol and generate a white continuum pulse which is centered at 805 nm. The continuum distribution on the infrared side 810-900 nm is used for the present set of measurements. A probe continuum is split off with a 4% reflection and the rest of the continuum beam is used as a continuously tunable intense pump pulse. An interference filter at 825 nm (1.50 eV) is selected for the pump pulse filter. The probe pulse passes through a 0.1 μm resolution stepper motor for time delay adjustments, and is focused to a 20 μm diameter spot on the sample. The pump beam is focused to a diameter of 55 μm at the same point on the sample. The sample and interference filter are the same ones which were used in our previous hole-burning experiment (Knox and coworkers 1986). The system time response as determined by replacing the sample with a 1 mm $LiIO_3$ crystal is 150 fs FWHM, corresponding to 100 fs continuum and selected continuum pulsewidths.

It has been shown experimentally (Knox and coworkers 1986) and theoretically (Schmitt-Rink, Chemla and Miller 1985) that in MQWS the effects of the Pauli exclusion principle (phase-space filling and exchange) are much more efficient than the direct screening of the Coulomb interaction in bleaching the excitonic as well as the continuum absorption. Consequently when an electron hole (e-h) plasma is photogenerated in the continuum above the exciton resonances of the $n_z = 1$ subband transition, it produces first a spectral-hole in the absorption spectrum that reproduces the electron, $n_e(k)$, and hole, $n_h(k)$, distributions. In the leading order in the perturbation the absorption coefficient in the continuum can be written;

$$\alpha_c \approx [1-n_e(k)-n_h(k)]\, \alpha_c^{(0)} \qquad (1)$$

In addition the carriers can induce a strong bleaching of the excitonic resonances by occupying states that form the basis for the exciton wavefunction in k-space which describes the correlated e-h pair relative motion $\Phi(k)$. These states are located within one exciton binding energy ($E_b \approx 10meV$) of the bottom of the band (Schmitt-Rink, Chemla and Miller 1985). Therefore, measurement of the evolution of the changes in absorption both at the energy where the photocarriers are generated and at the exciton resonance yields two internal probes of the dynamics of the carriers. The line shape and the evolution of the spectral-hole gives information about the scattering of the carriers out of the state in which they were generated. The evolution of the exciton peak gives information on the time they take to reach the bottom of the band and the internal details of the relative importance of Pauli exclusion, screening and exchange contributions (Schmitt-Rink, Chemla and Miller 1985).

We discuss first high density excitations in undoped quantum wells. Fig. (1) shows the absorption spectrum of an undoped sample before excitation and at a time delay which corresponds to the best time overlap of the pump and probe pulses (which we refer to as the "t = 0" point) and at a delay $\Delta t =$ 132 fs. The excitation distribution as determined by the pump beam interference filter is also shown. A deep spectral hole burning is observed, where the absorption dips nearly to zero. Also shown in Fig. 1 is the approximate absorption saturation which was obtained in the previous experiment at about $2\times10^{10}cm^{-2}$ carrier density, for comparison. At high densities, we find that this distribution is well-centered at the pump energy, and very rapidly relaxes. This is shown in Fig. (2) where a set of differential spectra at various delays between Δ t = - 270 fs and + 270 fs are presented. They show very clearly the effect of the photocarriers on the continuum and excitonic absorption as they are generated and during their thermalization. It is difficult to determine accurately the carrier density in these type of experiments, and particularly so at high densities, since the absorption of the pump pulse is both weak and time-varying over a significant range during the excitation pulse. We estimate that in the case of Fig. (2): $N_{eh} \approx 10^{12}cm^{-2}$ within a 50% accuracy.

In order to determine the dynamics of the thermalization, we show in Fig. (3) the value of the absorption bleaching at the peak of the spectral hole and at the $n_z = 1$ heavy hole (hh) exciton. Two excitation intensities are shown: Fig. (3a) $N_{eh} \approx 2\times10^{11}cm^{-2}$, Fig. (3b) $N_{eh} \approx 1\times10^{12}cm^{-2}$. The insets show the spectral shape of the pump and non-thermal signals at t = 0 for the respective cases.

It is clear from this study that the relaxation of the non-thermal peak becomes faster at higher densities. The time courses in Fig. 3 indicate this point in several ways. The recovery of the absorption at the hole is time resolved for the medium excitation case of Fig. 3a, as indicated by the asymmetry in the time course compared to the measured system time response. For this case, the measured hole burning signal has about the same magnitude as the excitonic differential signal. For the high density case, the time asymmetry disappears, indicating that the thermalization time is significantly less than the system response, and the height of the measured hole-

burning decreases relative to the excitonic differential signal. Two processes are responsible for this behavior. First, we determine that the thermalization time is density-dependent. Second, the excitonic differential signal saturates at a lower carrier density than the non-thermal distribution signal. Figure 1 shows that the exciton absorption is completely bleached at the high density, and it is replaced by renormalized continuum absorption. Therefore, we explain these results as follows: at low densities, thermalization times are longer than the system response, but since the density is much below the saturation density, the excitonic signal is about 10 times larger than the hole signal (Knox and coworkers 1986). At these new higher densities, the resulting hole burning signal increases with density until the thermalization time becomes comparable to the system time response, beyond which point it decreases. Dynamically, the bleaching at the exciton peak increases steadily and reaches its maximum value in a shorter time as the excitation density is increased. This shows that the carriers fill up the bottom of the band more rapidly at high densities. We note that the width of the spectral hole also increases as the carrier density is increased, as can be seen in the insets of Fig. 3. This result is related to the strong saturation of the n = 1 continuum. In Fig. 1 it is clearly seen that a density-dependent broadening is expected since there is less absorption near the peak of the pump spectrum than there is at the wings.

A complete analysis of these results is extremely complicated, even in our case with only carrier-carrier scattering in the Γ valley with no significant phonon emission. To our knowledge, two groups have performed Monte-Carlo simulations of our experiment in the low density limit: Goodnick and Lugli (1987) and Bailey and coworkers (1987), an approach which requires heavy numerical computations but allows for the inclusion of a number of important effects. We have developed a simple model for the thermalization of the photocarriers, involving a single relaxation time τ_r in which we assume that no energy is exchanged with the lattice in the time scale of the experiment, and there is no loss of carriers to intervalley scattering or recombination. The absorption saturation is obtained according to Eq.(1) and we assume a local equilibrium relaxation toward the Fermi distribution corresponding to the instantaneous number of carriers present in the sample. This simple model thus incorporates the major ingredients of the experiment and summarizes the results in a single parameter τ_r. This model will be discussed in more detail elsewhere. We find that the measured spectral-hole and exciton bleaching evolution of Fig. (3) are nicely reproduced by τ_r = 60fs and 30fs respectively. Similar consideration of the data of Knox and coworkers (1986) yields τ_r = 100fs. Thus when N_{eh} increases by at least a factor of 50, τ_r decreases by approximately a factor of 3, showing that the relaxation is not a very strongly varying function of the density. It is interesting to note that the relaxation time we measure at the highest density is significantly slower than that measured by Lin and coworkers (1987) for densities of a few times $10^{11}cm^{-2}$. We attribute this difference to the fact that in our experiment carrier-carrier scattering is the only relaxation channel whereas in the case of large excess photon energy phonon scattering as well as a number of other processes also participate in the relaxation, and the measured relaxation rate is the sum of the individual rates. All these processes may have different scalings with carrier densities, so it is important to isolate each process to determine its density dependence. Nonetheless, the weak dependence

which we find for the density dependence of the carrier-carrier scattering rate in our high density experiments is consistent with the weak dependence which has been found in other experiments. It is interesting to note that the relaxation time for our highest density is only 30 fs (our model indicates that if it were less than 30 fs, such a prominent hole would not be observed) and this is only about a factor of two lower than the maximum theoretically obtainable excitation density for a 96 A quantum well. By incorporating a properly saturating driving term into our model, we are able to explain our experimental result that the spectral hole becomes broader at high saturation levels. We note that in the previous experiment (Knox and coworkers 1986) the spectral hole width was essentially equal to the excitation bandwidth, whereas in the data of Fig. 2 at high density, the differential spectrum is about twice as broad as the pump spectrum. We note that the small energy offset between the pump and spectral hole in the previous experiment (Knox and coworkers 1986) is not reproduced in these experiments. We determine that the spectral hole center is within 1 meV from the center of the excitation pulse in the present experiments.

As mentioned in the introduction, by performing identical experiments in samples in which a distribution of excess charged particles already exists before excitation, we may learn more about the carrier-carrier scattering process and about the various components it involves. In particular, experiments on ballistic transistors are performed in such a way that nearly monoenergetic electrons are injected into a gate region in which a sea of carriers are already thermalized to the lattice (Levi and coworkers 1985) and Heiblum and coworkers (1985). Under these conditions, it has been possible to calculate scattering rates as a function of excess energy and density (Levi and coworkers 1985). In optical experiments in undoped samples, the the non-thermal distribution at time t thermalizes by interactions with itself and not another already thermalized distribution. In order to investigate these effects we have repeated the experiment with modulation doped (MD) samples. Here we report preliminary results on a n-type sample which consists of 50 periods of 120 A GaAs QW sandwiched between 350 A AlGaAs barriers whose central 113 A contain $3\times10^{17}cm^{-3}$ Si dopant. The density of electrons in the QW, $N_e = 3.5\times10^{11}cm^{-2}$ was determined by Hall measurements. Figure (4) shows the absorption spectrum of a room temperature MD-MQWS before excitation and the $\Delta t = 0$ absorption spectrum of the sample excited to $N_{eh} \approx 1\times10^{12}cm^{-2}$ by a pump centered at 840 nm. It is clear that the relaxation is very different from that of the undoped sample, since there is no hole-burning. The line shape of the unexcited sample absorption spectrum deserves some comments. The peak seen at 1.45 eV is not an exciton, but corresponds to the electron-hole correlation singularity recently investigated theoretically (Ruckenstein and Schmitt-Rink 1987), and experimentally (Livescu and coworkers 1987). This resonance is due to the motion of the Fermi-sea of electrons in reaction to the sudden appearance of the hole upon absorption of a photon. This screening of the Coulomb potential of the hole correlates this latter to the whole Fermi-sea thus forming a collective "many-body" analog of the hydrogenic exciton of the undoped samples. In Fig. (5) the complete time delay scans are shown. A thermalized distribution is observed instantaneously in this experiment. Apparently, the effect of a moderate background density of excess electrons which are thermalized to the lattice

is to greatly increase the scattering rate. We estimate by comparison with our model that the relaxation time is less than 10 fs for these conditions. One possible explanation of this is that electron-electron scattering rates are enhanced by carrier occupation near k = 0. Before the non-thermal distribution thermalizes, there is no k=0 occupation, as has been shown experimentally (Knox and coworkers 1986) and theoretically (Schmitt-Rink, Chemla and Miller 1985). This striking result is consistent with recent Monte-Carlo simulations in which a variable background density was included (Bailey and coworkers 1987). These calculations indicated that the non-thermal component vanishes when the background density is increased. This can be interpreted as a very rapid thermalization which is faster than the laser pulses which are used to make the measurements.

To our knowledge, these results represent the first optical investigations of non-thermal carrier generation in doped structures, and we envision further extensions to p-doped structures in which we may obtain information on the separate roles of electron and hole contributions in optical experiments.

SUMMARY

We have investigated non-thermal carrier generation in GaAs MQWS at high excitation densities by making use of a new laser system which generates intense 100 fs white light continuum pulses centered at 805 nm at 6 kilohertz repetition rate. We find that carrier-carrier scattering alone yields thermalization rates only as fast as 30 fs at densities close to the theoretical maximum for n = 1 in-band excitation. We find that as the density is varied over approximately 50-100 times, the scattering rate varies by only a factor of 3 or so. We find that the width of the non-thermal distribution depends on carrier density. A simple dynamic relaxation-time approximation with a self-consistent renormalized Fermi local-equilibrium distribution function reproduces our dynamic results quite well, and agrees qualitatively with Monte-Carlo simulations. Experiments in modulation-doped samples show significant sensitivity to background electron doping, and relaxation times of less than 10 fs are found for doping densities of $3.5\times10^{11} cm^{-2}$.

ACKNOWLEDGEMENTS

We wish to thank A. VonLehmen, and D.A.B. Miller for stimulating discussions and J.E. Henry and D. Burrows for expert technical assistance.

REFERENCES

[1] Bailey, D.W., Artaki, M.A., Stanton, C.J. and Hess, K. (1987). Private communication.

[2] Goodnick, S.M. and Lugli, P. (1987). Private communication.

[3] Heiblum, M., Nathan, M.I., Thomas, D.C. and Knoedler, C.M. (1985). Phys. Rev. Lett. 55,2200.

[4] Knox, W.H., Downer, M.C., Fork, R.L. and Shank, C.V. (1984). Opt. Lett. 9, 552.

[5] Knox, W.H., Hirlimann, Miller, D.A.B., Shah, J., Chemla, D.S. and Shank, C.V. (1986). Phys. Rev. Lett. 56, 1191.

[6] Knox, W.H. (1987, October). Journal of the Optical Society of America B.

[7] Levi, A.F.J., Hayes, J.R., Platzmann, P.M. and Wiegmann, W. (1985). Phys. Rev. Lett. 55, 2071.

[8] Lin, W.Z., Fujimoto, J.G., Ippen, E.P. and Logan, R.A. (1987). Appl. Phys. Lett., 50, 124.

[9] Livescu, G., Miller, D.A.B., Chemla, D.S., Gossard, A.C., English, J.H.,submitted to Phys. Rev. Lett.

[10] Oudar, J.L., Migus, A., Hulin, D., Grillon, G., Etchepare, Antonetti, A. (1984). Phys. Rev. Lett. 53, 384.

[11] Ruckenstein, A.E. and Schmitt-Rink, S. (1987). Phys. Rev. B35, 7551.

[12] Schmitt-Rink, S., Chemla, D.S. and Miller, D.A.B. (1985). Phys. Rev. B32, 6601.

[13] Tang, C.L. and Erskine, D.J. (1983). Phys. Rev. Lett. 51, 840.

FIGURE CAPTIONS

Figure 1 - Optical absorption spectra of 96 A GaAs MQWS at 300 K, before excitation, at t = 0 when non-thermal distribution is at a peak, and at 132 fs after t = 0, and the excitation pulse spectrum.

Figure 2 - Differential transmission spectra at 66 fs delay intervals for undoped 96 A MQWS.

Figure 3 - Time courses at exciton and at the nonthermal peak for (a) medium density : $2\times10^{11}cm^{-2}$, and (b) high density : $1\times10^{12}cm^{-2}$. Insets show the shape of the spectral hole burning signals at t = 0.

Figure 4 - Modulation doped n-type sample spectra. Absorption spectrum before t = 0, at t = 0 and pump pulse spectrum, and pump spectrum at 845 nm. showing no evidence for non-thermal distribution. This result implies a thermalization time of less than 10 fs.

Figure 5 - Differential transmission scans for n-type doped sample at 33 fs intervals. Doping density is $3.5\times10^{11}cm^{-2}$, as determined from Hall measurements.

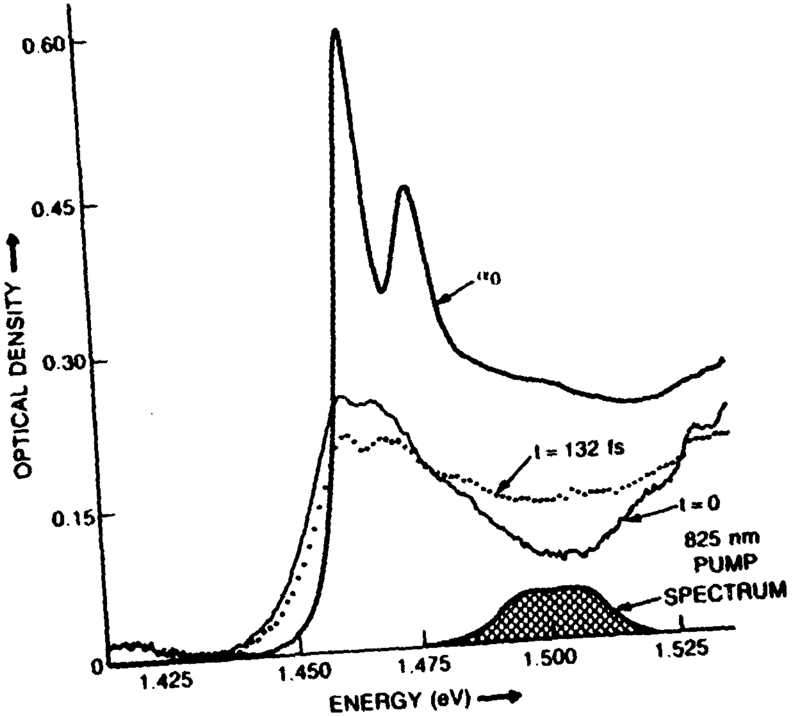

0.60
0.45
0.30
0.15
0
OPTICAL DENSITY
1.425
1.450
1.475
1.500
1.525
ENERGY (eV)
t = 132 fs
t = 0
825 nm
PUMP
SPECTRUM

FIGURE 1

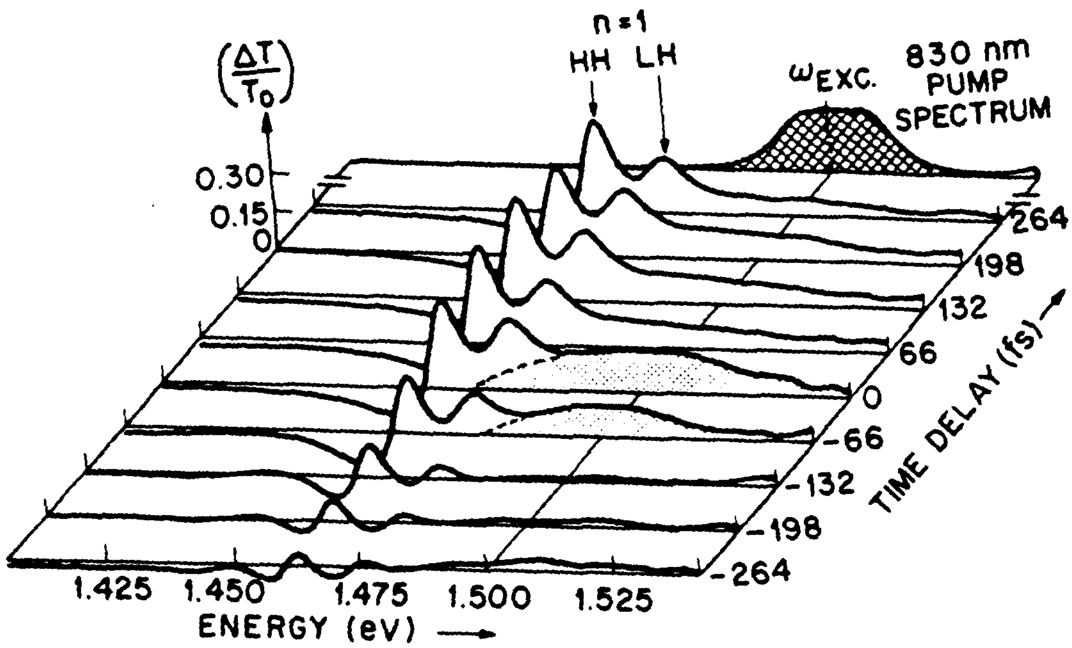

n = 1
HH LH
$\left(\frac{\Delta T}{T_0}\right)$
$\omega_{EXC.}$
830 nm
PUMP
SPECTRUM
0.30
0.15
0
264
198
132
66
0
-66
-132
-198
-264
TIME DELAY (fs)
1.425 1.450 1.475 1.500 1.525
ENERGY (eV)

FIGURE 2

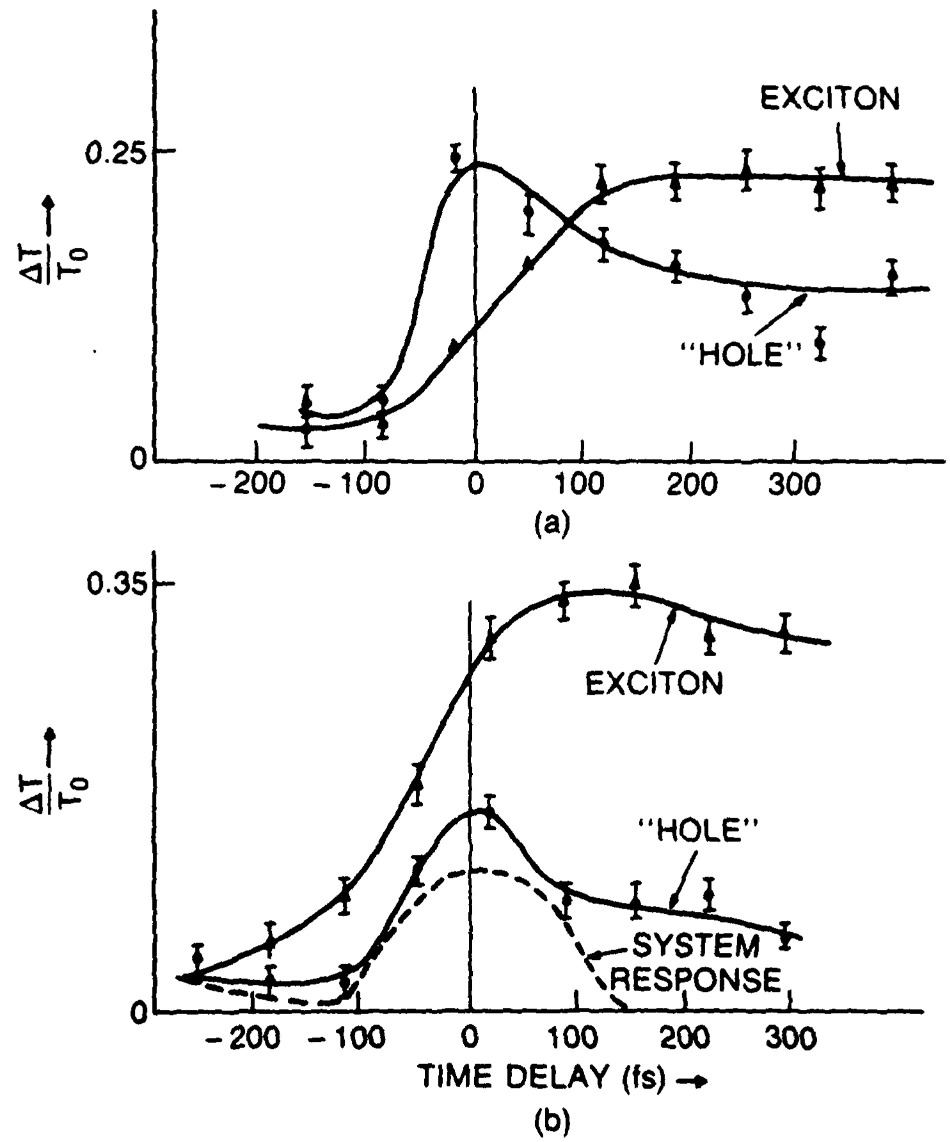
EXCITON
0.25
ΔT/T0
"HOLE"
0
- 200
- 100
0
100
200
300
(a)
0.35
EXCITON
ΔT/T0
"HOLE"
SYSTEM RESPONSE
0
- 200
- 100
0
100
200
300
TIME DELAY (fs)
(b)

FIGURE 3

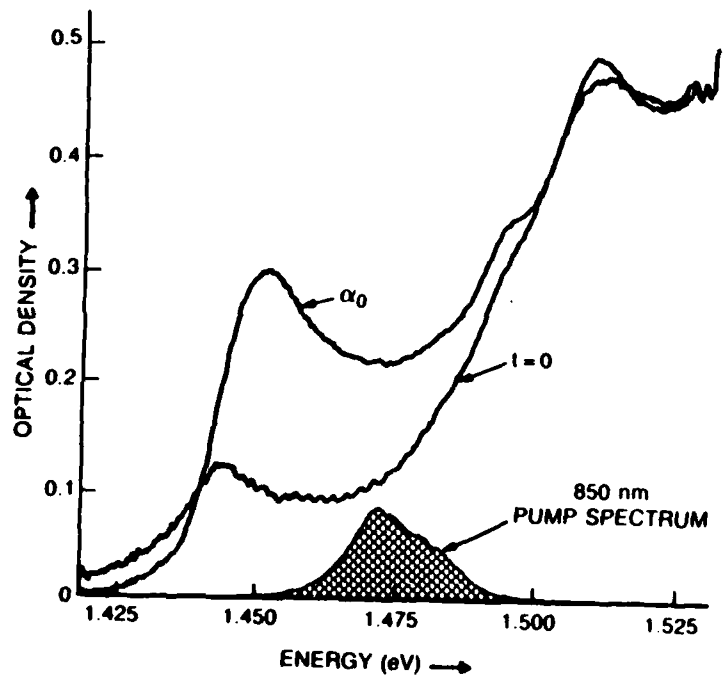
0.5
0.4
0.3
0.2
0.1
0
OPTICAL DENSITY
α_0
I = 0
850 nm
PUMP SPECTRUM
1.425
1.450
1.475
1.500
1.525
ENERGY (eV)

FIGURE 4

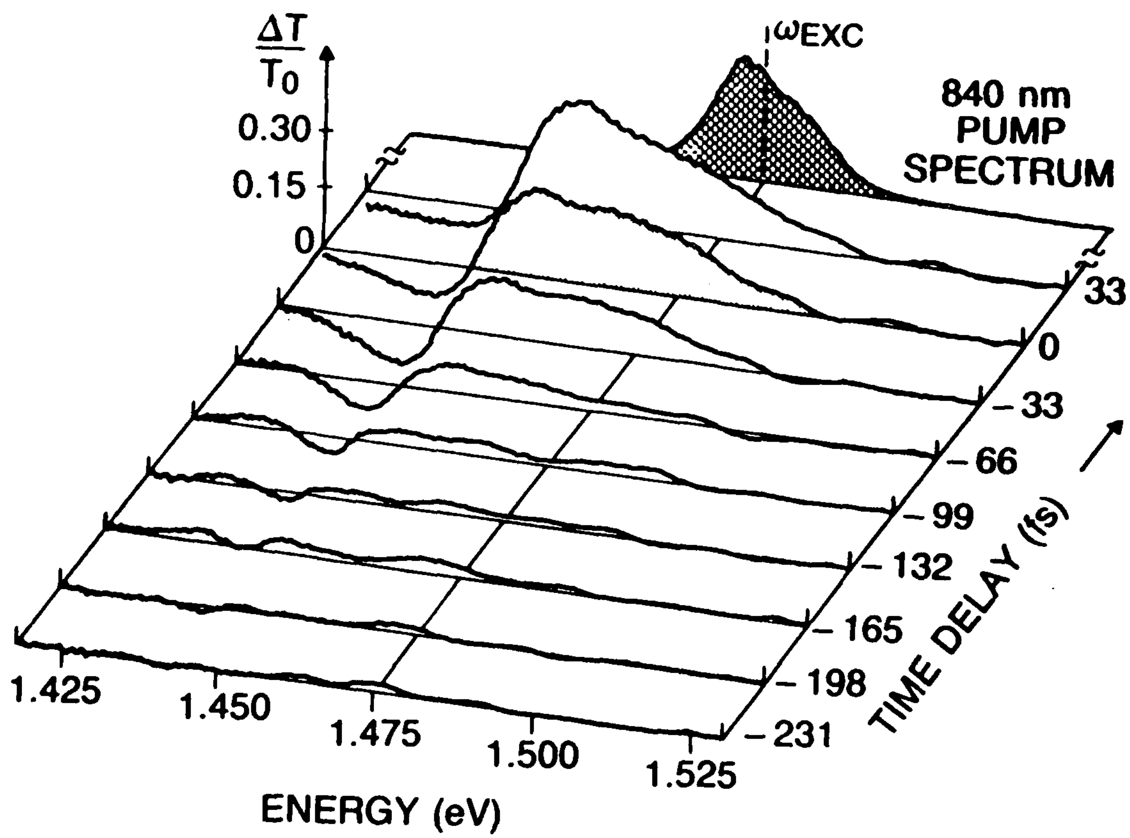
ΔT/T0
0.30
0.15
0
ωEXC
840 nm
PUMP
SPECTRUM
33
0
−33
−66
−99
−132
−165
−198
−231
TIME DELAY (fs)
1.425
1.450
1.475
1.500
1.525
ENERGY (eV)

FIGURE 5

Dynamical Aspects of Carrier Tunneling in Semiconductor Superlattices

Yasuaki Masumoto

Institute of Physics, University of Tsukuba,
Sakura-mura, Niihari-gun, Ibaraki 305, Japan

Abstract

Dynamical carrier processes in GaAs-AlGaAs superlattices are studied by means of picosecond spectroscopy and population mixing technique under the electric field along the superlattice direction. Two prominent structures are found in the curves of exciton luminescence and photocurrent vs. the electric field. They are ascribed to the onset of exciton dissociation followed by electron tunneling through AlGaAs barriers and resonant electron sequential tunneling. The electron tunneling rate is determined to be 1/(430ps) and is compared with calculations. In addition, competitive nature of ultrafast processes of photo-excited electron-hole pairs, exciton formation and pair ionization followed by tunneling through barriers, are clarified under the various electric field.

Dynamical Aspects of Carrier Tunneling in Semiconductor Superlattices

Yasuaki Masumoto

Institute of Physics, University of Tsukuba,
Sakura-mura, Niihari-gun, Ibaraki 305, Japan

Ultrafast processes of carriers in semiconductor superlattices under the perpendicular electric field

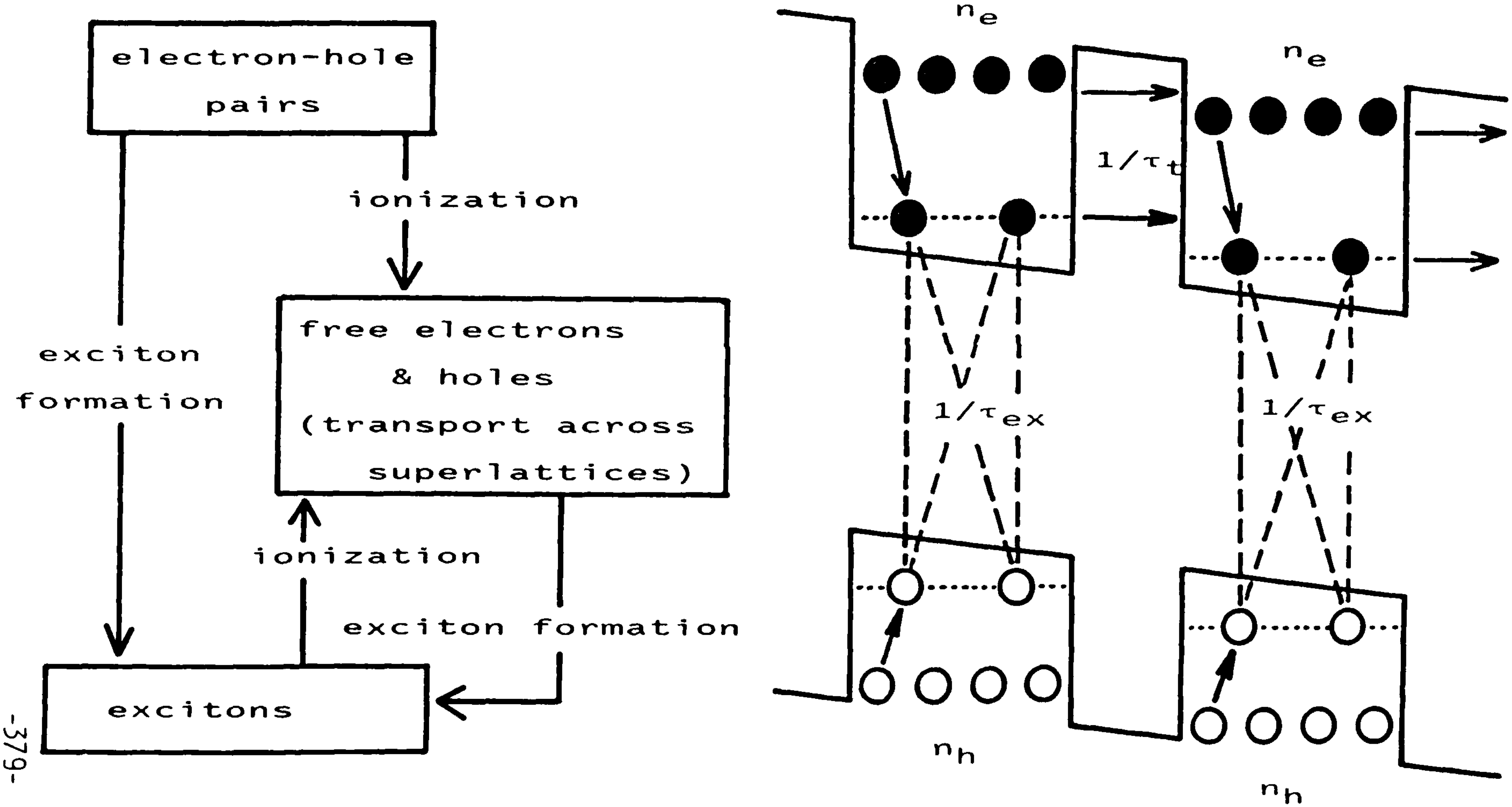

PIN DIODE STRUCTURE

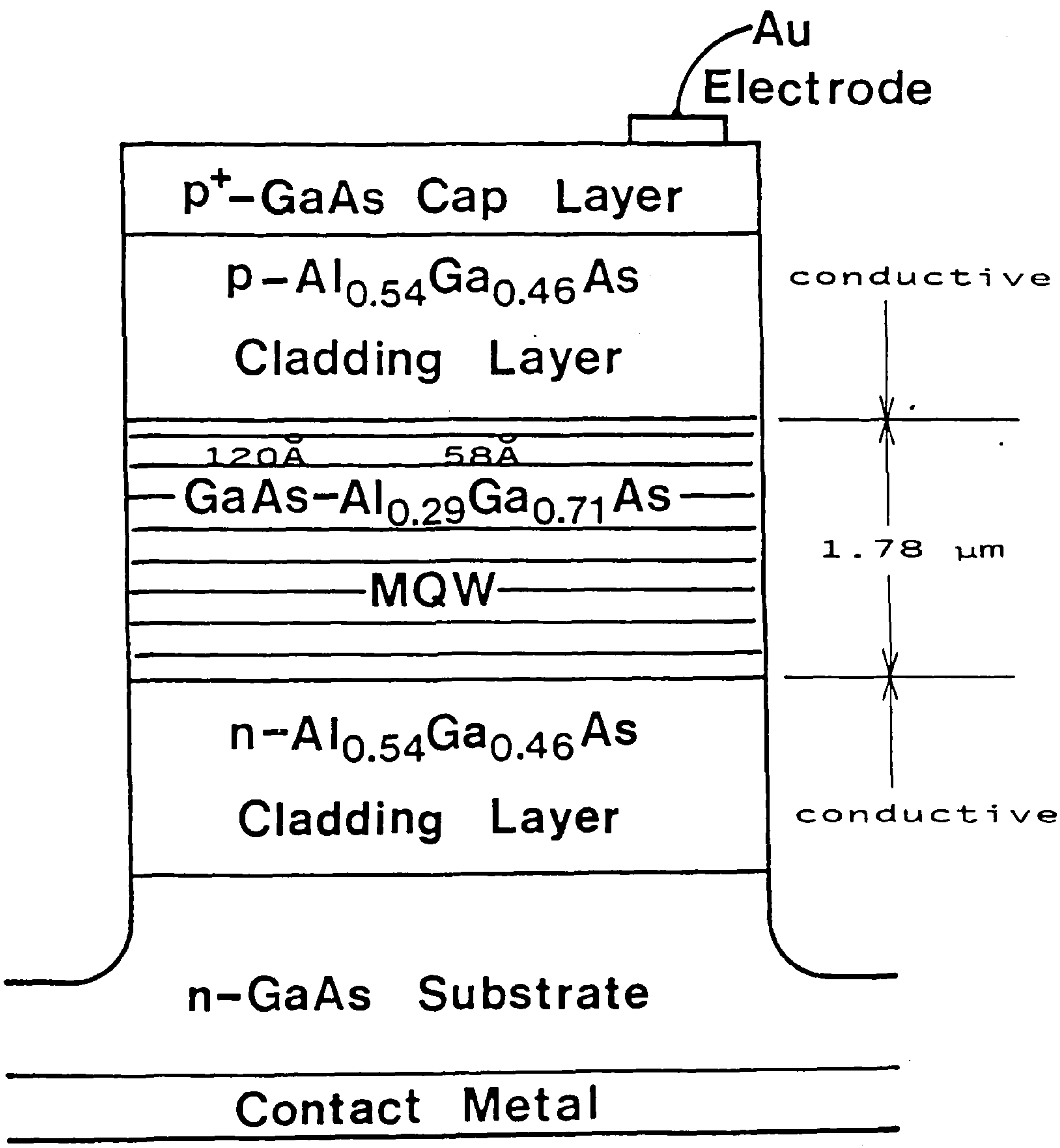

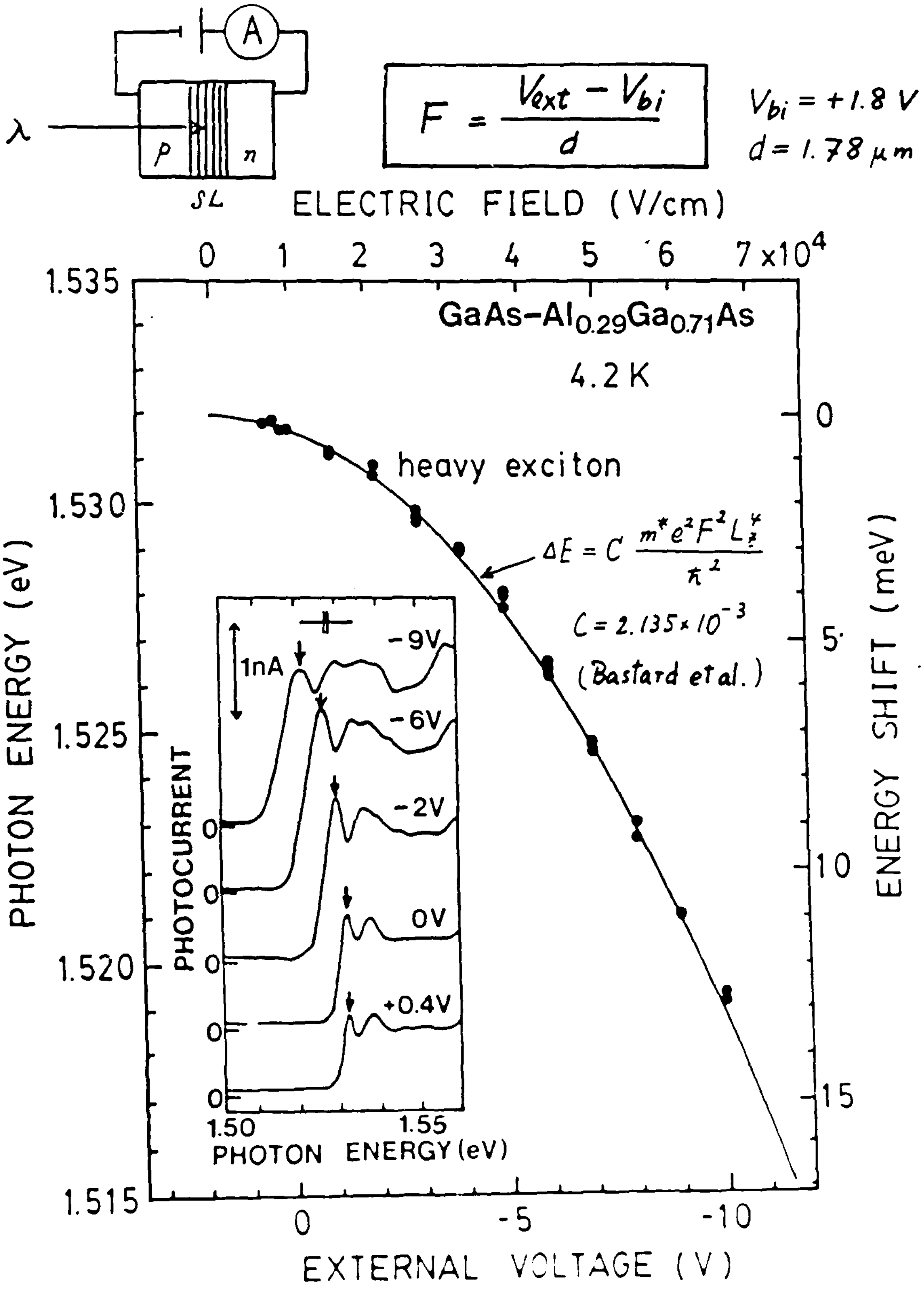

A
λ
p
n
SL
$F = \frac{V_{ext} - V_{bi}}{d}$
$V_{bi} = +1.8$ V
$d = 1.78\ \mu m$
ELECTRIC FIELD (V/cm)
0 1 2 3 4 5 6 7 x10^4
GaAs-Al0.29Ga0.71As
4.2K
heavy exciton
$\Delta E = C\,\frac{m^* e^2 F^2 L_z^4}{\hbar^2}$
$C = 2.135 \times 10^{-3}$
(Bastard et al.)
1nA
-9V
-6V
-2V
0V
+0.4V
PHOTOCURRENT
1.50
1.55
PHOTON ENERGY (eV)
1.535
1.530
1.525
1.520
1.515
PHOTON ENERGY (eV)
0
5
10
15
ENERGY SHIFT (meV)
0
-5
-10
EXTERNAL VOLTAGE (V)

AD-A186 938 UNITED STATES - JAPAN SEMINAR ON QUANTUM MECHANICAL ASPECTS OF QUANTUM EL (U) MASSACHUSETTS INST OF TECH CAMBRIDGE RESEARCH LAB OF ELECTRON 5/7

UNCLASSIFIED J H SHAPIRO ET AL OCT 87 N00014-87-G-0198 F/G 20/3 NL

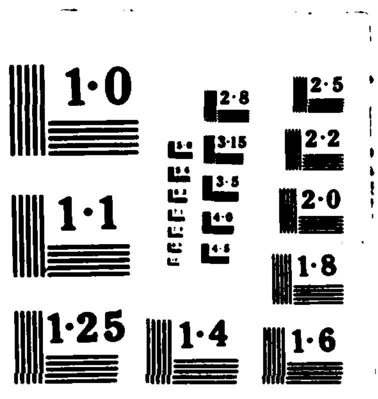
1·0
2·8
2·5
3·15
2·2
3·5
2·0
1·1
4·0
4·5
1·8
1·25
1·4
1·6

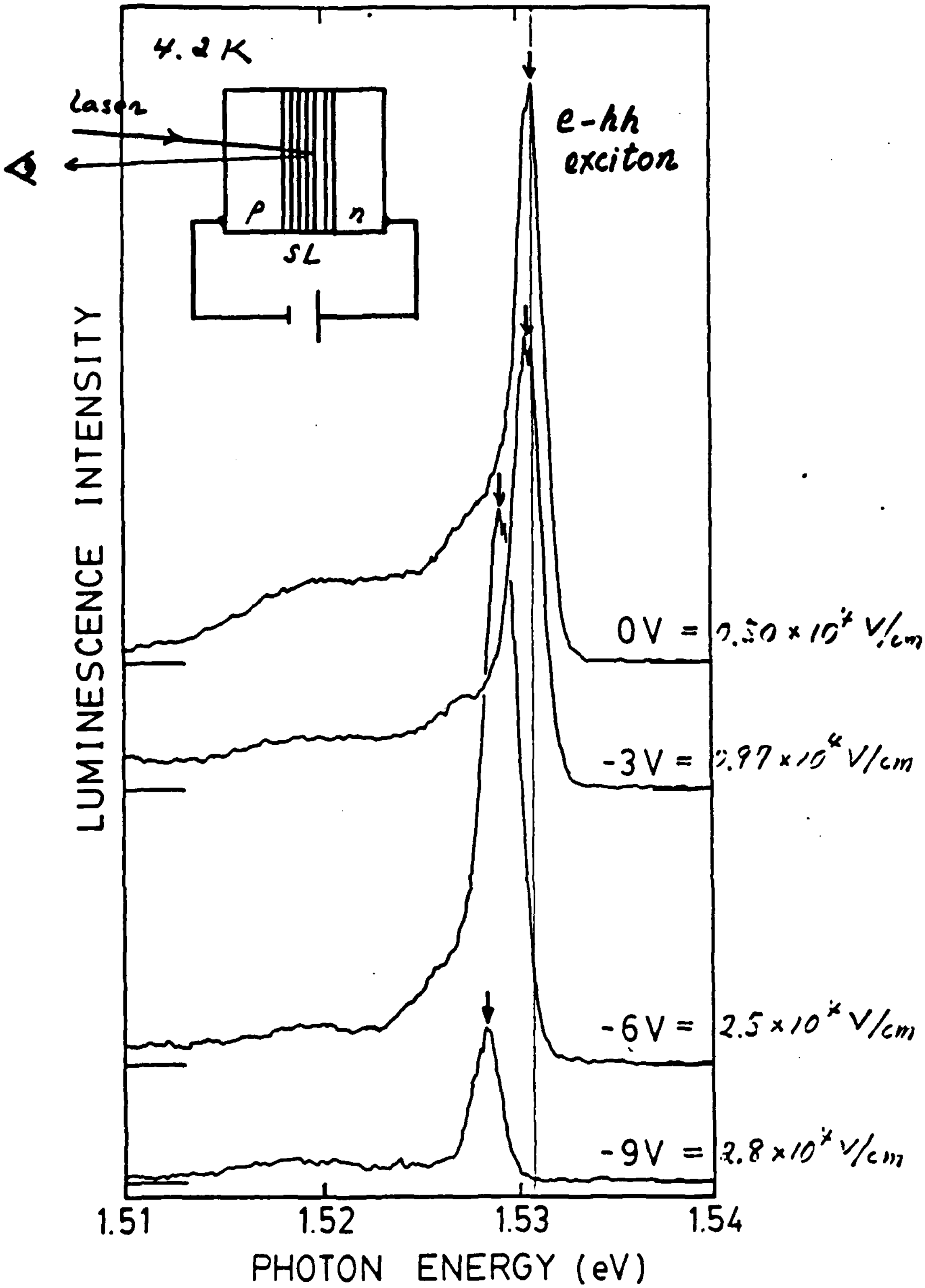

4.2K
laser
p
n
SL
e-hh
exciton
LUMINESCENCE INTENSITY
0V =
-3V =
-6V = 2.5 × 10⁴ V/cm
-9V = 2.8 × 10⁴ V/cm
1.51
1.52
1.53
1.54
PHOTON ENERGY (eV)

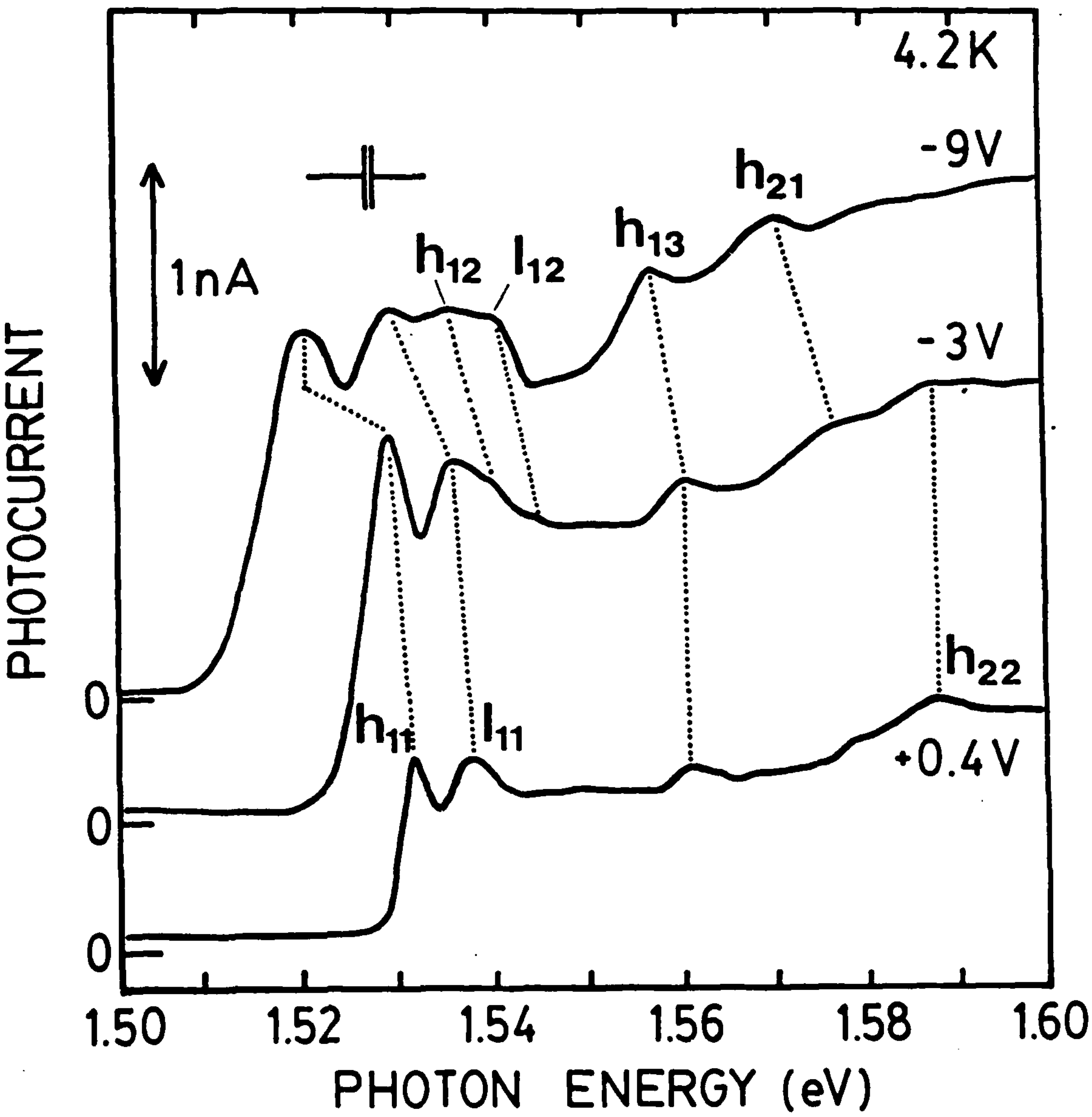

4.2K
-9V
-3V
+0.4V
1nA
h_{21}
h_{13}
h_{12}
l_{12}
h_{22}
h_{11}
l_{11}
PHOTOCURRENT
0
0
0
1.50
1.52
1.54
1.56
1.58
1.60
PHOTON ENERGY (eV)

Subband Energy Splits (meV)		
2e - 1e	($h_{21} - h_{11}$)	49
3hh - 1hh	($h_{13} - h_{11}$)	30
2hh - 1hh	($h_{12} - h_{11}$)	10
2lh - 1lh	($l_{12} - l_{11}$)	9
1lh - 1hh	($l_{11} - h_{11}$)	6

Table I. The estimated subband gaps for electrons and holes in 120Å GaAs wells. ne(hh,lh) denotes the n-th electron(heavy hole, light hole) subband. In the parentheses, exciton transition pairs used for the estimation are shown.

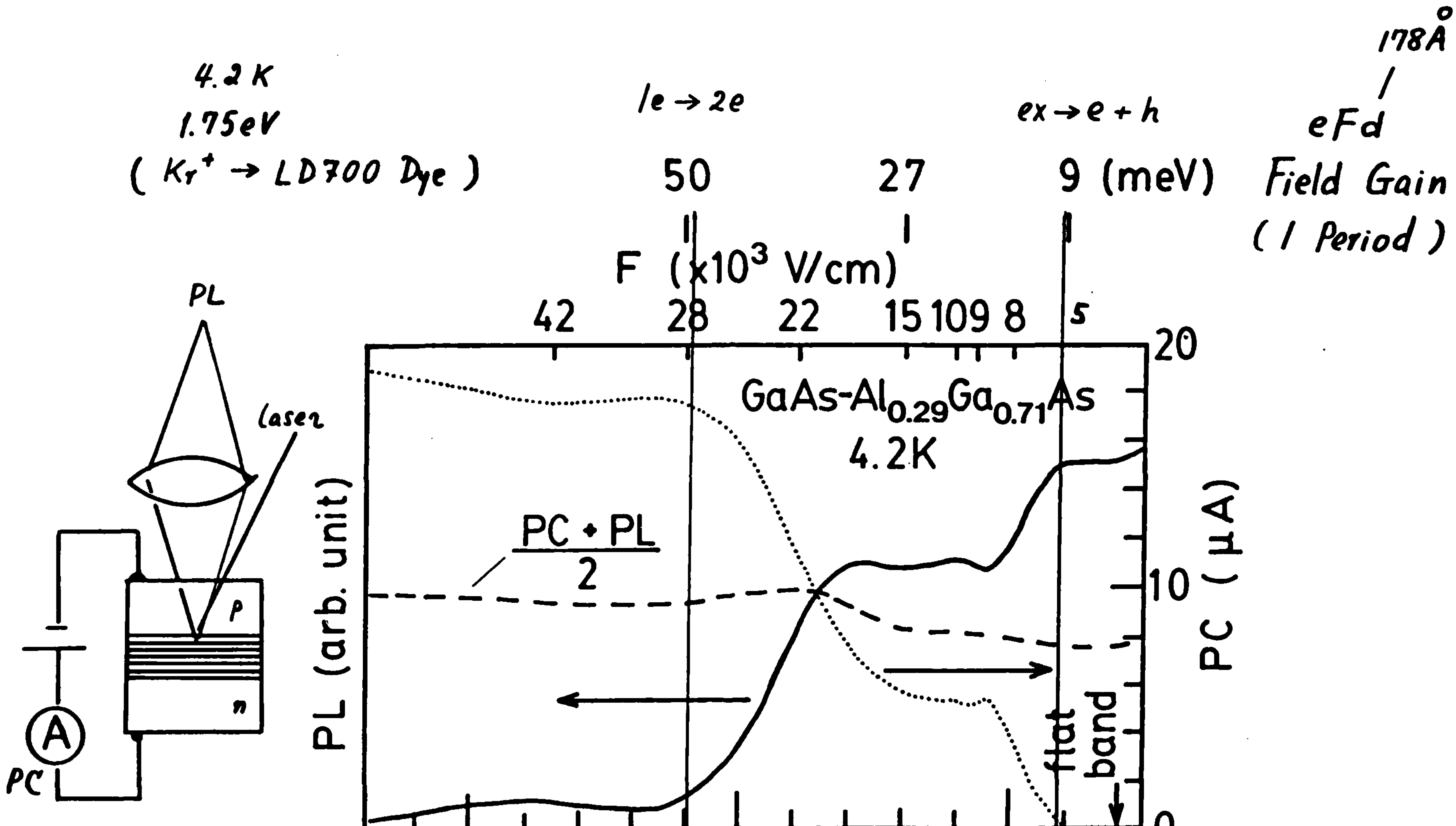

4.2 K
1.75eV
(Kr+ → LD700 Dye)
1e → 2e
ex → e + h
178Å
eFd
Field Gain
(1 Period)
50
27
9 (meV)
F (x10³ V/cm)
42
28
22
15 10 9 8
5
20
10
0
PC (μA)
PL (arb. unit)
GaAs-Al0.29Ga0.71As
4.2K
PC + PL
2
flat
band
-10
-5
0
Vext (V)
PL
laser
p
n
A
PC

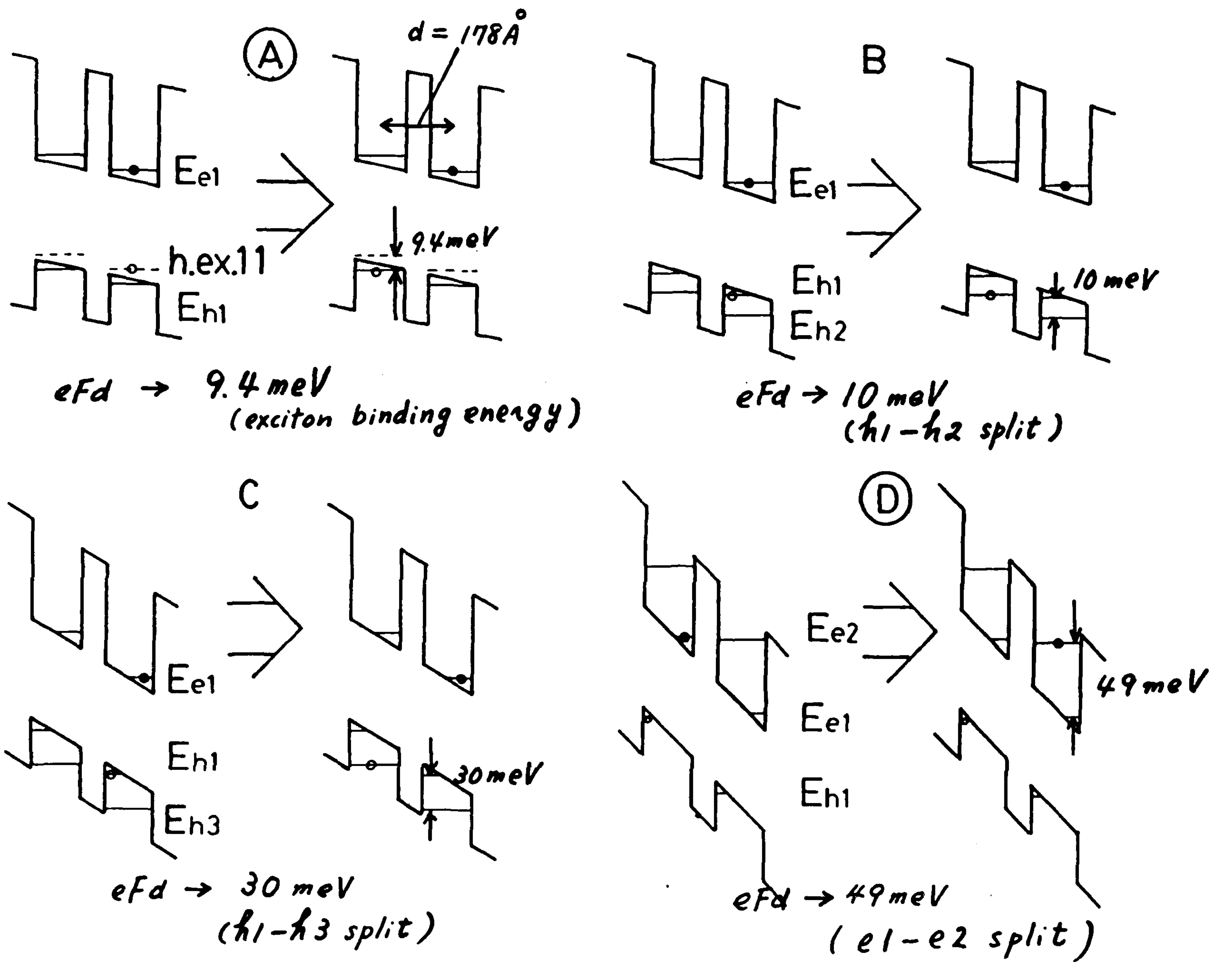
A
d = 178Å
E_{e1}
h.ex.11
E_{h1}
9.4meV
eFd → 9.4 meV
(exciton binding energy)
B
E_{e1}
E_{h1}
E_{h2}
10 meV
eFd → 10 meV
(h1 − h2 split)
C
E_{e1}
E_{h1}
E_{h3}
30meV
eFd → 30 meV
(h1 − h3 split)
D
E_{e2}
E_{e1}
E_{h1}
49 meV
eFd → 49 meV
(e1 − e2 split)

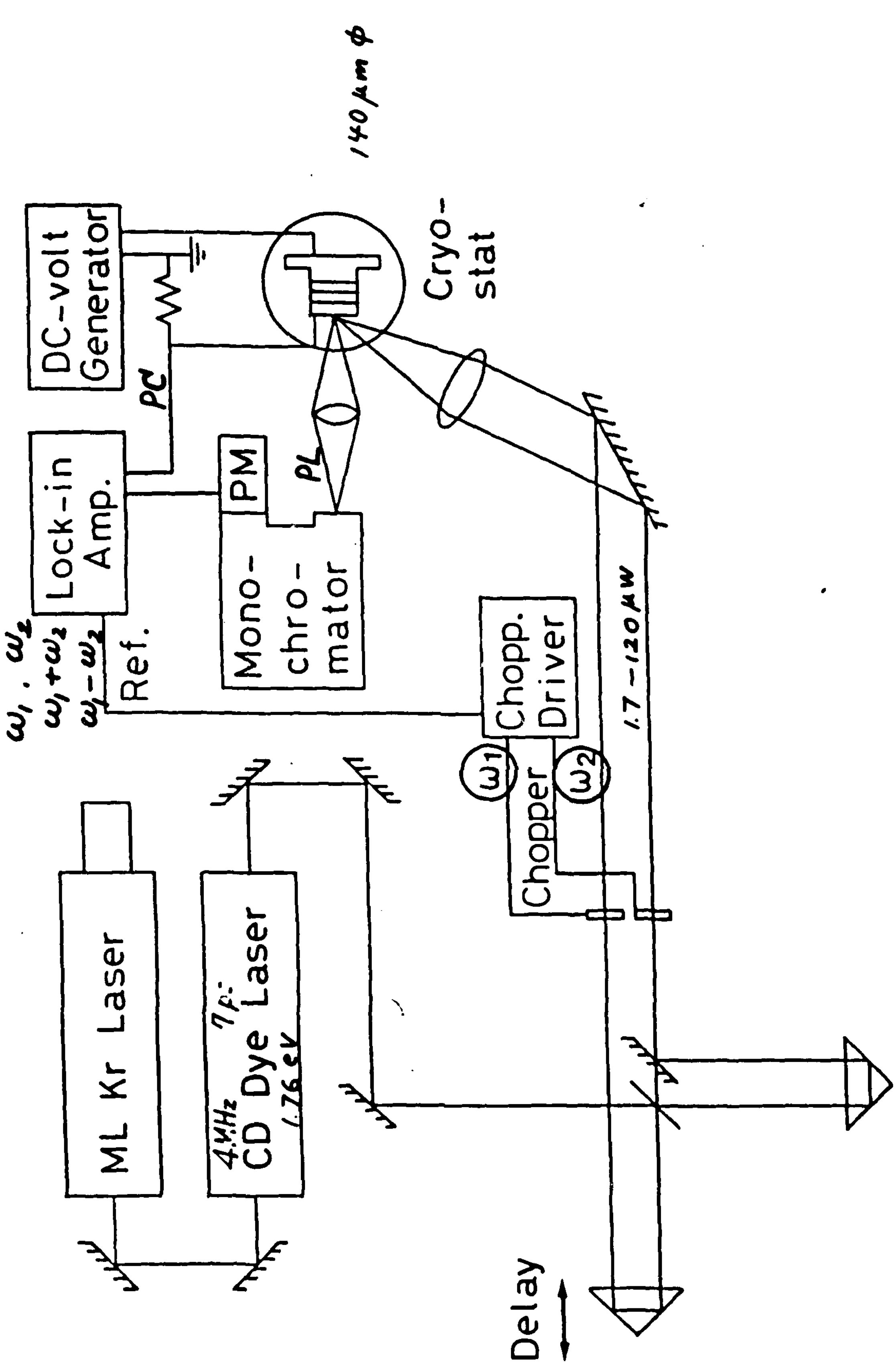
DC-volt Generator
Cryo-stat
140 μm φ
Lock-in Amp.
PC
PM
PL
Mono-chro-mator
Ref.
ω_1 , ω_2
$\omega_1+\omega_2$
$\omega_1-\omega_2$
Chopp. Driver
ω_1
ω_2
Chopper
1.7–120 μW
ML Kr Laser
4 MHz CD Dye Laser
1.76 eV
Delay

4.2K

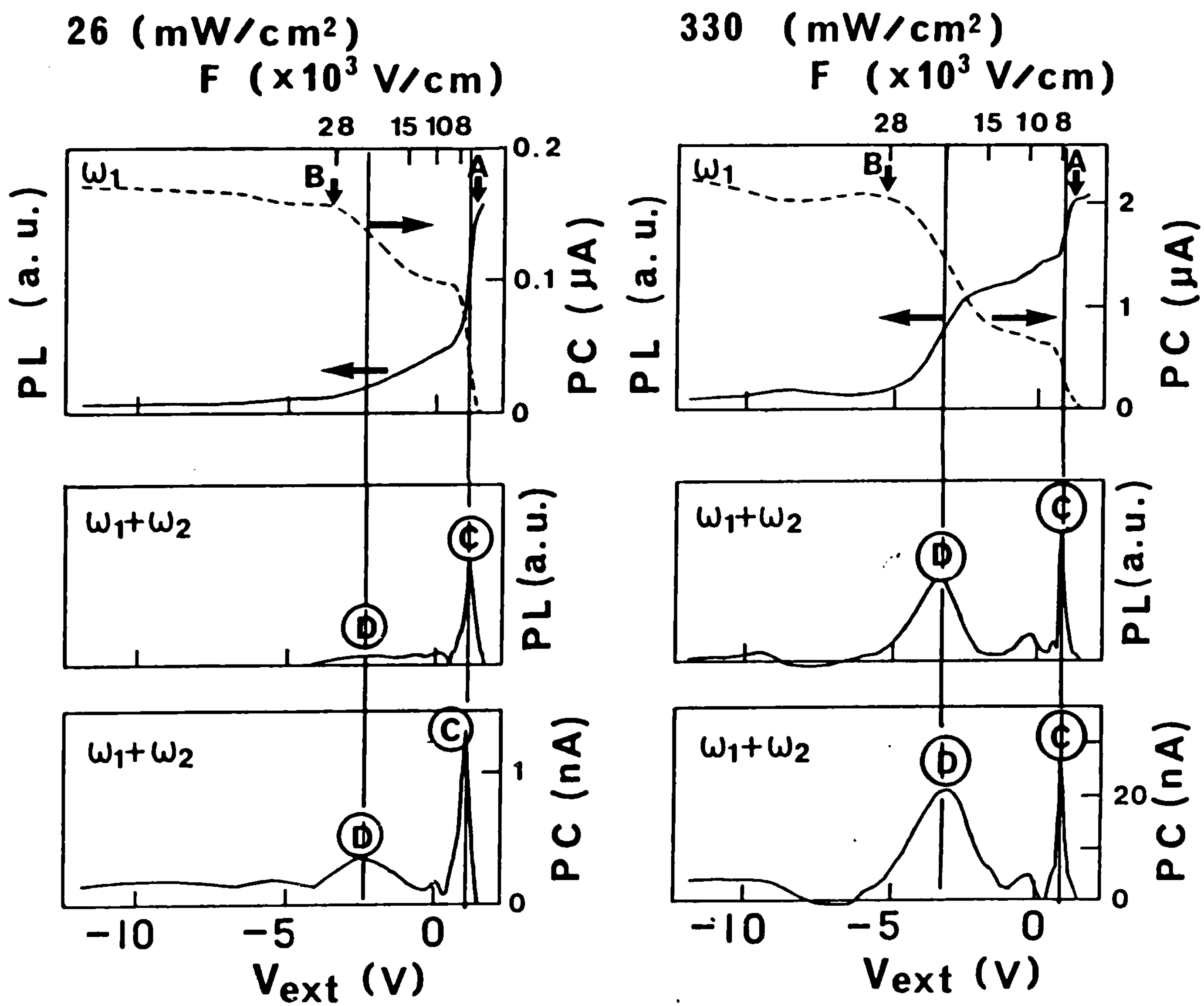

26 (mW/cm²)
330 (mW/cm²)
F (x10³ V/cm)
28
15
10
8
0.2
0.1
0
2
1
20
PL (a. u.)
PC (μA)
PL(a.u.)
PC (nA)
ω1
ω1+ω2
A
B
C
D
−10
−5
0
Vext (V)

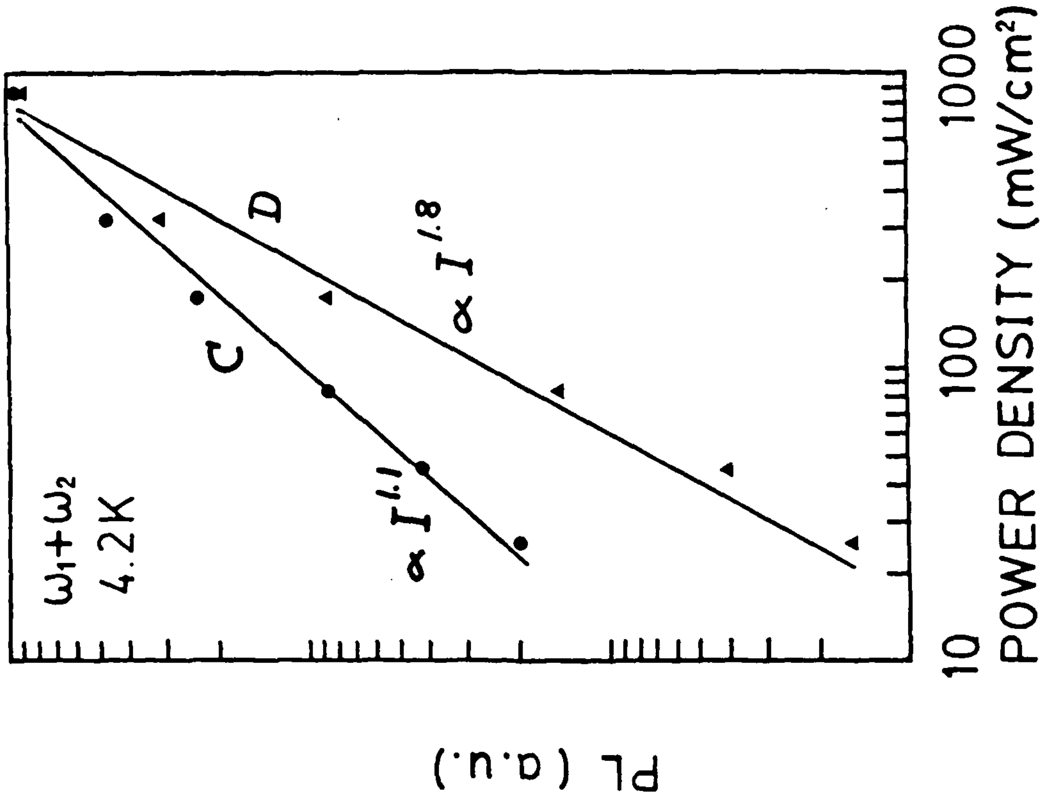

PL (a.u.)
POWER DENSITY (mW/cm²)
10
100
1000
ω₁+ω₂
4.2K
C
D
∝ I^1.1
∝ I^1.8

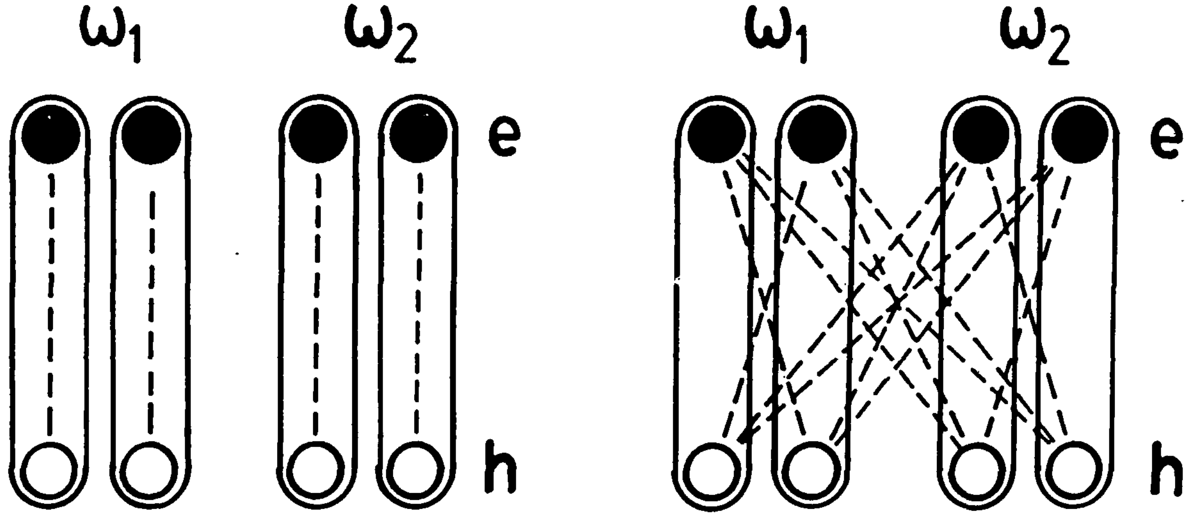

geminate exciton — ω_1 ω_2

non-geminate exciton — $2\omega_1$, $2\omega_2$; $\omega_1 + \omega_2$, $\omega_1 - \omega_2$

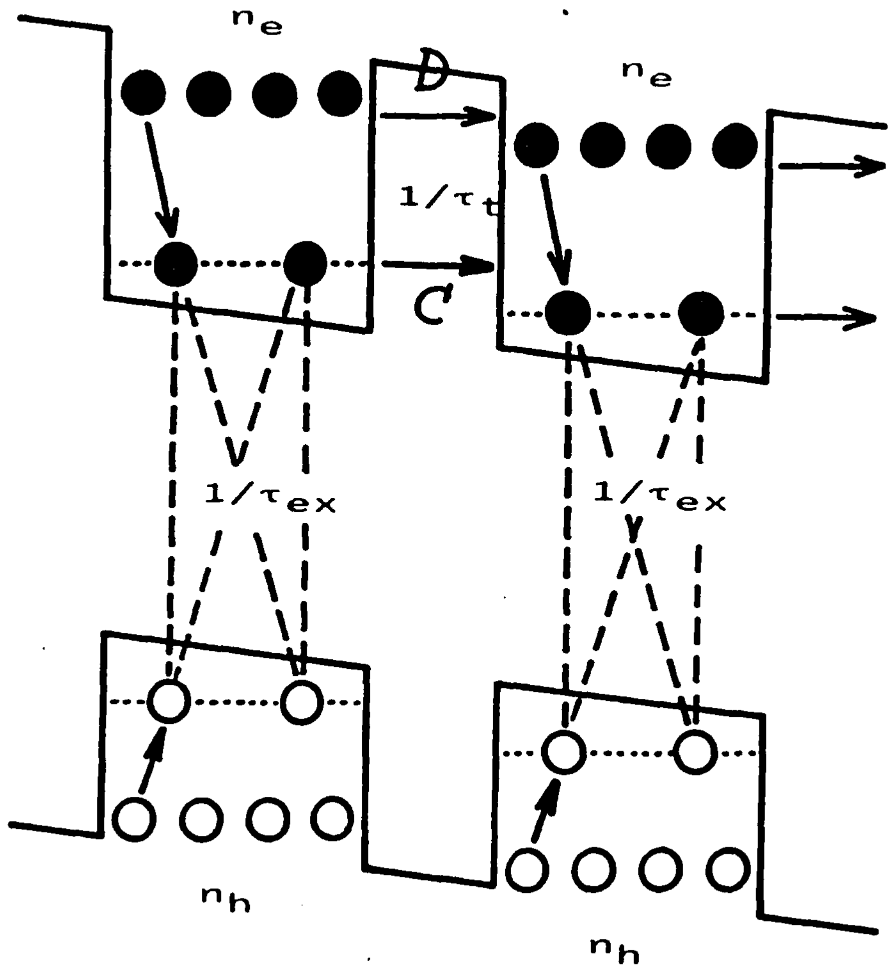

electron tunneling rate

$1/\tau_t$

non-geminate exciton formation rate

$1/\tau_{ex} \propto n_e n_h$

$\boxed{(1)\ 1/\tau_t >> 1/\tau_{ex}}$

$PL(\omega_1+\omega_2) \propto I^2$

$\boxed{(2)\ 1/\tau_t << 1/\tau_{ex}}$

$PL(\omega_1+\omega_2) \propto I$

picosecond dye laser + synchroscan streak camera

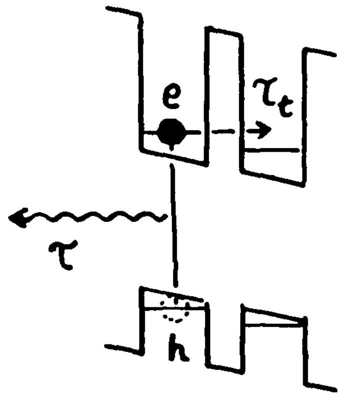

τ_t dominates τ when $F > 5\times10^3$ V/cm

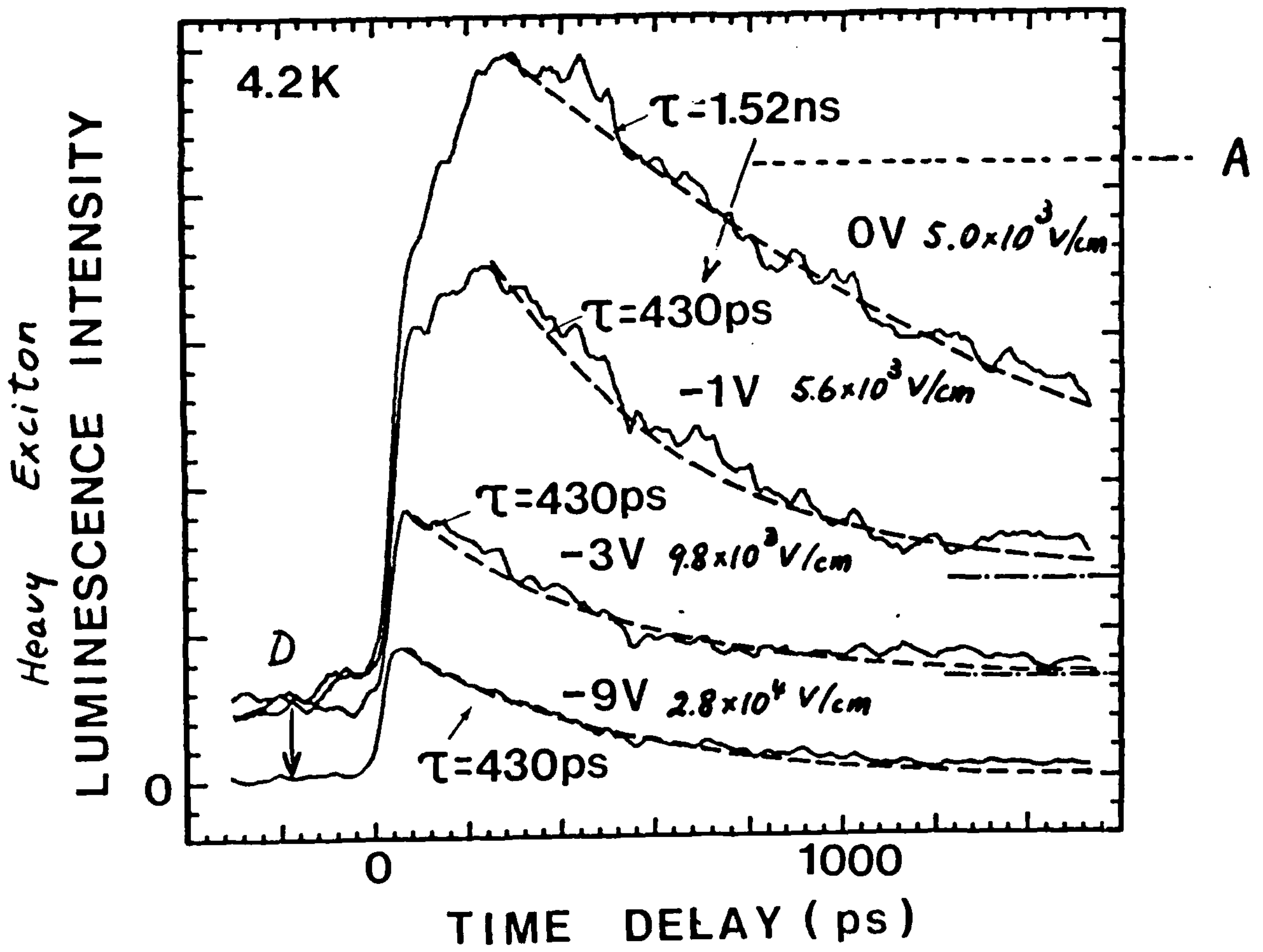

(1) Tunneling of Coulomb barrier

(Exciton ionization)

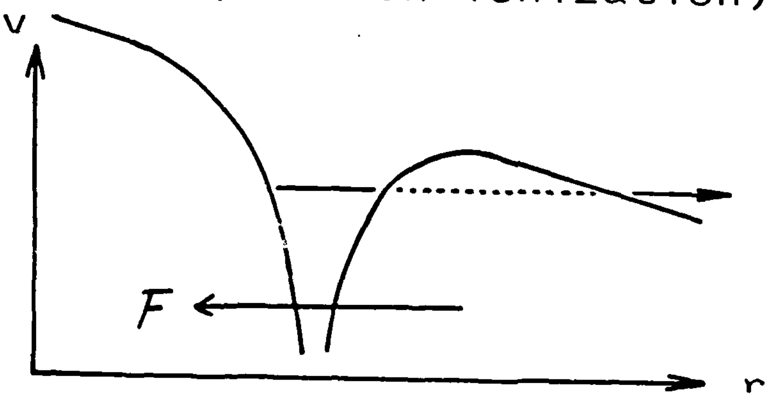

ionization rate

$$w = \frac{16R_y^2}{eFa_B\hbar} \exp\left(-\frac{4R_y}{3eFa_B}\right) \sim 2.8 \times 10^{13}\ s^{-1}$$

$(\tau \sim 36\ fs)$

at $F = 5 \times 10^3\ V/cm$

(2) Tunneling of potential barrier

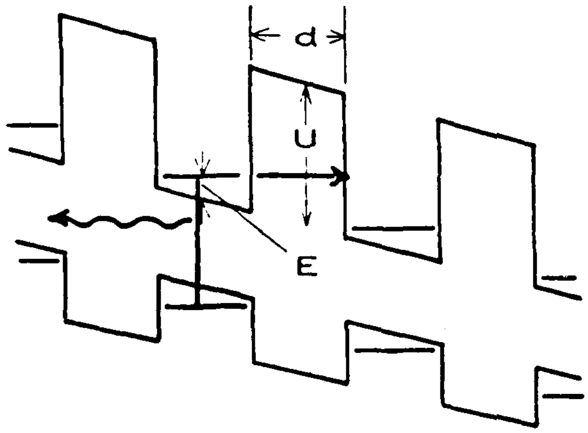

$U \sim 206\ meV$

electron tunneling rate

$$w = \frac{\pi\hbar}{2m_e L_z^2} \exp\left\{-\frac{2}{\hbar}\sqrt{2m_e(U-E)}\,d\right\} \sim 1.8 \times 10^{10}\ s^{-1}$$

$(\tau \sim 55\ ps)^*$

Electron tunneling rate little depends on F, if eFd << U-E holds.

* 57:43 split

cavity dumped picosecond dye laser
+
single photon counting

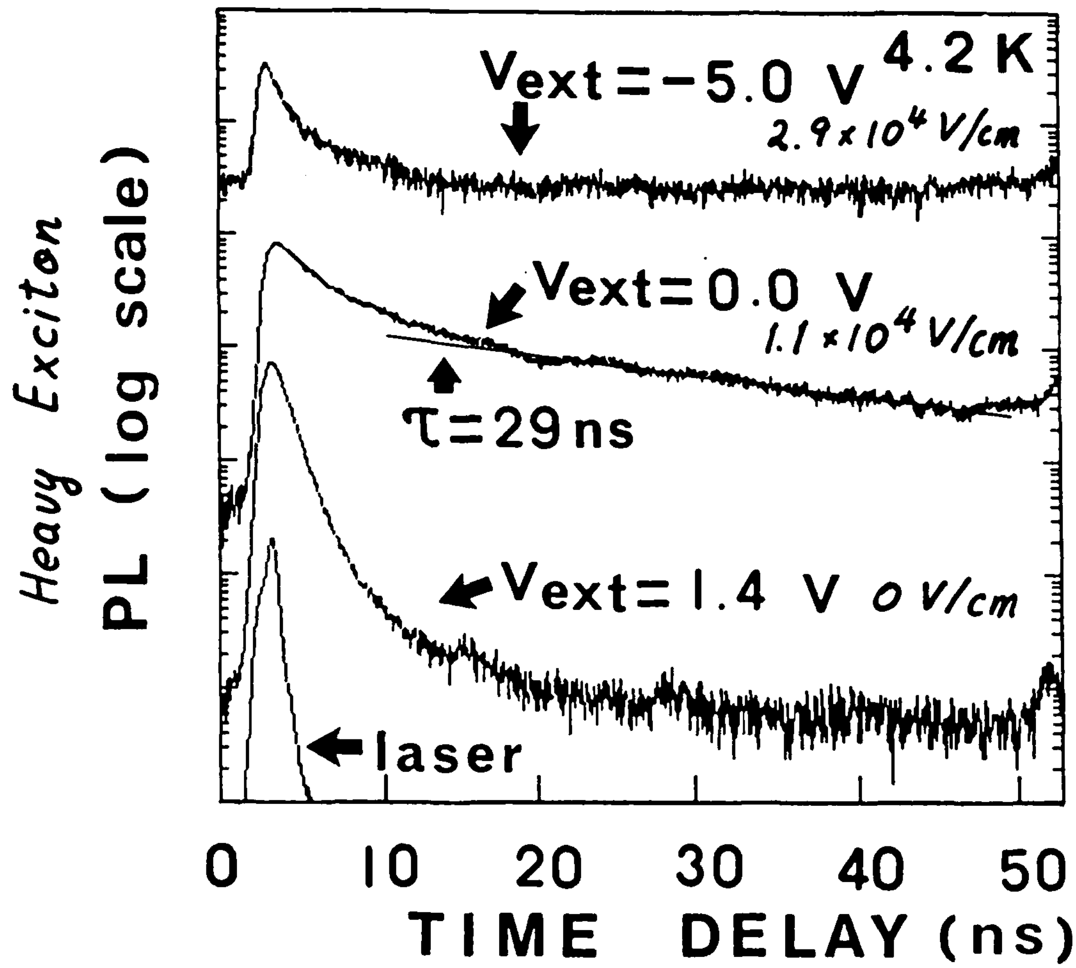

Summary

- Exciton dissociation followed by electron tunneling through AlGaAs barriers and resonant electron sequential tunneling are observed in GaAs-AlGaAs superlattices.
- Excitons dissociate when the field gain can compensate for the exciton binding energy.
- The tunneling rate of the electrons is determined to be 1/(430ps), slower than the simple calculation.
- Competitive nature of ultrafast processes of photo-excited electron-hole pairs, exciton formation and pair ionization followed by tunneling through barriers, are clarified under the various electric field.

SUMMARY

EXPERIMENTAL AND THEORETICAL STUDIES OF COHERENT AND NONTHERMAL PROCESSES IN SEMICONDUCTORS PROBED BY FEMTOSECOND LASER TECHNIQUES

N. Peyghambarian and S. W. Koch
Optical Sciences Center
University of Arizona
Tucson, AZ 85721

The coherent interaction of femtosecond laser pulses and a thin CdSe sample is investigated both experimentally and theoretically. Observation of coherent phenomena in semiconductors is very rare because the incoherent processes occur in the femtosecond time domain in these materials. One example of such a phenomena is the so called optical Stark effect of exciton where a blue shift of the exciton resonance occurs as a result of pumping below the bandgap (in the transparency region). Here, we report on our investigations of coherent effects involving band-to-band and also exciton transitions. Using femtosecond transmission measurements we observe clear evidence for coherent interference effects of the light field and the driven material polarization. These interferences manifest themselves as oscillatory structures in the differential transmission spectra. The structures are observed either in the spectral vicinity of the exciton pulse for resonant interband excitation, or around the exciton resonance. Experiments were performed in a pump-probe geometry with the pulses having ≅80 fs durations. The transmission of the probe pulse in the presence and absence of the pump pulse is detected and the normalized difference (DTS) is plotted against probe wavelength at various time delays between the two pulses. DTS show oscillatory behavior at early times where the probe preceeds the pump on the sample (negative time delays).

These oscillatory features are explained by comparison with a semiclassical theory. We assume a weak, short probe pulse interacting with the time-dependent medium polarizaticn

which is driven by the strong pump field. We consider the case, where the peak of the probe pulse precedes the maximum of the pump pulse. The different electron-hole-pair states of the semiconductor are modelled as mutually uncoupled transitions, each of which is described by a density matrix. The dissipative scattering processes among the elementary excitations are included through phenomenological decay rates in the equation of motion for the density matrix. The theory has been evaluated for the cases of resonant interband pumping where the transmission is probed around the frequency of the pump, and for the case of nonresonant pumping where the transmission changes are measured at the exciton.

Examples of the computed results are presented for different time delays between probe and pump. Similar to the experimental results, the spectra show clear oscillatory structures when the probe precedes the pump. The physical explanation of the observed oscillatory structures, which are reminescent of Ramsey fringes in atomic physics, is a transient population grating originating from the pump and probe inside the crystal. The grating is generated essentially during the temporal overlap of the pulses and the oscillations in the spectra are caused by the interference between the probe pulse and that part of the pump pulse which is scattered from the grating into the direction of the probe beam. The oscillation frequency is determined by the time delay between pump and probe. An increase of the temporal overlap between the pulses reduces the number and the amplitude of the oscillations with respect to the central peak. A detailed analysis of the relative importance of the different damping processes shows that the shape of the oscillatory structures is rather insensitive to the value of the dipole damping rate. However, the oscillatory features depend very strongly on the population decay rate. Increasing the population decay decreases the amplitude of the oscillations with respect to the central peak until only a broadened peak, the spectral hole, is left.

To analyze the situation where the transmission spectra are measured in the vicinity of the exciton frequency, we modelled the exciton as a single homogeneously broadened transition. The oscillations in the differential transmission spectra now occur around the exciton frequency. Assuming non-resonant excitation spectrally below the exciton, we obtain asymmetric

structures due to the detuning of the pump laser from the exciton resonance. When the delay time approaches zero, the oscillations gradually disappear and the transmission changes assume the dispersive shape characteristic for the optical Stark shift. Hence, the oscillatory structures should be viewed as the early stages of the optical Stark effect in short-pulse pump-probe spectroscopy. For large time delays, only a Lorentzian remains representing the exciton saturation caused by the pump pulse. For the case of resonant interband excitation, one can observe the oscillatory structures not only around the central pump frequency, but also around the exciton resonance. These experimental observations are in qualitative agreement with the theoretical results which predict large oscillation amplitudes around the exciton transition even for large detunings partly due to the greater exciton oscillator strength.

EXPERIMENTAL AND THEORETICAL STUDIES OF COHERENT AND NONTHERMAL PROCESSES IN SEMICONDUCTORS PROBED BY FEMTOSECOND LASER TECHNIQUES

N. Peyghambarian and S. W. Koch

Collaborators:

Experiment: B. Fluegel

Theory: M. Lindberg

Support:

NSF
NATO
OCC

OUTLINE

-- Introduction

-- Observation of Coherent Optical Phenomena Around the Pump Frequency and Exciton in CdSe

-- Theoretical Simulations

-- Conclusion

Dynamics of Laser-Excited Electron-Hole Pairs

1. Coherent Regime or
   Collision-Free Regime

   Rabi flopping of electrons between band states.

2. Nonthermal Distribution Regime

   Collisions destroy phase coherence
   Spectral hole burning

3. Quasi-Thermal Regime

   Optical Nonlinearities
   Coulomb Screening
   Bandgap Renormalization
   State Blocking

Optical Stark Effect

Non-resonant Excitation

- Mysyrowicz et al.
- Von Lehman et al.

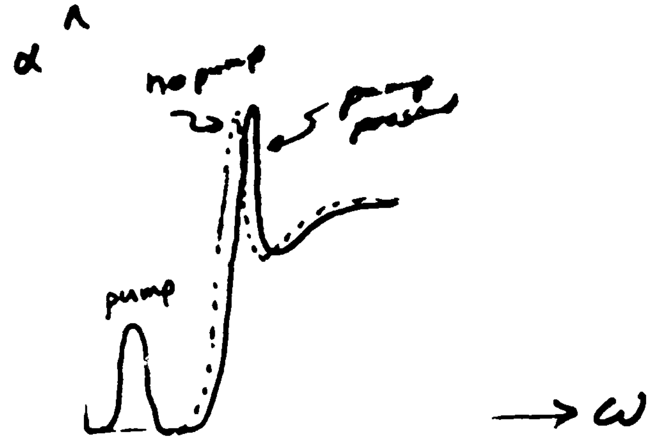

Exciton shift $\propto \mu \cdot E \propto$ Rabi Freq.

PUMP PROBE SPECTROSCOPY

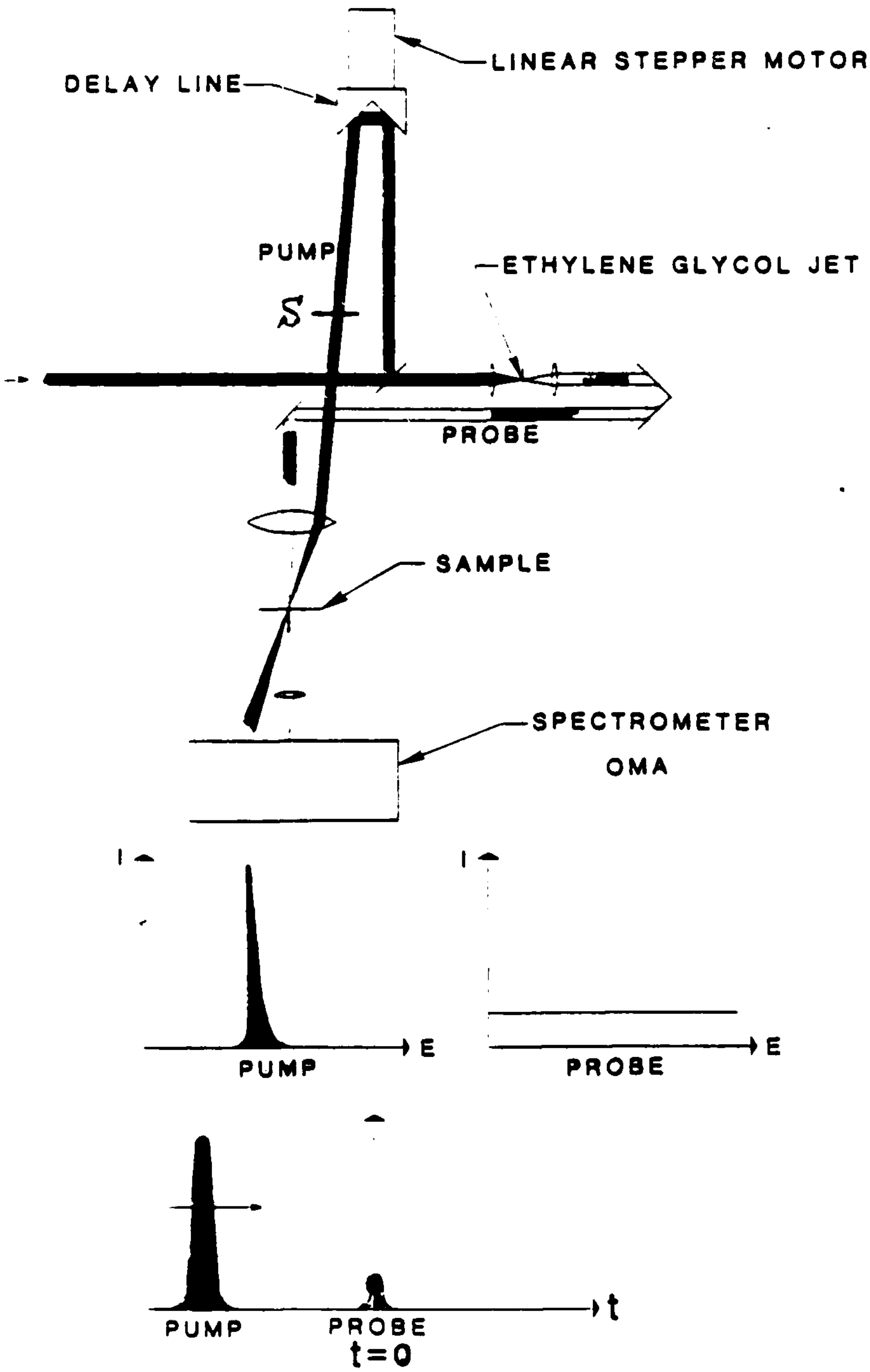

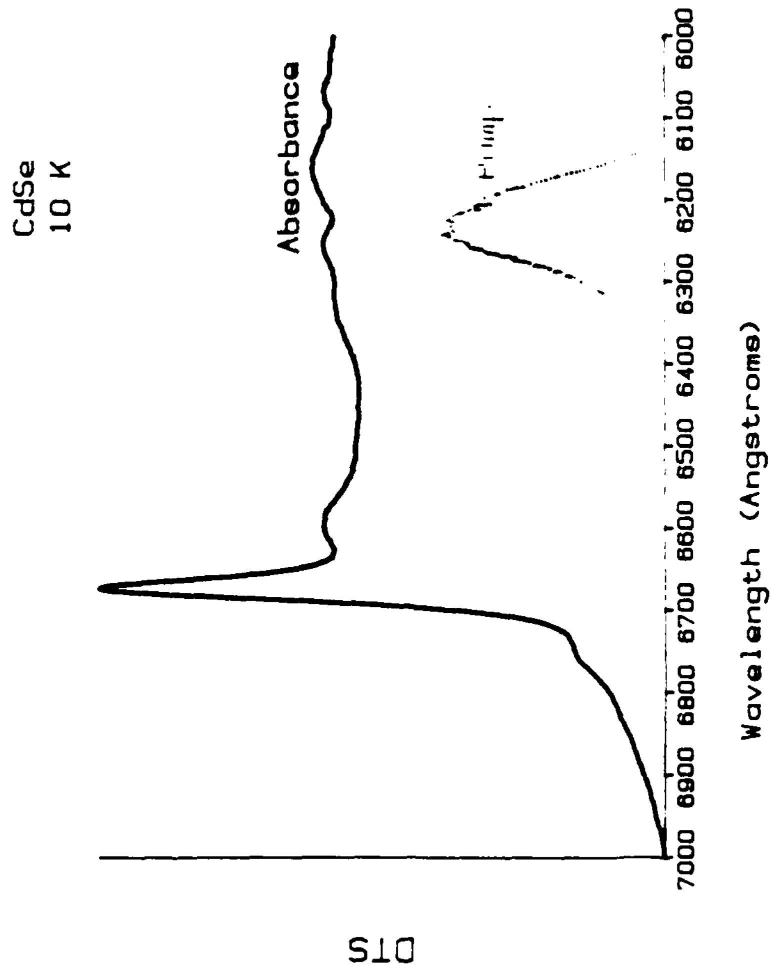
CdSe
10 K
Absorbance
Pump
DTS
7000 6900 6800 6700 6600 6500 6400 6300 6200 6100 6000
Wavelength (Angstroms)

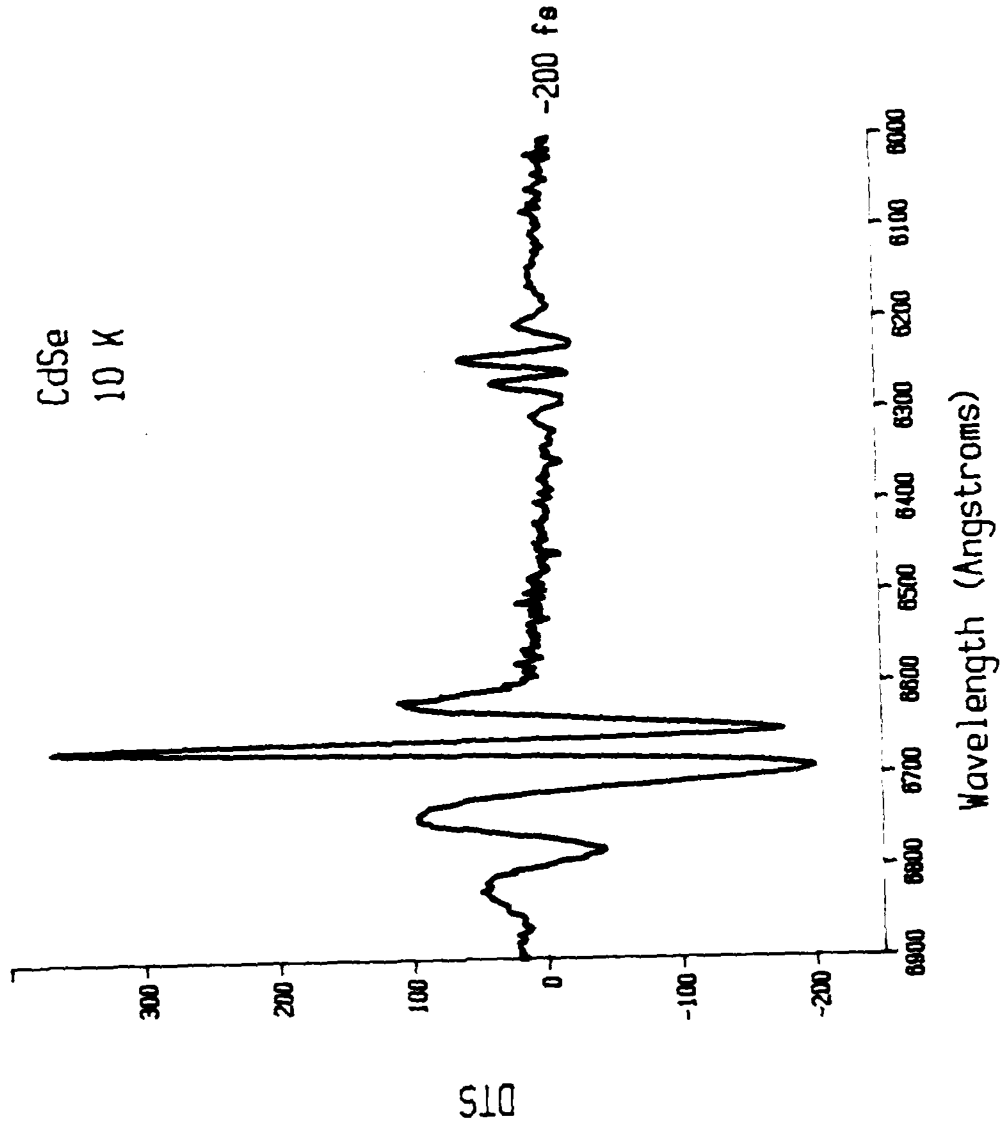

CdSe
10 K
-200 fs
DTS
300
200
100
0
-100
-200
6900
6800
6700
6600
6500
6400
6300
6200
6100
6000
Wavelength (Angstroms)

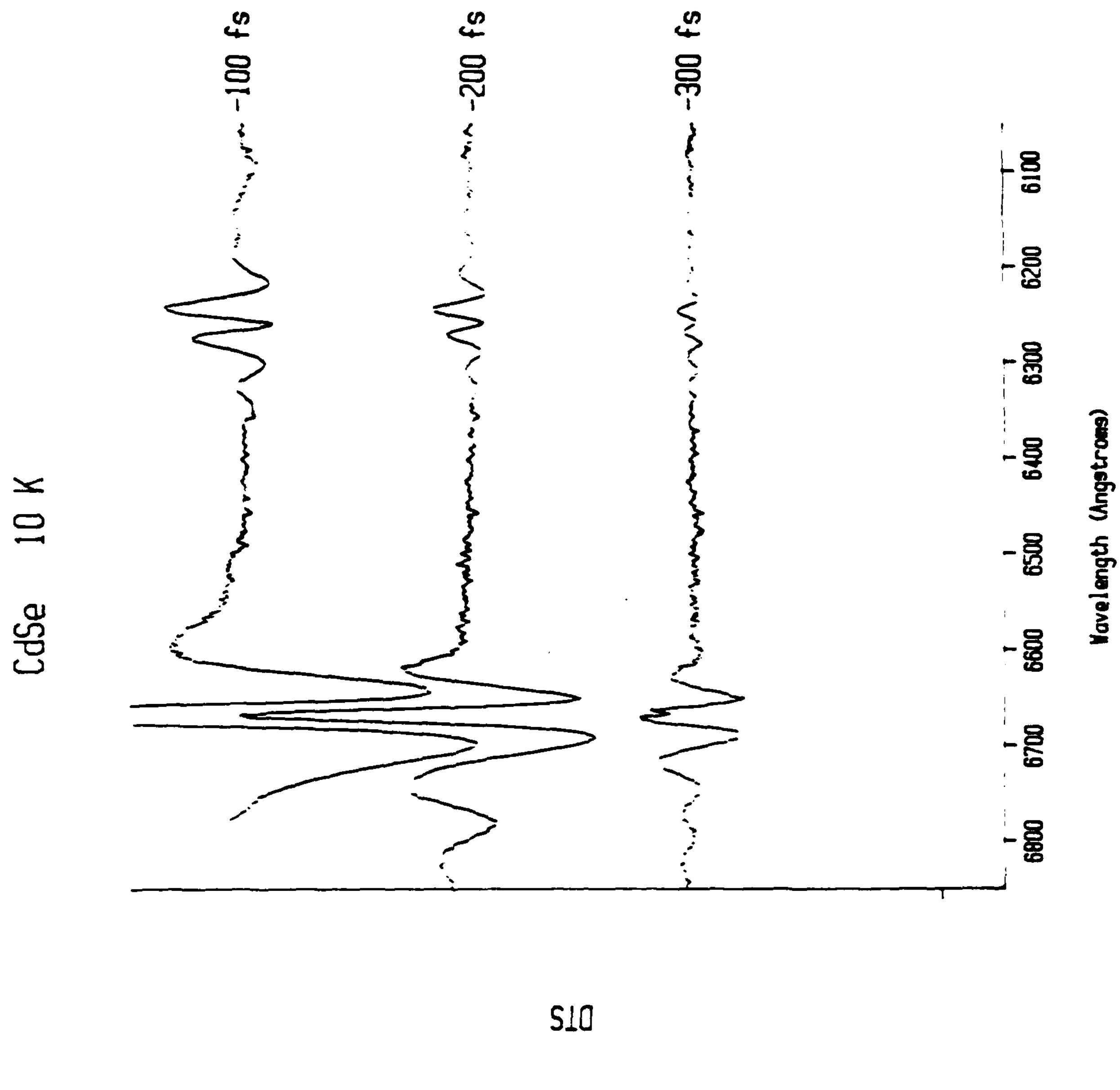
CdSe 10 K
-100 fs
-200 fs
-300 fs
6800
6700
6600
6500
6400
6300
6200
6100
Wavelength (Angstroms)
DTS

SEMICLASSICAL THEORY

- Treat Fields Classically and Material Response Q.M.

$$E(t) = \underbrace{E_L(t)e^{i(\vec{k}_L\cdot\vec{r}-\Omega_L t)}}_{\text{pump}} + \underbrace{E_p(t)\,e^{i(\vec{k}_p\cdot\vec{r}-\Omega_L t)}}_{\text{probe}}$$

$$\frac{\partial}{\partial x}E_p + \frac{1}{c}\frac{\partial}{\partial t}E_p = \frac{i\Omega}{2\varepsilon_0 c}\underbrace{P_p}_{\text{Induced Medium polarization}}$$

$$P_p(t) = \int_{-\infty}^{t} dt'\,\chi(t,t')\,E_p(t') \qquad \text{Linear Response}$$

where $\chi(t,t') = \underbrace{\chi_0(t-t')}_{\text{Unperturbed susceptibility}} + \underbrace{\delta\chi(t,t')}_{\text{perturbation caused by pump pulse}}$

$$\delta T(\omega) = DTS = \frac{|E_p(\omega)|^2_{\text{pump on}} - |E_p(\omega)|^2_{\text{pump off}}}{|E_p(\omega)|^2_{\text{pump off}}}$$

$$\delta T(\omega) \propto -\mathrm{Im}\left[\int_0^{\infty} dt\, e^{i(\omega-\Omega_L)t}\,\delta\chi(t+t_p,t_p)\right]$$

t_p = delay time

Model Semiconductor: collection of mutually independent k-states. Include Coulomb & phonon scattering phenomenologically by damping & pumping rates for each k-state.

Density Matrix Formalism, ρ for each k state

$$\frac{\partial}{\partial t}\rho_{22} = i\mu\left[E(t)\rho_{12} - E^{*}(t)\rho_{21}\right] - \Gamma\rho_{22}$$

$$\frac{\partial}{\partial t}\rho_{11} = i\mu\left[E^{*}(t)\rho_{21} - E(t)\rho_{12}\right] - \Gamma\rho_{11} + \Lambda$$

$$\frac{\partial}{\partial t}\rho_{21} = -\left[ie(k) + \gamma\right]\rho_{21} - i\mu E(t)(\rho_{22} - \rho_{11})$$

Intra-band scatt.

Γ = Decay rate for diagonal element (not recombination), population decay

γ = " " " non-diagonal ", dipole damping

$$P_k = \text{induced polarization} = \mu(\rho_{12} + \rho_{21})$$

for a single k state

get

2 = Conduction band $\qquad \mu$ = dipole matrix element

1 = Valance band

For Band-Band Region: Resonant pumping: pump resonantly excites b-b transition

Continuum of k-states

Sum over the response of all individual contributions

$$P = \sum_k P_k$$

For Exciton Region Non-resonant excitation of exciton. pump is detuned from exciton

An isolated transition

contribution of band states are neglected

Bond-Band Region:

$$\delta T(\omega) = T_0 \, Re\left\{ \int_0^\infty dt \, e^{i(\omega-\Omega_L)t} \left(e^{-2\gamma t} \times \right.\right.$$

$$\int_0^\infty dt' e^{-\Gamma t'} E_L(t_p - t') E_L^*(t_p - t' - t) + e^{-\Gamma t} \times$$

$$\left.\left. \int_0^t dt' \, e^{-(2\gamma-\Gamma)t'} E_L(t+t_p-t') \, E_L^*(t_p - t') \right) \right\}$$

Exciton Region:

For large detuning

$$\delta T(\omega) \propto \frac{1}{\Omega_L - \omega_x} \, Im\left[\frac{1}{\nu - i\Delta} \int_0^\infty dt \, |E_L(t+t_p)|^2 e^{i\Delta t} \right] + O\left[(\omega_x - \Omega_L)^{-2} \right]$$

Ω_L = pump central frequency

ν = exciton linewidth

$\Delta = \omega - \omega_x$ detuning from exciton

$$\left| \frac{\Delta T_x}{\Delta T_b} \right| \simeq \frac{\alpha_x}{\alpha_b} \left| \frac{\gamma_b + 2\gamma}{(\omega_x - \Omega_L)(5 - 6\gamma_b t_p)} \right| e^{-2\gamma_b t_p}$$

$\gamma_b = \dfrac{2 \ln 2}{\Delta t}$ $\qquad \Delta t$ = FWHM of pump pulse

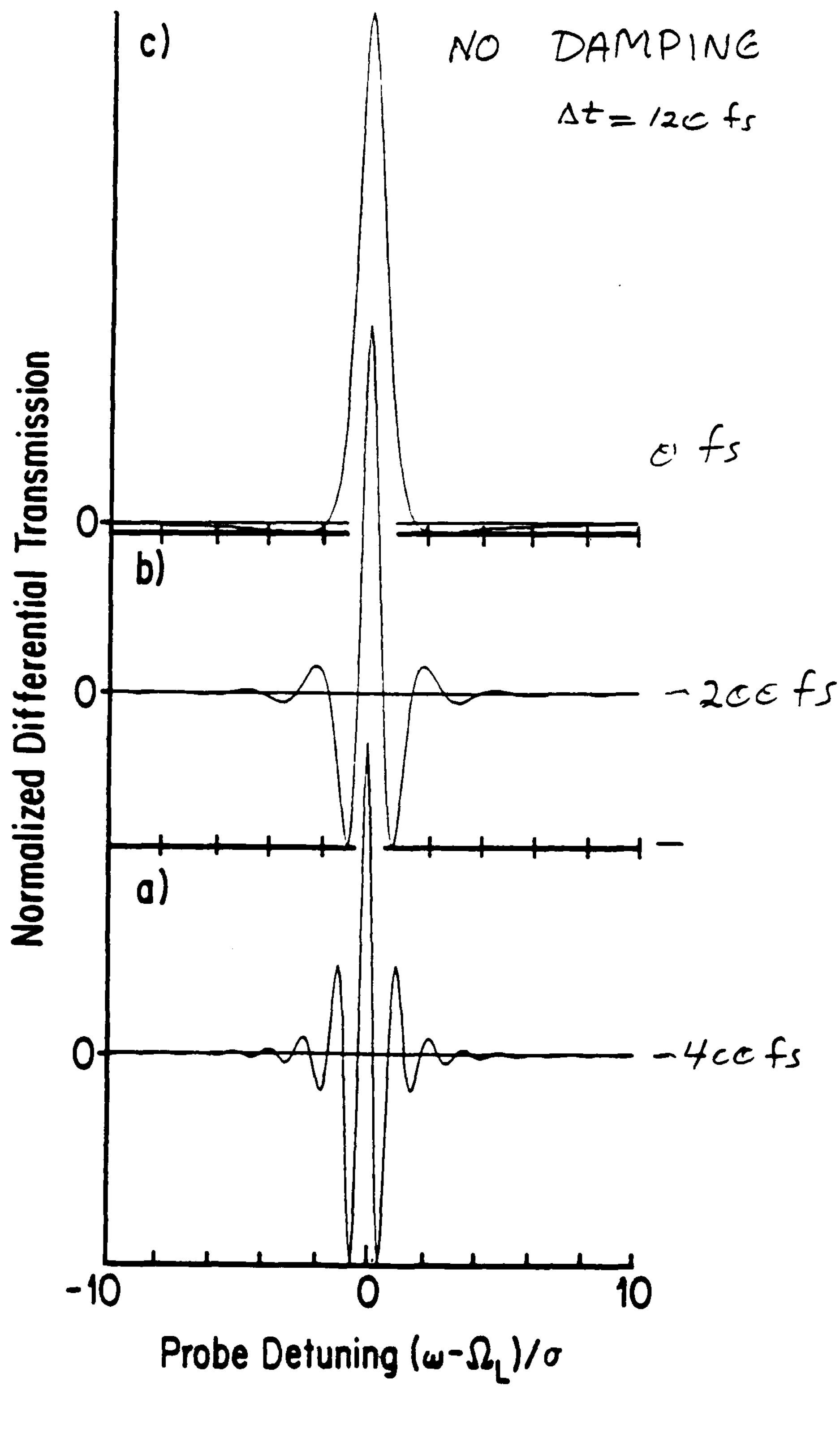

c)
NO DAMPING
Δt = 120 fs
0 fs
b)
-200 fs
a)
-400 fs
Normalized Differential Transmission
0
0
0
-10
0
10
Probe Detuning (ω-Ω_L)/σ

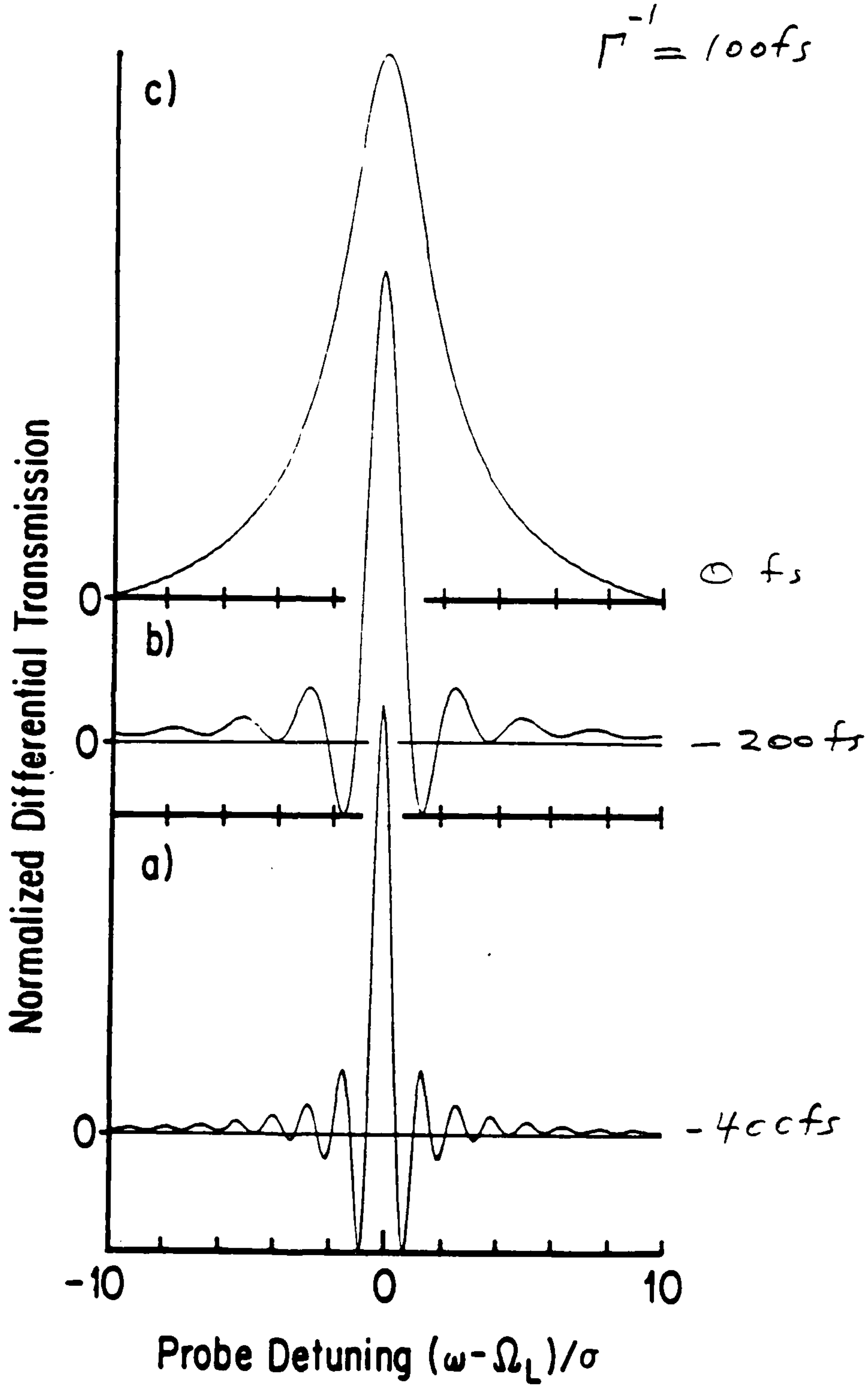
$\Gamma^{-1} = 100fs$
c)
b)
a)
0
0
0
0 fs
- 200 fs
- 400 fs
Normalized Differential Transmission
-10
0
10
Probe Detuning $(\omega-\Omega_L)/\sigma$

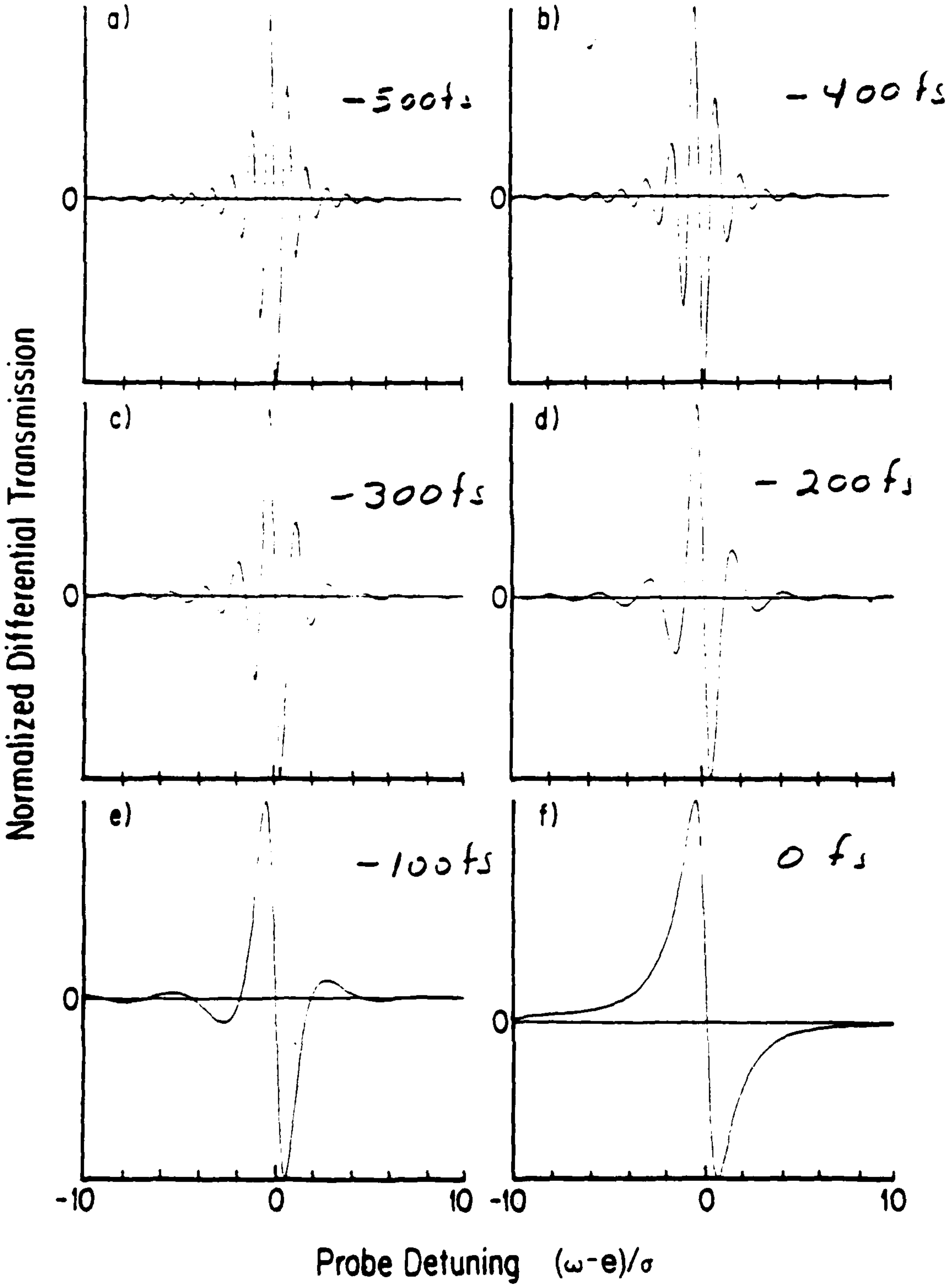

a)
-500fs
b)
-400fs
c)
-300fs
d)
-200fs
e)
-100fs
f)
0 fs
0
-10
10
Normalized Differential Transmission
Probe Detuning (ω-e)/σ

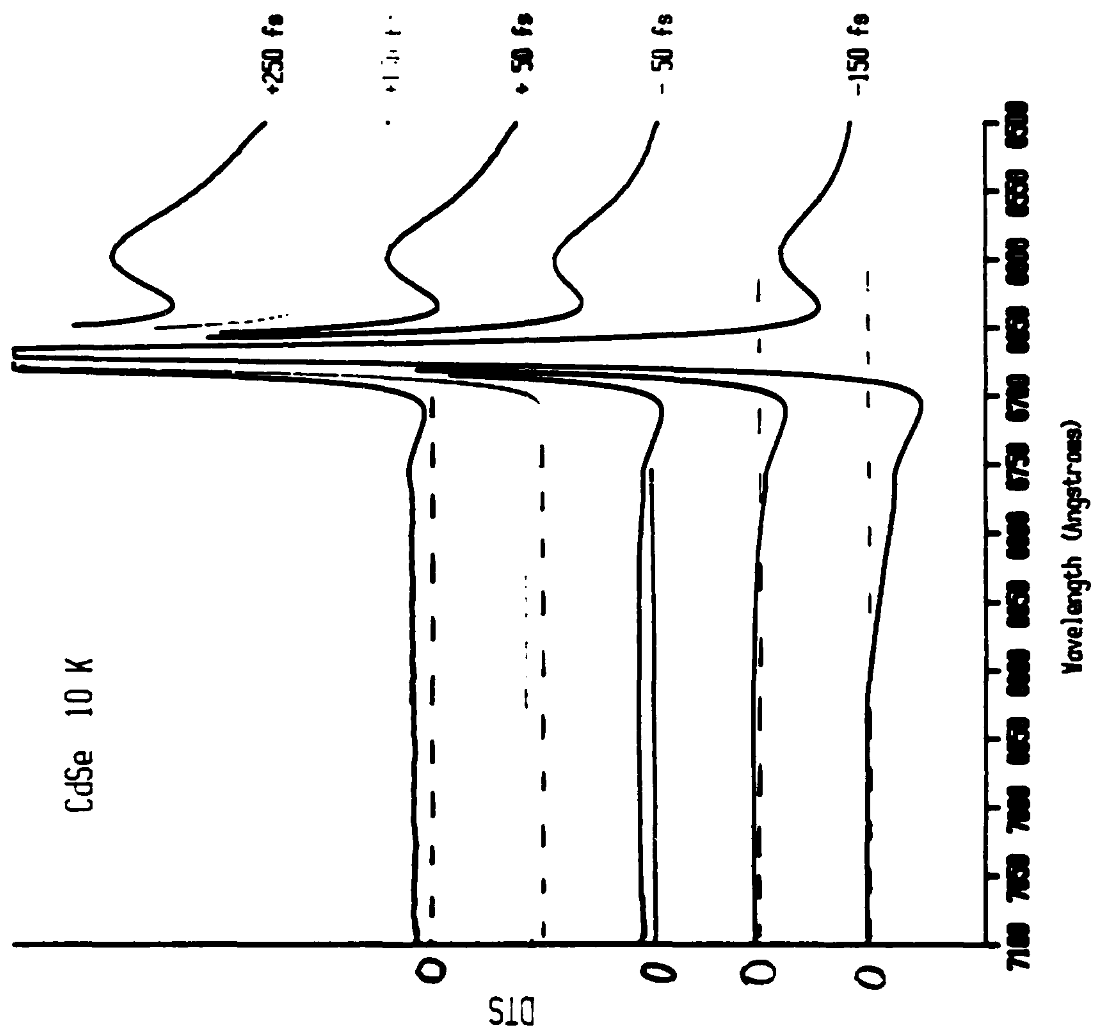
CdSe 10 K
DTS
Wavelength (Angstroms)
+250 fs
+ 50 fs
- 50 fs
-150 fs

U.S.-Japan Workshop
Monterey, 1987

Femtosecond Studies of Hot Carrier Relaxation in GaAs and AlGaAs

E. P. Ippen and J. G. Fujimoto

Department of Electrical Engineering and
Computer Science and the Research Laboratory
of Electronics
Massachusetts Institute of Technology
Cambridge, MA 02139

ABSTRACT

Femtosecond carrier dynamics in GaAs and AlGaAs thin films have been studied by femtosecond pump-probe absorption saturation spectroscopy. Identical pulse measurements monitor the rapid scattering of the carriers out of their initial, optically excited states. Multi-wavelength continuum probe investigations confirm the presence of the initial non-thermal carrier distribution as well as the appearance of state-filling throughout the band on a timescale of tens of femtoseconds.

SUMMARY

We describe a series of experiments which use femtosecond optical pulses to excite carriers in thin films of GaAs and AlGaAs semiconductors. Other, time-delayed femtosecond pulses are then used to probe the induced, and time-varying, changes in optical absorption that follow the excitation. Using pump and probe pulses of the same wavelength, we have investigated how long it takes highly excited carriers to scatter out of their

initial, excited energy distribution. These experiments were performed as a function of excitation density, pulse duration, and sample composition. For an excitation photon energy of 1.98 eV, the largest changes in behavior were found to occur with changes in Al concentration. In a second set of investigations, we have used probe pulses of various wavelengths, derived from a femtosecond continuum, to determine where the carriers go when they leave their initial excited states and how their distribution develops subsequently. In these experiments, the initial excitations can be observed directly as absorption saturation holes. Electrons are then observed to redistribute rapidly, in tens of femtoseconds, throughout the conduction band and to cool to the lattice on a slower, picosecond timescale.

The laser source for the identical-pulse experiments was a CPM ring dye laser incorporating internal prisms for control of dispersion. In addition, a pair of prisms was used external to the laser cavity to permit independent adjustment of pulse duration and chirp. Thus, we were able to produce either bandwidth-limited pulses of variable duration (35 - 150 fs) or pulses of variable chirp. Variations of both parameters were used to verify the speed and energy shifts of the carrier relaxation dynamics being observed. Pump-probe traces revealed dynamic behavior that could be separated into two different temporal regimes: a partial rapid recovery of absorption corresponding to the carriers leaving their initial excited states; and a slower, picosecond decay that can be attributed to the cooling of the distribution to the lattice via LO phonon

emission. The latter, picosecond contribution had approximately the same time constant in all samples studied. The early rapid response, however, varied in time constant from less than 30 fs for GaAs to 130 fs for AlGaAs with 0.3 mole fraction Al. This variation is due to changes in a number of factors including the initial excess energy of the carriers, simultaneous excitation of carriers from different valence bands, and the probability of intervalley scattering.

For the continuum probe experiments the output of the CPM laser was amplified with the help of a high-repetition-rate pulsed copper vapor laser. A fraction of the amplified output was split off for use as a pump beam. The remainder was focussed into a thin jet of ethylene glycol to generate a broadband continuum probe pulse. Results obtained using this system were consistent with the results described above; and they revealed, for the first time, transient absorption holes due to excitation from the split-off valence band as well as that from the light and heavy hole band. The continuum probe also confirmed that state filling throughout the band becomes evident within tens of femtoseconds of excitation.

This work was supported in part by the Air Force Office of Scientific Research Grant 85-0213. JGF acknowledges support from the National Science Foundation Presidential Young Investigator Program Grant ECS-8552701.

REFERENCES

W. Z. Lin, J. G. Fujimoto, E. P. Ippen and R. A. Logan, Proc. Internat. Conf. LASERS '86 (1986)

W. Z. Lin, J. G. Fujimoto, E. P. Ippen and R. A. Logan, Appl. Phys. Lett. vol.50, p.124 (1987)

W. Z. Lin, J. G. Fujimoto, E. P. Ippen and R. A. Logan, Appl. Phys. Lett. vol.51, p.161 (1987)

R. W. Schoenlein, W. Z. Lin, E. P. Ippen and J. G. Fujimoto, Appl. Phys. Lett. in press

HOT CARRIER RELAXATION IN SEMICONDUCTORS

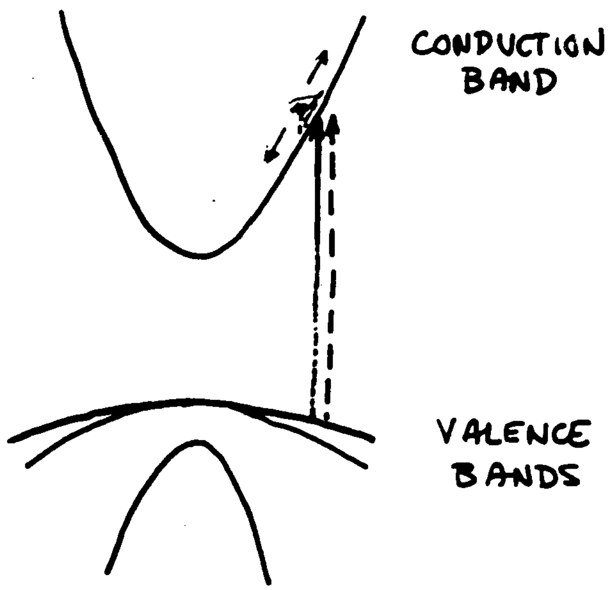

FEMTOSECOND PROCESSES IN SEMICONDUCTORS

- INTERBAND ABSORPTION
  e - h PAIRS
- CARRIER-CARRIER SCATTERING
  THERMAL DISTRIBUTION
- CARRIER-PHONON SCATTERING
  EQUILIBRATION WITH
  LATTICE

INTERVALLEY TRANSFER

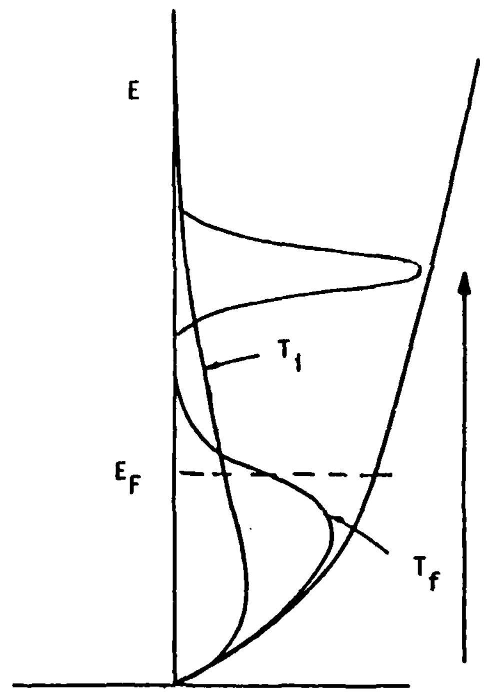

THIN FILM GaAs SAMPLES

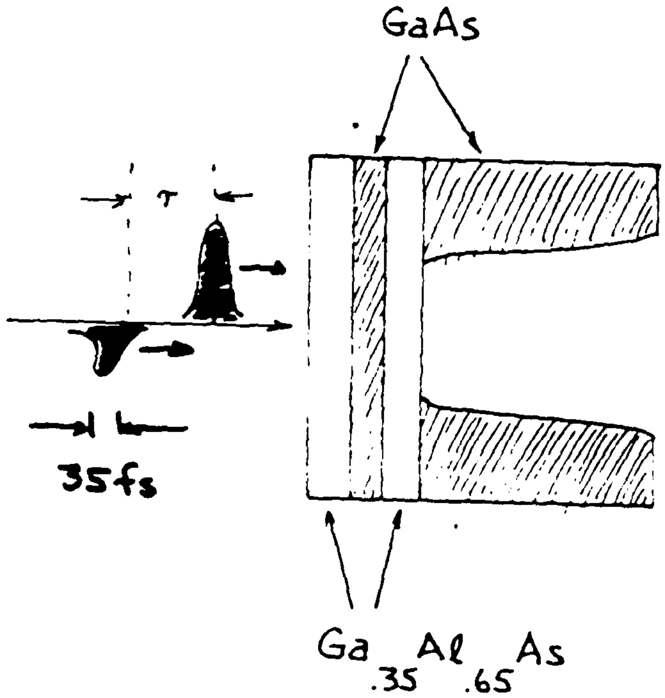

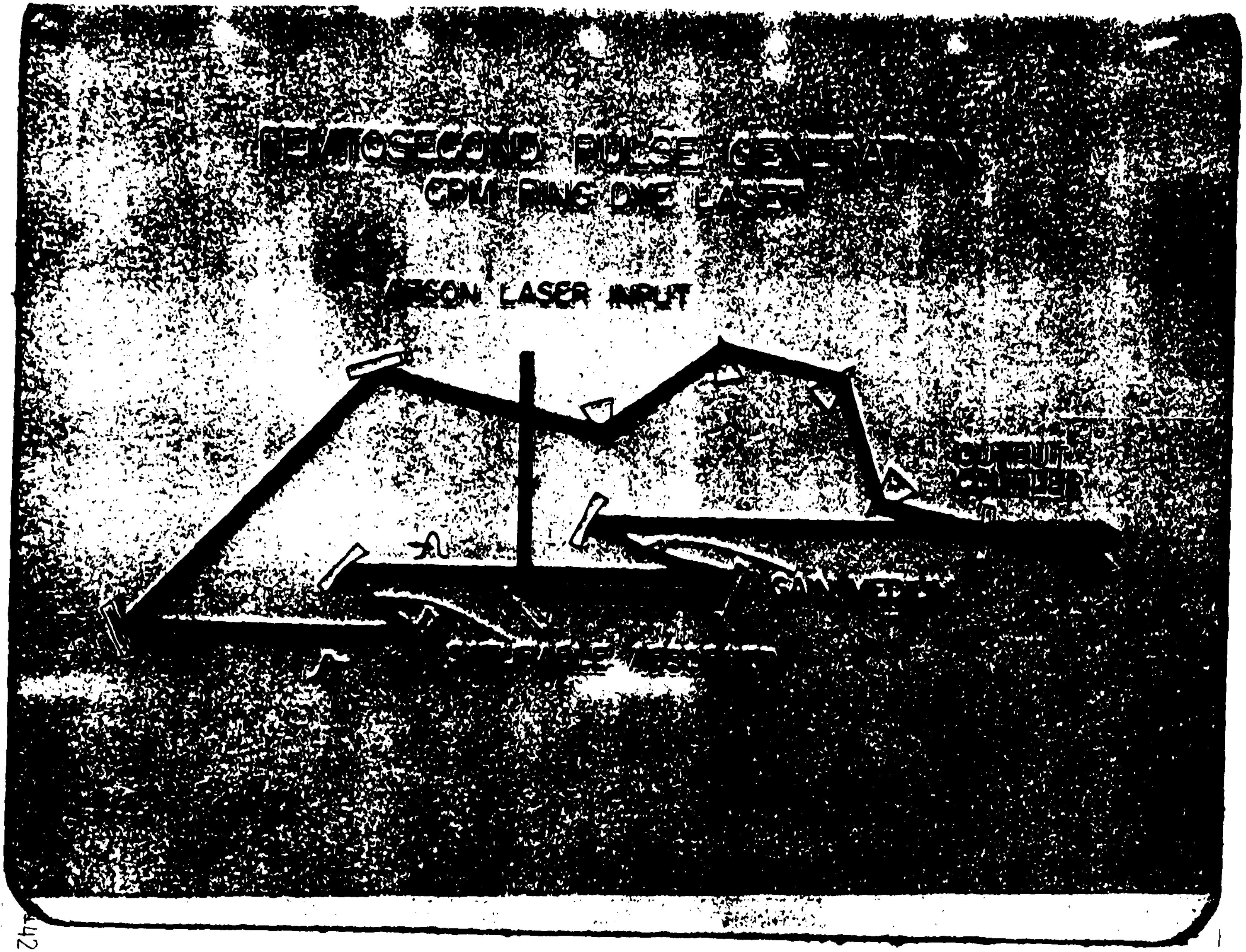
FEMTOSECOND PULSE GENERATION
CPM RING DYE
LASER INPUT

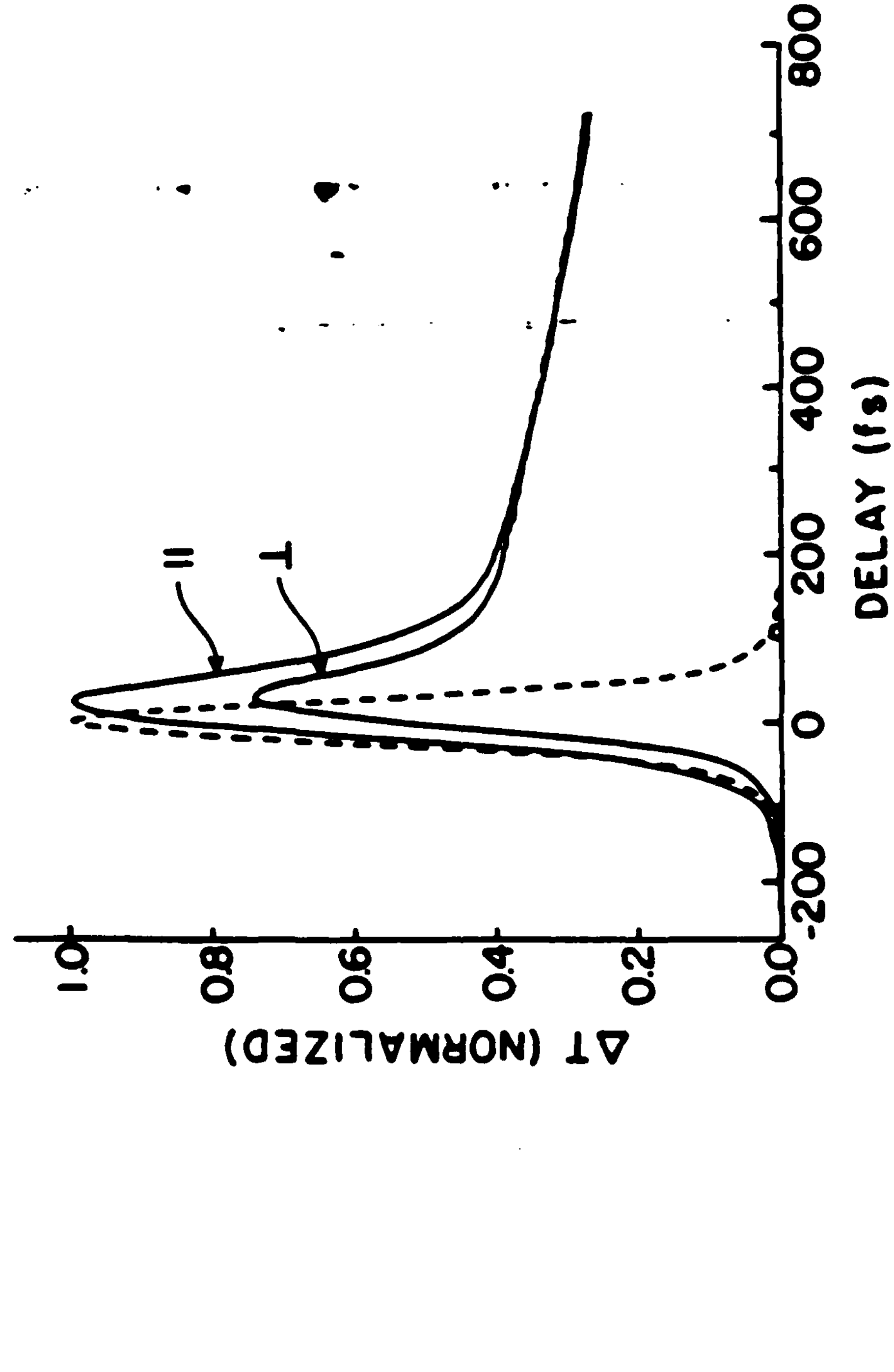
ΔT (NORMALIZED)
1.0
0.8
0.6
0.4
0.2
0.0
-200
0
200
400
600
800
DELAY (fs)
||
⊥

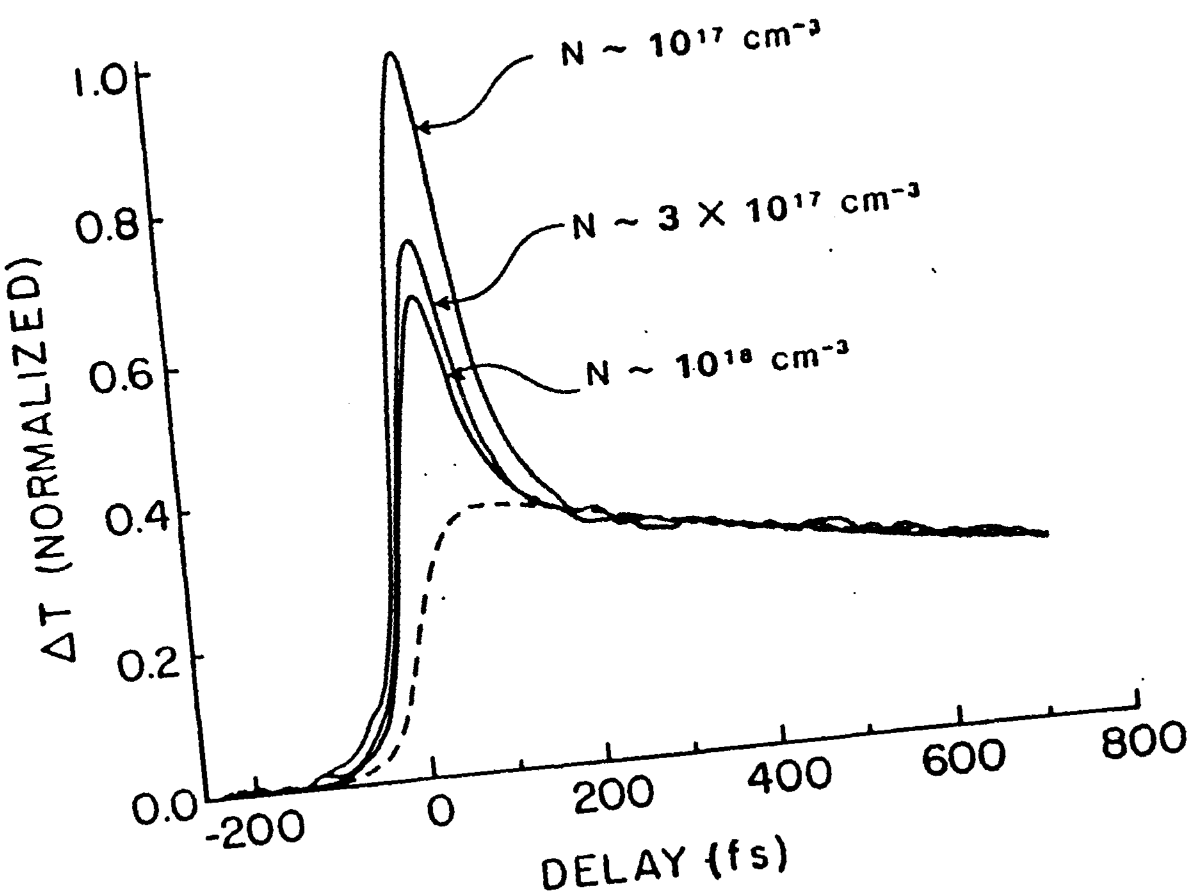
N ~ 10^{17} cm^{-3}
N ~ 3 × 10^{17} cm^{-3}
N ~ 10^{18} cm^{-3}
ΔT (NORMALIZED)
DELAY (fs)
1.0
0.8
0.6
0.4
0.2
0.0
-200
0
200
400
600
800

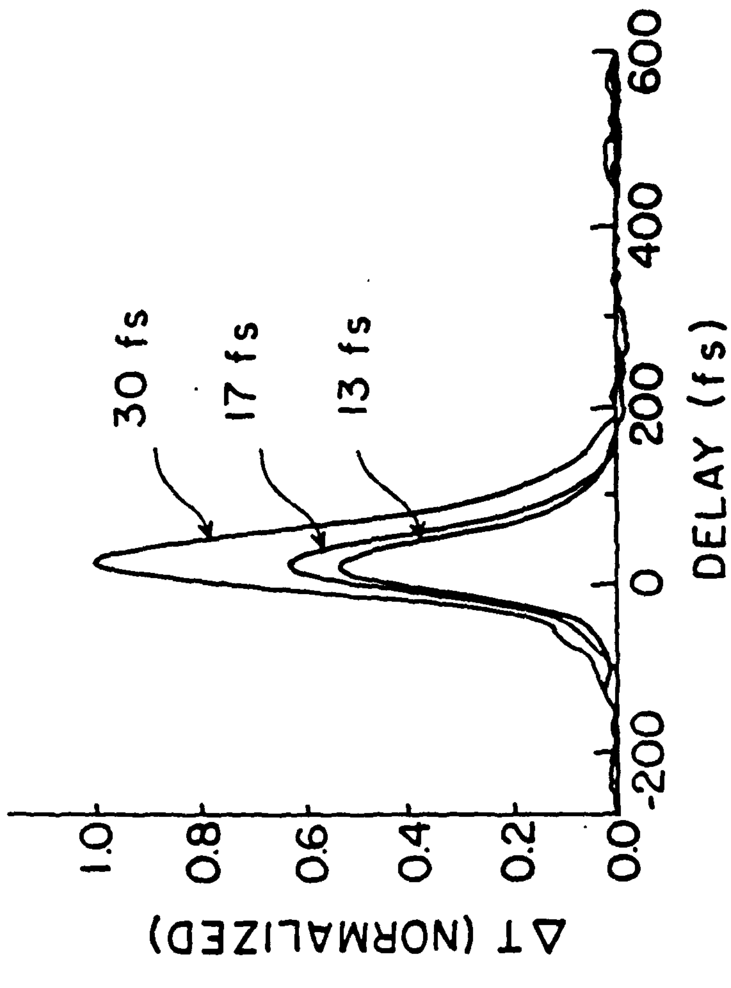
30 fs
17 fs
13 fs
ΔT (NORMALIZED)
1.0
0.8
0.6
0.4
0.2
0.0
-200
0
200
400
600
DELAY (fs)

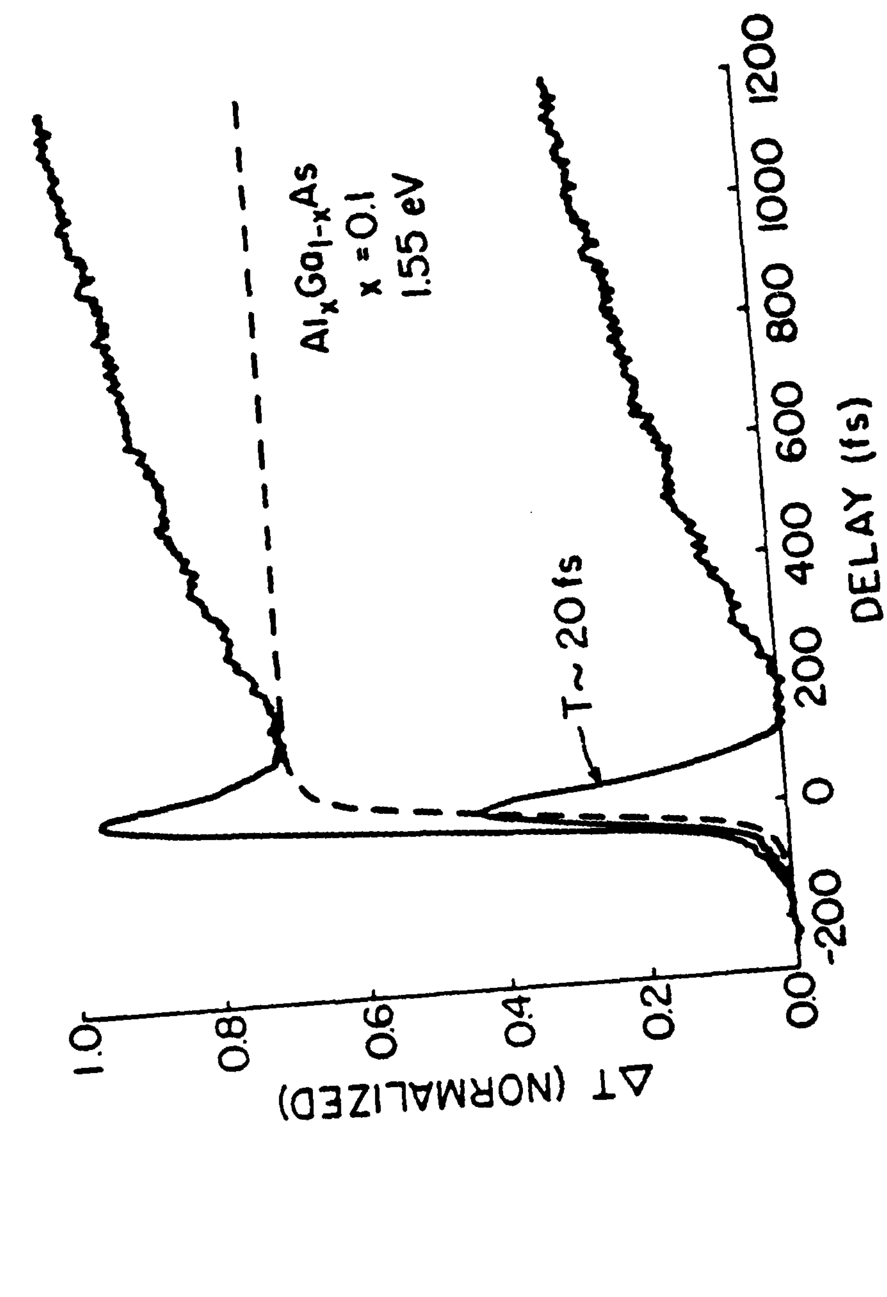

ΔT (NORMALIZED)
1.0
0.8
0.6
0.4
0.2
0.0
-200
0
200
400
600
800
1000
1200
DELAY (fs)
Al$_x$Ga$_{1-x}$As
x = 0.1
1.55 eV
T~ 20 fs

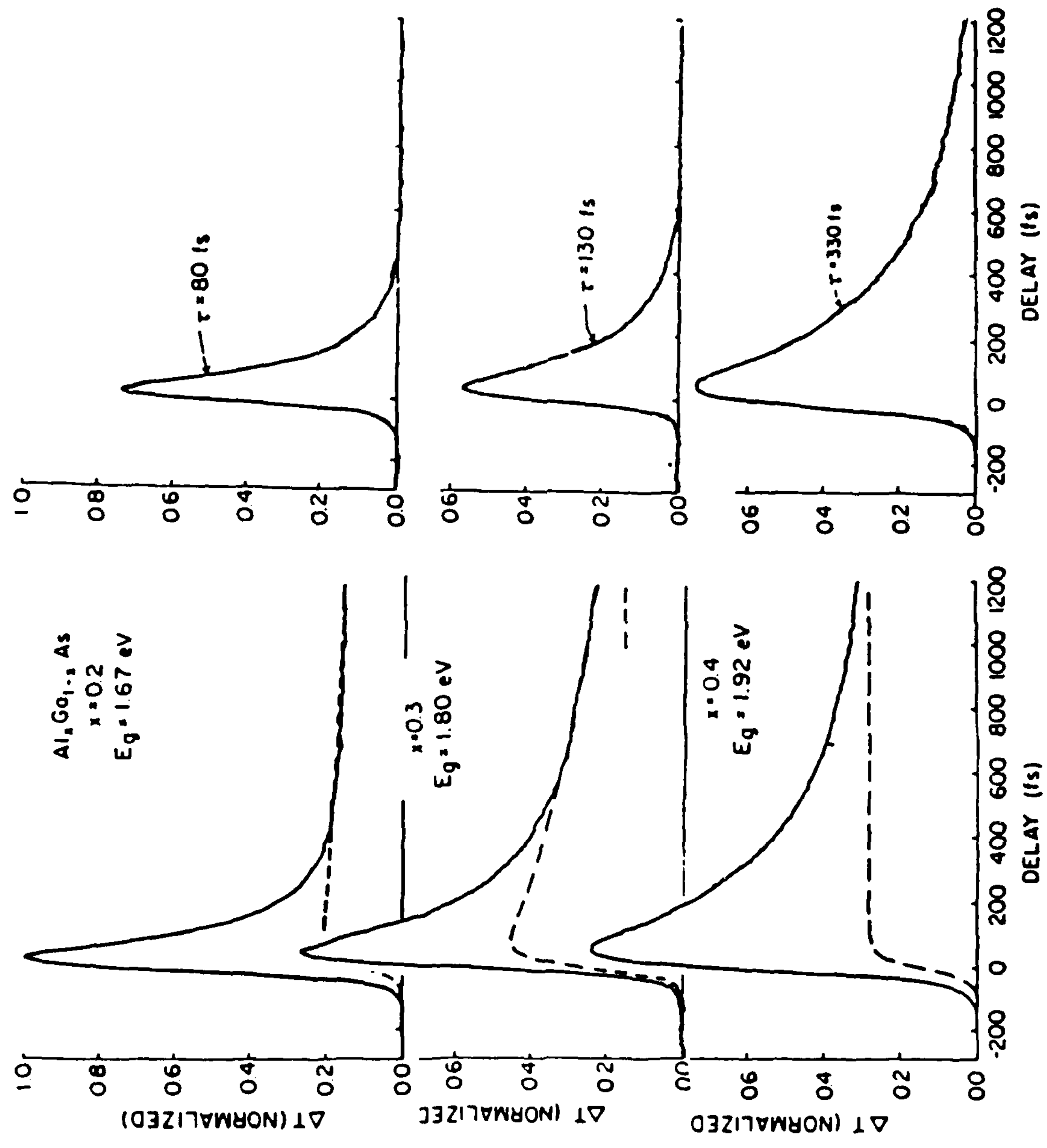

$Al_xGa_{1-x}As$
x = 0.2
E_g = 1.67 eV
x = 0.3
E_g = 1.80 eV
x = 0.4
E_g = 1.92 eV
ΔT (NORMALIZED)
ΔT (NORMALIZED)
ΔT (NORMALIZED)
DELAY (fs)
τ = 80 fs
τ = 130 fs
τ = 330 fs
DELAY (fs)

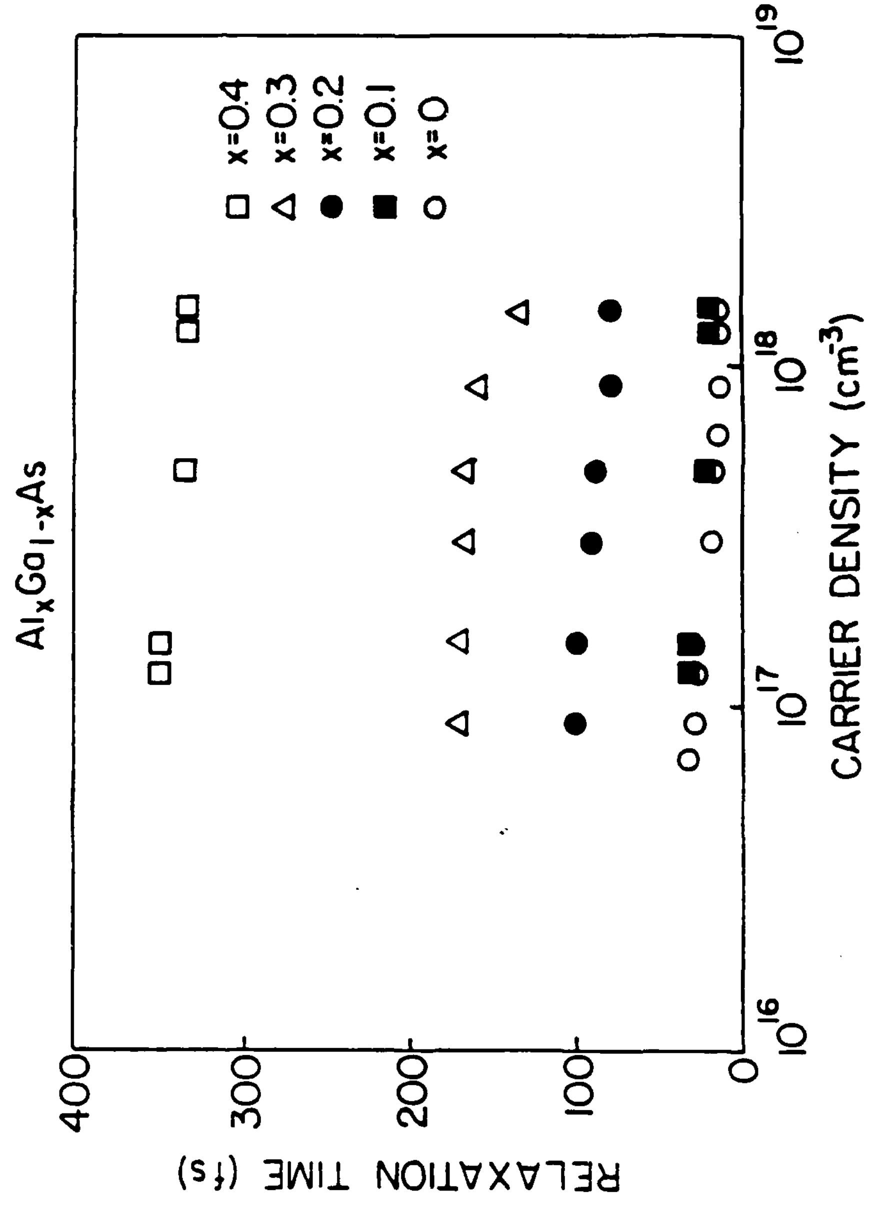
$Al_xGa_{1-x}As$
RELAXATION TIME (fs)
CARRIER DENSITY (cm^{-3})
x=0.4
x=0.3
x=0.2
x=0.1
x=0
0
100
200
300
400
10^{16}
10^{17}
10^{18}
10^{19}

CARRIER DYNAMICS

- TUNABLE PROBE

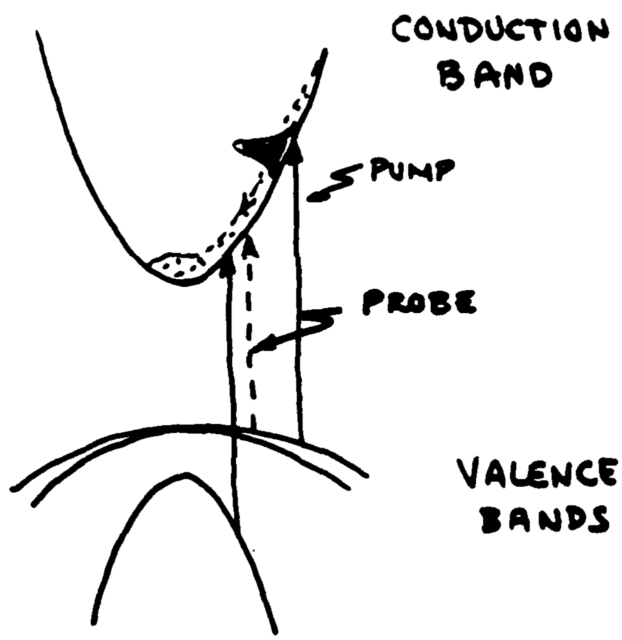

EXPERIMENTAL SCHEMATIC

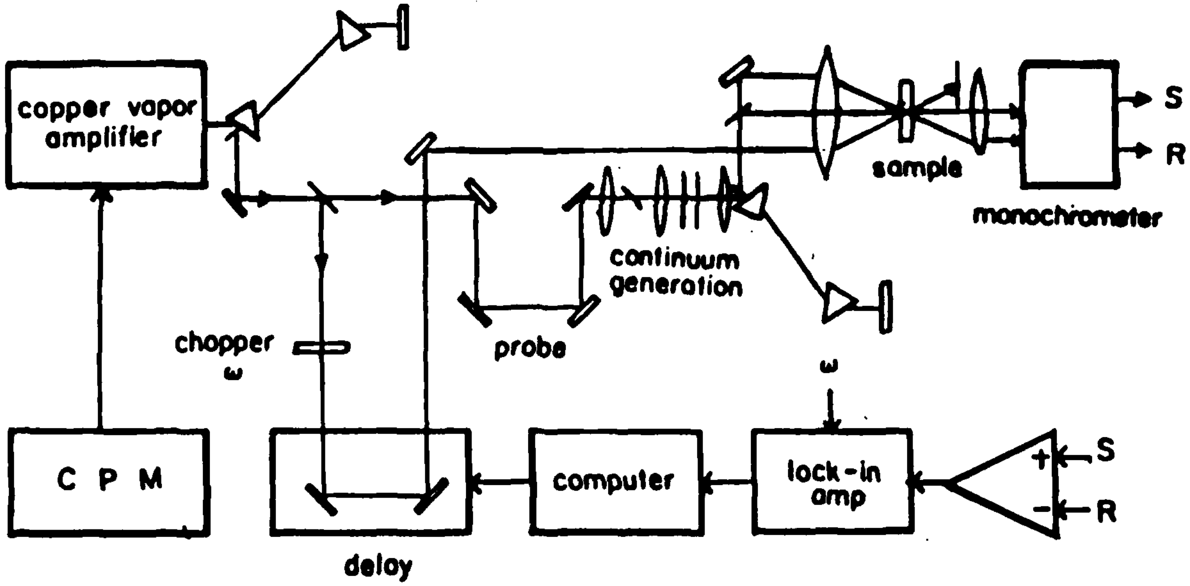

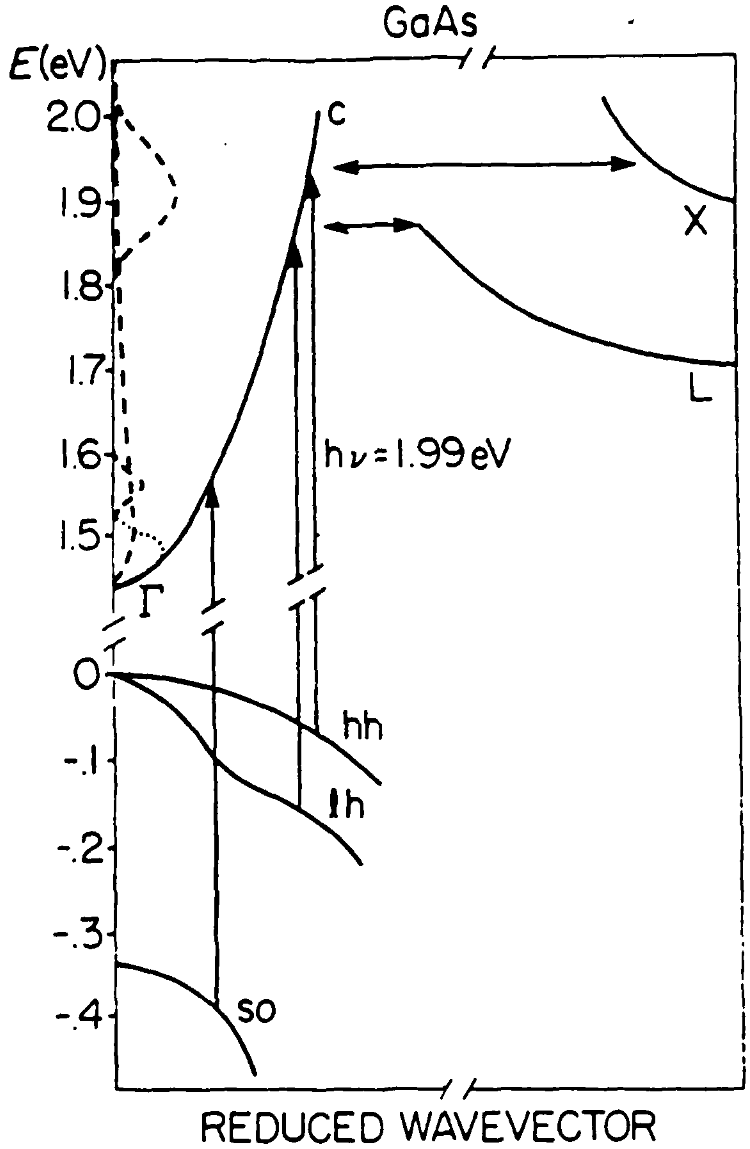
GaAs
E(eV)
2.0
1.9
1.8
1.7
1.6
1.5
0
-.1
-.2
-.3
-.4
c
X
L
Γ
hν = 1.99 eV
hh
lh
so
REDUCED WAVEVECTOR

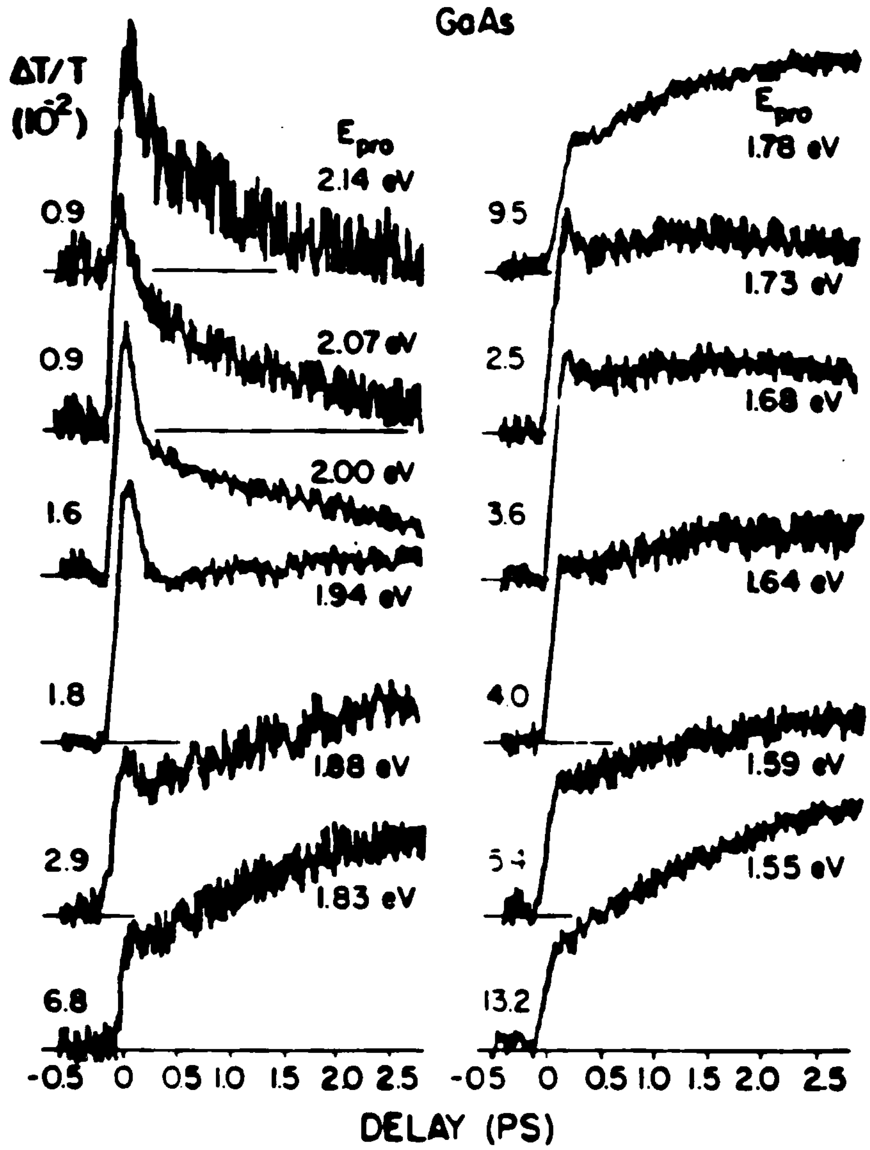

GaAs
ΔT/T
(10⁻²)
E_pro
2.14 eV
0.9
2.07 eV
0.9
2.00 eV
1.6
1.94 eV
1.8
1.88 eV
2.9
1.83 eV
6.8
1.78 eV
9.5
1.73 eV
2.5
1.68 eV
3.6
1.64 eV
4.0
1.59 eV
1.55 eV
13.2
-0.5 0 0.5 1.0 1.5 2.0 2.5
-0.5 0 0.5 1.0 1.5 2.0 2.5
DELAY (PS)

SUMMARY

FEMTOSECOND CARRIER ENERGY RELAXATION DYNAMICS

- TRANSIENT NONTHERMAL CARRIER DISTRIBUTION
  - ABSORPTION SATURATION HOLES
  - TIME SCALE $\lesssim$ PULSE DURATION
- CARRIER-CARRIER SCATTERING
  - RAPID SCATTERING TO RANGE OF ENERGIES
  - $N \sim 10^{18}$
- CARRIER-PHONON SCATTERING
  - ELECTRON COOLING
  - INTERVALLEY SCATTERING?
  - TIME SCALE $\sim$ 2 ps

Exciton Relaxation Phenomena in a Disordered System

Masaki Aihara

Department of Physics, Faculty of Liberal Arts
Yamaguchi University

Exciton relaxation phenomena in a disordered system are theoretically investigated by transient resonant light scattering and the transient optical parametric effect.

For transient resonant scattering, following observation are made. In the case of weak disorder, the fast scattering-like and the slow luminescence-like components distinctively arise in the time-resolved spectrum of resonantly scattered radiation, as shown in Fig. 1. In figures, Δ is the disorder strengh, C_A is the atomic concentration of a binary mixed crystal, γ is the inverse of the exciton lifetime, Ω_i and Ω_s are mean photon energies for incident and scattered radiation, and δ is the spectral width of incident radiation.

In the case of strong disorder, the scattering-like rapid component and the luminescence-like slow components are amalgamated as shown in Fig. 2, which reflect the diffusive motion of excitons caused by the higher-order multiple scattering of excitons due to strong disorder.

In the case of very strong disorder with the split spectrum, the quantum beat effect inherent in the excitons in mixed crystals arises as shown in Fig. 3.

For the transient optical parametric effect, a significant deviation from the exponential decay is found even in the case of relatively weak disorder, as shown in Figs. 4 and 5. This is a kind of the non-Markovian relaxation, where the memory effect associated with the exciton dephasing takes part in the problem.

In the case of strong disorder, there arises a transient response similar to the photon-echo phenomenon, as shown in Fig. 6. This is the reflction of the fact that excitons are not coherently extended in crystals, but are momentarily localized due to disorder.

Fig. 1

$C_A=0.5 \quad \Delta=0.1 \quad \gamma=0.01 \quad \Omega_i=-0.7 \quad \delta=0.1$

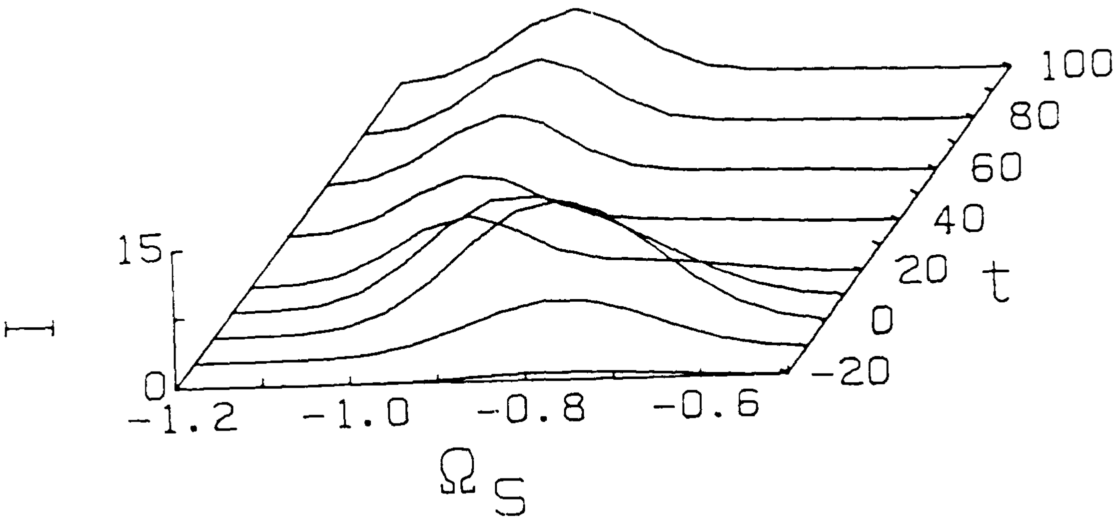

Fig. 2

$C_A=0.5 \quad \Delta=1 \quad \gamma=0.01 \quad \Omega_i=-0.988 \quad \delta=0.1$

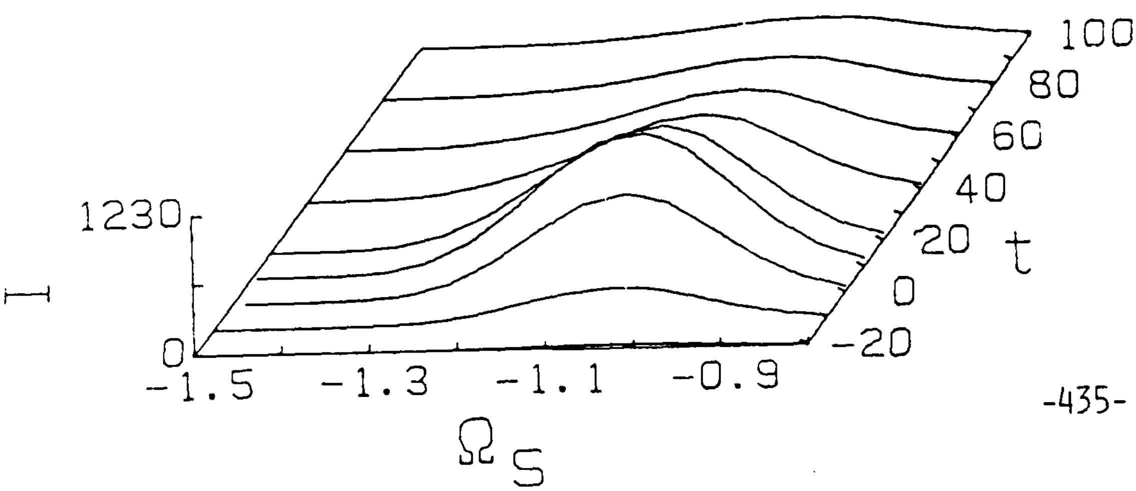

Fig. 3

$C_A=0.5 \quad \Delta=1.6 \quad r=0.2 \quad \Omega_i=0 \quad \delta=1$

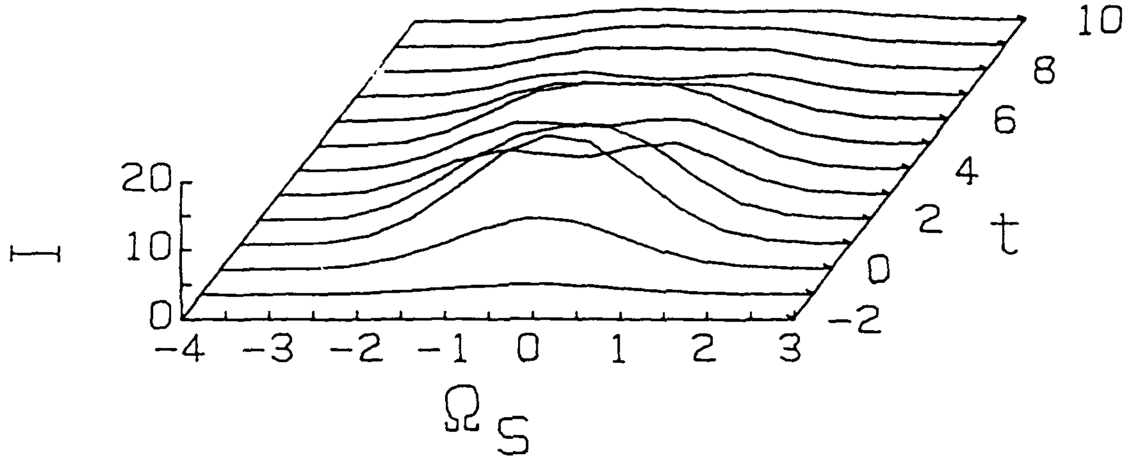

Fig. 4

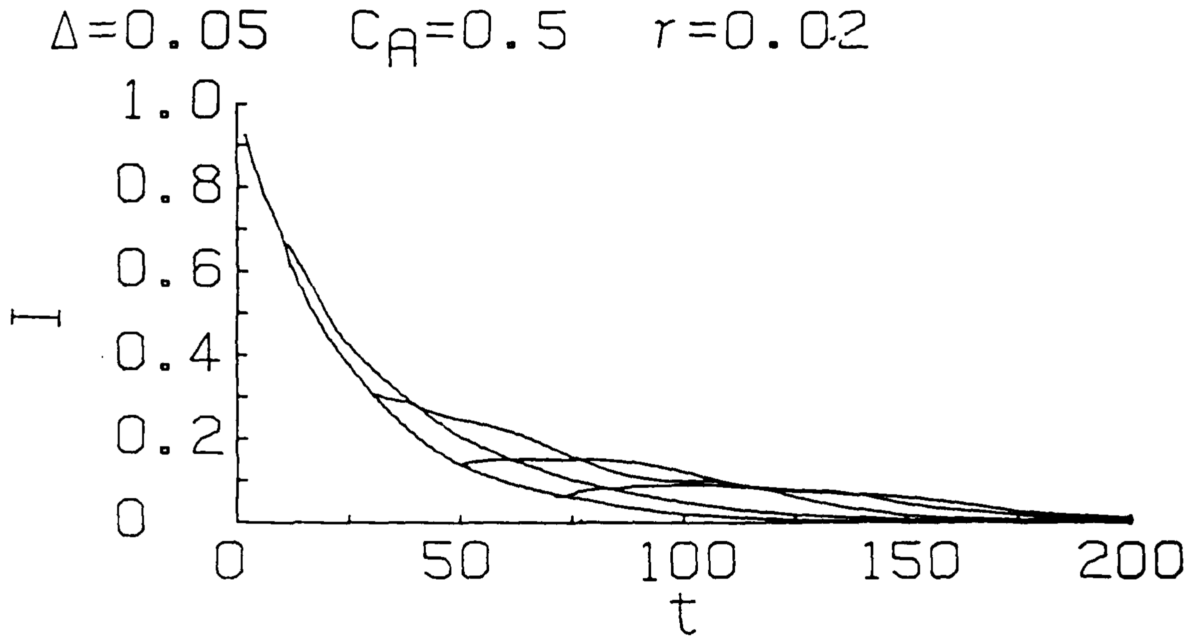

Δ=0.05 C_A=0.5 r=0.02
1.0
0.8
0.6
0.4
0.2
0
I
0
50
100
150
200
t

Fig. 5

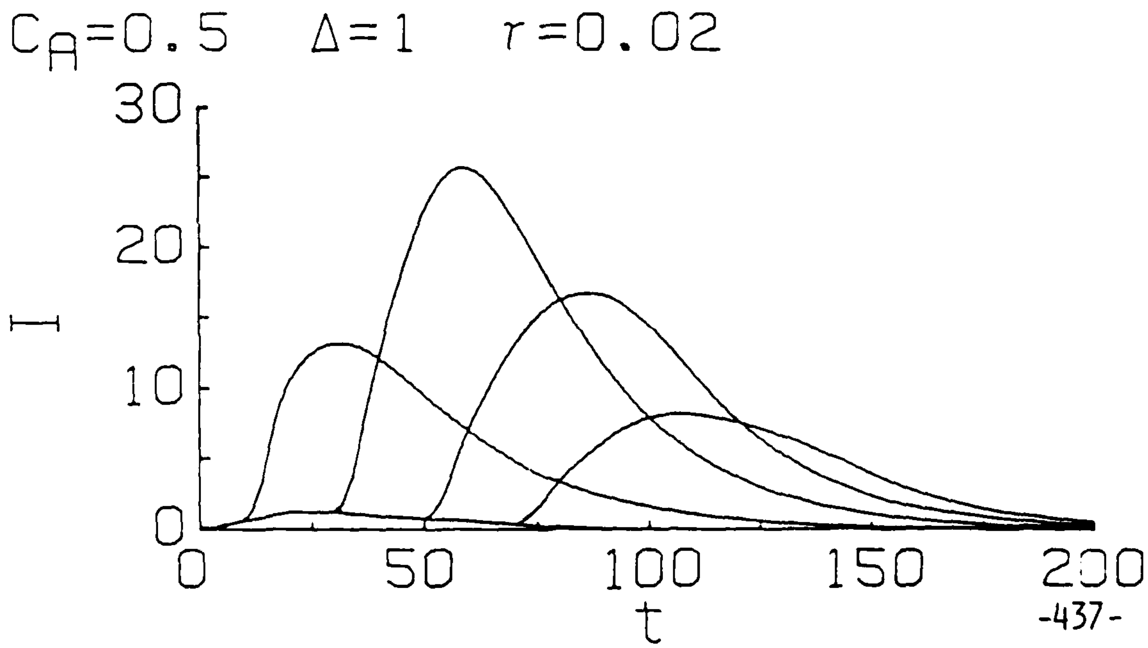

C_A=0.5 Δ=1 r=0.02
30
20
10
0
I
0
50
100
150
200
t

Generation of number-phase minimum uncertainty states

Y. Yamamoto, S. Machida, N. Imoto, M. Kitagawa and G. Björk
NTT Basic Research Laboratory
Musashinoshi, Tokyo 180, Japan

The difference between the two nonclassical lights, i.e. the squeezed state and number-phase minimum uncertainty state (NUS) is discussed. The four different generation principles for NUS are described. They are

1) unitary evolution using self-phase modulation[1],
2) nonunitary state reduction by the first kind measurement[2],
3) controlled state reduction by quantum correlation measurement-feedback[3)-5)], and
4) highly saturated laser oscillator with suppressed-pump-noise[6)-8)].

The constant current-driven semiconductor laser based on the last principle generated the NUS with photon number noise reduced below the standard quantum limit by 40% in the entire frequency region from dc to 1.1GHz. Several applications of NUS including quantum communication[9], quantum mechanical computers[10] and interferometric gravitational detection are discussed briefly.

1) M. Kitagawa and Y. Yamamoto, Phys. Rev. A34, 3974 (1986)
2) M. Kitagawa, N. Imoto and Y. Yamamoto, Phys. Rev. A35, 5270 (1987)
3) Y. Yamamoto, N. Imoto and S. Machida, Phys. Rev. A33, 3243 (1986)

4) H. A. Haus and Y. Yamamoto, Phys. Rev. A34, 270 (1986)

5) G. Björk and Y. Yamamoto, to be published

6) Y. Yamamoto, S. Machida and O. Nilsson, Phys. Rev. A34, 4025 (1986)

7) Y. Yamamoto and S. Machida, Phys. Rev. A35, 5114 (1987)

8) S. Machida, Y. Yamamoto and Y. Itaya, Phys. Rev. Lett. 58, 1000 (1987)

9) Y. Yamamoto and H. A. Haus, Rev. Mod. Phys. 56, 1001 (1986)

10) K. Igeta and Y. Yamamoto, to be published

Generation of Number-Phase Minimum Uncertainty States

Y. Yamamoto, S. Machida, N. Imoto, M. Kitagawa and G. Björk
NTT Basic Research Laboratory

1. Squeezed state (SS) vs. Number-phase minimum uncertainty state(NUS)

2. Four generation schemes of NUS
   - unitary evolution
   - nonunitary state reduction
   - measurement- feedback
   - saturated oscillator   40% below SQL from dc to 1.1 GHz

3. Applications

Minimum Uncertainty States

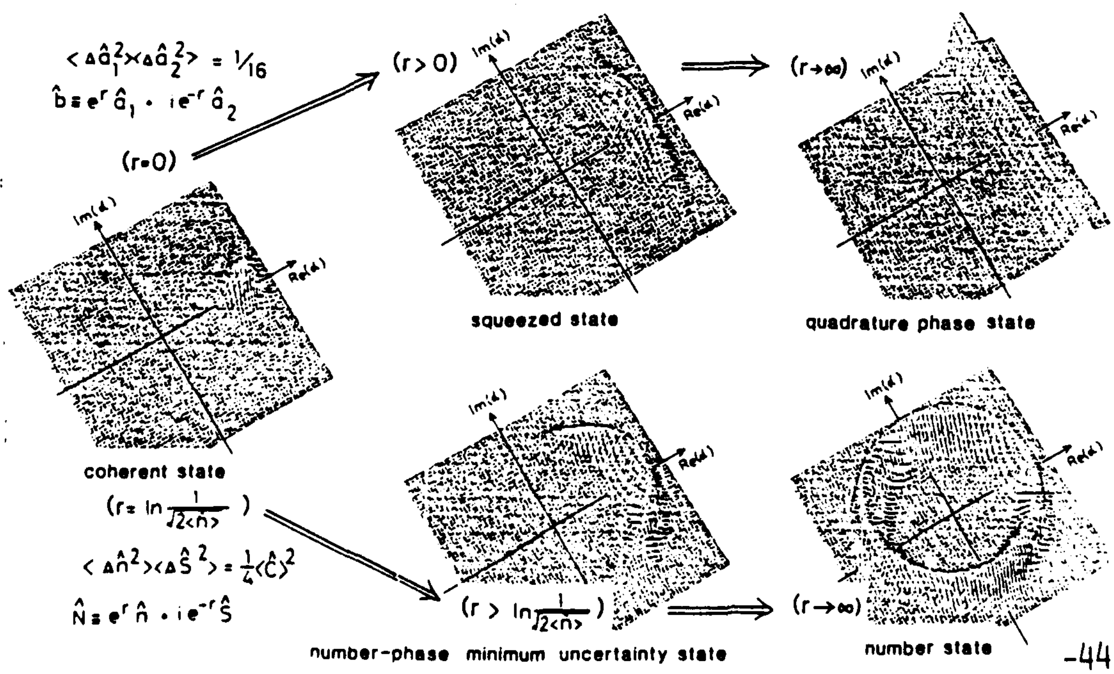

Four different generation schemes of NUS

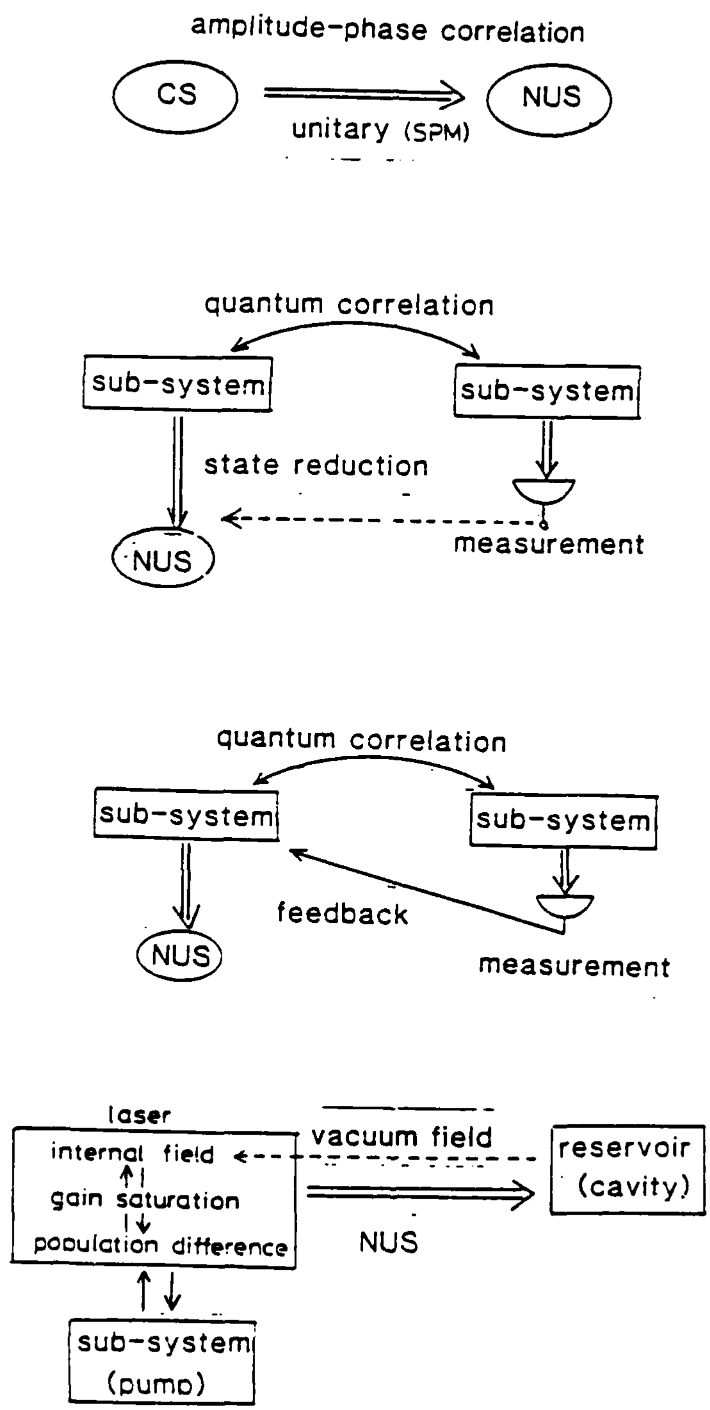

Unitary Evolution for NUS Generation

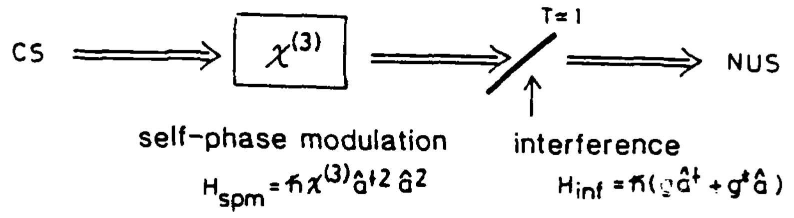

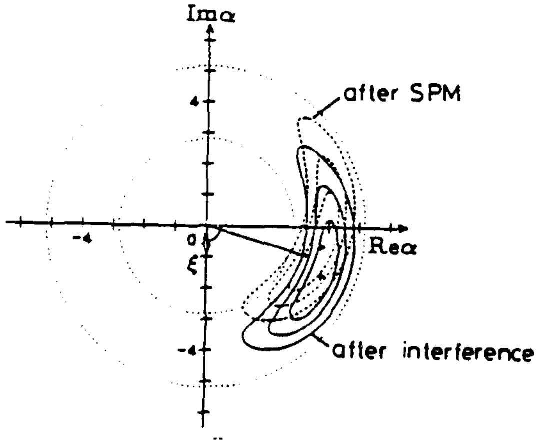

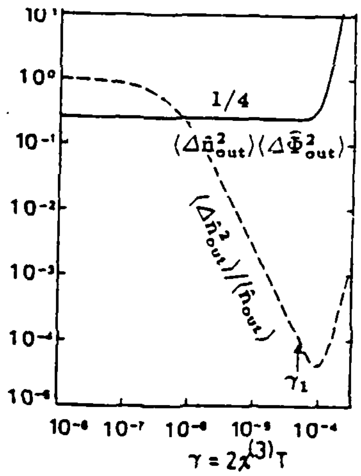

	Squeezed state	Number-phase minimum uncertainty state
Configuration	spatially nondegenerate four wave mixing	spatially degenerate four wave mixing
Interaction Hamiltonian	$H_I = \frac{\hbar}{2}(\chi\hat{a}^{\dagger 2} + \chi^*\hat{a}^2)$	$H_I = \hbar\chi\hat{a}^{\dagger 2}\hat{a}^2$
Interaction type	Active (amp./deamp.)	Passive (SPM)
QPD	elliptic 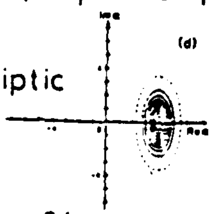	crescent 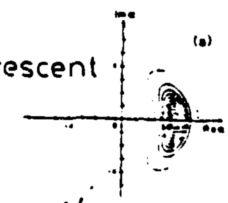
$\langle\Delta\hat{n}^2\rangle_{min}$	$\sim\langle\hat{n}\rangle^{2/3}$	$\sim\langle\hat{n}\rangle^{1/3}$

Nonunitary State Reduction by 1st kind Measurement

$$\hat{\rho}_0 = |\alpha\rangle_{aa}\langle\alpha| \otimes |0\rangle_{bb}\langle 0| \xrightarrow[U=\exp[i\eta(\hat{a}^\dagger\hat{b}^\dagger+\hat{a}\hat{b})]]{} \hat{\rho}_{ab} = U\hat{\rho}_0 U^\dagger$$

$$\hat{\rho}_a^{(meas)} \xrightarrow[\text{projection postulate}]{} Tr_b(|n\rangle_{bb}\langle n|\,\hat{\rho}_{ab})$$

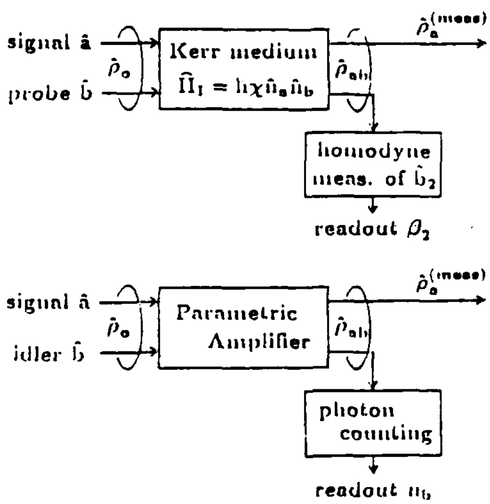

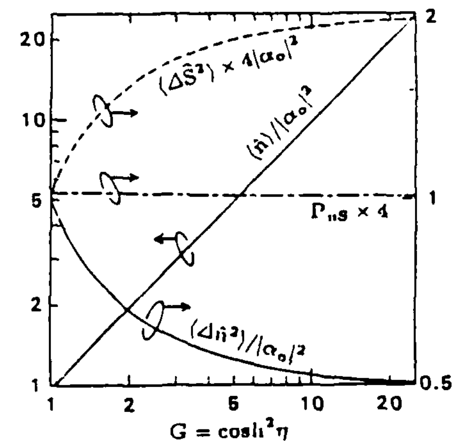

Optical Parametric Oscillator with measurement-feedback

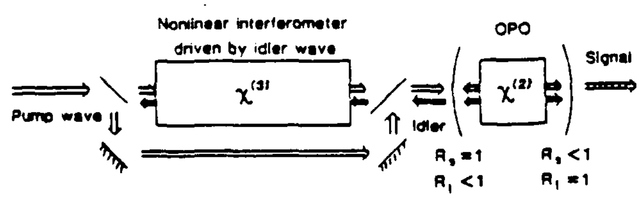

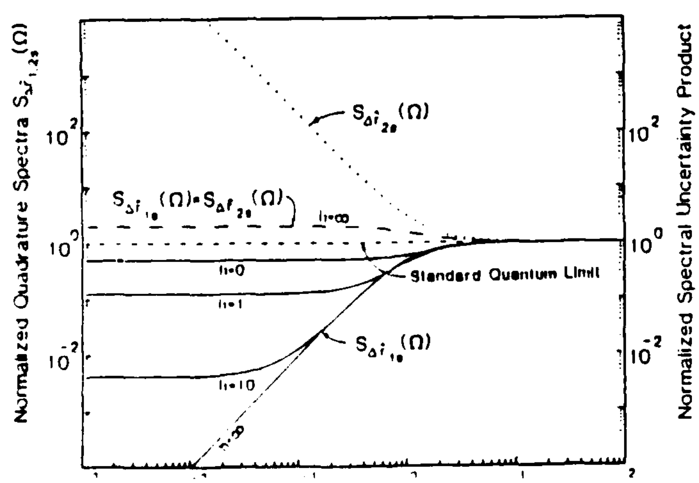

Pump-Noise-Suppressed Laser Oscillator

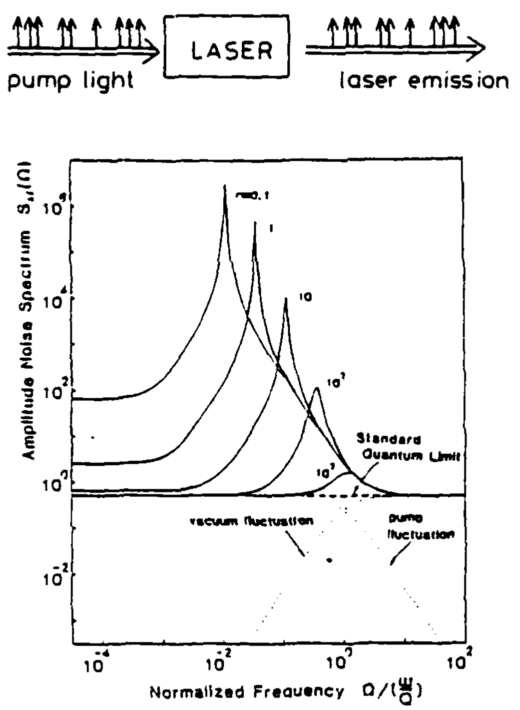

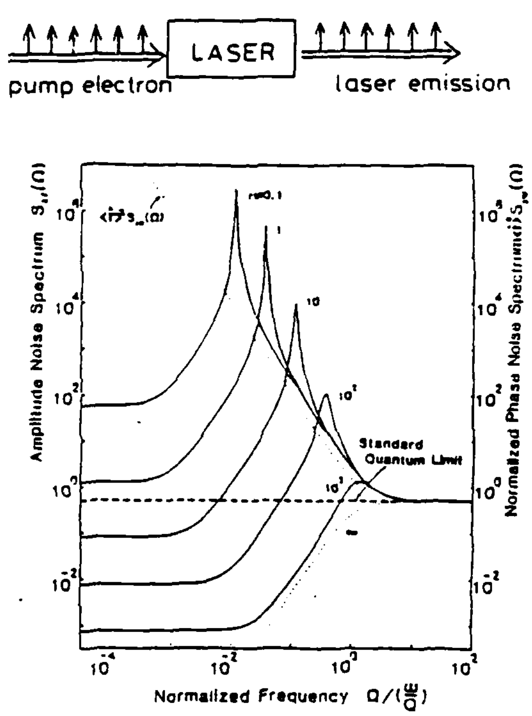

High Impedance Suppression of Pump Current Noise

$V_J = V - R_s I$

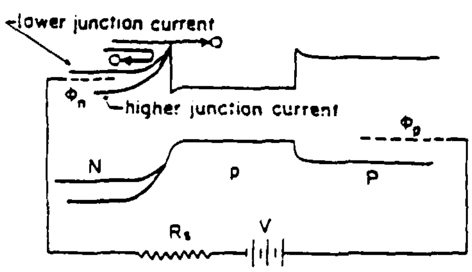

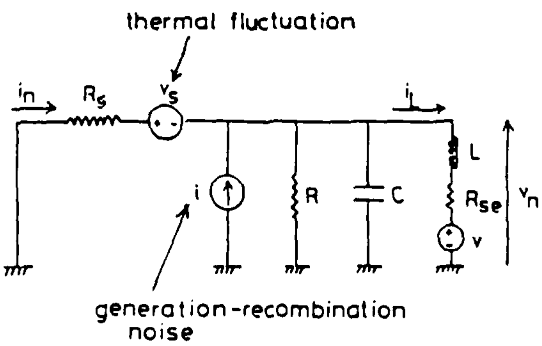

$R_s \ll 2R \Longrightarrow S_{v_n}(\Omega) \longrightarrow 0$ (constant voltage operation)

$R_s \gg 2R \Longrightarrow S_{i_n}(\Omega) \longrightarrow 0$ (constant current operation)

Calibration of Standard Quantum Limit

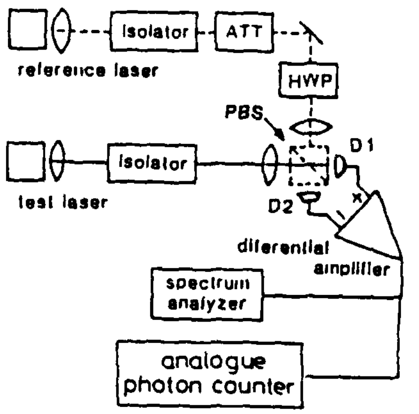

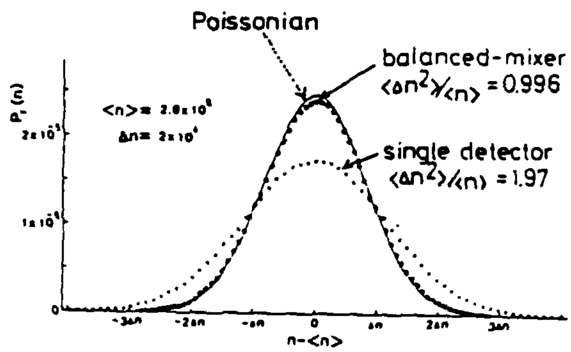

0.8 µm GaAs Transverse Junction Stripe Laser

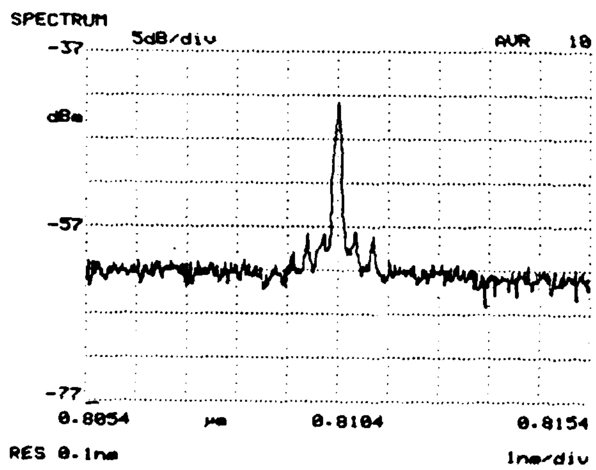

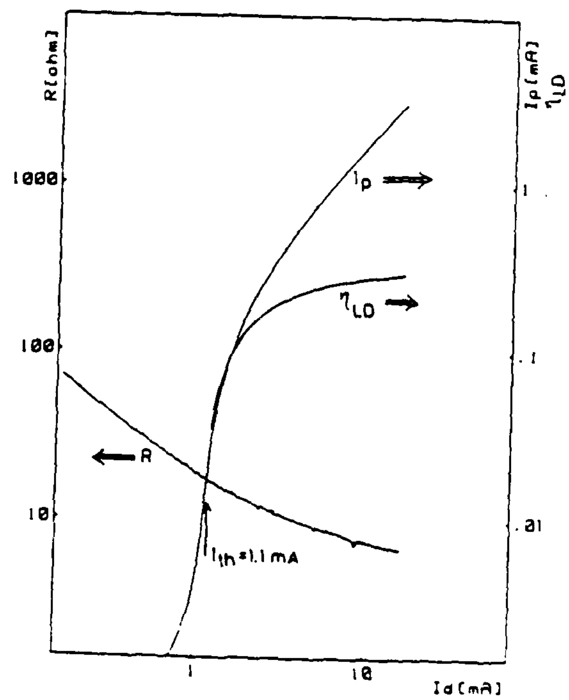

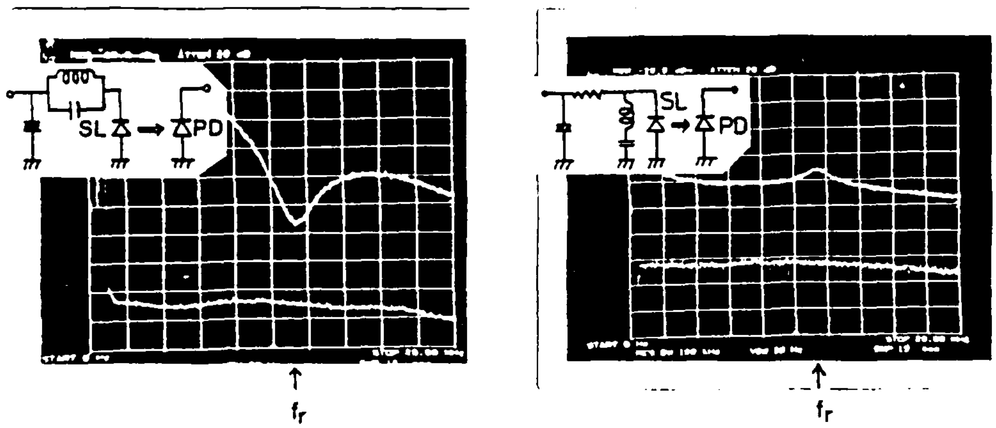

SL
PD
f_r
SL
PD
f_r

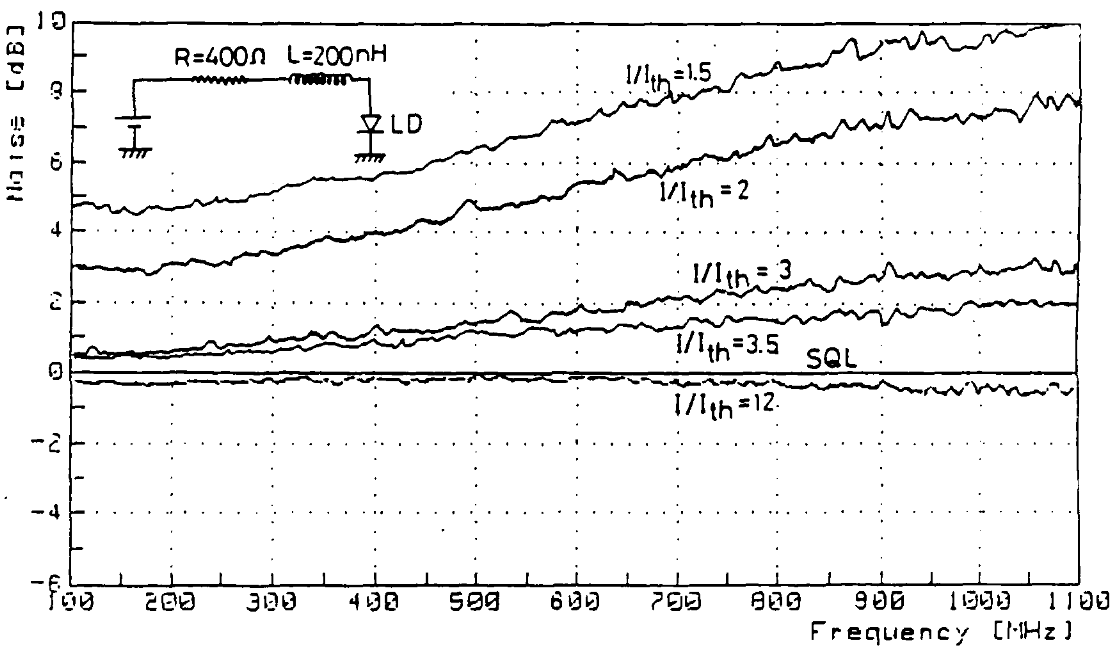

R=400Ω L=200nH
LD
I/Ith=1.5
I/Ith=2
I/Ith=3
I/Ith=3.5
SQL
I/Ith=12
Noise [dB]
Frequency [MHz]

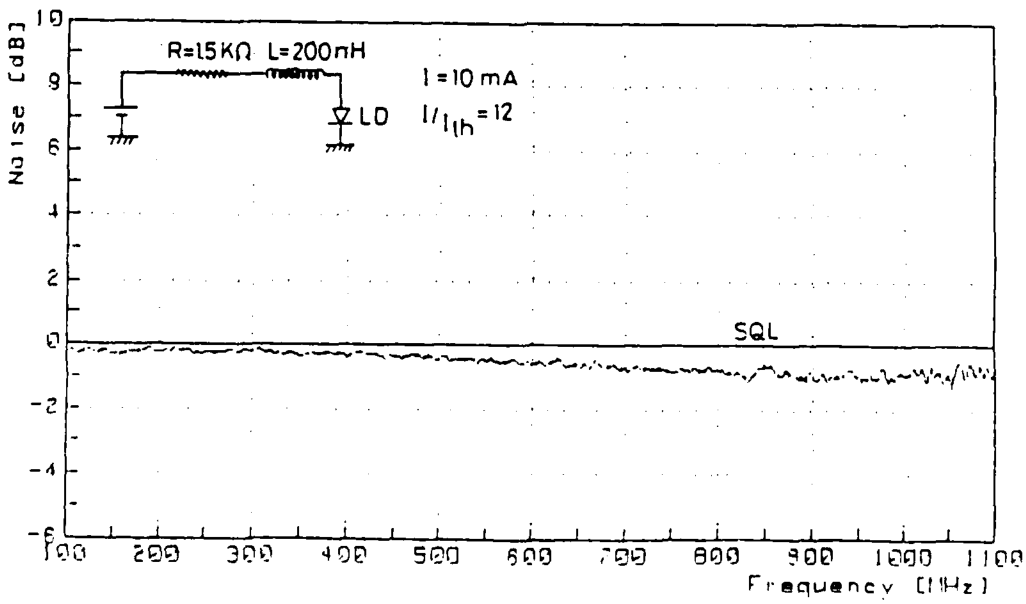

R=1.5KΩ L=200nH
LD
I=10 mA
I/Ith=12
SQL
Noise [dB]
Frequency [MHz]

AMPLITUDE SQUEEZING vs. OPTICAL LOSS

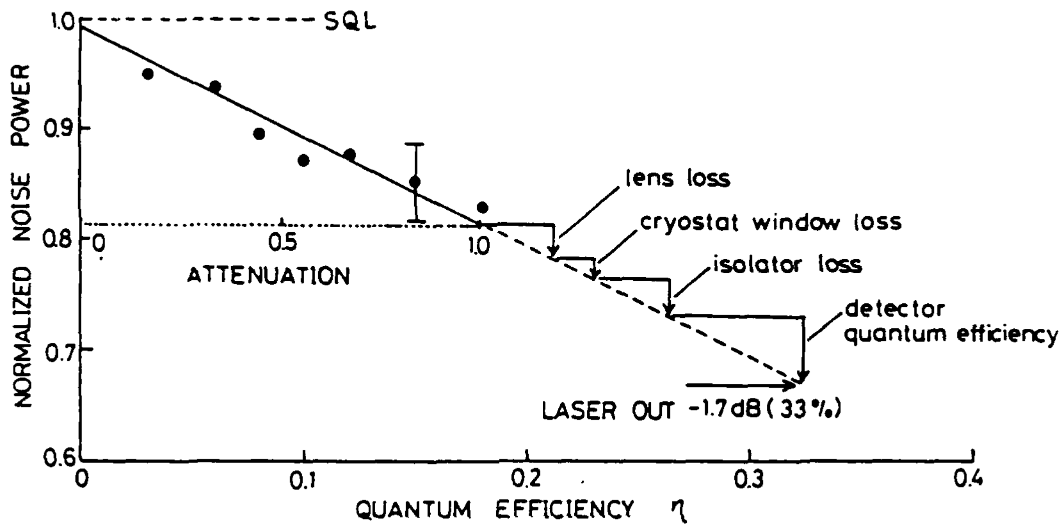

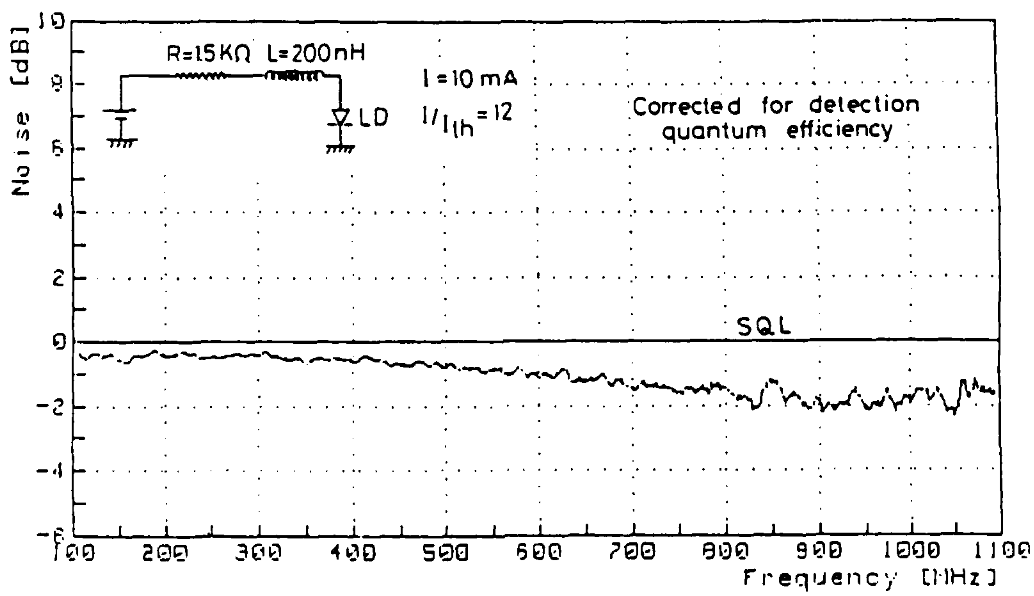

1.5μm InGaAsP Distributed Feedback Laser

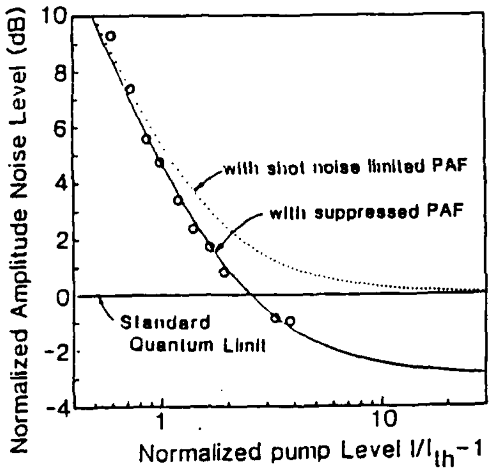

Application I —Quantum Communication —

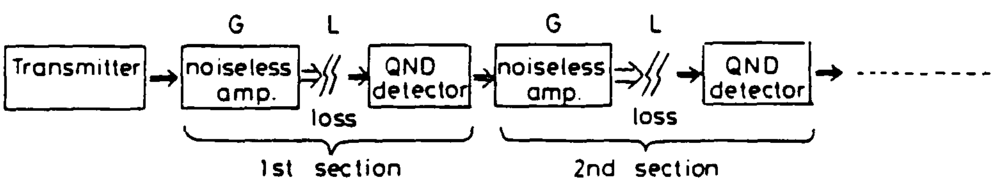

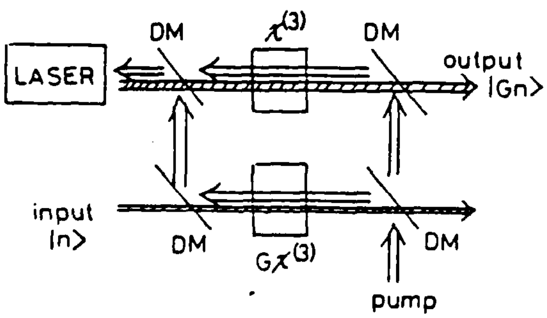

Noiseless photon amplifier

$$
S/N = \begin{cases}
\dfrac{\langle \hat{n}_s \rangle^2}{\langle \Delta \hat{n}_s^2 \rangle + \frac{1-L^m}{L^m}\langle \hat{n}_s \rangle} \xrightarrow{\text{no gain}} L^m \langle \hat{n}_s \rangle \; (SQL) \\[2ex]
\dfrac{\langle \hat{n}_s \rangle^2}{\langle \Delta \hat{n}_s^2 \rangle + m(1-L)\langle \hat{n}_s \rangle} \xrightarrow[(GL=1)]{} \dfrac{\langle \hat{n}_s \rangle}{m} \\[2ex]
\dfrac{\langle \hat{n}_s \rangle^2}{\langle \Delta \hat{n}_s^2 \rangle + \frac{1-L}{GL-1}\langle \hat{n}_s \rangle} \xrightarrow[(GL>1)]{} \dfrac{\langle \hat{n}_s \rangle^2}{\langle \Delta \hat{n}_s^2 \rangle}
\end{cases}
$$

Application II—Quantum Mechanical Computer—

Reversible logic (Fredkin gate)

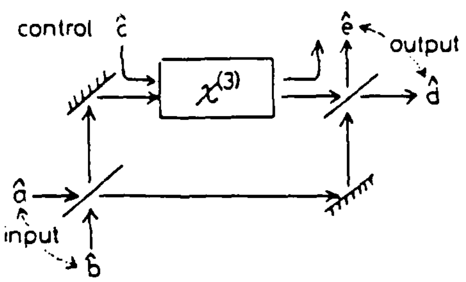

	NOT & FAN OUT	OR	AND
CONT-ROL	INPUT	INPUT1	INPUT1
input $\hat{a}$	1 PRESET	INPUT2	INPUT2
$\hat{b}$	0 PRESET	1 PRESET	0 PRESET
output $\hat{c}$	NOT	OR	GARBAGE
$\hat{d}$	FAN OUT	GARBAGE	AND

Microscopic memory (QND readout)

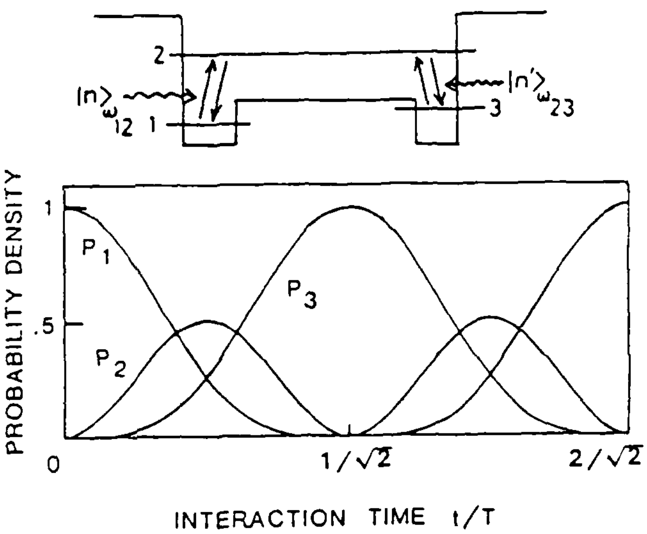

$T = \pi/g\sqrt{n} = \pi/g'\sqrt{n'}$

Application III—Gravitational Wave Detection—

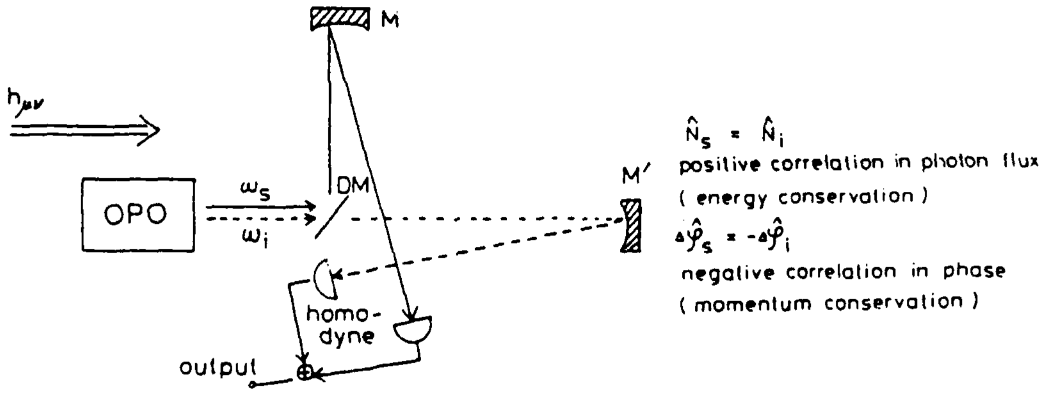

Suppression of detection noise

$$\Delta\phi_s^{(PM)} + \Delta\phi_i^{(PM)} < \text{SQL}$$

negative correlation

Suppression of radiation pressure noise

$$\Delta\phi_s^{(rp)}(N_s) - \Delta\phi_i^{(rp)}(N_i) < \text{SQL}$$

positive correlation

Conclusion

1. Four different generation schemes of NUS

2. Constant current-driven semiconductor laser

large squeezing	quantum efficiency limited
broadband	from dc to several(ten) GHz
wavelength tunability	from 0.6 μm to 10 μm

3. Applications

Quantum communication / Quantum computer / Interferometry

Acknowledgement

Hermann A. Haus (M.I.T.)

Olle Nilsson (Royal Institute of Technology)

Horace P. Yuen(Northwestern)

SQUEEZING VIA TRAVELLING-WAVE FORWARD FOUR-WAVE MIXING IN ATOMIC VAPORS: COMPARISON WITH NONDEGENERATE THEORY

Prem Kumar

Northwestern University

In this paper, I show that our recent observation of 4% squeezing via travelling-wave forward four-wave mixing in sodium vapor[1] is in good agreement with our quantum theory of nondegenerate multiwave mixing.[2] Squeezing spectra for the parameter values employed in the Maeda et al.[1] experiment are presented. It is shown that for the available dye-laser power, as much as a factor of four squeezing should be achievable from about 50 to 700 MHz in the sodium vapor experiment. However, Doppler broadening, optical pumping, and self-focussing effects may limit the observable squeezing.

1. M. W. Maeda, P. Kumar, and J. H. Shapiro, Opt. Lett. 12, 161 (1987).

2. S.-T. Ho, P. Kumar, and J. H. Shapiro, Phys. Rev. A 35, 3982 (1987).

Squeezing via Travelling-Wave Forward Four-Wave Mixing in Atomic Vapors: Comparison with Nondegenerate Theory

PREM KUMAR

Northwestern University

July 23, 1987

U.S.-Japan Seminar on

Quantum Mechanical Aspects of Quantum Electronics

①

COLLABORATORS

MIT — Jeffrey H. Shapiro

Mari W. Maeda

Seng-Tiong Ho

N.U. — Manjusha Madabushi

Outline

i) Observation of squeezing in forward four-wave mixing

ii) Quantum theory of nondegenerate multiwave mixing

iii) Calculation of squeezing spectrum

iv) Comparison with Maeda et al. experiment

v) Prognosis

SQUEEZED STATES

③

SINGLE MODE

$$\hat{E}^{(+)} = \sqrt{\frac{\hbar\omega_0}{AT}}\ \hat{a}\ e^{-i\omega_0 t}$$

$$\hat{a}_\phi \equiv \frac{1}{2}\left[\hat{a}\ e^{-i\phi} + \text{H.c.}\right]$$

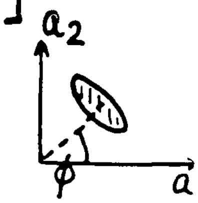

- vacuum state $|\rangle_v$: ${}_v\langle \Delta\hat{a}_\phi^2 \rangle_v = 1/4$
- squeezed state $|\rangle_s$: $\underline{{}_s\langle \Delta\hat{a}_\phi^2 \rangle_s < \frac{1}{4}}$ for some ϕ

TWO MODE : Nondegenerate ; $a_\pm : \omega_0 \pm \Omega$

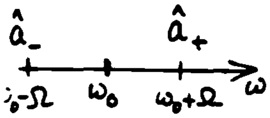

$$\hat{E}^{(+)} = \sqrt{\frac{\hbar\omega_0}{AT}}\left[\hat{a}_+ e^{-i\Omega t} + \hat{a}_- e^{i\Omega t}\right]e^{-i\omega_0 t}$$

$$\hat{a}_{\phi,\Phi}(\Omega) \equiv \left[\frac{1}{2}\left(\hat{a}_+ e^{-i\phi} + \hat{a}_-^\dagger e^{i\phi}\right)e^{-i\Phi} + \text{H.c.}\right]$$

- vacuum state $|\rangle_v = |\rangle_+|\rangle_-$: ${}_v\langle \Delta\hat{a}^2_{\phi,\Phi}(\Omega)\rangle_v = 1/4$
- squeezed state $|\rangle_s = \hat{\mathcal{O}}(|\rangle_+|\rangle_-)$:

Independent of Φ for 2-mode squeezing $\longrightarrow$ $\underline{{}_s\langle \Delta\hat{a}_\phi^2(\Omega)\rangle_s < 1/4 \quad \text{for some } \phi, \Omega}$

HOMODYNE DETECTION

$$\boxed{S_{ii}(\Omega) \propto {}_s\langle \Delta\hat{a}_\phi^2(\Omega)\rangle_s}$$

Ideal Forward Four-Wave Mixing

$$\hat{E}^{p,c}_{\substack{IN\\OUT}}(t) = \left(\frac{\hbar\omega_0}{AT}\right)^{\frac{1}{2}} \Big[\hat{a}^{p,c}_{\substack{IN\\OUT}}(+\Omega)\, e^{-i(\omega_0+\Omega)t} + \hat{a}^{p,c}_{\substack{IN\\OUT}}(-\Omega)\, e^{-i(\omega_0-\Omega)t} \Big]$$

$\hat{a}^{p,c}_{IN}(-\Omega)$ $\quad$ $\hat{a}^{p,c}_{IN}(+\Omega)$

$\omega_0-\Omega \quad \omega_0 \quad \omega_0+\Omega \quad \omega$

FFWM

$$\hat{a}^{p,c}_{OUT}(\pm\Omega) = \mu\, \hat{a}^{p,c}_{IN}(\pm\Omega) + i\nu\, \hat{a}^{c,p\,\dagger}_{IN}(\mp\Omega)$$

$$\mu = \cosh(|K|L) \quad , \quad \nu = e^{-i\theta}\sinh(|K|L)$$

Squeezing

$$\hat{E}_{\substack{OUT\\IN}}(t) = \Big[\hat{E}^{p}_{\substack{OUT\\IN}}(t) + \hat{E}^{c}_{\substack{OUT\\IN}}(t)\, e^{ik\Delta L} \Big] / \sqrt{2}$$

$$\equiv \left(\frac{2\hbar\omega_0}{AT}\right)^{\frac{1}{2}} \Big[\hat{a}^{\substack{IN\\OUT}}_{+}(\Omega)\cos(\Omega t) + \hat{a}^{\substack{IN\\OUT}}_{-}(\Omega)\sin(\Omega t) \Big] e^{-i\omega_0 t}$$

$$\boxed{\hat{a}^{OUT}_{\pm}(\Omega) = \mu\, a^{IN}_{\pm}(\Omega) + i\nu\, e^{ik\Delta L}\, \hat{a}^{IN}_{\pm}(\Omega)}$$ Yuen 1976

Homodyne Detection of $\hat{E}_{OUT}(t)$

$$V^2_\phi(\Omega) = 4e^2 \frac{P_{LO}}{\hbar\omega_0} B R^2 G \Big[\eta \Big\{ \big[\mathrm{Re}(\hat{a}^{OUT}_{+}(\Omega)\, e^{-i\phi})\big]^2 + \big[\mathrm{Re}(\hat{a}^{OUT}_{-}(\Omega)\, e^{-i\phi})\big]^2 \Big\} + \frac{1-\eta}{2} \Big]$$

$$= V^2_\phi(\mathrm{vac}) \Big[\eta \,\big| \mu - i\nu^* e^{-i(k\Delta L - 2\phi)} \big|^2 + 1-\eta \Big]$$

(5)

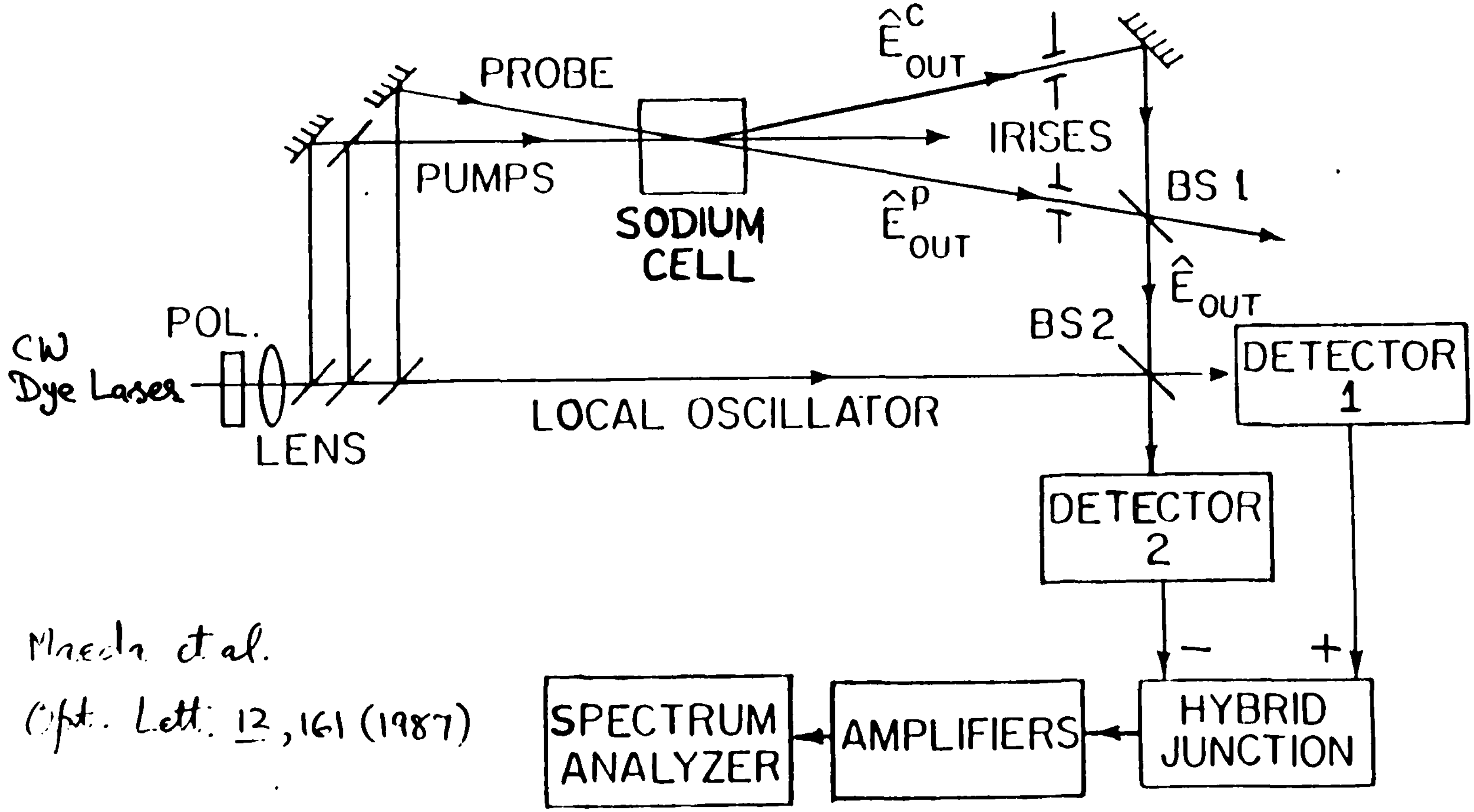

Maeda et al.
Opt. Lett. 12, 161 (1987)

(6)

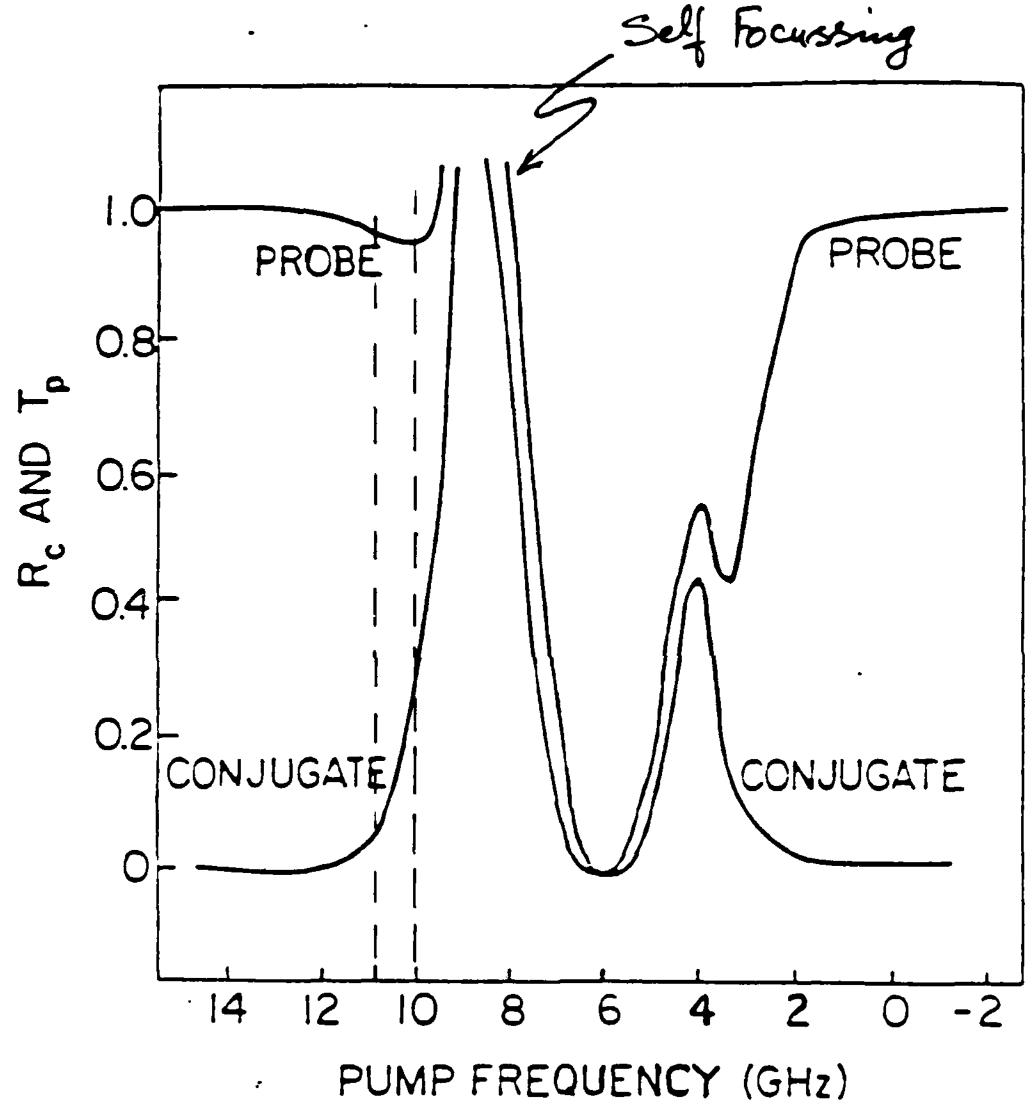

Detuning $\simeq$ 4-5 GHz ; $I_p \simeq$ 20-50 mW/0.5 mm dia.

$\alpha_0 L \simeq 5 \times 10^4$

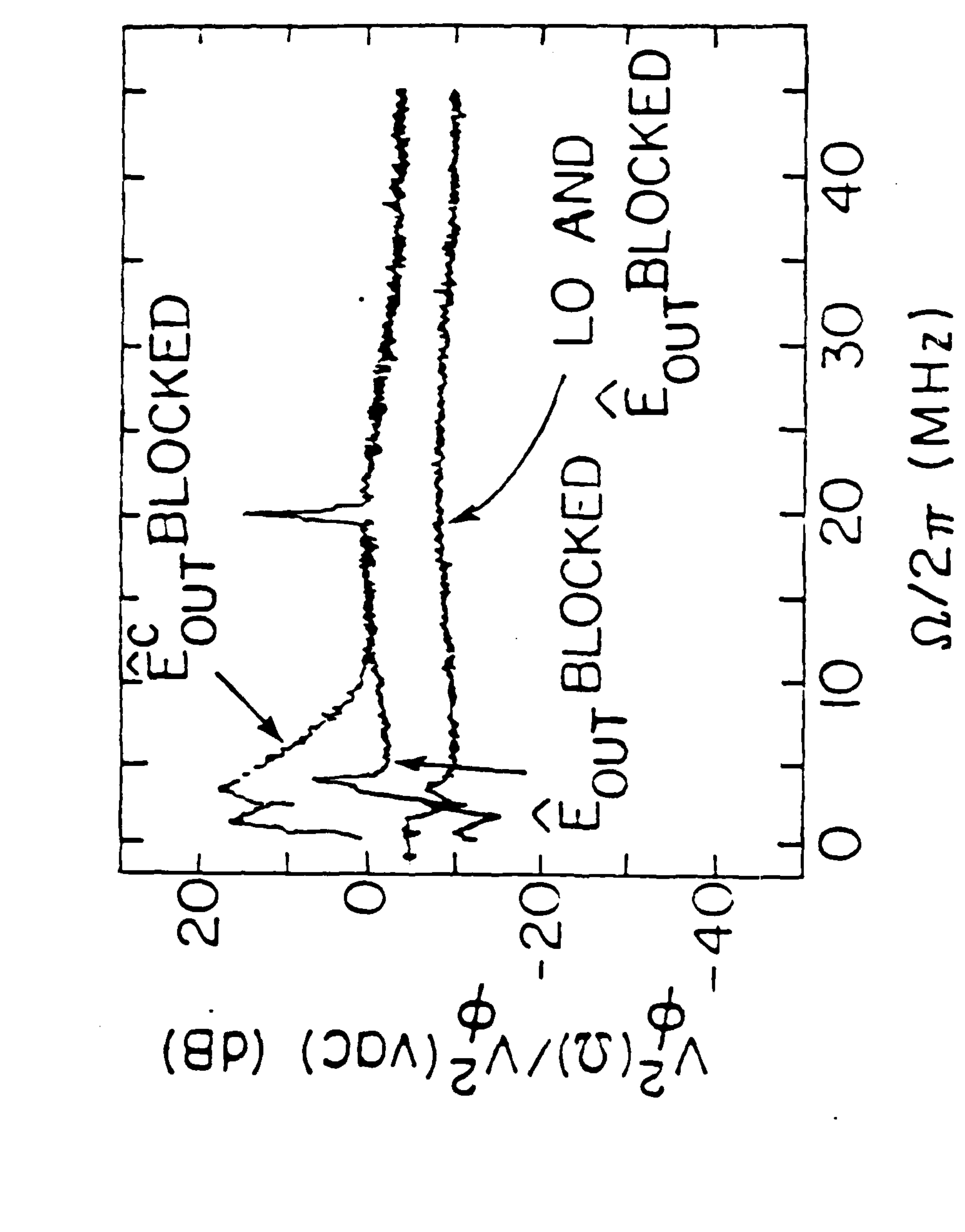
$\hat{E}^{c}_{OUT}$ BLOCKED
$\hat{E}_{OUT}$ BLOCKED
LO AND $\hat{E}_{OUT}$ BLOCKED
20
0
-20
-40
$V^2_\phi(\Omega)/V^2_\phi(\mathrm{vac})$ (dB)
0
10
20
30
40
$\Omega/2\pi$ (MHz)

(7)

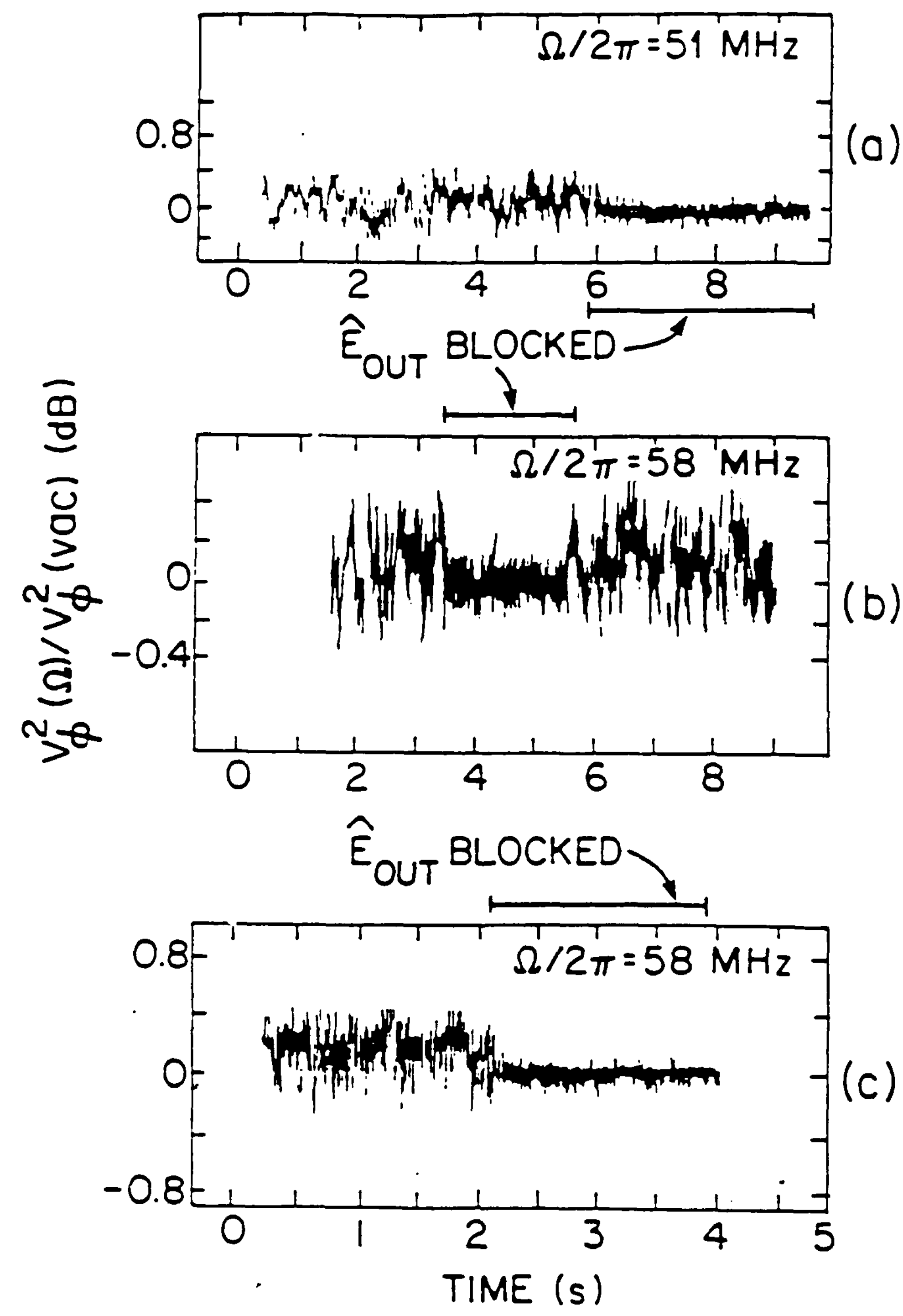

Ω/2π = 51 MHz
(a)
0.8
0
0 2 4 6 8
Ê OUT BLOCKED
$V_\phi^2(\Omega)/V_\phi^2$(vac) (dB)
Ω/2π = 58 MHz
(b)
0
-0.4
0 2 4 6 8
Ê OUT BLOCKED
Ω/2π = 58 MHz
(c)
0.8
0
-0.8
0 1 2 3 4 5
TIME (s)

(9)

Theories of Nondegenerate Four-Wave Mixing

- Reid and Walls (1985, 86)
- Holm and Sargent (1986, 87)

Apply to cavity configurations

Replace $z \rightarrow ct$

(not valid in an optically thick medium with dispersion and nonlinear mixing)

Quantum Theory of Nondegenerate Multiwave Mixing

He et al. (1987)

System Hamiltonian

N two-level atoms

q field modes

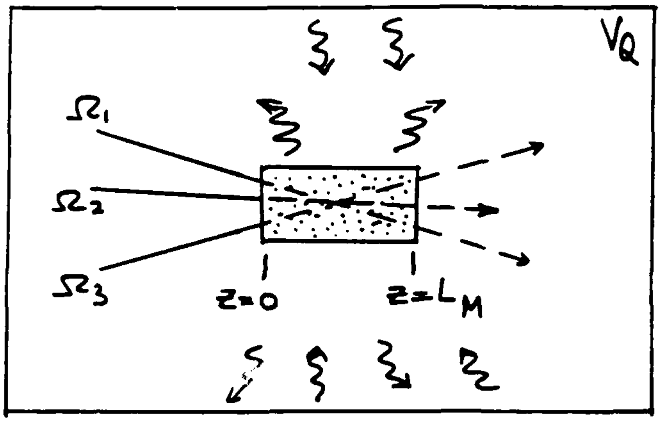

Rest of the modes constitute a common thermal-field reservoir. In addition each atom is coupled to a separate phase-damping reservoir.

$$\hat{H} = \hat{H}_0 + \hat{H}_I + \hat{H}_R + \hat{H}_C$$

$\hat{n}_i = |e\rangle_i {}_i\langle e|$

$\hat{n}_{gi} = |g\rangle_i {}_i\langle g|$

$\hat{n}_{di} = \left(|e\rangle_i {}_i\langle e| - |g\rangle_i {}_i\langle g|\right)$

$$\hat{H}_0 = \sum_{j=1}^{q} \hbar\omega_j \hat{a}_j^\dagger \hat{a}_j + \frac{\hbar\omega_a}{2} \sum_{i=1}^{N} \hat{n}_{di}$$

$$\hat{H}_I = \sum_{j=1}^{q} \sum_{i=1}^{N} \left\{ i\hbar\, C_j(\bar{r}_i)\, \hat{a}_j \hat{V}_i^\dagger + \text{H.c.} \right\} \qquad \hat{V}_i = |g\rangle_i {}_i\langle e|$$

Rotating Wave & Dipole

$$\hat{H}_R = \sum_{s=q+1}^{\infty} \hbar\omega_s \hat{a}_s^\dagger \hat{a}_s + \sum_{s=q+1}^{\infty} \sum_{i=1}^{N} \left\{ i\hbar\, C_s(\bar{r}_i)\, \hat{a}_s \hat{V}_i^\dagger + \text{H.c.} \right\}$$

$$\hat{H}_C = \sum_{i=1}^{N} \hat{\Gamma}_{pi}\, \hat{n}_{di}$$

Coulomb gauge
$$\begin{cases} C_j(\bar{r}_i) = g_j \mu_j e^{i \bar{k}_j \cdot \bar{r}_i} \\ \mu_j = {}_i\langle e|\, e\hat{\bar{r}}_i\, |g\rangle_i \cdot \bar{e}_j \\ g_j = \left(\omega_a^2 / 2\hbar\epsilon_0 \omega_j V_Q\right)^{\frac{1}{2}} \end{cases}$$

C-Number Langevin Equations

Haken: Laser Theory

Drummond and Walls: Bistability

$$\frac{\partial V_i}{\partial t} = -i\omega_a V_i - \sum_{j=1}^{q} C_j(\bar{r}_i)\, a_j (n_{g_i} - n_i) - \gamma_\perp V_i + f_{V_i}$$

$$\underbrace{-\sum_{i' \neq i} \gamma_{ii'}(\bar{r}_i - \bar{r}_{i'})\left[n_{g_i} - n_i\right] V_{i'}}_{\text{Superradiance terms}}$$

$$\frac{\partial n_i}{\partial t} = -\sum_{j=1}^{q}\left[C_j^*(\bar{r}_i)\, a_j^+ V_i + C_j(\bar{r}_i)\, a_j V_i^+\right] - \gamma_{\parallel} n_i + f_{n_i}$$

$$\underbrace{-\sum_{i' \neq i} \gamma_{ii'}(\bar{r}_i - \bar{r}_{i'})\left[V_i^+ V_{i'} + V_{i'}^+ V_i\right]}_{\text{Superradiance terms}}$$

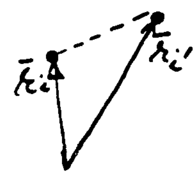

$n_{g_i} + n_i = 1$

Agree with Bonifacio et al. (1971)

$$\frac{\partial a_j}{\partial t} = -i\omega_j a_j + \sum_{i=1}^{N} C_j^*(\bar{r}_i) V_i$$

$$\gamma_\perp = \gamma_p + \gamma_{\parallel}/2 \equiv \frac{\gamma_{\parallel}}{2F} \; ; \quad 0 \leq F \leq 1$$

Superradiance terms are negligible: a) # of atoms in a diffraction volume is small

b) atoms pumped far off-resonance

Noise Correlations

We neglect superradiance $\langle f_{V_i^+}(t)\, f_{V_{i'}}(t')\rangle = 2\gamma_p n_i\, \delta_{ii'}\, \delta(t-t')$

$$\langle f_{V_i}(t)\, f_{V_{i'}}(t')\rangle = \left[\sum_{j=1}^{q} C_j(\bar{r}_i)\, a_j V_i\right] \delta_{ii'}\, \delta(t-t')$$

$$\langle f_{n_i}(t)\, f_{n_{i'}}(t')\rangle = \langle f_{n_{g_i}}(t)\, f_{n_{g_{i'}}}(t')\rangle = -\langle f_{n_i}(t)\, f_{n_{g_{i'}}}(t')\rangle$$

$$= \left[-\sum_{j=1}^{q}\left(C_j^*(\bar{r}_i)\, a_j^+ V_i + C_j(\bar{r}_i)\, a_j V_i^+\right) + \gamma_{\parallel} n_i\right] \delta_{ii'}\, \delta(t-t')$$

Delta correlated in space and time

Solution Technique For Atomic Polarization

- Fourier Decomposition

$$a_{\bar{r}_i}(t) \equiv \sum_{j=1}^{q} c_j(\bar{r}_i)\, a_j(t) = \sum_{m=1}^{\infty} A_m(\bar{r})\, e^{-i\nu_m t}$$

$$X(\omega) \equiv \int_{-\infty}^{\infty} \frac{dt}{2\pi}\, X(t)\, e^{i\omega t} \; ; \; X \in \{V, V^+, n, f_V, f_{V^+}, f_n\}$$

Iterative solution developed which converges when all strong modes are frequency-degenerate and remaining nondegenerate modes are weak.

$$V_i(t) = \sum_{m=1}^{\infty} Y(\nu_m, \bar{r}_i, t)\, A_m(\bar{r}_i)\, e^{-i\nu_m t} + \Gamma_{V_i}(t)$$

Slowly-Varying Amplitude Approximation   Frequency Domain Method

$$a_{\bar{r}_i}(t) = \sum_{j=1}^{q} c_j(\bar{r}_i)\, a_j(t) = \sum_{j=1}^{q} c_j(\bar{r}_i)\, \alpha_j(t)\, e^{-i(\omega_j - \Delta\omega_j)t}$$

$$\alpha_j(t-t') \simeq \alpha_j(t) - t' \frac{\partial \alpha_j(t)}{\partial t}$$

$$V_i(t) = \sum_{j=1}^{q} c_j(\bar{r}_i)\, e^{-i\omega_j^{\delta} t}\, \hat{D}_j(t)\, Y(\omega_j^{\delta}, \bar{r}_i, t) + \Gamma_{V_i}(t)$$

$$\hat{D}_j(t) \equiv \left[\alpha_j(t) + i \frac{\partial \alpha_j(t)}{\partial t} \frac{\partial}{\partial \omega_j^{\delta}} \right]$$

$$\omega_j^{\delta} \equiv \omega_j - \Delta\omega_j$$

↑ Dispersion is built in

Y is recursive and contains the operator $\hat{D}_j(t)$.

Temporal Coupled-Mode Equations

$$\frac{\partial \alpha_m(t)}{\partial t} = -i\,\Delta\omega_m\,\alpha_m(t) + \int_{V_M} d\bar{r}\,\rho_a\,C_m^*(\bar{r})\,V_{\bar{r}}(t)\,e^{i(\omega_m-\Delta\omega_m)}$$

$$V_{\bar{r}}(t) = \rho_a \sum_{i=1}^{N_0} \frac{V_{\bar{r}_i}(t)}{N_0}$$

volume integral leads to mode coupling

Spatial Propagation

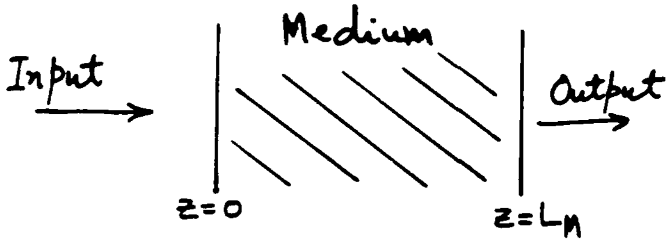

a) Quantum Method

$$E(x,y,z=0,t) = \sum_j C_j(x,y,z=0)\,\alpha_j(t)$$

$$\alpha_j(t) \longrightarrow E_j(x,y,z,t) = \sum_m C_m(\bar{r})\,\alpha_m(t)\,e^{iK_m z}$$

paraxial treatment coupled mode equations

Finally, $E(\bar{r},t) = \sum_j C_j(x,y,z=0)\,E_j(\bar{r},t)$

b) Slowly-Varying-Envelope-Method

$$\hat{E}(z,t) = \sum_{l=1}^{m} \hat{\alpha}_l(z,t)\,e^{-i(\Omega_l t - K_l' z)} + \text{H.c.}$$

$$\hat{P}(z,t) = \sum_{l=1}^{m} \hat{\rho}_l(z,t)\,e^{-i(\Omega_l t - K_l' z)} + \text{H.c.}$$

$$\frac{\partial \hat{\alpha}_\ell}{\partial z} + \frac{1}{c}\frac{\partial \hat{\alpha}_\ell}{\partial t} = \frac{i K'_\ell}{2\epsilon_0}\hat{P}_\ell \qquad P(z,t) = \mu \rho_a V_{\bar{z}_i}(t)$$

Wave-equation gives spatial-coupled-mode equations for $\alpha_\ell(z,t)$. Both methods agree.

Four-wave Mixing

$\Omega_{-\ell} = \omega_0 - \Omega$ $\quad$ $\Omega_p = \omega_0$ $\quad$ $\Omega_\ell = \omega_0 + \Omega$ $\quad$ ω_a

$(\Omega_\ell - \Omega_p) = (\Omega_p - \Omega_\ell)$ frequency-matching

$2\bar{K}'_p = \bar{K}'_\ell + \bar{K}'_{-\ell}$ phase-matching

Spatial Coupled-Mode Equations

$$\frac{\partial \alpha_\ell}{\partial z} = -i\check{\gamma}_\ell \alpha_\ell + \check{\chi}_\ell e^{i\delta K'_\ell z}\alpha^+_{-\ell} + \check{\Gamma}_\ell$$

$$\frac{\partial \alpha_{-\ell}}{\partial z} = i\check{\gamma}^*_{-\ell}\alpha^+_{-\ell} + \check{\chi}^*_{-\ell} e^{-i\delta K'_{-\ell} z}\alpha_\ell + \check{\Gamma}^+_{-\ell}$$

$\{\check{\gamma}_\ell, \check{\gamma}_{-\ell}\}$ dispersion coefficients

$\{\check{\chi}_\ell, \check{\chi}_{-\ell}\}$ nonlinear mixing coefficients

} agree with: Fu & Sargent (1979), Boyd et al. (1981)

$\{\check{\Gamma}_\ell, \check{\Gamma}_{-\ell}\}$ noise terms } give correct resonance fluorescence spectrum, Mollow (1969)

$$\delta K'_\ell = (\bar{K}'_\ell + \bar{K}'_{-\ell} - 2\bar{K}'_p) \cdot \bar{e}_z$$

Squeezing spectra

$$\Delta_p \equiv \frac{\omega_a - \Omega_p}{\gamma_\perp} = \frac{\omega_a - \omega_0}{\gamma_\perp}$$

$$\delta_m = \frac{\Omega_m - \Omega_p}{\gamma_\perp} = \frac{\Omega}{\gamma_\perp}$$

$$\beta = \frac{\Omega_R}{\gamma_\perp} = \sqrt{I_p / I_s^0} = \sqrt{S_0}$$

$$\delta \hat{X}_1^2(\theta) = \langle (\hat{X}_1(\theta) - \langle \hat{X}_1(\theta) \rangle)^2 \rangle \;;$$

$$\hat{X}_1(\theta, \Omega) \equiv \tfrac{1}{2}\left(\alpha(\Omega, L_M)\, e^{-i\theta} + \alpha^+(-\Omega, L_M)\, e^{i\theta}\right) + \text{c.c.}$$

- Pick θ for minimum $\delta \hat{X}_1^2(\theta)$

$\Delta p = 100$, $\alpha_0 L_M = 10^4$

$\beta = 26$

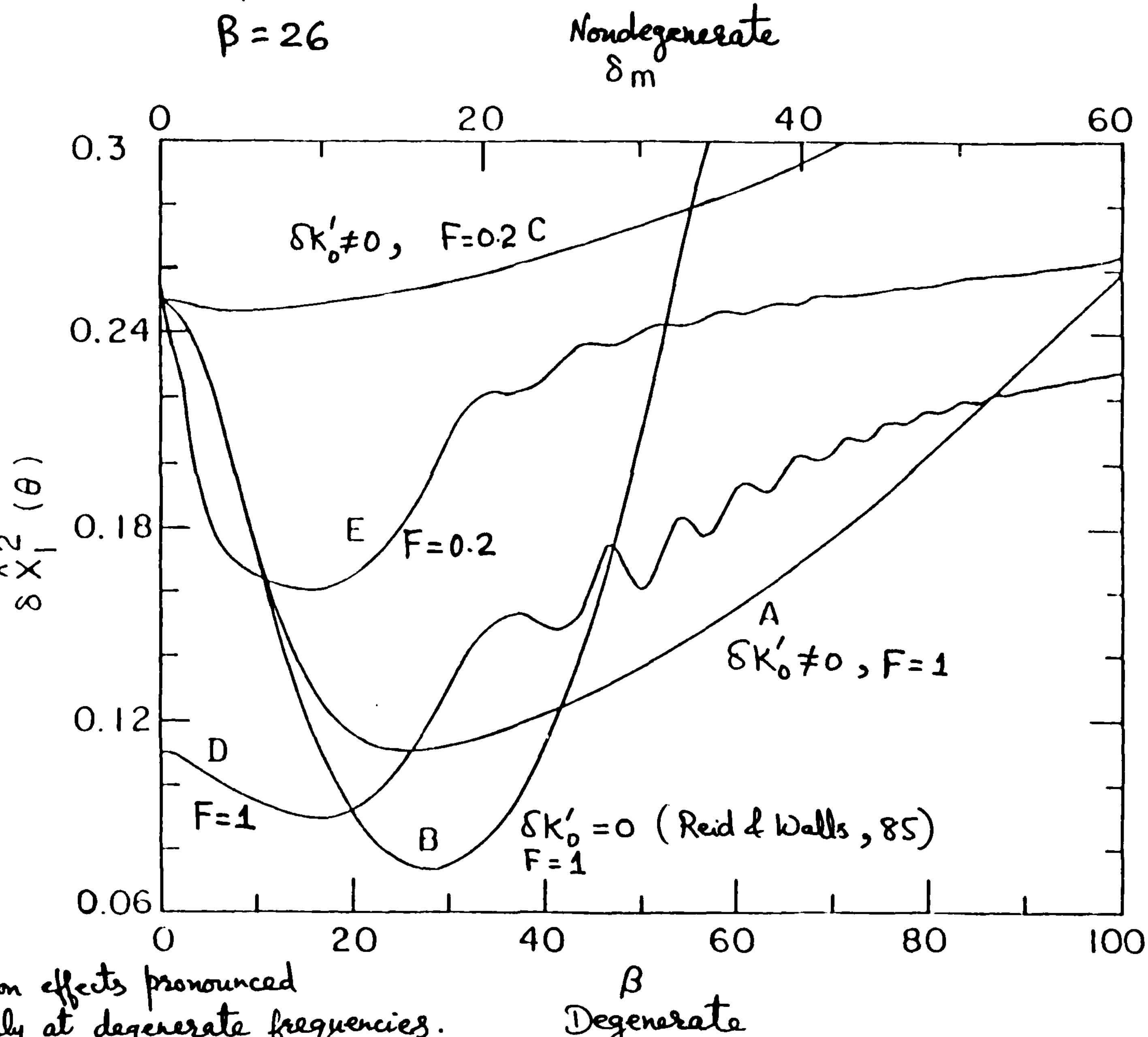

• Collision effects pronounced only at degenerate frequencies.

16

$\Delta_p = 100$, $\beta = 100$, $F = 1$ Squeezing Spectra

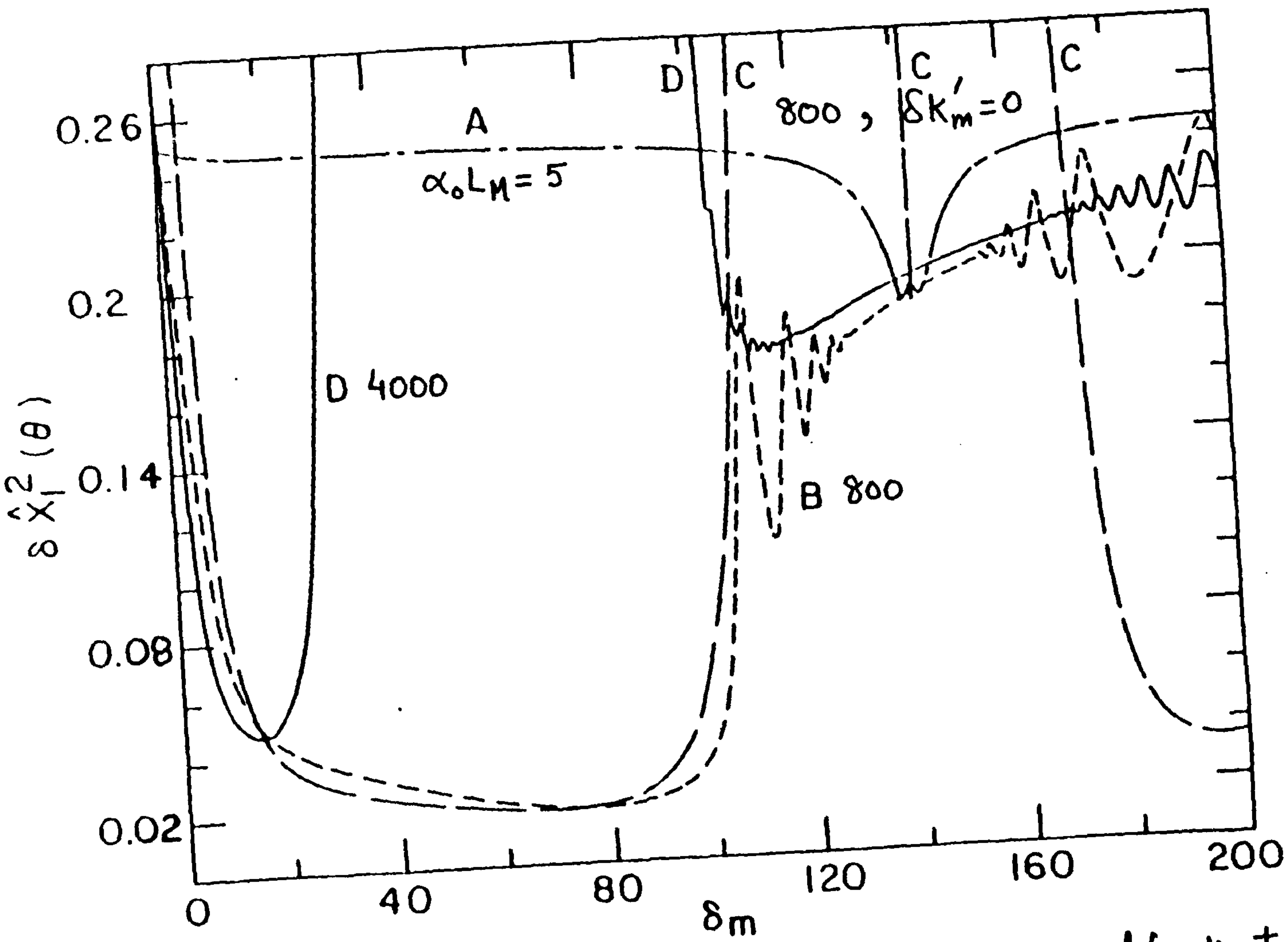

• Wiggles are due to phase-mismatch effects.

(17)

$\Delta_p = 100$, $\alpha_0 L_M = 4000$, $F = 1$

Squeezing Spectra

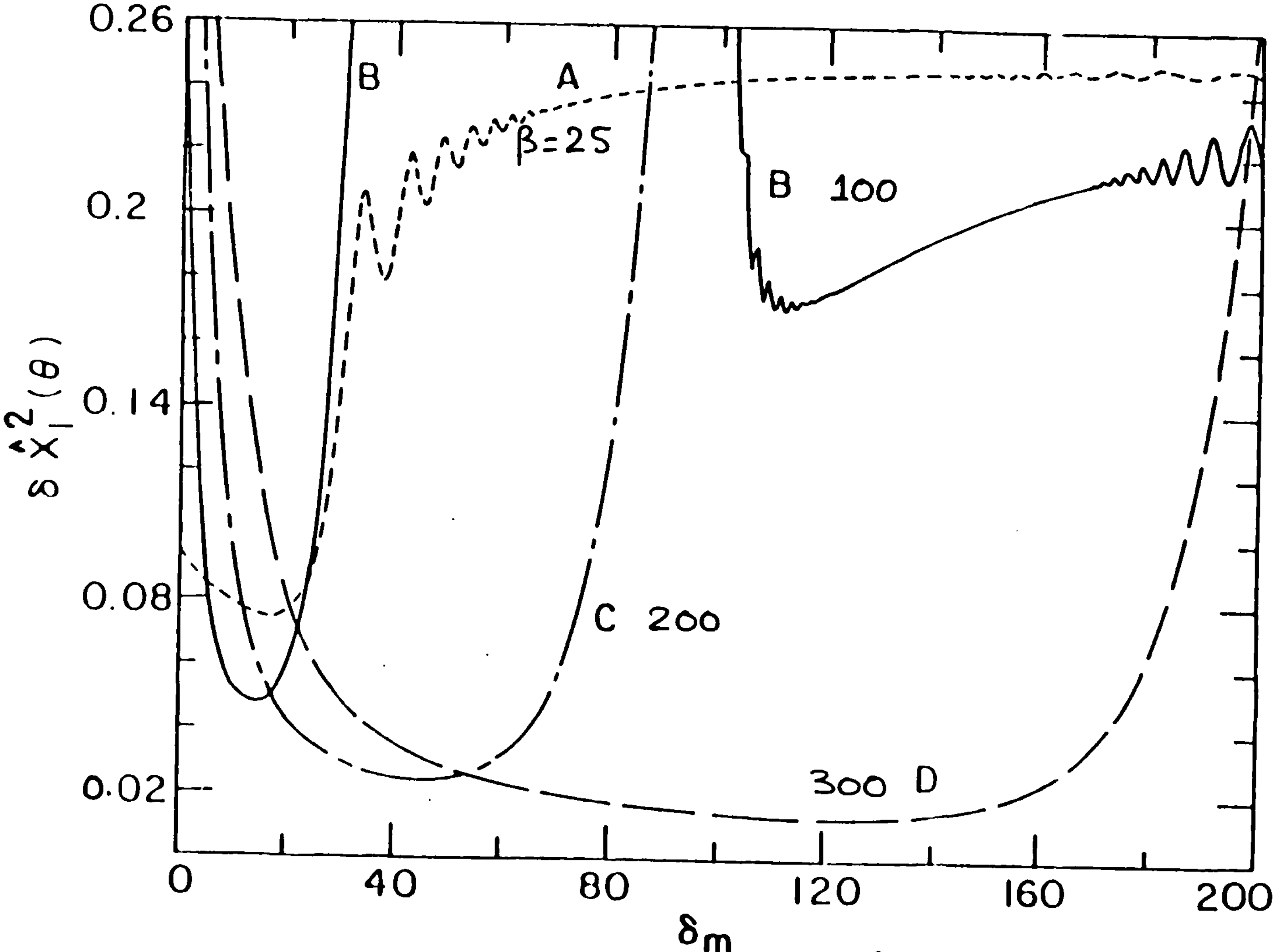

• Degenerate Squeezing at low β only

18

Maeda et al. Experiment

- Observed squeezing 4% (0.2 dB)
- Inferred squeezing 12% (0.6 dB)

$$\alpha_0 L_M = 5 \times 10^4$$

$$\beta = \sqrt{I/I_s^0} = \sqrt{1000} \simeq 32$$ [20 mW focussed to 0.5 mm dia.]

$$\delta_m = \frac{58\,\text{MHz}}{\gamma_\perp} \simeq 12$$

For sodium $\gamma_\perp \simeq 5$ MHz

$$\Delta_p = \frac{5\,\text{GHz}}{\gamma_\perp} \simeq 1000$$

Squeezing spectra under conditions of Maeda et al. experiment

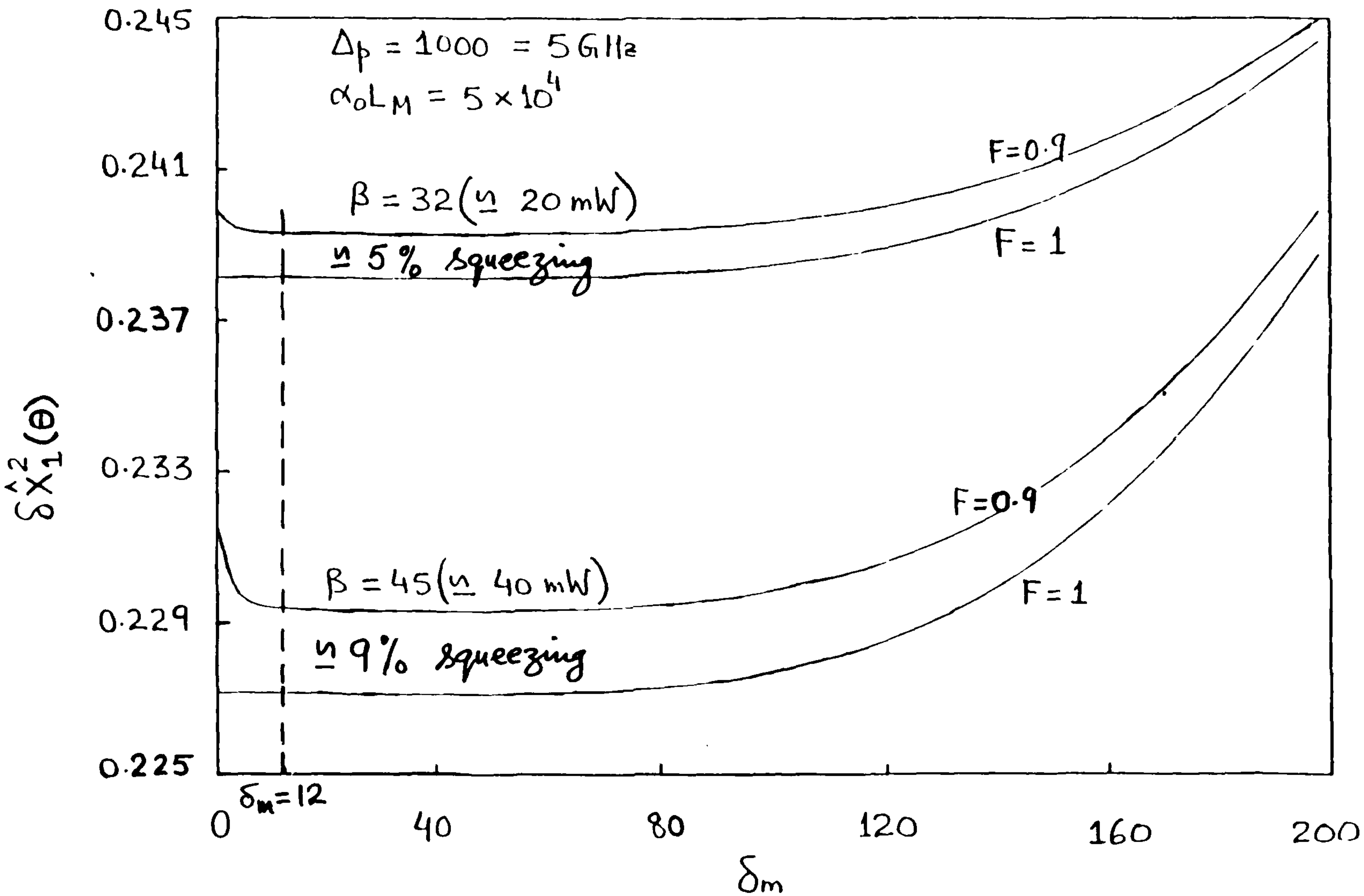

• Due to self-focussing, intensity may be higher.

20

Squeezing spectra for different pump detunings

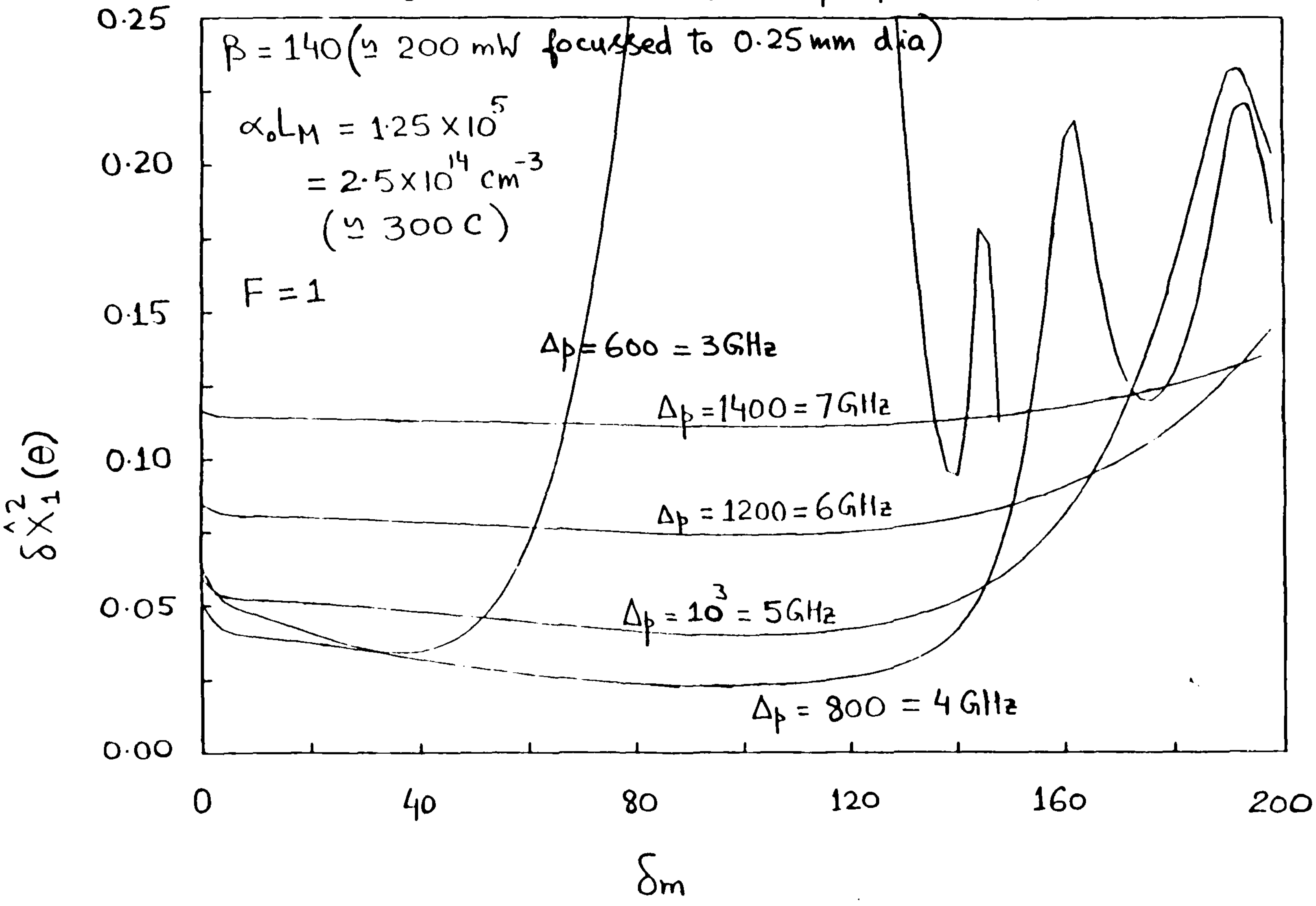

• Above conditions are achievable in the lab.

(21)

Effect of collisions on the sodium experiment

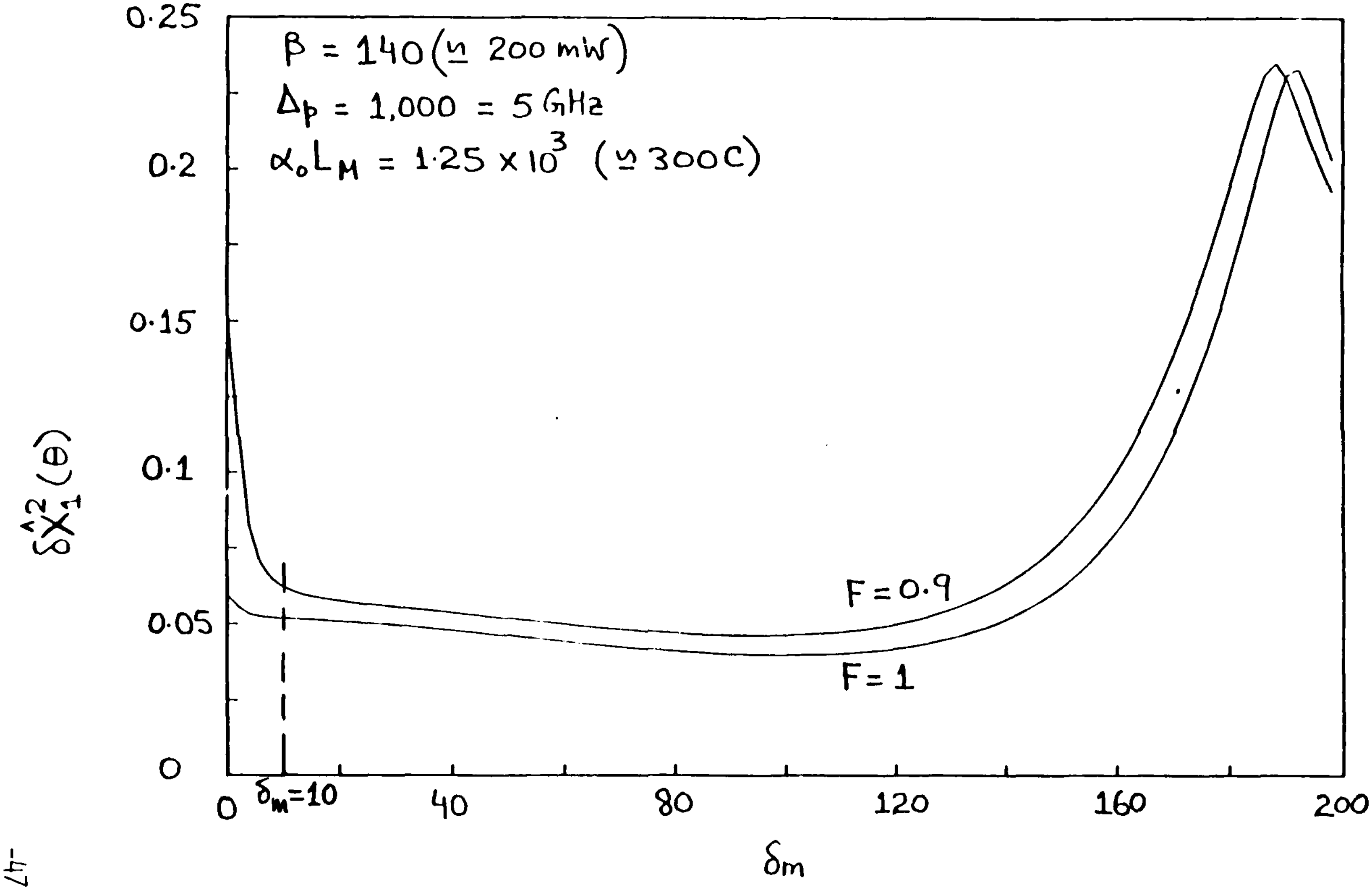

- Atleast a factor of 4 squeezing between 50 to 700 MHz

(22)

23

Conclusions

- Maeda et al. experiment is in good agreement with theory.
- Atleast a factor of four squeezing should be achievable with available dye laser power.
- Doppler broadening, optical pumping, and self-focussing effects may limit observable squeezing.

References

1. M.W. Maeda, P. Kumar, and J.H. Shapiro, Opt. Lett. 12, 161 (1987).

2. S.-T. Ho, P. Kumar, and J.H. Shapiro, Phys. Rev. A 35, 3982 (1987).

GENERATING SQUEEZED MICROWAVE RADIATION WITH A JOSEPHSON PARAMETRIC AMPLIFIER

B. Yurke
AT&T Bell Laboratories
Murray Hill, New Jersey 07974

In an effort to generate squeezed microwave radiation at 20 GHz via a Josephson parametric amplifier, we have recently demonstrated a factor of 2 squeezing of 4.2K thermal noise. A room temperature mixer with a 660K noise temperature was employed for homodyne detection. The overall detector system noise temperature (including waveguide losses) was 2100K. In order to rule out detector saturation effects, a probe signal was injected into the mixer to monitor the detector system gain. Since at 4.2K one is only an order of magnitude from the quantum noise floor, we are hopeful of observing quantum noise squeezing when the device is cooled well below .5K.

Generating Squeezed Microwave Radiation with a Josephson Parametric Amplifier

B. Yurke, P.G. Kaminsky, R.E. Miller;
AT&T Bell Laboratories

E.A. Whittaker; Stevens Institute

A.D. Smith, A.H. Silver, R.W. Simon;
TRW Space & Technology Group.

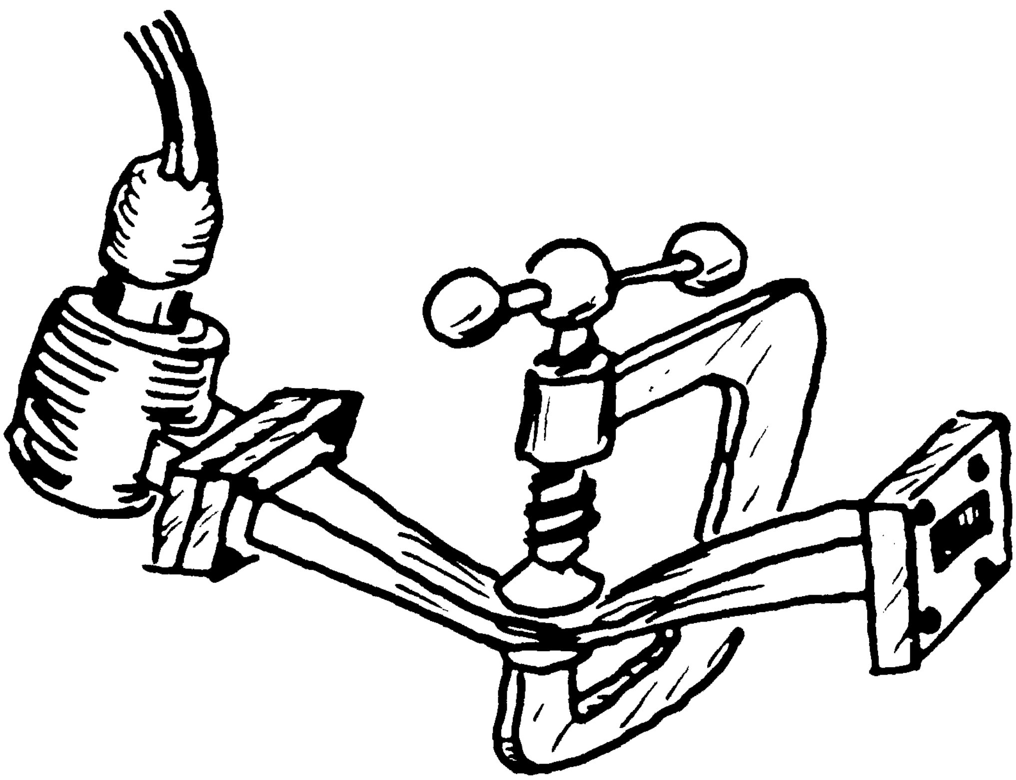

AD-A186 938 UNITED STATES - JAPAN SEMINAR ON QUANTUM MECHANICAL ASPECTS OF QUANTUM EL (U) MASSACHUSETTS INST OF TECH CAMBRIDGE RESEARCH LAB OF ELECTRON 6/7

UNCLASSIFIED J H SHAPIRO ET AL OCT 87 N00014-87-G-0198 F/G 20/3 NL

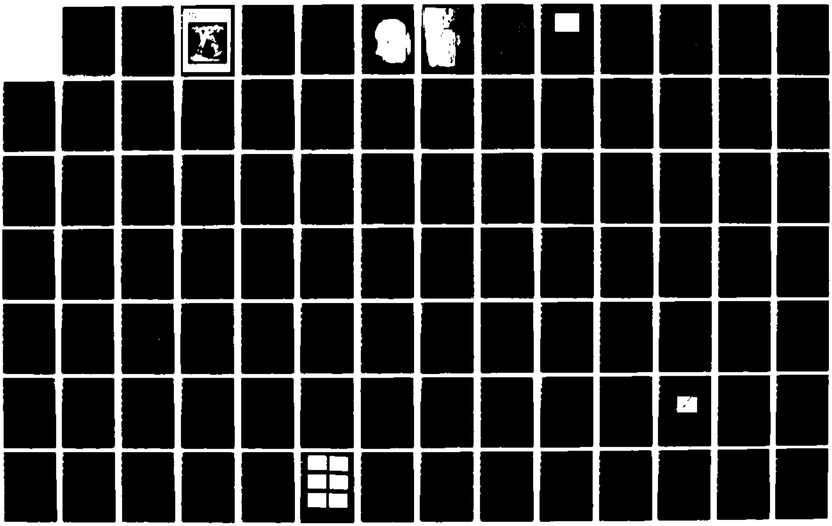

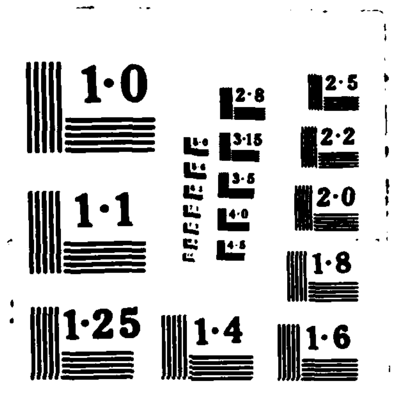
1·0
2·8
2·5
3·15
2·2
3·5
2·0
4·0
1·1
4·5
1·8
1·25
1·4
1·6

SQUEEZED STATE GENERATION AT 20 GHz

Motivation:

(1) One wants squeezed state sources at as many frequencies as possible.

(2) Study Rydberg atoms interacting with squeezed radiation

(a) level shifts.

(b) florescence spectrum line narrowing.

(3) Study quantum behavior of Josephson circuits.

Why 20 GHz:

(1) $h\nu = kT$
for $T = 1K$ and $\nu = 21$ GHz.

(2) K-band waveguide is of a convenient size to fit in a cryostat.

(3) Josephson technology works well here.

Optics News

JUNE 1987 ■ VOLUME 13, NUMBER 6

-479-

Squeezed light and the parametric swing

JOSEPHSON PARAMETRIC AMPLIFIER

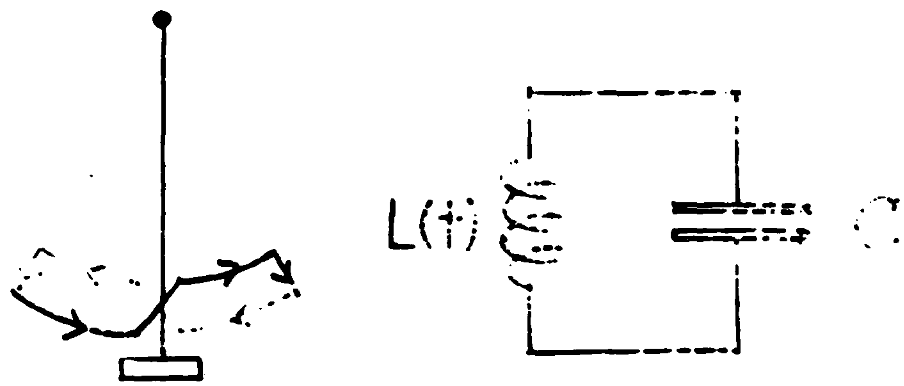

$$\frac{d}{dt}\left(I(t)\,\frac{d\phi}{dt}\right) + K\phi = 0 \qquad \frac{d}{dt}\left(L(t)\,\frac{dQ}{dt}\right) + \frac{Q}{C} = 0$$

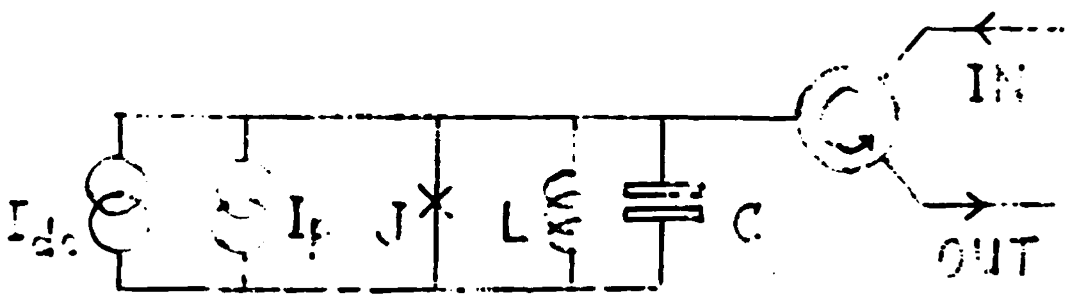

Josephson inductance

$$L_J(I) = \frac{\hbar}{2eI_c}\left[\frac{\sin^{-1}(I/I_c)}{I/I_c}\right]$$

5

THE JOSEPHSON PARAMETRIC AMPLIFIER

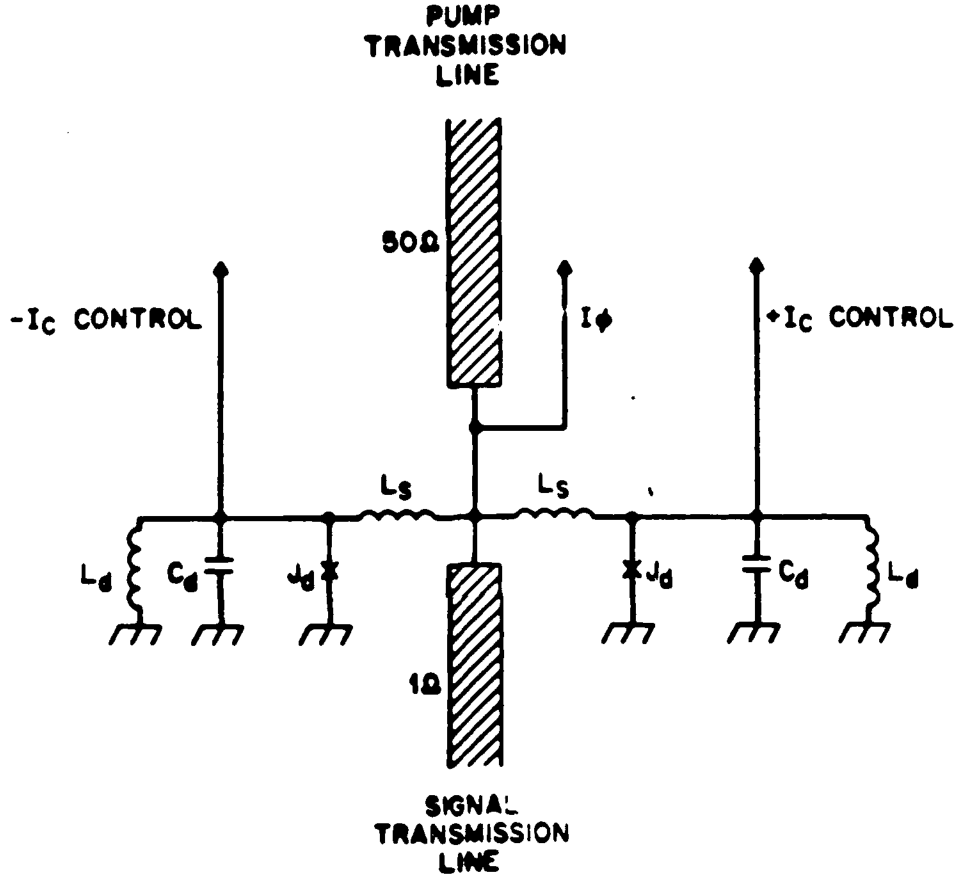

Junction technology Nb-AlO-Nb

$f_s = 20$ GHz

Novel Features:

(1) Two junctions employed to tune critical current via I_c^-, I_c^+ control lines.

(2) Four-Stage Impedance Transformer (1 GHz passband).

6

7

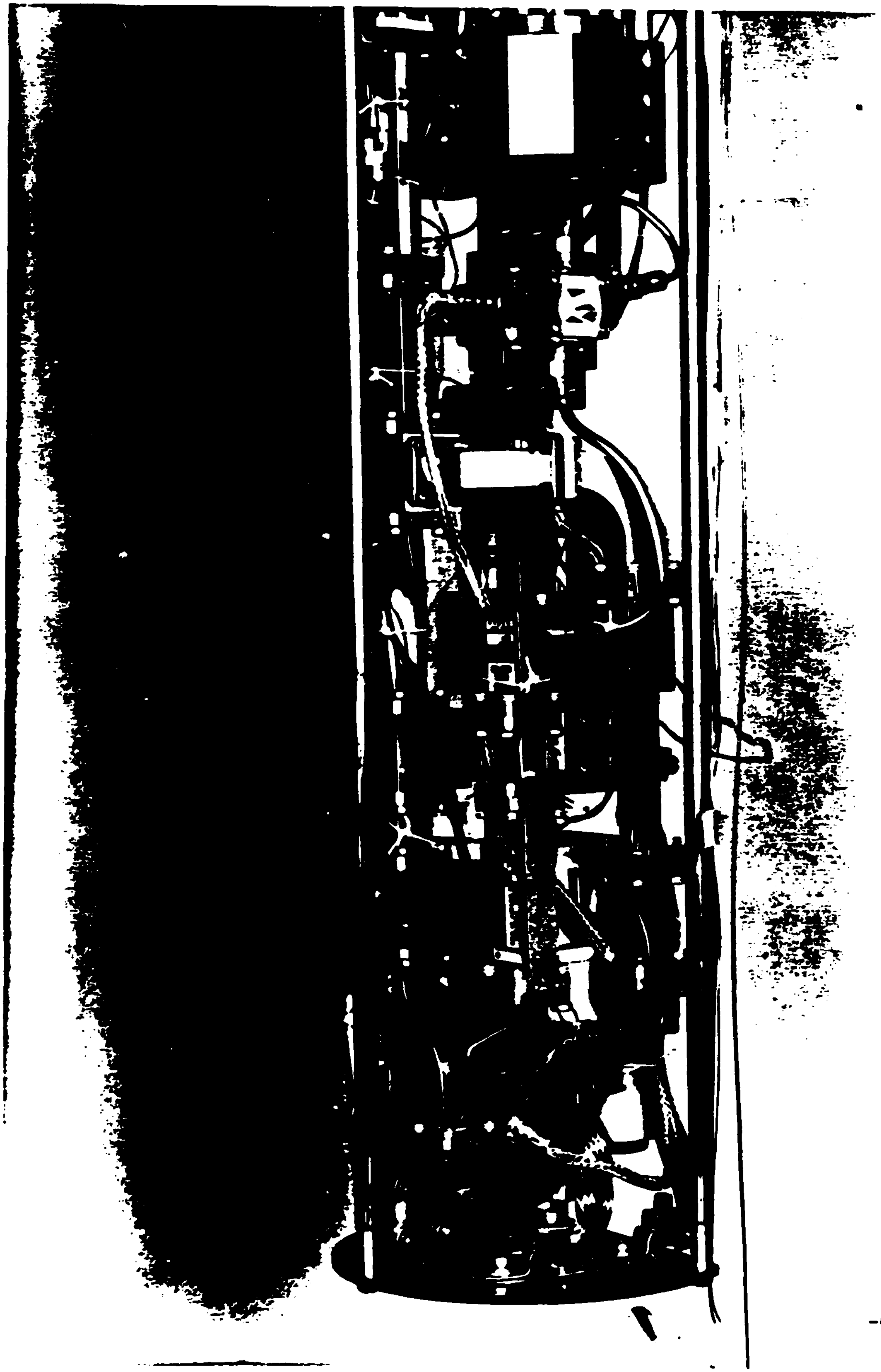

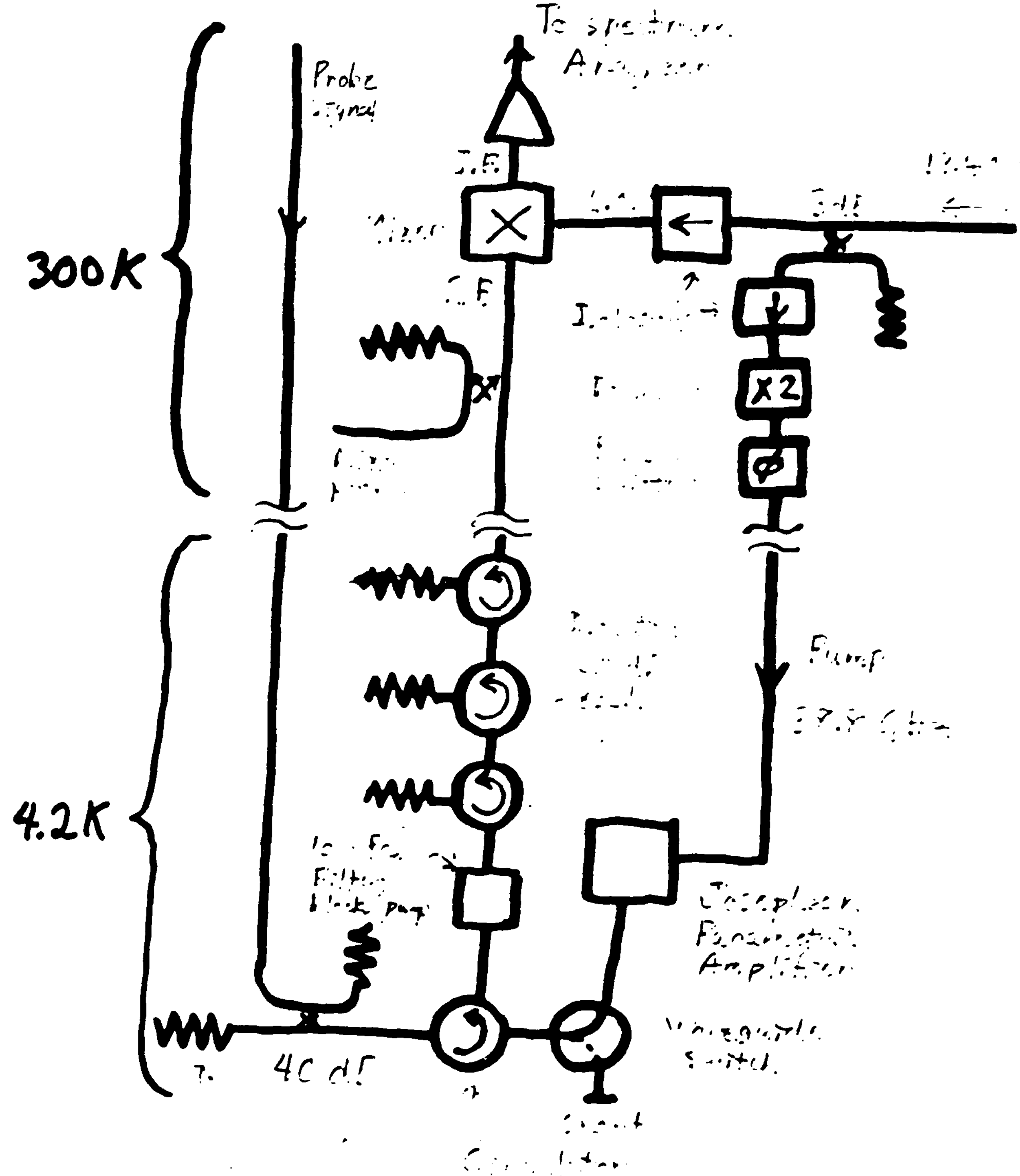

[illegible], source of 4.2 K thermal noise [illegible] to be squeezed.

9

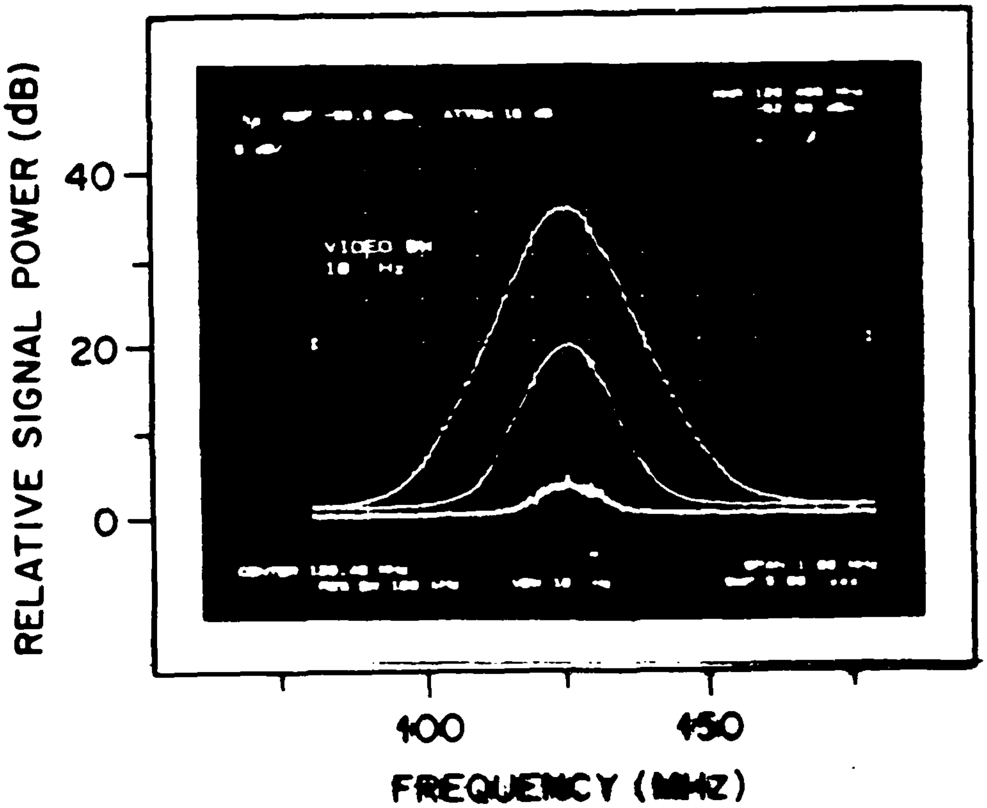

17 dB CLASSICAL SQUEEZING

<u>Red</u> - Amplified Component

White - Pump Off

<u>Green</u> - Squeezed Component

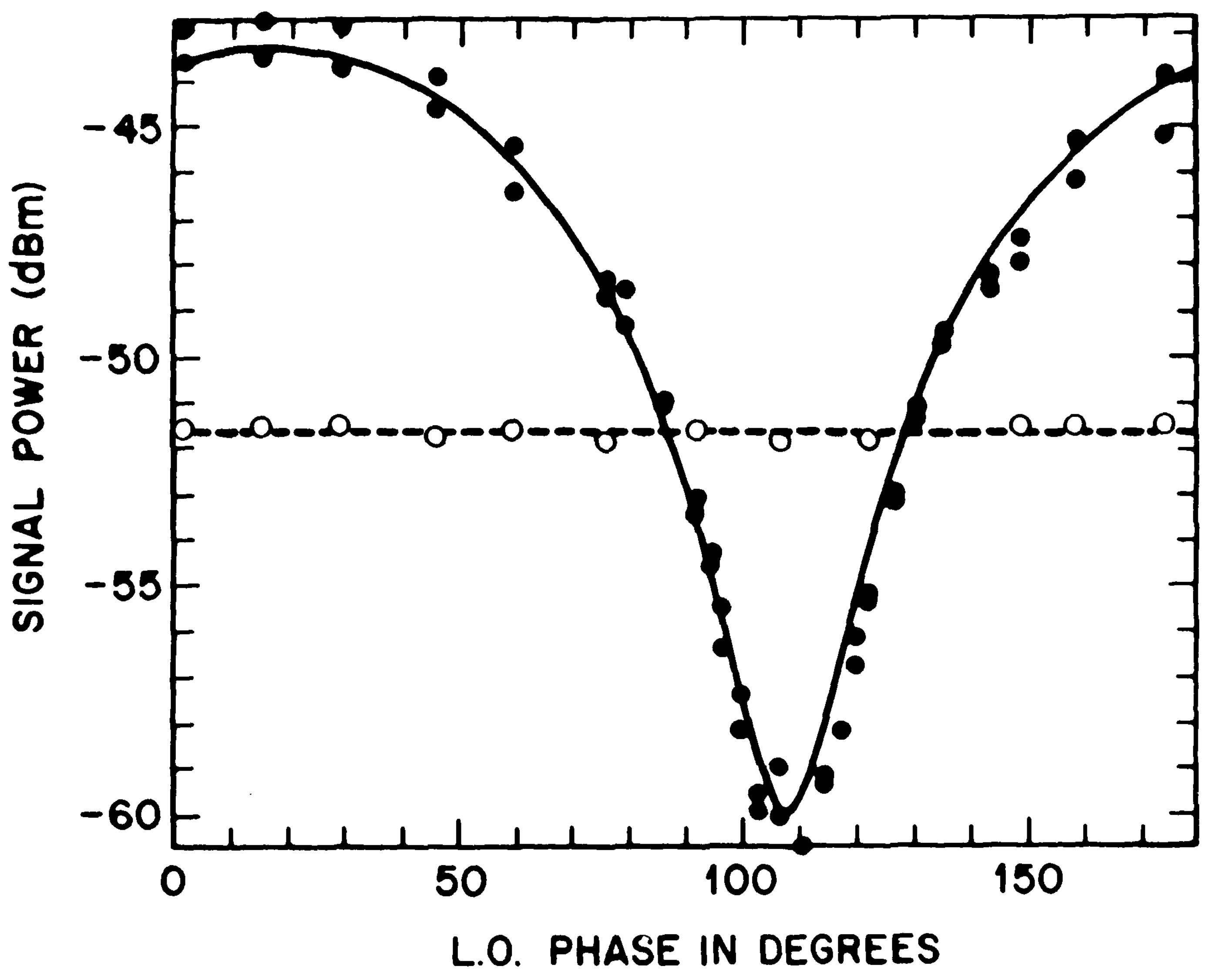

E-9148 (6-85)
AT&T BELL LABORATORIES

AT&T

Detecting Squeezing with Noisy Detectors

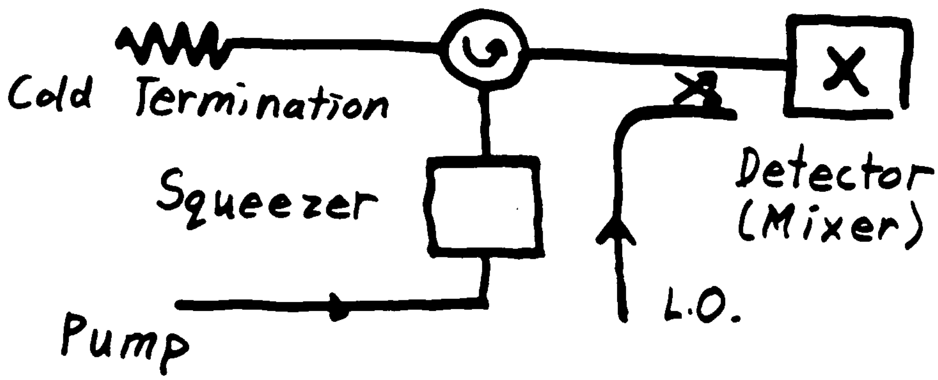

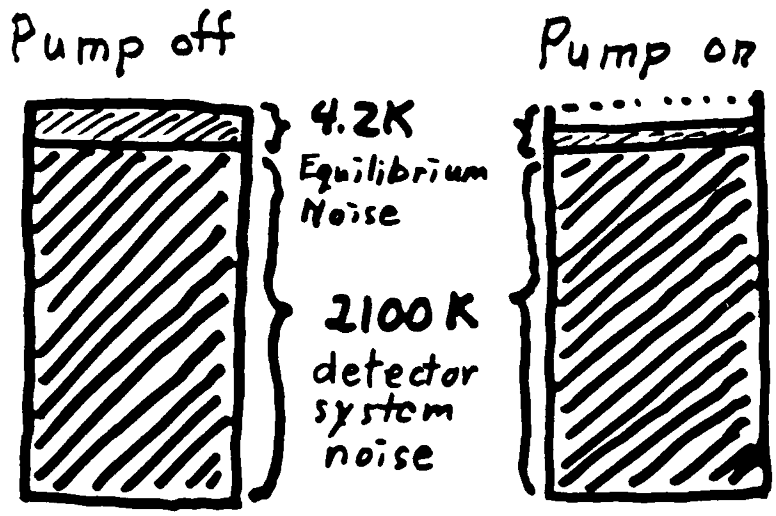

We are looking for changes in the noise floor of 2 parts in 10^{-4} or changes of the order of 10^{-3} dB

12

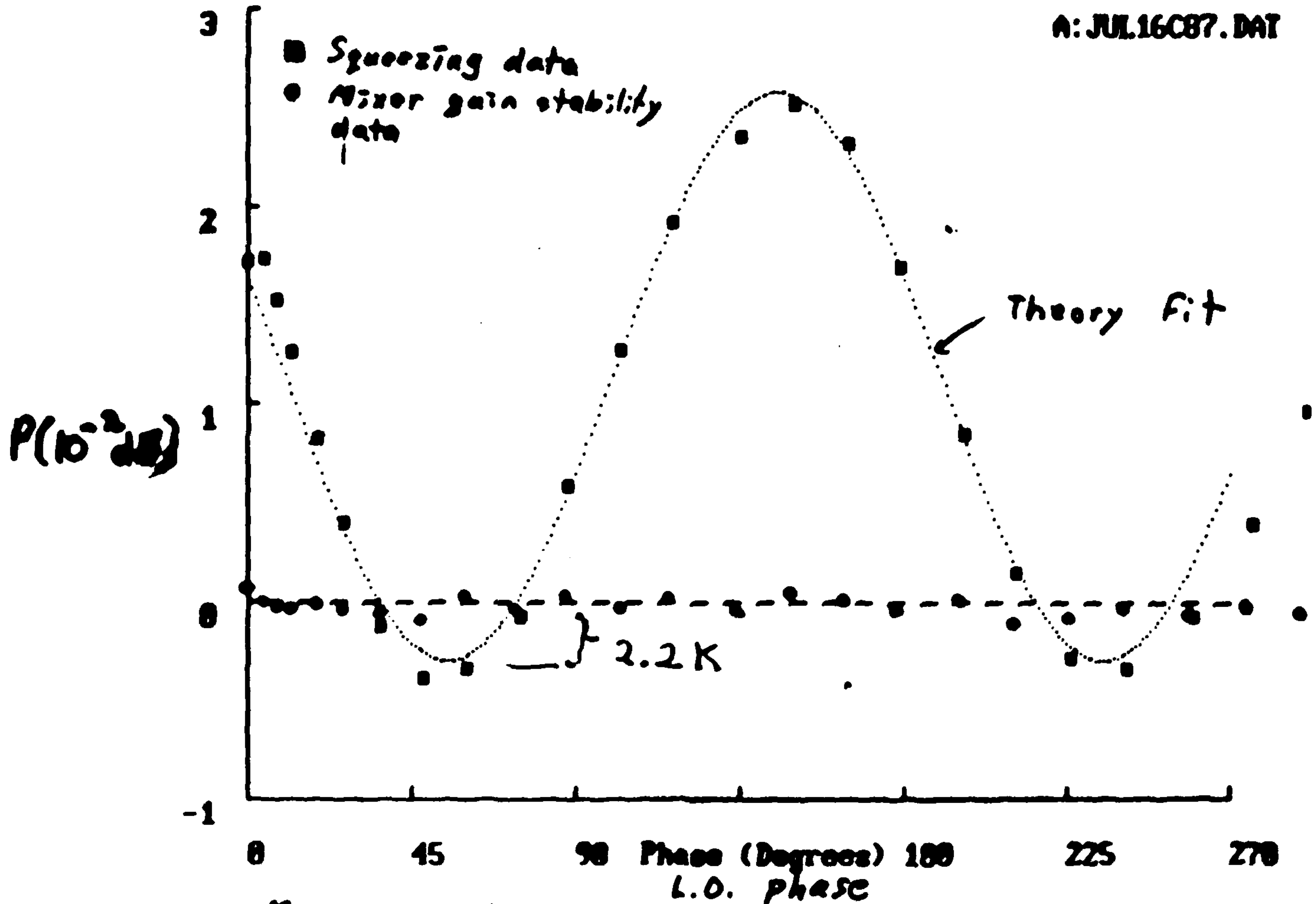

Measured classical gain 9.4 dB
Measured classical loss 3.8 dB

Detecting Squeezed States by Cross-Correlation*

Z.Y. Ou, C.K. Hong and L. Mandel

Department of Physics and Astronomy
University of Rochester
Rochester, New York 14627

Abstract

It is shown that squeezed states can be detected by cross-correlation measurements of the outputs of two detectors in a homodyne experiment, and that squeezing shows up as a positive correlation. The technique offers some of the same advantages as the balanced homodyne technique of Yuen and Chan, without the need to balance the detectors.

---

*This work was supported by the National Science Foundation and by the Office of Naval Research. A paper on this work is to appear in The Physical Review A.

Advantages of the Cross-Correlation Technique

(a) the method is insensitive to detector after-pulsing

(b) squeezing in the full sense can be measured by photon coincidence counting, with few photons

(c) no balancing of the two detectors is required.

(d) the method has some of the virtues of the balanced homodyne method for cancelling local oscillator fluctuations.

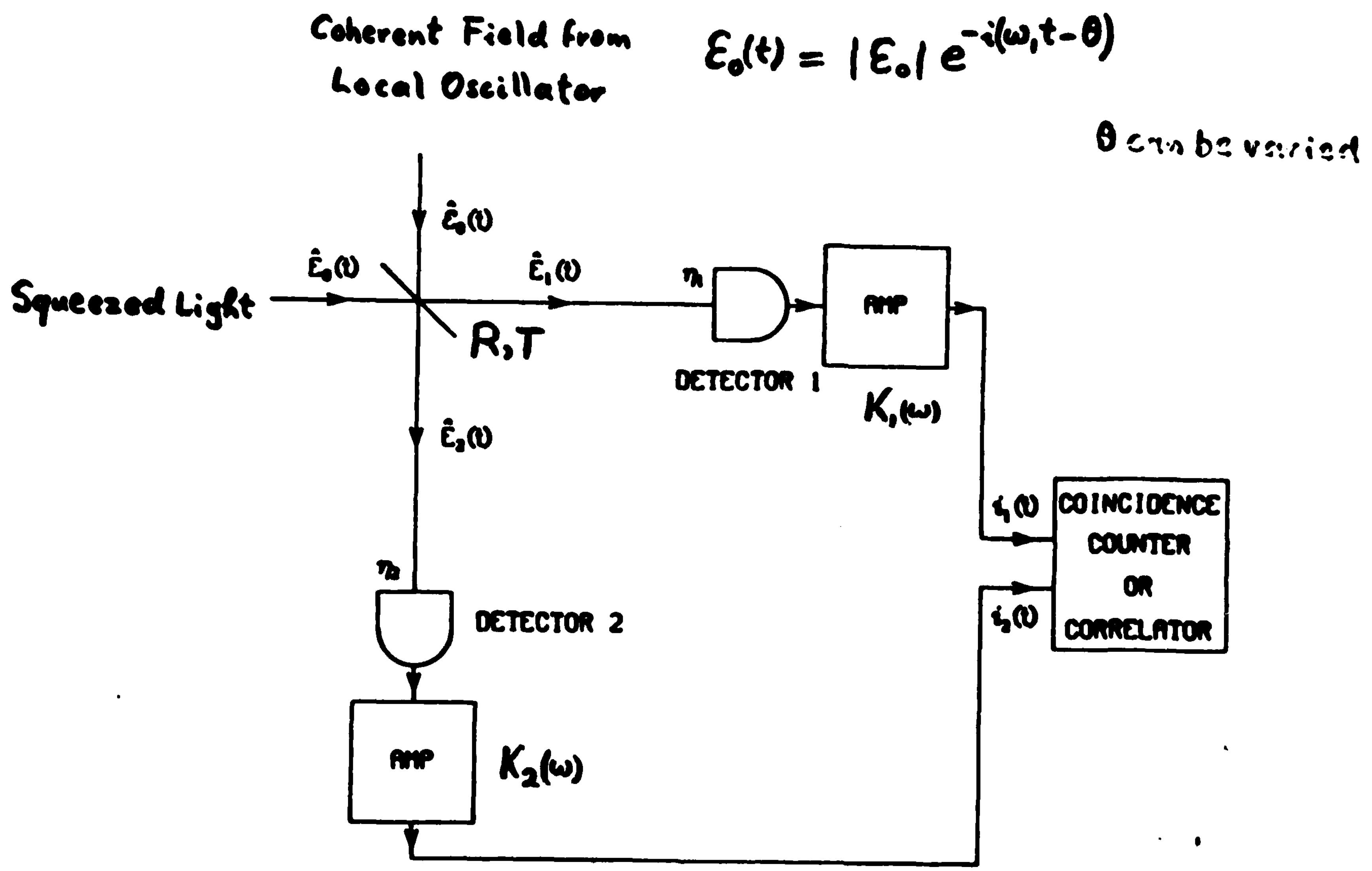

Homodyne Experiment

Beam Splitter Fields

Outputs from Beam Splitter 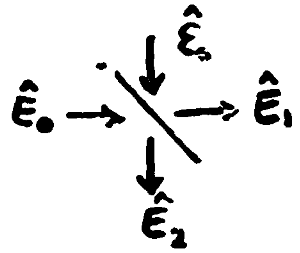

$$\left.\begin{aligned} \hat{E}_1^{(+)}(t) &= \sqrt{T}\,\hat{E}_0^{(+)}(t) + i\sqrt{R}\,\hat{\mathcal{E}}_0^{(+)}(t) \\ \hat{E}_2^{(+)}(t) &= i\sqrt{R}\,\hat{E}_0^{(+)}(t) + \sqrt{T}\,\hat{\mathcal{E}}_0^{(+)}(t) \end{aligned}\right\} \quad (1)$$

$\hat{E}_1$ & $\hat{E}_2$ obey same commutation relations as $\hat{E}_0$ and $\hat{\mathcal{E}}_0$ when $R + T = 1$.

The local oscillator field is in a coherent state, with eigenvalue

$$\mathcal{E}_0(t) = |\mathcal{E}_0|\, e^{-i(\omega_1 t - \theta)}$$

Photocurrents & their Moments

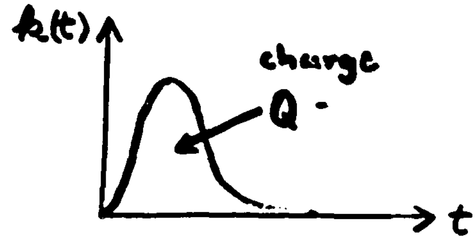

Currents

$$i_j(t) = \sum_\ell k_j(t - t_\ell) \qquad (j = 1,2)$$

Mean Current

$$\langle i_j \rangle = \eta_j Q_j \langle \hat{E}_j^{(-)}(t)\, \hat{E}_j^{(+)}(t) \rangle = \eta_j Q_j \langle \hat{I}_j \rangle \qquad (j = 1,2) \qquad (2)$$

detector

Cross-Correlation

$$\langle i_1(t) i_2(t) \rangle = \iint_{-\infty}^{\infty} k_1(t - t_\ell)\, k_2(t - t_m)\, P_{12}(t_\ell, t_m)\, dt_\ell\, dt_m \quad (3)$$

with

$$P_{12}(t_\ell, t_m) = \eta_1 \eta_2 \langle \mathcal{T} : \hat{I}_1(t_\ell)\, \hat{I}_2(t_m) : \rangle \quad (4)$$

Mean Intensities & Intensity Correlations

From Eqs(1) for the beam splitter

$$\langle \hat{I}_1(t)\rangle = R|\mathcal{E}_0|^2 + i|\mathcal{E}_0|\sqrt{RT}\langle \hat{E}_0^{(-)}(t)\rangle e^{-i(\omega_1 t-\theta)} + c.c. + \ldots$$

$$\langle \hat{I}_2(t)\rangle = T|\mathcal{E}_0|^2 - i|\mathcal{E}_0|\sqrt{RT}\langle \hat{E}_0^{(-)}(t)\rangle e^{-i(\omega_1 t-\theta)} + c.c. + \ldots \tag{5}$$

and to $O(|\mathcal{E}_0|^2)$

$$\langle \mathcal{T}: \Delta\hat{I}_1(t)\Delta\hat{I}_2(t+\tau):\rangle = -RT|\mathcal{E}_0|^2\,\Gamma_{11}(\tau, \theta+\tau\Omega) + \tag{6}$$

autocorrelation of one quadrature

Definition of $\Gamma_{11}(\tau,\beta)$:

Resolve $\hat{E}_0(t)$ into two quadratures

$$\hat{E}_0(t) = \hat{E}_0^{(1)}(t)\cos(\omega_1 t-\beta) + \hat{E}_0^{(2)}(t)\sin(\omega_1 t-\beta)$$

then

$$\Gamma_{11}(\tau,\beta) \equiv \langle \mathcal{T}: \Delta\hat{E}_0^{(1)}(t)\Delta\hat{E}_0^{(1)}(t+\tau):\rangle$$

If $\hat{E}_0^{(1)}$ is squeezed, $\Gamma_{11}(0,\beta) < 0$

Photoelectric Cross-Correlations

By combining eqs. (3), (4) & (6) we obtain

$$\langle \Delta i_1(t)\Delta i_2(t)\rangle = -\eta_1\eta_2 RT|E_0|^2 \iint_{-\infty}^{\infty} k_1(t')k_2(t'')\Gamma_{11}(t'-t'', \theta+\tfrac{\pi}{2})\,dt'dt'' \tag{7}$$

$$= -\eta_1\eta_2 RT|E_0|^2 \frac{1}{2\pi}\int_{-\infty}^{\infty} K_1^*(\omega)K_2(\omega)\,\Phi_{11}(\omega, \theta+\pi/2)\,d\omega \tag{8}$$

where

$$k_j(t) = \frac{1}{2\pi}\int_{-\infty}^{\infty} K_j(\omega)e^{-i\omega t}\,d\omega \qquad (j=1,2)$$

$$\Gamma_{11}(\tau,\theta) = \frac{1}{2\pi}\int_{-\infty}^{\infty}\Phi_{11}(\omega,\theta)e^{-i\omega t}\,d\omega$$

For fast response detectors (7) is more appropriate

For sharply tuned detectors (8) is more appropriate

Fast Response Detectors : Coincidences

If the response $k_j(t)$ of detector j is very short compared with range of $\Gamma_{11}(\tau, \theta)$, then eq.(7) reduces to

$$\boxed{\langle \Delta i_1(t) \Delta i_2(t) \rangle = -\eta_1 \eta_2 R T |\mathcal{E}_0|^2 Q_1 Q_2 \Gamma_{11}(0, \theta + \tfrac{\pi}{2})} \quad (9)$$

This is positive if $\hat{E}_0^{(1)}$ is squeezed in the full sense, in which case $\Gamma_{11}(0, \theta + \frac{\pi}{2}) < 0$.

If $\langle \hat{E}_0 \rangle = 0$, and separate measurements are made with squeezed field turned off, the effects of local oscillator fluctuations cancel <u>by subtraction</u>.

Effects of Local Oscillator Fluctuations

If there are fluctuations of the local oscillator then in eq(9)

$$|\mathcal{E}_0|^2 \rightarrow \langle|\mathcal{E}_0|^2\rangle$$

and, in addition, there are extra terms in

$\langle(\Delta|\mathcal{E}_0|^2)^2\rangle$ and

$\langle \Delta|\mathcal{E}_0|^2 \Delta\mathcal{E}_0 \rangle$, $\langle(\Delta |\mathcal{E}_0|)^2\rangle$, $\langle(\Delta\mathcal{E}_0)^2\rangle$, and c.c.

The effect of the first can be cancelled by making separate measurements with squeezed light turned off and subtracting.

The effects of the other terms vanish if

$$\langle \hat{E}_0^{(+)}(t) \rangle = 0$$

Offers some of the same benefits as balanced homodyne schem of Yuen & Chan

Spectral Analysis

If the detector amplifiers are sharply tuned to frequency ω_F within $\delta\omega$, with $\delta\omega \ll$ bandwidth of $\Phi_{11}(\omega,\theta)$, then eq.(8) reduces to

$$\boxed{\langle \Delta i_1(t)\Delta i_2(t)\rangle = -\eta_1\eta_2 RT|\mathcal{E}_0|^2\,\Phi_{11}(\omega_F,\theta+\tfrac{\pi}{2})\,\frac{1}{\pi}\int_{\omega_F-\delta\omega}^{\omega_F+\delta\omega}|K_1(\omega)K_2(\omega)|\,d\omega \qquad (10)}$$

This is positive if there is squeezing at frequency ω_F,

$$\Phi_{11}(\omega_F,\alpha) < 0 .$$

In all cases squeezing is manifest in the presence of positive cross-correlations

Different Categories of Squeezing

Quadratures $\hat{E}_0^{(1)}(t)$ and $\hat{E}_0^{(2)}(t)$.

$$\hat{E}_0(t) = \hat{E}_0^{(1)}(t)\cos(\omega_1 t-\beta) + \hat{E}_0^{(2)}(t)\sin(\omega_1 t-\beta)$$

(1) If

$$\langle :(\Delta \hat{E}_0^{(1)})^2: \rangle = \Gamma_{11}(0,\beta) < 0 ,$$

then $E_0^{(1)}(t)$ is squeezed in the full sense.

(2) Let

$$\Phi_{11}(\omega,\beta) = \int_{-\infty}^{\infty} \Gamma_{11}(\tau,\beta)\, e^{i\omega\tau}\, d\tau$$

If

$$\Phi_{11}(\omega,\beta) < 0 ,$$

then the field is squeezed at frequency ω.

(3) If $\hat{E}_0^{(1)}$ is squeezed in the full sense, but $\Phi_{11}(\omega) >$ at some frequencies, the squeezing is inhomogeneous

(4) If $\hat{E}_0^{(1)}$ is not squeezed in the full sense, but $\Phi_{11}(\omega) <$ for some ω, then we have spectral component squeezing

Squeezing in 4-Wave Mixing

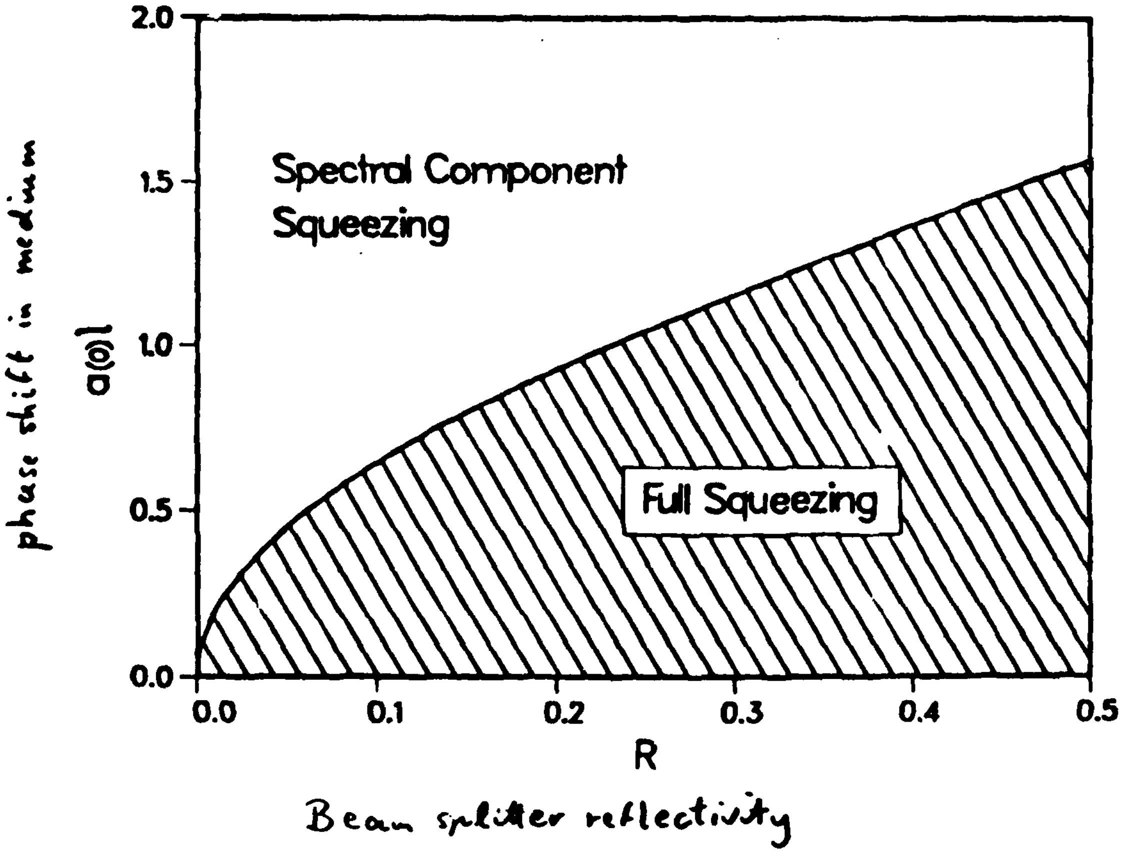

Degree of Squeezing

If $\hat{E}_1^{(+)}$ is squeezed at frequency ω,

$$q(\omega) \equiv \left(\frac{\eta_1 \eta_2}{\alpha_1 \alpha_2}\right)^{1/2} \Phi_{11}(\omega)$$

$q(\omega)$ is independent of detector efficiency

$-1 \le q(\omega) \le 0$ can be obtained from cross-correlation together with auto-correlation with squeezed light blocked, when detectors collect all the light;

$$\boxed{q(\omega) = -(\alpha_1 \alpha_2 R T)^{-1/2} \frac{\langle \Delta i_1 \Delta i_2 \rangle}{\left[\langle (\Delta i_1)^2 \rangle \langle (\Delta i_2)^2 \rangle\right]^{1/2}_{\text{blocked}}}} \qquad (11)$$

quantum efficiencies

Conclusions

1. Squeezing in the full sense and spectral component squeezing result in positive cross-correlations in a homodyne experiment.

2. Squeezing in the full sense can be identified by photon coincidence counting.

3. The correlation technique is largely independent of detector after-pulsing.

4. The technique has some of the virtues of the balanced homodyne method for cancelling out local oscillator fluctuations.

5. No balancing of the two detector signals is required.

WHAT HAS BEEN DONE AND WHAT WILL BE DONE BY SUBNATURAL LINEWIDTH SPECTROSCOPY

Hiroshi Takuma, Kazuko Shimizu

Institute for Laser Science and Department of Engineering Physics
University of Electro-Communications, 1-5-1 Chofugaoka, Chofu-shi Tokyo 182 Japan

and Fujio Shimizu

Department of Applied Physics, Faculty of Engineering
University of Tokyo, Hongo, Bunkyo-ku, Tokyo 113 Japan

1. INTRODUCTION

Reduction of linewidth is an essential approach in high resolution spectroscopy. Several methods to remove or reduce inhomogeneous linewidth have been developed resulting in a drastic improvement in the high resolution capability of laser spectroscopy. On the other hand, application of lasers has not been very effective in reducing homogeneous linewidth.

Main causes of the homogeneous line broadening in gaseous media are pressure broadening, saturation broadening, limited interaction time (transit time in the atomic/molecular beam spectroscopy), and natural width. Among those, the first and the second ones are easily removed or reduced. The third one can be reduced by the use of recently developed laser cooling techniques. Thus the present discussion will be concentrated in the last one: reduction of the natural linewidth.

2. BASIC PRINCIPLE

As is well known, the natural width is caused by the uncertainty principle: when the natural life time of an excited state is τ, observation of the fluorescence from the excited state gives the time at whicn the atom is in the excited state with an accuracy of τ. Thus uncertainty principle requires that the limit in the accuracy of measuring the energy of the excited state is given by $h/(2\pi\tau)$, thus the fluorescence spectrum should have a linewidth (uncertainty in the frequency) of $1/(2\pi\tau)$.

The same phenomenon can be described by classical picture as follows: if an ensemble of atoms is excited instantly to tne excited state. The fluorescence intensity should be described as $I=I_0 \exp(-t/\tau)$, where I_0 is a constant. Then the amplitude of the electric field should be $E=E_0 \exp(-t/2\tau)$, and corresponding Fourier transform, that is the frequency domain representation of the fluorescence as a response to an impulse excitation, should have a FWHM of $1/(2\pi\tau)$.

It is in principle easy to reduce a natural width: that is, to deal with only such atoms which happen to remain in the excited state longer than T, which is a time much longer than the life time τ. Because the number of such atoms is proportional to $\exp(-T/\tau)$, where T is the time much longer than τ, we must sacrifice tne fluorescence intensity in order to reduce the linewidth.

However, one cannot expect any reduction of linewidth by simply carrying out delayed fluorescence measurement. Reduction of the linewidth can be expected if we could detect the response of each atom independently. It is needed to carry out tne delayed measurement of a quantity wnich reflects the amplitude of the fluorescence including the phase. A typical example is seen in various types of coherent interactions of atoms and the electromagnetic field.

3. POSSIBLE SCHEMES AND EXPERIMENTAL RESULTS

[1] DELAYED OBSERVATION OF SINGLE EVENT

In order to certify that a photon is emitted in a time interval longer than T, we must know when the atom made a transition to the excited state. It can be easily done in γ-ray spectroscopy using Mossbauer effect. The 14.4 keV γ-ray is emitted by the spontaneous emission by a nuclear excited state of ^{57}Fe having a life time of 10^{-7} sec. This metastable nuclear state is occupied by 122 keV γ-ray of a higher excited state. Thus detection of 122 keV γ-ray tells us when a nucleus makes transition to the 14.4 keV excited state. If we observe only such a photon which is emitted more than T sec after the emission of a 122 keV photon, we will be able to obtain a sharp linewidth characterized by T[1].

[2] DOUBLE RESONANCE

In many spectroscopic applications, direct purpose of high resolution spectroscopy is to observe the hyperfine structure of the upper or the lower state. Double resonance is a convenient method to observe the hyperfine structure of the upper state, and the linewidth of the radiofrequency spectrum can be much shorter than that of the optical spectrum [2]. Although this is not a direct observation of the subnatural linewidth and does not contribute in improving the accuracy of the optical spectrum, it is an excellent method to determine the hyperfine structure accurately.

[3] RAMSEY RESONANCE

The most straightforward scheme of subnatural linewidth spectroscopy should be that of Ramsey resonance: if an atom is excited to the resonant state in the first field and keeps coherence until it is interacted by the second radiation field, signal takes a "Ramsey pattern." Apparently coherence of the atom is conserved only when it stays in the excited state, and the number of such atoms should decrease by a factor $\exp(-T/\tau)$.

For resonant transitions in the visible region, the natural lifetime is too short to practice conventional Ramsey resonance experiment. In such a case, acceleration of atoms (ionization — acceleration — neutralization) is a reasonable solution, though technically tedious to accelerate neutral atoms [3].

[4] LEVEL CROSSING

Level crossing signal is a result of mixing of two quantum states, and interference of the probability amplitudes is directly detected. Thus we have a possibility of narrowing the line by delayed observation. This method has been applied by several groups in early 70's on Ca and Ba [4], and also on Na [5,6] successfully observing narrowed linewidth.

[5] QUANTUM BEAT

When a couple of nearby states of the same symmetry are excited at the same time by a pulsed light, we can observe a quantum beat signal, which is essentially the interference of the probability amplitudes of the two states. Thus the observation of the quantum beat allows us to narrow the linewidth by carrying out the delayed observation. Theoretical treatment on this scheme was discussed in detail [7,8].

[6] COHERENT TRANSIENT

Coherent transient phenomena generally includes all the effects in which interaction of coherent light and coherent quantum states of matter give rise to a signal as the beat note of the coherent incident light and the radiation emitted by the induced dipole of the matter. Thus there are many possible arrangements by which we can expect narrowing by delayed observation.

However, an experimental success has been obtained only on our phase switching method [9,10]. In this method, one observes the effect of phase switching in the nutation signal of the atoms. Recently, hyperfine components in the D_2 line of lithium which are overlapping in the natural linewidth limited spectroscopy have been successfully separated by this method [11]. This may be the first experimental demonstration that SNWS is practically useful if it allows to separate hyperfine structures hidden within the natural width, as shown in a computer simulation [12].

4. FUTURE TRENDS

Importance of SNWS has been increased by recent technical improvements on laser cooling and trapping of atoms and ions. Ultimate linewidth limit in SNWS is atomic/molecular transit time in the optical field and signal-to-noise ratio. The former can be very much extended by cooling the atoms under observation and can be even infinite by trapping the atoms. The former can be eliminated simply extending the total accumulation time, if we have sufficient absolute frequency stability of lasers, and the SNWS scheme guarantees the center frequency of the spectrum to be investigated. This last point is especially important in choosing the SNWS scheme.

REFERENCES

1. W. Neuwirth, Z. Phys. 197, 473 (1966).
2. I.J. Ma, G. zuPutlitz and G. Schutte, Z. Phys. 208, 276 & 352 (1968).
3. K.A. Safinya, K.K. Chan, S.R. Lundeen and F.M. Pipkin, Phys. Rev. Lett., 45, 1934 (1980).
4. P. Schenck, R.C. Hilborn and H. Metcalf, Phys. Rev. Lett., 31, 189 (1973).
5. H. Figger and H. Walther, Z. Phys. 267, 1 (1974).
6. J.S. Deech, P. Hannaford and G.W. Series, J. Phys. B, 7, 1131 (1974).
7. P. Meystre, M.O. Scully and H. Walther, Opt. Communicat., 33, 153 (1980).
8. H.W. Lee, P. Meystre and M.O. Scully, Phys. Rev. A, 24, 1914 (1981).
9. F. Shimizu, K. Umezu and H. Takuma, Phys. Rev. Lett., 47, 825 (1981).
10. F. Shimizu, K. Shimizu and H. Takuma, Phys. Rev. A, 28, 2248 (1983).
11. F. Shimizu, K. Shimizu and H. Takuma, Phys. Rev. A, 35, 3149 (1987).
12. H. Metcalf and W. Phillips, Opt. Lett., 5, 540 (1980).

SUBNATURAL LINEWIDTH SPECTROSCOPY

WHAT IS NATURAL LINEWIDTH?

(1) QUANTUM MECHANICAL

NATURAL LINEWIDTH:

UNCERTAINTY

$$\Delta E = h / 2\pi\tau$$

(τ : RAD. LIFETIME)

$$\rightarrow \quad \Delta \nu = 1 / 2\pi\tau$$

(2) CLASSICAL

FOURIER TRANSFORM OF

DECAYING EMISSION

$I(t) = I_0 \exp(-t/\tau)$ (INTENSITY)

$\rightarrow$ $E(t) = E_0 \exp(-t/2\tau)$ (AMPLITUDE)

$\downarrow$ F.T.

$$I(\omega) = I_p / [(\omega - \omega)^2 + (1/2\pi\tau)^2]$$

NATURAL LINEWIDTH CANNOT BE REDUCED BY A SIMPLE DELAYED OBSERVATION OF INTENSITY

$$\mathrm{Re}\{E(\omega)\} = \{E_0\, e^{-\gamma T} / [(\Delta\omega)^2 + \gamma^2]\}$$

$$\times\ [\gamma \cos(\Delta\omega T) - \Delta\omega \sin(\Delta\omega T)],$$

$$\mathrm{Im}\{E(\omega)\} = \{E_0\, e^{-\gamma T} / [(\Delta\omega)^2 + \gamma^2]\}$$

$$\times\ [\gamma \sin(\Delta\omega T) + \Delta\omega \cos(\Delta\omega T)].$$

However,

$$I = \mathrm{Re}\{E(\omega)\}^2 + \mathrm{Im}\{E(\omega)\}^2 = E_0\, e^{-\gamma T} / [(\Delta\omega)^2 + \gamma^{2}]$$

NEEDED TO PICK UP

A COHERENT INTERACTION

SUCH AS:

[1]SINGLE ATOM PHENOMENUM

[2]DOUBLE-RESONANCE

[3]RAMSEY RESONANCE

[4]LEVEL CROSSING BEAT

[5]QUANTUM BEAT

[6]COHERENT TRANSIENTS

[1] SINGLE ATOM EMISSION
γ — RAY SPECTROSCOPY (1)

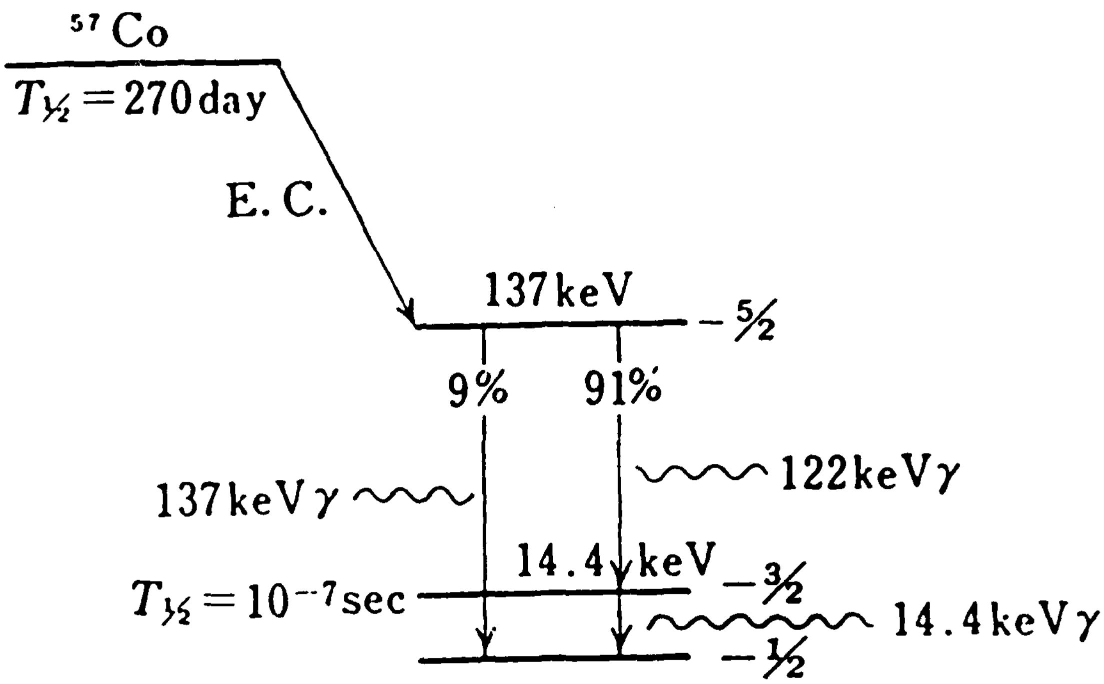

γ — RAY SPECTROSCOPY(2)

ex.)W.NEUWIRTH, 1966

SCHEMATIC EXPERIMENTAL SETUP

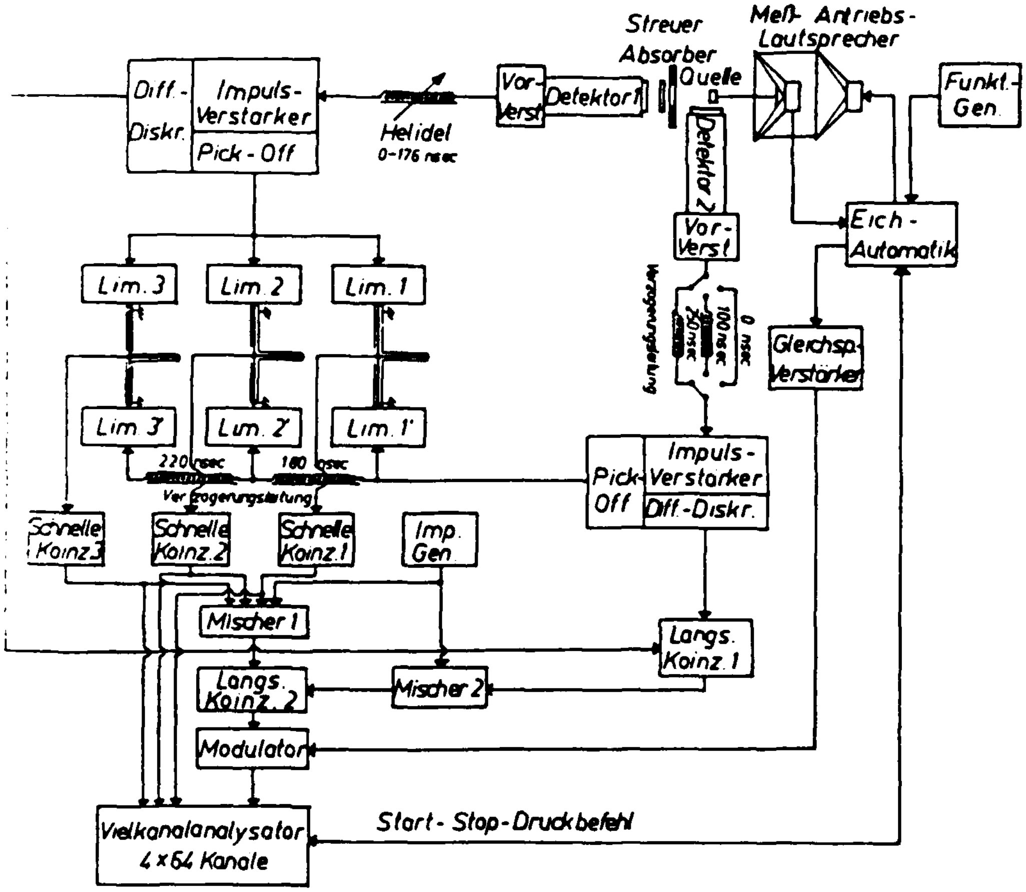

HZ 5

γ — RAY SPECTROSCOPY(3)

ex.) W. NEUWIRTH. 1966
EXPERIMENTAL RESULT

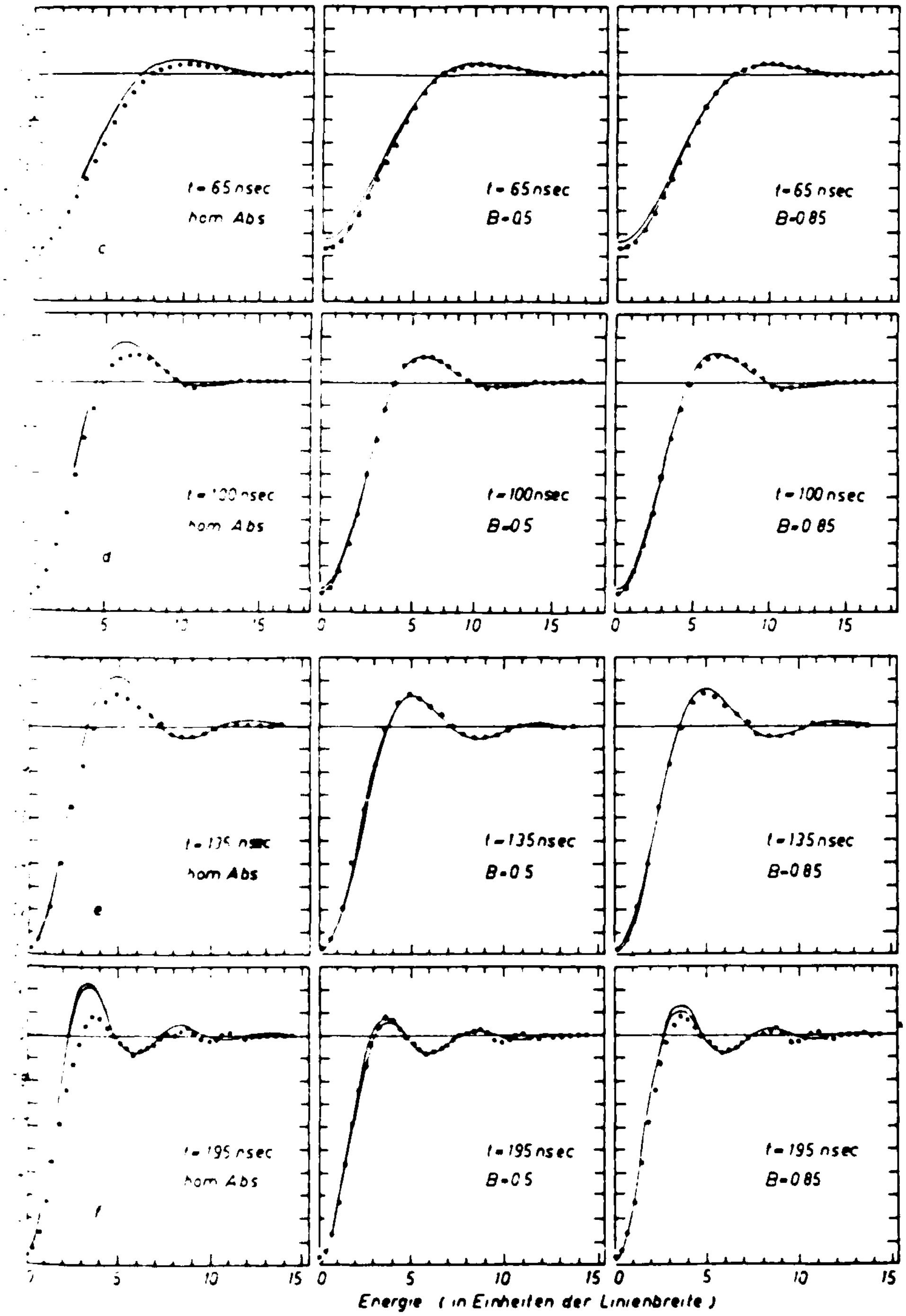

[2]DOUBLE RESONANCE(1)

ex.)I.J.MA et al.,1968

Cd & Sr

SCHEMATIC EXPERIMENTAL SETUP

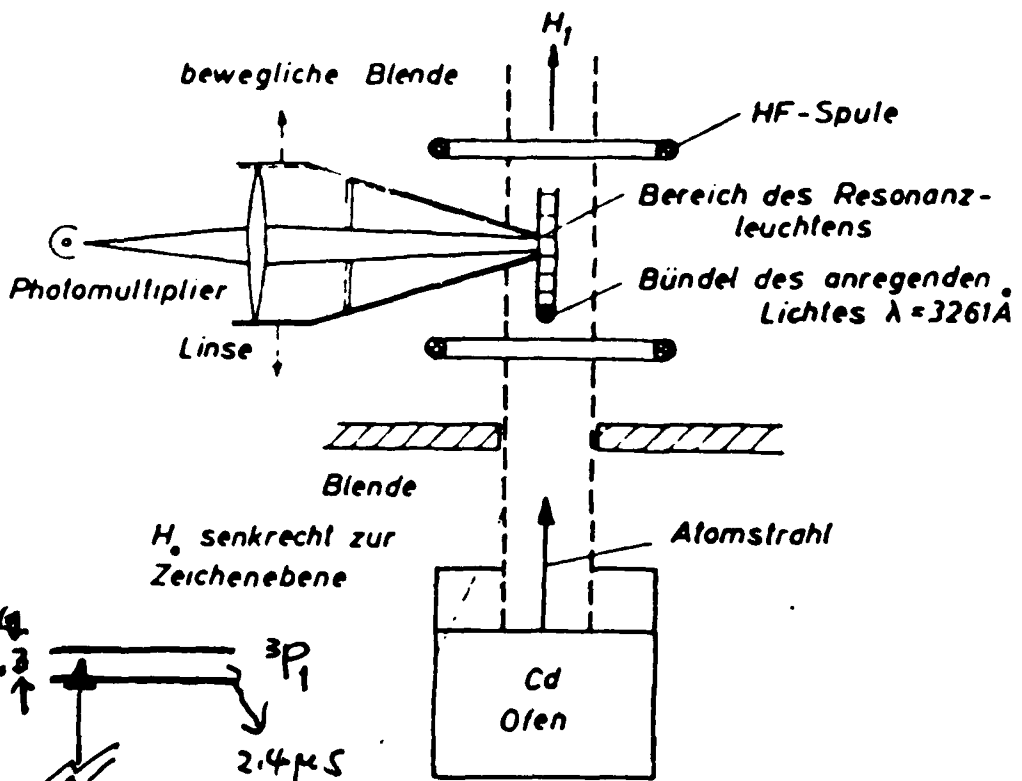

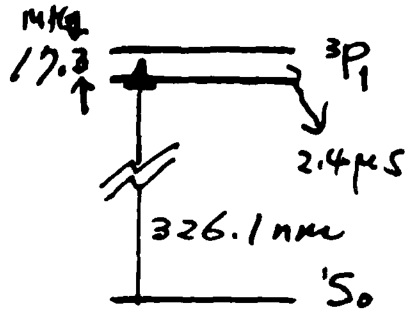

H.T. 7

[2]DOUBLE RESONANCE(2)

ex.)I.J.MA et al..1968

Cd & Sr

EXPERIMENTAL RESULT

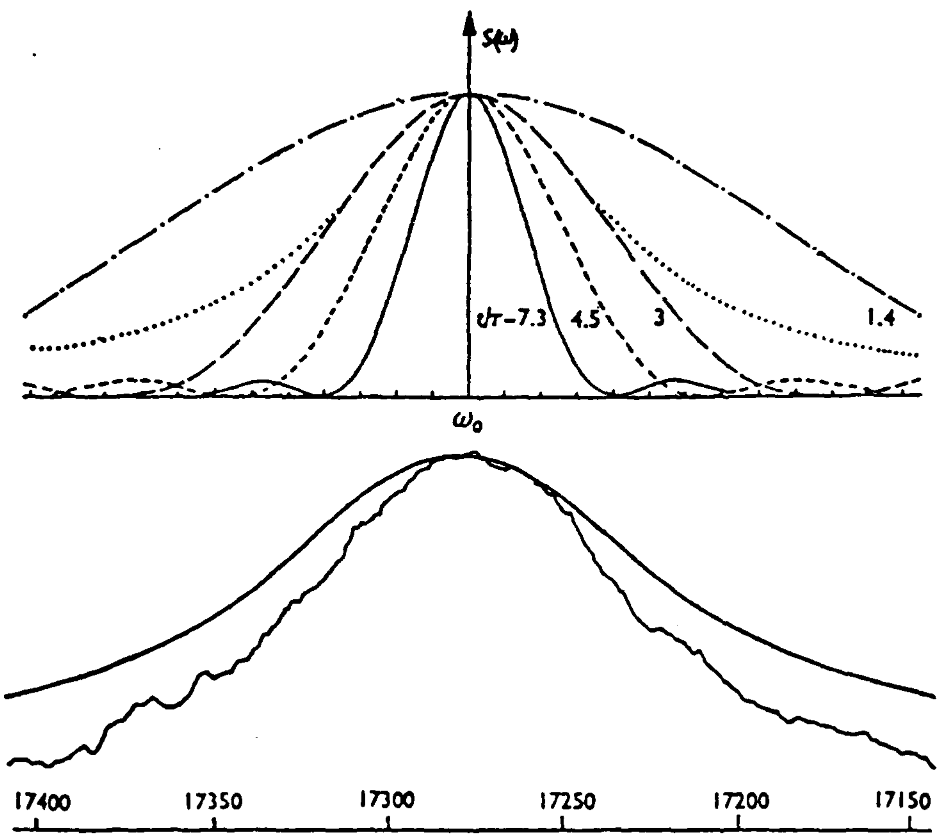

UTP

[4] LEVEL CROSSING (1)

ENERGY LEVELS

J S Deech et al

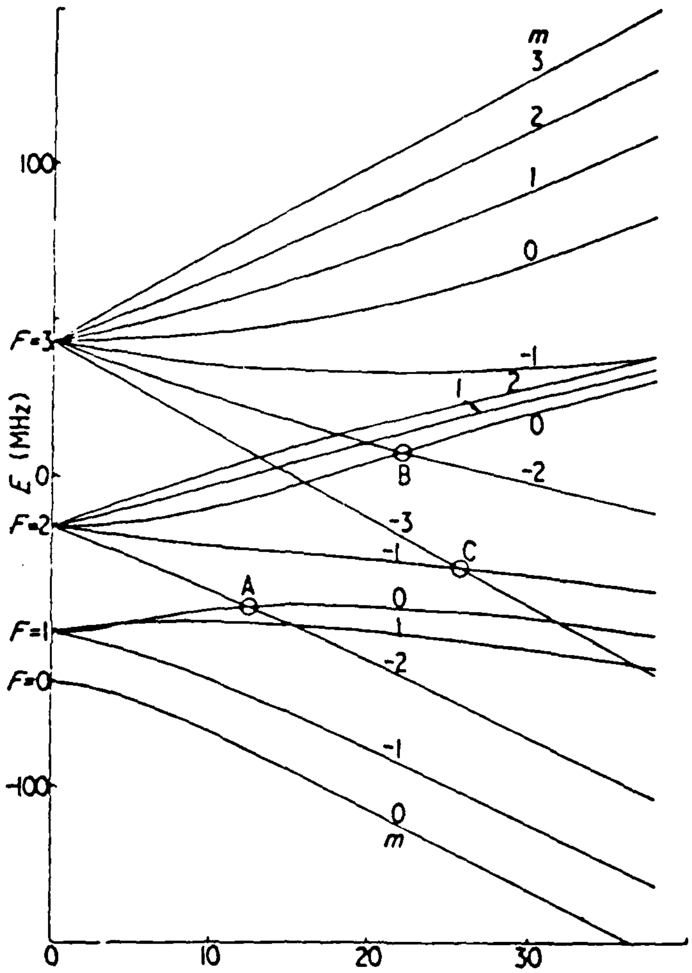

Figure 3. Energy eigenvalues for $I = \frac{3}{2}$, $J = \frac{3}{2}$, plotted against magnetic field, with $a = 18$ MHz, $b = 3.0$ MHz.

H.7.9

[4]LEVEL CROSSING(2)
EXPERIMENTAL RESULTS
ex.)P.SCHENK et al., 1973 Ba

THEORY

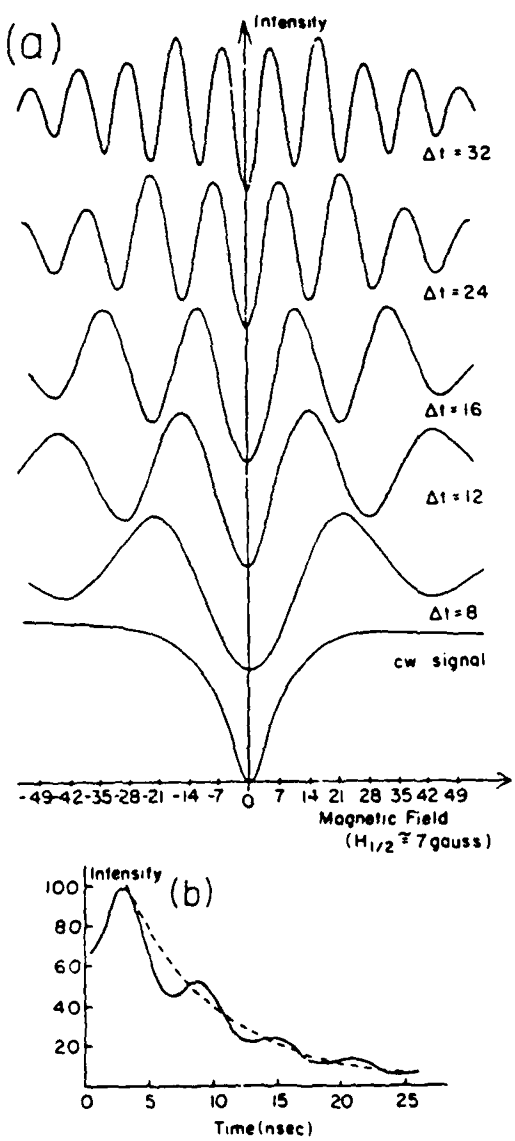

EXPERIMENT

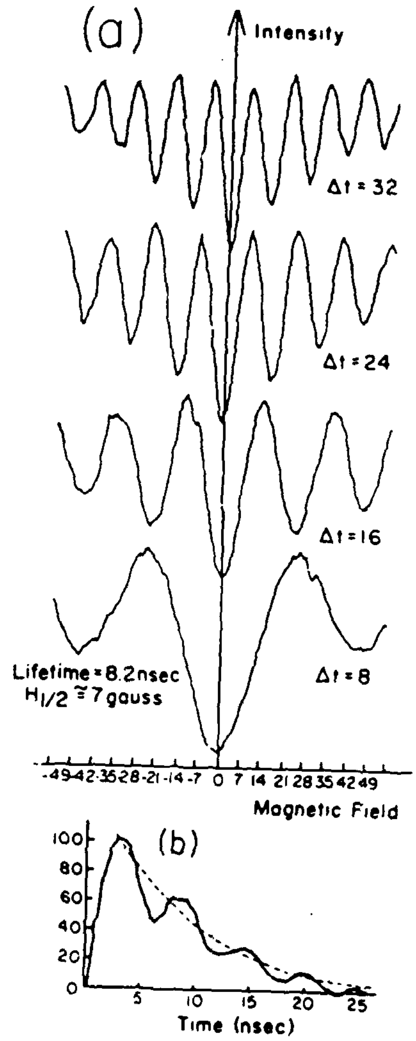

H.T.10

[4]LEVEL CROSSING(3)

EXPERIMENTAL RESULTS

ex.)H.WALTHER et al., 1974 Na

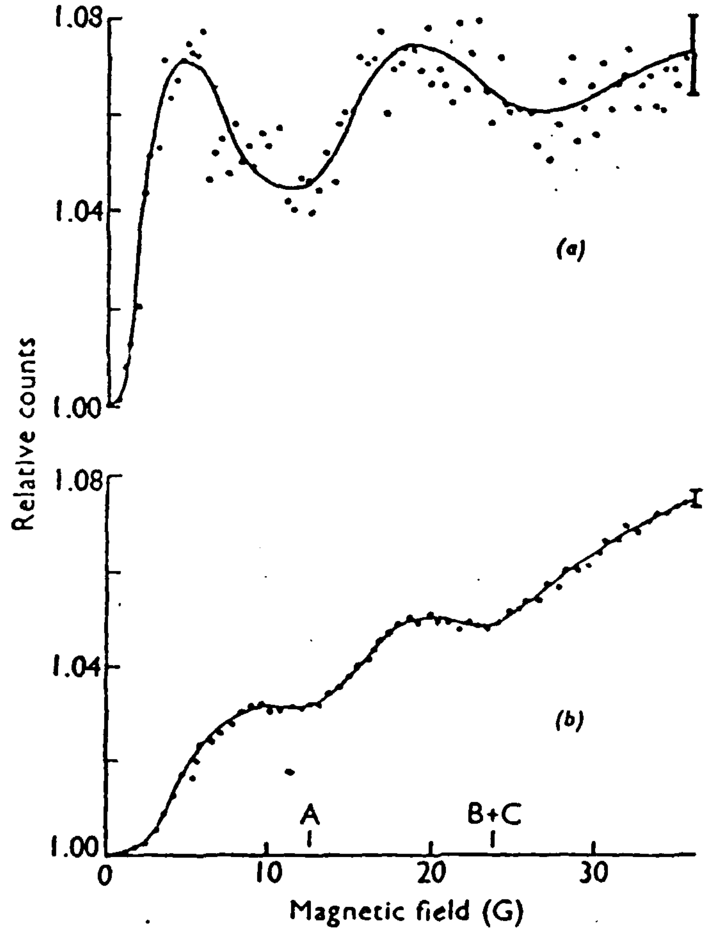

FIG. 3. Hanle effect and level-crossing curves in the $3^2P_{3/2}$ state of Na[11] with (a) and without (b) narrowing. Delay time 40 nsec (Ref. 10).

HT 11

[3]RAMSEY RESONANCE(1)

ex.)K.A.SAFINYA et al. 1980

SCHEMATIC EXPERIMENTAL SETUP

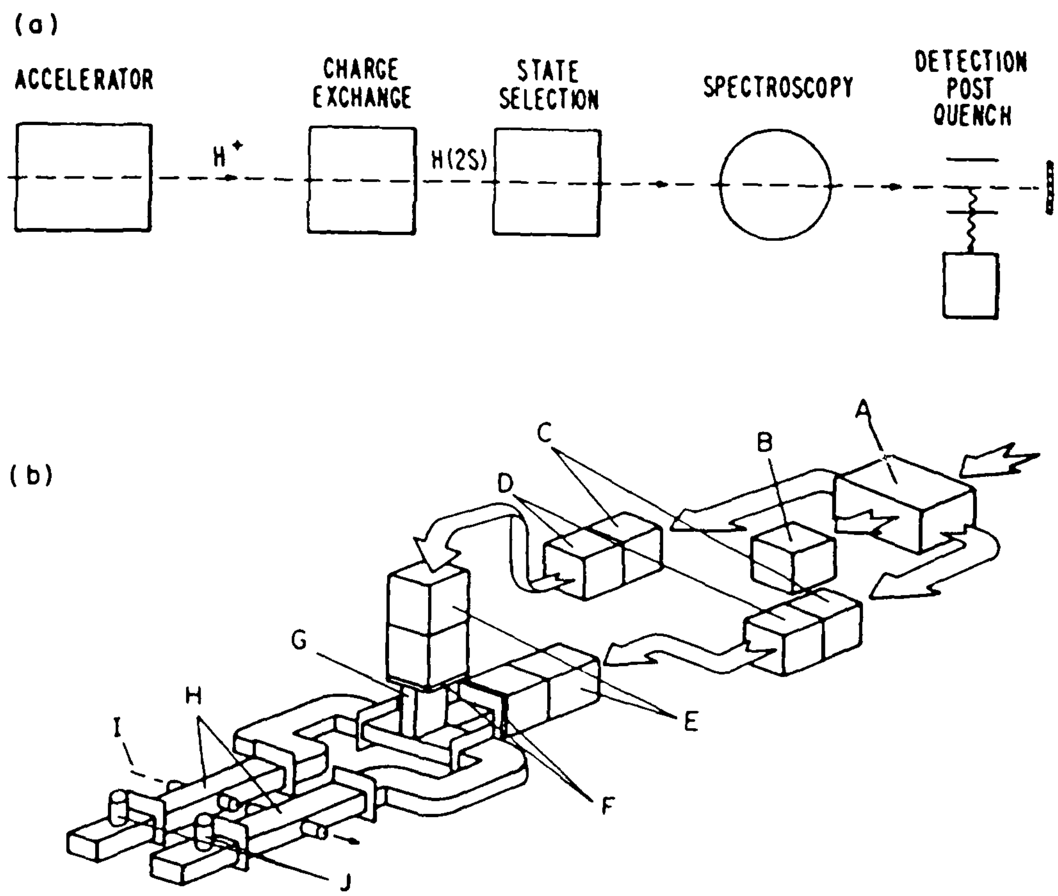

FIG. 1. (a) A schematic drawing of the apparatus. (b) A schematic drawing of the microwave plumbing in the spectroscopy region. *A*, three-pole switch; *B*, matched load; *C*, low-pass filters; *D*, precision variable attenuators; *E*, 50-dB circulators; *F*, vacuum windows; *G*, magic tee; *H*, interaction waveguides; *I*, beam; *J*, detector diodes.

H.7 /2

[3]RAMSEY RESONANCE(2)

ex.)K.A.SAFUNYA et al., 1980

EXPERIMENTAL RESULT

$2^2P_{3/2} \rightarrow 2^2S_{1/2}$ OF H

9911.117(41) MHz

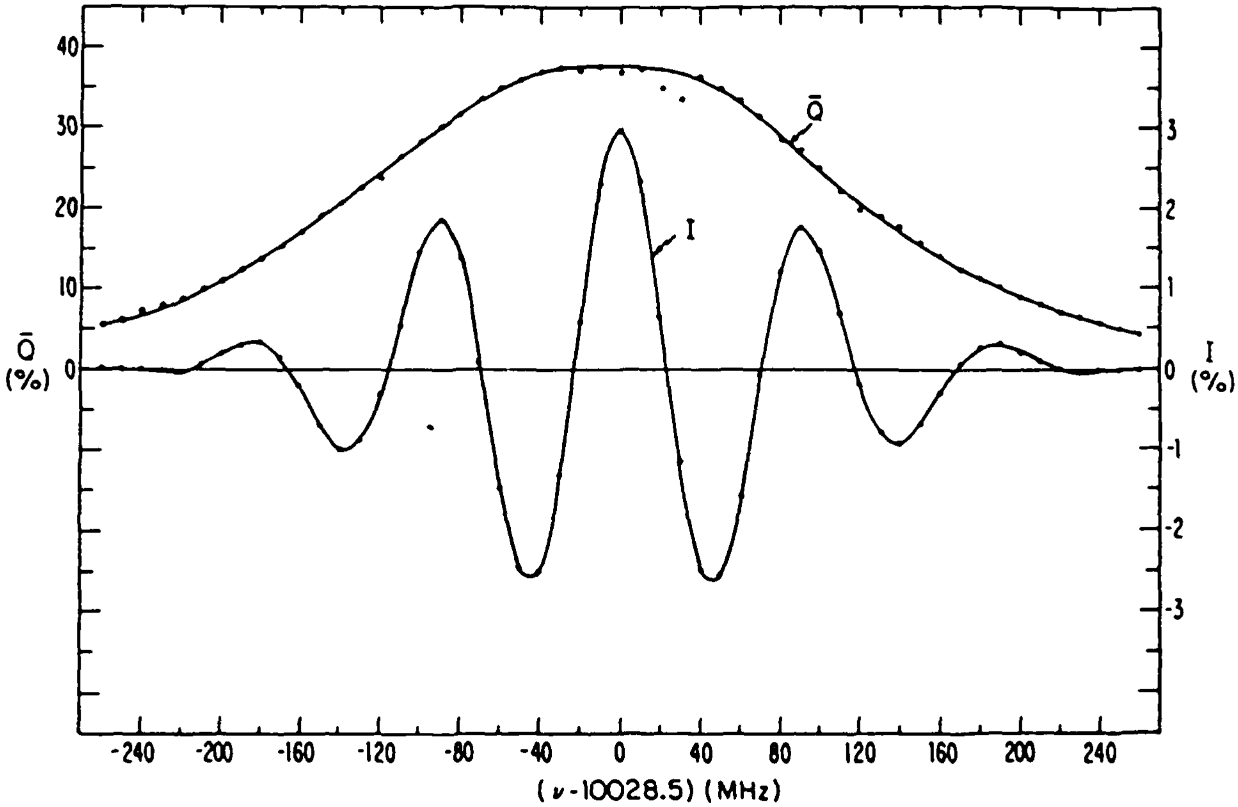

[6]COHERENT TRANSIENT

ex.)PHASE SWITCHED NUTATION

BY F.SHIMIZU et al. 1981 Na

(a)

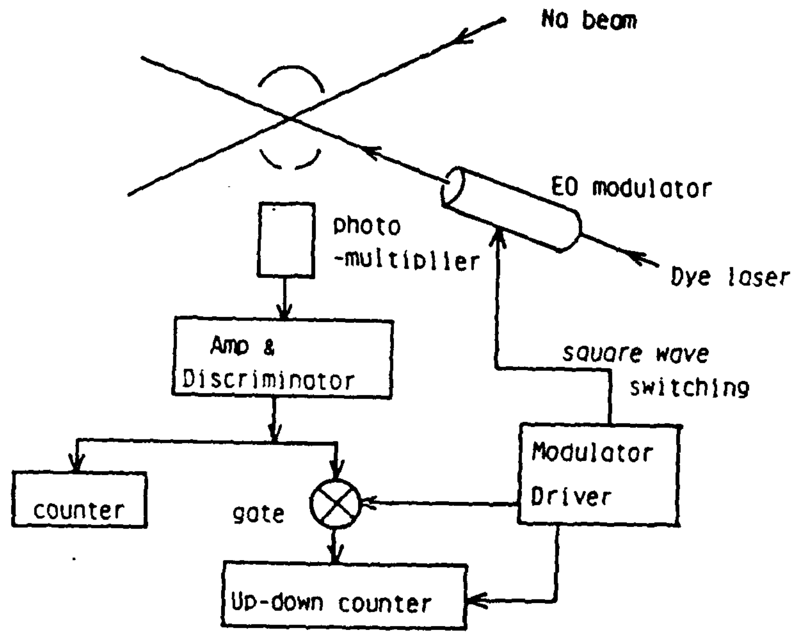

(b)

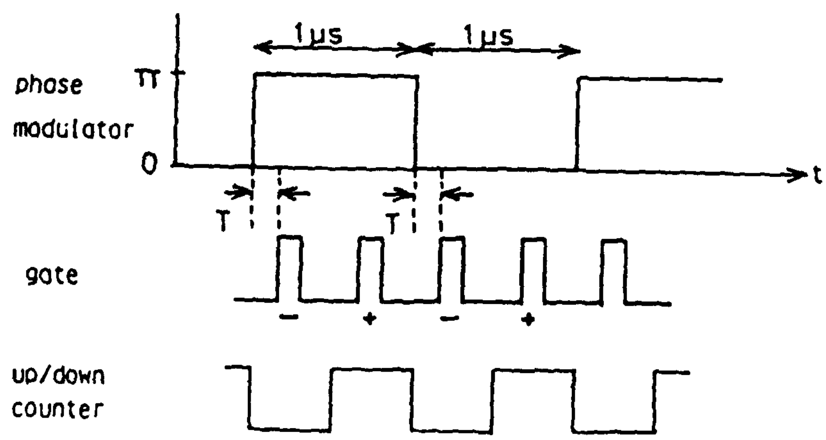

H 7 IV

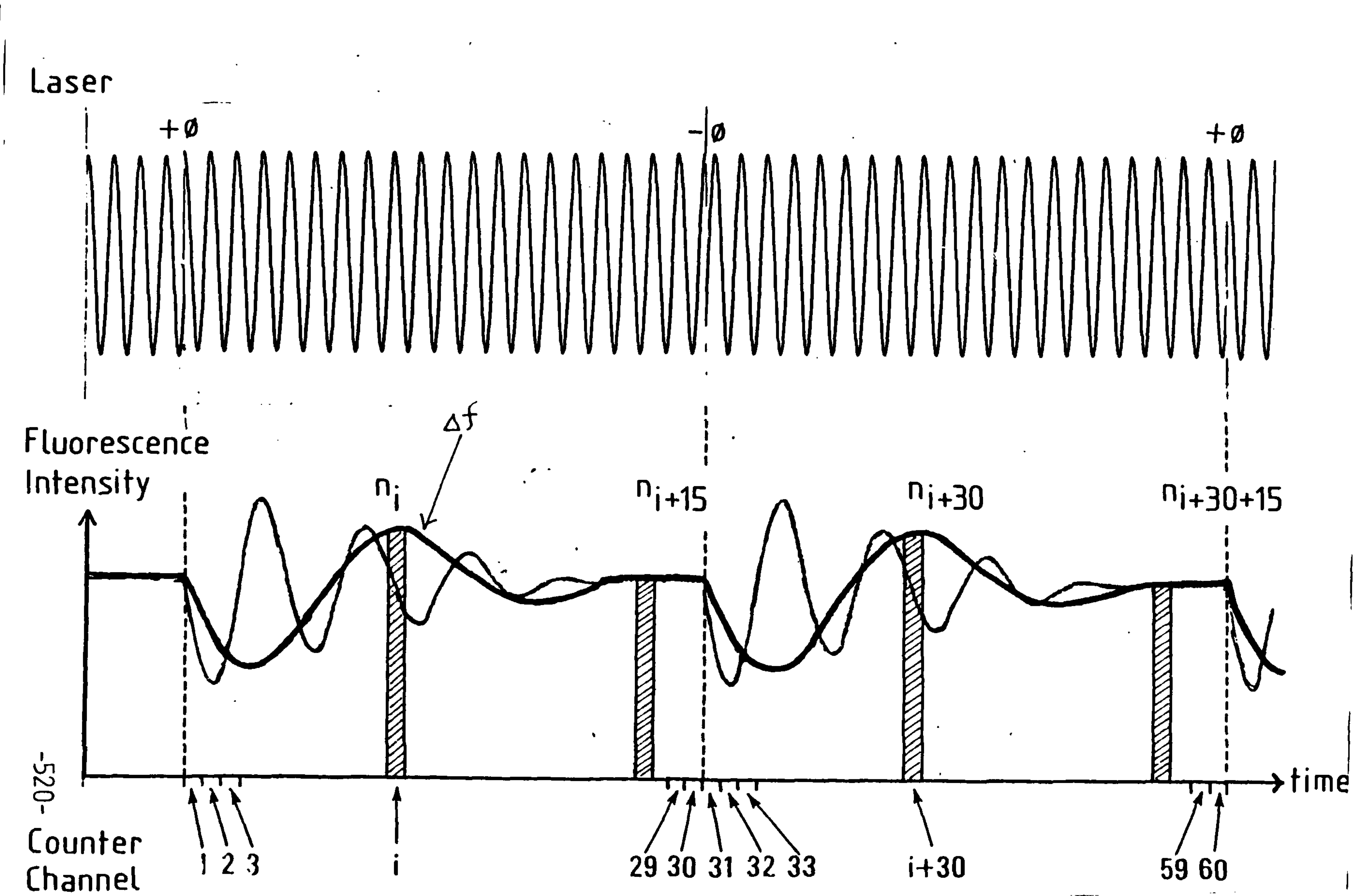
Laser
+ø
-ø
+ø
Fluorescence Intensity
Δf
n_i
n_{i+15}
n_{i+30}
$n_{i+30+15}$
time
Counter Channel
1 2 3
i
29 30 31 32 33
i+30
59 60

DENSITY MATRIX FORMULATION

$$d\rho_{11}/dt = -i\Omega(\rho_{12}-\rho_{21}) - \gamma_{11}\rho_{11}$$

$$d\rho_{22}/dt = i\Omega(\rho_{12}-\rho_{21}) - \gamma_{22}\rho_{22}$$

$$d\rho_{12}/dt = (i\omega_0 - \gamma_{12})\rho_{12} - i\Omega(\rho_{11}-\rho_{22})$$

$$\rho_{21} = \rho_{12}^{*}, \qquad \Omega = \mu E/\hbar$$

$$E = \begin{cases} E_0 \exp(-i\psi - i\omega t) + c.c. & (t<0) \\ E_n \exp(\quad -i\omega t \quad) + c.c. & (t>0) \end{cases}$$

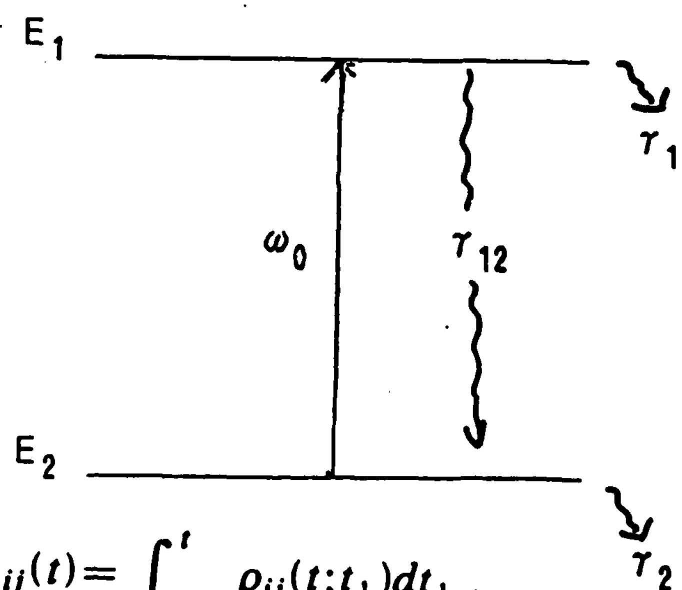

$$R_{ij}(t) = \int_{-\infty}^{t} \rho_{ij}(t;t_1)\,dt_1 .$$

For fluorescence

Steady state signal

Incoherent transient

$$R_{11}(t)=\frac{\mu^2}{\hbar^2}\frac{1}{\gamma_1\gamma_2}\frac{1}{-i\Delta\omega+\gamma_{12}}[\,|E_n|^2+(|E_0|^2-|E_n|^2)e^{-\gamma_1 t}]$$

decay rate is that of spontaneous emission

$$+\frac{\mu^2}{\hbar^2}\frac{1}{\gamma_2}\frac{1}{-i\Delta\omega+\gamma_{12}}\frac{1}{i\Delta\omega-\gamma_{12}+\gamma_1}(E_n^*E_0e^{-i\varphi}-|E_n|^2)$$

$$\times(\underbrace{e^{(i\Delta\omega-\gamma_{12})t}}_{\text{Coherent transient}}-e^{-\gamma_1 t})+\text{c.c.}$$

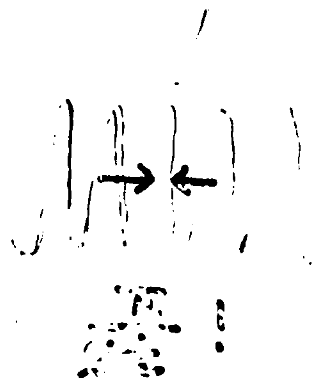

12

$$\Delta R_{11} \equiv R_{11}(\varphi,t) + R_{11}(-\varphi,t) - 2R_{11}(0,t)$$

$$= 4\frac{\mu^2}{\hbar^2}\frac{1}{\gamma_2}\frac{1}{(\Delta\omega)^2+\gamma_{12}^2}\frac{1}{(\Delta\omega)^2+(\gamma_1-\gamma_{12})^2}|E|^2(\cos\varphi-1)$$

$$\times\{[(\Delta\omega)^2-\gamma_{12}^2+\gamma_1\gamma_{12}][\underbrace{e^{-\gamma_{12}t}}\underbrace{\cos(\Delta\omega t)}-\underbrace{e^{-\gamma_1 t}}]$$

$$-\Delta\omega(\gamma_1-2\gamma_{12})\underbrace{e^{-\gamma_{12}t}}\underbrace{\sin(\Delta\omega t)}\},$$

$\gamma_{12} = \frac{1}{2}(\gamma_1+\gamma_2)$

If $\gamma_2 > \gamma_1$, observe ΔR_{22}

FOR $\gamma_1 = 2\gamma_{12}$

$$\Delta R_{11} = 4\frac{\mu^2}{\hbar^2}\,|E|^2(\cos\varphi - 1)\frac{1}{\gamma_2}\,\frac{1}{(\Delta\omega)^2+\gamma_{12}^2}$$

$$\times[e^{-\gamma_{12}t}\cos(\Delta\omega t) - e^{-2\gamma_{12}t}]\,.$$

$$\Delta\bar{R}_{11} = \gamma\int_{t_1}^{t_2}[R_{11}(\varphi,t)+R_{11}(-\varphi,t)-2R_{11}(0,t)]e^{\gamma t}dt$$

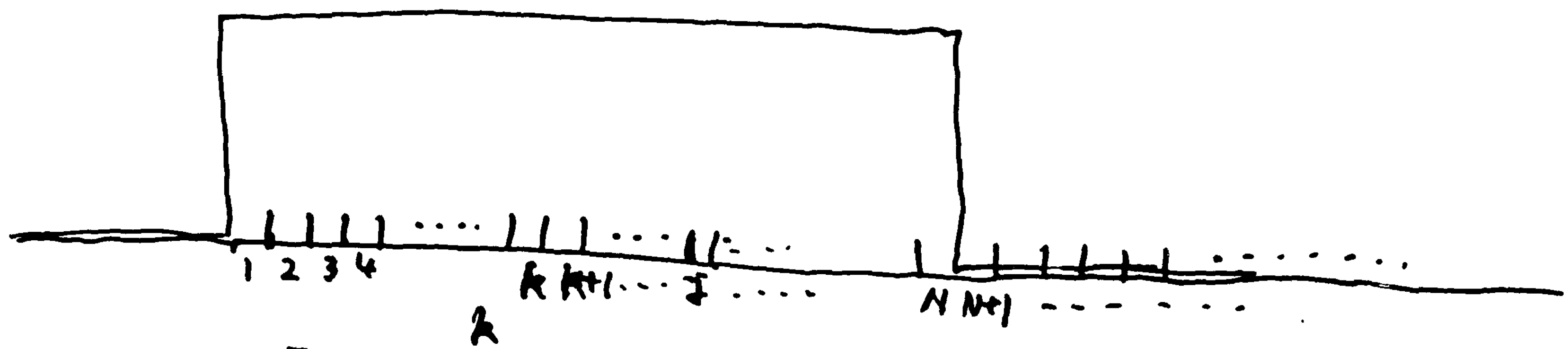

$$I_j = \sum_{i=1}^{k} \left(I_i + I_{i+N} - I_{i+j+N} - I_{i+j} \right) \exp\left(i - k\gamma T/(\tau N)\right)$$

$$I(\Delta\omega) = I_0 \frac{\gamma^2}{\Delta\omega^2 + \gamma^2} \left[\frac{\sin(\Delta\omega T)}{\Delta\omega T} + \frac{1 - \exp(-\gamma T)}{\gamma T} \right]$$

$$\gamma = \frac{1}{2} \gamma_1$$

Theoretical curves, absorption.

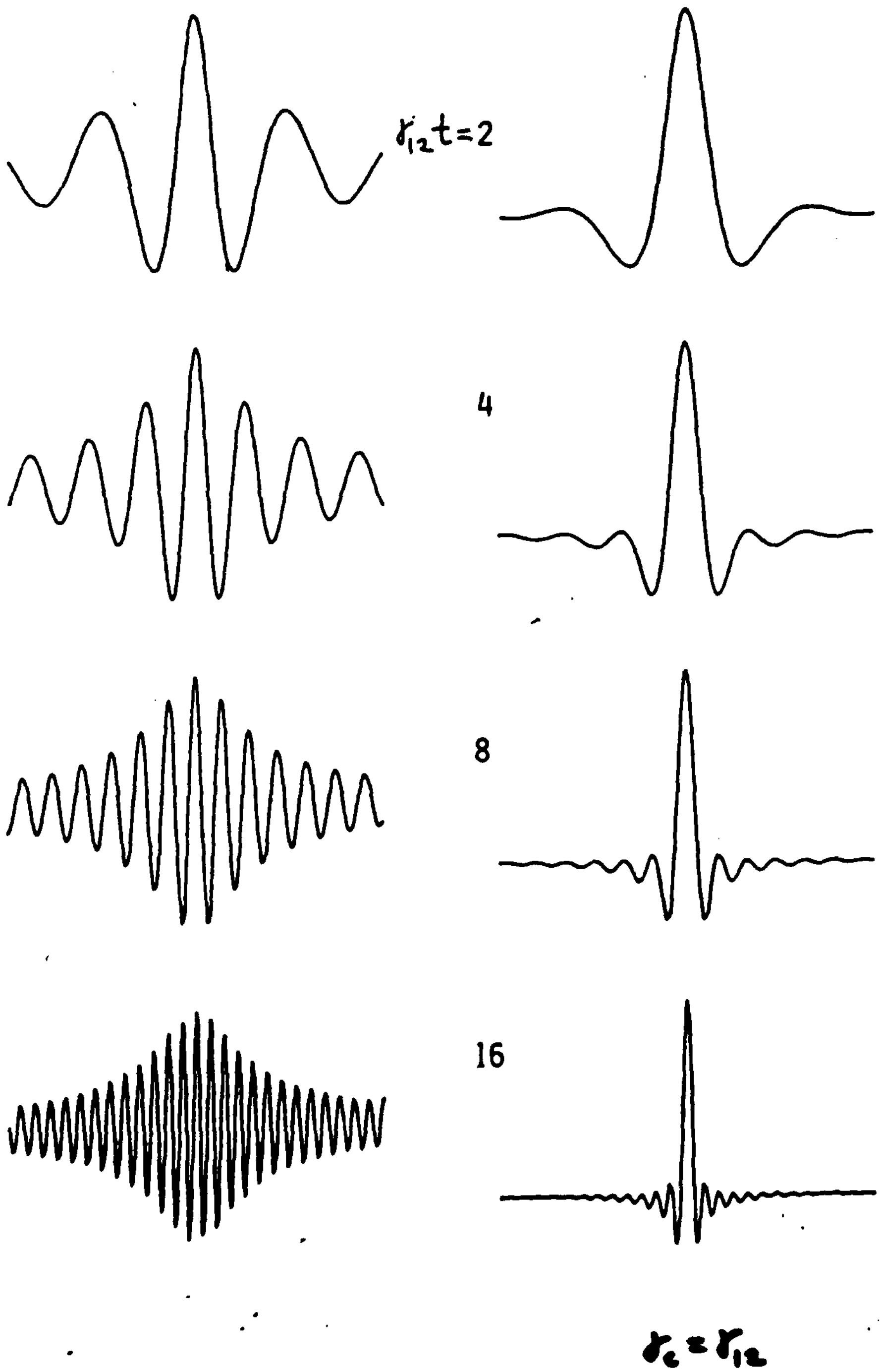

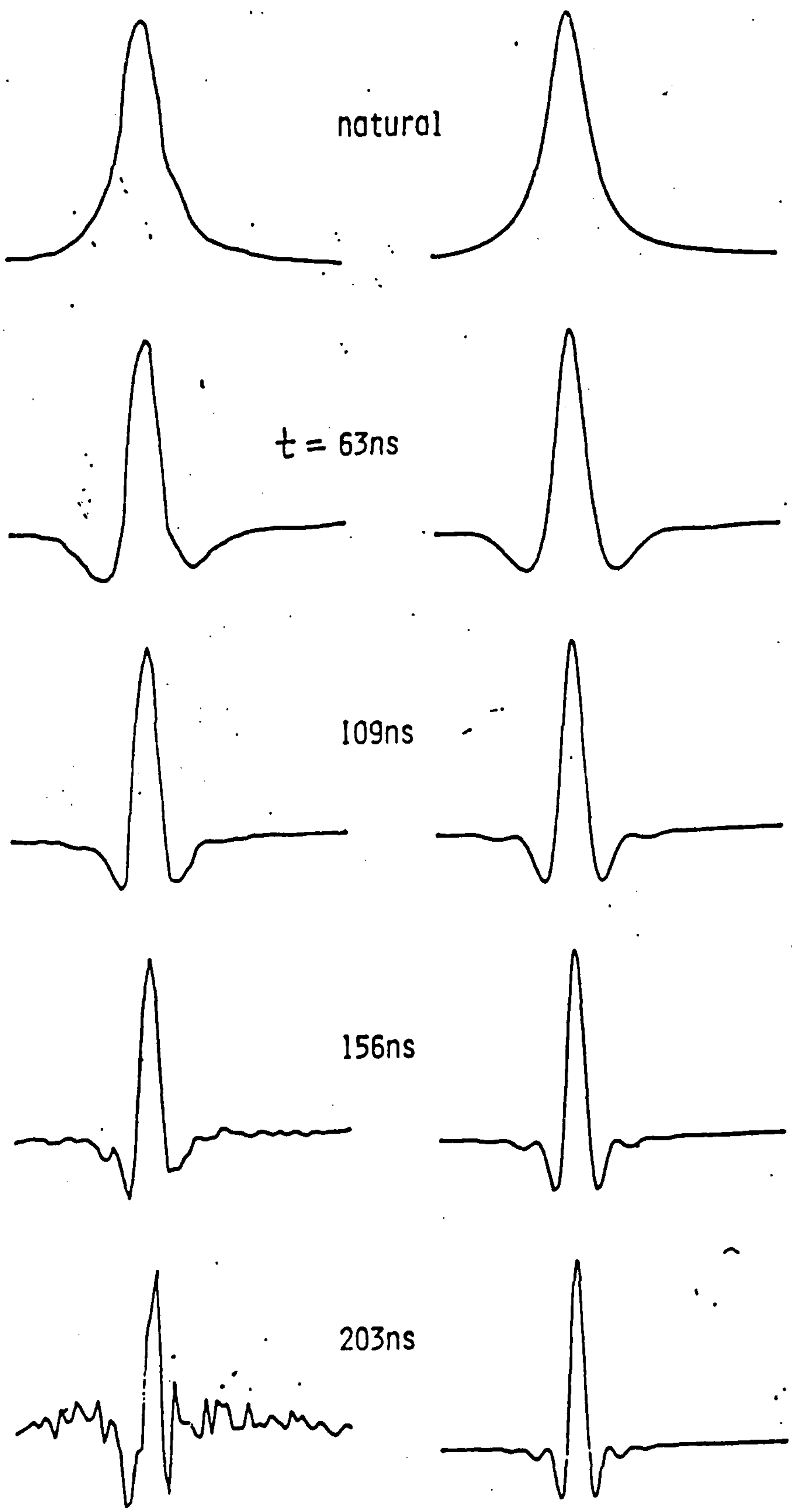

Lineshape with exp. average.

H.Z 21

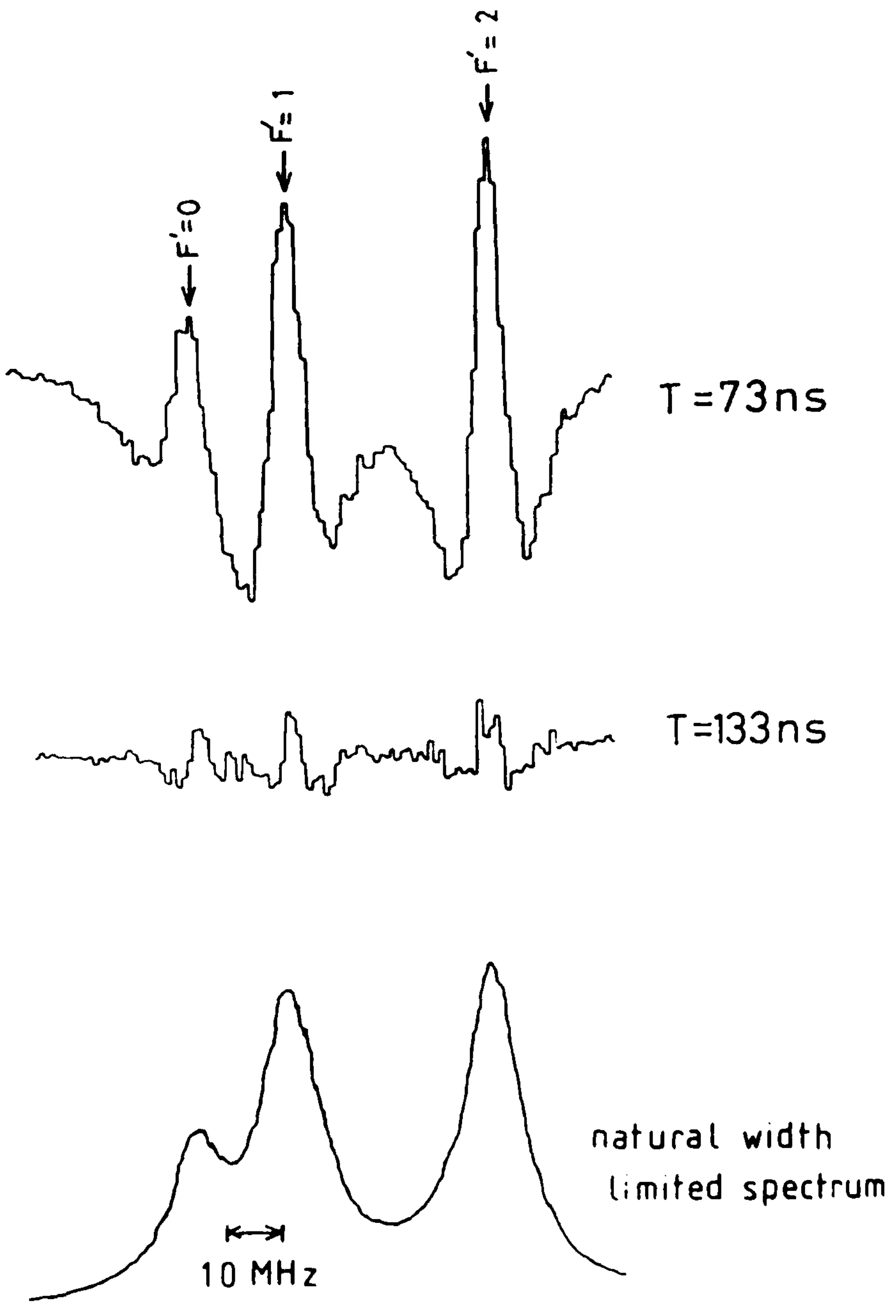
F'=0
F'=1
F'=2
T=73ns
T=133ns
natural width
limited spectrum
10 MHz

Subnatural LineWidth Spectroscopy by Phase Switching

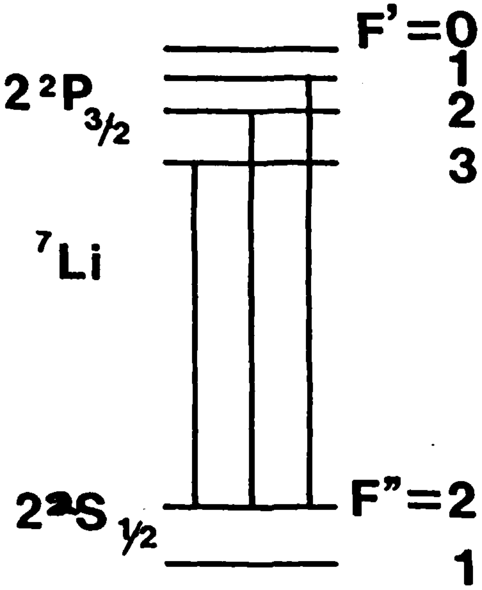

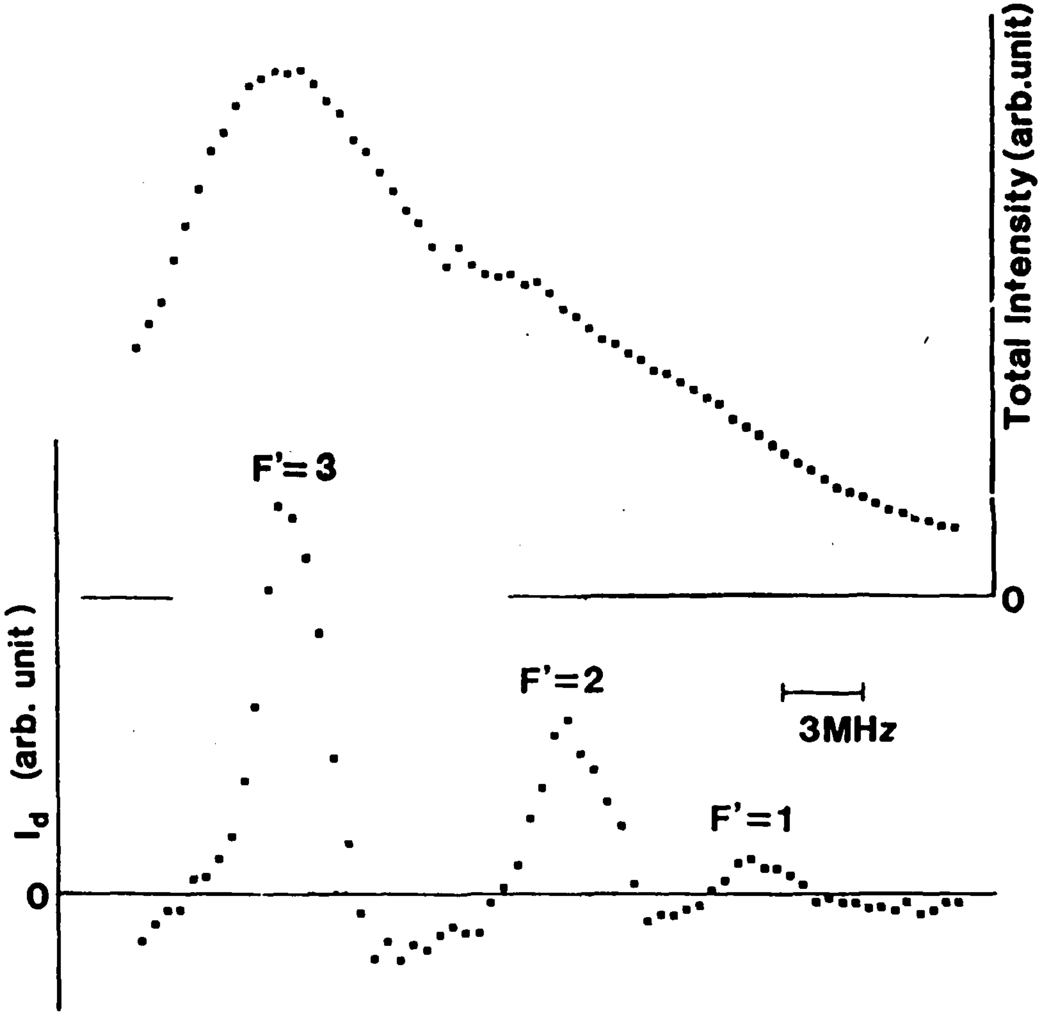

H. Shimizu et al.
(1987)

CONCLUDING REMARKS

1. Natural Width of Optical Spectral Lines can be narrowed by delayed oservation of Coherent transient effects.
2. phas switching method has been demonstrated to be practical in SNWS.
3. SNWS is meaningful in spite of a drastic loss in Intensity
4. New techniques (laser cooling & trapping) increases the Importance of SNWS.

Comprehensive Model for Laser Instability in a CO_2 Laser with Gaseous Saturable Absorber

Tadao Shimizu, Maki Tachikawa, and Kazuhito Tanii

Department of Physics, Faculty of Science, University of Tokyo, 7-3-1 Hongo, Bunkyo-ku, Tokyo 113, Japan

Summary: A periodic self-pulsation well known as passive Q-switching (PQS) is observed in a CO_2 laser containing a gaseous saturable absorber inside its cavity. PQS was developed at first as a high power pulse source to pump far-infrared lasers. In response to the recent interest in laser instability, it is now being reinvestigated extensively. Dynamic properties of the relating molecular systems are sensitively reflected in the transient pulse structure, and various features of PQS pulsation are realized, depending on lasing conditions and characteristics of the absorbing molecules. The most familiar PQS pulse is that with a single peak as is shown in Fig.1(a). Several new types of PQS have recently been reported.[1,2] The laser output is modulated sinusoidally when saturable absorbers such as CH_3I or CH_3OH is used (Fig.1(b)). An undamped undulation appears over the quasi-cw tail of PQS pulse with HCOOH absorber (Fig.1(c)). The undulation appears only in the ending part of the pulse tail in the case of SF_6 absorber (Fig.1(d)).

So far, in spite of extensive efforts to analyze the PQS

behavior, there has been no good model which reproduces the observed pulse structure with fidelity. We have tried a semiclassical rate-equation analysis introducing the vibrational relaxation of the lower laser level. It is found that this rate-equation approximation is very effective to describe the PQS phenomenon in the gas laser system. It seems that all the essential physical processes are included in this model to describe a transient behavior in the quantum mechanical system with strong nonlinearity. Through the numerical integration of the rate equations we have succeeded in systematic reproduction of all the PQS pulses, especially the PQS pulse with the undamped undulation for the first time (see Fig.1(a')-(d')). The undulation was revealed as a relaxation oscillation induced by the relaxation of the lower laser level. The model also describes optical bistability observed in the present laser system well.

The computer calculation based on the present model shows that chaotic pulsation is realized led by the period-doubling route. This is the first demonstration of chaos in a laser containing a saturable absorber. (In other words this is the first aperiodic passive Q-switching.) The chaos appears in a very limited parameter region where the undulation period is close to the pulse interval. The presence of the two close time constants may be a key to the production of chaos. The present analysis suggests that it is possible by introducing saturable absorbers inside the cavity to observe chaos even in small-gain lasers such as CO_2 and N_2O lasers far from the bad-cavity condition.

References

1. E.Arimondo, P.Bootz, P.Glorieux, and E.Menchi: J.Opt.Soc.Am.B 2, 193-201 (1985).

2. M.Tachikawa, K.Tanii, M.Kajita, and T.Shimizu: Appl.Phys. B39, 83-90 (1986).

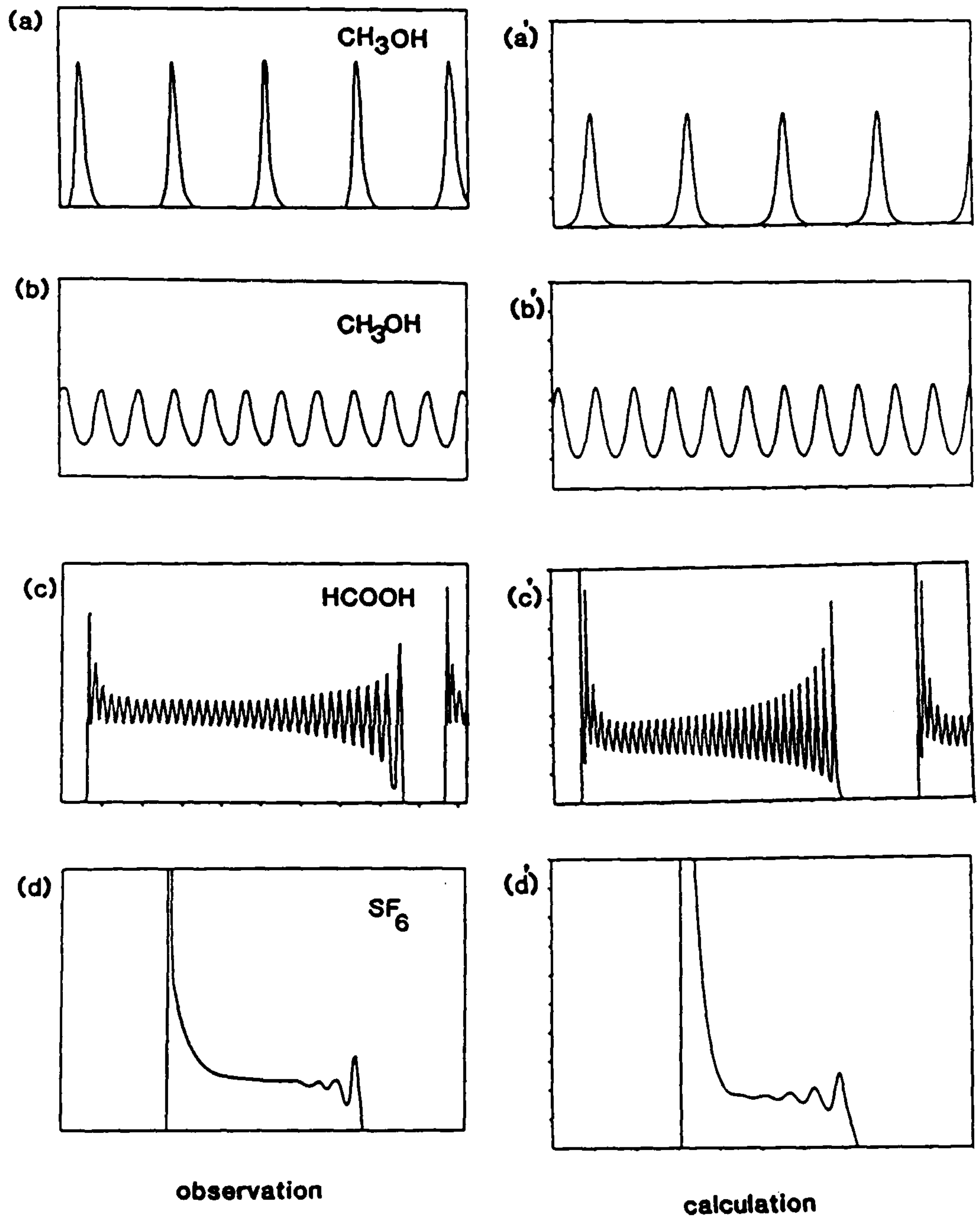

Fig.1 observed ((a)-(d)) and calculated ((a')-(d')) PQS pulse shapes. Full scale is 500 μs for (c) and (c'), and 200 μs for others.

US. Jap. Seminar

Comprehensive Model for Laser Instability in a CO_2 Laser with Gaseous Saturable Absorber

T. Shimizu

M. Tachikawa

K. Tanii

Dept. of Physics, Univ. of Tokyo

1. Comprehensive model

for $\begin{cases} \text{PQS time-dependent behavior} \\ \text{optical bistability} \end{cases}$

Is semiclassical rate-equation analysis effective?

its limitation?

2. Possibility of chaos in a laser system with a saturable absorber

What is the mechanism of chaos?

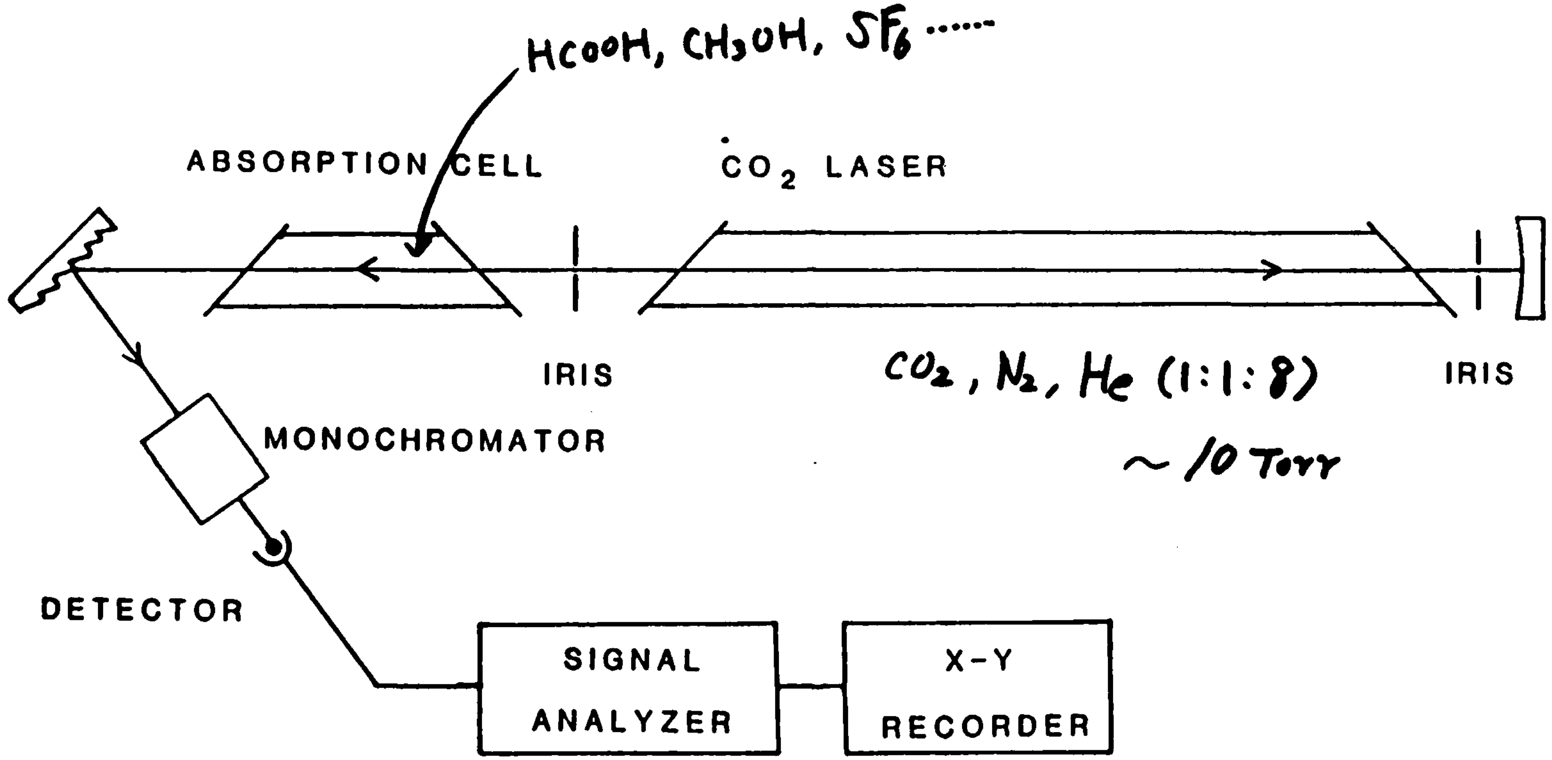

Fig.1 EXPERIMENTAL SETUP

cavity : 3.5 m
cell : 35 cm.

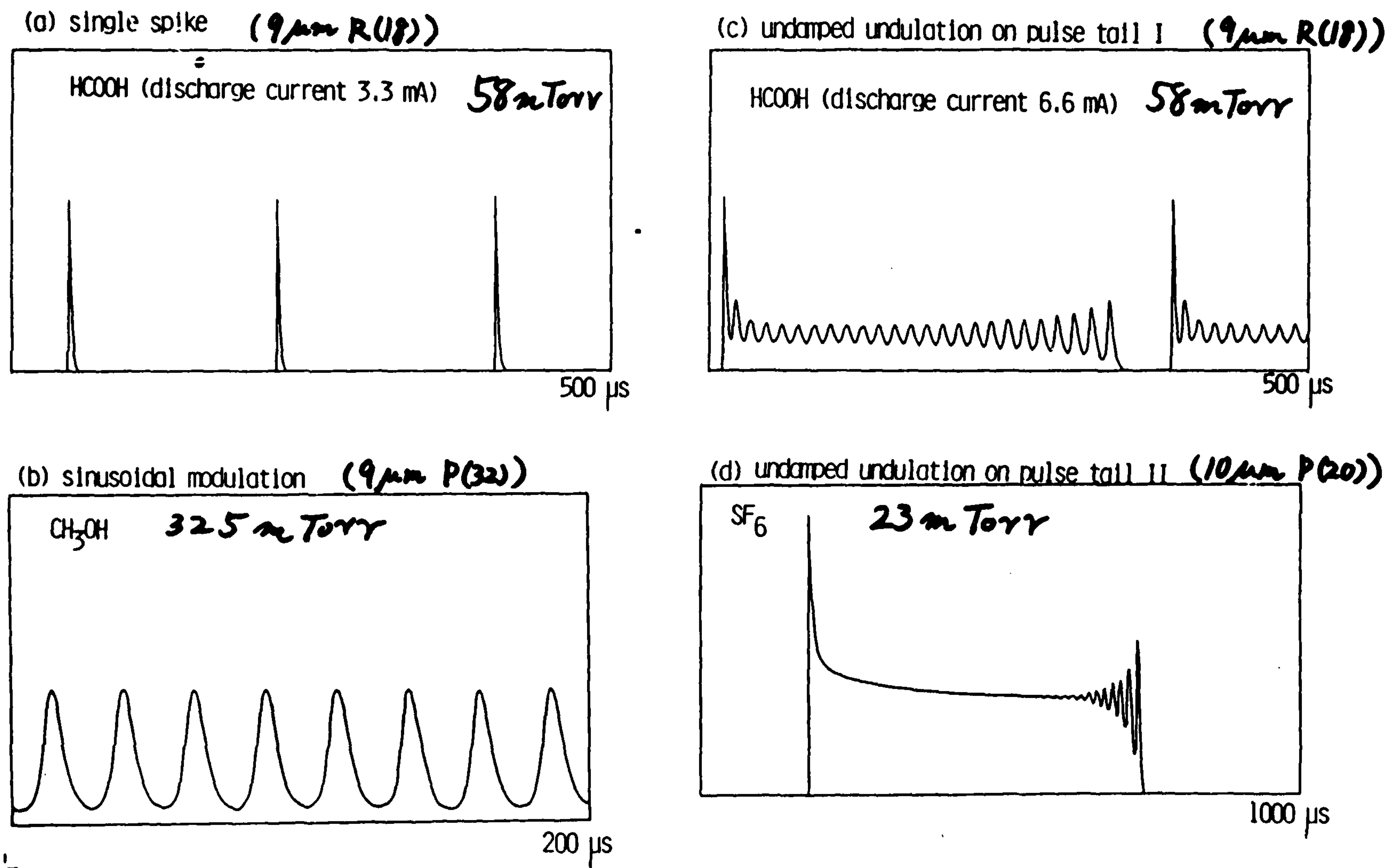

FIG.2 OBSERVED PQS PULSE SHAPES

10μm P(16)

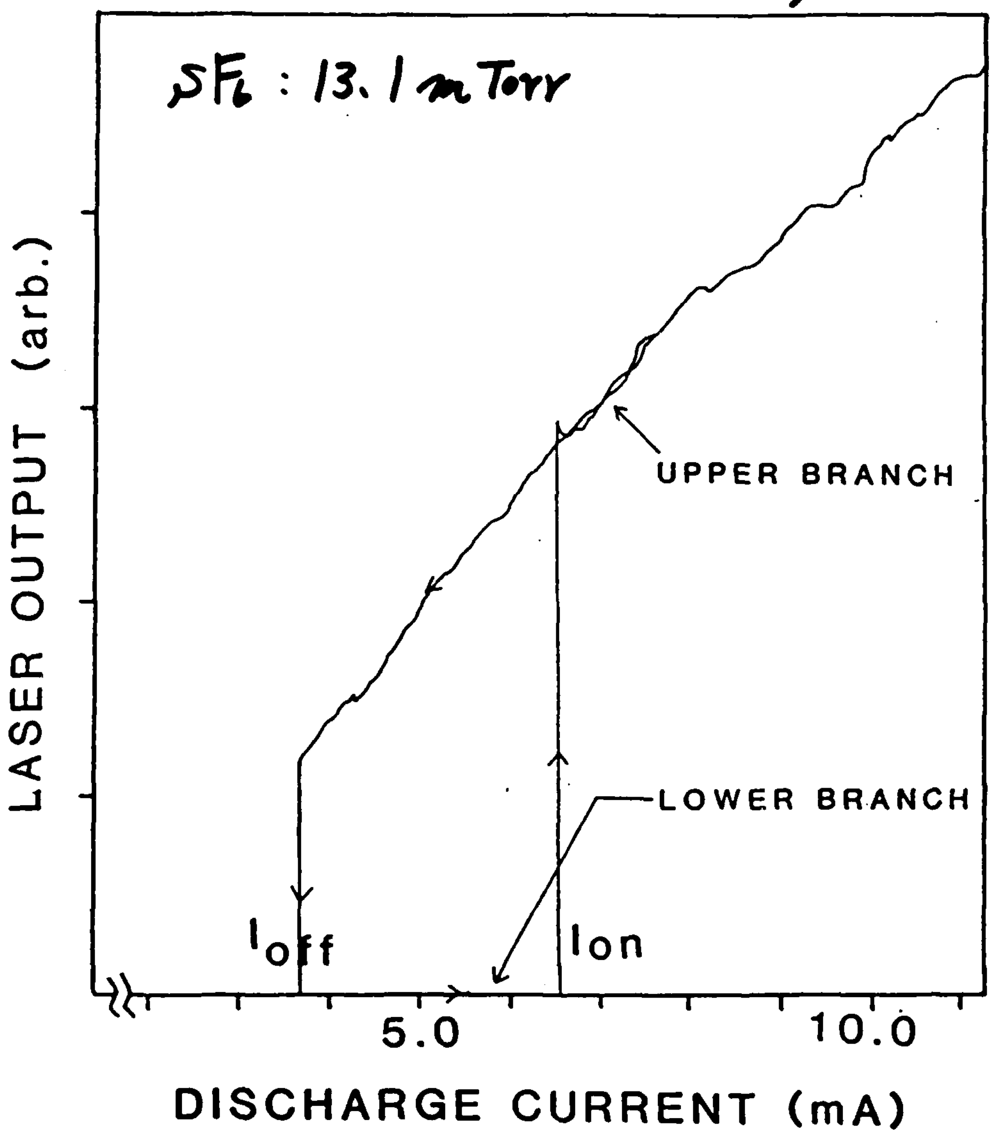

FIG.3 OBSERVED HYSTERESIS CURVE OF THE LASER OUTPUT AS A FUNCTION OF THE DISCHARGE CURRENT

Rate Equations

$$\frac{dn}{dt} = B_g f_g(J)\, n\,(M_1 - M_2)\frac{l_g}{L} - B_a n N \frac{l_a}{L} - kn + AM_1$$

$$\frac{dM_1}{dt} = -B_g f_g(J)\, n\,(M_1 - M_2) + PM - (P + R_{10} + R_{12})M_1 - PM_2$$

$$\frac{dM_2}{dt} = B_g f_g(J)\, n\,(M_1 - M_2) + R_{12}M_1 - R_{20}M_2$$

$$\frac{dN}{dt} = -2B_a n N - r(N - N^*)$$

n : photon density

M_1 : population density on the upper laser level

M_2 : population density on the lower laser level

N : difference of population density between the absorption levels

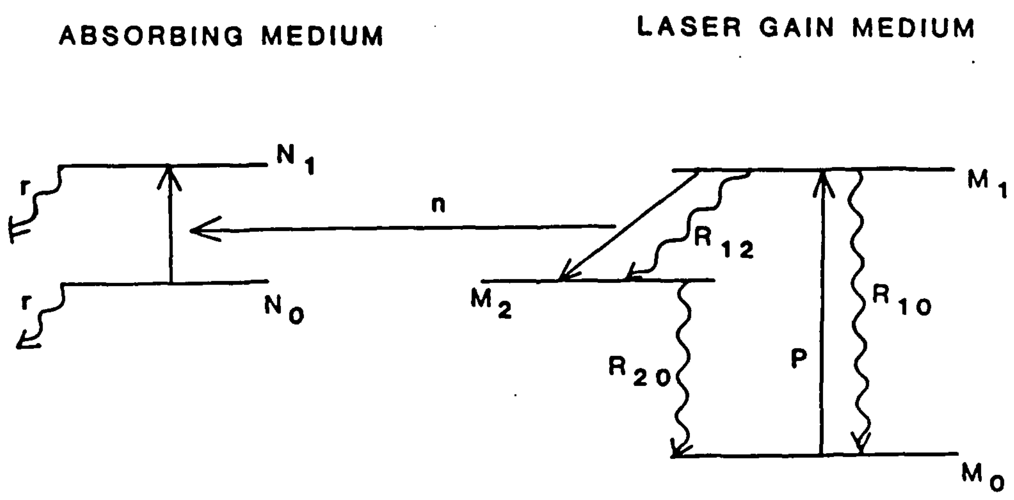

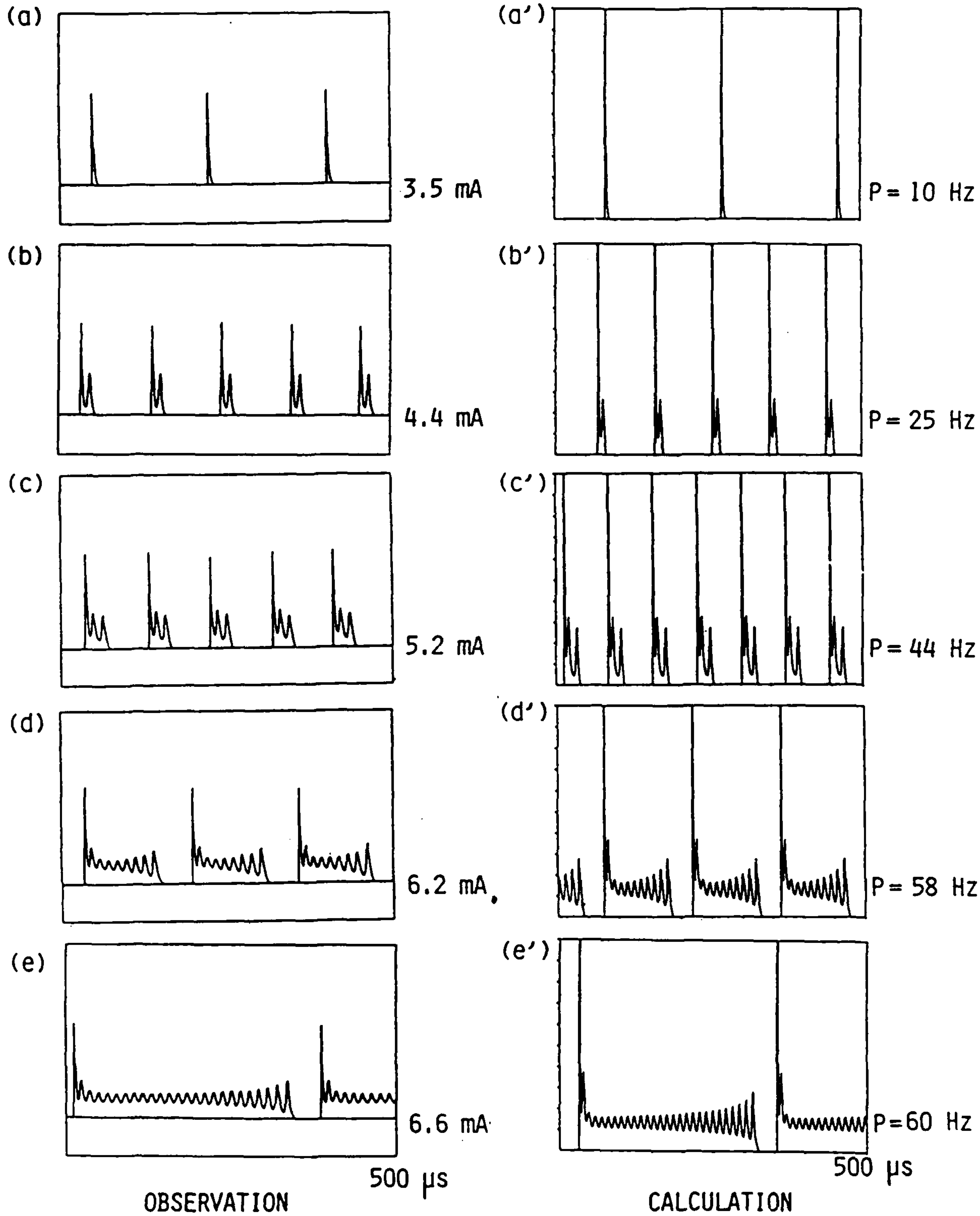

FIG.6 DEPENDENCE OF PQS PULSES ON THE DISCHARGE CURRENT IN THE HCOOH CASE

(HCOOH : 58 mTorr)

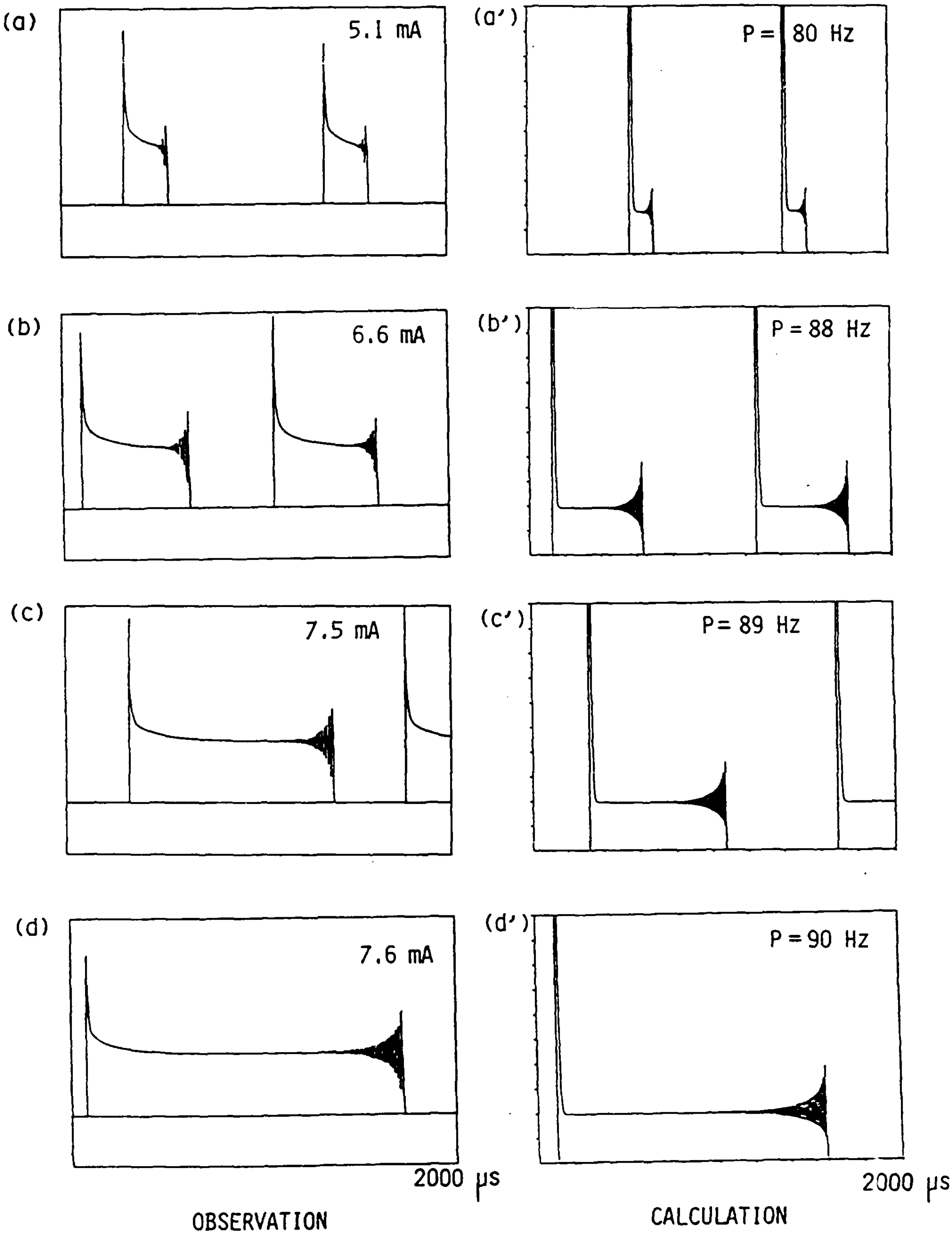

FIG.7 DEPENDENCE OF PQS PULSES ON THE DISCHARGE CURRENT IN THE SF_6 CASE (SF$_6$: 23 m Torr)

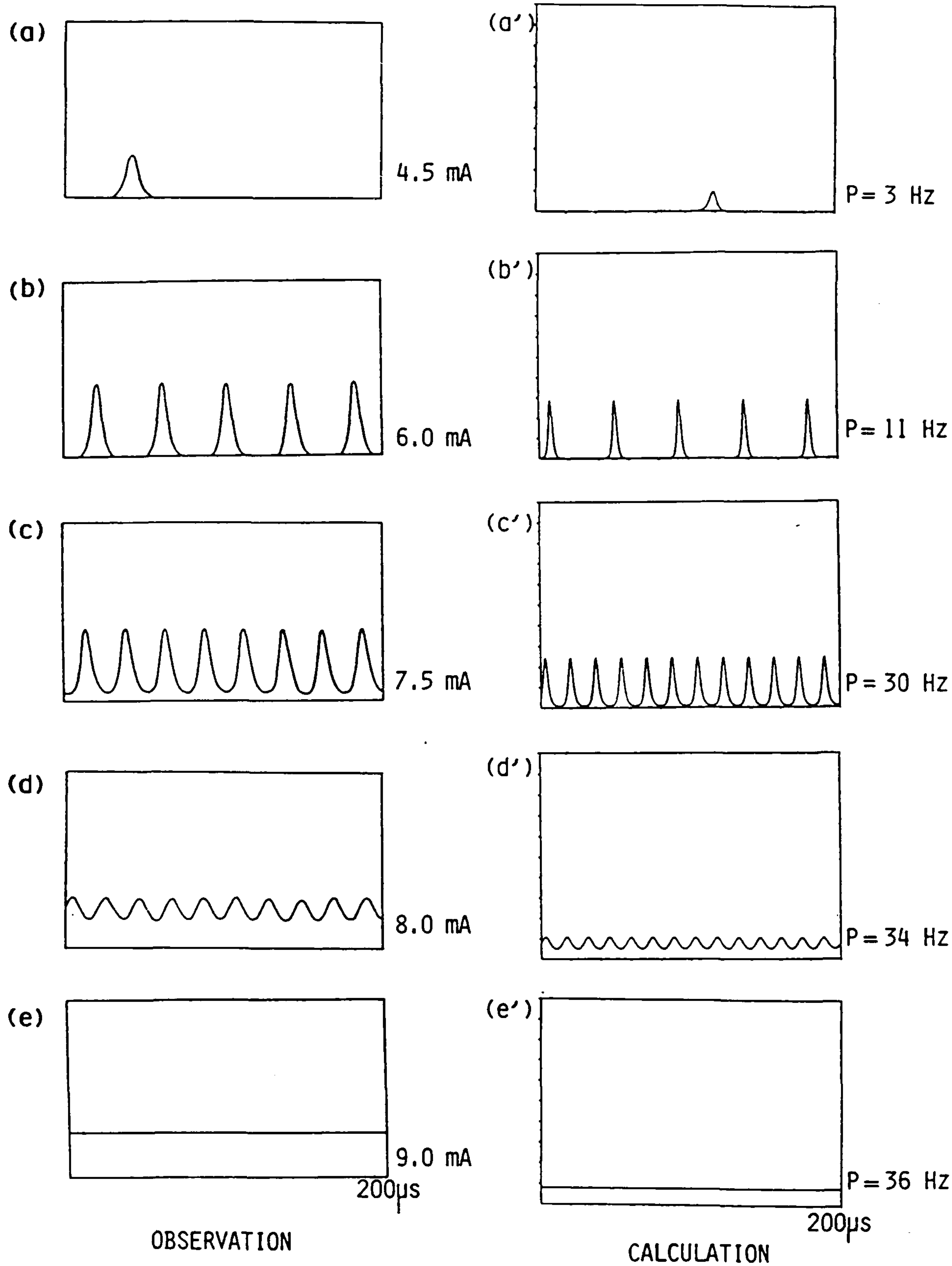

FIG.5 DEPENDENCE OF PQS PULSES ON THE DISCHARGE CURRENT IN THE CH_3OH CASE

(CH_3OH : 325 m Torr)

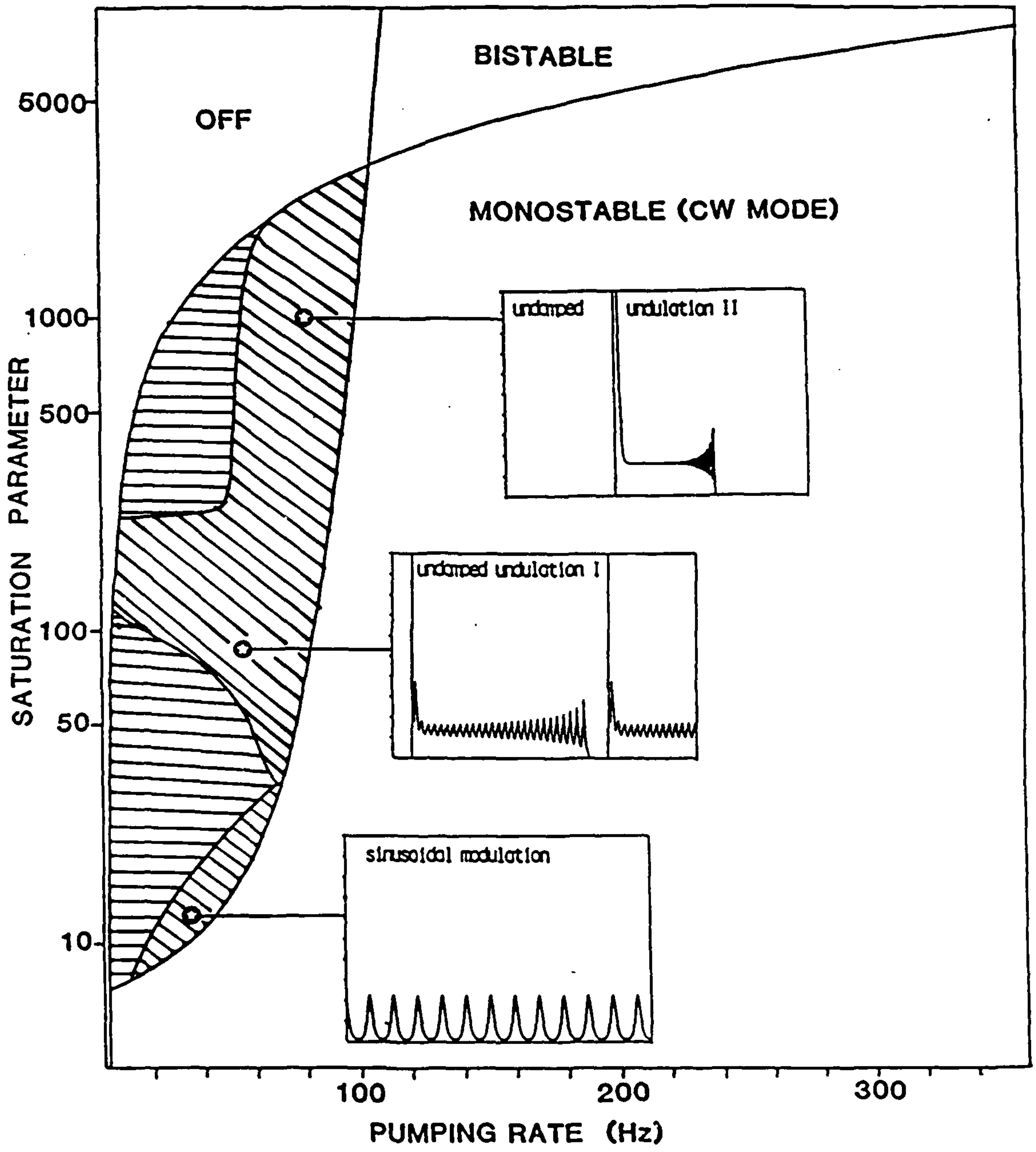

satulation parameter

$$= \frac{Ba}{\gamma} = \frac{1}{\gamma}\frac{2\pi^2\nu\mu_a^2}{3\varepsilon_0 h}\cdot g(\nu-\nu_0)$$

· PQS with undulation

· sinusoidal modulation

· single spike

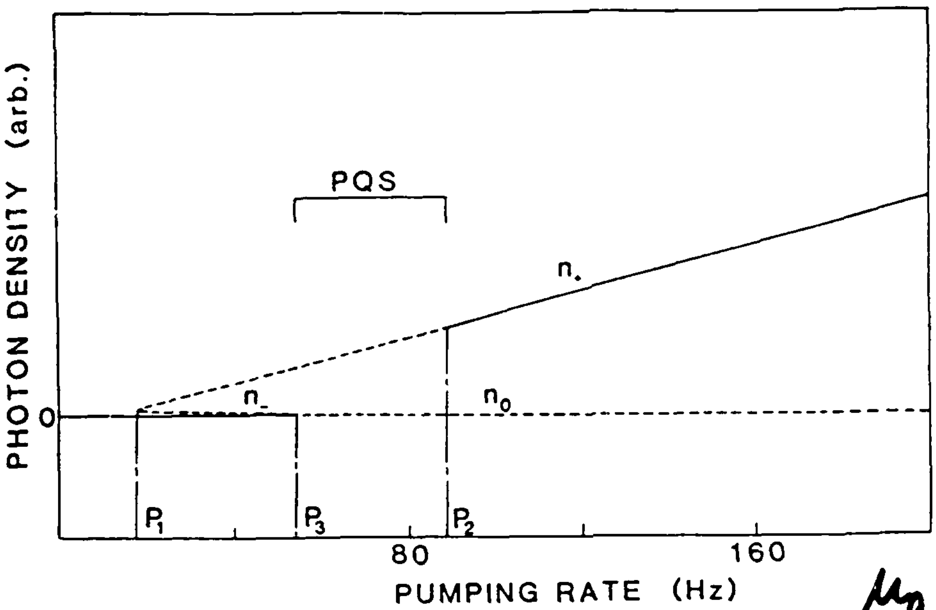

$\mu_a = 0.20$ D

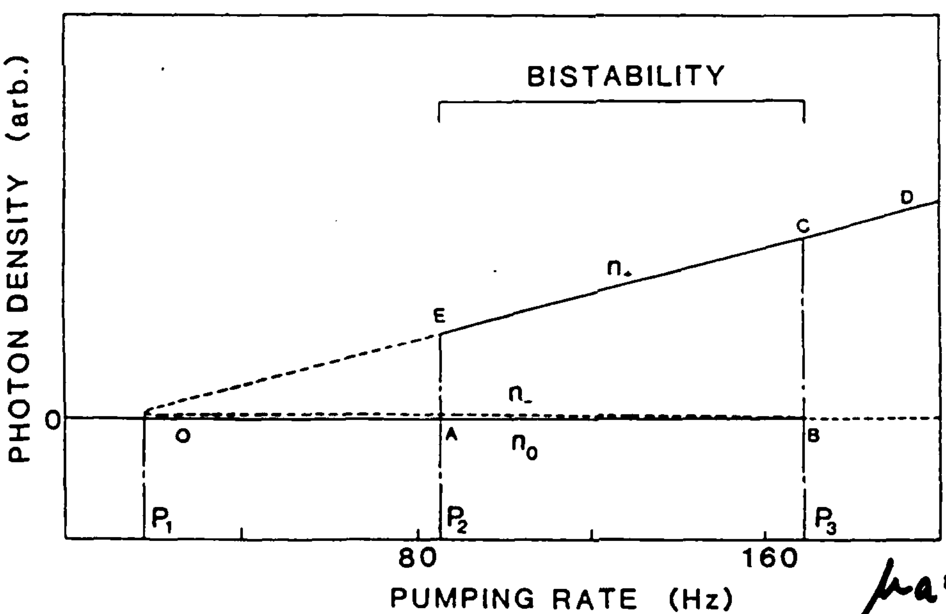

$\mu_a = 0.35$ D

FIG.9 STATIONARY SOLUTION OF THE PHOTON DENSITY AS A FUNCTION OF THE PUMPING RATE

(1) period-1

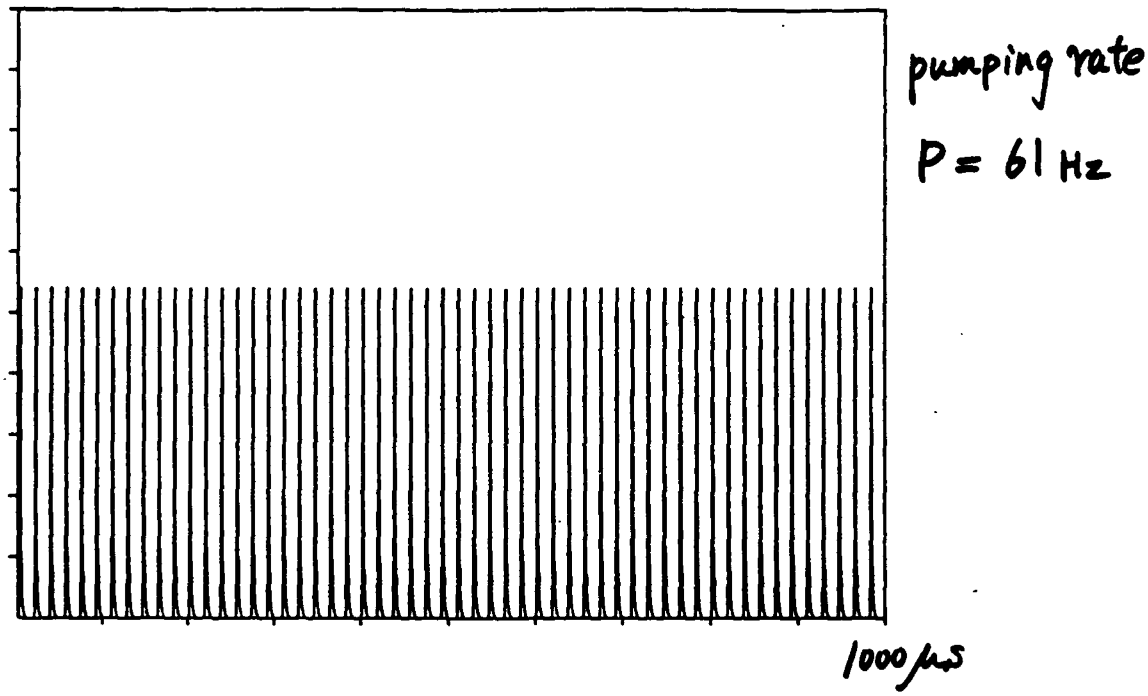

(2) period-2

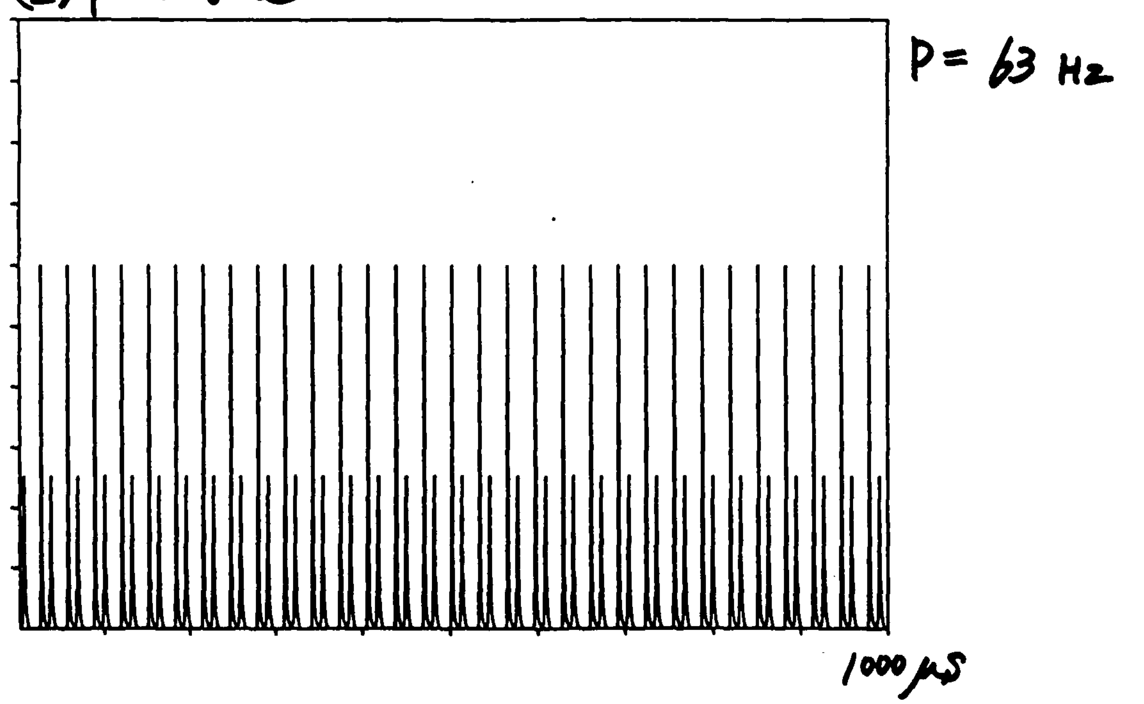

(3) period-4

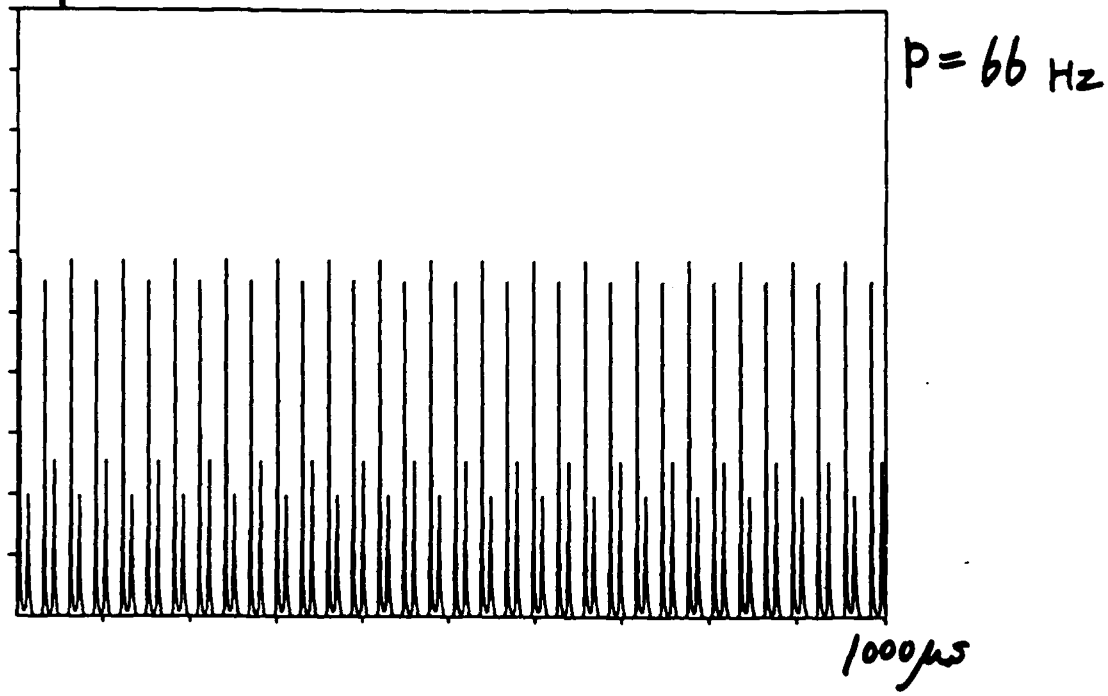

(4) period-8

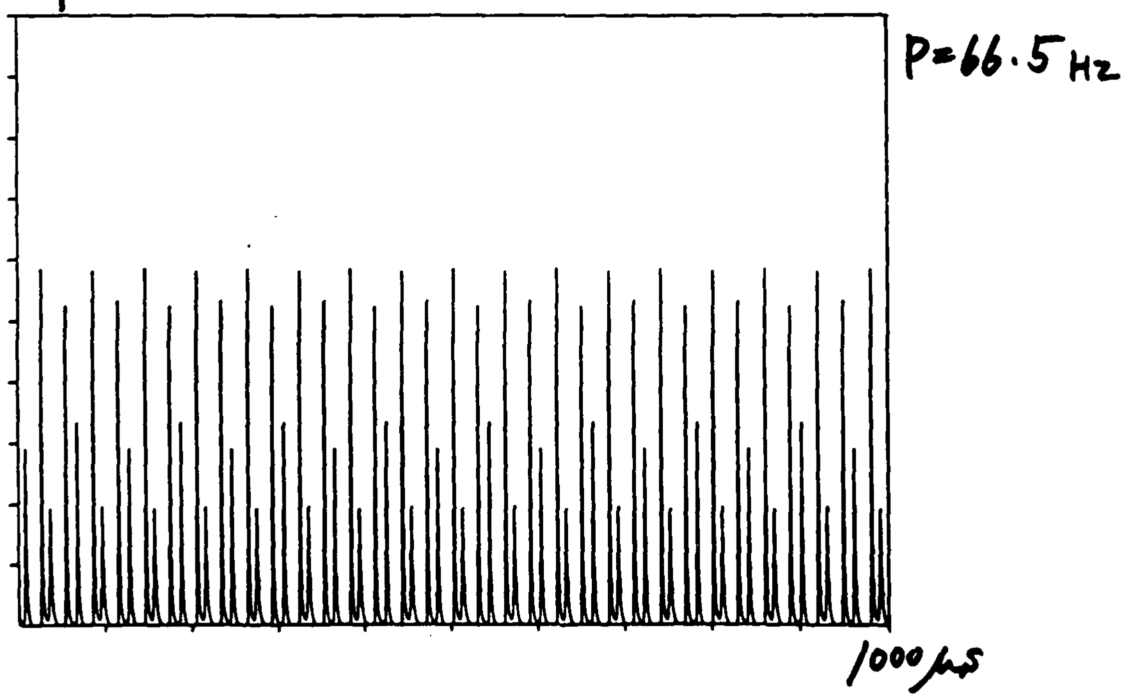

(5) chaos

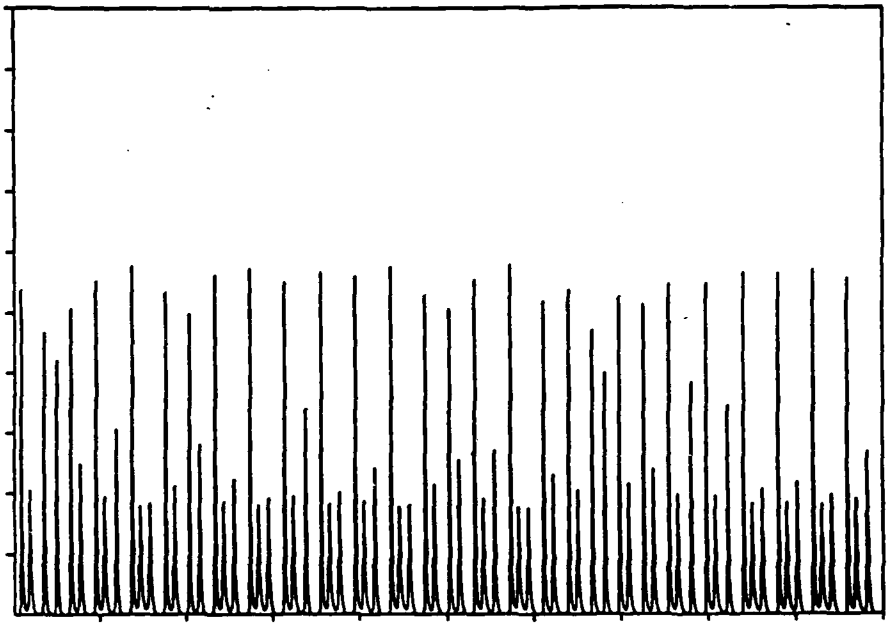

P= 68.5 Hz

1000 μs

* first chaos in a laser system containing a saturable absorber inside its cavity

(first aperiodic passive Q-switching)

even in a laser with small gain

(such as CO_2, N_2O lasers)

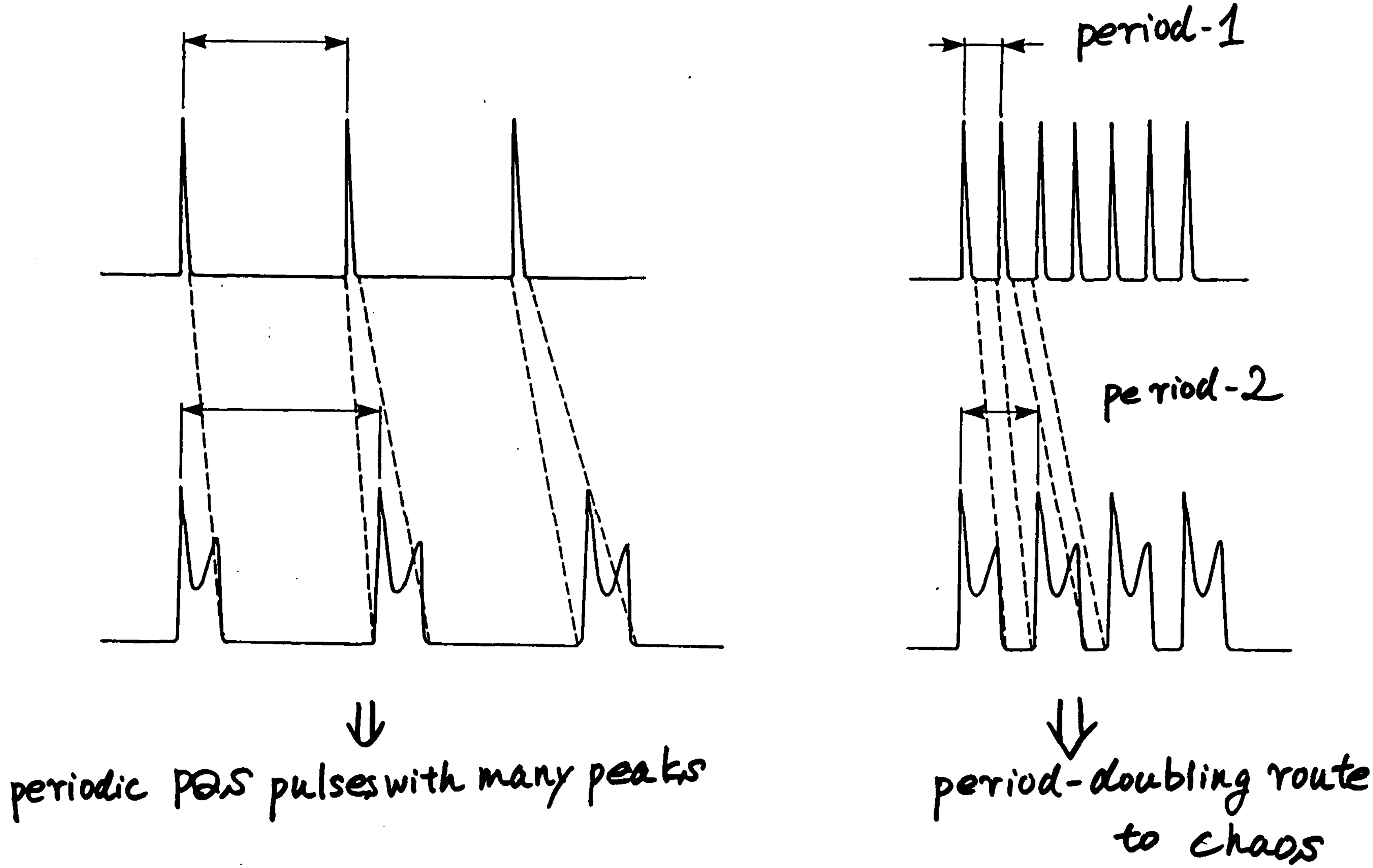
period-1
period-2
periodic PQS pulses with many peaks
period-doubling route to chaos

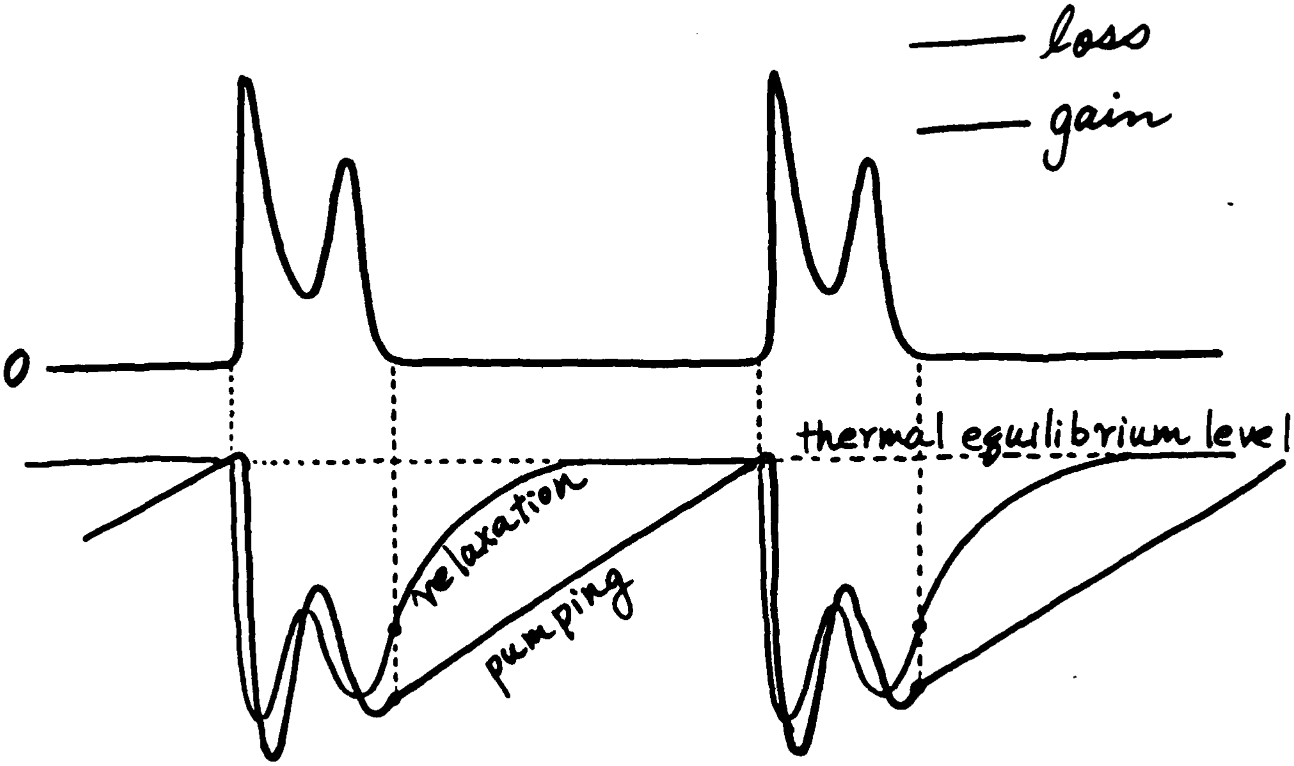
loss
gain
0
thermal equilibrium level
relaxation
pumping

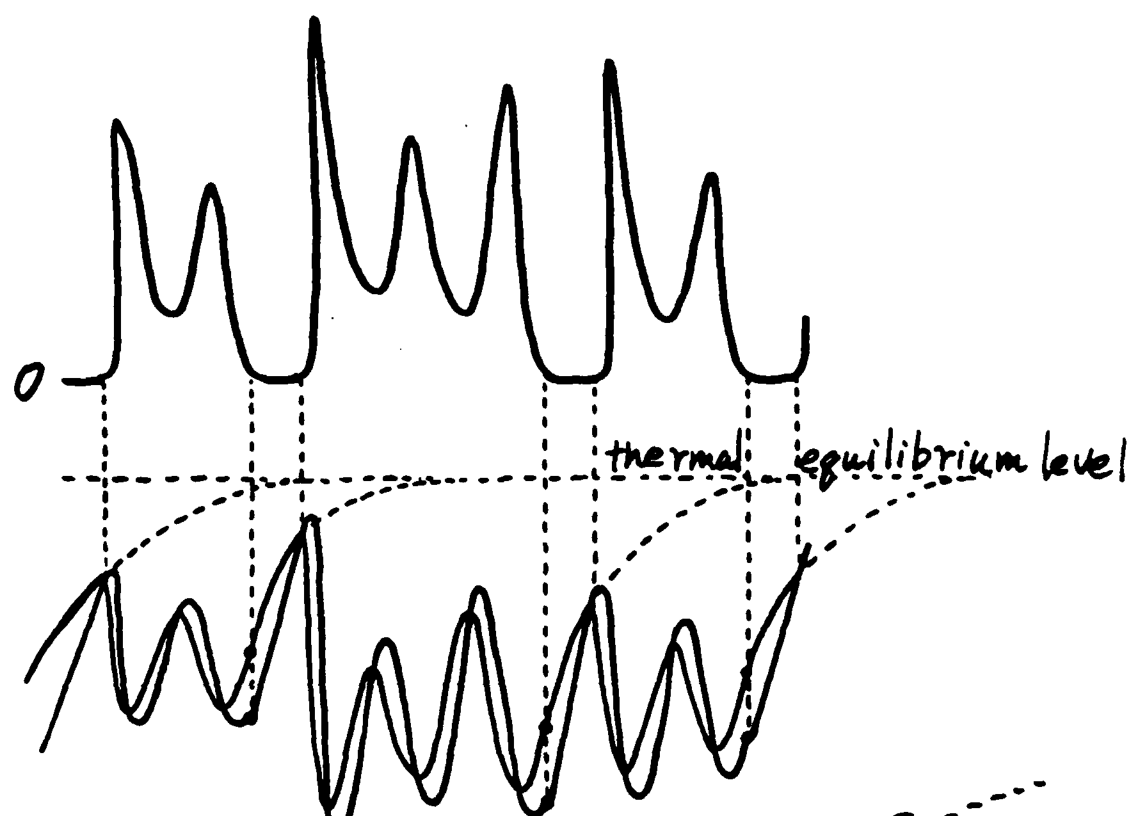
0
thermal equilibrium level

π 3.141528------
???

Summary

1. The rate-equation approximation is very effective to describe the PQS in a CO_2 laser with gaseous saturable absorbers, and all the pulse shapes are reproduced in the computer simulation based on the rate-equation model.

   Simultaneous presence of PQS and bistability can not be derived from the present model. ⟶ Maxwell-Bloch equations may be desirable.

2. Chaos was demonstrated for the first time in a laser system with saturable absorber.

   The presence of two close time-constants may be essential to produce chaos in this case.

RECENT PROGRESS IN OPTICAL BISTABILITY AND TRISTABILITY

T. Yabuzaki and M. Kitano *,

Department of Physics, Kyoto University, Kyoto 606, Japan, and

* Radio Atomospheric Science Center, Kyoto University, Uji, Kyoto 611, Japan

Summary

In recent years we have been studying theoretically and experimentally on the new type of optical bistability and tristability, and on the related phenomena such as self-pulsing, chaos, and transient chaos. I would like to focus my present talk on the optical bistability in the first place, which is caused by the spin polarization in the presence of optical feedback. This bistability is considerably different from the ordinary one, because it has no hysteresis cycle, while it does have a pitchfork bifurcation, i.e. symmetry-breaking. Secondly I would like to talk about the self-switching of the light polarization by spin-precession, which takes place in the same optical system. Finally, I discuss about the multistability observed experimentally, using simplified models with coupling between spatial modes of light.

Recent Progress in Optical Bi- and Tri-Stability

T. Yabuzaki and M. Kitano
Kyoto University

Bistability and tristability with symmetry-breaking caused by the spin-polarization through optical pumping in the presence of optical feedback

---

Focused Phenomena

o (1) Self-pulsing, or self-sustained spin-precession associated with the optical bistability with symmetry-breaking

o (2) Optical multistability in the same system

(2) Chaos and transient chaos in the optically tristable system

Optical Bistability with Symmetry Breaking

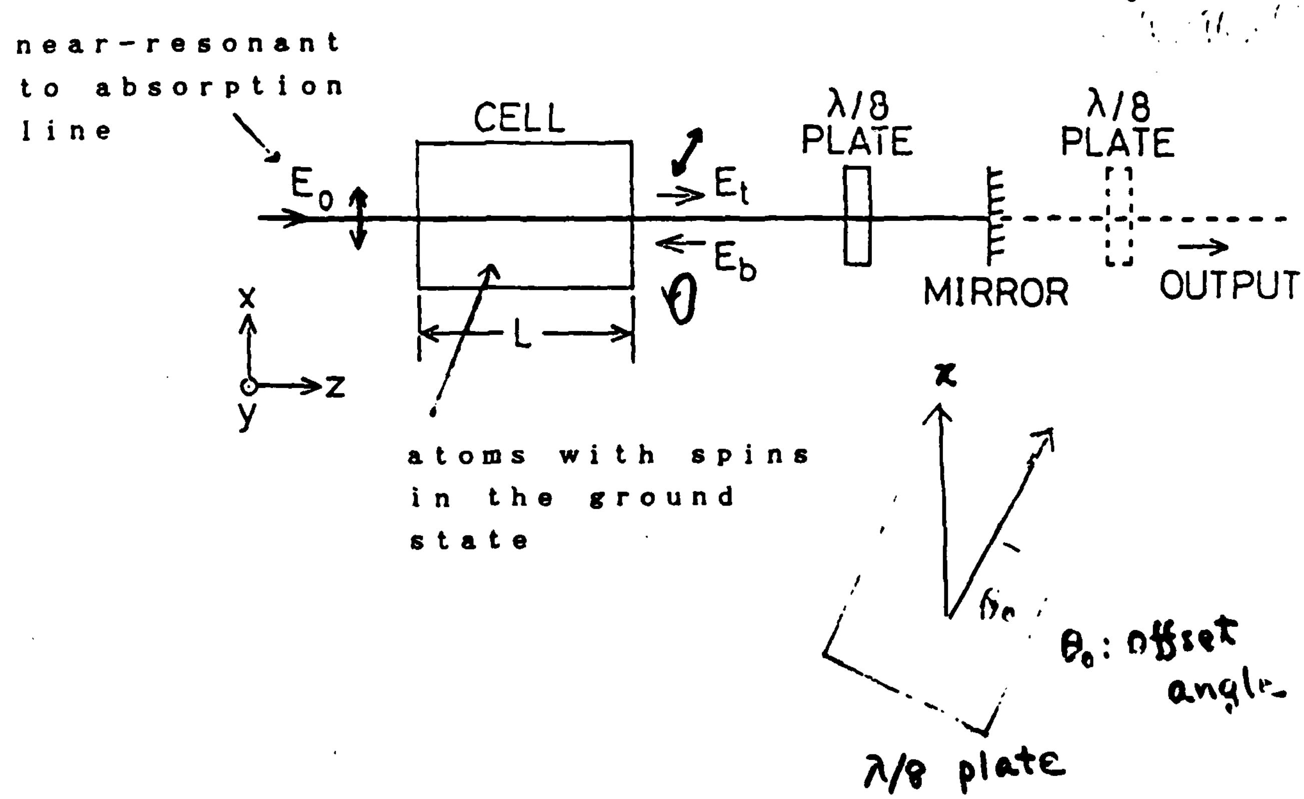

<u>Positive Feedback Loop</u>

for rotation of polarization of forward beam

or

spin orientation

- Circularly Polarized Component in E
  → Optical Pumping
  → Spin-Orientation
- Rotation of Polarization of Forward Beam

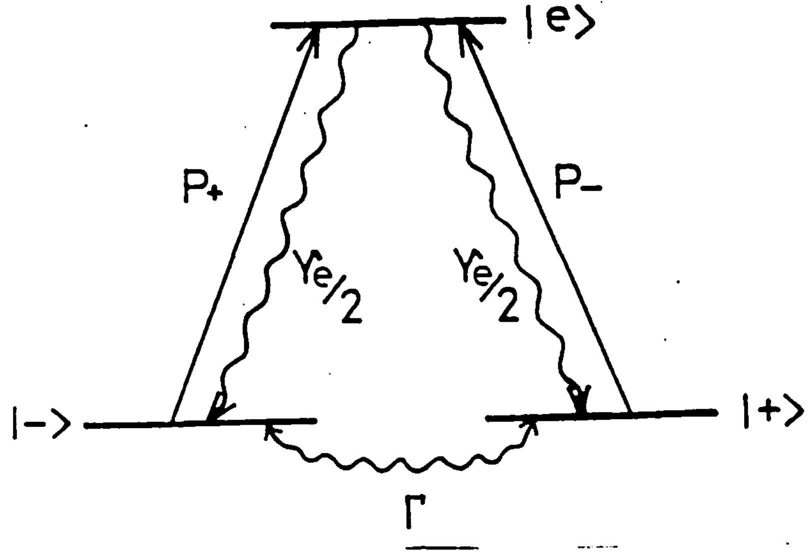

steady state population

$$I_\pm = I_0\{1 \pm \tfrac{1}{2}\sin 2(\theta+\theta_0)\}$$

$$N_\pm = \frac{I_\pm + 1}{I_+ + I_- + 2} N_0 .$$

wavenumber & absorption coeff.

$$k_\pm = k_0 + (\sigma/2)(\Delta\omega/\gamma_c) N_\mp$$

$$\alpha_\pm = (\sigma/2) N_\mp$$

$$\Delta\omega = \omega - \omega_0$$

$$\theta = (L/2)(k_+ - k_-)$$

rotation angle θ

$$\boxed{\theta = \frac{kL}{2}\,\frac{I_0 \sin 2(\theta+\theta_0)}{I_0 + 1}}$$

I_0 : incident light intensity

θ_0 : offset angle of $\lambda/8$ plate

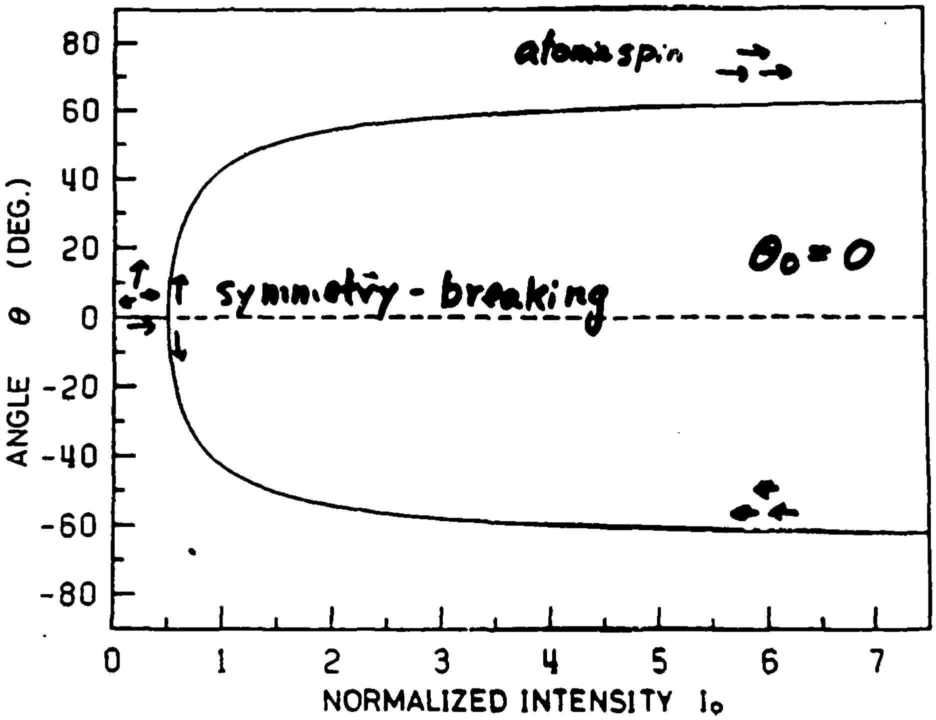
atomic spin
$\theta_0 = 0$
symmetry - breaking
ANGLE θ (DEG.)
NORMALIZED INTENSITY I_0
80
60
40
20
0
-20
-40
-60
-80
0
1
2
3
4
5
6
7

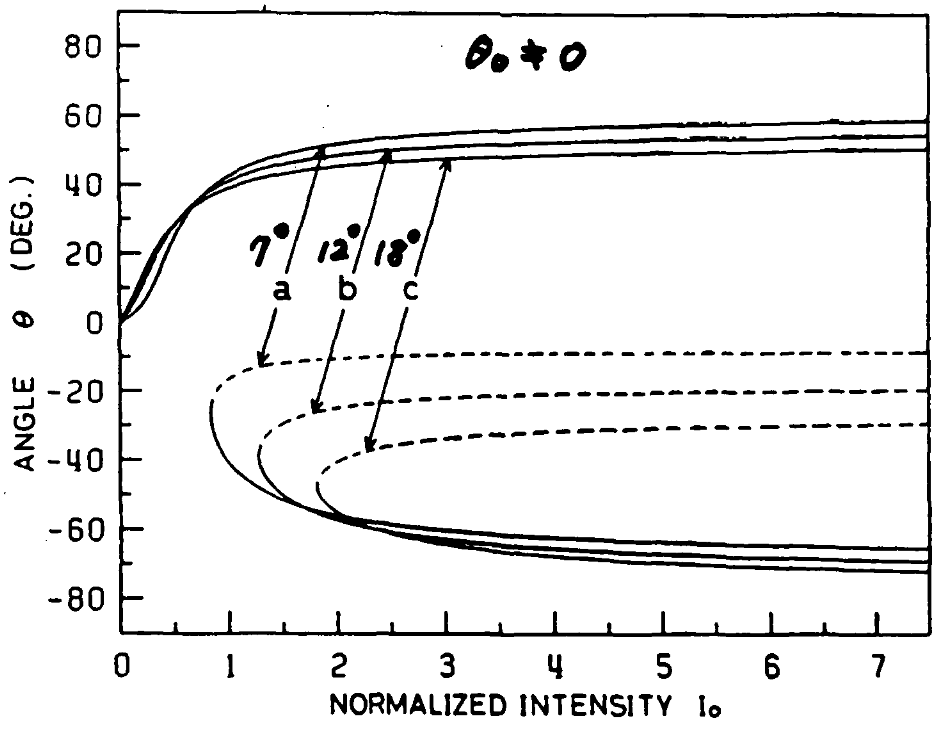
$\theta_0 \neq 0$
7°
12°
18°
a
b
c
ANGLE θ (DEG.)
NORMALIZED INTENSITY I_0
80
60
40
20
0
-20
-40
-60
-80
0
1
2
3
4
5
6
7

Experiment

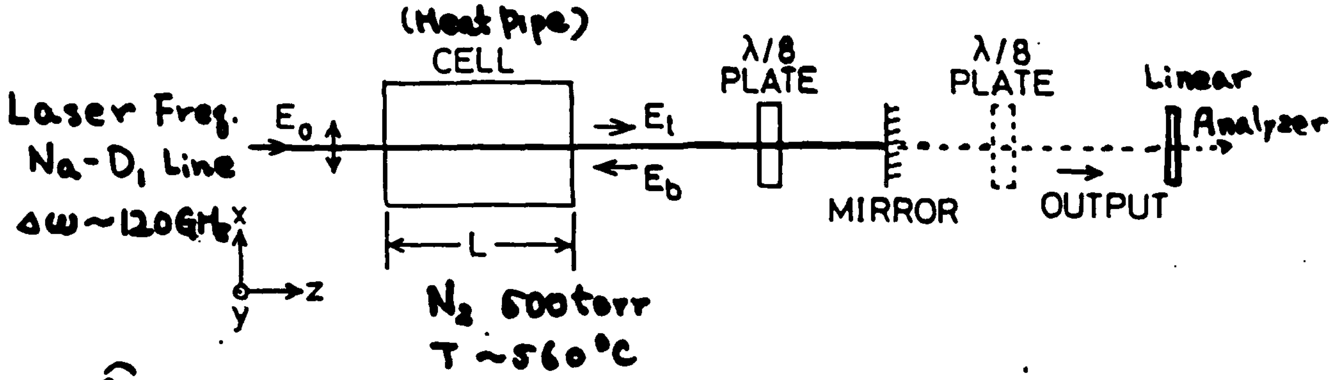

(Heat Pipe)
CELL
λ/8
PLATE
λ/8
PLATE
Linear
Analyzer
Laser Freq.
Na-D1 Line
Δω~120GHz
E0
E1
Eb
MIRROR
OUTPUT
L
x
y
z
N2 500torr
T ~560°C

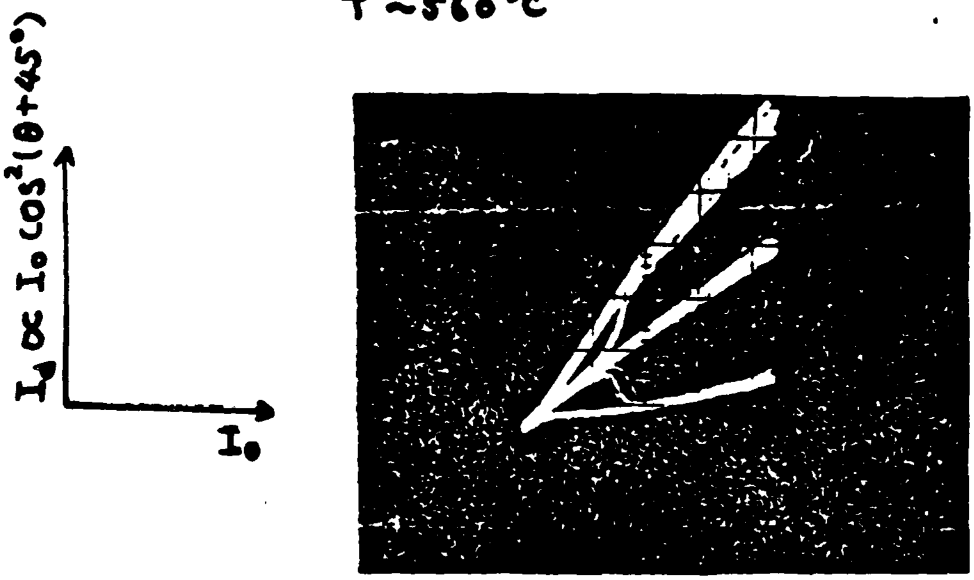

I⊥ ∝ I0 cos²(θ+45°)
I0

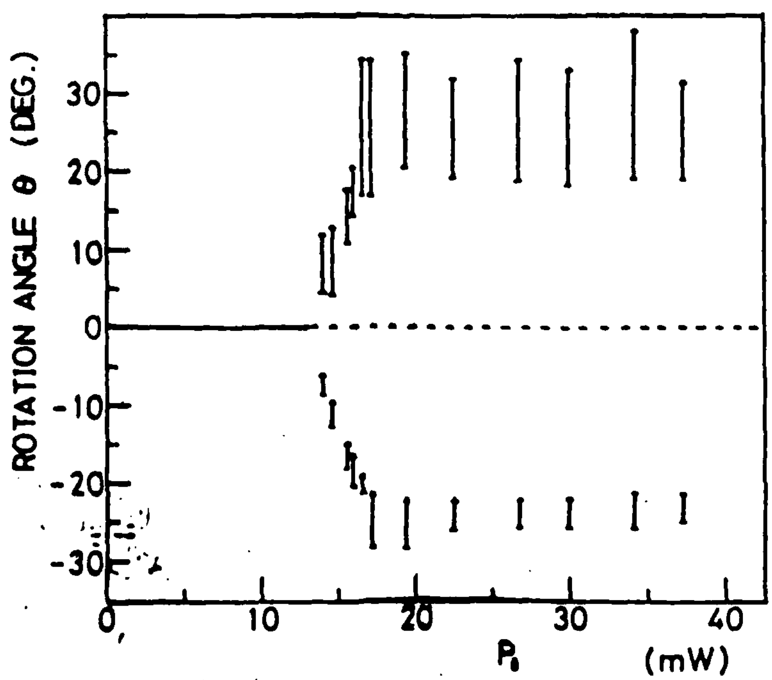

ROTATION ANGLE θ (DEG.)
30
20
10
0
-10
-20
-30
0
10
20
30
40
P0
(mW)

$$\theta = \frac{kL}{2}\,\frac{I_0 \sin 2(\theta+\theta_0)}{I_0+1}$$

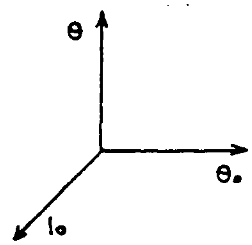

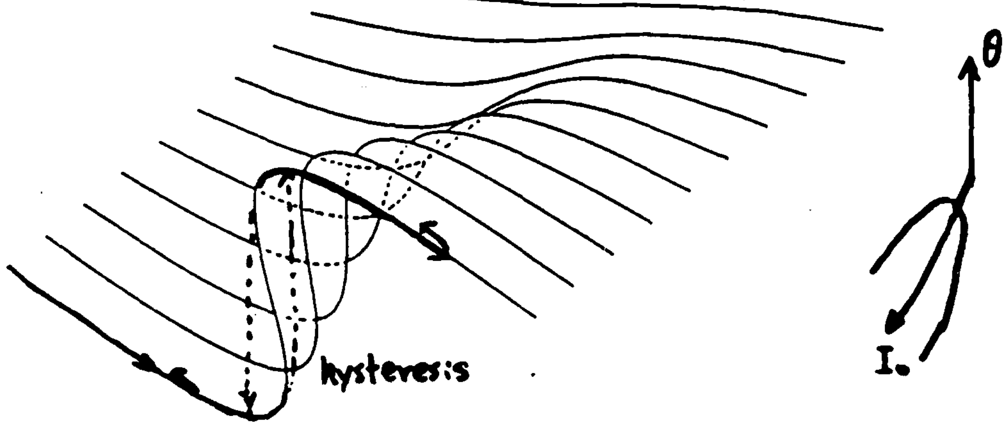

Cusp Catastrophe

- system potential

$$V(x) = \frac{1}{4}x^4 + \frac{1}{2}ux^2 + vx$$

x : behavior variable

u, v : control parameter

steady state surface $\quad \partial V(x)/\partial x = 0$

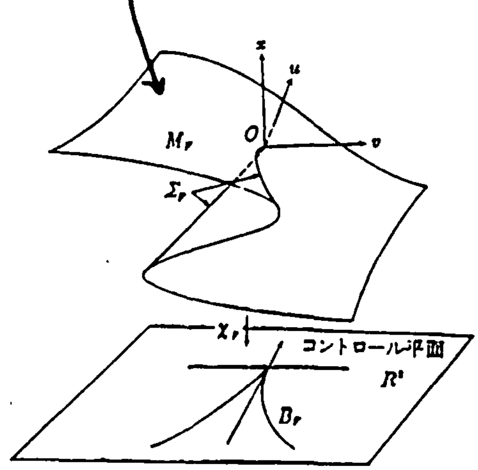

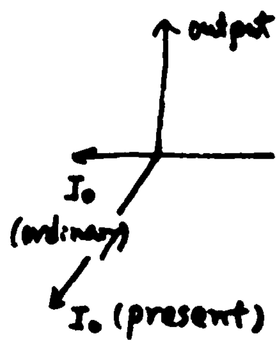

(B)(Aの図を向こう側(u<0の側)よりみた図)

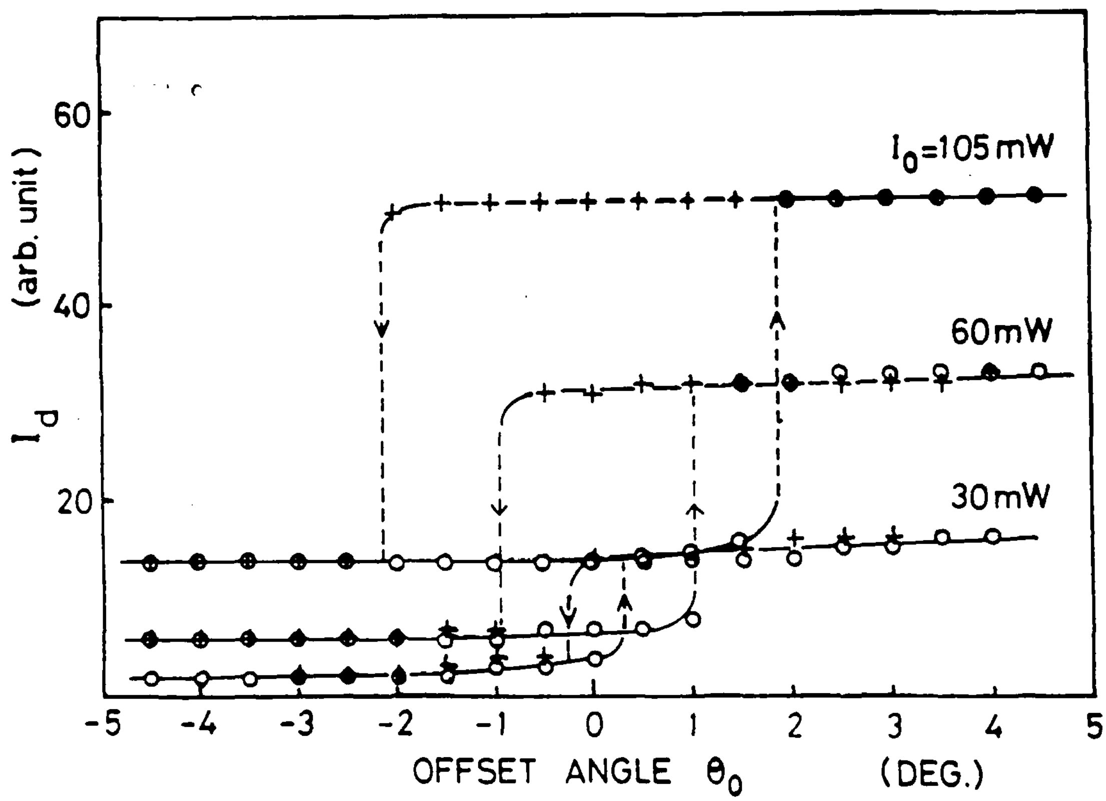

60
40
20
I_d (arb. unit)
I_0=105 mW
60 mW
30 mW
-5
-4
-3
-2
-1
0
1
2
3
4
5
OFFSET ANGLE θ_0 (DEG.)

Self-Pulsing by Spin Precession

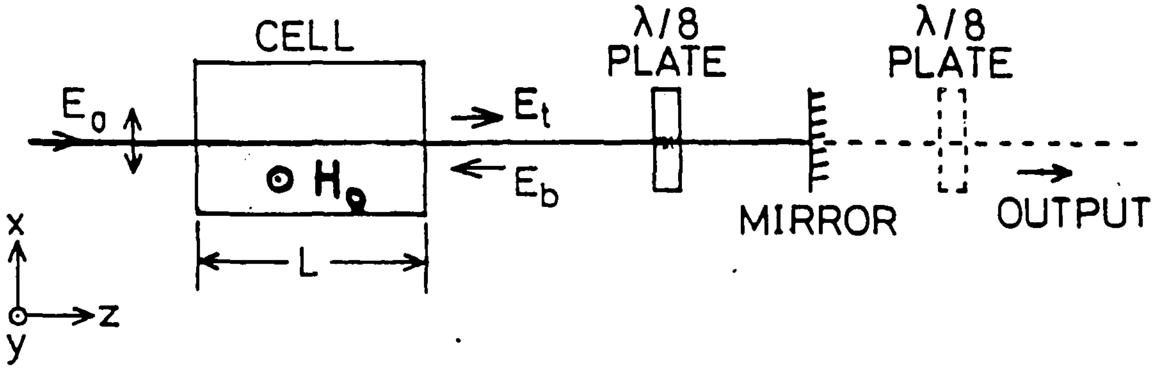

Bloch eq. for $\theta_0 = 0$

$$\frac{dm_x}{dt} = -\Omega_0 m_z - \Gamma(1+I_0)m_x$$

$$\frac{dm_z}{dt} = \Omega_0 m_x - \Gamma(1+I_0)m_z + \frac{\Gamma I_0}{2}\sin 2kL\, m_z$$

$(\Omega_0 = \gamma H_0)$

$\Downarrow$

van der Pol equation

Steady-state solutions
- o monostable solution $(m_x, m_z) = (0,0)$
- o bistable solutions (m_{x0}, m_{z0}), $(-m_{x0}, -m_{z0})$
- rotation along a limit cycle

Phase Diagram

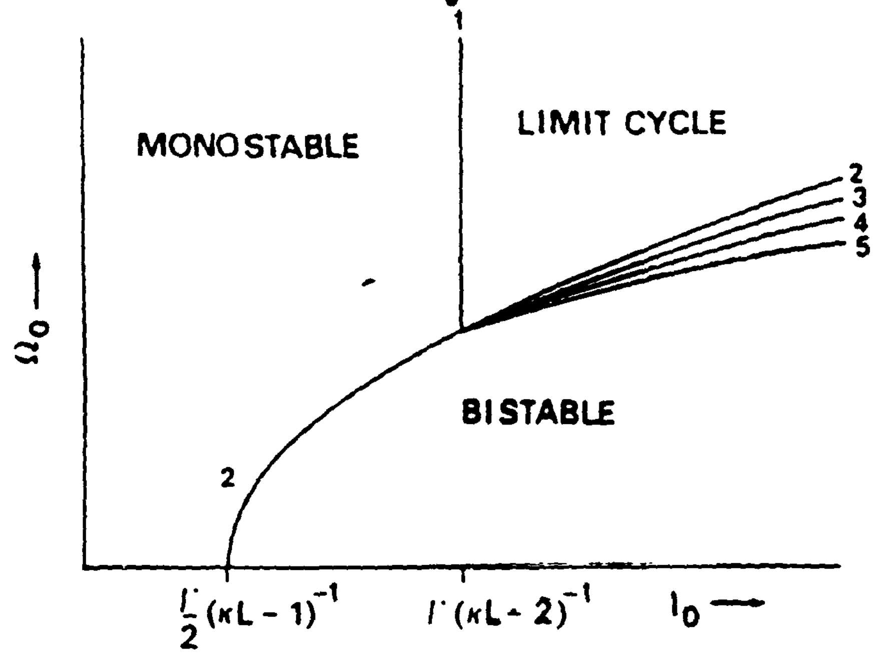

Spin-precession by sinchronous Switching of Polarization

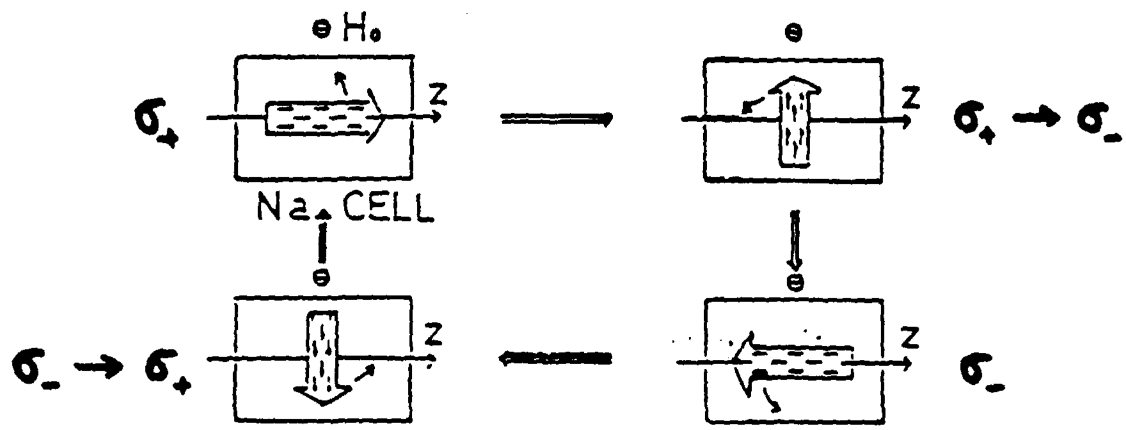

$I_0 = 9$
$KL = 3.5$

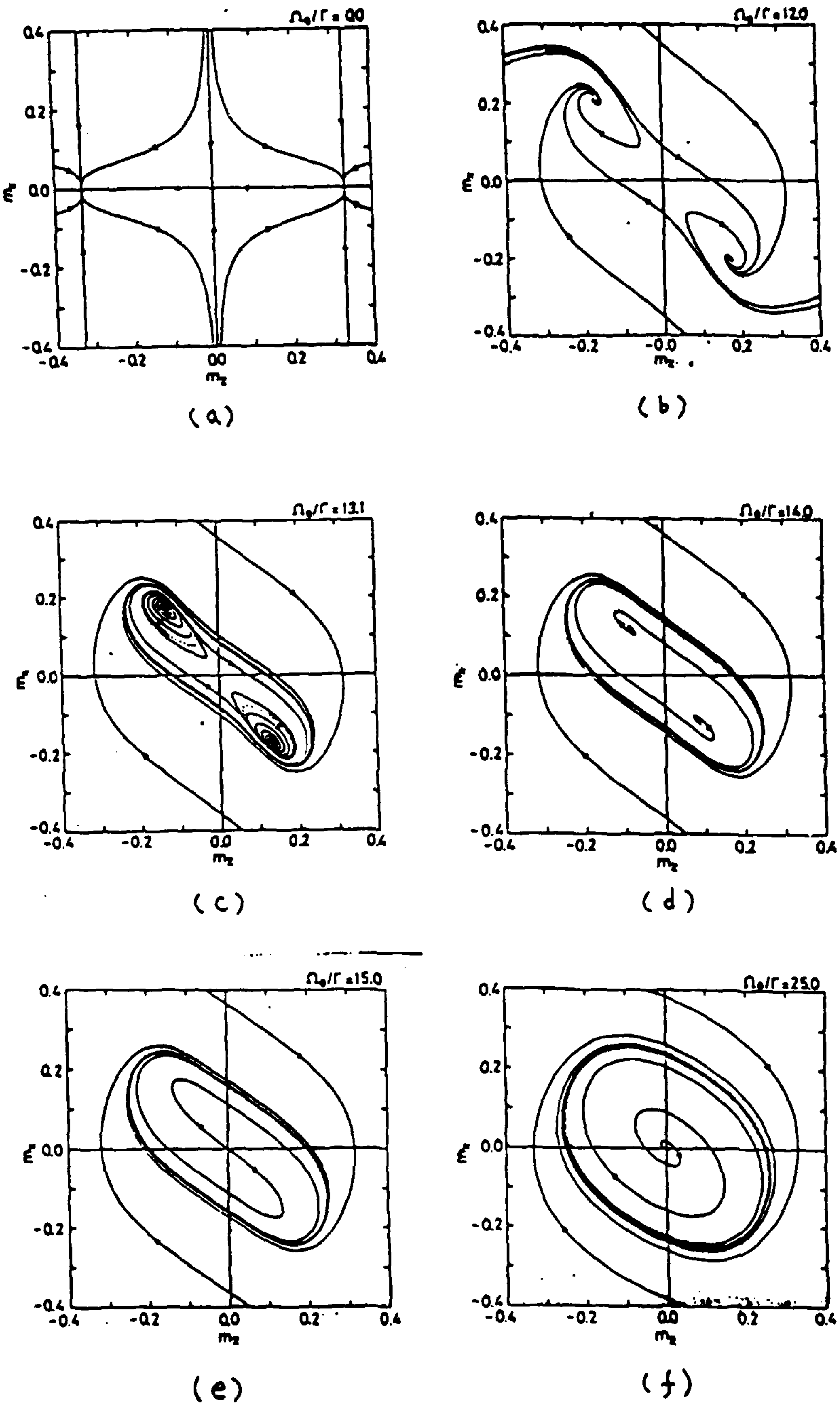

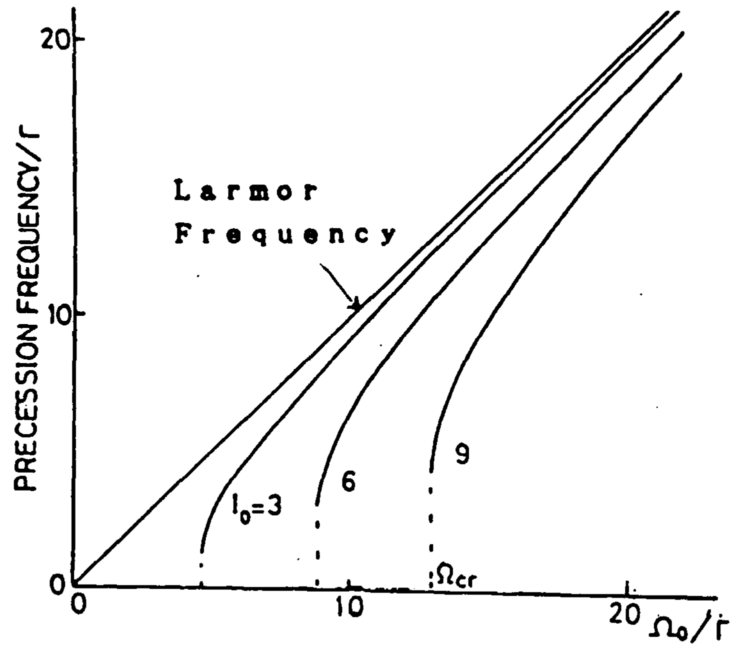

Upper limit of precession frequency

~ width of the absorption line.

(In the present experiment, pressure broadening of the D_2 line at He pressure ~500 torr is about 10 GHz.)

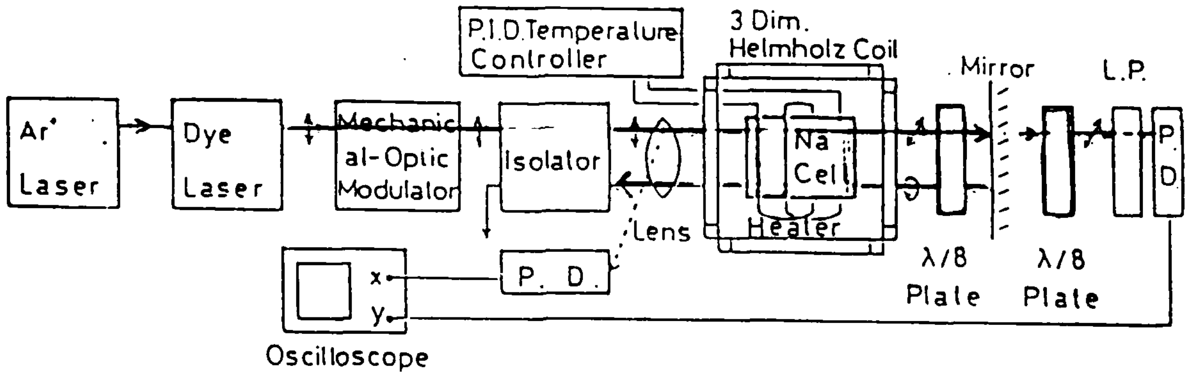
P.I.D. Temperature Controller
3 Dim. Helmholz Coil
Mirror
L.P.
Ar+ Laser
Dye Laser
Mechanical-Optic Modulator
Isolator
Na Cell
P. D.
Lens
Heater
λ/8 Plate
λ/8 Plate
P. D.
x
y
Oscilloscope

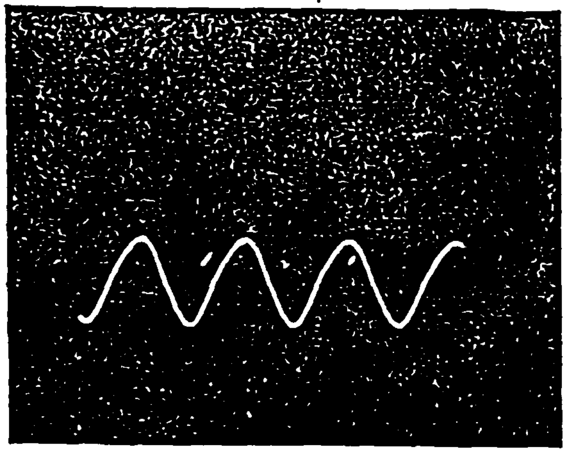

(a) Hy = 0.158 (Gauss)

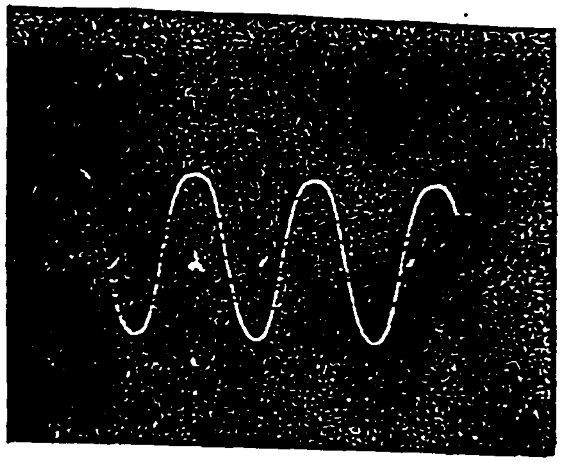

(b Hy = 0.455 (Gauss)

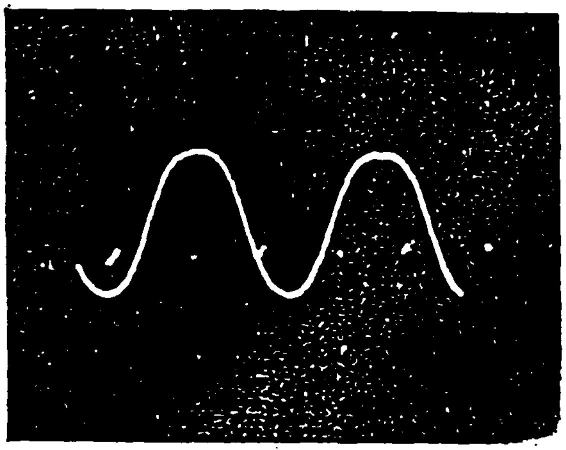

(c) Hy = 1.364 (Gauss)

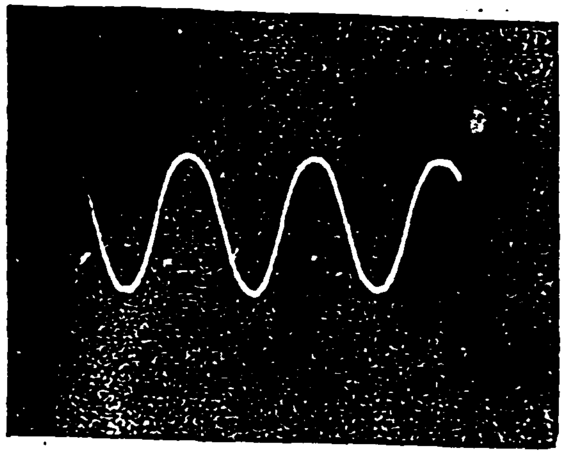

(d) Hy = 2.948 (Gauss)

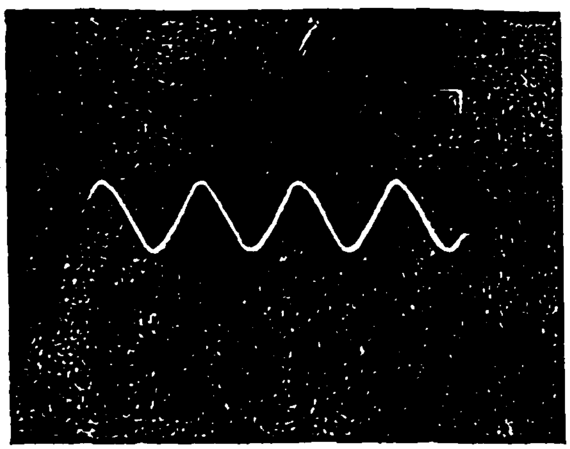

(e) Hy = 5.464 (Gauss)

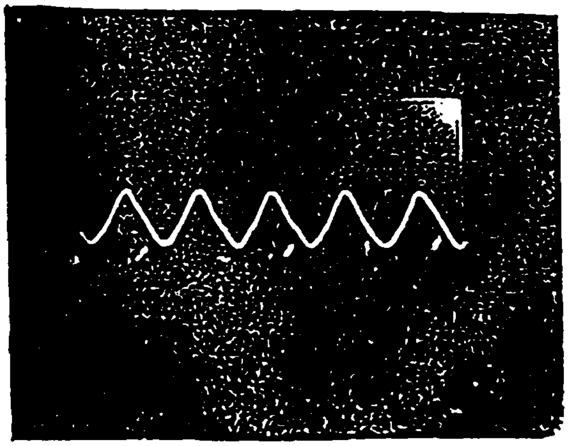

(f) Hy = 7.741 (Gauss)

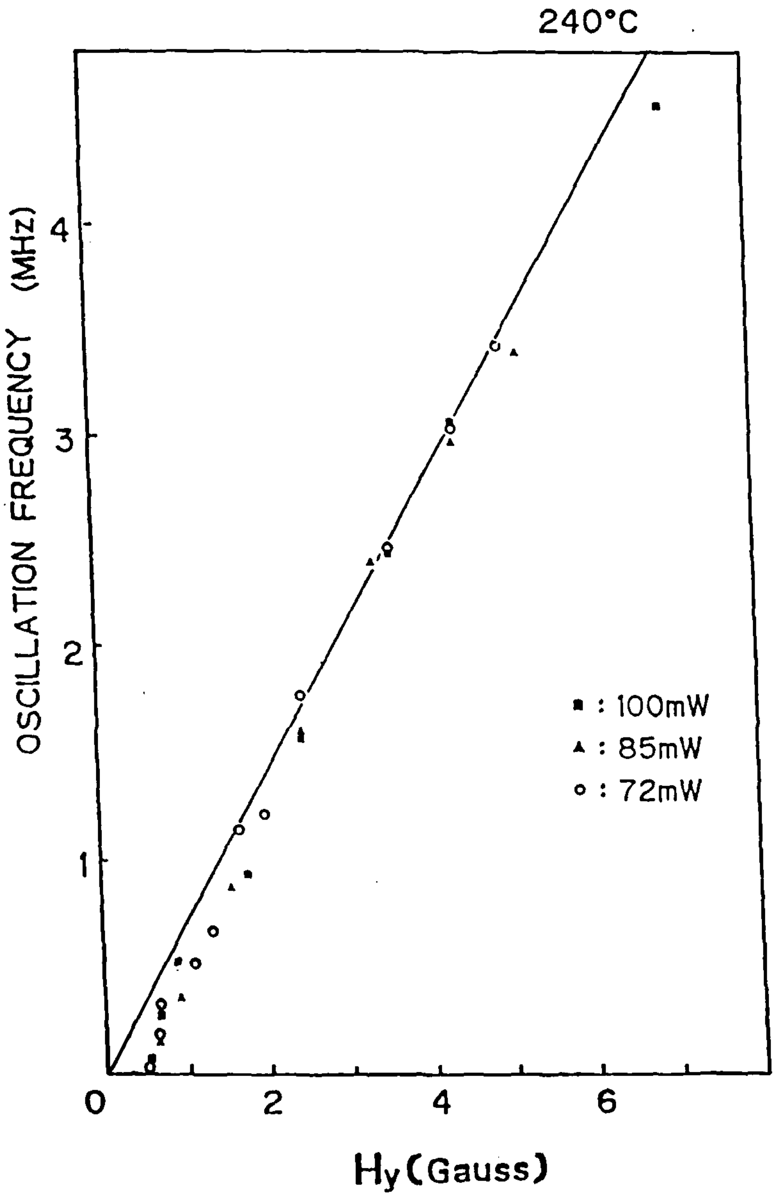
240°C
OSCILLATION FREQUENCY (MHz)
■ : 100mW
▲ : 85mW
○ : 72mW
0
1
2
3
4
0
2
4
6
Hy (Gauss)

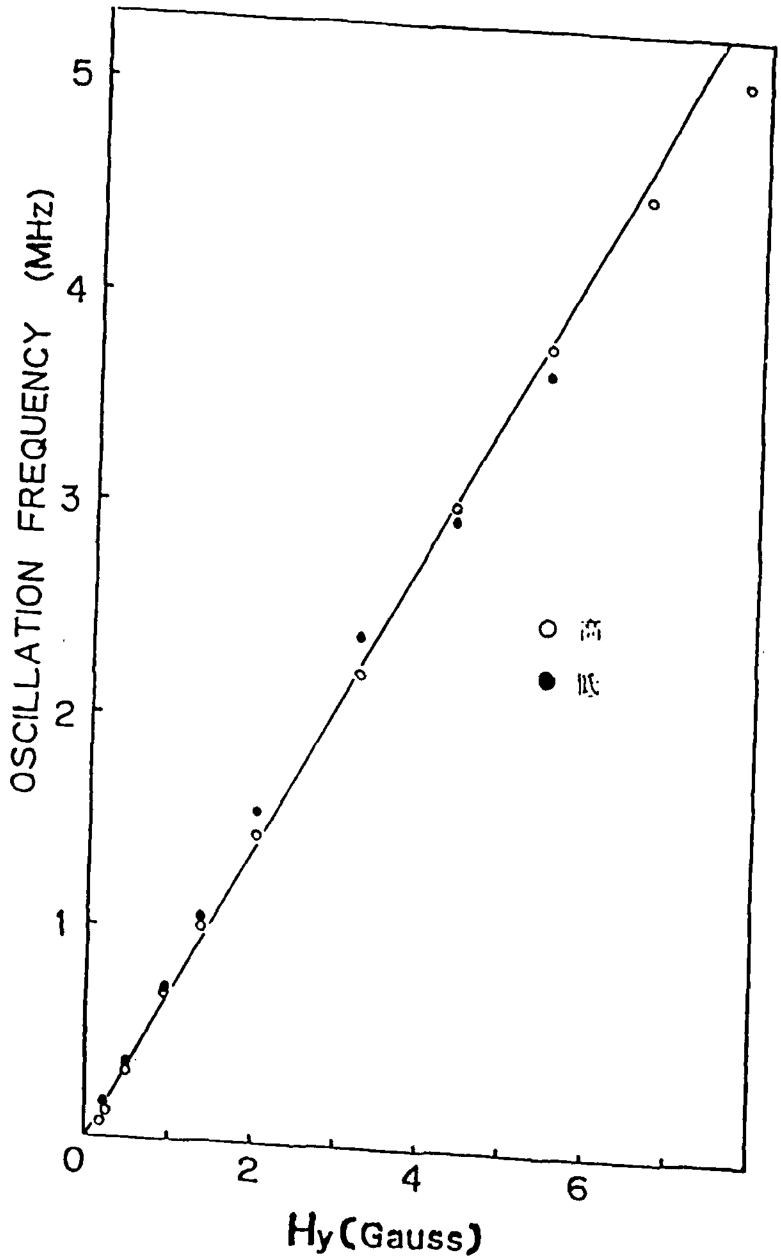
OSCILLATION FREQUENCY (MHz)
5
4
3
2
1
0
2
4
6
Hy (Gauss)
○ 高
● 低

1

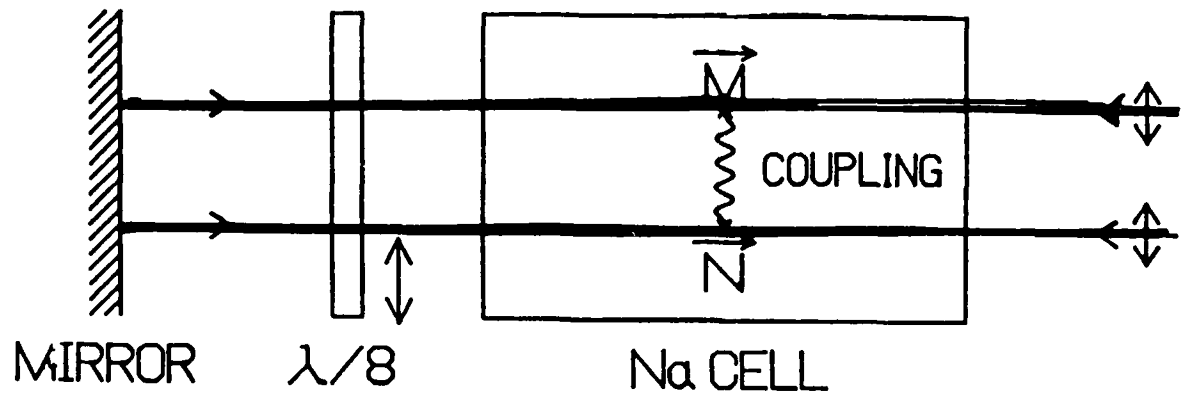

$$
\begin{cases}
dM/dt = -\gamma M + \mu M\,(1 - aM^2) + c\,(N - M) \\
dN/dt = -\gamma N + \mu N\,(1 - aN^2) + c\,(M - N)
\end{cases}
$$

coupling coeff.
c ：結合係数

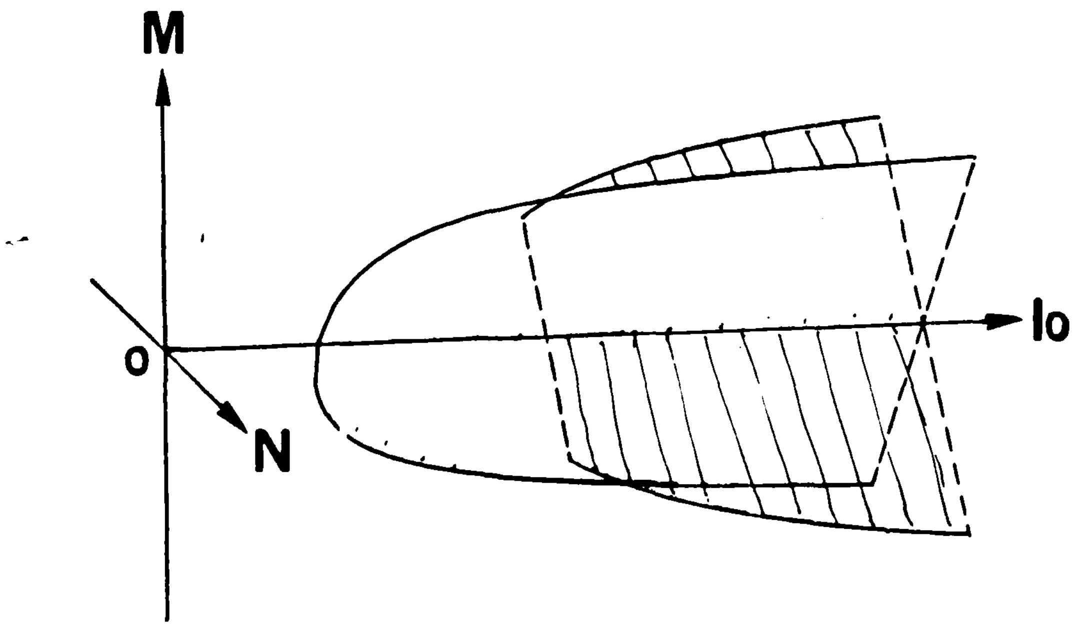

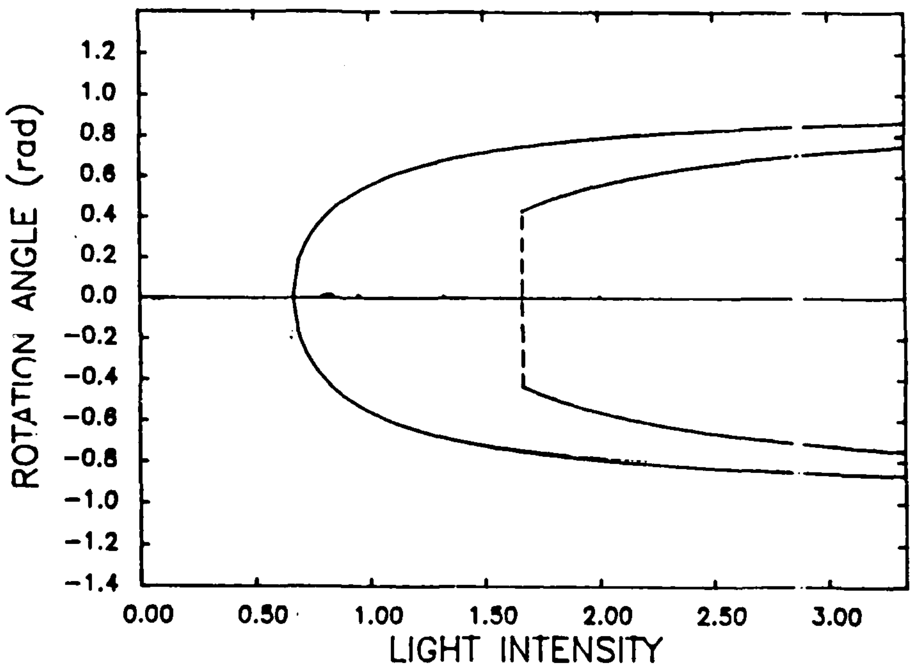

ROTATION ANGLE (rad)
1.2
1.0
0.8
0.6
0.4
0.2
0.0
−0.2
−0.4
−0.6
−0.8
−1.0
−1.2
−1.4
0.00
0.50
1.00
1.50
2.00
2.50
3.00
LIGHT INTENSITY

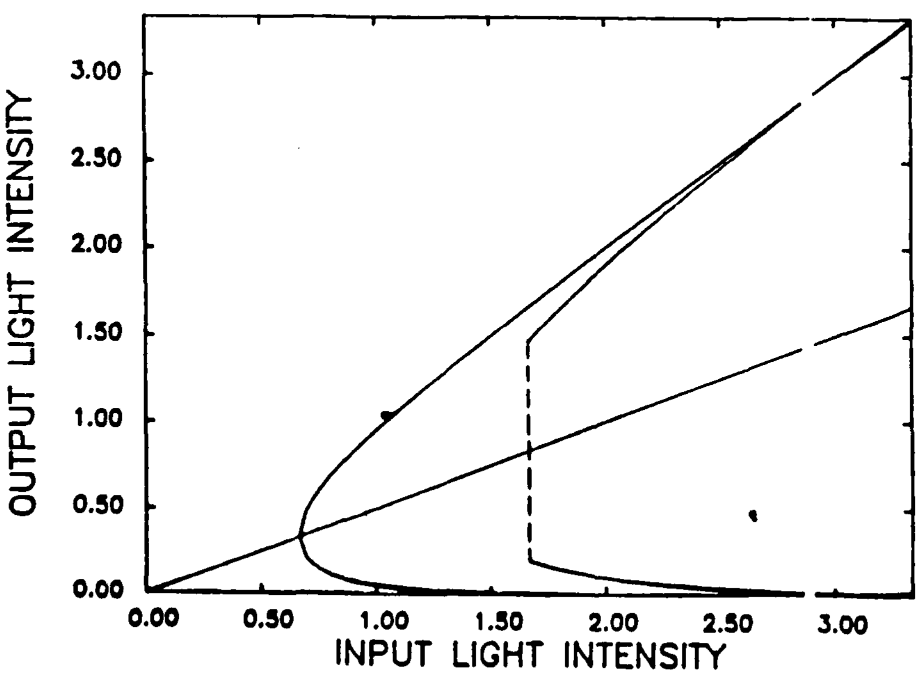

OUTPUT LIGHT INTENSITY
3.00
2.50
2.00
1.50
1.00
0.50
0.00
0.00
0.50
1.00
1.50
2.00
2.50
3.00
INPUT LIGHT INTENSITY

2

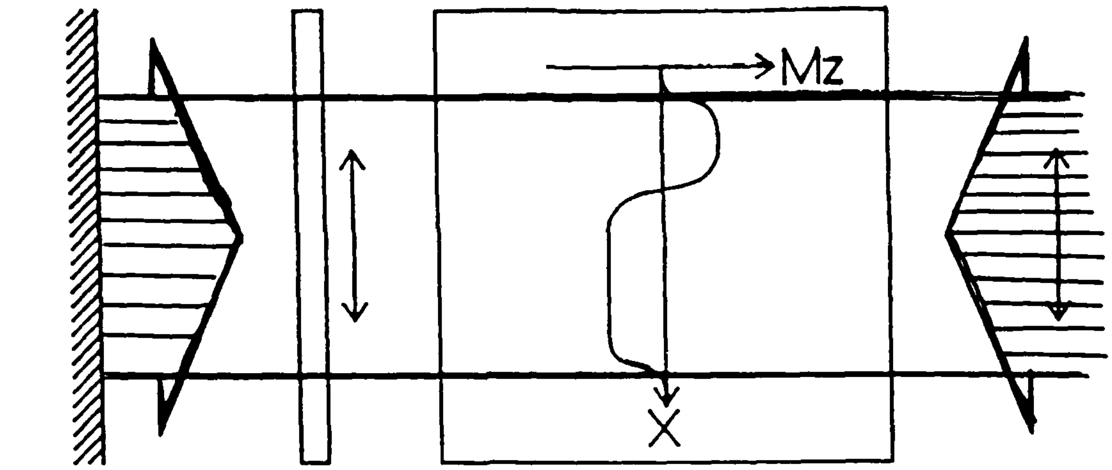

$$\partial M/\partial t = D\,\partial^2 M/\partial x^2 - \gamma M + \mu M(1 - aM^2)$$

$$M(x) = A\tanh(\pm Bx - C),\ \pm A$$

$$A = \sqrt{(1-\gamma/\mu)/a}$$
$$B = \sqrt{(\mu-\gamma)/2D}$$

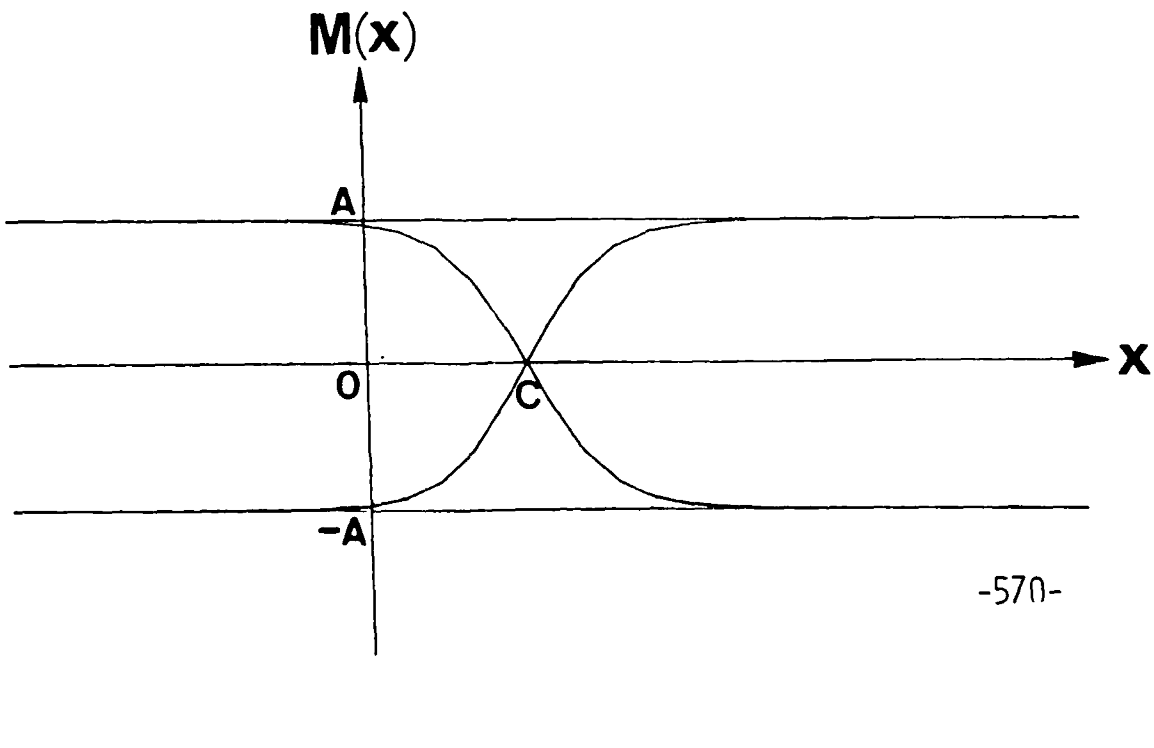

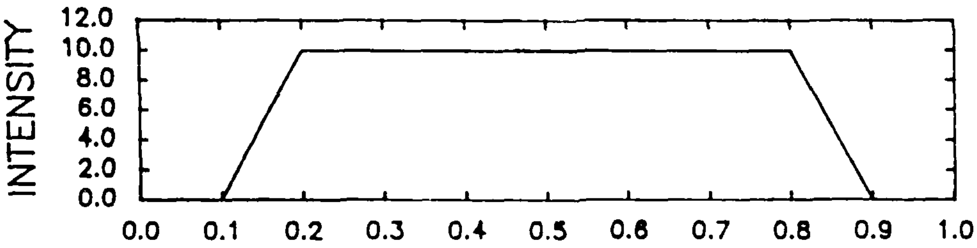
INTENSITY
12.0
10.0
8.0
6.0
4.0
2.0
0.0
0.0 0.1 0.2 0.3 0.4 0.5 0.6 0.7 0.8 0.9 1.0

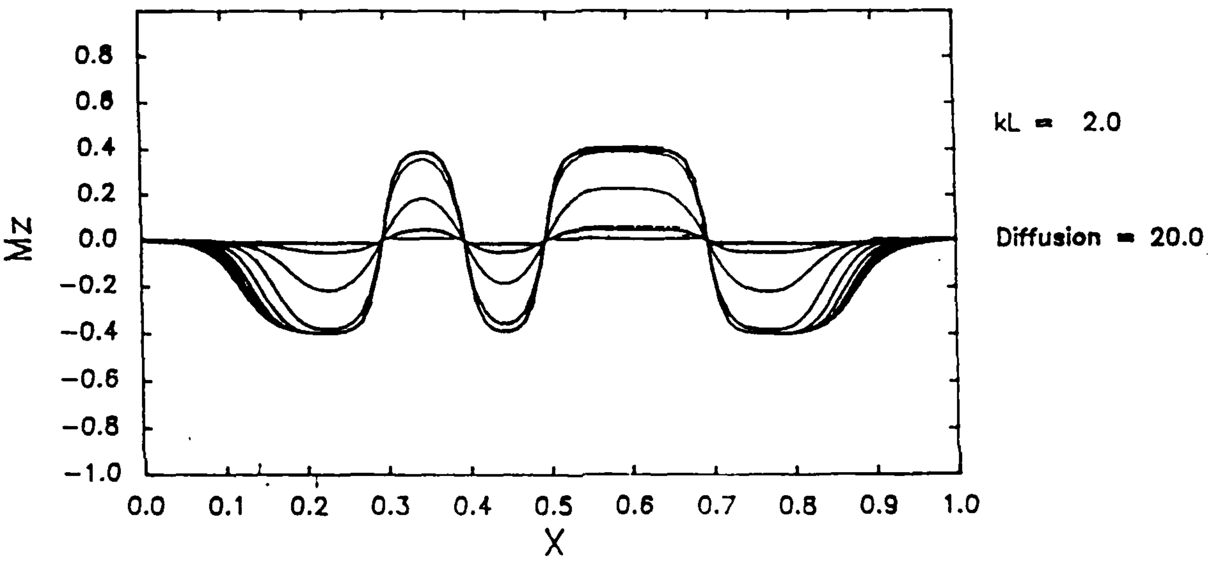
Mz
0.8
0.6
0.4
0.2
0.0
−0.2
−0.4
−0.6
−0.8
−1.0
0.0 0.1 0.2 0.3 0.4 0.5 0.6 0.7 0.8 0.9 1.0
X
kL = 2.0
Diffusion = 20.0

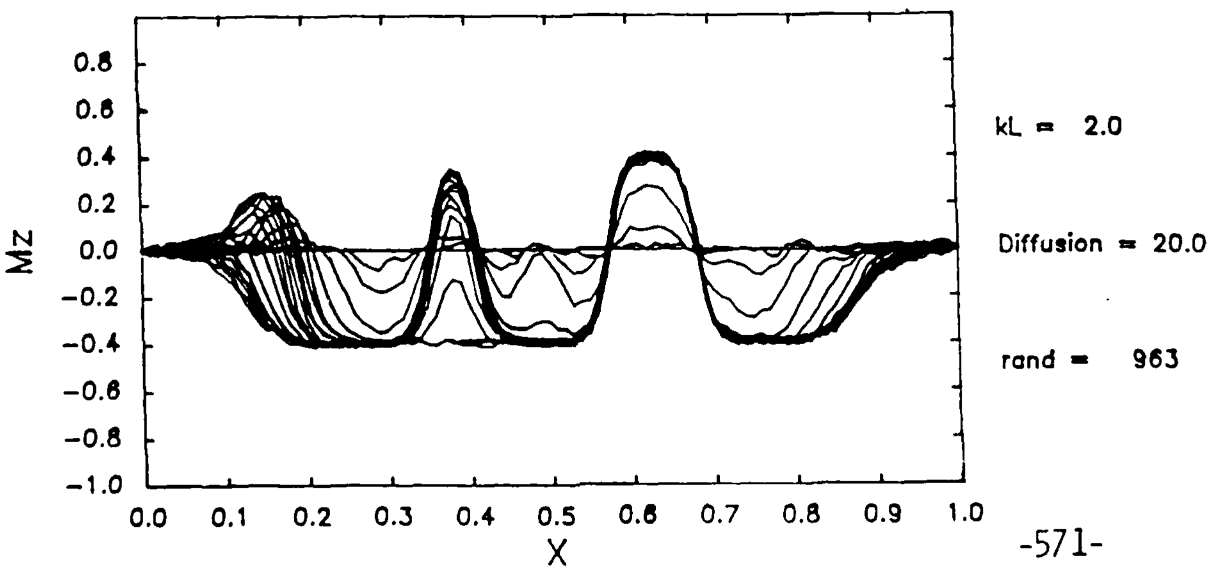
Mz
0.8
0.6
0.4
0.2
0.0
−0.2
−0.4
−0.6
−0.8
−1.0
0.0 0.1 0.2 0.3 0.4 0.5 0.6 0.7 0.8 0.9 1.0
X
kL = 2.0
Diffusion = 20.0
rand = 963

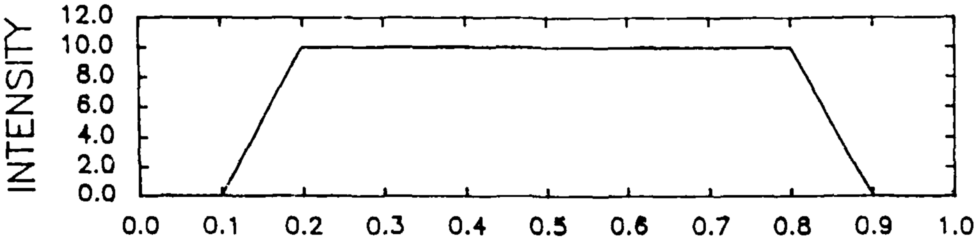

INTENSITY
12.0
10.0
8.0
6.0
4.0
2.0
0.0
0.0 0.1 0.2 0.3 0.4 0.5 0.6 0.7 0.8 0.9 1.0

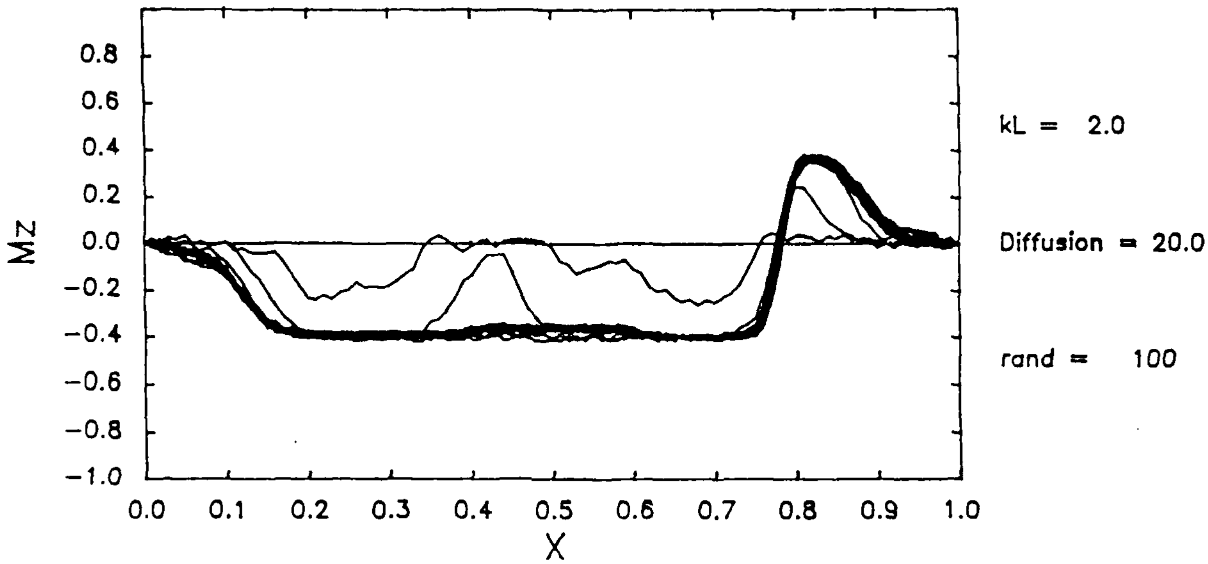

Mz
0.8
0.6
0.4
0.2
0.0
−0.2
−0.4
−0.6
−0.8
−1.0
0.0 0.1 0.2 0.3 0.4 0.5 0.6 0.7 0.8 0.9 1.0
X
kL = 2.0
Diffusion = 20.0
rand = 100

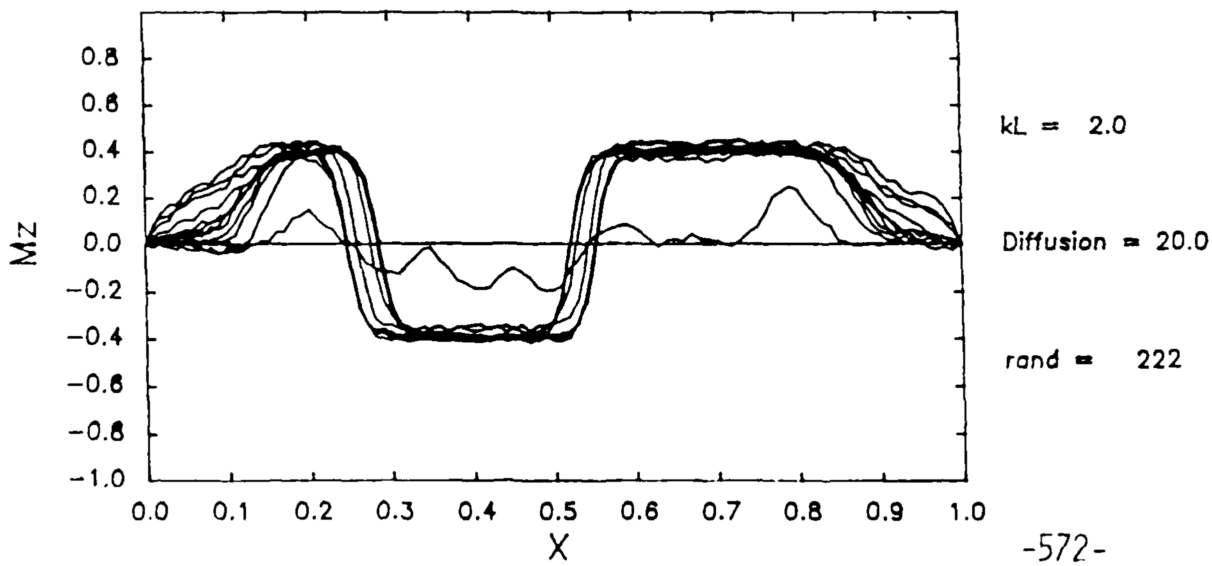

Mz
0.8
0.6
0.4
0.2
0.0
−0.2
−0.4
−0.6
−0.8
−1.0
0.0 0.1 0.2 0.3 0.4 0.5 0.6 0.7 0.8 0.9 1.0
X
kL = 2.0
Diffusion = 20.0
rand = 222

3

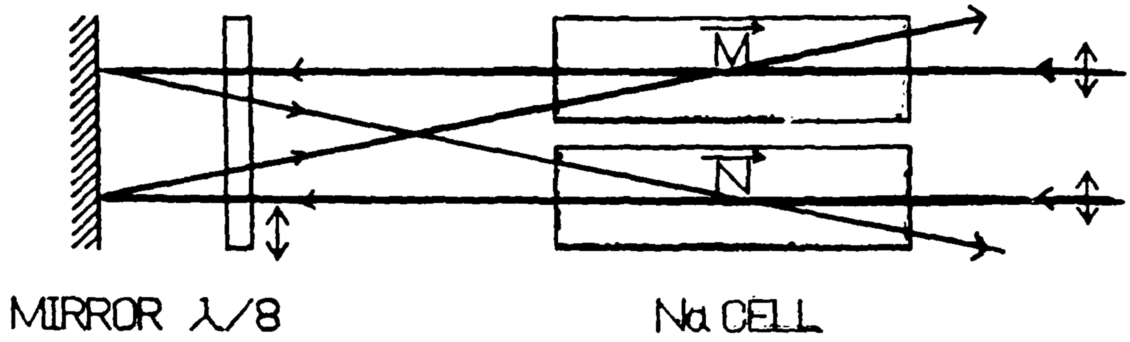

$$\begin{cases} dM/dt = -\gamma M + \mu N\,(1 - aN^2) \\ dN/dt = -\gamma N + \mu M\,(1 - aM^2) \end{cases}$$

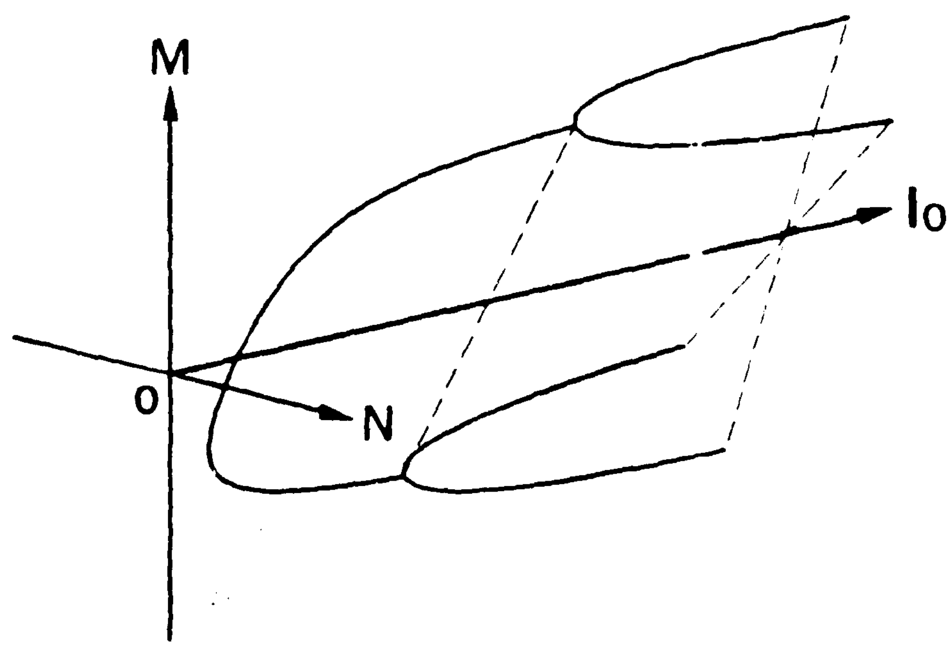

AD-A186 938 UNITED STATES - JAPAN SEMINAR ON QUANTUM MECHANICAL 7/7
ASPECTS OF QUANTUM EL (U) MASSACHUSETTS INST OF TECH
CAMBRIDGE RESEARCH LAB OF ELECTRON
UNCLASSIFIED J H SHAPIRO ET AL OCT 87 N00014-87-G-0198 F/G 20/3 NL

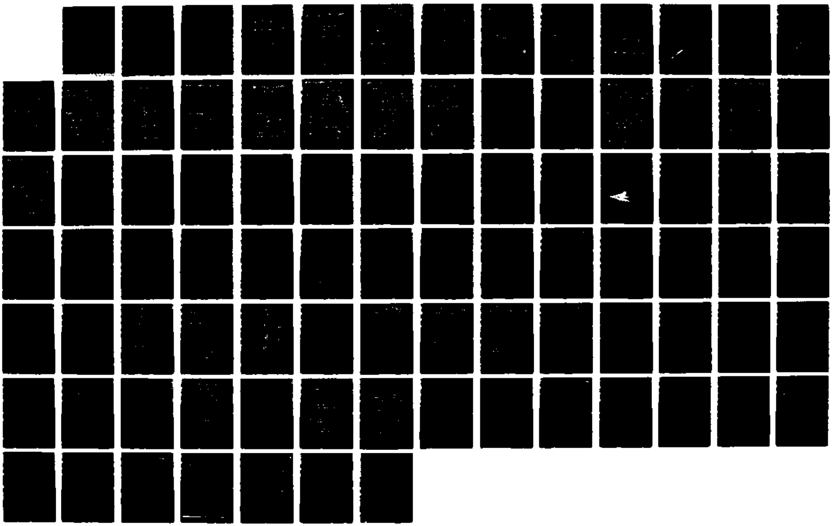

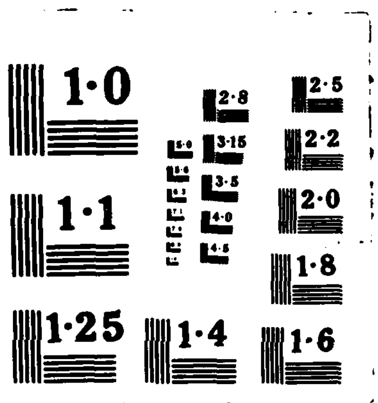
1·0
2·8
2·5
3·15
2·2
3·5
2·0
1·1
4·0
4·5
1·8
1·25
1·4
1·6

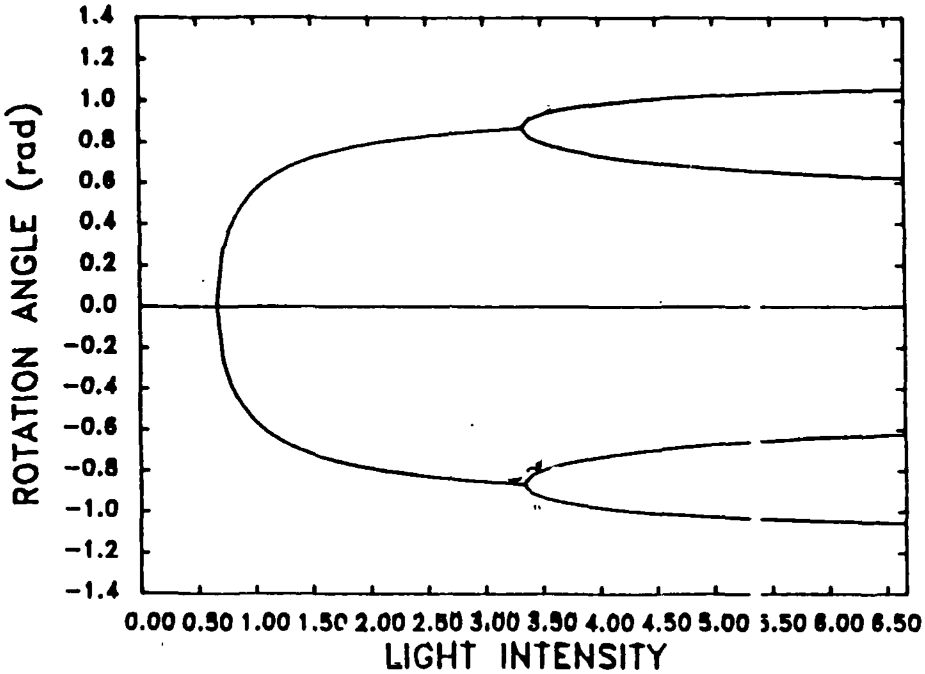
1.4
1.2
1.0
0.8
0.6
0.4
0.2
0.0
−0.2
−0.4
−0.6
−0.8
−1.0
−1.2
−1.4
ROTATION ANGLE (rad)
0.00 0.50 1.00 1.50 2.00 2.50 3.00 3.50 4.00 4.50 5.00 5.50 6.00 6.50
LIGHT INTENSITY

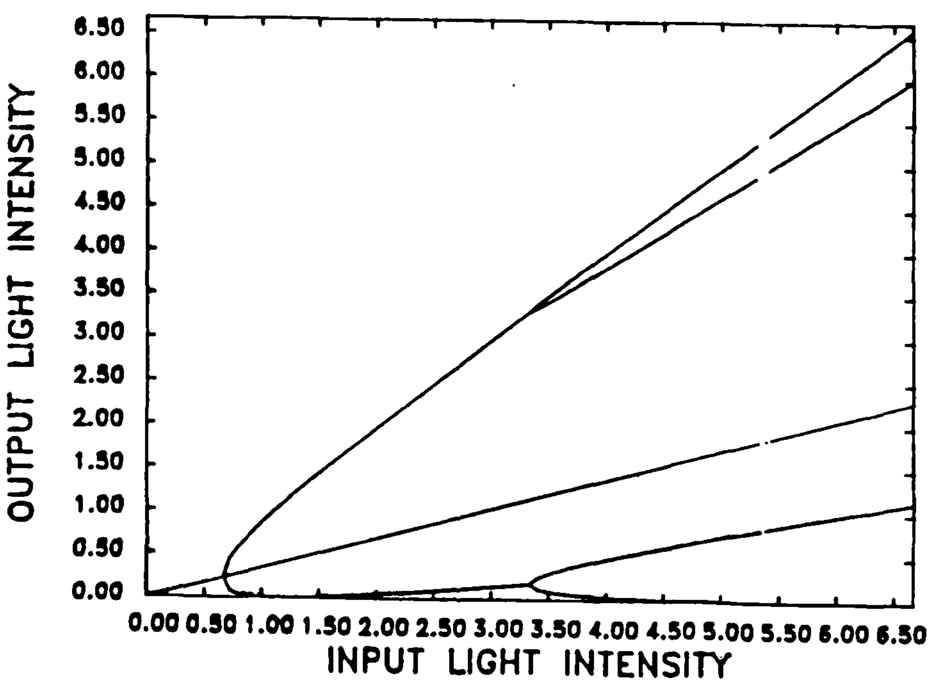
6.50
6.00
5.50
5.00
4.50
4.00
3.50
3.00
2.50
2.00
1.50
1.00
0.50
0.00
OUTPUT LIGHT INTENSITY
0.00 0.50 1.00 1.50 2.00 2.50 3.00 3.50 4.00 4.50 5.00 5.50 6.00 6.50
INPUT LIGHT INTENSITY

NONCLASSICAL LIGHTS

Horace P. Yuen
Department of Electrical Engineering and Computer Science
Northwestern University
Evanston, Illinois 60208

SUMMARY

The differences between "nonclassical" lights and coherent-state lights are reviewed. Some general observations are made concerning the generation, propagation, and detection of squeezed-state and near number-state lights. The role of phase-sensitive linear amplifiers and photon-number amplifiers is emphasized. Certain possible applications of nonclassical lights to communications are described, including optic local area networks.

NONCLASSICAL
NONSTANDARD LIGHTS

beating standard quantum limits
from standard sources (amplifiers)

ALL LIGHTS ARE QUANTUM

<u>Single</u> measurement
— one conventional probabilistic description

<u>two</u> incompatible measurements
— quantum

Coherent state $|\alpha\rangle$ $p(\alpha_1, \alpha_2)$

$|0\rangle$

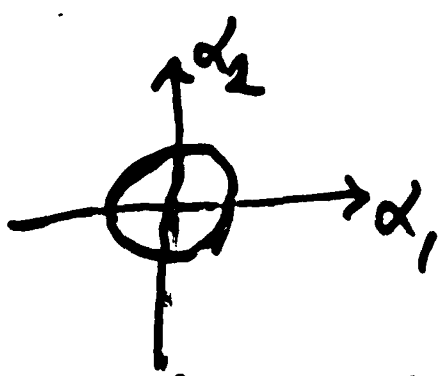

$\langle n|0\rangle$

$e^{-(\alpha_1^2+\alpha_2^2)}$

no single probabilistic description

RICHARD P. FEYNMAN (82 quote)

I think it is fair to say that no one understan[ds] quantum mechanics. Do not keep saying to yourself, if you can possibly avoid it, "But how can it be like th[at?"] because you will go "down the drain" into a blind alley from which nobody has yet escaped. Nobody knows how it can be like that.

R.P. FEYNMAN in "Simulating Physics with Computers", Intern. J. Theoret. Phys. 82

... We always have had (secret, secret, close the doors!) we always have had a great deal [of] difficulty in understanding the world view quantu[m] mechanics represents. .... I cannot define the real problem, therefore I suspect there is no real problem, but I am not sure there is no real proble[m]. So that is why I like to investigate things.

:

how can we simulate the quantum mechan[ics]

:

the challenge of explaining quantum mechanical phenomena

"vacuum" em field

ground state $|0\rangle$

$\downarrow$

a coherent state

Single mode

quadrature components

$$\underset{a_1}{\overset{\mathfrak{g}}{\downarrow}} \quad \underset{a_2}{\overset{p}{\downarrow}}$$

$$a = a_1 + i a_2$$

Coherent states

$$a|\alpha\rangle = \alpha|\alpha\rangle$$

uncertainty pricible

$$\langle \Delta a_1^2 \rangle \langle \Delta a_2^2 \rangle \geq \frac{1}{16}$$

$$\Downarrow$$

minimum sum fluctuation energy $\quad \langle \Delta a_1^2 \rangle + \langle \Delta a_2^2 \rangle \geq \frac{1}{2}$

= for coherent st

(classical or) standard light: ——

(a random superposition of) coherent s

Properties of Coherent State Light

$|\alpha\rangle$: $\quad \langle\alpha|a|\alpha\rangle = \alpha = \alpha_1 + i\alpha_2$ mean field

$\langle\alpha|a^\dagger a|\alpha\rangle = |\alpha|^2$

photocount statistics (direct detection) $\quad |\langle\alpha|n\rangle|^2 = e^{-|\alpha|^2}\dfrac{|\alpha|^{2n}}{n!}$

Poisson $\quad$ mean = var = $|\alpha|^2$

field amplitude statistics (homodyne detection)

Gaussian $\quad$ mean α_1, var $\frac{1}{4}$ (ħω

Signal & noise "representation"

$a_\phi = a_1\cos\phi - a_2\sin\phi$

$\langle\Delta a_\phi^2\rangle = \frac{1}{4}$

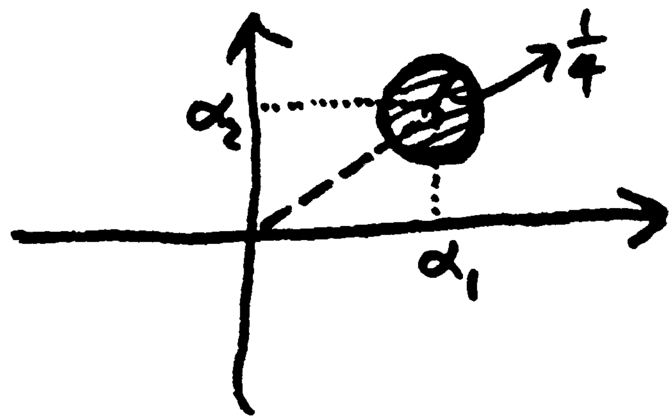

NOTE :

1/ coherent states are not at all classical.

2/ they do not have unique space-time coherence property — any single excited mode

3/ they do not necessarily obtain in an ideal ordinary laser

4/ they are special because the "vacuum state" is a coherent state

terminology —

nonclassical light

? nonstandard light

? ...

QUANTUM FIELD MODES

$\bar{\Psi}(\bar{x},t) \longrightarrow \psi(\bar{\rho})\,\phi(t)$ determ. mode functio

$\phi(t) \longleftrightarrow \tilde{\phi}(f)$

$E = \sum_n a_n \bar{\Psi}$

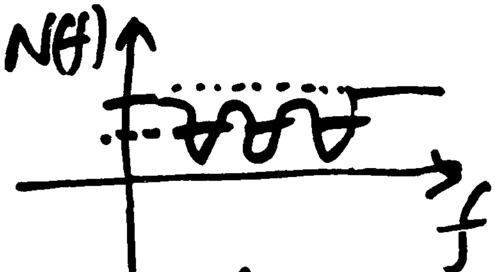

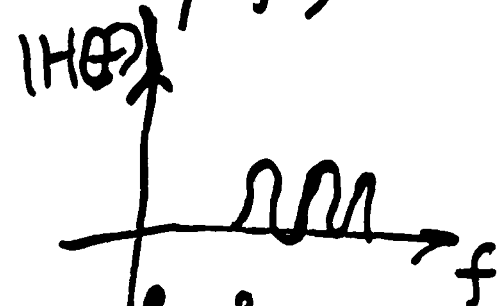

single mode ≠ single freq.
more power in pulsed mode

Space-time coherence

$\underset{a}{\alpha}\,\bar{\Psi}(\bar{x},t)$

<u>Coherent number state field</u>

$E = \underset{\uparrow\,|n\rangle}{a}\,\bar{\Psi}(\bar{\rho},t) + \text{vacuum}$

TWO-PHOTON COHERENT STATE LIGHT

(TCS, squeezed state light)

$|\mu\nu\alpha\rangle$: $|\mu|^2-|\nu|^2=1$ $\quad \mu a+\nu a^\dagger$

$\langle|a|\rangle = \alpha_1 + i\alpha_2$

$\langle|a^\dagger a|\rangle = |\alpha|^2+|\nu|^2$

photocount statistics .... $H_n(\cdots)$ ....

can be sub-Poissonian (var < mean

$\langle\mu\nu 0|n\rangle \neq 0$ only for even n

field amplitude statistics

Gaussian with unsymmetric noi

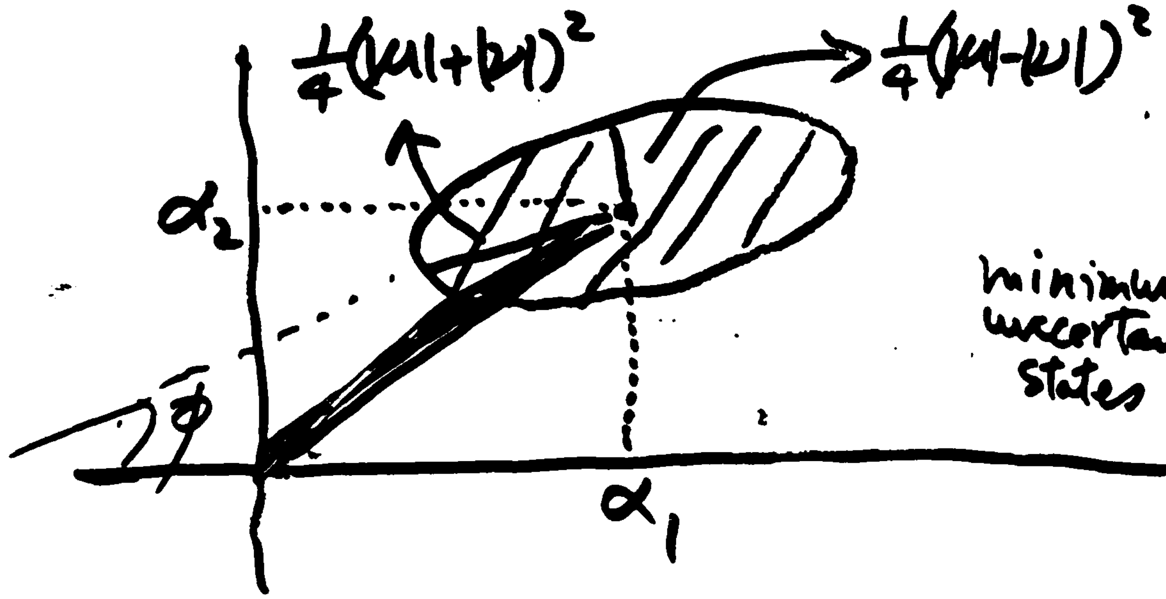

minimum uncertainty states $\phi =$

SQUEEZING

$\langle \Delta a_\phi^2 \rangle < \frac{1}{4}$ for some ϕ

$\langle \Delta a_\phi^2 \rangle \langle \Delta a_{\phi+\frac{\pi}{2}}^2 \rangle \geq \frac{1}{16}$

Squeezed state — any quantum state that exhibits squeezing

TCS — above rotated minimum uncertainty states

not a "classical state

For a given level of squeezing, TCS has the smallest total energy

For a fixed energy, TCS yields the best homodyne signal-to-noise ratio among all sta

$$\left(\frac{S}{N}\right)_{TCS}^{hom} \equiv \frac{\langle a_\phi \rangle^2}{\langle \Delta a_\phi^2 \rangle} = 4S(S+1)$$

$tr \rho a^\dagger a \leq S$

$$\left(\frac{S}{N}\right)_{CS}^{hom} = 4S$$

DETECTION OF TCS

homodyning

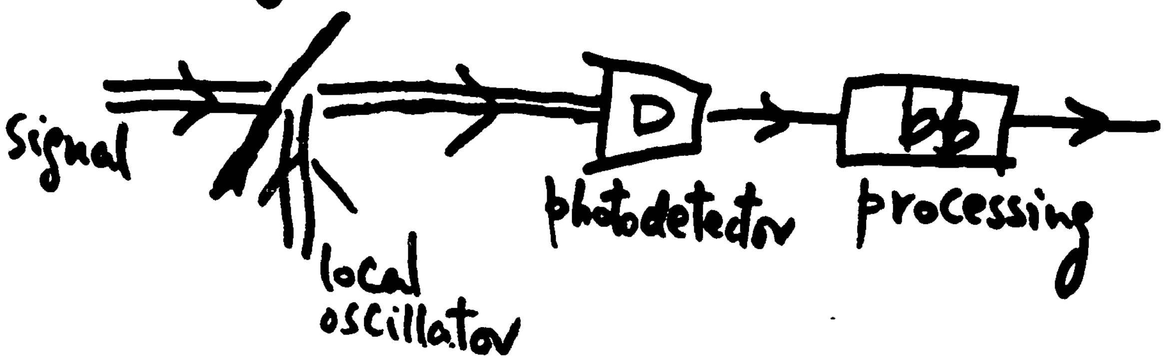

noise from signal, not local oscillator

balanced homodyning

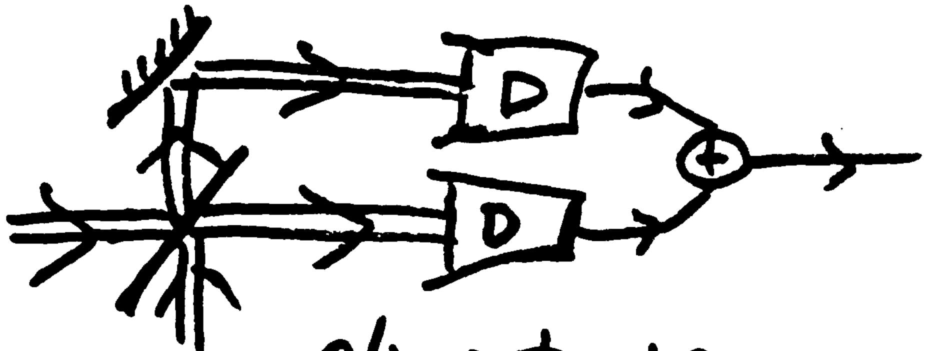

eliminate LO excess nois

problem of quantum efficiency

— 90% 1 order
99% 2 order improvement limit

EFFECT OF LOSS for all nonstandard lights

$$b = \eta^{\frac{1}{2}} a + (1-\eta)^{\frac{1}{2}} v_{\mathrm{\Delta}}$$

vacuum $|0\rangle$ is a CS

$$\langle \Delta b_\phi^2 \rangle = \eta \langle \Delta a_\phi^2 \rangle + (1-\eta)\tfrac{1}{4} \geq (1-\eta)\tfrac{1}{4}$$

noise floor in additio to signal attenuatio

General Principle for Overcoming Loss

any linear loss in system

Appropriate (match detection and/or state)

OPTICAL PRE-AMPLIFICATION

heterodyne (CS) — PIA phase insensit linear ampli

homodyne (TCS) — PSA phase sensit linear ampli

direct (NNS) — PNA photon-num amplifier

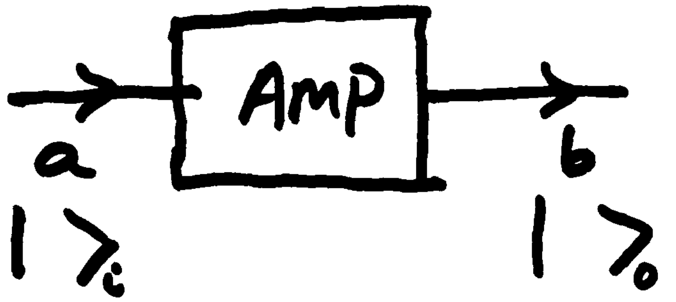

PIA

$$b = G^{1/2} a + (G-1)^{1/2} v$$

$$SNR_b = SNR_a \text{ — any } \rho_a$$

$$\left.\begin{array}{l} SNR_{b\phi} = \tfrac{1}{2} SNR_{a\phi} \\ SNR_{N_b} = \tfrac{1}{2} SNR_{N_a} \end{array}\right\rangle \text{CS } \rho_a$$

PSA

$$b_1 = G^{1/2} a_1, \quad b_2 = G^{-1/2} a_2$$

$$SNR_{b\phi} = SNR_{a\phi} \text{ — any } \rho_a$$

PNA

$$|n\rangle_i \longrightarrow |Gn\rangle_o$$

$$SNR_{N_b} = SNR_{N_a} \text{ — any } \rho_a$$

PHOTON NUMBER EIGENSTATES

$\rightarrow$ NNS

$N \equiv a^{\dagger} a \qquad N|n\rangle = n|n\rangle$

measure N —— $\langle \Delta N^2 \rangle = 0$, etc.

$$SNR_N \triangleq \frac{\langle N \rangle^2}{\langle \Delta N \rangle^2} \rightarrow \infty$$

but discrete

PHOTON NUMBER AMPLIFIER

$$a \longrightarrow \boxed{PNA} \longrightarrow b$$

$$\underline{|n\rangle \rightarrow |Gn\rangle}$$

$SNR_{N_b} = SNR_{N_a}$ for any ρ_a

ρ_b nonclassical for $\rho_a = |\alpha\rangle\langle\alpha|$

comparison with PIA

SQUEEZING GENERATION VIA A CAVITY

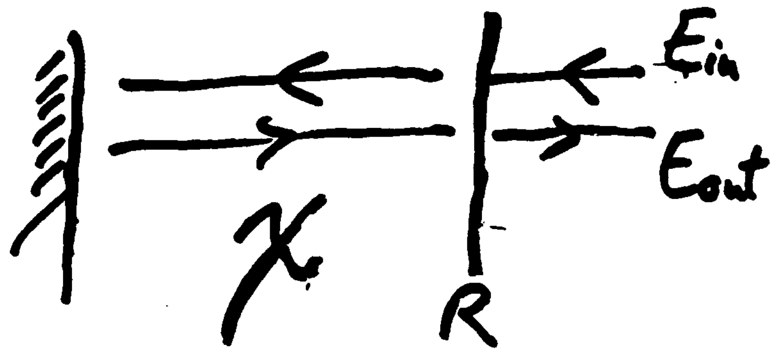

Coherent cancellation of noise for long observation time or narrow enough bandwidth

↓ effect of loss

near-perfect narrow-band parametric amplifier

NEAR NUMBER STATE LIGHT

$|n\rangle$ photon number eigenstate
— or strongly sub-Poissonian

generation

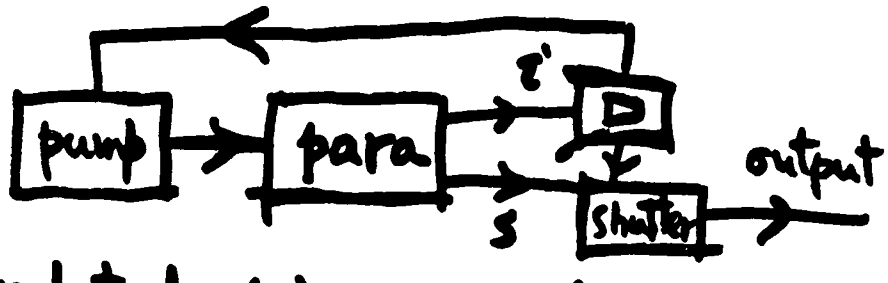

Correlated photon pairs feedforward
feedback

solid state
laser diode with pump fluc. suppress
⋮

propagation special fibers and/or amplifier

detection – noiseless photon amplifier
– transfer to another mode &
homodyne (QND)

application similar to TCS
local area network

APPLICATIONS

interferometry

$\frac{S}{N}$ improvement → grav. wave to[...]

in gyros (fiber or not)

gravitational wave interferomete[...]

communications

better system performance

— local area fiber network

long distance fiber transmission

near field space communication

precision measurements

interaction of radiation with matter

optical signal processing or computing

optical memory

Performance Advantage

general noise reduction

bandwidth W

power S

Capacity — general & specific modulation schemes

P_e, R, G tradeoff — digital / analog commun

ϵ^2

new capability

CAPACITY COMPARISON

$$C_g = W \log\left(1 + 2\frac{S}{hfW}\right)$$

$$C_{het} = W \log\left(1 + \frac{S}{hfW}\right)$$

(1) het

$$C_{hom} = \frac{W}{2} \log\left(1 + 4\frac{S}{hfW}\right)$$

(2) hom

$$C_{op} = C_{het} + \frac{S}{hf} \log\left(1 + \frac{hfW}{S}\right)$$

(3)

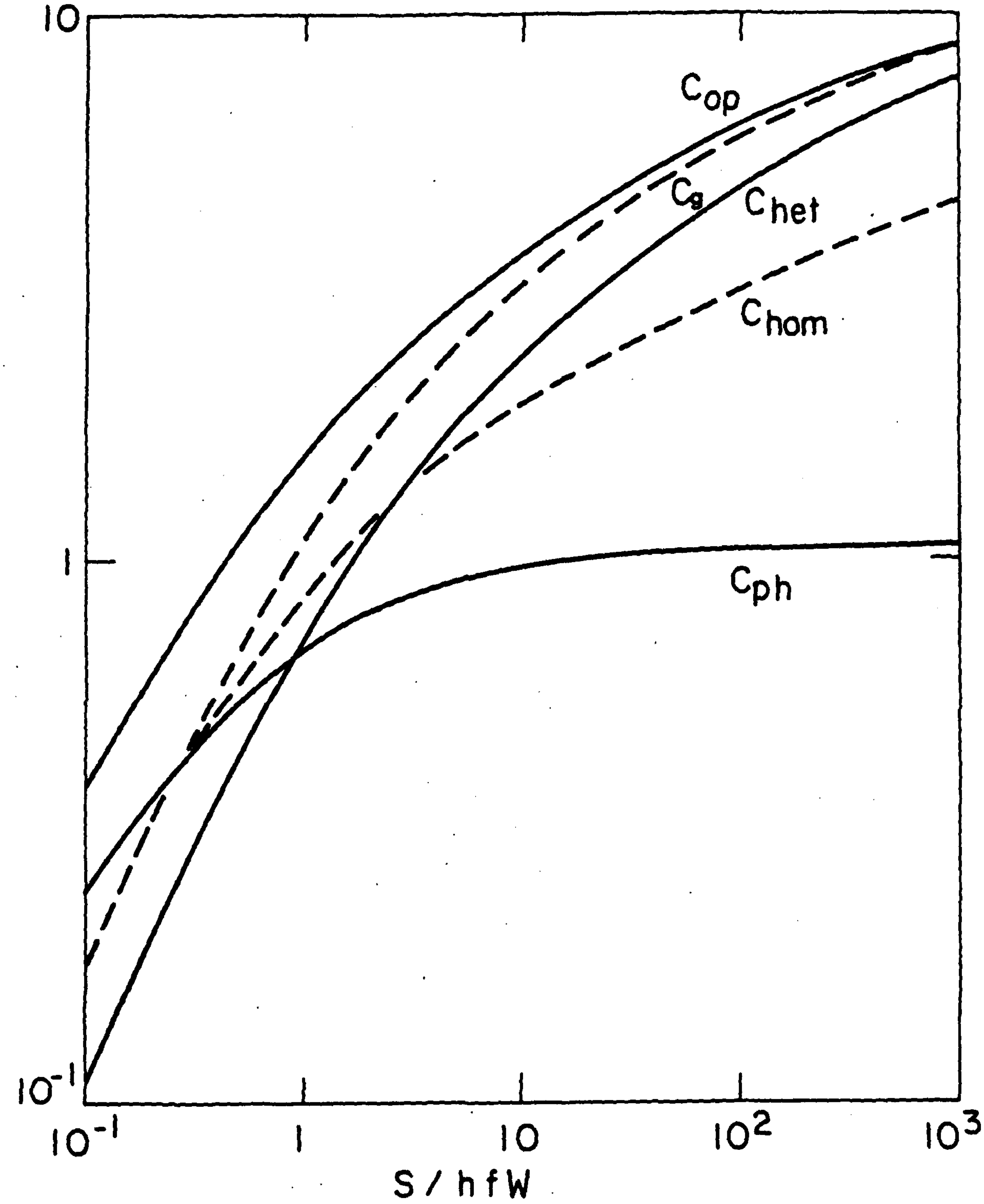
10
1
10^{-1}
10^{-1}
1
10
10^2
10^3
S / h f W
C_{op}
C_a
C_{het}
C_{hom}
C_{ph}

FIBER-OPTIC LAN

PSA — wideband parametric amplifier
fiber & integrated optics

PNA — need practical scheme

LONG-HAUL FIBER TRANSMISSION

Use of distributive-amplifier
compensated fibers, discrete
amplifier stages, etc. for

— CS
— TCS
— NNS

to get significant improvement

in both cases, no need for nonclassical sources

FIBER-OPTIC QUANTUM COMMUNICATIONS

	SOURCES	AMPLIFIERS
ordinary optical communication	coherent states CS	phase-insensitive PIA
quantum	two-photon coherent states or squeezed states TCS	phase-sensitive PSA
	near-number states NNS	photon-number PNA

LINEAR BUS IN LOCAL AREA NETWORK

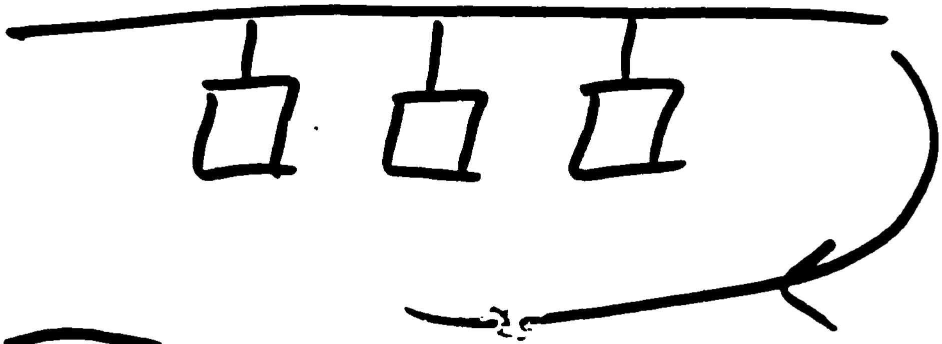

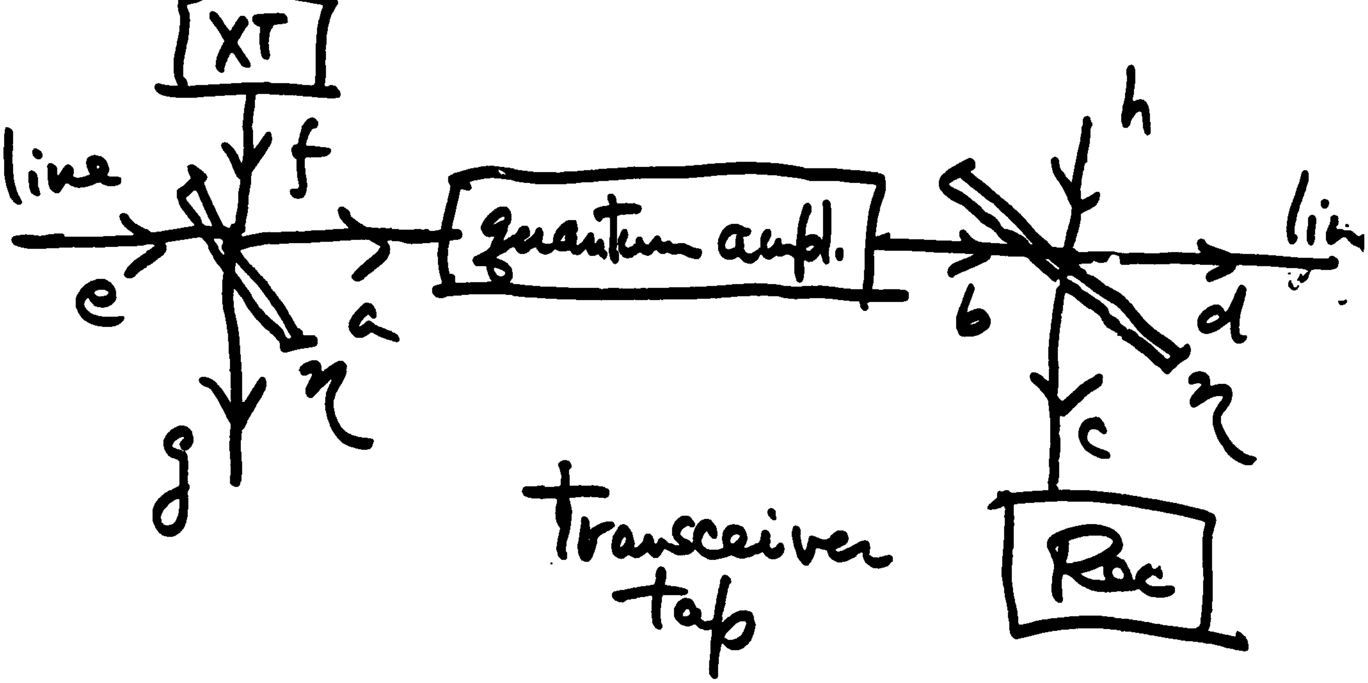

amp = PCA

$$SNR_{N_c} \sim \frac{1}{2} SNR_{N_a}$$

c, d, $c\phi$, $d\phi$ (under N); $a\phi$ (under N_a)

not ma ~~user~~

AMP = PNA

$$SNR_{N_c} = SNR_{N_a} \Big/ \left[1 + \frac{\eta}{G(1-\eta)} \frac{\langle N_a \rangle}{\langle \Delta N_a^2 \rangle}\right]$$

$$SNR_{N_d} = SNR_{N_a} \Big/ \left[1 + \frac{1-\eta}{G\eta} \frac{\langle N_a \rangle}{\langle \Delta N_a^2 \rangle}\right]$$

$$SNR_{N_c} \sim SNR_{N_d} \sim SNR_{N_a}$$

<u>ampl</u> switched on-off line — $\eta = \frac{1}{2}$, $G \geq 10$

turned on-off but permanent online — η small

$G(1-\eta)$ large enough

$\langle N_d \rangle \sim G \langle N_a \rangle$

long haul too

amplification good for subsequent detecti

AMP = PSA

$$\xrightarrow[a]{} \boxed{PSA} \xrightarrow[b]{}$$

$$b_1 = G^{1/2} a_1$$
$$b_2 = G^{-1/2} a_2$$

$$SNR_{b\phi} = SNR_{a\phi}$$

$$SNR_{c_1} = SNR_{a_1} / \left[1 + \frac{\eta}{G(1-\eta)} \frac{1}{4\langle \Delta a_1^2 \rangle}\right]$$

$$SNR_{d_1} = SNR_{a_1} / \left[1 + \frac{1-\eta}{G\eta} \frac{1}{4\langle \Delta a_1^2 \rangle}\right]$$

$$SNR_{c_1} \sim SNR_{d_1} \sim SNR_{a_1}$$

& similar to PNA case

Comparison to Shapiro's tap

h mode in TCS

utilize large squeezing vs have noise insensitive

also have amplification

Quantum Statistics of Parametric Oscillators Above Threshold

D.F. Walls*, M.J. Collett+, A.S. Lane*,
M.D. Reid* and C.M. Savage$^{\Delta}$

* Physics Department
University of Waikato
Hamilton, New Zealand

+ Physics Department
University of Essex
Colchester, Essex, U.K.

$^{\Delta}$ Optical Sciences Center
University or Arizona
Tucson, A2, U.S.A.

Summary

The quantum statistics of the degenerate parametric oscillator above threshold are described. The squeezing spectrum is plotted for a range of parameters. The nondegenerate parametric oscillator is studied above threshold where the solutions are known to undergo phase diffusion. The fluctuations in the difference current from the signal and idler modes are calculated for the case where the signal and idler may have different cavity decay rates.

DEGENERATE PARAMETRIC OSCILLATOR

Collett

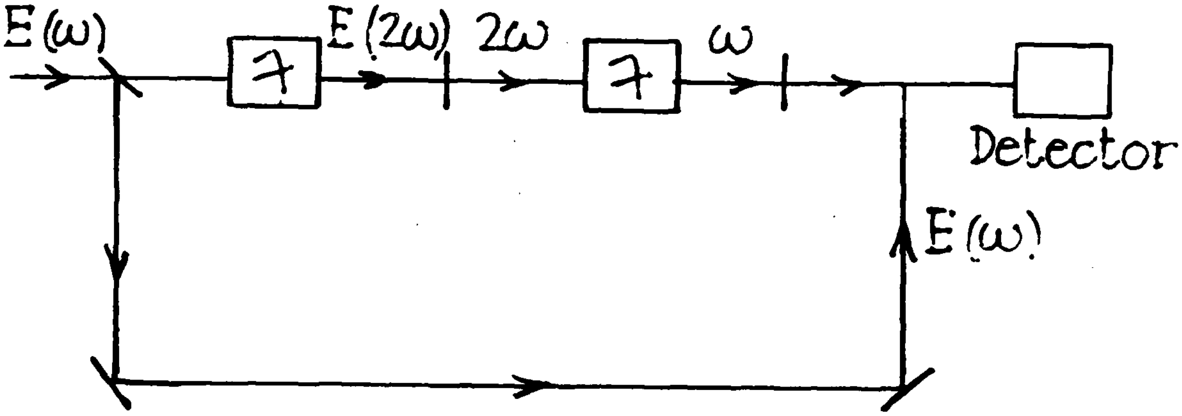

HAMILTONIAN

Non linear coupling

$$\chi a_1^2 a_2^\dagger + \chi a_1^{\dagger 2} a_2$$

Cavity losses

$$a_1 \Gamma_1^\dagger + a_2 \Gamma_2^\dagger + hc$$

Driving fields

$$a_2 E^* + a_2^\dagger E$$

Equations for mode amplitudes

$$\dot{\alpha}_1 = -\varkappa_1 \alpha_1 + \varkappa \alpha_1 \alpha_2^{\dagger} + \sqrt{\varkappa \alpha_2}\, \Gamma_1(t)$$

$$\dot{\alpha}_2 = E - \varkappa_2 \alpha_2 - \frac{\varkappa}{2} \alpha_1^2$$

[illegible]

$$< \Gamma_1(t)\, \Gamma_1(t') > = \delta(t - t')$$

[illegible]

$$|\alpha_1^{\circ}|^2 = 0 \qquad E \ll E_{Th}$$

$$|\alpha_1^{\circ}|^2 = \left[\frac{2}{\varkappa}\,(E - E_{Th})\right] \qquad E > E_{Th}$$

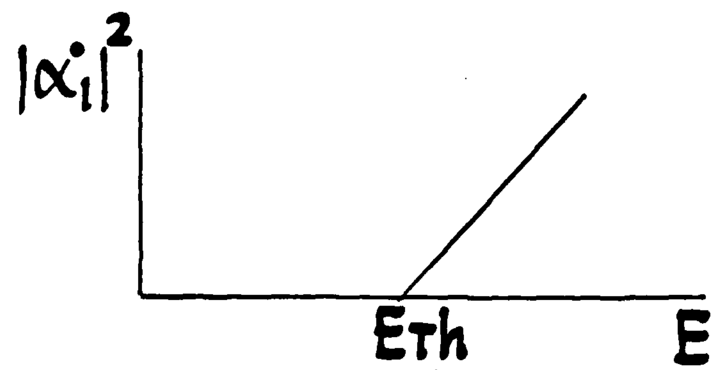

Define quadrature

$$X_\theta = (a e^{-i\theta} + a^{+} e^{i\theta})$$

Squeezing spectrum

$$V(X_{\theta,\omega}) = \int \left[\langle X_\theta(\tau) X_\theta(0) \rangle - \langle X_\theta(\tau) \rangle \langle X_\theta(0) \rangle \right] e^{i\omega\tau} \, d\tau$$

$$V(X_{\theta,\omega}) = 1 - \frac{4 \chi_1 \varepsilon}{(\chi_1 + \varepsilon)^2 + \omega^2}$$

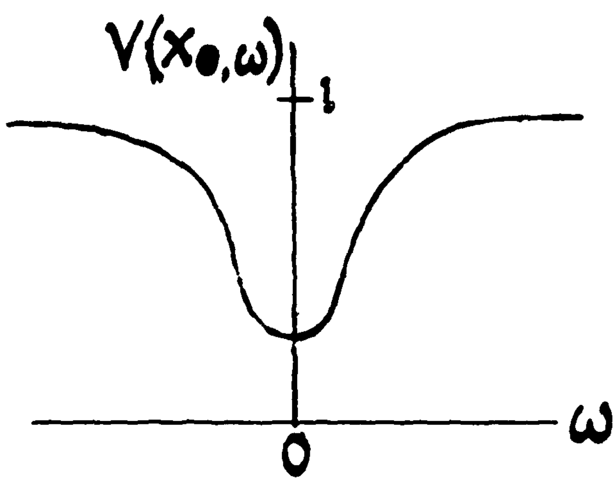

Squeezing Spectrum for Parametric Oscillator Below Threshold

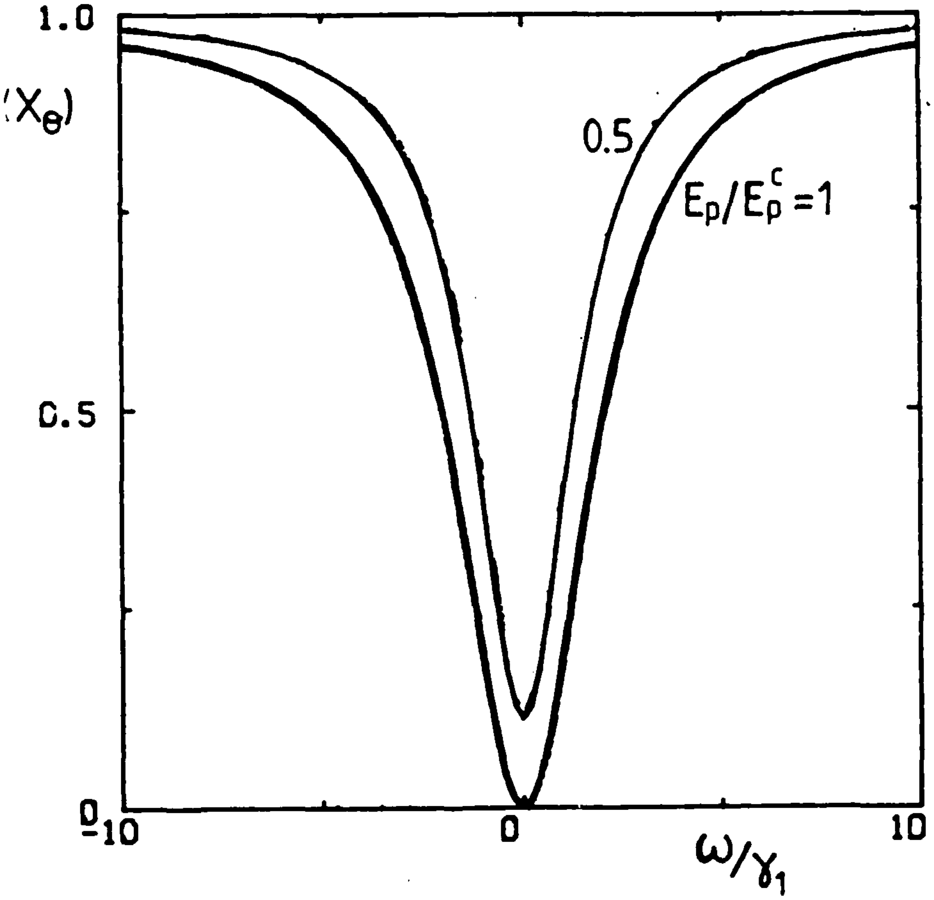

Above Threshold

Squeezing Spectrum

$$V(X_{\theta}, \omega) = 1 - \frac{4\kappa_1 |\varepsilon_2| (\kappa_2^2 + \omega^2)}{\left[\kappa_2 (\kappa_1 + |\varepsilon_2|) + |\varepsilon_1|^2 - \omega^2\right]^2 + \omega^2 (\kappa_1 + |\varepsilon_2| + \kappa_2)^2}$$

$$\varepsilon_1 = 2\chi\alpha_1^0$$

$$\varepsilon_2 = 2\chi\alpha_2^0$$

Collett

Squeezing Spectrum for Parametric Oscillator above Threshold

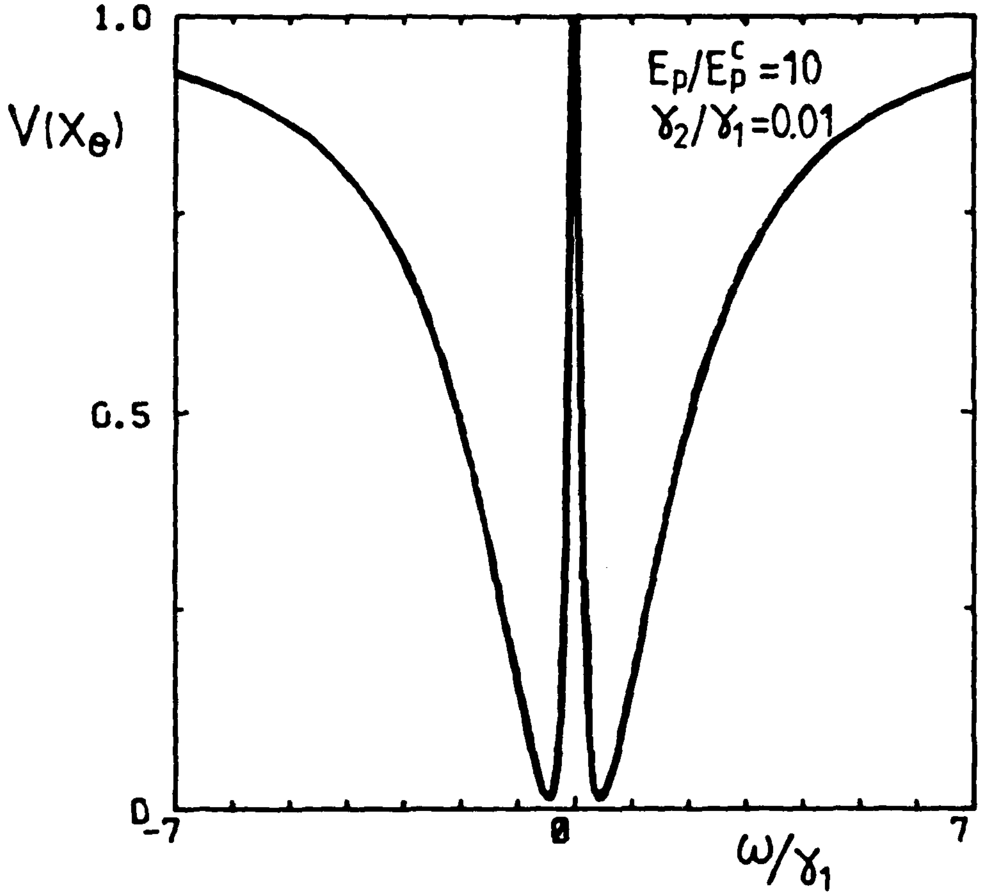

Optimal Squeezing for the Parametric Oscillator as a Function of Pump Amplitude

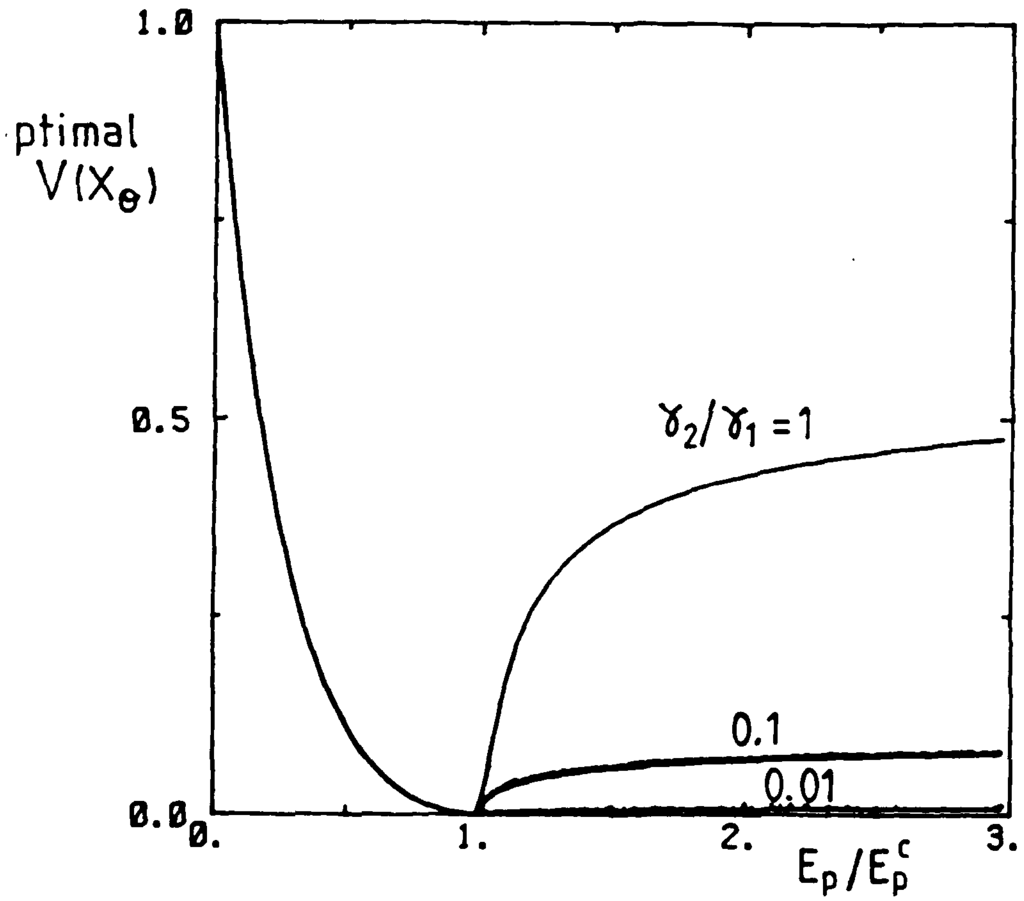

Degenerate parametric oscillator

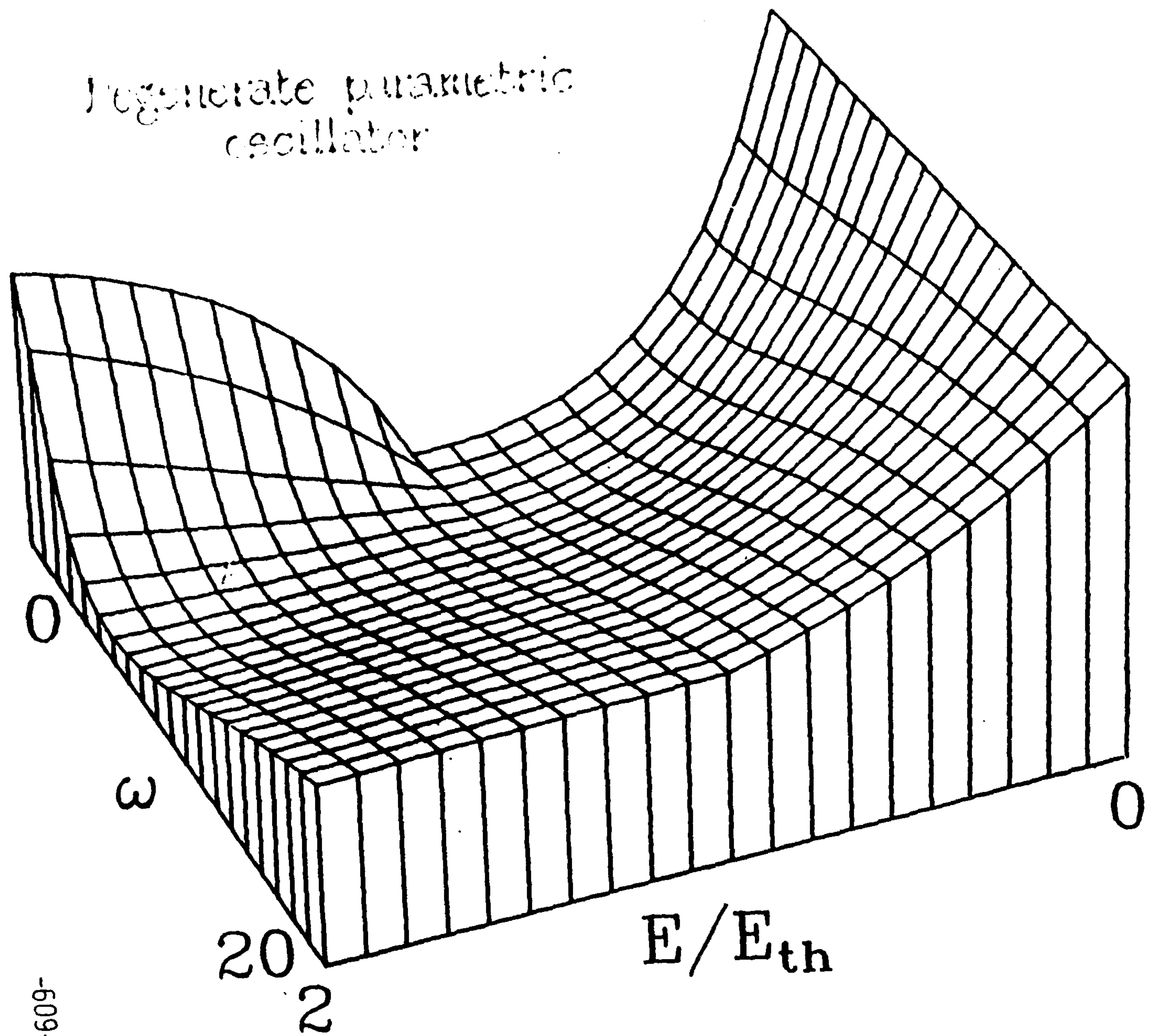

Savage

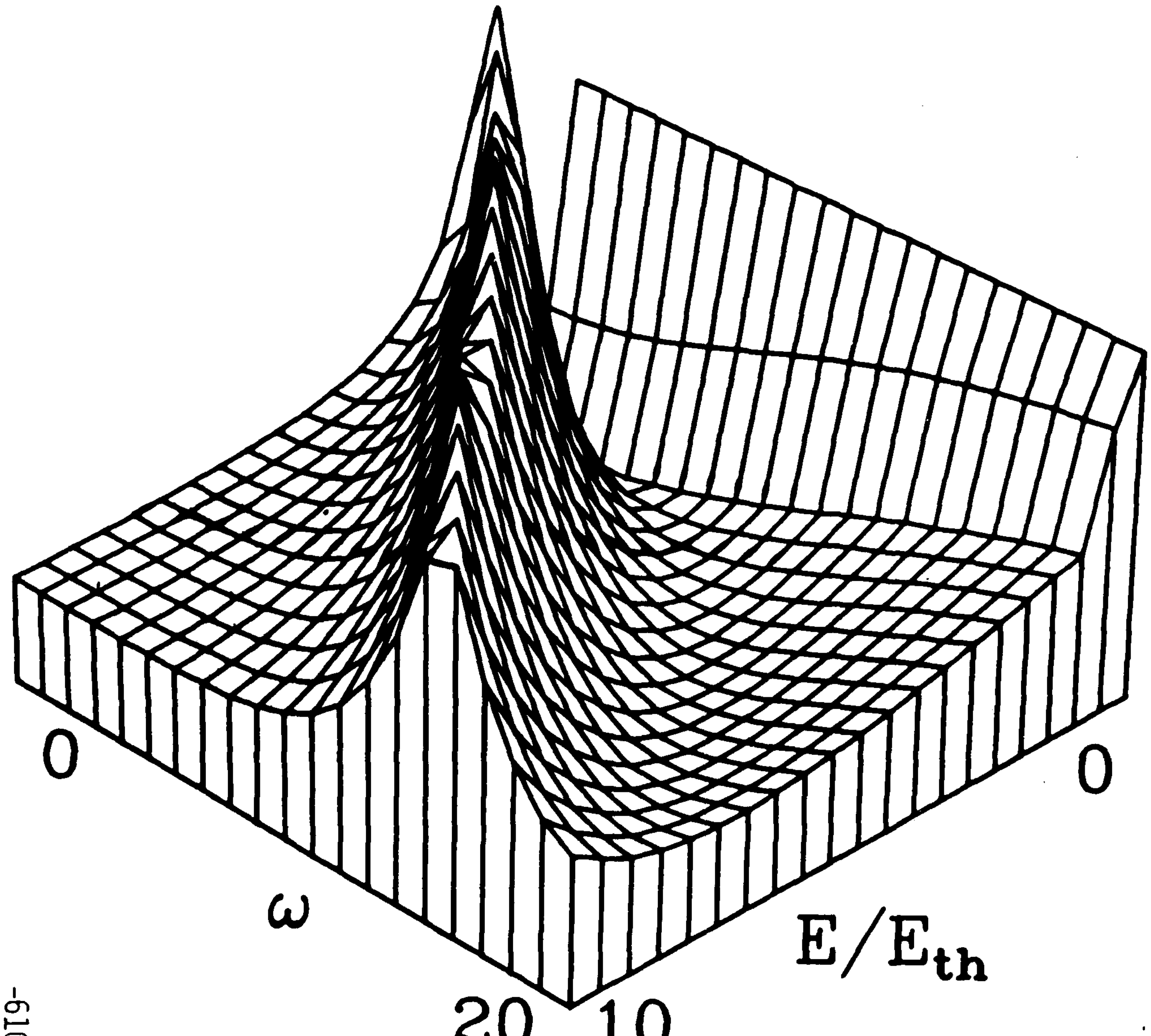

Dege[illegible]

Non Degenerate Parametric Oscillator

Reid & Lane

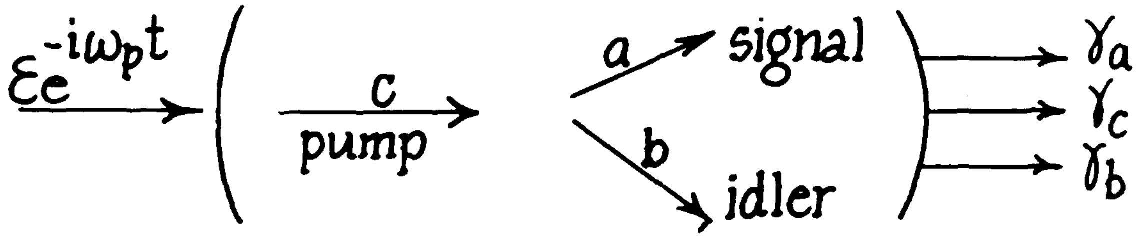

Hamiltonian

$$H = i\hbar\left(\mathcal{E}e^{-i\omega_p t}c^{+} - c\mathcal{E}^{*}e^{i\omega_p t}\right)$$

$$+\, i\hbar\kappa\left(ca^{+}b^{+} - c^{+}ab\right)$$

$$+\left(a\Gamma_a^{+} + b\Gamma_b^{+} + c\Gamma_c^{+} + h.c.\right)$$

Langevin Equations

$$\dot{c} = -\gamma_c c + \mathcal{E} - \kappa\alpha\beta$$

$$\dot{\alpha} = -\gamma_a\alpha + \kappa c\beta^{+} + F_a$$

$$\dot{\beta} = -\gamma_b\beta + \kappa c\alpha^{+} + F_b$$

$$\langle F_\alpha(t)F_\beta(t')\rangle = \kappa c\,\delta(t-t')$$

Steady State Solutions

Threshold $$|\varepsilon| = \frac{\gamma_c\sqrt{\gamma_a\gamma_b}}{k}$$

Below threshold

$$\alpha = \beta = 0$$

$$c = \frac{\varepsilon}{\gamma_c}$$

Above threshold

$$|c|^2 = \frac{\gamma_a\gamma_b}{k^2}$$

$$|\alpha|^2 = \frac{|\varepsilon|}{k}\sqrt{\frac{\gamma_b}{\gamma_a}} - \frac{\gamma_c\gamma_b}{k^2}$$

$$|\beta|^2 = \frac{|\varepsilon|}{k}\sqrt{\frac{\gamma_a}{\gamma_b}} - \frac{\gamma_c\gamma_a}{k^2}$$

Phases

$$\theta_p = \theta_c = \theta_\beta + \theta_\alpha$$

$$\varepsilon = |\varepsilon|e^{i\theta_p}, \quad c = |c|e^{i\theta_c}$$

$$\alpha = |\alpha|e^{i\theta_\alpha}$$

$$\beta = |\beta|e^{i\theta_\beta}$$

Linearized Stability Analysis

$$\delta\dot{c} = -\gamma_c \delta_c - k\alpha_0 \delta_\beta - k\beta_0 \delta_\alpha$$
$$\delta\dot{\alpha} = -\gamma_a \delta_\alpha + k c_0 \delta_\beta^+ + k\beta_0^+ \delta_c$$
$$\delta\dot{\beta} = -\gamma_b \delta_\beta + k c_0 \delta_\alpha^+ + k\alpha_0^+ \delta_c$$

Below threshold

Eigenvalues $\lambda = -\gamma_c$

$$\lambda = -\left(\frac{\gamma_a+\gamma_b}{2}\right) \pm \frac{1}{2}\left[(\gamma_a+\gamma_b)^2 - 4\left(\gamma_a\gamma_b - \left(\frac{k\varepsilon}{\gamma_c}\right)^2\right)\right]^{1/2}$$

Stability for $|\varepsilon| < \dfrac{\gamma_c\sqrt{\gamma_a\gamma_b}}{k}$

Above threshold

Find a zero eigenvalue

solutions unstable

undergo phase diffusion

Graham & Haken

Above threshold:

Transform equations to radial and phase variables

$$C = \sqrt{I_C}\, e^{-i\phi_C}$$

$$\alpha = \sqrt{I_\alpha}\, e^{-i\phi_\alpha}$$

$$\beta = \sqrt{I_\beta}\, e^{-i\phi_\beta}$$

Relative phase $\quad \phi = (\phi_\alpha + \phi_\beta) - \phi_C$

$$\delta \dot{I}_C = \left(-2\gamma_c - \frac{|\varepsilon|}{\sqrt{I_C}} - k\sqrt{\frac{I_A I_B}{I_C}}\right)\delta I_C - k\sqrt{\frac{I_C I_A}{I_B}}\,\delta I_B - k\sqrt{\frac{I_C I_B}{I_A}}\,\delta I_A$$

$$\delta \dot{I}_A = \left(-2\gamma_a + k\sqrt{\frac{I_C I_B}{I_A}}\right)\delta I_A + k\sqrt{\frac{I_A I_B}{I_C}}\,\delta I_C + k\sqrt{\frac{I_C I_A}{I_B}}\,\delta I_B + F_A$$

$$\delta \dot{I}_B = \left(-2\gamma_b + k\sqrt{\frac{I_C I_A}{I_B}}\right)\delta I_B + k\sqrt{\frac{I_A I_B}{I_C}}\,\delta I_C + k\sqrt{\frac{I_C I_B}{I_A}}\,\delta I_A + F_B$$

$$\delta \dot{\phi}_c = -\frac{|\varepsilon|}{\sqrt{I}}\,\delta\phi_c - k\sqrt{\frac{I_A I_B}{I}}\,\delta\varphi$$

$$\delta\dot{\varphi} = \left(-k\sqrt{\frac{I_C I_B}{I_A}} - k\sqrt{\frac{I_C I_A}{I_B}} + k\sqrt{\frac{I_A I_B}{I_C}}\right)\delta\varphi + \frac{|\varepsilon|}{\sqrt{I_C}}\,\delta\phi_c + F_\varphi$$

$$\langle F_A(t)\, F_B(t') \rangle = 2k\sqrt{I_A I_B I_C}\,\delta(t-t')$$

$$\langle F_{[illegible]}(t)\, F_{[illegible]}(t') \rangle = -k\sqrt{\frac{I_C}{[illegible]}}\,\delta(t-t')$$

Phase equations

$$\lambda_{\rho\pm} = -\left(\frac{2\gamma+\gamma_c}{2}\right) \pm \frac{1}{2}\sqrt{(2\gamma+\gamma_c)^2 - 8k|\mathcal{E}|}$$

stable

Intensity equations $(\gamma_a = \gamma_b)$

$$\delta I_D = \delta I_A - \delta I_B \quad , \quad \delta I_S = \delta I_A + \delta I_B$$

$$\delta \dot{I}_c = -\gamma_c \delta I_c - \gamma \delta I_S$$

$$\delta \dot{I}_S = \frac{2k^2}{\gamma} I_A \delta I_c + F_S$$

$$\delta \dot{I}_D = -2\gamma \delta I_D + F_D$$

$$\lambda = -2\gamma$$

$$\lambda = -\frac{\gamma_c}{2} \pm \frac{1}{2}\sqrt{\gamma_c^2 - 8k^2 I_A}$$

stable

Spectrum of fluctuations in the
difference current

$$\delta I_D(\omega) = \frac{1}{\sqrt{2\pi}} \int e^{i\omega t}\, \delta I_D(t)\, dt$$

$$\delta I_D(\omega) = \frac{F_D(\omega)}{(2\gamma - i\omega)}$$

Spectrum

$$S_D(\omega) = 1 + \gamma \langle \delta I_D(\omega),\ \delta I_D(-\omega) \rangle$$
$$= \frac{\omega^2}{4\gamma^2 + \omega^2}\ I_A$$

Reynaud, Fabre + Giacobino

Experiment: Giacobino

Paramp

$\kappa_0 = 1 \quad \kappa_1 = 1 \quad \kappa_2 = 1$

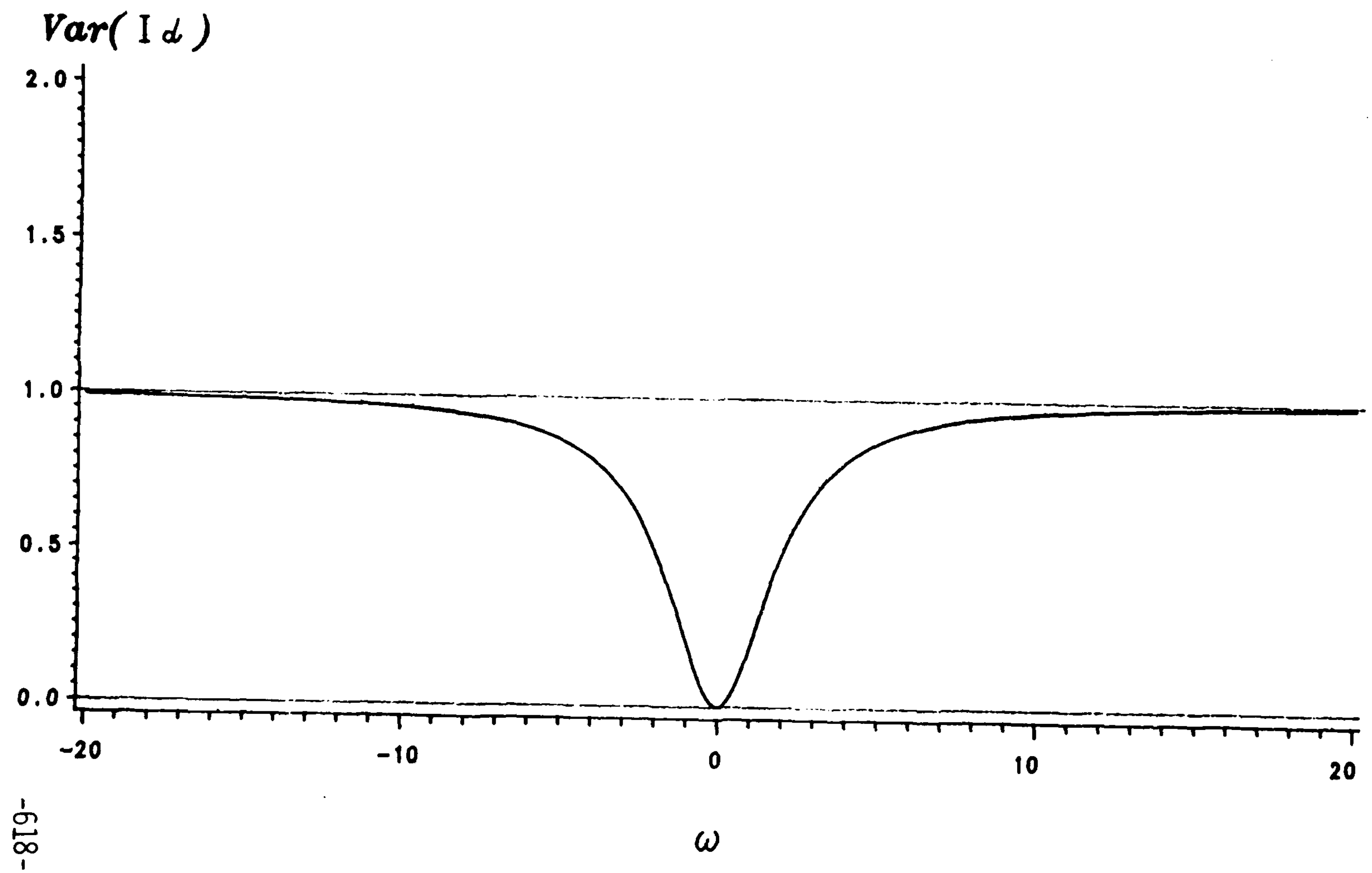

Unequal Dampings $\Delta = \gamma_A - \gamma_B$

Intensity Equations

$$\delta \dot{I}_c = -\gamma_c \delta I_c - \gamma \delta I_s$$

$$\delta \dot{I}_s = \Delta \delta I_d + \frac{2k^2}{\gamma} I_A \delta I_c + F_s$$

$$\delta \dot{I}_d = -\gamma \delta I_d + \Delta \delta I_c + F_d$$

Spectrum of intensity fluctuations
in difference current

$$S_D(\omega) = I_A \frac{\omega^2 + 4\Delta^2 \left(1 + 4(\gamma^2 - \Delta^2) y\right)}{4\gamma^2 + \omega^2}$$

where

$$y = \frac{\omega^2 + 2\omega I_m(A) + 4(\gamma^2 - \Delta^2) - 4\gamma \, Re(A)}{(4\gamma^2 + \omega^2)\,|A|^2}$$

$$Re(A) = 2\gamma - \frac{8\Delta^2 \gamma}{4\gamma^2 + \omega^2} - \frac{\omega^2}{\gamma_c (E-1)}$$

$$I_m(A) = \omega \left(\frac{4\Delta^2}{4\gamma^2 + \omega^2} + \frac{1}{E-1} \right)$$

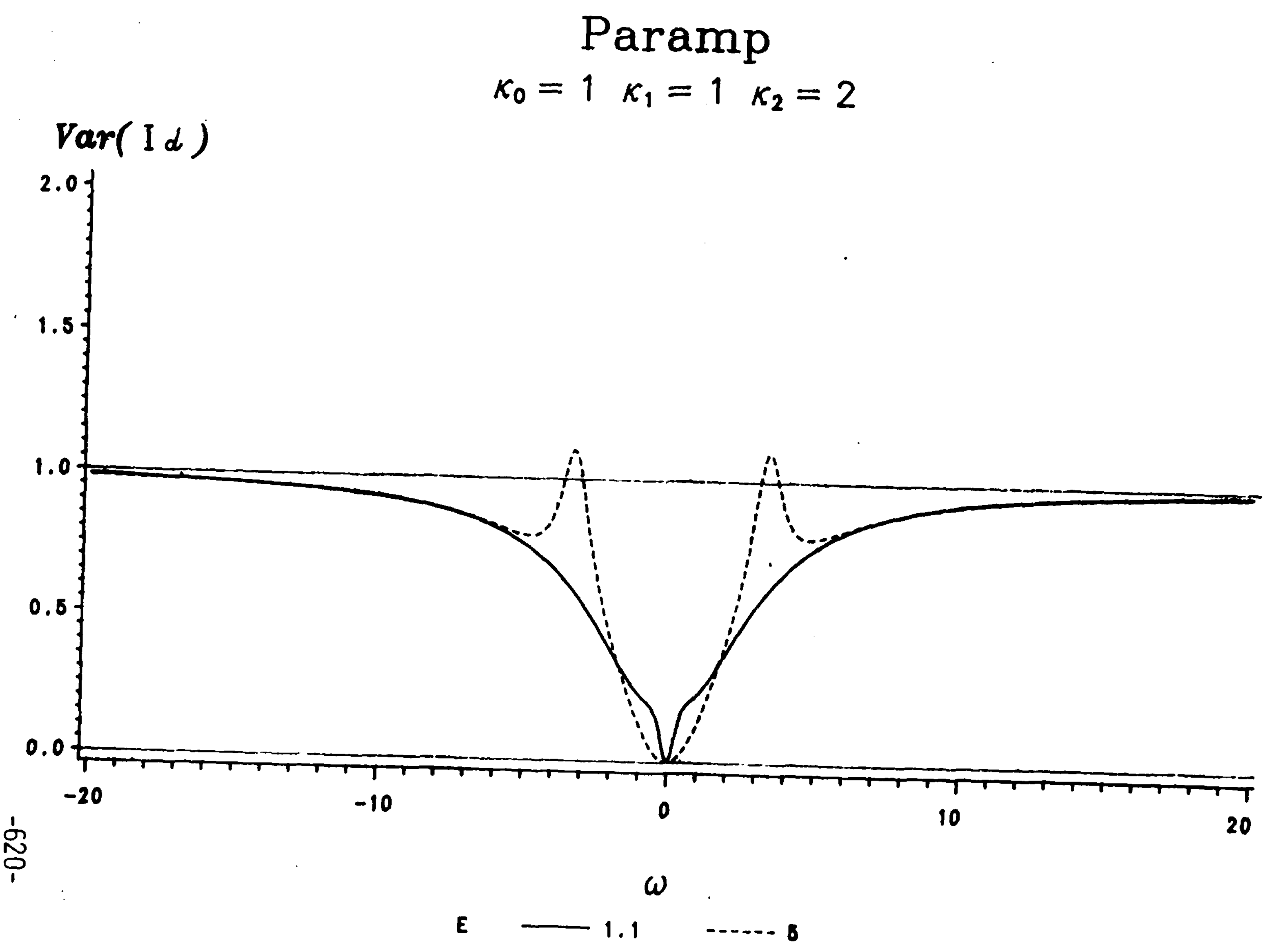
Paramp
$\kappa_0 = 1 \;\; \kappa_1 = 1 \;\; \kappa_2 = 2$
Var(I d)
2.0
1.5
1.0
0.5
0.0
-20
-10
0
10
20
ω
E —— 1.1 ----- 5

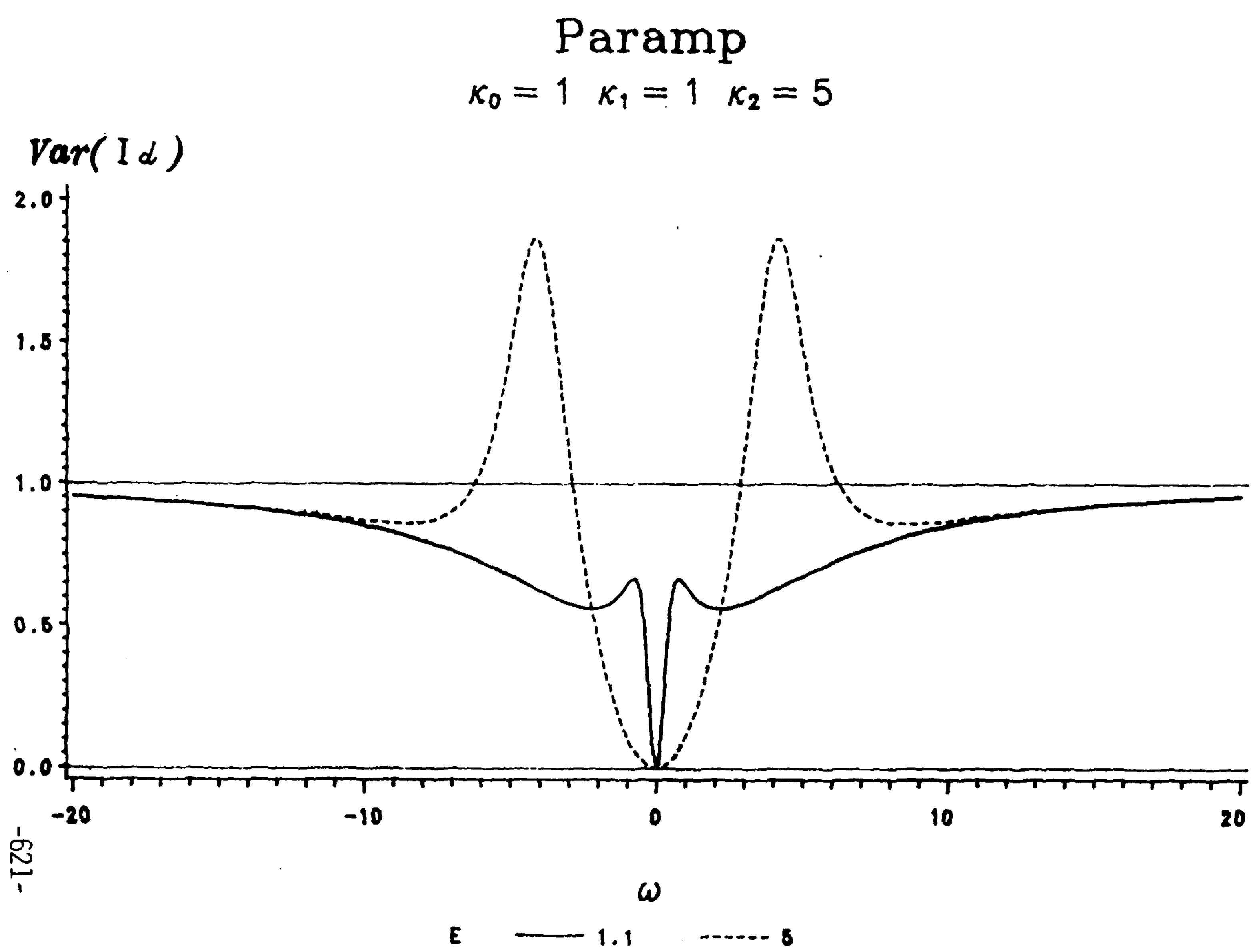
Paramp
κ0 = 1 κ1 = 1 κ2 = 5
Var(I d)
2.0
1.5
1.0
0.5
0.0
-20
-10
0
10
20
ω
E
1.1
5

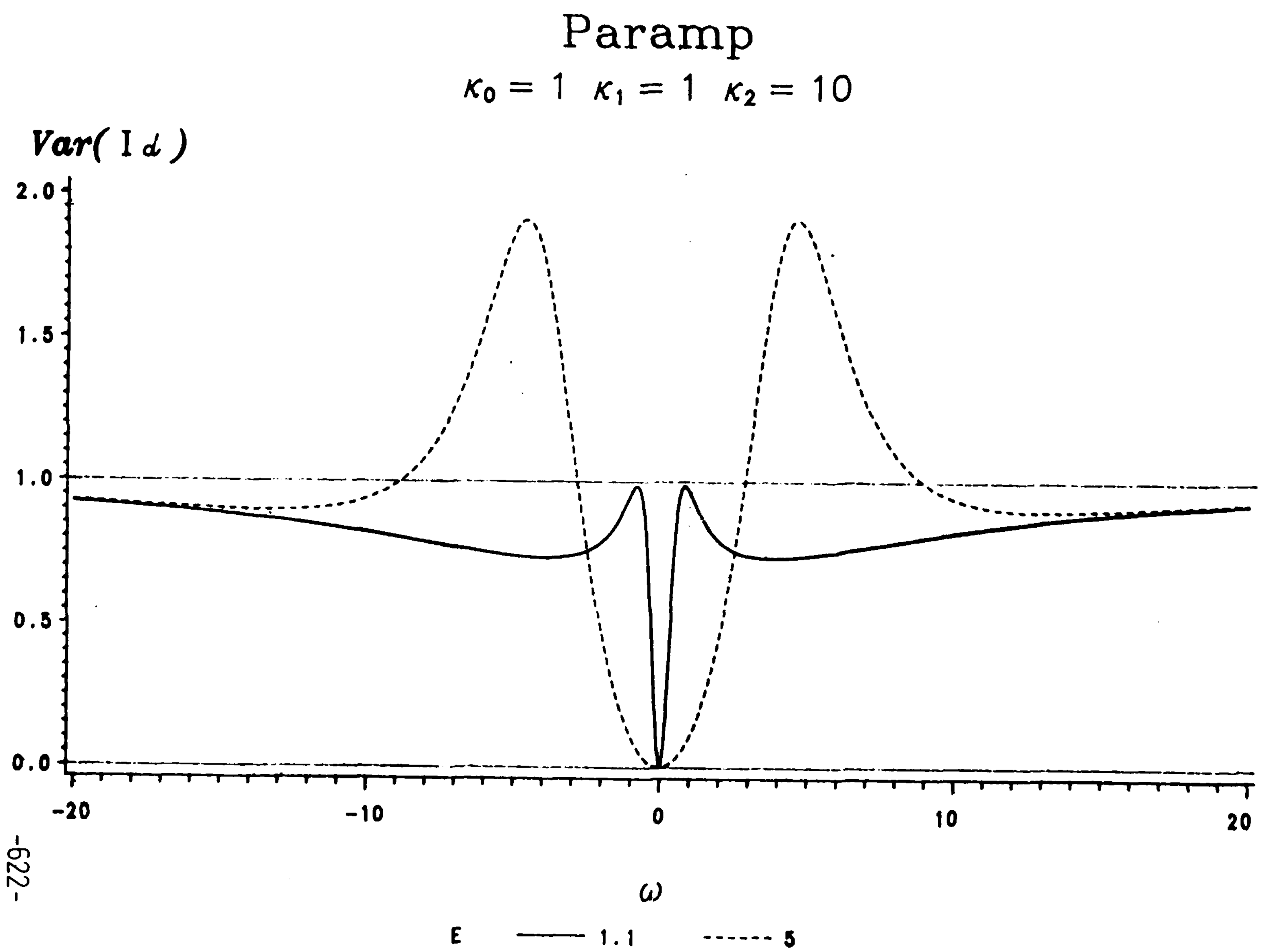
Paramp
$\kappa_0 = 1 \quad \kappa_1 = 1 \quad \kappa_2 = 10$
Var(I d)
2.0
1.5
1.0
0.5
0.0
-20
-10
0
10
20
ω
E
1.1
5

High Loss pump $\quad \gamma_c \gg 1$

$$\gamma_+ = \gamma_a + \gamma_b$$

$$\gamma_- = \gamma_a - \gamma_b$$

Eigenvalue

$$\lambda = -\frac{\gamma_+}{2} P \pm \frac{\gamma_+}{2} \left[(P-2)^2 + \frac{\gamma_-^2}{\gamma_+^2} 4(P-1) \right]^{1/2}$$

$P = 1$ threshold power

For $\left(\frac{\gamma_-}{\gamma_+}\right)^2 \ll 1$

$$\lambda \approx -\gamma_+ \;,\; -\gamma_+ (P-1)$$

just above threshold

linewidth $\sim \gamma_+ (P-1)$

power broadens to γ_+

Paramp

$\kappa_0 = 10 \quad \kappa_1 = 1 \quad \kappa_2 = 5$

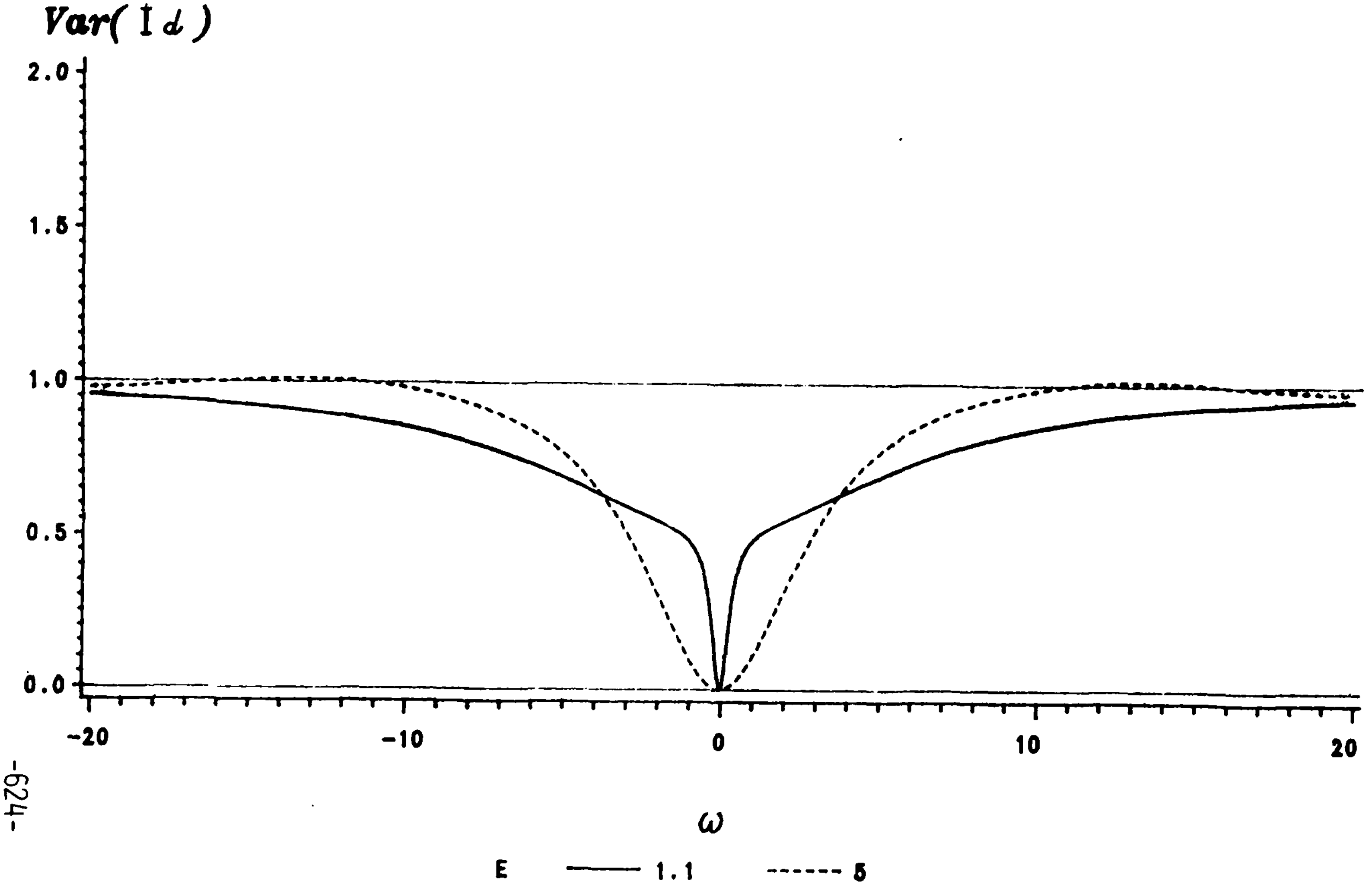

Low Loss Pump $\gamma_0 \ll 1$

Eigenvalue

$$\lambda = -\frac{\gamma_c}{2} \pm \left[\gamma_c^2 - 4\gamma_c(P-1)\gamma_+ + 4\gamma_c(P-1)\frac{\Gamma^2}{\gamma_+}\right]^{\frac{1}{2}}$$

γ_c determines linewidth

sidebands appear for higher pump powers

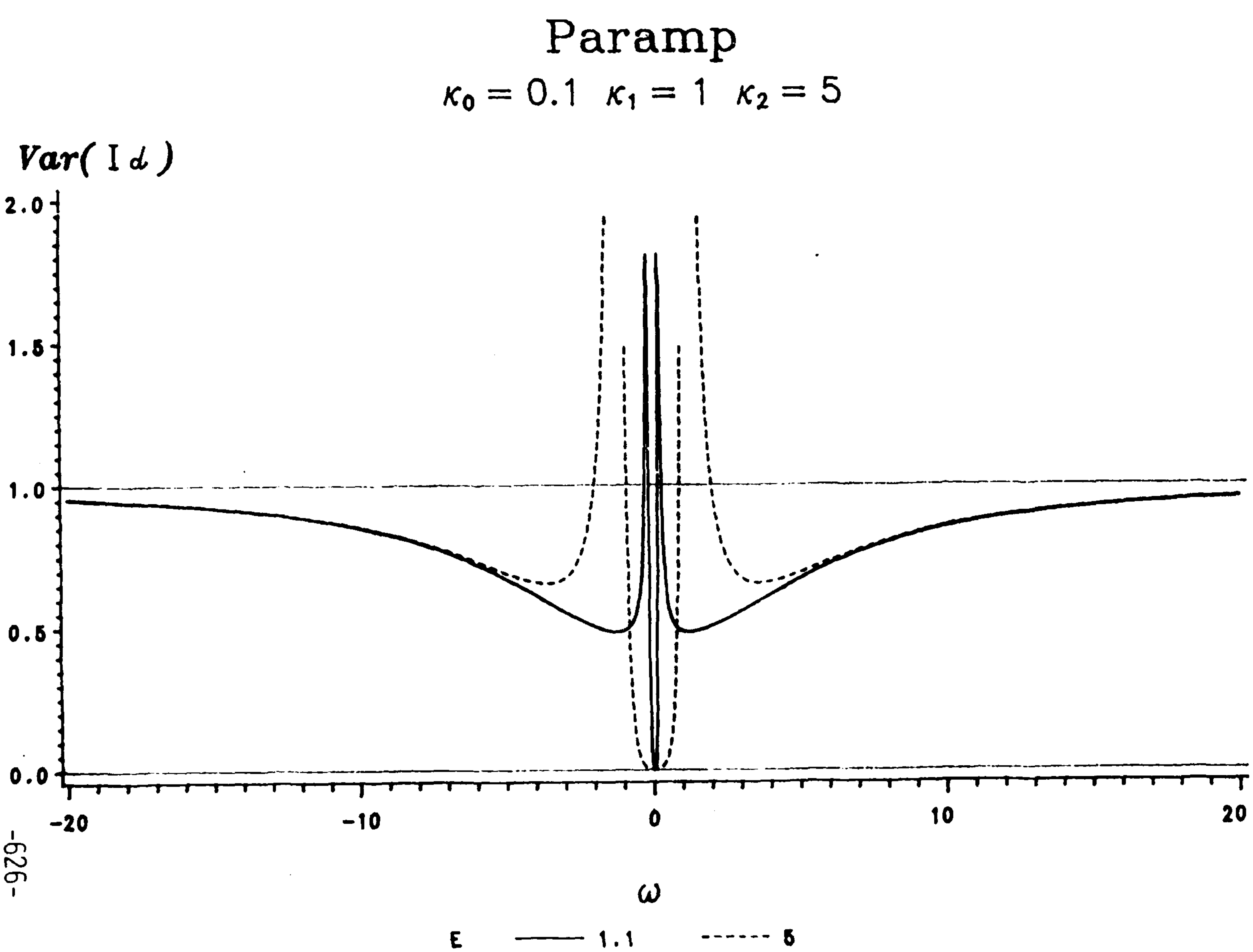

Paramp
$\kappa_0 = 0.1 \quad \kappa_1 = 1 \quad \kappa_2 = 5$
Var(I d)
2.0
1.5
1.0
0.5
0.0
-20
-10
0
10
20
ω
E
1.1
5

Paramp

$\kappa_0 = 0.1 \quad \kappa_1 = 1 \quad \kappa_2 = 5$

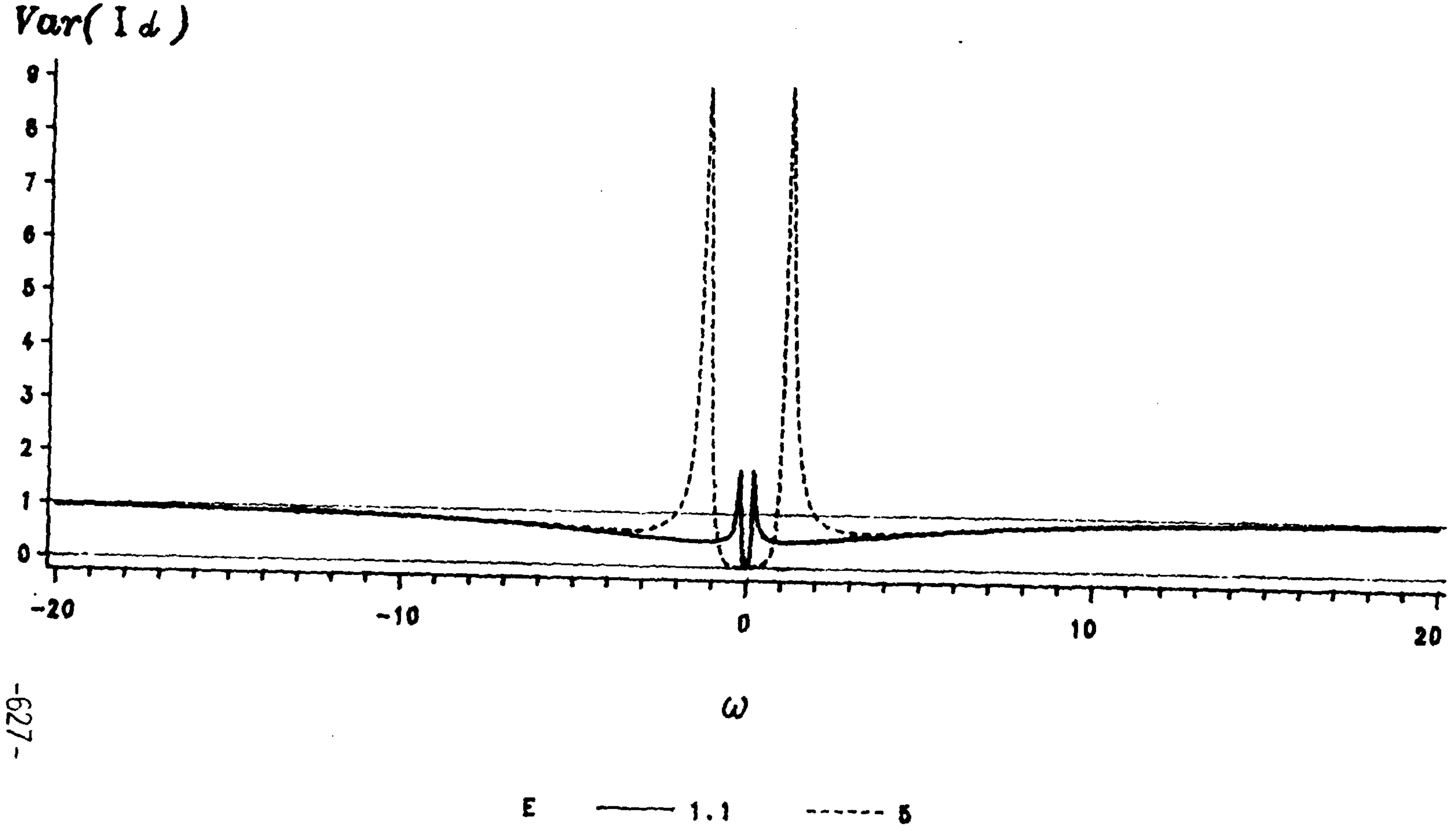

OPEN QUESTIONS IN CLOSED-LOOP PHOTODETECTION

Jeffrey H. Shapiro

Massachusetts Institute of Technology
Department of Electrical Engineering and Computer Science
Cambridge, Massachusetts 02139

The usual open-loop quantum and semiclassical theories of light detection apply to configurations in which there is no feedback from the photodetector to the light beam impinging on that detector [1] - [3]. In these circumstances there are unmistakable signatures of nonclassical light, such as sub-shot-noise spectra and sub-Poisson photocounts. No such unmistakable signatures exist for the case of closed-loop photodetection, i.e., for configurations in which there is a feedback path from the detector to the light source. This talk reviews recent progress [4], [5] in the theory of closed-loop photodetection, and extrapolates therefrom to possible future schemes for quantum-state synthesis and quantum-measurement synthesis.

References

[1] J.H. Shapiro, H.P. Yuen, and J.A. Machado Mata, IEEE Trans. Inform. Theory IT-25, 179 (1979).

[2] H.P. Yuen and J.H. Shapiro, IEEE Trans. Inform. Theory IT-26, 78 (1980).

[3] J.H. Shapiro, IEEE J. Quantum Electron. QE-21, 237 (1985).

[4] J.H. Shapiro, M.C. Teich, B.E.A. Saleh, P. Kumar, and G. Saplakoglu, Phys. Rev. Lett. 56, 1136 (1986).

[5] J.H. Shapiro, G. Saplakoglu, S.-T. Ho, P. Kumar, M.C. Teich, and B.E.A. Saleh, J. Opt. Soc. Am. B4, xxxx (1987).

OPEN QUESTIONS IN CLOSED-LOOP PHOTODETECTION

J.H. SHAPIRO

MIT

ACKNOWLEDGEMENTS

H. P. YUEN

P. KUMAR
R. S. BONDURANT
G. SAPLAKOGLU
S.-T. HO

C.M. CAVES
B. YURKE

Y. YAMAMOTO
M. C. TEICH
B.E.A. SALEH

PHOTODETECTION STATISTICS

- **PHOTOCURRENT & PHOTOCOUNTS**
- **SELF-EXCITING PROCESSES**
  - Semiclassical vs. Quantum
- **CONVENTIONAL SYSTEMS**
  - Direct Detection
  - Nonclassical Signatures
- **UNCONVENTIONAL SYSTEMS**
  - Closed-Loop Photodetection
  - Quantum-State Synthesis
  - Quantum-Measurement Synthesis

REAL PHOTODETECTION

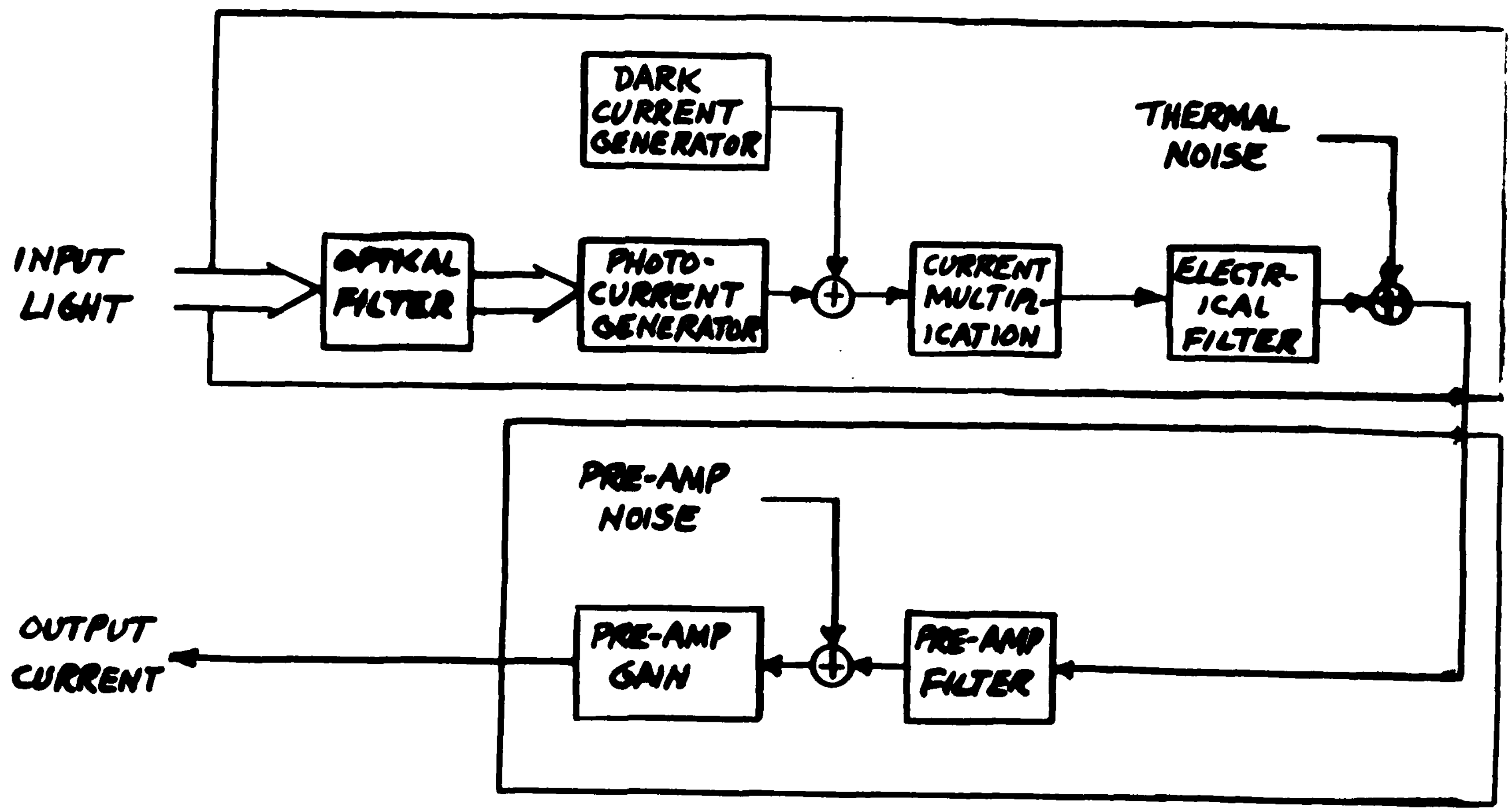

PHOTOCURRENT & PHOTOCOUNTS

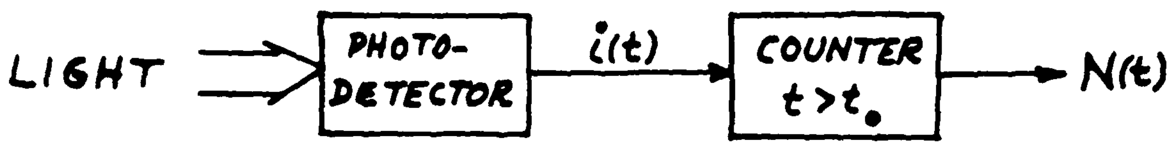

- LIGHT - QUASIMONOCHROMATIC PARAXIAL SCALAR WAVE: $E(\bar{x},t)$ OR $\hat{E}(\bar{x},t)$
- PHOTODETECTOR - IDEAL EXCEPT FOR $\eta < 1$
- PHOTOCURRENT

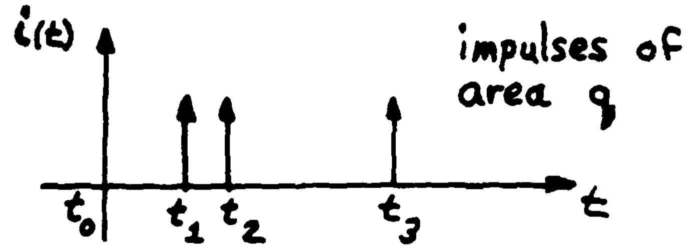

- PHOTOCOUNTS

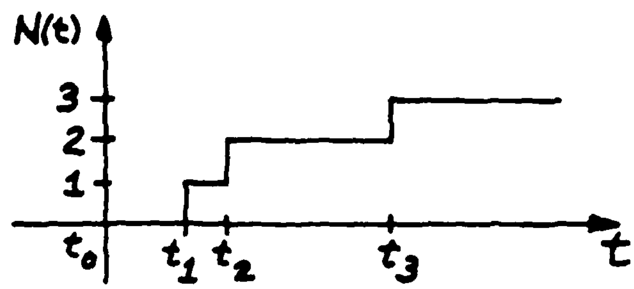

SELF-EXCITING COUNTING PROCESSES

- $N(t)$ SELF-EXCITING -

  EVENTS OCCUR ONE AT A TIME WITH INCREMENTAL CONDITIONAL PROBABILITIES

$$Pr\left[\Delta N_t = n \,\middle|\, \underset{\sim}{t}, N_t\right] \approx \begin{cases} 1 - \mu(t; \underset{\sim}{t}, N_t)\Delta t, & n=0 \\ \mu(t; \underset{\sim}{t}, N_t)\Delta t, & n=1 \\ 0, & n \geq 2 \end{cases}$$

WHERE $\Delta N_t \equiv N(t+\Delta t) - N(t)$

$\underset{\sim}{t} \equiv (t_1, t_2, \ldots, t_{N_t})$

event times up to t

$N_t \equiv N(t)$

\# events up to t

POISSON COUNTING PROCESSES

- N(t) POISSON –

$$Pr\left[\Delta N_t = n \,\middle|\, \underset{\sim}{t}, N_t\right] \approx \begin{cases} 1 - \lambda(t)\Delta t, & n = 0 \\ \lambda(t)\Delta t, & n = 1 \\ 0, & n \geq 2 \end{cases}$$

WHERE $\lambda(t) \geq 0$ IS DETERMINISTIC

- POISSON PROCESS IS SELF-EXCITING PROCESS WITH

$$\mu(t; \underset{\sim}{t}, N_t) = \lambda(t)$$

DOUBLY-STOCHASTIC POISSON PROCESSES

- N(t) DOUBLY-STOCHASTIC POISSON –

$$\Pr\left[\Delta N_t = n \,\middle|\, \underset{\sim}{t}, N_t, \underset{\sim}{\lambda}_t\right] \approx \begin{cases} 1-\lambda(t)\Delta t, & n=0 \\ \lambda(t)\Delta t, & n=1 \\ 0, & n\geq 2 \end{cases}$$

WHERE $\lambda(t) \geq 0$ IS STOCHASTIC,

$$\underset{\sim}{\lambda}_t \equiv \{\lambda(\tau) : \tau \leq t\}$$

- DOUBLY-STOCHASTIC POISSON PROCESS IS SELF-EXCITING PROCESS WITH

$$\mu(t; \underset{\sim}{t}, N_t) = \langle \lambda(t) \,|\, \underset{\sim}{t}, N_t \rangle$$

MULTICOINCIDENCE RATES

- kth ORDER MCR FOR CLASSICAL COUNTING PROCESS N(t)

$$w_k(t_1, t_2, \ldots, t_k) = \lim_{\Delta t \downarrow 0} (\Delta t)^{-k} \Pr\left[\left(\prod_{i=1}^{k} \Delta N_{t_i} \right) = 1 \right]$$

- N(t) IS COMPLETELY CHARACTERIZED STATISTICALLY BY KNOWLEDGE OF MCRs

$$\{ w_k(t_1, t_2, \ldots, t_k) : 1 \le k < \infty \}$$

- FOR EXAMPLE

$$\Pr[N(t) = n] =$$

$$\sum_{m=n}^{\infty} \frac{(-1)^{m-n}}{(m-n)!\, n!} \int_{t_0}^{t} dt_1 \cdots \int_{t_0}^{t} dt_m \, w_m(t_1, t_2, \ldots, t_m)$$

MOMENT STATISTICS

- **PHOTOCOUNTS**

MEAN-
$$\langle N(t)\rangle = \int_{t_0}^{t} ds\, w_1(s)$$

VARIANCE-

$$\mathrm{VAR}(N(t)) = \langle N(t)\rangle + \int_{t_0}^{t} ds \int_{t_0}^{t} ds' \left[w_2(s,s') - w_1(s) w_1(s') \right]$$

- **PHOTOCURRENT**

ASSUME $w_1(t) = w_1$, $w_2(t,s) = w_2(t-s)$

MEAN -
$$\langle i(t)\rangle = q w_1$$

NOISE SPECTRUM (BILATERAL) -

$$S_{ii}(f) = q\langle i\rangle + q^2 \int_{-\infty}^{\infty} dt \left[w_2(t) - w_1^2 \right] e^{-j2\pi f t}$$

CLASSICAL FIELDS

- POSITIVE-FREQUENCY ELECTRIC FIELD

  $E^{(+)}(\bar{x},t)$ volts/m units

  ILLUMINATES DETECTOR

- PHOTON-UNITS POSITIVE-FREQUENCY FIELD

$$E(\bar{x},t) = \int d\nu \int d\tau \, (c\epsilon_0/2h\nu)^{1/2} E^{(+)}(\bar{x},\tau)\, e^{-j2\pi\nu(t-\tau)}$$

$\sqrt{\text{photons}/\text{m}^2\text{s}}$ units

- MODAL EXPANSION

$$E(\bar{x},t) = \sum_n \alpha_n \xi_n(\bar{x},t), \quad \bar{x}\in \mathcal{A}_d,\ t\in \mathcal{T}$$

$\{\xi_n\}$ CON MODE SET

$\{\alpha_n\}$ COMPLEX-VALUED RANDOM VARIABLES

QUANTUM FIELDS

- POSITIVE-FREQUENCY ELECTRIC FIELD OPERATOR $\hat{E}^{(+)}(\bar{x},t)$ ILLUMINATES DETECTOR

- PHOTON-UNITS FIELD OPERATOR

$$\hat{E}(\bar{x},t) = \int d\nu \int d\tau \; (c\epsilon_0/2h\nu)^{1/2} \hat{E}^{(+)}(\bar{x},\tau) e^{-j2\pi\nu(t-\tau)}$$

- MODAL EXPANSION

$$\hat{E}(\bar{x},t) = \sum_n \hat{a}_n \xi_n(\bar{x},t), \quad \bar{x} \in \mathcal{A}_d, \; t \in \mathcal{T}$$

$\{\xi_n\}$ CON MODE SET

$\{\hat{a}_n\}$ MODAL ANNIHILATION OPERATORS

$\hat{\rho}$ = DENSITY OPERATOR (STATE) OF MODES

PHOTODETECTION MCRs

- SEMICLASSICAL THEORY

$$W_k(t_1, t_2, \ldots, t_k) = \eta^k \langle P(t_1)P(t_2)\cdots P(t_k)\rangle$$

WHERE
$$P(t) = \int_{\mathcal{A}_d} d\bar{x}\ |E(\bar{x},t)|^2$$

= CLASSICAL PHOTON FLUX

- QUANTUM THEORY

$$W_k(t_1, t_2, \ldots, t_k) =$$

$$\int_{\mathcal{A}_d} d\bar{x}_1 \cdots \int_{\mathcal{A}_d} d\bar{x}_k \left\langle \left(\prod_{i=1}^{k} \hat{E}'^{\dagger}(\bar{x}_i, t_i)\right)\left(\prod_{i=1}^{k} \hat{E}'(\bar{x}_i, t_i)\right)\right\rangle$$

WHERE
$$\hat{E}'(\bar{x},t) = \eta^{1/2}\hat{E}(\bar{x},t) + (1-\eta)^{1/2}\hat{E}_{VAC}(\bar{x},t)$$

$\hat{E}_{VAC}(\bar{x},t)$ = FICTITIOUS VACUUM-STATE FIELD OPERATOR

CONVENTIONAL SYSTEMS

- PHOTODETECTOR RUNS OPEN LOOP; $i(t)$ IS NOT FED BACK TO CONTROL LIGHT BEAM ILLUMINATING THE DETECTOR
- SEMICLASSICAL THEORY

  $P(t)$ IS ORDINARY NON-NEGATIVE RANDOM PROCESS

  $w_1(t) = \eta \langle P(t) \rangle$

  $w_2(t,s) - w_1(t) w_1(s) = \eta^2 K_{PP}(t,s)$
- QUANTUM THEORY

  $\hat{\rho}$ IS ORDINARY FREE-FIELD DENSITY OPERATOR

DIRECT DETECTION

- PHOTOCURRENT

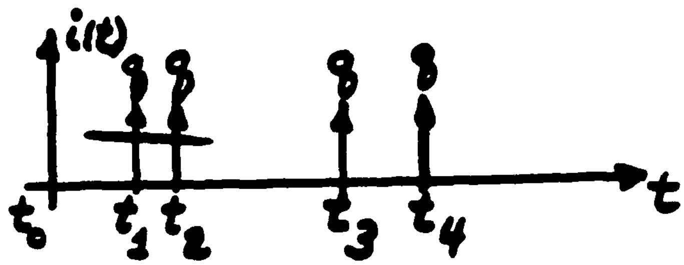

- SEMICLASSICAL STATISTICS

  $i(t)$ CONDITIONALLY POISSON WITH EMISSION RATE $\eta \int_{A_d} |E(\bar{x},t)|^2 d\bar{x}$

- QUANTUM STATISTICS

  $i(t)$ MEASURES $q \int_{A_d} \hat{E}'^{\dagger}(\bar{x},t)\hat{E}'(\bar{x},t)d\bar{x}$

$$\hat{E}'(\bar{x},t) = \eta^{1/2}\hat{E}(\bar{x},t) + (1-\eta)^{1/2}\hat{E}_{VAC}(\bar{x},t)$$

$\hat{E}_{VAC}(\bar{x},t)$ = FICTITIOUS VACUUM-STATE FIELD OPERATOR

DIRECT DETECTION

- NOISE IN $i(t)$ IS –

  DETECTOR SHOT NOISE IN THE SEMICLASSICAL MODEL

  $\hat{E}'$ QUANTUM NOISE IN THE QUANTUM MODEL

- SEMICLASSICAL STATISTICS ARE QUANTITATIVELY CORRECT IF $\hat{\rho}$ IS A CLASSICAL STATE, i.e., IF

$$\hat{\rho} = \int d^2\underset{\sim}{\alpha}\; P(\underset{\sim}{\alpha};\underset{\sim}{\alpha}^*)\, |\underset{\sim}{\alpha}\rangle\langle\underset{\sim}{\alpha}|$$

FOR $|\underset{\sim}{\alpha}\rangle$ = MULTIMODE COHERENT STATE

$P(\underset{\sim}{\alpha};\underset{\sim}{\alpha}^*)$ = CLASSICAL PROBABILITY DENSITY

NONCLASSICAL SIGNATURES

- **SEMICLASSICAL THEORY**

  $K_{pp}(t,s)$ POSITIVE SEMIDEFINITE

  $\Longrightarrow$ $VAR(N(t)) \geq \langle N(t) \rangle$

  $S_{ii}(f) \geq q\langle i(t) \rangle$

- **QUANTUM THEORY**

  $VAR(N(t)) < \langle N(t) \rangle$ possible,
  SUB-POISSONIAN BEHAVIOR

  $S_{ii}(f) < q\langle i(t) \rangle$ possible,
  SUB-SHOT NOISE BEHAVIOR

UNCONVENTIONAL SYSTEMS

- PHOTODETECTOR RUNS CLOSED LOOP; $i(t)$ IS FED BACK TO CONTROL LIGHT BEAM ILLUMINATING THE DETECTOR
- SELF-EXCITING PROCESS CHARACTERIZATION IN TERMS OF MCRs STILL VALID
- SEMICLASSICAL THEORY

  $W_2(t,s) - W_1(t)W_1(s)$ IS NOT A COVARIANCE

  $VAR(N(t)) < \langle N(t) \rangle$ possible

  $S_{ii}(f) < q\langle i(t) \rangle$ possible

DIRECT DETECTION

- PHOTOCURRENT

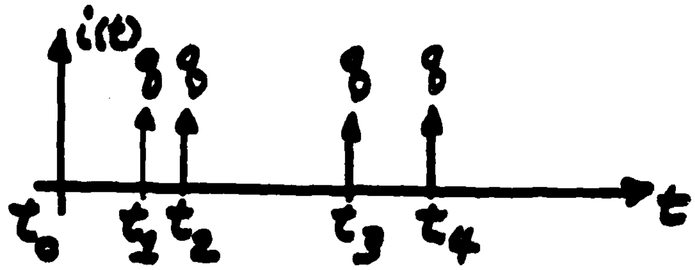

- SEMICLASSICAL STATISTICS

  $i(t)$ IS SELF-EXCITING WITH

  EMISSION RATE $\eta \int_{A_d} |E(\bar{x},t)|^2 d\bar{x}$

  $E(\bar{x},t)$ DEPENDS EXPLICITLY ON PAST MEASUREMENTS

- QUANTUM STATISTICS

  $i(t)$ MEASURES $q \int_{A_d} \hat{E}'^{\dagger}(\bar{x},t)\hat{E}'(\bar{x},t)d\bar{x}$

  $\hat{E}(\bar{x},t)$ DEPENDS EXPLICITLY ON PAST MEASUREMENTS

DIRECT DETECTION

- SEMICLASSICAL THEORY IS QUANTITATIVELY CORRECT IF BREAKING THE FEEDBACK LOOP LEAVES THE DETECTOR ILLUMINATED BY A CLASSICAL-STATE DENSITY OPERATOR $\hat{\rho}$
- SUB-POISSONIAN PHOTOCOUNTS

  $$\mathrm{VAR}(N(t)) < \langle N(t) \rangle$$

  POSSIBLE SEMICLASSICALLY
- SUB-SHOT NOISE SPECTRA

  $$S_{ii}(f) < q\langle i(t) \rangle$$

  POSSIBLE SEMICLASSICALLY
- NO UNMISTAKABLE NONCLASSICAL SIGNATURES

DEAD-TIME SYSTEM

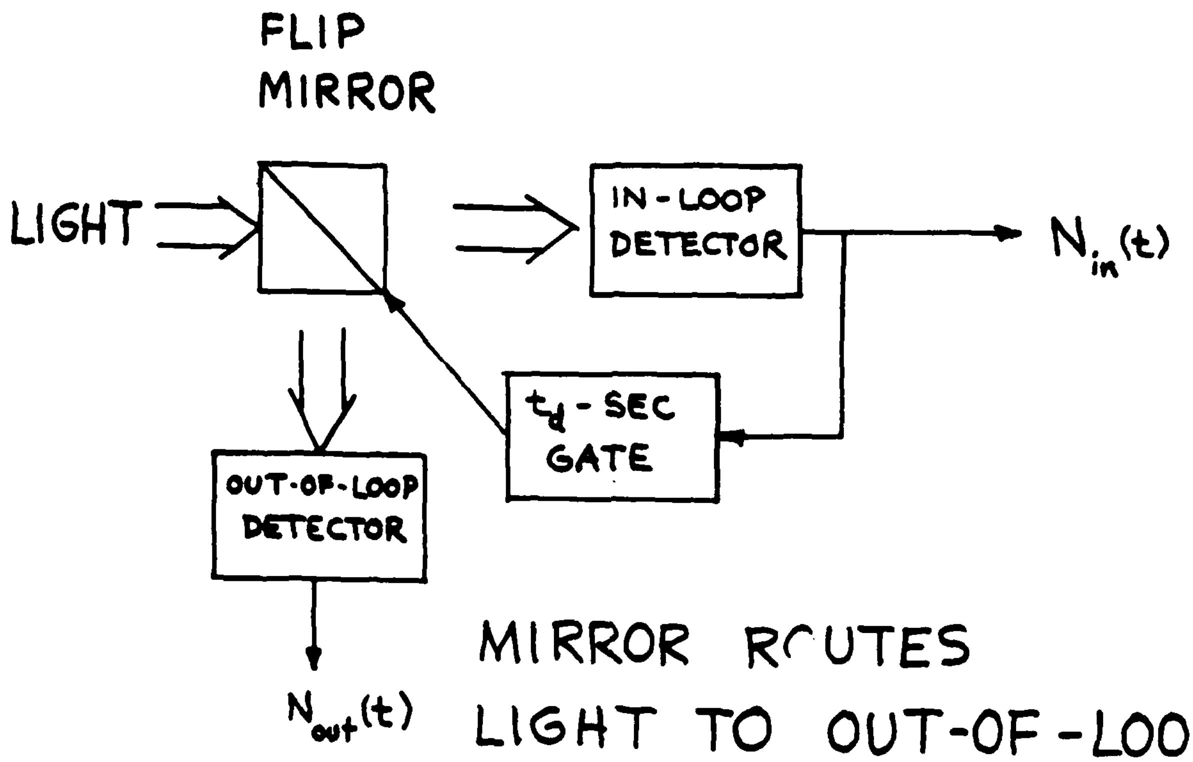

MIRROR RCUTES
LIGHT TO OUT-OF-LOOP
DETECTOR FOR t_d-SEC
AFTER EACH IN-LOOP
PHOTOCOUNT

WALKER & JAKEMAN (1985)

DEAD-TIME RESULTS

- SEMICLASSICAL AND QUANTUM THEORIES AGREE

- STEADY-STATE t-SEC COUNTING STATISTICS, $t >> t_d$

$$\langle N_{in} \rangle \approx \lambda t / (1 + \lambda t_d)$$

$$\langle N_{out} \rangle = \lambda t - \langle N_{in} \rangle$$

$$VAR(N_{in}) \approx \langle N_{in} \rangle / (1 + \lambda t_d)^2$$

$$VAR(N_{out}) \approx \langle N_{out} \rangle \left[1 + \lambda t_d / (1 + \lambda t_d)^2 \right]$$

λ = AVERAGE DETECTED PHOTONS/SEC

t_d = DEAD TIME

t = COUNTING INTERVAL DURATION

LINEAR FEEDBACK

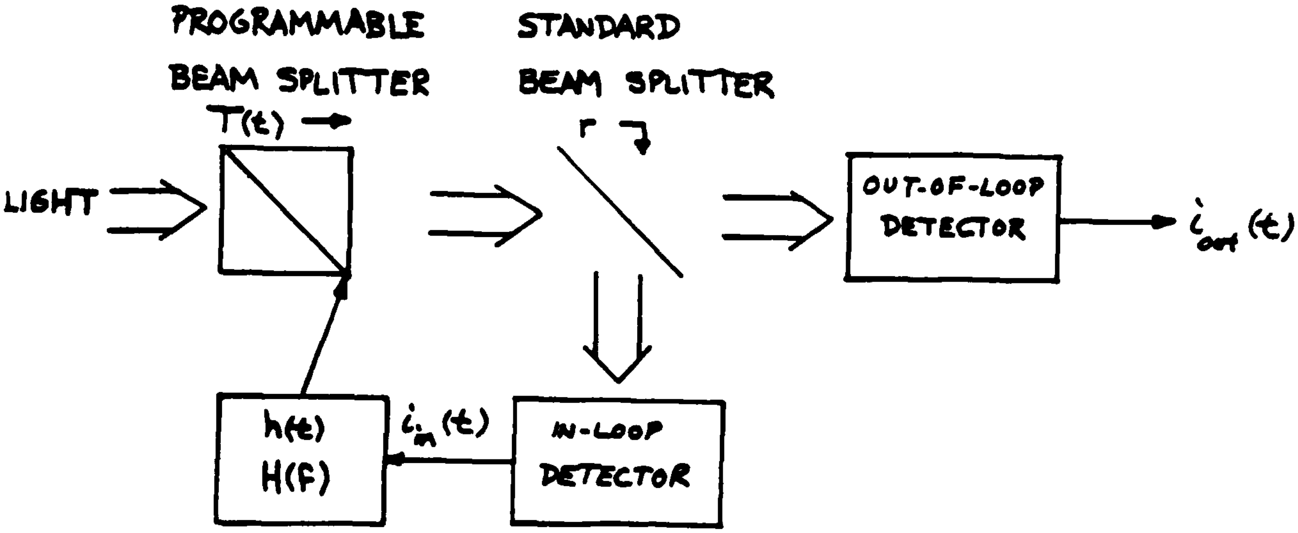

NEGATIVE LINEAR INTENSITY FEEDBACK IN HIGH SNR REGIME

$$T(t) = T_0 - T_1 \int_{-\infty}^{t} q^{-1} i_{in}(\tau)\, h(t-\tau)\, d\tau$$

YAMAMOTO, IMOTO, & MACHIDA (1986)

LINEAR FEEDBACK

- SEMICLASSICAL AND QUANTUM THEORIES AGREE

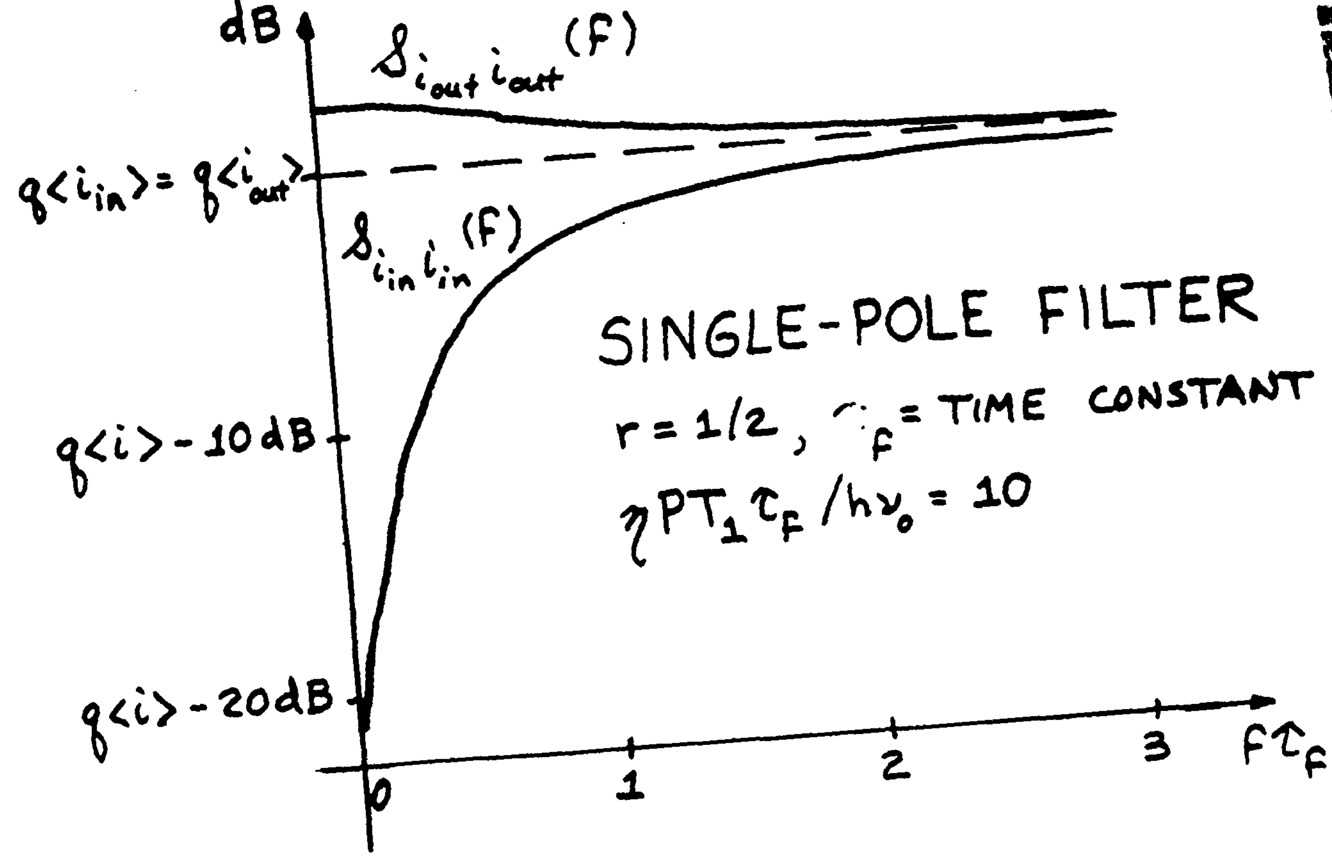

- IN-LOOP QUANTUM FIELD VIOLATES FREE-FIELD UNCERTAINTY PRINCIPLE

SQUEEZED-STATE GENERATION

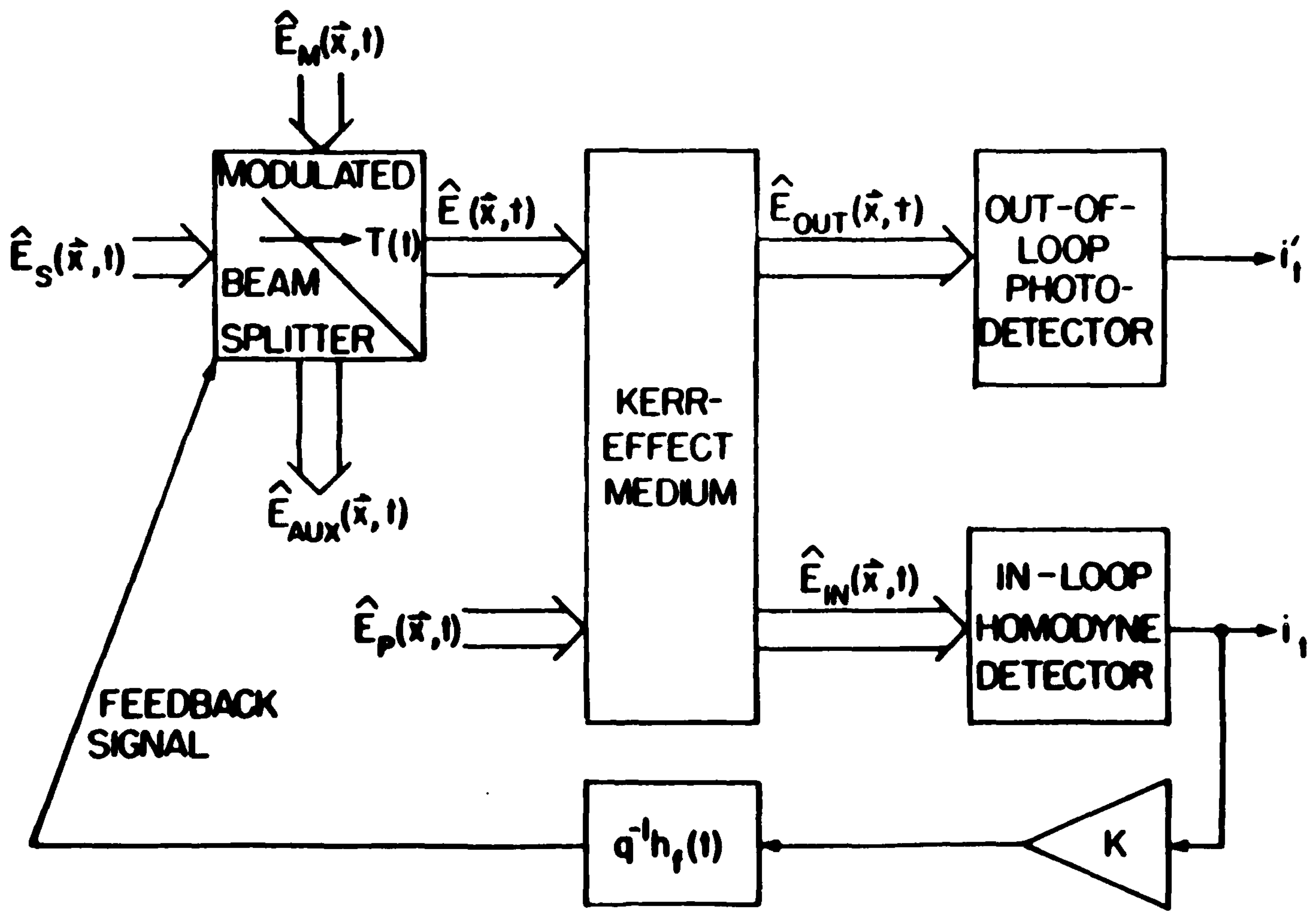

QUANTUM STATE SYNTHESIS

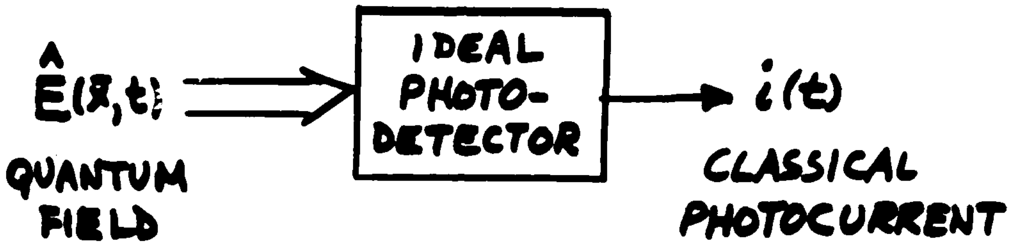

- $\hat{E}(\bar{x}, t)$ IN ARBITRARY STATE $\hat{\rho}$
- DETECTOR IS IDEAL, $\eta = 1$
- $i(t)$ IS SELF-EXCITING IMPULSE PROCESS WITH ARBITRARY CONDITIONAL RATE

$$\mu(t; \underset{\sim}{t}, N_t) = \lim_{\Delta t \downarrow 0} (\Delta t)^{-1} \Pr\left[\Delta N_t = 1 \,\middle|\, \underset{\sim}{t}, N_t\right]$$

QUANTUM STATE SYNTHESIS

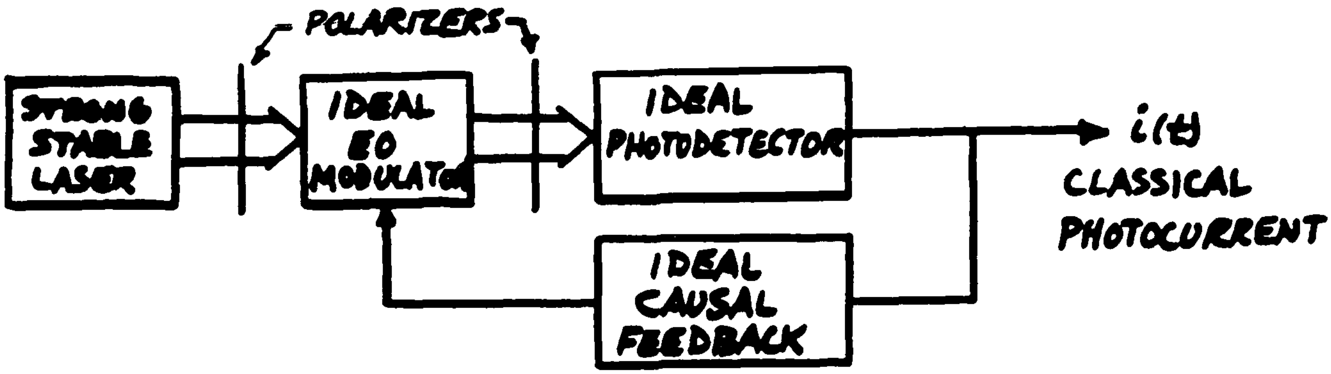

- CLASSICAL FIELD $E(\bar{x},t)$ ILLUMINATES DETECTOR
- $i(t)$ IS SELF-EXCITING IMPULSE PROCESS WITH CONDITIONAL RATE $\mu(t;\underset{\sim}{t},N_t)$
- WITH APPROPRIATE FEEDBACK, ANY $\mu(t;\underset{\sim}{t},N_t)$ IS OBTAINABLE
- WITH QND, OPEN LOOP $\hat{E}(\bar{x},t)$ GIVING ANY $\mu(t;\underset{\sim}{t},N_t)$ IS OBTAINABLE

COHERENT-STATE RECEIVER

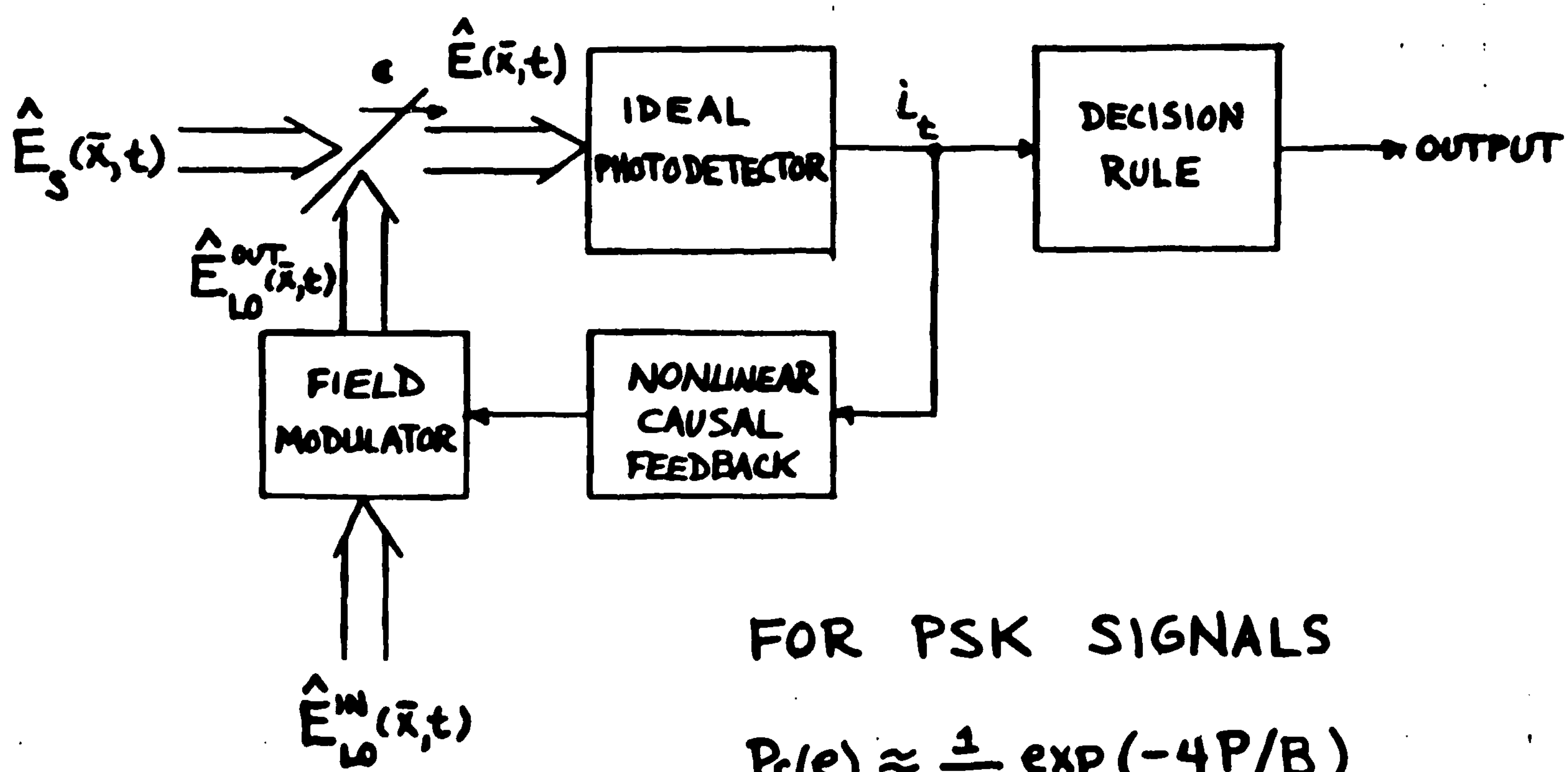

FOR PSK SIGNALS

$$Pr(e) \approx \frac{1}{4} \exp(-4P/B)$$

P = AVERAGE PHOTON FLUX

B = BANDWIDTH

DUALITY

- CLOSED-LOOP SYSTEM AS STATE SYNTHESIS -
  DETECTOR MAKES USUAL MEASUREMENT,
  FEEDBACK TRANSFORMS INPUT STATE

- CLOSED-LOOP SYSTEM AS MEASUREMENT SYNTHESIS -
  INPUT STATE UNCHANGED,
  FEEDBACK TRANSFORMS DETECTOR MEASUREMENT

DEAD-TIME SYSTEM

- MEASUREMENT SYNTHESIS

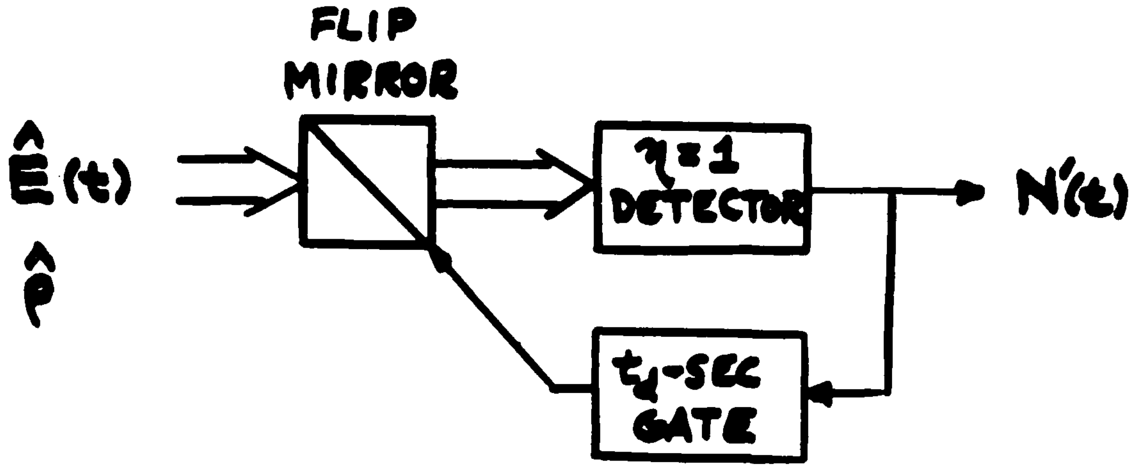

$dN'_t \equiv \lim_{\Delta t \downarrow 0} \Delta N'_t$ MEASURES $\int dN'_t \, |d\underset{\sim}{N}_t\rangle\langle d\underset{\sim}{N}_t|$

$|d\underset{\sim}{N}_t\rangle$ = MULTIMODE NUMBER STATE

$d\underset{\sim}{N}_t \equiv \{dN_\tau : t_0 \le \tau \le t\}$

$dN_\tau = 1$ INDICATES PHOTON AT TIME τ

$$dN'_t = \left[1 - u\left(\int_{t-t_d}^{t} dN_\tau\right)\right] dN_t$$

DEAD-TIME SYSTEM

- **STATE SYNTHESIS**

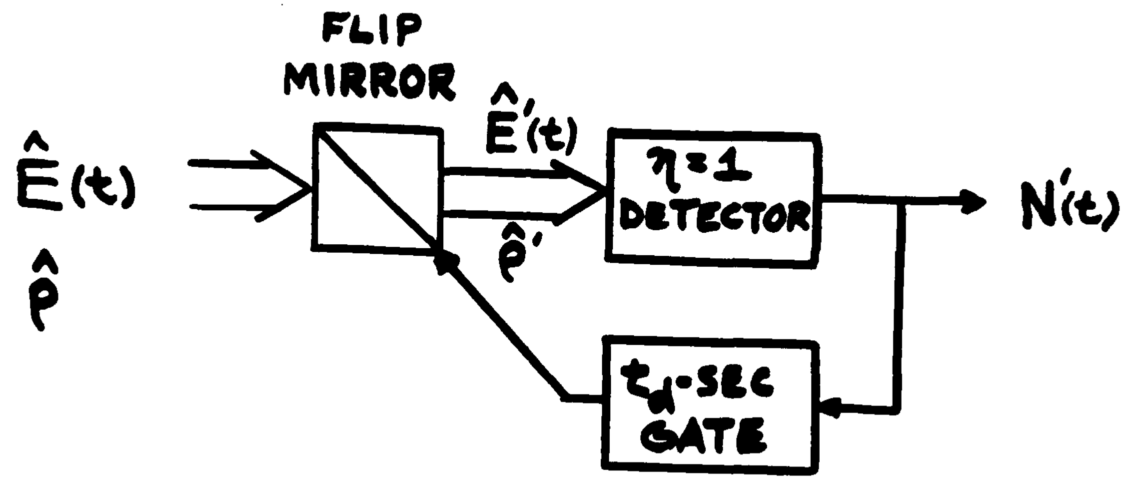

$$dN'_t \equiv \lim_{\Delta t \downarrow 0} \Delta N'_t \quad \text{MEASURES} \quad \hat{E}'^{\dagger}(t)\,\hat{E}'(t)\,dt$$

$$\langle d\underset{\sim}{N}'_t | \hat{\rho}' | d\underset{\sim}{N}'_t \rangle = \int_{d\underset{\sim}{N}_t \in \Theta^{-1}(d\underset{\sim}{N}'_t)} \langle d\underset{\sim}{N}_t | \hat{\rho} | d\underset{\sim}{N}_t \rangle$$

$$d\underset{\sim}{N}_t \xrightarrow{\Theta} d\underset{\sim}{N}'_t \quad \text{IS THE MAP}$$

$$dN'_t = \left[1 - u\left(\int_{t-t_d}^{t} dN_t \right) \right] dN_t$$

OPEN QUESTIONS

- WHAT MEASUREMENTS CAN BE SYNTHESIZED VIA PHOTODETECTION FEEDBACK?
- WHAT STATES CAN BE SYNTHESIZED VIA PHOTODETECTION FEEDBACK?

UNCLASSIFIED
SECURITY CLASSIFICATION OF THIS PAGE

REPORT DOCUMENTATION PAGE

1a. REPORT SECURITY CLASSIFICATION Unclassified	1b. RESTRICTIVE MARKINGS A186 935
2a. SECURITY CLASSIFICATION AUTHORITY	3. DISTRIBUTION/AVAILABILITY OF REPORT Approved for public release; distribution unlimited
2b. DECLASSIFICATION / DOWNGRADING SCHEDULE	
4. PERFORMING ORGANIZATION REPORT NUMBER(S)	5. MONITORING ORGANIZATION REPORT NUMBER(S)
6a. NAME OF PERFORMING ORGANIZATION Research Laboratory of Electronics Massachusetts Institute of Technology 6b. OFFICE SYMBOL (If applicable)	7a. NAME OF MONITORING ORGANIZATION
6c. ADDRESS (City, State, and ZIP Code) 77 Massachusetts Avenue Cambridge, MA 02139	7b. ADDRESS (City, State, and ZIP Code)
8a. NAME OF FUNDING/SPONSORING ORGANIZATION Office of Naval Research 8b. OFFICE SYMBOL (If applicable)	9. PROCUREMENT INSTRUMENT IDENTIFICATION NUMBER N00014-87-G-0198
8c. ADDRESS (City, State, and ZIP Code) 800 North Quincy Street Arlington, Virginia 22217 - 5000	10. SOURCE OF FUNDING NUMBERS PROGRAM ELEMENT NO. 41 / PROJECT NO. 24502---01 / TASK NO. / WORK UNIT ACCESSION NO

11. TITLE (Include Security Classification)
United States – Japan Seminar on Quantum Mechanical Aspects of Quantum Electronics
Hilton Inn Resort, Monterey, California – July 21-24, 1987

12. PERSONAL AUTHOR(S)
J. H. Shapiro and H. Takuma, Coordinators

13a. TYPE OF REPORT	13b. TIME COVERED	14. DATE OF REPORT (Year, Month, Day)	15. PAGE COUNT
Proceedings	FROM ______ TO ______	October 1987	660

16. SUPPLEMENTARY NOTATION

17. COSATI CODES			18. SUBJECT TERMS (Continue on reverse if necessary and identify by block number)
FIELD	GROUP	SUB-GROUP	

19. ABSTRACT (Continue on reverse if necessary and identify by block number)

These Proceedings represent summaries and viewgraphs from a U.S. – Japan Seminar entitled "Quantum Mechanical Aspects of Quantum Electronics," which was held from July 21 to July 24, 1987 at the Hilton Inn Resort in Monterey, California. The Sem ar focused on: neutral atom trapping; ultrahigh stability sources and ultrahigh resolution spectroscopy; squeezed states of light; and nonlinear optics of semiconductors.

20. DISTRIBUTION/AVAILABILITY OF ABSTRACT ☒ UNCLASSIFIED/UNLIMITED ☐ SAME AS RPT ☐ DTIC USERS	21. ABSTRACT SECURITY CLASSIFICATION Unclassified
22a. NAME OF RESPONSIBLE INDIVIDUAL Kyra M. Hall	22b. TELEPHONE (Include Area Code) (617) 253-2569 22c. OFFICE SYMBOL

DD FORM 1473, 84 MAR   83 APR edition may be used until exhausted.
All other editions are obsolete.

SECURITY CLASSIFICATION OF THIS PAGE
UNCLASSIFIED

END
Feb.
1988
DTIC